17TH EDITION OF THE SPANISH SOCIETY FOR DEVELOPMENTAL BIOLOGY MEETING: NEW TRENDS IN DEVELOPMENTAL BIOLOGY

EDITED BY: Rosa Barrio and Sofia J. Araújo
PUBLISHED IN: Frontiers in Cell and Developmental Biology

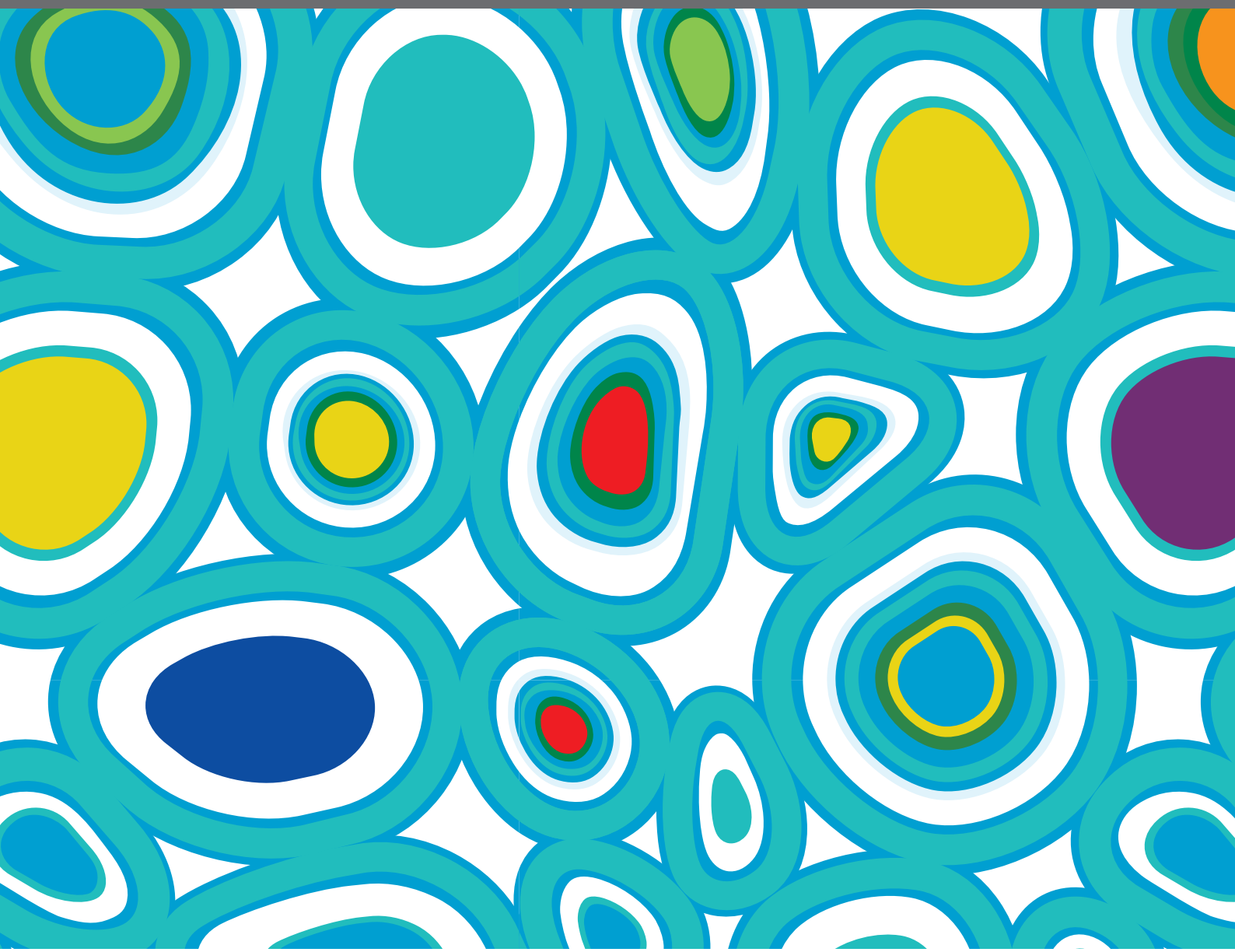

frontiers Research Topics

ISSN 1664-8714
ISBN 978-2-88976-130-2
DOI 10.3389/978-2-88976-130-2

About Frontiers

Frontiers is more than just an open-access publisher of scholarly articles: it is a pioneering approach to the world of academia, radically improving the way scholarly research is managed. The grand vision of Frontiers is a world where all people have an equal opportunity to seek, share and generate knowledge. Frontiers provides immediate and permanent online open access to all its publications, but this alone is not enough to realize our grand goals.

Frontiers Journal Series

The Frontiers Journal Series is a multi-tier and interdisciplinary set of open-access, online journals, promising a paradigm shift from the current review, selection and dissemination processes in academic publishing. All Frontiers journals are driven by researchers for researchers; therefore, they constitute a service to the scholarly community. At the same time, the Frontiers Journal Series operates on a revolutionary invention, the tiered publishing system, initially addressing specific communities of scholars, and gradually climbing up to broader public understanding, thus serving the interests of the lay society, too.

Dedication to Quality

Each Frontiers article is a landmark of the highest quality, thanks to genuinely collaborative interactions between authors and review editors, who include some of the world's best academicians. Research must be certified by peers before entering a stream of knowledge that may eventually reach the public - and shape society; therefore, Frontiers only applies the most rigorous and unbiased reviews.
Frontiers revolutionizes research publishing by freely delivering the most outstanding research, evaluated with no bias from both the academic and social point of view. By applying the most advanced information technologies, Frontiers is catapulting scholarly publishing into a new generation.

What are Frontiers Research Topics?

Frontiers Research Topics are very popular trademarks of the Frontiers Journals Series: they are collections of at least ten articles, all centered on a particular subject. With their unique mix of varied contributions from Original Research to Review Articles, Frontiers Research Topics unify the most influential researchers, the latest key findings and historical advances in a hot research area! Find out more on how to host your own Frontiers Research Topic or contribute to one as an author by contacting the Frontiers Editorial Office: frontiersin.org/about/contact

17TH EDITION OF THE SPANISH SOCIETY FOR DEVELOPMENTAL BIOLOGY MEETING: NEW TRENDS IN DEVELOPMENTAL BIOLOGY

Topic Editors:
Rosa Barrio, CIC bioGUNE, Spain
Sofia J. Araújo, University of Barcelona, Spain

Citation: Barrio, R., Araújo, S. J. eds. (2022). 17th Edition of the Spanish Society for Developmental Biology Meeting: New Trends in Developmental Biology. Lausanne: Frontiers Media SA. doi: 10.3389/978-2-88976-130-2

Table of Contents

05 ***Editorial: 17th Spanish Society for Developmental Biology Meeting: New Trends in Developmental Biology***
Sofia J. Araújo and Rosa Barrio

07 ***Meis2 Is Required for Inner Ear Formation and Proper Morphogenesis of the Cochlea***
María Beatriz Durán Alonso, Victor Vendrell, Iris López-Hernández, María Teresa Alonso, Donna M. Martin, Fernando Giráldez, Laura Carramolino, Giovanna Giovinazzo, Enrique Vázquez, Miguel Torres and Thomas Schimmang

18 ***Role of the Forkhead Transcription Factors Fd4 and Fd5 During* Drosophila *Leg Development***
Mireya Ruiz-Losada, Cristian Pérez-Reyes and Carlos Estella

32 ***PAX2$^+$ Mesenchymal Origin of Gonadal Supporting Cells Is Conserved in Birds***
Martin A. Estermann, Mylene M. Mariette, Julie L. M. Moreau, Alexander N. Combes and Craig A. Smith

45 ***SALL1 Modulates CBX4 Stability, Nuclear Bodies, and Regulation of Target Genes***
Immacolata Giordano, Lucia Pirone, Veronica Muratore, Eukene Landaluze, Coralia Pérez, Valerie Lang, Elisa Garde-Lapido, Monika Gonzalez-Lopez, Orhi Barroso-Gomila, Alfred C. O. Vertegaal, Ana M. Aransay, Jose Antonio Rodriguez, Manuel S. Rodriguez, James D. Sutherland and Rosa Barrio

62 ***Muscle Satellite Cell Heterogeneity: Does Embryonic Origin Matter?***
Lara Rodriguez-Outeiriño, Francisco Hernandez-Torres, F. Ramírez-de Acuña, Lidia Matías-Valiente, Cristina Sanchez-Fernandez, Diego Franco and Amelia Eva Aranega

72 ***Mosmo Is Required for Zebrafish Craniofacial Formation***
Carlos Camacho-Macorra, Marcos Sintes, Noemí Tabanera, Irene Grasa, Paola Bovolenta and Marcos J. Cardozo

81 ***Developmental Disruption of* Erbb4 *in* Pet1*+ Neurons Impairs Serotonergic Sub-System Connectivity and Memory Formation***
Candela Barettino, Álvaro Ballesteros-Gonzalez, Andrés Aylón, Xavier Soler-Sanchis, Leticia Ortí, Selene Díaz, Isabel Reillo, Francisco García-García, Francisco José Iborra, Cary Lai, Nathalie Dehorter, Xavier Leinekugel, Nuria Flames and Isabel Del Pino

98 ***Origin and Development of the Adipose Tissue, a Key Organ in Physiology and Disease***
Esmeralda Parra-Peralbo, Ana Talamillo and Rosa Barrio

120 ***The Role of Bmp- and Fgf Signaling Modulating Mouse Proepicardium Cell Fate***
Carlos Garcia-Padilla, Francisco Hernandez-Torres, Estefania Lozano-Velasco, Angel Dueñas, Maria del Mar Muñoz-Gallardo, Isabel S. Garcia-Valencia, Lledó Palencia-Vincent, Amelia Aranega and Diego Franco

138 ***Dynamic MicroRNA Expression Profiles During Embryonic Development Provide Novel Insights Into Cardiac* Sinus Venosus*/Inflow Tract Differentiation***
Carlos Garcia-Padilla, Angel Dueñas, Diego Franco, Virginio Garcia-Lopez, Amelia Aranega, Virginio Garcia-Martinez and Carmen Lopez-Sanchez

152 ***Transcriptional Control of Axon Guidance at Midline Structures***
Eloísa Herrera and Augusto Escalante

160 **FoxK1** ***is Required for Ectodermal Cell Differentiation During Planarian Regeneration***
Pablo Coronel-Córdoba, M. Dolores Molina, Gemma Cardona, Susanna Fraguas, Eudald Pascual-Carreras, Emili Saló, Francesc Cebrià and Teresa Adell

171 ***LanB1 Cooperates With Kon-Tiki During Embryonic Muscle Migration in* Drosophila**
Juan José Pérez-Moreno, Carmen Santa-Cruz Mateos, María Dolores Martín-Bermudo and Beatriz Estrada

181 ***Corrigendum: LanB1 Cooperates With Kon-Tiki During Embryonic Muscle Migration in* Drosophila**
Juan José Pérez-Moreno, Carmen Santa-Cruz Mateos, María Dolores Martín-Bermudo and Beatriz Estrada

frontiers | Frontiers in Cell and Developmental Biology

EDITORIAL
published: 20 April 2022
doi: 10.3389/fcell.2022.897989

Editorial: 17th Spanish Society for Developmental Biology Meeting: New Trends in Developmental Biology

Sofia J. Araújo[1,2]* *and Rosa Barrio*[3]*

[1]Department of Genetics, Microbiology and Statistics, School of Biology, University of Barcelona, Barcelona, Spain, [2]Institute of Biomedicine University of Barcelona (IBUB), Barcelona, Spain, [3]Center for Cooperative Research in Biosciences (CIC bioGUNE), Basque Research and Technology Alliance (BRTA), Bizkaia Technology Park, Derio, Spain

Keywords: Developmental Biology, Conference, Spanish Society for Developmental Biology, Trends in Development, Scientific Society, Virtual Meeting

Editorial on the Research Topic

17th Spanish Society for Developmental Biology Meeting: New Trends in Developmental Biology

The Spanish Society for Developmental Biology organized its 17th meeting in November 2020. The meeting, organized by CIC bioGUNE, the University of the Basque Country and the University of Cantabria, gathered about 280 registrants and received 132 scientific abstracts. Participants ranged from undergraduate to senior researchers, with a broad participation of Ph.D. students. The meeting was organized in 8 sessions: Growth and Scaling, Self-organization, Neurodevelopment, Genomes, Cell Biology, Development and Disease, Evo-Devo and Regeneration (Araújo et al., 2021). These sessions focused on the new tendencies in Developmental Biology research and, based on the science presented there, we organized this special issue on *The 17*th *Edition of the Spanish Society for Developmental Biology Meeting: New Trends in Developmental Biology*. This collection of articles gathers several scientific contributions in this area, featuring collaborative and interdisciplinary approaches among developmental biologists.

With the focus on organogenesis and gene regulation, our selected content embraces novel discoveries on muscle development, regeneration and the transcriptional control and role of miRNAs in development, while highlighting advances in organogenesis and gonadal development.

Original research articles include works on ear morphogenesis, where Durán-Alonso et al. show that Meis2 is essential for inner ear formation, providing an entry point to the network underlying proper cochlear coiling. Muscle morphogenesis is approached in a report by Pérez-Moreno et al., reporting that the interaction between laminins and the proteoglycan Kon-tiki/Perdido controls both myotube migration and attachment during *Drosophila* myogenesis. Garcia-Padilla et al., study the role of Bmp- and Fgf signaling in the modulation of mouse proepicardium cell fate and propose that species-specific differences regulate proepicardial/septum transversum cardiomyogenic lineage commitment. Muscle satellite cell origin and heterogeneity in the context of muscle regeneration is reviewed by Rodriguez-Outeiriño et al., who summarize works supporting the different developmental origins of satellite cells.

Planarian regeneration is tackled by Coronel-Córdoba et al., who study the involvement of FoxK1 transcription factor in ectodermal tissues and report on its involvement neural and epidermal tissue regeneration.

Organogenesis is the subject of more research reported in this issue. Camacho-Macorra et al. analyze the involvement of the Hedgehog pathway in craniofacial development, by studying Mosmo, a modulator of the pathway. Inactivation of the two zebrafish Mosmo paralogs induces craniofacial skeleton defects, suggesting that Mosmo is a candidate to explain uncharacterized forms of human

OPEN ACCESS

Edited and reviewed by:
Ana Cuenda,
Spanish National Research Council (CSIC), Spain

***Correspondence:**
Sofia J. Araújo
sofiajaraujo@ub.edu
Rosa Barrio
rbarrio@cicbiogune.es

Specialty section:
This article was submitted to Signaling, a section of the journal Frontiers in Cell and Developmental Biology

Received: *16 March 2022*
Accepted: *21 March 2022*
Published: *20 April 2022*

Citation:
Araújo SJ and Barrio R (2022) Editorial: 17th Spanish Society for Developmental Biology Meeting: New Trends in Developmental Biology. Front. Cell Dev. Biol. 10:897989. doi: 10.3389/fcell.2022.897989

congenital craniofacial malformations. Appendage development is the subject of study of Ruiz-Losada et al., who report on a redundant role of forkhead transcription factors Fd4 and Fd5 during *Drosophila* leg development. The involvement of miRNAs during early cardiac development is studied by Garcia-Padilla et al., who analyze the expression profiles of different miRNAs and demonstrate their modulation of different Hox clusters. They propose that miRNAs are involved in Hox gene modulation during differentiation and compartmentalization of the posterior structures of the developing venous pole of the heart.

Developmental gene regulation is explored by Giordano et al., who report on the relationship between two key transcription factors, CBX4 and SALL1, showing they interact in the nucleoplasm and uncovering a new way of SALL1-mediated regulation of Polycomb bodies through modulation of CBX4 stability. They present a novel mechanism of regulation of a developmental factor, which has consequences for the regulation of its target genes.

Estermann et al. build the first comparative molecular characterization of gonadal supporting cell differentiation in birds, which reveals conservation of $PAX2^{+}$ expression and a mesenchymal origin of gonadal supporting cells, indicating that gonadal morphogenesis is conserved among the major bird clades.

An original research report by Barettino et al. reports on the developmental mechanisms guiding the formation of serotonergic sub-systems. They unveil a developmental process acting through Erb4 in subsets of serotonergic neurons to orchestrate a long-range circuit involved in the formation of emotional and social memories. Nervous system development in the context of the transcriptional control of axon guidance and the selection of trajectories at midline structures is reviewed by Herrera and Escalante.

Finally, Parra-Peralbo et al., review the current knowledge on the origin and development of the adipose tissue, focusing on this organ in *Drosophila melanogaster* and identifying some gaps for future research.

Together, manuscripts in this Research Topic (https://www.frontiersin.org/research-topics/17566/17th-edition-of-the-spanish-society-for-developmental-biology-meeting-new-trends-in-developmental-bi#articles) provide an overview of the latest research on the new trends in developmental biology, ranging from early embryogenesis to regeneration, through gene regulation, in a variety of systems and organs. The contributions presented here reflect the diversity and richness of the presentations we enjoyed at the 17th edition of the SEBD meeting. We are looking forward to the next edition!

AUTHOR CONTRIBUTIONS

SA and RB wrote this Editorial.

ACKNOWLEDGMENTS

We would like to thank to all the authors that contributed to this special issue and to the Scientific and Organizing Committee members of the 17th Edition of the Spanish Society for Developmental Biology Meeting. RB acknowledges funding by PID 2020-114178 GB-I00 (MINECO/FEDER, EU), SAF 2017-90900-REDT (UBIRed Program); SA acknowledges funding by PGC 2018-099465-B-I00 and the National Ataxia Foundation (NAF); and RB and SA acknowledge networking support from the ProteoCure COST Action (CA20113).

REFERENCES

Araújo, S. J., Almudi, I., Bozal-Basterra, L., Casares, F., Casas-Tintó, S., Escalante, A., et al. (2021). Virtual Meeting, Real and Sound Science: Report of the 17th Meeting of the Spanish Society for Developmental Biology (SEBD-2020). *Int. J. Dev. Biol.* 52 (7-8-9), 457–464. doi:10.1387/ijdb.210005rb

frontiers in Cell and Developmental Biology

BRIEF RESEARCH REPORT
published: 28 May 2021
doi: 10.3389/fcell.2021.679325

Meis2 Is Required for Inner Ear Formation and Proper Morphogenesis of the Cochlea

*María Beatriz Durán Alonso[1], Victor Vendrell[1], Iris López-Hernández[1], María Teresa Alonso[1], Donna M. Martin[2], Fernando Giráldez[3], Laura Carramolino[4], Giovanna Giovinazzo[4], Enrique Vázquez[4], Miguel Torres[4] and Thomas Schimmang[1]**

[1] Instituto de Biología y Genética Molecular, Universidad de Valladolid y Consejo Superior de Investigaciones Científicas, Valladolid, Spain, [2] Departments of Pediatrics and Human Genetics, University of Michigan, Ann Arbor, MI, United States, [3] CEXS, Universitat Pompeu Fabra, Parc de Recerca Biomédica de Barcelona, Barcelona, Spain, [4] Cardiovascular Development Program, Centro Nacional de Investigaciones Cardiovasculares, CNIC, Madrid, Spain

OPEN ACCESS

Edited by:
Rosa Barrio, CIC bioGUNE, Spain

Reviewed by:
Andy Groves, Baylor College of Medicine, United States
Olivia Bermingham-McDonogh, University of Washington, United States

***Correspondence:**
Thomas Schimmang
schimman@ibgm.uva.es

Specialty section:
This article was submitted to Morphogenesis and Patterning, a section of the journal Frontiers in Cell and Developmental Biology

Received: *11 March 2021*
Accepted: *29 April 2021*
Published: *28 May 2021*

Citation:
Durán Alonso MB, Vendrell V, López-Hernández I, Alonso MT, Martin DM, Giráldez F, Carramolino L, Giovinazzo G, Vázquez E, Torres M and Schimmang T (2021) Meis2 Is Required for Inner Ear Formation and Proper Morphogenesis of the Cochlea. Front. Cell Dev. Biol. 9:679325. doi: 10.3389/fcell.2021.679325

Meis genes have been shown to control essential processes during development of the central and peripheral nervous system. Here we have explored the roles of the *Meis2* gene during vertebrate inner ear induction and the formation of the cochlea. *Meis2* is expressed in several tissues required for inner ear induction and in non-sensory tissue of the cochlear duct. Global inactivation of *Meis2* in the mouse leads to a severely reduced size of the otic vesicle. Tissue-specific knock outs of *Meis2* reveal that its expression in the hindbrain is essential for otic vesicle formation. Inactivation of *Meis2* in the inner ear itself leads to an aberrant coiling of the cochlear duct. By analyzing transcriptomes obtained from *Meis2* mutants and ChIPseq analysis of an otic cell line, we define candidate target genes for *Meis2* which may be directly or indirectly involved in cochlear morphogenesis. Taken together, these data show that *Meis2* is essential for inner ear formation and provide an entry point to unveil the network underlying proper coiling of the cochlear duct.

Keywords: inner ear, cochlea, Meis, organ of corti, mouse

INTRODUCTION

Development of the inner ear begins as a thickening of the ectoderm adjacent to the posterior hindbrain termed the otic placode, which can be observed at embryonic day 8 (E 8) in the mouse. In vertebrates, induction of the otic placode requires the interaction with neighboring tissues such as the neural tissue of the hindbrain, the mesoderm and/or the endoderm. Members of the fibroblast growth factor (*Fgf*) gene family such as *Fgf3* have been shown to play a central role during otic placode induction (Schimmang, 2007; Whitfield, 2015). After E8 in the mouse, the otic placode invaginates and forms the otic vesicle, which undergoes a series of morphogenetic steps to form the complex shape of the mature inner ear. Cochlear morphogenesis is initiated at the ventral portion of the otic vesicle that elongates and coils in an anterior–medial direction until it reaches its full one and three−quarters turns. This process is paralleled by cellular differentiation that leads to the formation of sensory cells such as hair cells and auditory neurons, and non-sensory components within the cochlear duct (Basch et al., 2016).

Meis genes are vertebrate orthologs of the Drosophila homolog *homothorax* (*hth*) gene which encode for transcription factors belonging to the superclass of TALE (three amino acid loop extension) proteins. *Meis* genes play key roles during development of the central and peripheral nervous systems, and interact with signaling pathways such as those controlled by Wnt, Fgf and retinoic acid (Schulte and Frank, 2014). The TALE superclass of proteins contains an atypical homeodomain and comprises five separate classes: Meinox, including Prep (*Prep1–2* genes) and Meis (*Meis1–3* genes), Pbc (*Pbx1–4* genes) and the three more distantly related TG-interacting factors, Iroquois, and Mohawk (Schulte and Geerts, 2019). A prominent characteristic of Meinox proteins is their capacity to heterodimerize with the structurally related Pbx proteins. A further group of Meis protein-binding partners participating in these cooperative interactions is the Hox proteins. In this case, Meis proteins often do not interact directly with DNA (Penkov et al., 2013).

In the present work, we have analyzed the role of *Meis2* during inner ear induction and cochlear development. We show that during inner ear induction *Meis2* is prominently expressed in the hindbrain neighboring the otic placode and to a lesser extent in the periotic mesoderm and endoderm. Specific inactivation in the rhombomeres flanking the otic placode, led to reduced otic vesicles, uncovering a dominant role of hindbrain *Meis2* in otic vesicle formation. Inactivation of *Meis2* within the otic placode caused morphological defects including improper coiling of the cochlea. Microarray analysis revealed a set of genes that were downregulated in mutant cochleas, representing potential *Meis2* target genes required for proper morphogenesis of the cochlear duct. Finally, ChIPseq analysis in an otic cell line with the potential to give rise to sensory and non-sensory cochlear tissue (VOT-E36) allowed the detection of genes whose regulatory regions bind Meis2 directly or indirectly. Our results thus show that *Meis2* is essential for otic vesicle formation and cochlear duct morphogenesis.

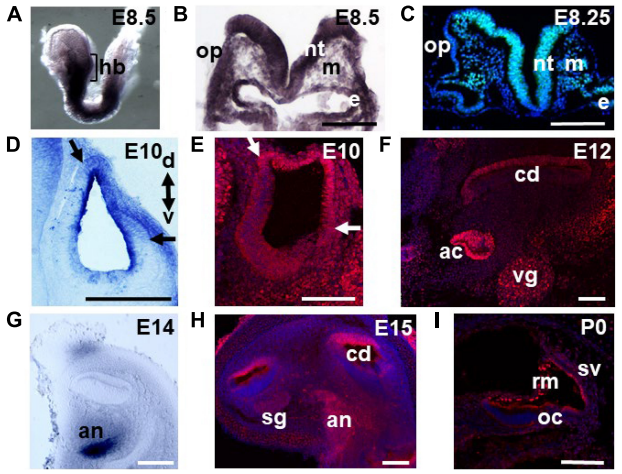

FIGURE 1 | Meis2 expression throughout inner ear development. Meis2 expression was detected via mRNA *in situ* hybridization **(A,B,D,G)** or immunohistochemistry **(C,E,F,H,I)** at the indicated stages. **(A)** At embryonic day (E) 8.5 high levels of Meis2 are detected at the level of the hindbrain (hb) and on corresponding sections at the level of the otic placode (op) **(B)**. High levels of Meis2 protein are detected in the neural tube (nt), the endoderm (e), and weaker expression in the mesoderm (m) and the placode itself **(C)**. **(D)** In the otic vesicle low *Meis2* mRNA levels are observed in its dorsal-lateral portion (borders indicated by arrows). The orientations of the sections through the otic vesicles along the dorsal (d)–ventral (v) axis are indicated. **(E)** Immunohistochemical detection of Meis2 protein in the dorsal-lateral quadrant of the otic vesicle. **(F)** Presence of Meis2 protein in the roof of the cochlear duct (cd), the vestibular ganglion (vg) and the ampullary cristae (ac). **(G)** High levels of *Meis2* mRNA are detected in the auditory nerve (an). **(H)** Next to the auditory nerve, Meis2 protein is also observed in the roof of the cochlear duct and to a lesser extent in the spiral ganglion (sg). **(I)** At P0 Meis2 immunoreactivity is detected in Reissner's membrane (rm) and the stria vascularis (sv). oc, organ of Corti. Scale bars in **(B,C,E–H)**: 100 μm; in **(D)**: 200 μm and in **(I)**: 75 μm.

RESULTS

Meis2 Expression During Inner Ear Development

In order to define *Meis2* expression throughout inner ear development, we performed whole mount RNA *in situ* hybridization and immunohistochemistry studies. During inner ear induction around E8–8.5, high levels of mRNA were detected in the developing hindbrain (**Figure 1A**). Sections of the posterior hindbrain confirmed this expression and revealed *Meis2* transcripts in the otic placode and the neighboring mesoderm and endoderm (**Figure 1B**). Immunohistochemistry confirmed high levels of Meis2 protein in the hindbrain and moderate to low amounts in the endoderm, mesoderm and otic placode (**Figure 1C**). Upon formation of the otic vesicle Meis2 immunoreactivity was observed in its dorsolateral domain, accompanied by low but detectable *Meis2* mRNA (**Figures 1D,E**).

During inner ear morphogenesis around E12, Meis2 protein was detected in the roof of the cochlear duct, which will give rise to non-sensory tissue (**Figure 1F**). Expression in this domain was maintained at E15 and was also detected in the auditory nerve at the protein and shortly before at the mRNA level (**Figures 1G,H**). Low levels of anti-Meis2 immunoreactivity were also observed in the spiral ganglion (**Figure 1H**). At postnatal day 0 (P0), Meis2 protein was observed in Reissner's membrane and the stria vascularis but not in the sensory tissue corresponding to the organ of Corti (**Figure 1I**). Adjacent to the cochlea, Meis2 protein was also detected in different parts of the vestibular system such as the ampullary cristae, the utriculus, the semicircular canals and the vestibular ganglion (**Figure 1F** and data not shown).

Meis2 Is Required for Otic Vesicle Formation

To analyze the requirement of *Meis2* for inner ear formation, we inactivated its expression throughout the epiblast by crossing a mouse strain carrying a floxed *Meis2* allele with a *Sox2*-Cre deleter strain (Hayashi et al., 2002). $Meis2^{flox/flox}$; $Sox2^{Cre/+}$ embryos showed a severely reduced otic vesicle at E9 as revealed by *in situ* hybridization with the otic markers *Pax2* and *Dlx5* (**Figures 2A–D**), confirming similar observations made in *Meis2* null mutants (Machon et al., 2015). Therefore, *Meis2* is required for otic vesicle formation.

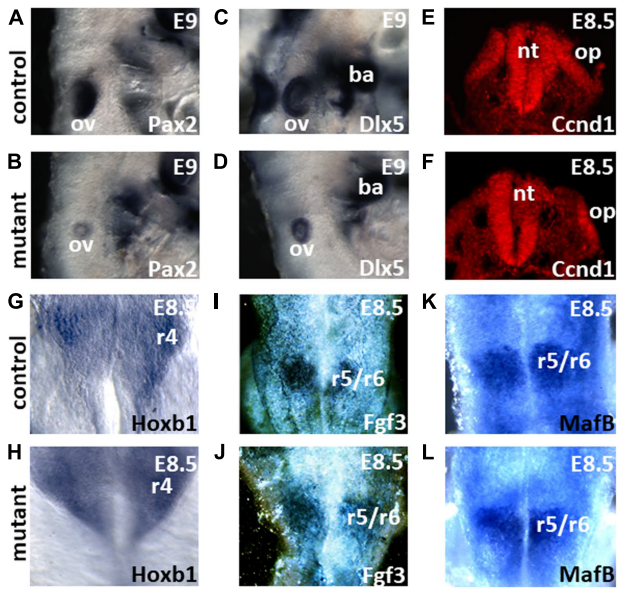

FIGURE 2 | Global inactivation of *Meis2* affects inner ear formation. **(A–D)** *Meis2*$^{flox/flox}$; *Sox2*$^{Cre/+}$ mutants show severely reduced otic vesicles (ov) at embryonic day 9 (E9) in comparison to controls as revealed by *Pax2* and *Dlx5* riboprobes. **(E,F)** Sections reveal widespread cyclinD1 immunoreactivity in the neural tube (nt) and the otic placode (op) of controls and mutants. Note the reduced size of the otic placode in the mutant. **(G–L)** Flatmounts of the hindbrain reveal an unaltered expression of *Hoxb1, Fgf3* and *MafB* riboprobes in the indicated rhombomeres (r) in *Meis2*$^{flox/flox}$; *Sox2*$^{Cre/+}$ mutants in comparison to control embryos. ba, branchial arch.

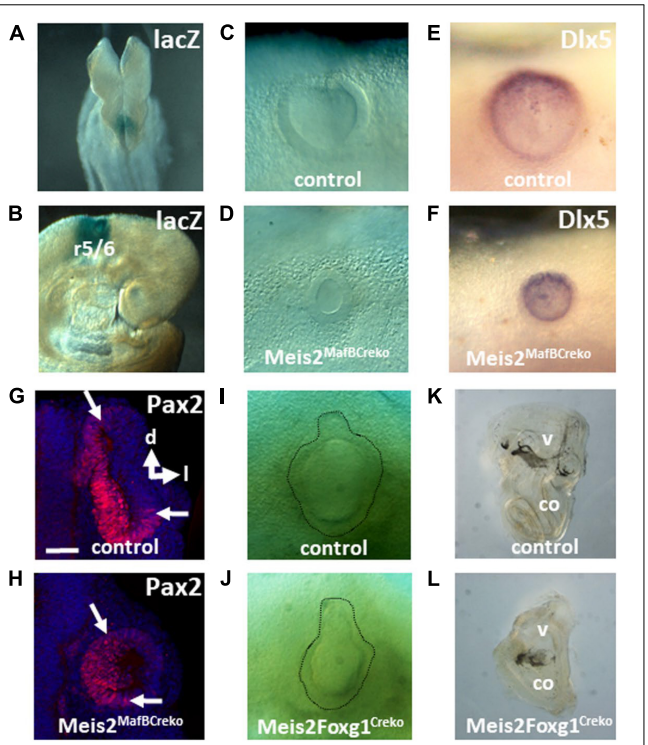

FIGURE 3 | Effects of tissue-specific inactivation of Meis2 on inner ear formation. **(A,B)** lacZ *ROSA*26 reporter staining caused by the *MafB*Cre driver in the posterior hindbrain of E8.25 embryos and in rhombomeres (r) flanking the otic vesicle at E9 **(B)**. **(C–H)** Meis2$^{flox/flox}$; *MafB*$^{Cre/+}$ mutants show reduced sized vesicles **(C,D)** which maintain expression of *Dlx5* (at E9) and Pax2 (at E9,5), as revealed by whole mount RNA *in situ* hybridization **(E,F)** and immunohistochemistry **(G,H)**. The orientations of the sections through the otic vesicles along the dorsal (d)–lateral (l) axis are indicated. **(I–L)** Bright field view of otic vesicles at E11.5 and cleared inner ears at P1 from *Meis2*$^{flox/flox}$; *Foxg1*$^{Cre/+}$ mutants. Note the flask-shaped morphology of the otic vesicle and the lack of a discernible cochlea (co) in the mutants. v, vestibule.

Next, we were interested to determine the tissue-specific requirements for *Meis2* during otic induction. Since *Meis2* was strongly expressed in the hindbrain during otic development, we sought to find a Cre line with a specific activity in the hindbrain. The *MafB* gene is expressed in the posterior hindbrain next to the developing otic placode and vesicle (Cordes and Barsh, 1994). Recently, a *MafB*-Cre line has been employed for lineage tracing of macrophages which are also characterized by endogenous *MafB* expression (Wu et al., 2016). To assay if Cre activity also occurred in the developing hindbrain, we crossed *MafB*-Cre transgenic mice with *ROSA26* reporter mice (Soriano, 1999). Cre activity was detected by X-gal staining at E8.5 in the posterior hindbrain and in rhombomeres flanking the otic vesicle at E9 (**Figures 3A,B** and **Supplementary Figure 1**). This confirmed its utility for the inactivation of floxed genes during inner ear formation. In order to study the requirement for hindbrain *Meis2* expression during otic vesicle formation, we analyzed the effects of *Meis2* conditional inactivation induced by *MafB*-Cre at the otic vesicle stage. *Meis2*$^{flox/flox}$; *MafB*$^{Cre/+}$ mutants showed a severely reduced vesicle at E9 comparable to the size observed upon global *Meis2* inactivation with a penetrance of 50% (n = 2/4; **Figures 3C,D**). Therefore Meis2 expression in the hindbrain is required for otic vesicle formation. Staining with the otic markers *Dlx5* and *Pax2* revealed that their expression was maintained in their corresponding domains in *Meis2*$^{flox/flox}$; *MafB*$^{Cre/+}$ mutants (**Figures 3E–H**). To analyze the influence of Meis2 expression in neighboring tissue during otic induction, we used a *Foxg1*-Cre line which next to the otic placode also drives expression in peri-otic mesoderm and endoderm (Zelarayan et al., 2007; **Supplementary Figure 1**). Conditional inactivation of *Meis2* using the *Foxg1*-Cre line did not affect inner ear formation until E11.5 when a reduced sized otic vesicle with a flask-like shape was observed in *Meis2*$^{flox/flox}$; *Foxg1*$^{Cre/+}$ mutants (**Figures 3I,J**). *Meis2*$^{flox/flox}$; *Foxg1*$^{Cre/+}$ inner ears isolated at P0 and cleared with methylsalicylate revealed no discernible structures such as the cochlea or the semicircular canals (**Figures 3K,L**).

With the aim to define the molecular changes underlying defective inner ear induction, we analyzed *Meis2*$^{flox/flox}$; *Sox2*$^{Cre/+}$ mutants which show severely reduced sized otic vesicles with a penetrance of 100% for alterations in gene expression or signaling pathways known to be controlled by *Meis* genes and related to inner ear formation. Formation of the hindbrain requires *Meis* gene expression in lower vertebrates and has been shown to activate *Fgf3* expression which is redundantly required together with other *Fgf* family members to induce the

otic placode in vertebrates (Maroon et al., 2002; Alvarez et al., 2003; Wright and Mansour, 2003; Ladher et al., 2005; Gutkovich et al., 2010). Moreover, *Fgf3* has been shown to participate in the induction of *MafB* (Zelarayan et al., 2007), and *MafB* inactivation also leads to reduced sized otic vesicles (Cordes and Barsh, 1994; Wiellette and Sive, 2003; Hernandez et al., 2004). Lastly, Meis proteins together with Fgf signaling have also been shown to induce in the rhombencephalon expression of *Hox* genes that belong to the paralogous group 1 (PG1) and which are likewise required for in inner ear induction (Rossel and Capecchi, 1999; Pasqualetti et al., 2001; Schulte and Frank, 2014). RNA *in situ* hybridization with probes corresponding to *Fgf3, MafB* and the PG1 gene *HoxB1* showed no changes in their expression pattern within rhombomeres flanking the developing otic placode in *Meis2*$^{flox/flox}$; *Sox2*$^{Cre/+}$ mutants (**Figures 2G–L**).

Alternatively to hindbrain patterning defects, reduced proliferation may cause the smaller sized vesicles. Meis has been shown to regulate cyclinD1 and thereby to control eye size in vertebrates (Bessa et al., 2008; Marcos et al., 2015). CyclinD1 was prominently expressed in the hindbrain and the neighboring otic placode of both controls and *Meis2*$^{flox/flox}$; *Sox2*$^{Cre/+}$ mutants (**Figures 2E,F**).

Conditional Inactivation of *Meis2* During Inner Ear Development Affects Cochlear Coiling

To analyze the function of *Meis2* expression in the inner ear, we generated conditional mutant mice using a Cre line driven by *Pax2* regulatory sequences which has been used to inactivate floxed alleles throughout inner ear development (Ohyama and Groves, 2004; **Supplementary Figure 1**). No morphological defects in inner ear formation were found until E10.5 in *Meis2*$^{flox/flox}$; *Pax2*$^{Cre/+}$ mutants, when a reduced sized otic vesicle was observed in comparison to controls (**Figures 4A,B**).

The smaller size of the otic vesicle observed in *Meis2*$^{flox/flox}$; *Pax2*$^{Cre/+}$ mutants may be caused by a lack of proliferation. To examine cell proliferation, we used staining with an antibody against pH3 that labels cells in late G2 and M phase of the cell cycle. Immunoreactivity for pH3 was observed throughout the otic epithelium of both wild-type and *Meis2*$^{flox/flox}$; *Pax2*$^{Cre/+}$ mutants (**Figures 4C,D**). To examine potential changes in molecular markers in mutant otic vesicles, we first examined the neurosensory region. This develops in an anterior-medial domain of the otic vesicle and is characterized by the expression of *Neurogenin 1* (*Ngn1*) and *Lunatic fringe* (*Lfng*). Complementary to *Ngn1* expression, genes like *Tbx1* (*T-box transcription factor 1*) stabilize the neurogenic region (for a review, see Bok et al., 2007). No difference in the expression patterns of these markers was observed in *Meis2*$^{flox/flox}$; *Pax2*$^{Cre/+}$ mutants when compared to control otic vesicles (**Figures 4E–J**).

During normal development, *Pax2* expression is localized in the medial wall of the otic vesicle (**Figure 4K**) whereas the ventral portion is characterized by a broad domain of Sox2 at E11.5 from where the cochlear anlage derives (Basch et al., 2016; **Figure 4M**). Later on, *Pax2* and *Sox2* label the non-sensory and pro-sensory regions within the developing cochlear duct, respectively (Burton et al., 2004; Mak et al., 2009; **Figures 5A,C**). *Pax2* showed a normal pattern of expression at the otic vesicle stage in *Meis2*$^{flox/flox}$; *Pax2*$^{Cre/+}$ mutants (**Figure 4L**) but its domain was severely reduced at E14, pointing to a potential truncation of the cochlear duct (**Figure 5B**). *Sox2* staining at E11.5 revealed a reduced expression domain that correlated with the smaller size of the otic vesicle in *Meis2*$^{flox/flox}$; *Pax2*$^{Cre/+}$ mutants (**Figure 4N**). At E14 we observed a small patch of Sox2 expression at the basal portion of the cochlea, confirming the shortening of the cochlear duct (**Figure 5D**). However, sections through the cochlear duct revealed that the formation of the prosensory region in *Meis2*$^{flox/flox}$; *Pax2*$^{Cre/+}$ mutants was unaffected (**Figures 5E,F**). Sox2 staining was also unaffected in the prosensory region of all vestibular sensory epithelia, including the utricular and saccular maculae and posterior, lateral, and anterior cristae (**Figures 5C,D**).

To further explore the cochlear abnormality in *Meis2*$^{flox/flox}$; *Pax2*$^{Cre/+}$ mice, we performed whole-mount β-galactosidase staining of the inner ears from mutants which also carried a *ROSA26*lacZ reporter (Soriano, 1999). *Pax2*-Cre is active in the early otic placode and vesicle, and the *ROSA26*lacZ reporter allows labeling of all inner ear components throughout development (Ohyama and Groves, 2004). Beta-galactosidase staining revealed that in control animals, the cochlea had undertaken its one and three quarter turns (**Figure 5G**). In contrast, in *Meis2*$^{flox/flox}$; *Pax2*$^{Cre/+}$ mutants, instead of turning ventrally along the anterior-medial axis, the cochlear duct extended toward the apex but then took a U-turn toward the base. This lead to its termination being positioned half-way from its point of initiation (**Figure 5H**). This irregular turning was also confirmed by whole mount staining with myosin VII antibodies which label sensory hair cells within the cochlear duct (**Figures 5I,J**). Sections through control ears confirmed the typical structure of the cochlear duct including one row of inner hair cells and three rows of outer hair cells in controls (**Figures 5K,M**). In contrast, sections from *Meis2*$^{flox/flox}$; *Pax2*$^{Cre/+}$ mutant cochleas revealed an extra row of outer hair cells in the basal turn and an enlarged cochlear duct with clusters of hair cells at the apex (**Figures 5L,N**). Staining with calretinin antibodies that label spiral ganglion neurons and inner hair cells confirmed a normally structured cochlea with the typical appearance of basal and apical turns in control animals, whereas sections of *Meis2*$^{flox/flox}$; *Pax2*$^{Cre/+}$ mutants revealed an abnormal extension of the cochlear duct along the basal to apical axis (**Figures 5O,P**). In summary, these data confirm that loss of *Meis2* during inner ear development leads to a defective cochlear coiling and extra rows of hair cells.

Direct and Indirect Targets of Meis2 in the Cochlea

In order to identify potential target genes of Meis2 in the mammalian cochlea, we performed a microarray-based screen for differential gene expression in *Meis2*$^{flox/flox}$; *Pax2*$^{Cre/+}$ mutant vs. wild-type cochleas (for details, see section "Materials and Methods"). We used whole E15 cochleas when *Meis2* expression is detected in the cochlear duct, the spiral ganglion and the

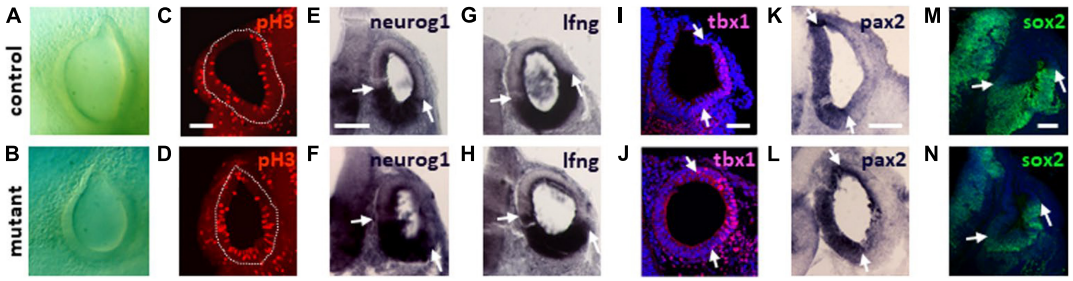

FIGURE 4 | Expression of otic vesicle markers in *Meis2*$^{flox/flox}$; *Pax2*$^{Cre/+}$ mutants. Expression of the indicated markers was detected via mRNA *in situ* hybridization **(E–H,K,L)** or immunohistochemistry **(C,D,I,J,M,N)**. **(A,B)** Bright field image of controls and mutants showing a reduced sized otic vesicle at E10,5. **(C,D)** Sections at E10 reveal widespread pH3 immunoreactivity in the otic vesicles (circumference indicated by stippled lines) of controls and mutants. **(E–L)** No changes in the spatial domains of the otic markers (borders indicated by arrows) is observed in the mutants at E9 **(E–H)** and E10 **(I–L)**. **(M,N)** At E11 the ventral domain of Sox2 expression is smaller in mutants correlating with the reduced sized dimensions of the otic vesicle at this stage. Scale bars in **(C,E,I)**: 50 μm; in **(K)**: 100 μm and in **(M)**: 75 μm.

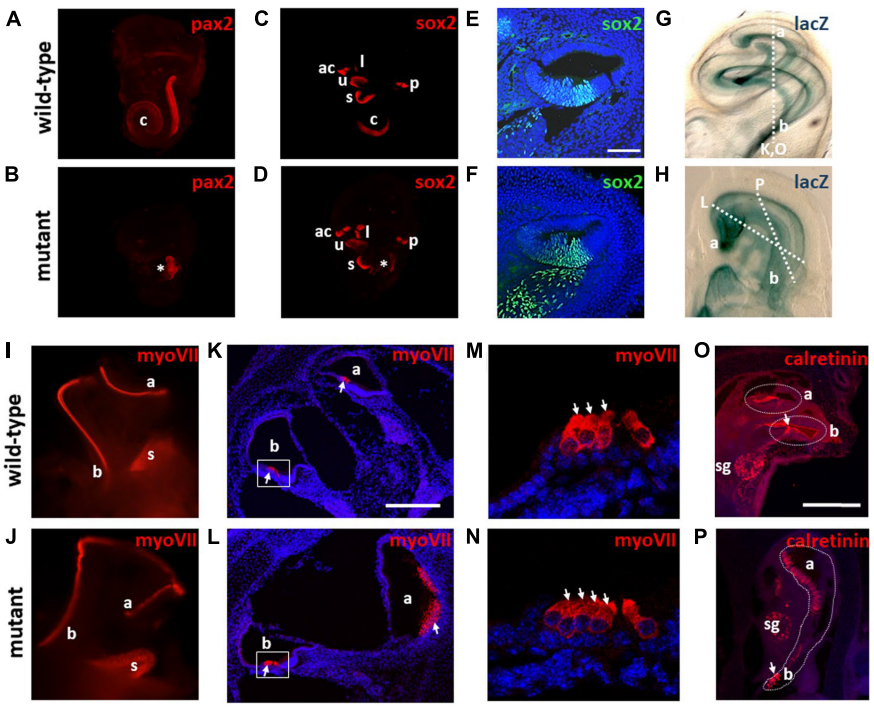

FIGURE 5 | Meis2 is required for cochlear outgrowth and coiling. Expression was monitored by staining of whole mounts or on sections with the corresponding antibodies indicated. **(A–D)** Staining with Pax2 and Sox2 antibodies reveals a truncation of the cochlear duct (c), indicated by an asterisk in the mutants. Note that the prosensory regions within the vestibular system maintain Sox2 expression in the mutants. **(E,F)** Sections through the cochlear duct reveal that formation of the prosensory region is unaffected in the mutants. **(G,H)** lacZ*ROSA26* reporter staining caused by the *Pax2*-Cre driver reveals the abnormal coiling of the cochlear duct in mutants. The basal (b) and apical (a) portions of the cochlea are indicated. **(I–L)** Staining with myosin VII antibodies labeling hair cells (indicated by arrows) confirms the abnormal morphology of the cochlear duct in mutants. Note the increased sized patches of hair cells in the apex of mutants. **(M,N)** High magnification view of the basal region (boxed in **K,L**) reveals the presence of an extra row of outer hair cells (indicated by arrows) in the mutants. **(O,P)** Sections stained with calretinin antibodies labeling inner hair cells (arrows) and the spiral ganglion (sg). Note the presence of a normal morphology in the wild-type with the typical appearance of basal and apical turns whereas the mutant shows an abnormal extension along the basal-apical axis. The plane of the sections shown in **(K,L,O,P)** are indicated in **(G,H)**. ac, anterior cristae; l, lateral cristae; p, posterior cristae; s, sacculus; u, utriculus; Scale bars: 50 μm in **(E)**; 250 μm in **(K,O)**.

auditory nerve (**Figure 1E**). The results of the microarrays showed that the vast majority of the 255 transcripts differentially expressed were downregulated in mutant cochleas (**Figure 6A**). Several of the downregulated genes are expressed in the cochlear duct or the spiral ganglion (**Table 1**). Within this group of genes, the cochlea of mouse mutants for the chromatin remodeling enzyme *Chd7* has been described to undergo an abnormal twist at their apex (Hurd et al., 2010). We first confirmed downregulation of *Chd7* by qPCR (**Figure 6B**) and then created a conditional mouse mutants for *Chd7* using the *Pax2*-Cre driver. Cleared whole mounts of inner ears isolated from *Chd7*$^{flox/flox}$; *Pax2*$^{Cre/+}$ mutants revealed a defective phenotype in cochlear coiling

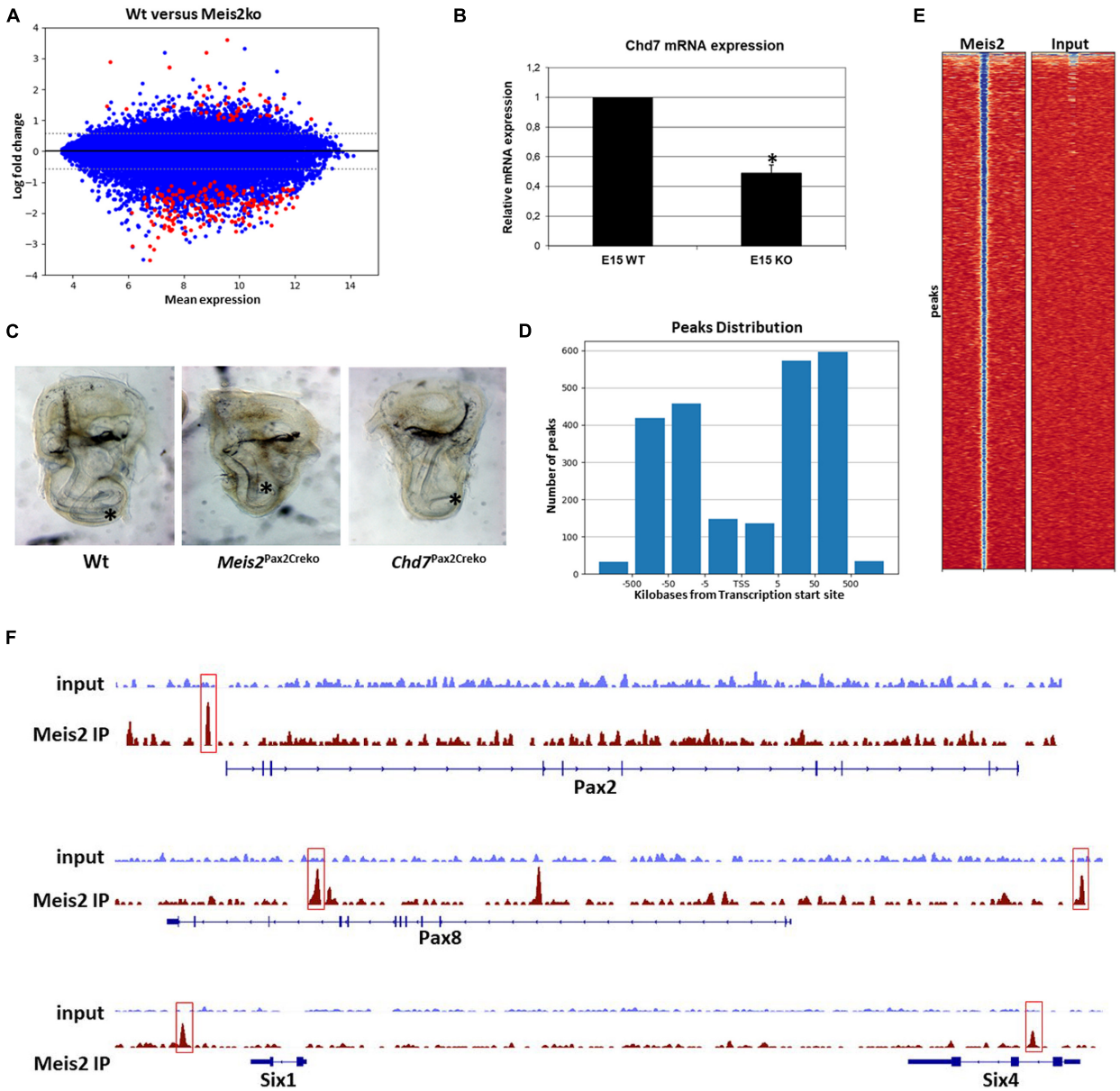

FIGURE 6 | Targets of Meis2. **(A)** MA plot showing differential gene expression between *Meis2*$^{flox/flox}$; *Pax2*$^{Cre/+}$ mutant vs. wild-type cochleas at E15. Red dots indicate significantly regulated genes. **(B)** Significantly reduced expression of *Chd7* is observed in the cochlea of *Meis2*$^{flox/flox}$; *Pax2*$^{Cre/+}$ mutants (KO) by qPCR at E15. Data were normalized to expression levels in wild-type (WT) cochleas. Student's *t*-test: $^{*}p < 0.0001$ **(C)** *Meis2*$^{flox/flox}$; *Pax2*$^{Cre/+}$ animals show a similar mutant cochlear phenotype to *Chd7*$^{flox/flox}$; *Pax2*$^{Cre/+}$ animals. The asterisk indicates the ending of the cochlear duct. **(D)** Distribution of Meis2 binding sites by their position with respect to the nearest transcription start site (TSS) in VOT-E36 cells. **(E)** Density plots showing the distribution of Meis2 binding sites vs. input control in VOT-E36 cells. **(F)** Input control and Meis2 ChIP-seq read profiles from VOT-E36 cells. Detected Meis2 binding sites within or close to the genomic regions of *Pax2, Pax8, Six1* and *Six4* are boxed.

which was very similar to the one observed in *Meis2*$^{flox/flox}$; *Pax2*$^{Cre/+}$ mutants (**Figure 6C**). Therefore, *Chd7* may be a crucial downstream target of *Meis2*.

To identify direct targets of Meis2, we performed ChIPseq analysis (see section "Materials and Methods") using the VOT-E36 cell line derived from the ventral portion of the otic vesicle, the domain that gives rise to the cochlea (Lawoko-Kerali et al., 2004; **Figure 6E**). We identified a total of 2,401 Meis2 binding sites in the genome and a collection of 917 genes with a transcription start site closest to any Meis2 binding site (GEO GSE166072). As previously reported for Meis1 (Penkov et al., 2013; Marcos et al., 2015), most Meis2 binding sites were located in regions remote from their closest associated transcription start site (**Figure 6D**). Meis proteins select two main sequences in DNA: a motif resembling the Pbx-Hox binding sequence (A/TGATNNAT), to which it binds indirectly, and a direct

binding site (TGACAG) (Penkov et al., 2013). Transcription factor motif enrichment analysis using Homer and MEME suite software (see section "Materials and Methods") confirmed these motifs as the most frequently detected with 15.7 and 28.9% of peaks containing at least one of the conserved and/or the PBX-Hox binding sites, respectively. Gene ontology analysis revealed the presence of Meis2 binding peaks in the vicinity of 30 genes related to inner ear development, such as members of the *Pax*- and *Six*-gene families (**Figure 6F**). Interestingly, a Meis2 peak was observed in the vicinity of the *Otx1* gene, whose inactivation also leads to defective cochlear coiling (Morsli et al., 1999). A comparison between the observed peaks and differentially expressed genes in the cochlea of *Meis2*$^{flox/flox}$; *Pax2*$^{Cre/+}$ mutants at E15 revealed no Meis2 binding sites in the vicinity of the *Chd7* gene. However, an overlap in the vicinity of 7 genes including *Dlg1, Pnn, Nsmce2, Usf3, Zfp945, Lrrcc1, Rybp* and *Mras* was observed. Interestingly, *Dlg1* is expressed in the otic vesicle and its loss is associated with a shortening of cochlear length (Iizuka-Kogo et al., 2015), albeit to a lesser degree than that observed in *Meis2*$^{flox/flox}$; *Pax2*$^{Cre/+}$ mutants. Therefore, loss of *Dlg1* expression may, at least in part, contribute to the shortening of the cochlear duct in *Meis2*$^{flox/flox}$; *Pax2*$^{Cre/+}$ mutants.

DISCUSSION

Meis2 was expressed in all three tissue layers involved in otic induction: the endoderm, mesoderm and the neural tissue of the hindbrain. Correlating with the highest expression levels, the loss of *Meis2* in the hindbrain led to a phenotype similar to that observed by global inactivation at E9 (compare **Figures 2A–D** with **Figures 3C–H**). Therefore, it may be concluded that *Meis2* expression in the hindbrain is likely to be sufficient to account for *Meis2* contribution to otic vesicle formation. Genes required for inner ear formation, which are directly or indirectly induced by *Meis2* showed no changes in their expression in the hindbrain, and thus so far indicate no major defects in patterning within the hindbrain in *Meis2* mutants. However, yet unknown downstream targets for Meis2 within the hindbrain may be involved in inner ear induction. During later stages, otic vesicle development was also affected in *Meis2*$^{flox/flox}$; *Foxg1*$^{Cre/+}$ mutants that lacked *Meis2* expression in the otic placode and the neighboring mesoderm and endoderm. The otic vesicle was reduced at E11 and at the postnatal stage the inner ear showed severe defects (**Figures 3I–L**). Compared to *Meis2*$^{flox/flox}$; *Pax2*$^{Cre/+}$ mutants which show Cre activity only in the otic placode (**Supplementary Figure 1** and **Figure 5**), *Meis2*$^{flox/flox}$; *Foxg1*$^{Cre/+}$ mutants show a more severe inner ear phenotype (**Figures 3K,L**). Therefore, inactivation of *Meis2* expression from the mesoderm and/or endoderm leads to additional defects during inner ear development. Within the inner ear, *Meis2* initially showed expression in the dorsal portion of the otic vesicle and was later on found in non-sensory tissue of the cochlea and the peripheral nervous system innervating the inner ear. Very similar patterns of expression for *Meis2* have also been described during chicken inner ear development (Sanchez-Guardado et al., 2011).

Meis2$^{flox/flox}$; *Pax2*$^{Cre/+}$ mouse mutants lacking *Meis2* throughout inner ear development showed a smaller otic vesicle at E10.5, indicating that initial expression of *Meis2* in the otic placode or vesicle is also required for its normal formation. Nevertheless, otic markers related to neurosensory development and formation of the cochlear anlage were unaffected. However, by E13.5 *Meis2*$^{flox/flox}$; *Pax2*$^{Cre/+}$ mutants a striking defective outgrowth of the cochlear duct became apparent which resulted in its abnormal coiling. The phenotype was similar to that described in mouse mutants lacking β-catenin, required for Wnt signaling, or the transcription factors *Sox9* or *Tbx1* (Xu et al., 2007; Trowe et al., 2010; Bohnenpoll et al., 2014). However, in mutants lacking *Sox9* or *Tbx1*, the observed inner ear phenotype is caused by the inactivation of these genes in the surrounding mesenchyme, pointing to their indirect influence on morphogenesis. Defective turning of the cochlear duct has also been described in a mouse mutant lacking the chromatin remodeling enzyme *Chd7* throughout inner ear development (Hurd et al., 2010). Interestingly, we found that *Chd7* expression was reduced in the cochlea of *Meis2*$^{flox/flox}$; *Pax2*$^{Cre/+}$ mutants, suggesting that these genes may share a common pathway. Indeed, inactivation of *Chd7* using the *Pax2*-Cre line led to a phenotype very similar to *Meis2*$^{flox/flox}$; *Pax2*$^{Cre/+}$ mutants. Moreover, like *Meis2*, *Chd7* null mutants also show severely reduced sized otic vesicles (Hurd et al., 2007). In spite of this functional relationship, we did not find evidence for the binding

TABLE 1 | Summary of genes downregulated in the cochlea of *Meis2* mutants.

Gene (MGI reference)	Fold Downregulation	Expression pattern
Acidic nuclear phosphoprotein 32 family (5332981)	4.1x	Mesenchyme
THUMP domain containing 3 (1277973)	3.7x	Otic capsule
Itchy, E3 ubiquitin protein ligase (4825634)	3.4x	Ganglion
Zinc finger protein 788 (1914857)	3.1x	Ganglion
Neurofilament, light polypeptide (97313)	3.1x	Ganglion
Trafficking protein particle complex 4 (4480575)	2.9x	Ganglion
Centrosome/spindle pole associated protein (2681832)	2.7x	Ganglion
FK506 binding protein 3 (5335642)	2.7x	Mesenchyme
Chromodomain helicase DNA binding protein 7 (2444748)	2.6x	Cochlear duct, ganglion and mesenchyme
Craniofacial development protein 1 (1344403)	2.4x	Cochlear duct and ganglion
Formin binding protein 1-like (1925642)	2.4x	Ganglion
Ephrin A1 (103236)	2.4x	Cochlear duct
Thymidylate synthase (98878)	2x	Mesenchyme

The localization of the genes within the cochlea is annotated according to Mouse Genome Informatics (MGI) using RNA in situ hybridization. The table shows a list of genes which are expressed in the cochlea and down regulated by twofold or higher in Meis2 mutants according to the results obtained by the microarrays.

of Meis2 within the regulatory regions of *Chd7* in the VOT-E36 cell line. Additionally, *Chd7* mutants show reduced expression of *Ngn1,* which was unaltered in *Meis2* mutants in the present study. This suggests that *Chd7* and *Meis2* rather belong to parallel pathways controlling cochlear coiling.

Only very few genes (Hayashi et al., 2002) from the ChIPseq analysis showed binding close to the transcription start site of genes. Similar findings have been recently reported for Meis1 (Penkov et al., 2013; Marcos et al., 2015). The most frequently detected binding motif detected in our studies corresponded to a site to which Meis binds indirectly to DNA. A major group of binding partners that facilitate indirect contact with DNA belong to the Hox gene family. Due to its rostral position in the embryo, the inner ear is a relatively Hox-free tissue, although the expression of PG-1 group genes like *Hoxa1* and its control of downstream targets have been reported in the inner ear (Makki and Capecchi, 2010, 2011). Additionally, Meis cooperates with a wide variety of transcription factors containing homeodomains, such as members of the *Pax, Dlx,* and *Otx* gene families which are also expressed in the inner ear (Schulte and Geerts, 2019). Nevertheless, only very few genes with Meis2 binding sites showed an overlap with differentially expressed transcripts in the cochlea. Therefore, the VOT-E36 cell line used for the ChIPseq analysis might not reflect an ideal model for *in vivo* inner ear development. Unfortunately, ChIP analysis from isolated otic vesicles was not feasible in our hands owing to technical limitations due to small-scale tissue samples. Nevertheless, further analysis of the genes showing both differential expression in *Meis2*$^{flox/flox}$; *Pax2*$^{Cre/+}$ mutants and containing binding sites detected by the ChIPseq analysis may reveal novel regulators of cochlear morphogenesis which are controlled by Meis2.

MATERIALS AND METHODS

Transgenic Mice

Mice carrying a floxed *Meis2* allele (Delgado et al., 2020), a floxed *Chd7* allele (Hurd et al., 2007), the *Sox2*-Cre (Hayashi et al., 2002), *Pax2*-Cre (Ohyama and Groves, 2004), *Foxg1*-Cre (Hebert and McConnell, 2000) and *MafB*-Cre (Wu et al., 2016) transgenes and the *ROSA26* Cre reporter strain (Soriano, 1999) have been described previously. With the exception of the *Meis2*$^{flox/flox}$; *MafB*$^{Cre/+}$ mutants which showed a penetrance of 50%, all other phenotypes were fully penetrant and observed in a minimum of $n = 3$ animals for each experimental condition. Experiments conformed to the institutional and national regulatory standards concerning animal welfare.

β-Galactosidase Staining and *in situ* Hybridization

β-Galactosidase staining, RNA whole-mount *in situ* hybridization and sectioning of stained embryos have been described previously (Alvarez et al., 2003). Riboprobes were generated for detection of *Meis2* (Delgado et al., 2020), *LFng, Ngn1, Dlx5,* (Vazquez-Echeverria et al., 2008), *Fgf3, Pax2, MafB* (Alvarez et al., 2003) and *HoxB1* (Vendrell et al., 2013).

Immunohistochemistry

For immunohistochemistry cryostat sections were prepared and processed using standard protocols. The following antibodies were used: Meis-2 (Mercader et al., 2005); Pax2 (PRB-276P) from Covance, Sox2 (sc-17320) from Santa Cruz Biotechnology; myosin VIIA (25-6790) from Proteus; calretinin (7699/3H) from Swant; cyclin D1 (RM-9104-S0) from Thermo Fisher Scientific. For immunofluorescence, cryostat sections were incubated with primary antibodies, and the corresponding secondary antibodies used were donkey anti-goat Alexa Fluor-488, and goat anti-rabbit Alexa Fluor-568 (all from Invitrogen). Some of the sections were counterstained with DAPI. Whole-mount immunolabeling, dehydration, and clearing of inner ears was performed as described previously (MacDonald and Rubel, 2008). Bright-field images were captured with a DFC 490 camera (Leica) on a Labophot-2 microscope (Nikon). Immunofluorescence images were taken with a Nikon Eclipse 90i fluorescence microscope, or Leica SP confocal microscope.

Screening for Differentially Regulated Genes in *Meis2*$^{flox/flox}$; *Pax2*$^{Cre/+}$ Mutants

RNA was isolated from E15 cochleas of wild type and *Meis2*$^{flox/flox}$; *Pax2*$^{Cre/+}$ mutants using the RNeasy Mini Kit (Qiagen) according to the manufacturer's instructions. RNA integrity was assessed using Agilent 2100 Bioanalyzer (Agilent). Labeling and hybridizations were performed according to protocols from Affymetrix. Briefly, 100–300 ng of total RNA were amplified and labeled using the WT Expression Kit (Ambion) and then hybridized to Mouse Gene 1.0 ST Arrays (Affymetrix) covering a total of 21,041 gene transcripts. Washing and scanning were performed using the Affymetrix GeneChip System (GeneChip Hybridization Oven 640, GeneChip Fluidics Station 450 and GeneChip Scanner 7G). The robust microarray analysis algorithm was used for background correction, intra- and inter-microarray normalization, and expression signal calculation. The absolute expression signal for each gene was calculated in each microarray and significance analysis of microarrays was applied to calculate differential expression and find the gene probe sets that characterized the highly metastatic samples. The method uses permutations to provide robust statistical inference of the most significant genes and provides $>$ *P*-values adjusted to multiple testing using false discovery rate. Probe synthesis, hybridizations and microarray data analysis were performed by the Genomics facility of the Centro de Investigación del Cancer (Salamanca, Spain). The microarray data from this screen have been deposited at GEO with accession number GSE149916. Genes twofold or greater were examined for their expression in the cochlea (Visel et al., 2004; Diez-Roux et al., 2011; Agoston et al., 2014; Bult et al., 2019) and are listed in **Table 1**.

Quantitative PCR

Individual RNA samples were each prepared from the cochleae of two embryonic day (E) 15 mice (i.e., 4 cochleae were used to generate one RNA sample). RNA was extracted following

homogenization in TRIzol® Reagent (Invitrogen), and according to manufacturer's instructions. Each RNA was then reverse transcribed into cDNA using a High Capacity cDNA Reverse Transcription Kit (Applied Biosystems, Life Technologies). cDNA samples were amplified in a LightCycler® 480 II (Roche Molecular Diagnostics, Pleasanton, CA, United States) using SYBR® Green PCR Master Mix (Life Technologies); duplicate reactions were carried out with each cDNA sample. The thermocycling conditions consisted of an initial denaturation step of 10 min at 95°C, followed by 40 cycles at 95°C for 15 s and 60°C for 1 min. The sequences of the PCR primers used in this work were: *Gapdh*, TCCTGCACCACCAACTGCTT and GTGGCAGTGATGGCATGGAC; *Chd7*, GAATACCCCA CAGAAAGTGCC and TCGCTCTTCACTAGCTGAGCG. Data were analyzed using the Software version LCS480 1.5.0.39. Relative levels of mRNA expression were calculated according to the $2^{-\Delta\Delta Ct}$ method, using *Gapdh* as the housekeeping gene. The data presented are the results from three independent experiments.

ChIP-Seq

US/VOT-E36 cells (University of Sheffield/ventral otocyst-epithelial cell line clone 36) were used, derived from the otocyst of Immortomice at embryonic day 10.5 (Lawoko-Kerali et al., 2004). The cells were cultured in minimum essential medium (Gibco) supplemented with 10% fetal bovine serum (Gibco) and 50 U/ml γ-IFN (Immunotools) in a humidified atmosphere with 10% CO_2 and at a temperature of 33°C, conditions under which these cells proliferate in the absence of differentiation.

For the ChIP assay, once the cultures had reached 85–90% confluence, the chromatin from the cells in six 75-cm^2 flasks was cross-linked in 1% formaldehyde for 10 min at room temperature; next, the reaction was quenched by adding glycine to a final concentration of 125 mM and mixing during an additional 5 min. Following removal of the medium and various washes with phosphate buffer saline, cells were scraped off the tissue culture flasks, pelleted and lysed; the chromatin was then sheared into 200–500 bp fragments by sonication (using pulses of 30 s on and 30 s off in a water-bath sonicator). Any remaining cellular debris was subsequently removed by centrifugation and the sonicated chromatin was pre-cleared for 4 h at 4°C with protein A agarose beads (Roche). After this time, the beads were removed by centrifugation; half the volume of the chromatin sample was immunoprecipitated (IP sample) at 4°C overnight with a 1:1 mixture of an antibody against Meis2 (K846) and K830, an antibody that recognizes both Meis 1a and Meis 2a isoforms (Penkov et al., 2013). A volume that was equivalent to one tenth of the volume used for the IP reaction was also at that time set apart and frozen, constituting the Input control sample. Following immunoprecipitation with the antibodies, beads that had been pre-blocked at 4°C overnight with BSA and a rabbit IgG isotype control (ChromPure Rabbit IgG, Jackson ImmunoResearch Laboratories) were added to each tube; the samples were then incubated at 4°C for 4 h. Afterward, a series of washes using multiple buffers were conducted in order to remove any molecule that had bound non-specifically to the beads; the chromatin was finally eluted from the beads and cross-linking to the antibody reversed by incubating the IP sample in the presence of NaCl at 65°C overnight; the Input sample that had been stored at –20°C was also incubated in the same solution at 65°C. The next day, both the IP and the Input chromatin were purified using a PCR purification kit (Qiagen), following manufacturer's instructions. The samples were then used to carry out ChIP-seq analysis.

0.5 ng of total DNA for both Input and IP were used to generate barcoded libraries using the *NEBNext® Ultra™ II DNA Library Prep Kit for Illumina* (New England Biolabs). Basically, adapters were ligated to DNA followed by an amplification and clean up. The size of the libraries was checked using the Agilent 2100 Bioanalyzer High Sensitivity DNA chip and their concentration was determined using the Qubit® fluorometer (Thermo Fisher Scientific).

Libraries were sequenced on a HiSeq 2500 (Illumina) and processed with RTA v1.18.66.3. FastQ files for each sample were obtained using bcl2fastq v2.20.0.422 software (Illumina).

Sequencing reads were trimmed for Illumina adapter sequence with cutadapt, aligned to the mouse reference genome (mm10 v92) with bowtie and PCR duplicates were excluded with samtools MarkDuplicates tool.

Peaks were called with HOMER2 and params "-region -localSize 50000 -size 150 -minDist 1000-ntagThreshold 5-regionRes 6." Peaks were also annotated with HOMER2 and inspected for MOTIFs with Meme (from Meme Suite) and with HOMER2. Data have been deposited in the NCBI GEO database under accession number GSE166072.

DATA AVAILABILITY STATEMENT

The datasets presented in this study can be found in online repositories. The names of the repository/repositories and accession number(s) can be found below: https://www.ncbi.nlm.nih.gov/, GSE166072, https://www.ncbi.nlm.nih.gov/, GSE149916.

ETHICS STATEMENT

The animal study was reviewed and approved by Ethics Committee of the University of Valladolid.

AUTHOR CONTRIBUTIONS

TS and MD designed the research. TS, MD, VV, IL-H, FG, EV, LC, and GG performed the research. MA, MT, and DM contributed unpublished reagents and analytic tools. TS, MD, VV, and EV analyzed the data. TS wrote the first draft of the manuscript and wrote the manuscript. TS, MD, DM, and FG edited the manuscript. All authors contributed to the article and approved the submitted version.

FUNDING

We acknowledge grants from Mineco BFU2016-76580-P and Consejería de Educación, Junta de Castilla y León (FEDER CSI143P20) (TS).

ACKNOWLEDGMENTS

We thank Bernice Morrow for providing Tbx1 antibodies and Kiril Schimmang-Alonso for help on designing of figures.

SUPPLEMENTARY MATERIAL

The Supplementary Material for this article can be found online at: https://www.frontiersin.org/articles/10.3389/fcell.2021.679325/full#supplementary-material

Supplementary Figure 1 | Expression domains of Cre lines. *MafB*-Cre is expressed in the neural tube (nt) corresponding to rhombomeres 5 and 6 of the hindbrain whereas *Pax2*-Cre is active in the otic placode (op). Next to the otic placode, *Foxg1*-Cre is also active in the peri-otic mesoderm (m) and endoderm (e).

REFERENCES

Agoston, Z., Heine, P., Brill, M. S., Grebbin, B. M., Hau, A. C., Kallenborn-Gerhardt, W., et al. (2014). Meis2 is a Pax6 co-factor in neurogenesis and dopaminergic periglomerular fate specification in the adult olfactory bulb. *Development* 141, 28–38. doi: 10.1242/dev.097295

Alvarez, Y., Alonso, M. T., Vendrell, V., Zelarayan, L. C., Chamero, P., Theil, T., et al. (2003). Requirements for FGF3 and FGF10 during inner ear formation. *Development* 130, 6329–6338. doi: 10.1242/dev.00881

Basch, M. L., Brown, R. M. II, Jen, H. I., and Groves, A. K. (2016). Where hearing starts: the development of the mammalian cochlea. *J. Anat.* 228, 233–254. doi: 10.1111/joa.12314

Bessa, J., Tavares, M. J., Santos, J., Kikuta, H., Laplante, M., Becker, T. S., et al. (2008). meis1 regulates cyclin D1 and c-myc expression, and controls the proliferation of the multipotent cells in the early developing zebrafish eye. *Development* 135, 799–803. doi: 10.1242/dev.011932

Bohnenpoll, T., Trowe, M. O., Wojahn, I., Taketo, M. M., Petry, M., and Kispert, A. (2014). Canonical Wnt signaling regulates the proliferative expansion and differentiation of fibrocytes in the murine inner ear. *Dev. Biol.* 391, 54–65. doi: 10.1016/j.ydbio.2014.03.023

Bok, J., Chang, W., and Wu, D. K. (2007). Patterning and morphogenesis of the vertebrate inner ear. *Int. J. Dev. Biol.* 51, 521–533. doi: 10.1387/ijdb.072381jb

Bult, C. J., Blake, J. A., Smith, C. L., Kadin, J. A., Richardson, J. E., Mouse Genome, et al. (2019). Mouse Genome Database (MGD). *Nucleic Acids Res.* 47, D801–D806.

Burton, Q., Cole, L. K., Mulheisen, M., Chang, W., and Wu, D. K. (2004). The role of Pax2 in mouse inner ear development. *Dev. Biol.* 272, 161–175. doi: 10.1016/j.ydbio.2004.04.024

Cordes, S. P., and Barsh, G. S. (1994). The mouse segmentation gene kr encodes a novel basic domain-leucine zipper transcription factor. *Cell* 79, 1025–1034. doi: 10.1016/0092-8674(94)90033-7

Delgado, I., Lopez-Delgado, A. C., Rosello-Diez, A., Giovinazzo, G., Cadenas, V., Fernandez-de-Manuel, L., et al. (2020). Proximo-distal positional information encoded by an Fgf-regulated gradient of homeodomain transcription factors in the vertebrate limb. *Sci. Adv.* 6:eaaz0742. doi: 10.1126/sciadv.aaz0742

Diez-Roux, G., Banfi, S., Sultan, M., Geffers, L., Anand, S., Rozado, D., et al. (2011). A high-resolution anatomical atlas of the transcriptome in the mouse embryo. *PLoS Biol.* 9:e1000582. doi: 10.1371/journal.pbio.1000582

Gutkovich, Y. E., Ofir, R., Elkouby, Y. M., Dibner, C., Gefen, A., Elias, S., et al. (2010). Xenopus Meis3 protein lies at a nexus downstream to Zic1 and Pax3 proteins, regulating multiple cell-fates during early nervous system development. *Dev. Biol.* 338, 50–62. doi: 10.1016/j.ydbio.2009.11.024

Hayashi, S., Lewis, P., Pevny, L., and McMahon, A. P. (2002). Efficient gene modulation in mouse epiblast using a Sox2Cre transgenic mouse strain. *Mech. Dev.* 119(Suppl. 1), S97–S101.

Hebert, J. M., and McConnell, S. K. (2000). Targeting of cre to the Foxg1 (BF-1) locus mediates loxP recombination in the telencephalon and other developing head structures. *Dev. Biol.* 222, 296–306. doi: 10.1006/dbio.2000.9732

Hernandez, R. E., Rikhof, H. A., Bachmann, R., and Moens, C. B. (2004). vhnf1 integrates global RA patterning and local FGF signals to direct posterior hindbrain development in zebrafish. *Development* 131, 4511–4520. doi: 10.1242/dev.01297

Hurd, E. A., Capers, P. L., Blauwkamp, M. N., Adams, M. E., Raphael, Y., Poucher, H. K., et al. (2007). Loss of Chd7 function in gene-trapped reporter mice is embryonic lethal and associated with severe defects in multiple developing tissues. *Mamm. Genome* 18, 94–104. doi: 10.1007/s00335-006-0107-6

Hurd, E. A., Poucher, H. K., Cheng, K., Raphael, Y., and Martin, D. M. (2010). The ATP-dependent chromatin remodeling enzyme CHD7 regulates pro-neural gene expression and neurogenesis in the inner ear. *Development* 137, 3139–3150. doi: 10.1242/dev.047894

Iizuka-Kogo, A., Senda, T., Akiyama, T., Shimomura, A., Nomura, R., Hasegawa, Y., et al. (2015). Requirement of DLG1 for cardiovascular development and tissue elongation during cochlear, enteric, and skeletal development: possible role in convergent extension. *PLoS One* 10:e0123965. doi: 10.1371/journal.pone.0123965

Ladher, R. K., Wright, T. J., Moon, A. M., Mansour, S. L., and Schoenwolf, G. C. (2005). FGF8 initiates inner ear induction in chick and mouse. *Genes Dev.* 19, 603–613. doi: 10.1101/gad.1273605

Lawoko-Kerali, G., Milo, M., Davies, D., Halsall, A., Helyer, R., Johnson, C. M., et al. (2004). Ventral otic cell lines as developmental models of auditory epithelial and neural precursors. *Dev. Dyn.* 231, 801–814. doi: 10.1002/dvdy.20187

MacDonald, G. H., and Rubel, E. W. (2008). Three-dimensional imaging of the intact mouse cochlea by fluorescent laser scanning confocal microscopy. *Hear. Res.* 243, 1–10. doi: 10.1016/j.heares.2008.05.009

Machon, O., Masek, J., Machonova, O., Krauss, S., and Kozmik, Z. (2015). Meis2 is essential for cranial and cardiac neural crest development. *BMC Dev. Biol.* 15:40. doi: 10.1186/s12861-015-0093-6

Mak, A. C., Szeto, I. Y., Fritzsch, B., and Cheah, K. S. (2009). Differential and overlapping expression pattern of SOX2 and SOX9 in inner ear development. *Gene Exp. Patterns* 9, 444–453. doi: 10.1016/j.gep.2009.04.003

Makki, N., and Capecchi, M. R. (2010). Hoxa1 lineage tracing indicates a direct role for Hoxa1 in the development of the inner ear, the heart, and the third rhombomere. *Dev. Biol.* 341, 499–509. doi: 10.1016/j.ydbio.2010.02.014

Makki, N., and Capecchi, M. R. (2011). Identification of novel Hoxa1 downstream targets regulating hindbrain, neural crest and inner ear development. *Dev. Biol.* 357, 295–304. doi: 10.1016/j.ydbio.2011.06.042

Marcos, S., Gonzalez-Lazaro, M., Beccari, L., Carramolino, L., Martin-Bermejo, M. J., Amarie, O., et al. (2015). Meis1 coordinates a network of genes implicated in eye development and microphthalmia. *Development* 142, 3009–3020. doi: 10.1242/dev.122176

Maroon, H., Walshe, J., Mahmood, R., Kiefer, P., Dickson, C., and Mason, I. (2002). Fgf3 and Fgf8 are required together for formation of the otic placode and vesicle. *Development* 129, 2099–2108. doi: 10.1242/dev.129.9.2099

Mercader, N., Tanaka, E. M., and Torres, M. (2005). Proximodistal identity during vertebrate limb regeneration is regulated by Meis homeodomain proteins. *Development* 132, 4131–4142. doi: 10.1242/dev.01976

Morsli, H., Tuorto, F., Choo, D., Postiglione, M. P., Simeone, A., and Wu, D. K. (1999). Otx1 and Otx2 activities are required for the normal development of the mouse inner ear. *Development* 126, 2335–2343. doi: 10.1242/dev.126.11.2335

Ohyama, T., and Groves, A. K. (2004). Generation of Pax2-Cre mice by modification of a Pax2 bacterial artificial chromosome. *Genesis* 38, 195–199. doi: 10.1002/gene.20017

Pasqualetti, M., Neun, R., Davenne, M., and Rijli, F. M. (2001). Retinoic acid rescues inner ear defects in Hoxa1 deficient mice. *Nat. Genet.* 29, 34–39. doi: 10.1038/ng702

Penkov, D., Mateos San, Martin, D., Fernandez-Diaz, L. C., Rossello, C. A., Torroja, C., et al. (2013). Analysis of the DNA-binding profile and function of TALE homeoproteins reveals their specialization and specific interactions with Hox genes/proteins. *Cell Rep.* 3, 1321–1333. doi: 10.1016/j.celrep.2013.03.029

Rossel, M., and Capecchi, M. R. (1999). Mice mutant for both Hoxa1 and Hoxb1 show extensive remodeling of the hindbrain and defects in craniofacial development. *Development* 126, 5027–5040. doi: 10.1242/dev.126.22.5027

Sanchez-Guardado, L. O., Ferran, J. L., Rodriguez-Gallardo, L., Puelles, L., and Hidalgo-Sanchez, M. (2011). Meis gene expression patterns in the developing chicken inner ear. *J. Comp. Neurol.* 519, 125–147. doi: 10.1002/cne.22508

Schimmang, T. (2007). Expression and functions of FGF ligands during early otic development. *Int. J. Dev. Biol.* 51, 473–481. doi: 10.1387/ijdb.072334ts

Schulte, D., and Frank, D. (2014). TALE transcription factors during early development of the vertebrate brain and eye. *Dev. Dyn.* 243, 99–116. doi: 10.1002/dvdy.24030

Schulte, D., and Geerts, D. (2019). MEIS transcription factors in development and disease. *Development* 146:dev174706.

Soriano, P. (1999). Generalized lacZ expression with the ROSA26 Cre reporter strain. *Nat. Genet.* 21, 70–71. doi: 10.1038/5007

Trowe, M. O., Shah, S., Petry, M., Airik, R., Schuster-Gossler, K., Kist, R., et al. (2010). Loss of Sox9 in the periotic mesenchyme affects mesenchymal expansion and differentiation, and epithelial morphogenesis during cochlea development in the mouse. *Dev. Biol.* 342, 51–62. doi: 10.1016/j.ydbio.2010.03.014

Vazquez-Echeverria, C., Dominguez-Frutos, E., Charnay, P., Schimmang, T., and Pujades, C. (2008). Analysis of mouse kreisler mutants reveals new roles of hindbrain-derived signals in the establishment of the otic neurogenic domain. *Dev. Biol.* 322, 167–178. doi: 10.1016/j.ydbio.2008.07.025

Vendrell, V., Vazquez-Echeverria, C., Lopez-Hernandez, I., Alonso, B. D., Martinez, S., Pujades, C., et al. (2013). Roles of Wnt8a during formation and patterning of the mouse inner ear. *Mech. Dev.* 130, 160–168. doi: 10.1016/j.mod.2012.09.009

Visel, A., Thaller, C., and Eichele, G. (2004). GenePaint.org: an atlas of gene expression patterns in the mouse embryo. *Nucleic Acids Res.* 32, D552–D556.

Whitfield, T. T. (2015). Development of the inner ear. *Curr. Opin. Genet. Dev.* 32, 112–118.

Wiellette, E. L., and Sive, H. (2003). vhnf1 and Fgf signals synergize to specify rhombomere identity in the zebrafish hindbrain. *Development* 130, 3821–3829. doi: 10.1242/dev.00572

Wright, T. J., and Mansour, S. L. (2003). Fgf3 and Fgf10 are required for mouse otic placode induction. *Development* 130, 3379–3390. doi: 10.1242/dev.00555

Wu, X., Briseno, C. G., Durai, V., Albring, J. C., Haldar, M., Bagadia, P., et al. (2016). Mafb lineage tracing to distinguish macrophages from other immune lineages reveals dual identity of Langerhans cells. *J. Exp. Med.* 213, 2553–2565. doi: 10.1084/jem.20160600

Xu, H., Chen, L., and Baldini, A. (2007). In vivo genetic ablation of the periotic mesoderm affects cell proliferation survival and differentiation in the cochlea. *Dev. Biol.* 310, 329–340. doi: 10.1016/j.ydbio.2007.08.006

Zelarayan, L. C., Vendrell, V., Alvarez, Y., Dominguez-Frutos, E., Theil, T., Alonso, M. T., et al. (2007). Differential requirements for FGF3, FGF8 and FGF10 during inner ear development. *Dev. Biol.* 308, 379–391. doi: 10.1016/j.ydbio.2007.05.033

Conflict of Interest: The authors declare that the research was conducted in the absence of any commercial or financial relationships that could be construed as a potential conflict of interest.

frontiers in Cell and Developmental Biology

ORIGINAL RESEARCH
published: 02 August 2021
doi: 10.3389/fcell.2021.723927

Role of the Forkhead Transcription Factors Fd4 and Fd5 During *Drosophila* Leg Development

*Mireya Ruiz-Losada, Cristian Pérez-Reyes and Carlos Estella**

Centro de Biología Molecular Severo Ochoa (C.S.I.C.-U.A.M.), Universidad Autónoma de Madrid, Madrid, Spain

Appendage development requires the coordinated function of signaling pathways and transcription factors to pattern the leg along the three main axes: the antero-posterior (AP), proximo-distal (PD), and dorso-ventral (DV). The *Drosophila* leg DV axis is organized by two morphogens, Decapentaplegic (Dpp), and Wingless (Wg), which direct dorsal and ventral cell fates, respectively. However, how these signals regulate the differential expression of its target genes is mostly unknown. In this work, we found that two members of the *Drosophila* forkhead family of transcription factors, Fd4 and Fd5 (also known as *fd96Ca* and *fd96Cb*), are identically expressed in the ventro-lateral domain of the leg imaginal disc in response to Dpp signaling. Here, we analyze the expression regulation and function of these genes during leg development. We have generated specific mutant alleles for each gene and a double *fd4/fd5* mutant chromosome to study their function during development. We highlight the redundant role of the *fd4/fd5* genes during the formation of the sex comb, a male specific structure that appears in the ventro-lateral domain of the prothoracic leg.

Keywords: Fd4/Fd5, *fd96Ca/fd96Cb*, forkhead transcription factors, leg development, dorso-ventral axis, sex comb, *Drosophila*

OPEN ACCESS

Edited by:
Rosa Barrio,
CIC bioGUNE, Spain

Reviewed by:
Artyom Kopp,
UC Davis Genome Center,
United States
William Brook,
University of Calgary, Canada

***Correspondence:**
Carlos Estella
cestella@cbm.csic.es

Specialty section:
This article was submitted to Morphogenesis and Patterning, a section of the journal Frontiers in Cell and Developmental Biology

Received: *11 June 2021*
Accepted: *12 July 2021*
Published: *02 August 2021*

Citation:
Ruiz-Losada M, Pérez-Reyes C and Estella C (2021) Role of the Forkhead Transcription Factors Fd4 and Fd5 During Drosophila Leg Development. Front. Cell Dev. Biol. 9:723927. doi: 10.3389/fcell.2021.723927

INTRODUCTION

Territorial specification depends on the ability of cells to activate a specific developmental program depending on their position within a tissue. The positional information, often provided by extrinsic signaling molecules, is integrated at the *cis*-regulatory modules (CRMs) of genes that encode for transcription factors that instruct cells with a unique developmental fate. Appendage development is a great model to study pattern formation, as it requires the specification of different cell fates along three main axes: the antero-posterior (AP), the dorso-ventral (DV), and the proximo-distal (PD) (Estella et al., 2012; Ruiz-Losada et al., 2018). More than 30 years of studies in *Drosophila* have identified many of the signals and transcription factors that pattern these axes, numerous of them conserved in vertebrates (Shubin et al., 1997; Tabin et al., 1999; Pueyo and Couso, 2005). An important, and yet not fully understood question is how the different signaling pathways regulate the restricted expression of the pattering genes along the three main appendage axes.

Appendages in *Drosophila* are derived from specialized epithelial sacs, named imaginal discs, which are specified in the embryo and grow and pattern during larva development (reviewed in Ruiz-Losada et al., 2018). The leg imaginal disc is divided into an anterior and posterior compartment by the expression of the selector gene *engrailed* (*en*) in the posterior compartment. En activates the expression of the short-range morphogene Hedgehog (Hh) in posterior compartment cells. Hh signals to anterior cells where it induces the transcription of two signaling molecules:

Decapentaplegic (Dpp) in dorsal anterior cells and Wingless (Wg) in ventral anterior cells (Basler and Struhl, 1994). The dorsal and ventral domains of *dpp* and *wg* expression are maintained by a mutual repression, where Dpp prevents the activation of *wg* in dorsal cells and *vice versa* (Brook and Cohen, 1996; Jiang and Struhl, 1996; Johnston and Schubiger, 1996; Morimura et al., 1996; Penton and Hoffmann, 1996; Theisen et al., 1996). However, low levels of *dpp* expression could still be observed in the ventral domain of the leg disc (**Figure 1D**). Both, Dpp and Wg are required for the initiation and patterning of the PD and DV axes (Diaz-Benjumea et al., 1994; Brook and Cohen, 1996; Lecuit and Cohen, 1997; Campbell and Tomlinson, 1998). The juxtaposition of cells expressing high levels of Wg and Dpp in the center of the leg disc leads to the formation of the PD axis by activating a regulatory cascade of transcription factors that divide the leg in different domains of gene expression (Estella et al., 2012). In addition to initiating the PD axis formation, Wg and Dpp play an instructive role in the distinction between dorsal and ventral fates (Brook and Cohen, 1996; Jiang and Struhl, 1996; Johnston and Schubiger, 1996; Morimura et al., 1996; Penton and Hoffmann, 1996; Theisen et al., 1996). Dpp specifies dorsal fates and represses ventral ones, while Wg specifies ventral identities and represses dorsal fates. Therefore, hypomorphic mutations of *wg* show strong derepression of Dpp in the ventral domain and formation of ectopic dorsal structures in place of the corresponding ventral ones in the adult leg (Held et al., 1994). Similar phenotypes, but in the opposite direction, were observed in *dpp* mutants (Held et al., 1994). Interestingly, lateral fates are recovered in double hypomorphic mutants for *dpp* and *wg*, suggesting that the lateral fate is the default DV state (Held et al., 1994). The Dpp and Wg signaling molecules depend on the activation of a specific set of transcription factors that promote the DV fate of these cells. The family of T-box transcription factors plays an important role in the specification of DV identities (Brook, 2010). In the ventral domain of the leg, Wg activates while Dpp represses the expression of the redundant genes *H15* and *midline* (*mid*) that act as selector genes for ventral fates, promoting the acquisition of ventral identity. Accordingly, mutants for *H15/mid* lack ventral leg structures or these are transformed to dorsal, whereas when ectopically expressed in the dorsal domain, *H15/mid* induce ventral fates (Svendsen et al., 2009, 2019). In the dorsal domain, the expression of the T-box genes *optomotor-blind* (*omb*) and the *Dorsocross* (*Doc*) *1*, *2*, and *3* are able to repress ventral genes (Maves and Schubiger, 1998; Reim et al., 2003; Svendsen et al., 2015). However, whether *omb* and the *Doc* genes are required to specify dorsal fates is mostly unknown. Gene expression analysis and loss of function studies suggested that the function of the PD and DV patterning genes is generally conserved across arthropods (Maves and Schubiger, 1998; Abzhanov and Kaufman, 2000; Prpic et al., 2001; Inoue et al., 2002; Angelini and Kaufman, 2004; Ober and Jockusch, 2006; Janssen et al., 2008; Grossmann et al., 2009).

In this study we address the role of the sister genes *fd4* and *fd5* (also known as *fd96Ca* and *fd696cb*), members of the forkhead family of transcription factors, during appendage development (Hacker et al., 1992). We found that *fd4/fd5* are expressed exclusively in the ventral imaginal discs and more specifically in the ventro-lateral domain of the leg disc. We identified a minimal CRM that directs the expression of these genes and characterized its regulation in the leg disc. Furthermore, using

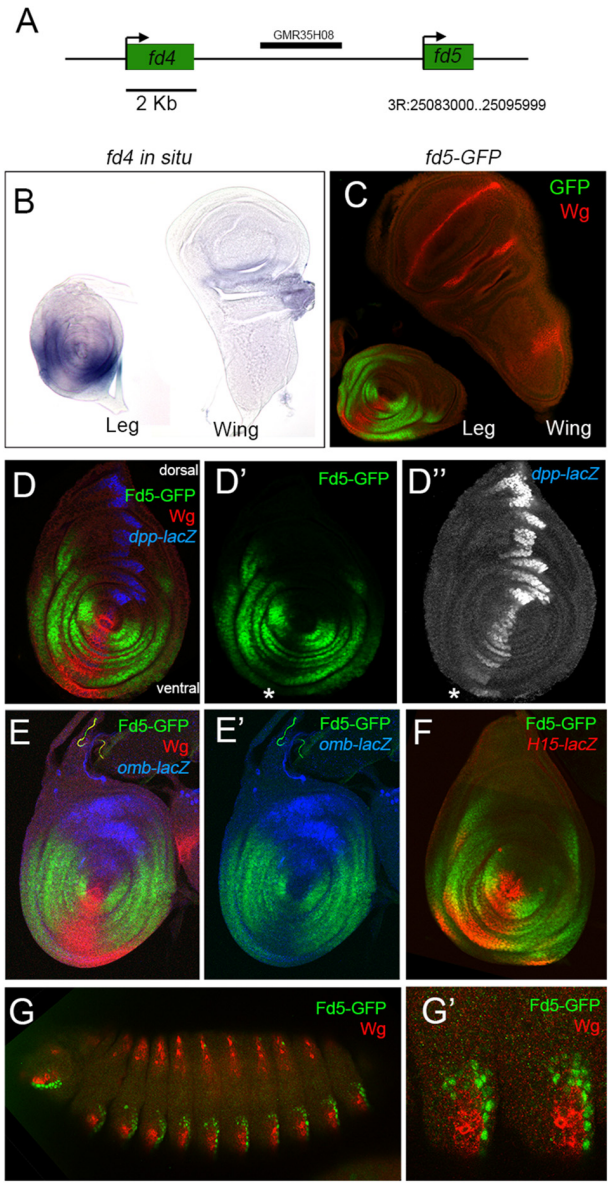

FIGURE 1 | *fd4* and *fd5* expression during development. **(A)** Schematic representation of the *fd4* and *fd5* genomic locus. **(B)** *fd4* expression pattern by *in situ* hybridization. **(C)** *fd5* expression visualized by a *fd5-GFP* tagged (green) line. Wg (red) staining is also shown. **(D)** Expression pattern of *fd5* (green), *dpp-lacZ* (blue), and *wg* (red) in the leg disc. Separate channels for *fd5* **(D')** and *dpp* **(D'')** are shown. The asterisk indicates the ventral most region of the disc where low Fd5-GFP levels are detected. **(E)** Leg imaginal disc stained for Fd5-GFP (green), *omb-lacZ* (blue), and Wg (red). Separate channels for Fd5-GFP (green) and *omb-lacZ* (blue) are shown in panel **(E')**. **(F)** Leg imaginal disc stained for Fd5-GFP (green) and *H15-lacZ* (red). **(G)** Stage 14 embryo stained for Fd5-GFP (green) and Wg (red). **(G')** A close up view of the ventro-lateral domain of two abdominal segments. In all confocal images, dorsal is up and anterior is left.

specific mutations generated for each gene we found that *fd4/fd5* play redundant roles during the formation of the sex comb, a characteristic ventro-lateral structure of the prothoracic male leg. Our results highlight the function of the *fd4/fd5* genes during leg development.

RESULTS

fd4 and *fd5* Expression During Leg Development

To identify genes with a potential role in DV patterning we searched the Flylight database for non-coding DNA elements that have a restricted DV activity pattern in the leg disc (Jory et al., 2012). We identified a DNA fragment that activates the reporter gene in the ventro-lateral domain of the leg disc (named GMR35H08 at Flylight database). This fragment is located between the *fd4* and *fd5* genes, two members of the forkhead family of transcription factors (Hacker et al., 1992; Lee and Frasch, 2004; **Figure 1A**). The Fd4 and Fd5 proteins share a 49% of aa sequence identity, suggesting they could play similar functions. In order to investigate the expression pattern of these genes we used an *in situ* hybridization probe for *fd4* and GFP-tagged versions for *fd4* and *fd5*. Both genes are identically expressed in the three leg imaginal discs, the antenna and the genital imaginal discs and show no expression in the wing or haltere discs (**Figures 1B,C** and **Supplementary Figure 1**; Heingard et al., 2019). When compared to the dorsal and ventral determinants, *dpp* and *wg*, *fd4* and *fd5* expression is restricted to the ventro-lateral domain of the leg disc with faint expression in the ventral most region that coincides with the highest levels of Wg and low Dpp (**Figure 1D** and **Supplementary Figure 1**; Heingard et al., 2019). Comparison of *fd5* expression with that of the Dpp and Wg targets, *omb* and *H15*, confirmed that *fd5* expression is complementary to *omb* and extends more laterally than *H15* (Estella and Mann, 2008; Brook, 2010; Ruiz-Losada et al., 2018; **Figures 1E,F**). As previously reported, these genes are also expressed in the embryo (Archbold et al., 2014), and at least for *fd5*, its expression is restricted to ectodermal segmental ventral stripes surrounding *wg* expression (**Figure 1G**).

Fd4 and Fd5 Act Redundantly in the Formation of the Sex Comb Structure

Next, we investigated the role of *fd4* and *fd5* during leg development. To this end, we generated specific mutant alleles for each gene and a double *fd4/fd5* mutant using CRISPR/Cas9 (**Supplementary Figure 2**) (see details in Materials and Methods). The $fd4^{5nt}$ mutant allele has a five nucleotide (nt) deletion at the beginning of the coding region that changes the open reading frame. $fd4^{5nt}$ homozygous mutant flies are viable and have normal patterned legs with the exception of a slight reduction in the number of sex comb bristles (∼10.6 in the control vs. ∼8.7 in $fd4^{5nt}$ mutants) (**Figures 2A,E**). The sex comb is a male specific structure present on the prothoracic leg (T1 leg) that develops from modified bristles of the most distal transverse row (TRs) on the first tarsal segment that rotate approximately 90° (Tokunaga, 1962; Tanaka et al., 2009; Kopp, 2011). The $fd5^{1nt}$ mutant has a reading frame shift due to a single nt deletion at the start of the gene that completely changes the amino acid sequence (**Supplementary Figure 2**). No defects were observed in the legs of $fd5^{1nt}$ mutant animals (**Figures 2A,E**). As both genes have identical expression patterns, and likely similar functions, we generated a double *fd4*, *fd5* mutant chromosome by mutating the *fd5* gene over the $fd4^{5nt}$ allele (**Supplementary Figure 2**). The new $fd5^{stop}$ mutant has a nine nt sequence change and a three nt deletion that generate a premature stop codon at the beginning of the coding region (**Supplementary Figure 2**). $fd4^{5nt}$, $fd5^{stop}$ homozygous mutant animals reach adulthood, though they get caught in the food where they die soon afterwards.

A detailed leg phenotypic analysis of the different DV landmarks present in the three legs from $fd4^{5nt}$, $fd5^{stop}$ double mutant animals revealed defects in the formation of the sex comb and some necrotic tissue in few joints (Hannah-Alava, 1958). We also found that the pattern of transverse row bristles is slightly altered in these mutants (**Figure 2A** and **Supplementary Figure 3**). The number of sex comb bristles is strongly reduced in the double mutant $fd4^{5nt}$, $fd5^{stop}$ when compared to each single mutant or the control (∼10.6 in the control vs. ∼4.8 in $fd4^{5nt}$, $fd5^{stop}$ mutants), suggesting a redundant role of these genes in the formation of this male specific structure (**Figures 2A,E**). The orientation of the remaining sex comb teeth is longitudinal as in the control, suggesting that the 90° rotation of precursor distal transverse row bristles have occurred properly in the mutants. In females, we detected approximately the same number of ta1 transverse rows in the control and in the double $fd4^{5nt}$, $fd5^{stop}$ mutant (**Supplementary Figure 3**). Importantly, the number of sex combs bristles of $fd4^{5nt}$, $fd5^{stop}$ mutant animals was almost completely rescued when a wild type copy of the *fd5* gene (BAC-*fd5*-GFP) was provided in the mutant background (∼4.8 in $fd4^{5nt}$, $fd5^{stop}$ mutants vs. ∼9 in the $fd4^{5nt}$, $fd5^{stop}$; *fd5-GFP* rescue), confirming that these phenotypes are specific of the *fd4*, *fd5* mutations (**Figures 2B,E**).

In addition, we used specific RNAi lines for each gene that efficiently reduced Fd4 and Fd5 protein levels (**Supplementary Figure 4**). When these RNAi lines were expressed in the distal domain of the leg with the *Dll-Gal4* driver (*Dll>*) we obtained identical phenotypes that with the mutants (**Supplementary Figure 4**). These results corroborate the redundant roles of the *fd4* and *fd5* genes in the formation of the sex comb.

Next, we investigated whether the requirement of the *fd4/fd5* genes is restricted to the bristles precursors that will form the sex comb teeth or to the epidermal cells of the leg imaginal disc. To this end, we used the *scabrous* (*sca*)*-Gal4* line to knock down simultaneously Fd4 and Fd5 levels in nascent bristle cells (Shroff et al., 2007). In addition, both RNAi lines were simultaneously expressed with the *doublesex* (*dsx*)*-Gal4* that is expressed both in the epidermis and sensory organ precursors (SOPs) of the sex comb (Robinett et al., 2010). While no defects were observed in *sca>fd4-RNAi*, *fd5-RNAi* animals, a strong reduction in the number of sex comb bristles was found in *dsx>fd4-RNAi*, *fd5-RNAi* flies (∼11 in *dsx>* control animals vs. ∼5.2 in *dsx>fd4/fd5-RNAi* mutant animals) (**Figures 2C,D,F**). These results suggest that Fd4 and Fd5 function is not restricted to late sex comb SOPs but instead required in leg epithelium cells including those that will be re-specified as SOPs.

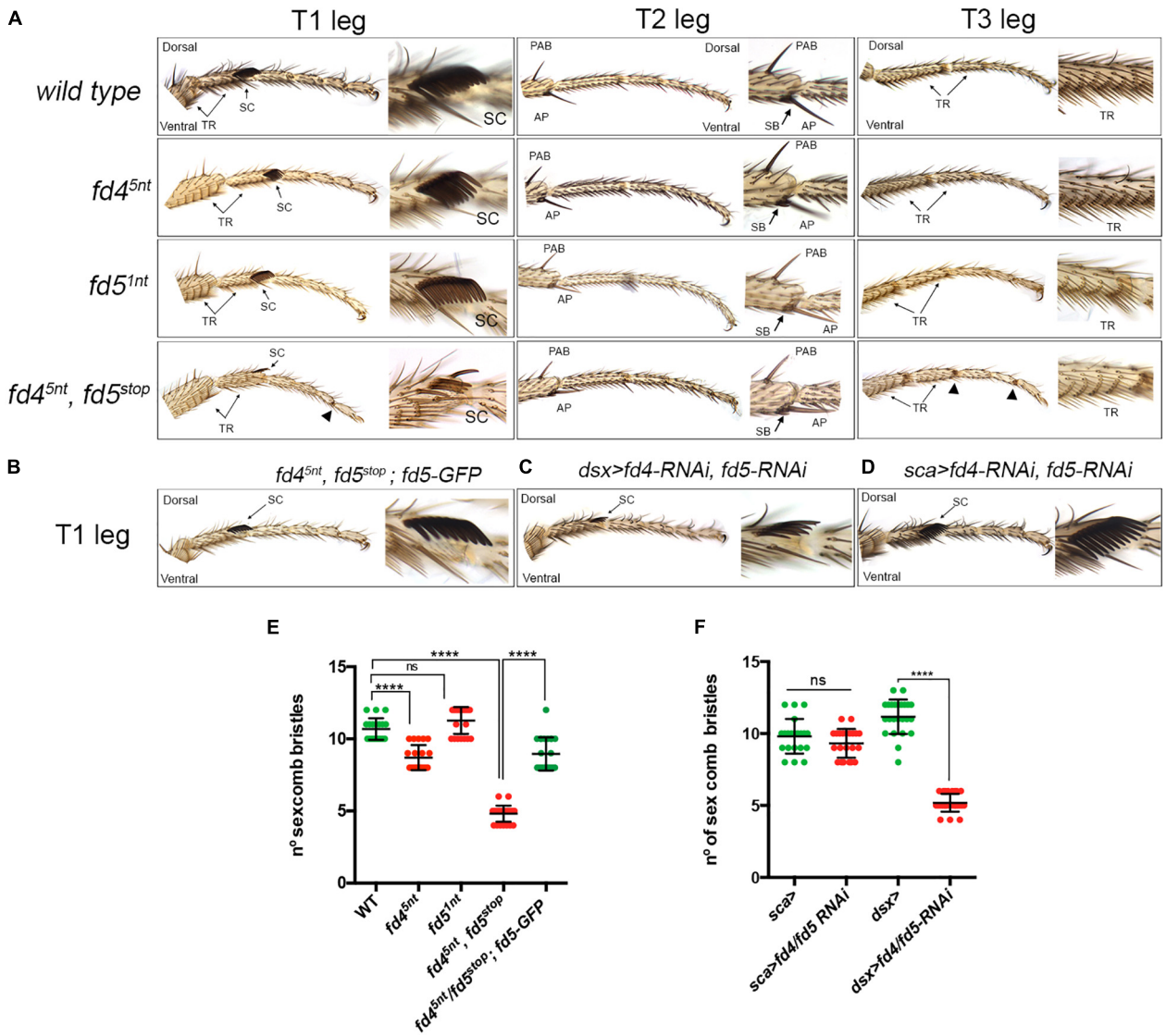

FIGURE 2 | Phenotypic analysis of *fd4* and *fd5* mutants. **(A)** Male adult leg phenotypes of a wild type, $fd4^{5nt}$, $fd5^{1nt}$ and the double $fd4^{5nt}$, $fd5^{stop}$ mutants. Representative examples of the three legs (T1–T3) are shown. Close up views of the sex comb in T1, the distal tibia in T2, and the first tarsus in T3 are shown. TR, transverse row; SC, sex comb; PAB, pre-apical bristle; AP, apical bristle and SB, spur bristles. Arrowheads indicate defective joints. Characteristic ventro-lateral structures are the transverse rows (TRs), the sex combs (SCs), and the apical bristles (ABs). **(B–D)** Male first thoracic legs of the genotypes indicated. Note that the sex comb phenotype of the double $fd4^{5nt}$, $fd5^{stop}$ mutant is largely rescued by one copy of the *fd5-GFP* transgene **(B)**. Knockdown of Fd4 and Fd5 levels with the *dsx-Gal4* **(C)**, but not with the *sca-Gal4* **(D)**, reduced the number of sex comb bristles. **(E,F)** Quantification of sex comb bristles in the genotypes indicated and presented in panels **(A,B)**. $n > 19$ sex combs per genotype were counted. Error bars indicate standard deviation (SD). Statistically significant differences based on Student's *t* test are indicated: $^{****}P < 0.0001$ and not significant (ns).

In order to study the function of the *fd4/fd5* genes in gain of function experiments we have generated specific UAS lines for each gene and ectopically expressed them in the dorsal region (*dpp-gal4*) or in the entire distal domain (*Dll-Gal4*) of the leg imaginal disc (**Figure 3**). Importantly, the ectopic expression of *fd4* or *fd5* did not increase the number of sex comb bristles in any of these conditions (**Figures 3A,B,D**). Nevertheless, we observed the appearance of an extra dorsal pre-apical bristle in 50% of T2 legs and a distal truncation that deletes the claw in the *Dll>fd5* genotype (**Figure 3B**). When both genes were expressed together with the *Dll-Gal4* line, a more severe distal truncation phenotype was detected, however the number on sex comb bristles remained close to the control (∼11.4 in *Dll>* vs. ∼10 in *Dll>fd4/fd5* animals) (**Figures 3C,D**).

In summary, all these results suggest that *fd4/fd5* act redundantly in the formation of the sex comb, however these genes are not sufficient to generate ectopic sex comb teeth when ectopically expressed.

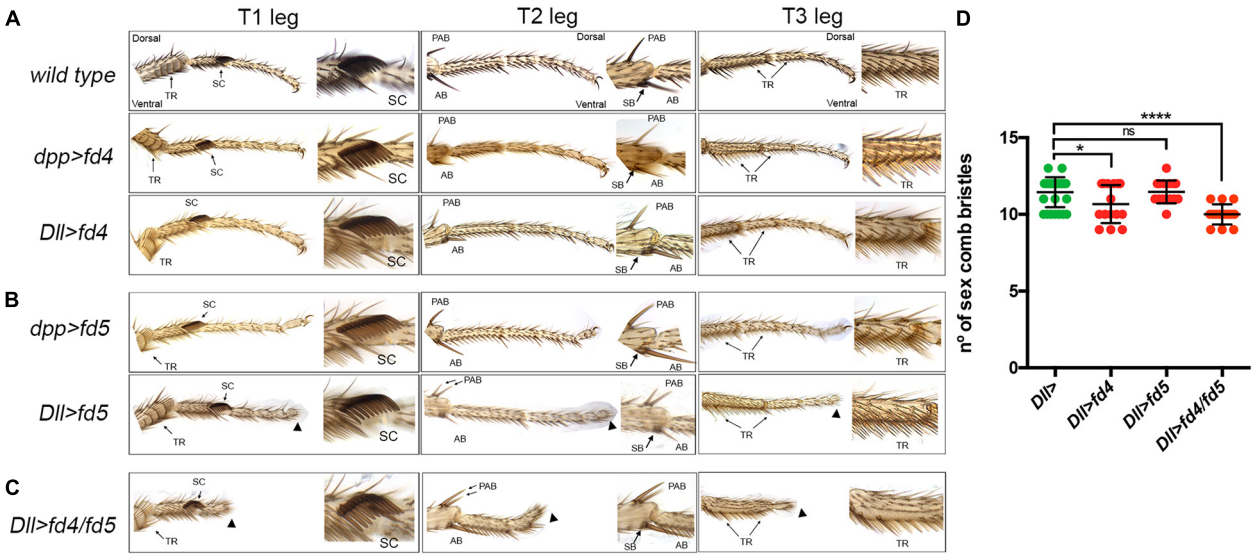

FIGURE 3 | Phenotypic analysis of *fd4* and *fd5* gain of function. **(A,B)** Male adult legs phenotypes of wild type control animals and of flies misexpressing *fd4* **(A)** or the *fd5* **(B)** in the distal (*Dll-Gal4*) or dorsal (*dpp-Gal4*) domain of the legs. Representative examples of the three legs (T1–T3) are presented. Close up views of the sex comb in T1, the distal tibia in T2, and the first tarsus in T3 are shown. Arrowheads indicate distal truncations. Arrows indicate the presence of duplicated PABs. **(C)** Male adult legs of flies misexpressing *fd4* and *fd5* under the *Dll-Gal4* driver. Note the severe truncation of the distal leg (arrowheads) and the presence of two PABs. **(D)** Quantification of sex comb bristles in the genotypes indicated and presented in panels **(A–C)**. *n* = 15 sex combs per genotype were counted. Error bars indicate standard deviation (SD). Statistically significant differences based on Student's *t* test are indicated: $*P < 0.05$, $****P < 0.0001$, and not significant (ns).

Analysis of *fd4/fd5* Role in the Sex Comb Regulatory Network

The formation of the sex comb is directed by a gene regulatory network that precisely localizes this structure in the anterior ventro-lateral domain of the first tarsal segment of prothoracic male legs (Kopp, 2011). PD patterning genes such as *Dll*, *dachsound* (*dac*), and *bric à brac* (*bab*), in combination with *H15/mid*, *wg*, and *en* regulate the prominent expression of the Hox gene *Sex comb reduced* (*Scr*) in the tibia (ti) and first tarsal segment (ta1) of the prothoracic leg (Tokunaga, 1961; Struhl, 1982; Couderc et al., 2002; Svendsen et al., 2009; Eksi et al., 2018; **Figures 4A,I**). Scr, together with PD transcription factors, regulate *doublesex* (*dsx*) expression in two anterior distal crescents (ta1 and ta2). Dsx is a sex-specific transcription factor that exists in two isoforms. The male isoform promotes male-specific structures while the female isoform dictates the corresponding female ones (Burtis and Baker, 1989). Once activated, Dsx modulates the sexual dimorphic male-specific expression of *scr* in ta1 segment (Kopp, 2011; Tanaka et al., 2011; **Figures 4B,I**).

Initially, we analyzed the expression of *wg* and its target genes *H15* and *mid* in *fd4/fd5* loss of function conditions. No changes were observed in the expression of any of these genes (**Supplementary Figure 5**). Next, as both Scr and Dsx direct the morphogenesis of the sex comb structure, we decided to study the functional relationship between these genes and *fd4/fd5*. To monitor *dsx* expression we used an antibody against the common domain shared by the male and female Dsx protein isoforms (Sanders and Arbeitman, 2008). First, we compared the expression of *fd5-GFP* with Scr and Dsx and confirmed that both genes overlap with Fd5 in the ventro-lateral domain of the presumptive ta1 in male prothoracic imaginal disc, the region that will form the transverse row bristles and the sex comb (**Figures 4A,B**). Second, we analyzed *Scr* and *dsx* expression in leg discs from $fd4^{5nt}$, $fd5^{stop}$ double mutant animals. No visible changes were observed in the expression of these genes in mutants as compared to controls, or when we knockdown Fd4/Fd5 levels in the anterior compartment using the RNAi lines (**Figures 4C–F**). To confirm that the *fd4/fd5* genes are not modulating Scr or Dsx levels, we generated mosaic mitotic $fd4^{5nt}$, $fd5^{stop}$ mutant clones and monitored Scr and Dsx levels in mutant and wild type adjacent cells of the same leg imaginal disc (**Figures 4G,H**). We did not detect any change on Scr and Dsx levels in $fd4^{5nt}$, $fd5^{stop}$ mutant clones. As *fd4* and *fd5* expression is neither sexually dimorphic nor restricted to the prothoracic legs, it is very unlikely that these genes are downstream of Scr and Dsx regulation.

These results indicate that the *fd4/fd5* genes may work in parallel with Scr and Dsx in the regulatory network that controls the formation of the sex comb (**Figure 4I**).

Identification of the Leg Disc *fd4/fd5* Minimal *Cis*-Regulatory Module

To identify the CRMs that direct *fd4/fd5* expression in the leg imaginal disc, we searched for differentially open chromatin regions between the leg and the wing disc in the *fd4/fd5* genomic locus (McKay and Lieb, 2013). Two regions, A and C, show a clear open chromatin state in the leg as opposed to the wing

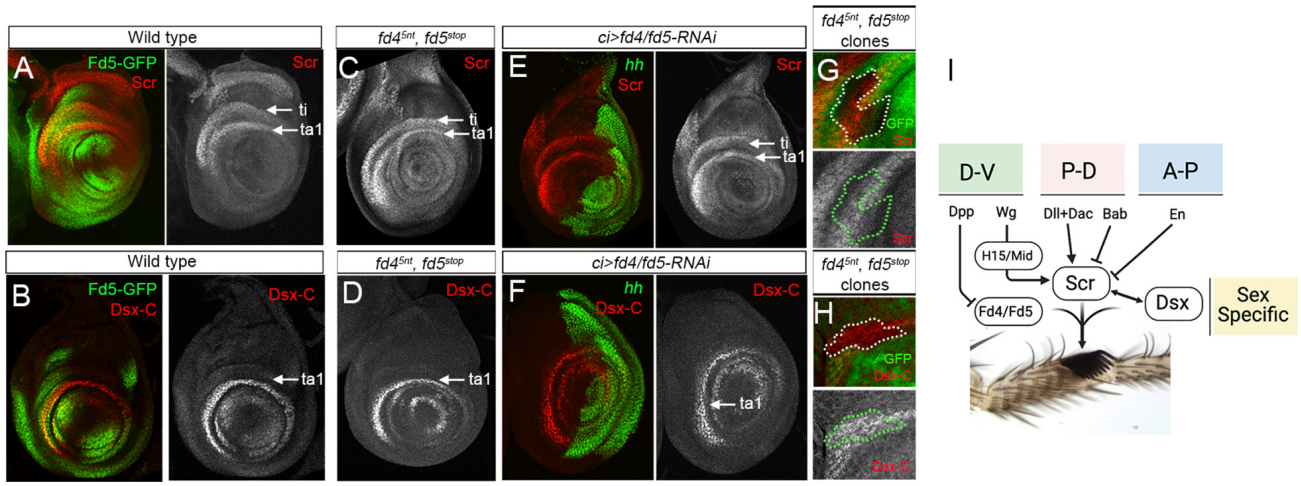

FIGURE 4 | Fd4/Fd5 are not requiered for *Scr* and *dsx* expression. **(A,B)** Expression of *fd5-GFP* (green) and *Scr* (red, **A**) or *dsx-C* (red, **B**) in a male third instar prothoracic leg imaginal disc. Single channels for Scr and Dsx-C stainings are shown. White arrows point to the tibia and first tarsal segment. **(C,D)** Scr **(C)** and Dsx-C **(D)** antibody stainings in male prothoracic leg imaginal discs of $fd4^{5nt}$, $fd5^{stop}$ mutant animals. **(E,F)** Male prothoracic leg imaginal discs stained for Hh (green) and Scr (red, **E**) and Dsx-C (red, **F**). The knockdown of Fd4/Fd5 levels in the anterior compartment by the expression of the *fd4* and *fd5 RNAi* lines under the *ci-Gal4* driver does not affect Scr or Dsx-C. Single channels for Scr and Dsx-C staining are shown. **(G,H)** $fd4^{5nt}$, $fd5^{stop}$ mitotic mutant clones visualized by the absence of GFP (green) and by a dotted white and green line. Scr **(G)** and Dsx-C **(H)** levels (red) are not affected in $fd4^{5nt}$, $fd5^{stop}$ mutant cells. Single channels for Scr and Dsx-C staining are shown. **(I)** The sex comb integrate multiple regulatory inputs form the three axes (D-V, P-D, and A-P) and sex-specific cues to develop in a precise location in the first tarsal segment of the male prothoracic leg. A simplified version of the gene regulatory network that directs the formation of the sex comb is depicted. In all confocal images, dorsal is up and anterior is left.

disc (**Figure 5A**). Both regions and an additional sequence (B fragment) that has been previously shown to reproduce *fd4/fd5* expression in the embryo were cloned in a GFP or lacZ reporter vector (**Figures 5A,B**; Archbold et al., 2014). Of these three elements, only fragment C, which is contained within the GMR35H08 element, is active in the leg disc in a similar pattern as *fd4/fd5* expression (**Figure 5B**). However, unlike the *fd4/fd5* genes, this element is also active in the wing disc (**Supplementary Figure 6**). We further subdivided the C element in two non-overlapping halves (C1 and C2) and a fragment that encompass the peak of open chromatin in the leg (C3) (**Figure 5A**). As both C2 and C3 elements reproduce *fd4/fd5* expression, we tested the activity of the 200 bp overlapping region (Cs) in the leg disc. No reporter activity was observed for the Cs fragment, suggesting that the C3 element contains the minimal information to drive *fd4/fd5* expression in the leg disc (**Figure 5B**).

Regulation of *fd4/fd5* Expression in the Leg Imaginal Disc

As the expression of the *fd4/fd5* genes is restricted to the ventro-lateral domain of the leg disc, we investigated the role of the Dpp and Wg pathways in their regulation. We used the *fd5-GFP* line or the *fd4/fd5* C-CRM as readouts for *fd4/fd5* expression depending on the experimental setup. To test the idea that the *fd4/fd5* genes integrate the Wg and Dpp inputs, we generated clones expressing a constitutive activated form of the β-catenin homolog Armadillo (Arm*) to activate the Wg pathway, or an activated form of the Dpp receptor Thickveins (Tkv^{QD}), respectively (**Figures 6A–C**). Most of dorsally located *arm** expressing clones show a cell autonomous upregulation of *fd5-GFP* and *C-GFP* CRM expression (**Figures 6A,B**). However, *arm** clones close to the *dpp* domain failed to induce the expression of these reporters (**Figures 6A,B**). In contrast, activation of the Dpp pathway by tkv^{QD} expressing clones strongly repressed *fd5-GFP* expression (**Figure 6C**). These results suggest that the Wg pathway activates, while the Dpp pathway represses *fd4/fd5* expression. To test for the requirement of these pathways in the regulation of the *fd4/fd5* genes, we generated mitotic loss of function clones for the transcriptional effectors of the Dpp pathway, Mad and for the Wg co-receptor Arrow (Arr). *C-GFP* was strongly upregulated in all dorsally located mad^{12} clones, while ventral arr^{2} mutant clones exhibit different behaviors of C-CRM activity depending on their localization (**Figures 6D–F**). For example, ventral anterior clones close to the AP compartment border downregulate C-*lacZ* activity while ventral posterior clones have no effect on it (**Figures 6E,F**, respectively). The regulation of *fd4/fd5* expression by the Dpp and Wg pathways is not mediated by their target genes *omb* and *H15/mid*, as mutant clones for these genes have no effect on *fd5-GFP* expression or C activity (**Supplementary Figure 6**).

Decapentaplegic and Wg transcriptionally repress each other in the leg disc, and therefore the downregulation of one pathway allows the activation by Hh of the other in anterior cells (Brook and Cohen, 1996; Jiang and Struhl, 1996; Johnston and Schubiger, 1996; Morimura et al., 1996; Penton and Hoffmann, 1996; Theisen et al., 1996). Our arr^{2} mutant clone analysis points to an indirect regulation of *fd4/fd5* expression through the derepression of the Dpp pathway instead of a direct requirement of the Wg pathway for its expression. To further test this possibility, we first generated mutant clones for Schnurri (Shn), a transcriptional repressor downstream of Dpp activity. Shn is a zinc finger protein that together with Mad/Med forms a complex

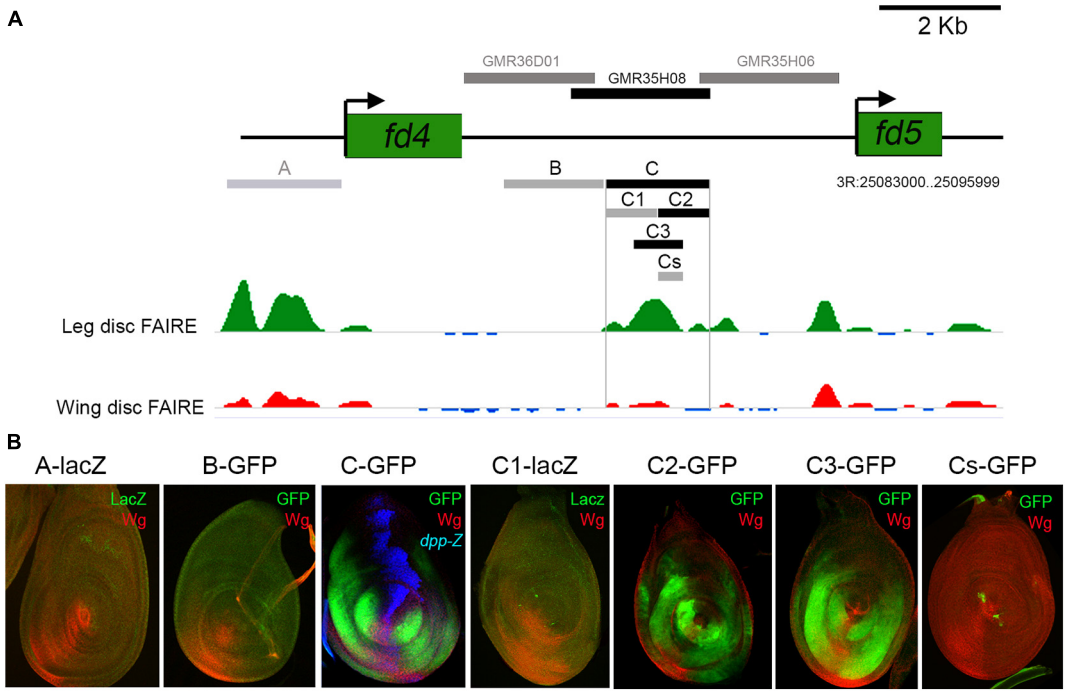

FIGURE 5 | Identification of the *fd4/fd5* CRM. **(A)** Schematic representation of the *fd4* and *fd5* genomic locus in which open chromatin regions, identified by FAIRE seq for leg and wing imaginal discs are indicated by green and red peaks, respectively. Data obtained from McKay and Lieb (2013). In the upper part of the panel, horizontal bars represent the DNA elements for which Gal4 drivers were generated by the Janelia Farm consortium (gray bars). Only the GMR35H08 line (black bar) reproduced *fd4/fd5* expression in the leg disc. Below the genomic locus are drawn the different DNA elements cloned in this work into a reporter *GFP* or *lacZ* construct. Only the C fragment and the C2 and C3 subfragments faithfully reproduced the expression of *fd4/fd5* in the leg imaginal disc. Note that the A and C fragments were selected because of the different chromatin accessibility profiles between the leg and wing imaginal discs. Gray bars indicate no activity and black bars indicate activity in leg imaginal discs. **(B)** Leg imaginal disc activity of the different fragments cloned in this work and shown in panel **(A)**. All elements were cloned in a *GFP* or *lacZ* reporter vector and inserted in the same attP site. GFP (green), Wg (red), and *dpp-lacz* (blue).

that regulates Dpp target genes such as *brinker* (*brk*) (Arora et al., 1995; Grieder et al., 1995; Marty et al., 2000). Dorsally located shn^3 mutant clones activated the expression of the *C-lacZ* reporter cell autonomously and, importantly, they do so without derepression of *wg* (**Figure 6G**). Next, we induced shn^1 mutant clones that are also mutant for *arr*, and therefore cannot transduce the Wg pathway. Consistently with our previous results, these shn^1 arr^2 mutant clones still derepressed C-*lacZ* activity in dorsal leg regions (**Figure 6H**).

Taken together, these results demonstrate that *fd4/fd5* expression is repressed dorsally by the Dpp effectors Shn and Mad and is activated independently of Wg.

fd4/fd5 are expressed in ventral (legs and antenna) but not dorsal (wing and haltere) imaginal discs, suggesting that their expression could be regulated by a positive input from a ventral selector gene. The sister genes, *buttonhead* (*btd*) and *Sp1* could fulfill this role: in one hand, forced expression of *btd* or *Sp1* in the wing disc induces ectopic leg development and in the other, removing *btd* and *Sp1* completely abolish leg formation (Estella et al., 2003; Estella and Mann, 2010). To test this idea, we analyzed *fd5-GFP* expression in wing discs where *btd* is ectopically induced (**Figures 7A–C**). Misexpression of *btd* in the wing imaginal disc with the *dpp-Gal4* line activates *fd5-GFP* in the wing pouch but not in the notum (**Figures 7A–C**). In contrast, clones for a deficiency that deletes the *btd* and *Sp1* genes (*Df(btd,Sp1)*) in the leg disc has no effect on *fd5-GFP* expression, even when these clones lose the ability to activate *Dll* (**Figure 7D**). These results suggest that although *btd* is sufficient to ectopically induce *fd5-GFP* expression in the wing disc, *btd* and *Sp1* are not necessary for endogenous *fd5* expression in the leg disc.

DISCUSSION

In this work we studied the expression and function of the forkhead family members *fd4* and *fd5* during leg development in *Drosophila*. We found that these genes play redundant roles during sex comb formation.

Subdivision of the DV territories is regulated in a different manner between wing and leg appendages. For example, in the wing imaginal disc the expression of the selector gene *apterous* (*ap*) is activated in response to the epidermal growth factor receptor (EGFR) pathway and it is required for the specification of dorsal cell fates (Diaz-Benjumea and Cohen, 1993; Blair et al., 1994; Wang et al., 2000; Bieli et al., 2015). In the leg imaginal disc, DV subdivision is controlled by Dpp and Wg signaling pathways that direct dorsal and ventral fates, respectively (Brook and Cohen, 1996; Jiang and Struhl, 1996; Johnston and Schubiger, 1996; Morimura et al., 1996; Penton and Hoffmann, 1996; Theisen et al., 1996). As Dpp and Wg

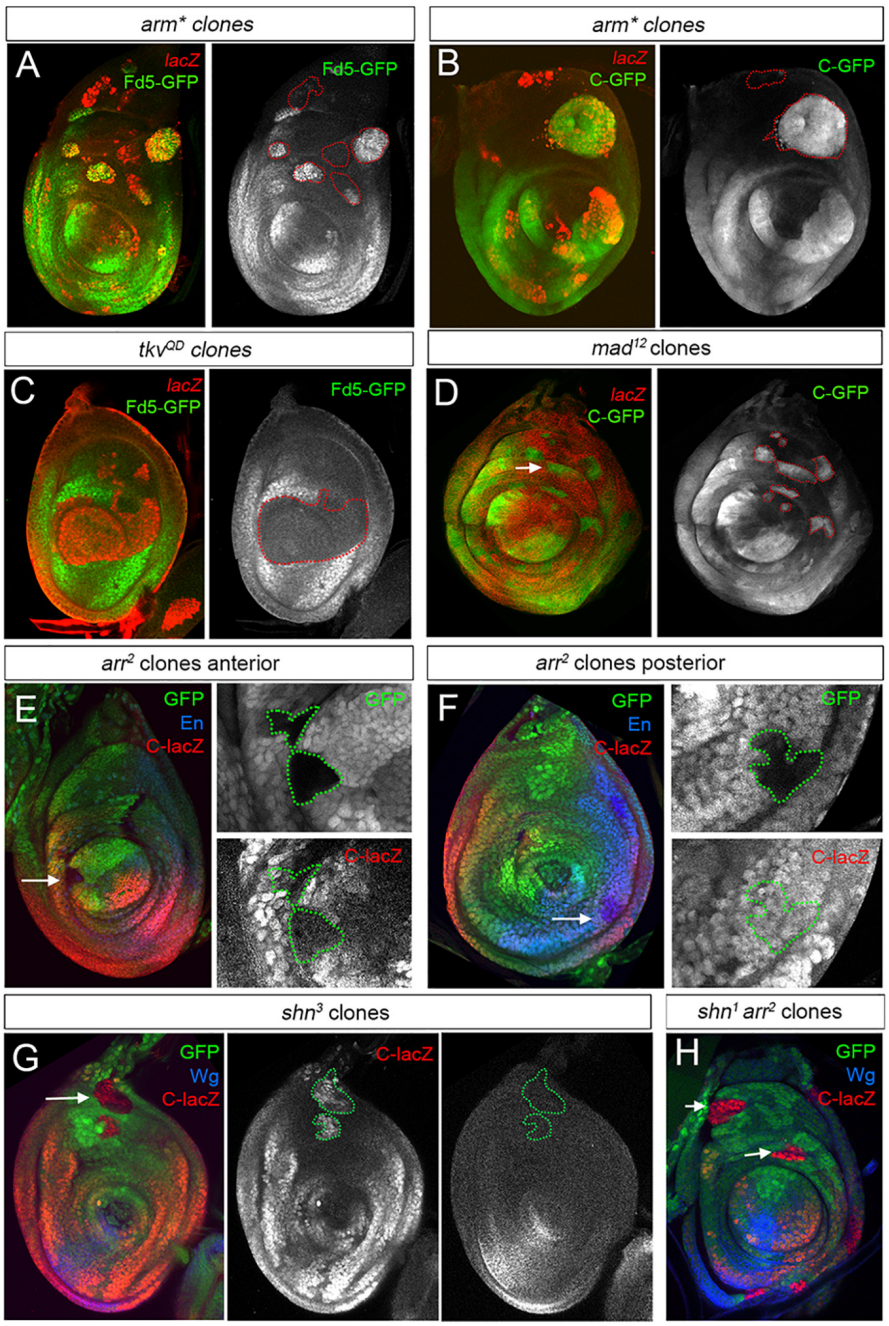

FIGURE 6 | Wg and Dpp contribution to *fd4/fd5* regulation in the leg disc. **(A,B)** Clones expressing *arm** marked by lacZ (red) activates *fd5-GFP* (green, **A**) or C-GFP (green, **B**) expression in dorso-lateral regions of the disc. Note that dorsal-most clones failed to activate *fd5* or C activity. Single channels for Fd5-GFP and C-GFP are shown separately and *arm** clones are outlined with red dots. **(C)** Clones expressing tkv^{QD} marked by lacZ (red) repress *fd5-GFP* (green) expression. Single channel for Fd5-GFP is shown and tkv^{QD} clones are outlined with red dots. **(D)** mad^{12} clones marked by absence of lacZ (red), show C-GFP (green) derepression in the dorso-lateral domain of the leg (white arrow). Single channel for C-GFP is shown and clones are outlined with red dots. **(E,F)** arr^{2} clones marked by absence of GFP stained for C-lacZ (red) and En (blue) to mark the posterior compartment. In panel **(E)**, an anterior arr^{2} mutant clones in the ventro-lateral domain of the leg show downregulation of C-lacZ (arrow). In panel **(F)**, the same clones located in the posterior compartment have no effect on C-lacZ activity (arrow). Single channels for GFP and C-lacZ are shown and clones are outlined with green dots. **(G)** shn^{3} mutant clones marked by the absence of GFP (green) derepress C-lacZ activity (red) in the dorsal domain of the leg disc (arrow). Note that in these clones, *wg* expression (blue) is not activated. Single channels for C-lacZ and Wg are shown and clones are outlined with green dots. **(H)** shn^{1}, arr^{2} double mutant clones marked by the absence of GFP (green) derepress C-lacZ activity (red) in the dorsal domain of the leg disc (arrows). Wg staining is in blue. All clones were generated 48–72 h AEL.

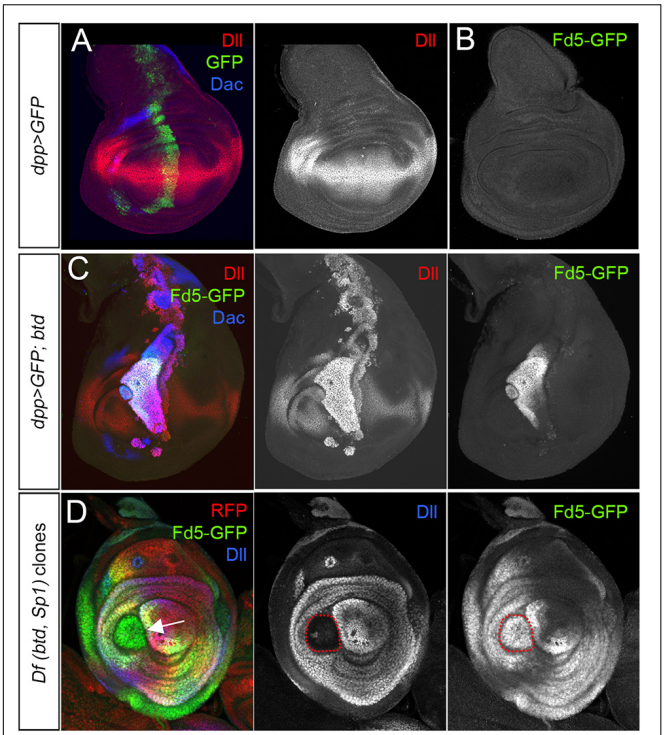

FIGURE 7 | *fd5* regulation by *btd* and *Sp1*. **(A)** Control wing imaginal disc expressing GFP (green) under the *dpp-Gal4* driver and stained for Dll (red) and Dac (blue). Separate channel for Dll is shown. **(B)** Wing imaginal disc from a *fd5-GFP* line. Note the absence of *fd5* expression (green) in the wing disc. **(C)** The expression of *btd* under the control of the *dpp-Gal4* line ectopically activates *fd5-GFP* (green) expression in the wing disc. Dll (red) and Dac (blue). Separate channels for Dll and Fd5-GFP are shown. **(D)** *Df(btd, Sp1)* mutant clones generated 48–72 h before dissection marked by the absence of RFP (red and arrow) and stained for Fd5-GFP (green) and Dll (blue). Single channels for Dll and Fd5-GFP are shown. Clones are outlined with red dots.

form gradients, an interesting problem is to understand how cells in the leg disc, which are exposed to different levels of these morphogens are able to integrate this information and assume dorsal, ventral, and lateral fates. This is of special interest as the leg is a circular appendage with no clear morphological DV distinction and no lineage restriction as opposed to the wing. Moreover, in contrast to the PD axis, we have very limited information of the downstream Wg and Dpp targets that controls DV patterning in the leg.

In a search for genes with DV expression patterns in the leg, we identified the forkhead family members *fd4* and *fd5* to be restricted to the ventro-lateral domain of the ventral imaginal discs. In contrast to other known DV leg patterning genes, the *fd4/fd5* expression is extended more laterally than the Wg target genes *H15/mid*. These genes are not activated in the dorsal domain of the leg, where high levels of Dpp are present. In addition, we identified a minimal CRM that faithfully recapitulates *fd4/fd5* expression in the leg imaginal disc. Detailed analysis of the C element regulation reveals that this CRM is activated by an unknown factor and repressed by the Dpp pathway, more specifically by the transcriptional repressor Shn. Interestingly, we found that the C element is similarly expressed as *brk*, another Shn target gene (Marty et al., 2000; Estella and Mann, 2008). However, Brk is not required for C element activity in the leg as the *C-GFP* CRM is normally expressed in *brk* mutant clones (**Supplementary Figure 6**). No consensus binding site for the Mad/Med/Shn complex was found in the C-CRM sequence, suggesting that either this complex is binding a non-consensus site or that *fd4/fd5* regulation by Shn is indirect (Pyrowolakis et al., 2004). Importantly, we found that the Wg pathway is indirectly required for C element activity through the repression of Dpp expression.

Unlike the endogenous expression of the *fd4/fd5* genes, the C element is not restricted to the ventral imaginal discs (legs and antenna), as activity of this CRM is also observed in the wing disc. This result suggests that sequences outside the C and GMR35H08 elements restrict *fd4/fd5* expression to the ventral imaginal discs. We studied the potential role of the ventral selector genes Sp1 and Btd as regulators of *fd4/fd5* ventral specific expression. However, *btd/Sp1* loss of function clones still display *fd5* expression in the leg. It is possible that wing disc specific genes are required for repressing *fd4/fd5* expression in dorsal imaginal discs and restricting its activity to ventral ones.

According to their identical expression and sequence homology, we found that these genes play redundant roles during leg development. Using newly generated alleles for each gene and a double *fd4/fd5* mutant, we describe a redundant role for these genes in sex comb formation. In contrast to their wide lateral expression in all three legs, we only found defects on the development of this specific male structure of the first thoracic leg. In males, the distal most transverse row of the first tarsal segment is transformed into a sex comb. We found that in *fd4/fd5* double mutants the number of sex comb bristles is strongly reduced but not eliminated, suggesting that these genes contribute to sex comb development but are not completely required. As the sex comb is formed from cells with ventral and lateral fates (Held et al., 1994), the remaining sex comb bristles observed in the *fd4/fd5* mutants would only be formed from cells with ventral identity.

The sex comb gene regulatory network integrates information from the three axes (AP, DV, and PD) and sex- and segment-specific cues by the *dsx* and *Scr* genes, respectively (Kopp, 2011). No defects on the expression of *H15/mid*, *Scr*, or *dsx* were observed when *fd4/fd5* levels were knock down, suggesting that the *fd4/fd5* act in parallel to these genes in the regulatory network that controls sex comb formation. The sex comb is a great model to study how the precise combination of positional and sex specific patterning cues promote the formation of morphological structures. Understanding the genetics of sex comb development could help understand the origin and diversification of this recently evolved structure.

A recent study has analyzed the expression and function of the forkhead transcription factor FoxB in the common house spider *Parasteatoda tepidariorum* (Heingard et al., 2019). This gene is the ortholog of *fd4/fd5* and the only family member in the spider. Similar to *Drosophila fd4/fd5*, *pt-FoxB* expression is restricted to the ventral domain of developing appendages and it is required for DV patterning. In *pt-Foxb-RNAi* animals the

expression of the ventral determinants *wg* and *H15* is almost lost while the corresponding ventral expansion for the dorsal determinants, *dpp* and *omb*, is described. It is remarkable the different mutant phenotypes observed in the spider and the fly after the knockdown of these genes. One possibility that could explain these differences is that the double $fd4^{5nt}$, $fd5^{stop}$ mutant chromosome generated in our study is not a true null for *fd5* but a strong hypomorph due to stop codon readthrough mechanisms (Palma and Lejeune, 2021). Either way, the leg phenotypes described here using the double $fd4^{5nt}$, $fd5^{stop}$ mutant and the RNAi lines are almost identical. Also, in the *Parasteatoda* study the authors used RNAi techniques to downregulate the function of the *Foxb* gene. Another possibility is that the function and requirement of the FoxB forkhead transcription factors have been modified during the evolution of arthropods. Thanks to the development of new technologies such as CRISPR/Cas9 the function of the FoxB forkhead transcription factors could be easily investigated in other arthropods to study how the DV gene regulatory network has been modified in related species.

MATERIALS AND METHODS

Drosophila Strains

fd4-GFP (*P{fd96Ca-GFP.FPTB}attP40*), *fd5-GFP* (*P{fd96Cb-GFP.FPTB}attP40*), dpp^{10368}*-lacZ (p10368)*, *omb-lacZ*, *H15-lacZ*, *mid-lacZ*, *dpp-Gal4*, *UAS-GFP*, Dll^{212}*-Gal4*, *dsx-Gal4*, *sca-Gal4*, *UAS-fd4-RNAi*, *UAS-fd5-RNAi* and *hh-dsred*, *Ci-Gal4* are described in FlyBase.

Loss-of-function clonal analysis the following genotypes were used:

yw122; *FRT82B* $fd4^{5nt}$, $fd5^{stop}$*/yw122*; *FRT82B-ubi-GFP.*
yw122; *FRT42D* arr^{2}*/w122*; *FRT42D ubi-GFP*; *C-lacZ*
yw122; Mad^{1-2} *FRT40A/arm-lacZ FRT40A*; *C-GFP*
yw122; *FRT42D* shn^{3}; *C-lacZ/yw122*; *FRT42D ubi-GFP.*
yw122; *FRT42D* arr^{2} shn^{1}*/yw122*; *FRT42D ubi-GFP*; *C-lacZ*
Df(btd,Sp1) FRT19A/yw122 ubi-RFP FRT19A, *fd5-GFP*
omb^{282} *FRT19A/yw122 ubi-RFP FRT19A*, *fd5-GFP*
yw122; $H15^{X4}$ mid^{1a5} *FRT40A/ubi-GFP FRT40A*; *C-lacZ*
brk^{M68} *FRT19A/yw122 ubi-RFP FRT19A*, *C-GFP*

Clones were induced by heat shocking 48–72 h AEL (after egg laying) larvae for 1 h at 37°C.

Gain-of-function clonal analysis:

yw122; *act>STOP>Gal4, UAS-lacZ; fd5-GFP/UAS-*tkv^{QD}
yw122; *act>STOP>Gal4, UAS-lacZ; fd5-GFP/UAS-arm**
yw122; *act>STOP>Gal4, UAS-lacZ; C-GFP/UAS-arm**

Clones were induced by heat shocking 48–72 h AEL larvae for 10 min at 37°C.

At least three clones were scored for each experiment.

All fly lines listed above are described in FlyBase.

Generation of the $fd4^{5nt}$, $fd5^{1nt}$ and $fd4^{5nt}$, $fd5^{stop}$ Mutant Flies

The $fd4^{5nt}$, $fd5^{1nt}$ and $fd4^{5nt}$, $fd5^{stop}$ mutant flies were generated by CRISPR-Cas9 technique. Briefly, *fd4* and *fd5* gRNAs were cloned in the pBFv-U6.2 and injected in $y^{1}v^{1}$ *P{y[+ t7.7] = nos-phiC31\int.NLS}X;P{y[+ t7.7] = CaryP}attP40* flies. These flies were then crossed with flies expressing Cas9 in their germinal line cells. Candidate mutants were confirmed by sequencing. gRNAs sequences were selected as the produced mutations (insertions and deletions) at the beginning of the respective gene. The following sequences were used as primers to clone the gRNAs in the pBFv-U6.2 vector following FlyCas9 protocols[1]:

Sense fd4 5′-CTTCGTAGGATTCTCGCGAGGGCC-3′
Asense fd4 5′-AAACGGCCCTCGCGAGAATCCTAC-3′
Sense fd5 5′-CTTCGCTGAGCGGCAGCAATCTTTG-3′
Asense fd5 5′-AAACCAAAGATTGCTGCCGCTCAGC-3

To generate the $fd4^{5nt}$, $fd5^{stop}$ double mutant we introduced the *fd5* gRNA into $fd4^{5nt}$ flies. The candidate mutant flies were sequenced to verify the new mutations produced in the *fd5* gene.

Generation of UAS-*fd4* and UAS-*fd5* Lines

Wild type *fd4* and *fd5* DNA was amplified from genomic DNA and cloned in the pUAST attB vector using the following primers (restriction sites are underlined and restriction enzyme used is noted in brackets):

For UAS-*fd4*:

5′-CAGTGAATTCGTAATAATGCCCCGGCCCTC GCGAGAATCC-3′ (*Eco*RI)

5′-CAGTCTCGAGCCCTGCTTGTTGCCACTTATCTAT ATCGTACGC-3′(*Xho*I)

For UAS-*fd5*:

5′ CAGTAGATCTCTTCGCAATGCCACGCCC ATTGAAAATGAG 3′ (*Bgl*II)

5′ CAGTGCGGCCGCTCAAAAGACGGGCAACGGGCCG 3′ (*Not*I)

Both UAS constructs were inserted into the same attP site (86Fb).

Generation of *GFP* and *lacZ* Reporter Transgenic Lines

To generate the A, B, C, C1, C2, C3, and Cs reporter constructs, DNA from the *fd4/fd5* locus was amplified by PCR from genomic DNA. For the GFP reporter lines, the DNA fragments were first cloned into the pEntry/D-TOPO vector and then swapped into the *attB-pHPdesteGFP* vector (Boy et al., 2010), using the LR Clonase Enzyme Mix (Thermo Fisher Scientific). For the *lacZ* reporter lines, DNA fragments were amplified with primers containing restriction enzyme sites as overhangs, and subsequently cloned into plasmid *attB-hs43-nuc-lacZ* (Giorgianni and Mann, 2011).

We cloned all the sequences in the *GFP* reporter vector except for the C1 and A fragments that were cloned in the *lacZ* vector and the C-CRM that was cloned in both vectors.

To carry out these experiments, we used the following primers (restriction sites are underlined and restriction enzyme used is noted in brackets)

A fragment in *attB-hs43-nuc-lacZ* vector:

5′-CAGTGCGGCCGCCCGTGGCCATATTCATATGTCCAC-3′ (*Not*I)

[1]https://shigen.nig.ac.jp/fly/nigfly/cas9/

5′-CAGTGCGGCCGCAGGATTCTCGCGAGGGCCGGGG-3′(*Not*I)

B fragment in *attB-pHPdesteGFP* vector:

5′CACCGCGCACCAGGCCACGCCCACCCCCG-3′

5′CAGTAGATCTGGAGCCGCAGGGGCCAGATA-3′

C fragment in *attB-hs43-nuc-lacZ* vector:

5′-CAGTGCGGCCGCGTATCTGGCCCCTGCGGCTCC-3′(*Not*I)

5′CAGTAGGCCTGCCCAGAGGCGGATTCGGATTCGG-3′(*Stu*I)

C fragment in *attB-pHPdesteGFP* vector:

5′-CACCGTATCTGGCCCCTGCGGCTCC-3′

5′-GCCCAGAGGCGGATTCGGATTCGG-3′

C2 fragment in *attB-pHPdesteGFP* vector:

5′-CACCCAGATCTCAGTTTCTCGGTTCG-3′

5′-GCCCAGAGGCGGATTCGGATTCGG-3′

C3 fragment in *attB-pHPdesteGFP* vector:

5′-CACCAGATCTCGGCTCGGGTGTTGATGC-3′

5′-CAGTGCGGCCGCGCCGCTAGTTGCCGGCAC-3′

Cs fragment in *attB-pHPdesteGFP* vector:

5′-CACCCAGATCTCAGTTTCTCGG-3′

5′-CAGTGCCGCTAGTTGCCGGCAC-3′

The C1-lacZ fragment was cloned from the C sequence included in the *attB-hs43-nuc-lacZ* vector, using the restriction site of *Not*I enzyme that had been included at the beginning of C sequence, and *Bgl*II that digests in the middle of the C fragment. The primers to clone the C2 fragment were designed to clone from *Bgl*II.

All these constructs were inserted into the same attP site (86Fb).

Immunostaining

Embryos and larval leg imaginal discs were fixed and stained following standard procedures described in Requena et al. (2017). We used the following primary antibodies: rabbit anti-βGal (1/1000; Promega), mouse anti-βGal (1/1000; MP Biomedicals), guinea pig anti-Dll (1/2000) (Estella et al., 2008), rabbit anti-GFP (1/1000; Thermo Fisher Scientific), mouse anti-Dac (1/50; DSHB #mAbdac1-1), mouse anti-Wg (1/50; DSHB #4D4), rat-anti-Dsx-C (1/200) (Sanders and Arbeitman, 2008), mouse-anti-Scr (1/50; DSHB #6H4.1) and mouse anti-En (1/50; DSHB #4D9).

In situ Hybridization

The *fd4* RNA probe used in this experiment was generated by PCR from genomic DNA using primers with the recognition sequences of the RNA polymerase T7 and T3:

Forward T7:

5′-TAATACGACTCACTATAGGGGGGACT GACCAATCTGCCCGCGC-3′

Reverse: T3:

5′-ATTAACCCTCACTAAAGGGACGGGGCTCCG ATATTGCTGCGCC-3′

The transcription to generate antisense probes was done using the RNA polymerase T3 in the presence of DIG (DIG RNA labeling mix, Roche) at 15°C for 2 h, and the probes were precipitated and suspended in H_2O with DEPC (Sigma).

Imaginal discs were dissected in PBS 1× and fixed in 4% formaldehyde for 30 min at room temperature. Then, we washed in PBS-0.1% Tween (PBT) three times, and refixed for 20 min at room temperature in 4% formaldehyde, 0.1% Tween. The samples were washed again in PBT.

After three washes in PBT, discs were incubated overnight at −20°C in hybridization solution (SH; 50% formamide, SSC 5×, 100 μg/ml salmon sperm DNA, 50 μg/ml heparin, and 0.1% Tween).

The next day, we washed the disc in SH for 10 min at room temperature. The discs were prehybridized for 2 h at 55°C in SH and hybridized with digoxigenin (DIG)-labeled RNA probes at 55°C. The probes were previously denatured at 80°C for 10 min. All the solutions used before hybridization were treated with DEPC (Sigma). After hybridization, discs were washed in SH and PBT and incubated for 2 h at room temperature in a 1:4000 dilution of anti-DIG antibody (Roche). After incubation, the discs were washed in PBT and the detection of probes was performed with 4-Nitro blue tetrazolium chloride (NBT) and 5-Bromo-4-chloro-3-indolyl-phosphate (BCIP) solution (Roche). The discs were mounted in 70% glycerol.

DATA AVAILABILITY STATEMENT

The raw data supporting the conclusions of this article will be made available by the authors, without undue reservation.

AUTHOR CONTRIBUTIONS

MR-L, CP-R, and CE contributed to the conception and design of the study, performed the experiments, and analyzed the data. CE wrote the manuscript. All authors contributed to manuscript revision, read, and approved the submitted version.

FUNDING

This study was supported by grants from: the Programa Estatal de Generación de conocimiento y fortalecimiento científico y tecnológico del sistema de I + D + I (Ministerio de Ciencia, Innovación y Universidades) [No. PGC2018-095144-B-I00] to CE.

ACKNOWLEDGMENTS

We thank Michelle N. Arbeitman, William J. Brook, the Bloomington Stock Center, the Vienna Drosophila Resource Center, and the Developmental Studies Hybridoma Bank at The University of Iowa for fly stocks and reagents. We specially thank the Confocal microscopy service at CBMSO, Sergio Córdoba for comments on the manuscript, and Eva Caminero and Mar Casado for fly injections.

SUPPLEMENTARY MATERIAL

The Supplementary Material for this article can be found online at: https://www.frontiersin.org/articles/10.3389/fcell.2021.723927/full#supplementary-material

Supplementary Figure 1 | *fd4* and *fd5* expression in ventral imaginal discs. Third instar eye-antenna, genital and leg imaginal discs stained for Fd4-GFP (green) or Fd5-GFP (green), *dpp-lacZ* (blue), and Wg (red).

Supplementary Figure 2 | Generation of *fd4*, *fd5* and *fd4*, *fd5* double mutant alleles. Schematic representation of the different mutants generated for this study. gRNA target sites are in red. Chromatograms, as determined by Sanger sequencing, for the evaluation of the different mutants are presented. All sequences were obtained from homozygous flies at the exception of the $fd5^{1nt}$ mutant. Insertions are indicated in blue. Asterisks indicate the first stop codon generated. Gray boxes represent alterations in the protein sequence due to stop codons and open reading frame changes. The corresponding amino acid sequences are shown below.

Supplementary Figure 3 | *fd4* and *fd5* mutant's leg phenotypes. Adult male and female prothoracic legs of wild type, $fd4^{5nt}$, $fd5^{1nt}$ and the double $fd4^{5nt}$, $fd5^{stop}$ mutants. The tibia (tib) and the first tarsal (ta1) segment are shown. Sex comb (SC) are indicated, and numbers mark the transverse rows in the ta1.

Supplementary Figure 4 | Validation of *fd4* and *fd5* RNAi lines. **(A–D)** Third instar leg imaginal discs stained for GFP (green) and *hh-dsRED* (red) of the following genotypes: **(A)** *ci-Gal4*, *hh-dsRED*; *Fd4-GFP*, **(B)** *ci-Gal4*, *hh-dsRED*; *UAS-fd4-RNAi*; *Fd4-GFP*, **(C)** *ci-Gal4*, *hh-dsRED*; *Fd5-GFP*, and **(D)** *ci-Gal4*, *hh-dsRED*; *UAS-fd5-RNAi*; *Fd5-GFP*. Separate channels for GFP and Hh are shown. Note the downregulation of Fd4 and Fd5 levels in the anterior compartment in panels **(B,D)**. The compartment boundary is marked by white dots. **(E)** Male prothoracic adult legs of the indicated genotypes. Close up views of the sex comb are shown. **(F)** Quantification of sex comb bristles in the genotypes indicated and presented in panel **(E)**. $n > 15$ sex combs per genotype were counted. Error bars indicate standard deviation (SD). Statistically significant differences based on Student's *t* test are indicated: $^{****}P < 0.0001$ and not significant (ns).

Supplementary Figure 5 | Fd4/Fd5 are not required for *H15* and *mid* expression. **(A)** Leg imaginal disc stained for Fd5-GFP (green), Wg (blue), and *mid-lacZ* (red). **(B)** Expression of the *fd4* and *fd5* RNAi lines under the control of the *Dll-Gal4* line to knockdown Fd4/Fd5 levels. Leg imaginal disc is stained for *mid-lacZ* (red) and Wg (blue). The domain of *Dll-Gal4* is marked by green dots. **(C)** The knockdown of Fd4/Fd5 levels in the anterior compartment by the expression of the *fd4* and *fd5* RNAi lines under the *ci-Gal4* has no effect on *H15-lacZ* expression (green) or Wg protein (blue). *hh* expression is in red and the compartment boundary is marked by red dots. In panels **(A–C)**, separate channels for *mid-lacZ*, *H15-lacZ*, and Wg are shown.

Supplementary Figure 6 | *brk*, *omb*, and *mid/H15* mutant clones have no effect on *fd4/fd5* expression. **(A)** C-GFP activity is observed in the wing imaginal disc in a complementary pattern to *dpp* expression and similar to *brk* (not shown). **(B)** brk^{M68} mutant clones in the leg disc marked by the absence of RFP (red) and stained for C-GFP (green). Separate channels for RFP and C-GFP are shown and the brk^{M68} mutant clones are outlined by white dots. **(C)** Leg imaginal disc with a dorsal omb^{282} mutant clone marked by the absence of RFP (red, arrow) and stained for Fd5-GFP (green) and Wg (blue). Separate channel for Fd5-GFP is shown and the clone is outlined by a red dotted line. **(D)** $H15^{X4}$ mid^{1a5} mutant clones marked by the absence of GFP (green) in a third instar leg imaginal disc stained for C-lacZ (red) and Wg (blue). An arrow marks a ventro-lateral anterior compartment clone and a close up view is shown. All clones were generated 48–72 h before dissection.

REFERENCES

Abzhanov, A., and Kaufman, T. C. (2000). Homologs of *Drosophila* appendage genes in the patterning of arthropod limbs. *Dev. Biol.* 227, 673–689. doi: 10.1006/dbio.2000.9904

Angelini, D. R., and Kaufman, T. C. (2004). Functional analyses in the hemipteran *Oncopeltus fasciatus* reveal conserved and derived aspects of appendage patterning in insects. *Dev. Biol.* 271, 306–321. doi: 10.1016/j.ydbio.2004.04.005

Archbold, H. C., Broussard, C., Chang, M. V., and Cadigan, K. M. (2014). Bipartite recognition of DNA by TCF/Pangolin is remarkably flexible and contributes to transcriptional responsiveness and tissue specificity of wingless signaling. *PLoS Genet.* 10:e1004591. doi: 10.1371/journal.pgen.1004591

Arora, K., Dai, H., Kazuko, S. G., Jamal, J., O'Connor, M. B., Letsou, A., et al. (1995). The *Drosophila schnurri* gene acts in the Dpp/TGF beta signaling pathway and encodes a transcription factor homologous to the human MBP family. *Cell* 81, 781–790. doi: 10.1016/0092-8674(95)90539-1

Basler, K., and Struhl, G. (1994). Compartment boundaries and the control of *Drosophila* limb pattern by hedgehog protein. *Nature* 368, 208–214. doi: 10.1038/368208a0

Bieli, D., Kanca, O., Requena, D., Hamaratoglu, F., Gohl, D., Schedl, P., et al. (2015). Establishment of a developmental compartment requires interactions between three synergistic cis-regulatory modules. *PLoS Genet.* 11:e1005376. doi: 10.1371/journal.pgen.1005376

Blair, S. S., Brower, D. L., Thomas, J. B., and Zavortink, M. (1994). The role of apterous in the control of dorsoventral compartmentalization and PS integrin gene expression in the developing wing of *Drosophila*. *Development* 120, 1805–1815. doi: 10.1242/dev.120.7.1805

Boy, A. L., Zhai, Z., Habring-Muller, A., Kussler-Schneider, Y., Kaspar, P., and Lohmann, I. (2010). Vectors for efficient and high-throughput construction of fluorescent *Drosophila* reporters using the PhiC31 site-specific integration system. *Genesis* 48, 452–456. doi: 10.1002/dvg.20637

Brook, W. J. (2010). T-box genes organize the dorsal ventral leg axis in *Drosophila melanogaster*. *Fly* 4, 159–162. doi: 10.4161/fly.4.2.11251

Brook, W. J., and Cohen, S. M. (1996). Antagonistic interactions between wingless and decapentaplegic responsible for dorsal-ventral pattern in the *Drosophila* Leg. *Science* 273, 1373–1377. doi: 10.1126/science.273.5280.1373

Burtis, K. C., and Baker, B. S. (1989). *Drosophila* doublesex gene controls somatic sexual differentiation by producing alternatively spliced mRNAs encoding related sex-specific polypeptides. *Cell* 56, 997–1010. doi: 10.1016/0092-8674(89)90633-8

Campbell, G., and Tomlinson, A. (1998). The roles of the homeobox genes aristaless and distal-less in patterning the legs and wings of *Drosophila*. *Development* 125, 4483–4493. doi: 10.1242/dev.125.22.4483

Couderc, J. L., Godt, D., Zollman, S., Chen, J., Li, M., Tiong, S., et al. (2002). The bric a brac locus consists of two paralogous genes encoding BTB/POZ domain proteins and acts as a homeotic and morphogenetic regulator of imaginal development in *Drosophila*. *Development* 129, 2419–2433. doi: 10.1242/dev.129.10.2419

Diaz-Benjumea, F. J., and Cohen, S. M. (1993). Interaction between dorsal and ventral cells in the imaginal disc directs wing development in *Drosophila*. *Cell* 75, 741–752. doi: 10.1016/0092-8674(93)90494-b

Diaz-Benjumea, F. J., Cohen, B., and Cohen, S. M. (1994). Cell interaction between compartments establishes the proximal-distal axis of *Drosophila* legs. *Nature* 372, 175–179. doi: 10.1038/372175a0

Eksi, S. E., Barmina, O., McCallough, C. L., Kopp, A., and Orenic, T. V. (2018). A Distalless-responsive enhancer of the Hox gene Sex combs reduced is required for segment- and sex-specific sensory organ development in *Drosophila*. *PLoS Genet.* 14:e1007320. doi: 10.1371/journal.pgen.1007320

Estella, C., and Mann, R. S. (2008). Logic of Wg and Dpp induction of distal and medial fates in the *Drosophila* leg. *Development* 135, 627–636. doi: 10.1242/dev.014670

Estella, C., and Mann, R. S. (2010). Non-redundant selector and growth-promoting functions of two sister genes, buttonhead and Sp1, in *Drosophila* leg development. *PLoS Genet.* 6:e1001001. doi: 10.1371/journal.pgen.1001001

Estella, C., McKay, D. J., and Mann, R. S. (2008). Molecular integration of wingless, decapentaplegic, and autoregulatory inputs into Distalless during *Drosophila* leg development. *Dev. Cell* 14, 86–96. doi: 10.1016/j.devcel.2007.11.002

Estella, C., Rieckhof, G., Calleja, M., and Morata, G. (2003). The role of buttonhead and Sp1 in the development of the ventral imaginal discs of *Drosophila*. *Development* 130, 5929–5941. doi: 10.1242/dev.00832

Estella, C., Voutev, R., and Mann, R. S. (2012). A dynamic network of morphogens and transcription factors patterns the fly leg. *Curr. Top. Dev. Biol.* 98, 173–198. doi: 10.1016/B978-0-12-386499-4.00007-0

Giorgianni, M. W., and Mann, R. S. (2011). Establishment of medial fates along the proximodistal axis of the *Drosophila* leg through direct activation of dachshund by Distalless. *Dev. Cell* 20, 455–468. doi: 10.1016/j.devcel.2011.03.017

Grieder, N. C., Nellen, D., Burke, R., Basler, K., and Affolter, M. (1995). Schnurri is required for *Drosophila* Dpp signaling and encodes a zinc finger protein similar to the mammalian transcription factor PRDII-BF1. *Cell* 81, 791–800. doi: 10.1016/0092-8674(95)90540-5

Grossmann, D., Scholten, J., and Prpic, N. M. (2009). Separable functions of wingless in distal and ventral patterning of the *Tribolium* leg. *Dev. Genes Evol.* 219, 469–479. doi: 10.1007/s00427-009-0310-z

Hacker, U., Grossniklaus, U., Gehring, W. J., and Jackle, H. (1992). Developmentally regulated *Drosophila* gene family encoding the fork head domain. *Proc. Natl. Acad. Sci. U.S.A.* 89, 8754–8758. doi: 10.1073/pnas.89.18.8754

Hannah-Alava, A. (1958). Morphology and chaetotaxy of the legs of *Drosophila melanogaster*. *J. Morphol.* 103, 281–310. doi: 10.1002/jmor.1051030205

Heingard, M., Turetzek, N., Prpic, N. M., and Janssen, R. (2019). FoxB, a new and highly conserved key factor in arthropod dorsal-ventral (DV) limb patterning. *EvoDevo* 10:28. doi: 10.1186/s13227-019-0141-6

Held, L. I. Jr., Heup, M. A., Sappington, J. M., and Peters, S. D. (1994). Interactions of decapentaplegic, wingless, and Distal-less in the *Drosophila* leg. *Rouxs Arch. Dev. Biol.* 203, 310–319. doi: 10.1007/BF00457802

Inoue, Y., Mito, T., Miyawaki, K., Matsushima, K., Shinmyo, Y., Heanue, T. A., et al. (2002). Correlation of expression patterns of homothorax, dachshund, and Distal-less with the proximodistal segmentation of the cricket leg bud. *Mech. Dev.* 113, 141–148. doi: 10.1016/s0925-4773(02)00017-5

Janssen, R., Feitosa, N. M., Damen, W. G., and Prpic, N. M. (2008). The T-box genes H15 and optomotor-blind in the spiders *Cupiennius salei*, *Tegenaria atrica* and *Achaearanea tepidariorum* and the dorsoventral axis of arthropod appendages. *Evol. Dev.* 10, 143–154. doi: 10.1111/j.1525-142X.2008.00222.x

Jiang, J., and Struhl, G. (1996). Complementary and mutually exclusive activities of decapentaplegic and wingless organize axial patterning during *Drosophila* leg development. *Cell* 86, 401–409. doi: 10.1016/s0092-8674(00)80113-0

Johnston, L. A., and Schubiger, G. (1996). Ectopic expression of wingless in imaginal discs interferes with decapentaplegic expression and alters cell determination. *Development* 122, 3519–3529. doi: 10.1242/dev.122.11.3519

Jory, A., Estella, C., Giorgianni, M. W., Slattery, M., Laverty, T. R., Rubin, G. M., et al. (2012). A survey of 6,300 genomic fragments for cis-regulatory activity in the imaginal discs of *Drosophila melanogaster*. *Cell Rep.* 2, 1014–1024. doi: 10.1016/j.celrep.2012.09.010

Kopp, A. (2011). *Drosophila* sex combs as a model of evolutionary innovations. *Evol. Dev.* 13, 504–522. doi: 10.1111/j.1525-142X.2011.00507.x

Lecuit, T., and Cohen, S. M. (1997). Proximal-distal axis formation in the *Drosophila* leg. *Nature* 388, 139–145. doi: 10.1038/40563

Lee, H. H., and Frasch, M. (2004). Survey of forkhead domain encoding genes in the *Drosophila* genome: classification and embryonic expression patterns. *Dev. Dyn.* 229, 357–366. doi: 10.1002/dvdy.10443

Marty, T., Muller, B., Basler, K., and Affolter, M. (2000). Schnurri mediates Dpp-dependent repression of brinker transcription. *Nat. Cell Biol.* 2, 745–749. doi: 10.1038/35036383

Maves, L., and Schubiger, G. (1998). A molecular basis for transdetermination in *Drosophila* imaginal discs: interactions between wingless and decapentaplegic signaling. *Development* 125, 115–124. doi: 10.1242/dev.125.1.115

McKay, D. J., and Lieb, J. D. (2013). A common set of DNA regulatory elements shapes *Drosophila* appendages. *Dev. Cell* 27, 306–318. doi: 10.1016/j.devcel.2013.10.009

Morimura, S., Maves, L., Chen, Y., and Hoffmann, F. M. (1996). decapentaplegic overexpression affects *Drosophila* wing and leg imaginal disc development and wingless expression. *Dev. Biol.* 177, 136–151. doi: 10.1006/dbio.1996.0151

Ober, K. A., and Jockusch, E. L. (2006). The roles of wingless and decapentaplegic in axis and appendage development in the red flour beetle, *Tribolium castaneum*. *Dev. Biol.* 294, 391–405. doi: 10.1016/j.ydbio.2006.02.053

Palma, M., and Lejeune, F. (2021). Deciphering the molecular mechanism of stop codon readthrough. *Biol. Rev. Camb. Philos. Soc.* 96, 310–329. doi: 10.1111/brv.12657

Penton, A., and Hoffmann, F. M. (1996). Decapentaplegic restricts the domain of wingless during *Drosophila* limb patterning. *Nature* 382, 162–164. doi: 10.1038/382162a0

Prpic, N. M., Wigand, B., Damen, W. G., and Klingler, M. (2001). Expression of dachshund in wild-type and Distal-less mutant *Tribolium* corroborates serial homologies in insect appendages. *Dev. Genes Evol.* 211, 467–477. doi: 10.1007/s004270100178

Pueyo, J. I., and Couso, J. P. (2005). Parallels between the proximal-distal development of vertebrate and arthropod appendages: homology without an ancestor? *Curr. Opin. Genet. Dev.* 15, 439–446. doi: 10.1016/j.gde.2005.06.007

Pyrowolakis, G., Hartmann, B., Muller, B., Basler, K., and Affolter, M. (2004). A simple molecular complex mediates widespread BMP-induced repression during *Drosophila* development. *Dev. Cell* 7, 229–240. doi: 10.1016/j.devcel.2004.07.008

Reim, I., Lee, H. H., and Frasch, M. (2003). The T-box-encoding *Dorsocross* genes function in amnioserosa development and the patterning of the dorsolateral germ band downstream of Dpp. *Development* 130, 3187–3204. doi: 10.1242/dev.00548

Requena, D., Alvarez, J. A., Gabilondo, H., Loker, R., Mann, R. S., and Estella, C. (2017). Origins and specification of the *Drosophila* wing. *Curr. Biol.* 27, 3826–3836.e5. doi: 10.1016/j.cub.2017.11.023

Robinett, C. C., Vaughan, A. G., Knapp, J. M., and Baker, B. S. (2010). Sex and the single cell. II. There is a time and place for sex. *PLoS Biol.* 8:e1000365. doi: 10.1371/journal.pbio.1000365

Ruiz-Losada, M., Blom-Dahl, D., Cordoba, S., and Estella, C. (2018). Specification and patterning of *Drosophila* appendages. *J. Dev. Biol.* 6:17. doi: 10.3390/jdb6030017

Sanders, L. E., and Arbeitman, M. N. (2008). Doublesex establishes sexual dimorphism in the *Drosophila* central nervous system in an isoform-dependent manner by directing cell number. *Dev. Biol.* 320, 378–390. doi: 10.1016/j.ydbio.2008.05.543

Shroff, S., Joshi, M., and Orenic, T. V. (2007). Differential delta expression underlies the diversity of sensory organ patterns among the legs of the *Drosophila* adult. *Mech. Dev.* 124, 43–58. doi: 10.1016/j.mod.2006.09.004

Shubin, N., Tabin, C., and Carroll, S. (1997). Fossils, genes and the evolution of animal limbs. *Nature* 388, 639–648. doi: 10.1038/41710

Struhl, G. (1982). Genes controlling segmental specification in the *Drosophila* thorax. *Proc. Natl. Acad. Sci. U.S.A.* 79, 7380–7384. doi: 10.1073/pnas.79.23.7380

Svendsen, P. C., Formaz-Preston, A., Leal, S. M., and Brook, W. J. (2009). The Tbx20 homologs midline and H15 specify ventral fate in the *Drosophila melanogaster* leg. *Development* 136, 2689–2693. doi: 10.1242/dev.037911

Svendsen, P. C., Phillips, L. A., Deshwar, A. R., Ryu, J. R., Najand, N., and Brook, W. J. (2019). The selector genes midline and H15 control ventral leg pattern by both inhibiting Dpp signaling and specifying ventral fate. *Dev. Biol.* 455, 19–31. doi: 10.1016/j.ydbio.2019.05.012

Svendsen, P. C., Ryu, J. R., and Brook, W. J. (2015). The expression of the T-box selector gene midline in the leg imaginal disc is controlled by both transcriptional regulation and cell lineage. *Biol. Open* 4, 1707–1714. doi: 10.1242/bio.013565

Tabin, C., Carroll, S., and Panganiban, G. (1999). Out on a limb: parallels in vertebrate and invertebrate limb patterning and the origin of appendages. *Am. Zool.* 39, 650–663. doi: 10.1093/icb/39.3.650

Tanaka, K., Barmina, O., and Kopp, A. (2009). Distinct developmental mechanisms underlie the evolutionary diversification of *Drosophila* sex combs. *Proc. Natl. Acad. Sci. U.S.A.* 106, 4764–4769. doi: 10.1073/pnas.0807875106

Tanaka, K., Barmina, O., Sanders, L. E., Arbeitman, M. N., and Kopp, A. (2011). Evolution of sex-specific traits through changes in HOX-dependent doublesex expression. *PLoS Biol.* 9:e1001131. doi: 10.1371/journal.pbio.1001131

Theisen, H., Haerry, T. E., O'Connor, M. B., and Marsh, J. L. (1996). Developmental territories created by mutual antagonism between Wingless and Decapentaplegic. *Development* 122, 3939–3948. doi: 10.1242/dev.122.12.3939

Tokunaga, C. (1961). The differentiation of a secondary sex comb under the influence of the gene engrailed in *Drosophila melanogaster*. *Genetics* 46, 157–176. doi: 10.1093/genetics/46.2.157

Tokunaga, C. (1962). Cell lineage and differentiation on the male foreleg of *Drosophila melanogaster*. *Dev. Biol.* 4, 489–516. doi: 10.1016/0012-1606(62)90054-4

Wang, S. H., Simcox, A., and Campbell, G. (2000). Dual role for *Drosophila* epidermal growth factor receptor signaling in early wing disc development. *Genes Dev.* 14, 2271–2276. doi: 10.1101/gad.827000

Conflict of Interest: The authors declare that the research was conducted in the absence of any commercial or financial relationships that could be construed as a potential conflict of interest.

Publisher's Note: All claims expressed in this article are solely those of the authors and do not necessarily represent those of their affiliated organizations, or those of the publisher, the editors and the reviewers. Any product that may be evaluated in this article, or claim that may be made by its manufacturer, is not guaranteed or endorsed by the publisher.

frontiers in Cell and Developmental Biology

BRIEF RESEARCH REPORT
published: 27 August 2021
doi: 10.3389/fcell.2021.735203

PAX2$^+$ Mesenchymal Origin of Gonadal Supporting Cells Is Conserved in Birds

*Martin A. Estermann[1], Mylene M. Mariette[2], Julie L. M. Moreau[1], Alexander N. Combes[1] and Craig A. Smith[1]**

[1] Department of Anatomy and Developmental Biology, Monash Biomedicine Discovery Institute, Monash University, Clayton, VIC, Australia, [2] Centre for Integrative Ecology, School of Life and Environmental Sciences, Deakin University, Geelong, VIC, Australia

During embryonic gonadal development, the supporting cell lineage is the first cell type to differentiate, giving rise to Sertoli cells in the testis and pre-granulosa cells in the ovary. These cells are thought to direct other gonadal cell lineages down the testis or ovarian pathways, including the germline. Recent research has shown that, in contrast to mouse, chicken gonadal supporting cells derive from a *PAX2/OSR1/DMRT1/WNT4* positive mesenchymal cell population. These cells colonize the undifferentiated genital ridge during early gonadogenesis, around the time that germ cells migrate into the gonad. During the process of somatic gonadal sex differentiation, PAX2 expression is down-regulated in embryonic chicken gonads just prior to up-regulation of testis- and ovary-specific markers and prior to germ cell differentiation. Most research on avian gonadal development has focused on the chicken model, and related species from the Galloanserae clade. There is a lack of knowledge on gonadal sex differentiation in other avian lineages. Comparative analysis in birds is required to fully understand the mechanisms of avian sex determination and gonadal differentiation. Here we report the first comparative molecular characterization of gonadal supporting cell differentiation in birds from each of the three main clades, Galloanserae (chicken and quail), Neoaves (zebra finch) and Palaeognathe (emu). Our analysis reveals conservation of PAX2$^+$ expression and a mesenchymal origin of supporting cells in each clade. Moreover, down-regulation of PAX2 expression precisely defines the onset of gonadal sex differentiation in each species. Altogether, these results indicate that gonadal morphogenesis is conserved among the major bird clades.

Keywords: PAX2, sex determination, Evo-Devo, gonadal sex differentiation, DMRT1, embryonic gonad

OPEN ACCESS

Edited by:
Rosa Barrio, CIC bioGUNE, Spain

Reviewed by:
Ahmed Uosef, Houston Methodist Hospital, United States
Patrick Tschopp, University of Basel, Switzerland

****Correspondence:***
Craig A. Smith
craig.smith@monash.edu

Specialty section:
This article was submitted to Evolutionary Developmental Biology, a section of the journal Frontiers in Cell and Developmental Biology

Received: *02 July 2021*
Accepted: *09 August 2021*
Published: *27 August 2021*

Citation:
Estermann MA, Mariette MM, Moreau JLM, Combes AN and Smith CA (2021) PAX2$^+$ Mesenchymal Origin of Gonadal Supporting Cells Is Conserved in Birds. Front. Cell Dev. Biol. 9:735203. doi: 10.3389/fcell.2021.735203

INTRODUCTION

Gonadal sex differentiation during embryogenesis provides an excellent model for studying the genetic regulation of development. The somatic component of the vertebrate gonad arises from intermediate mesoderm, while the germ cells are of extra-gonadal origin, migrating into the gonad before somatic sex differentiation commences (Lawson, 1999; Nef et al., 2019). Among most vertebrates, the gonadal primordium, together with its germ cells, is initially morphically identical

in both sexes. Subsequently, the somatic cells and the germ cells of the gonad are directed down the testicular or ovarian pathway via a cascade of sexually dimorphic gene expression that starts in the somatic compartment (Eggers et al., 2014; Liu et al., 2016; Yang et al., 2018). Two distinctive structures are initially distinguishable in the somatic compartment, an outer coelomic epithelium and underlying medulla (Smith and Sinclair, 2004). In the mouse, for which most data are available, proliferation of cells in the coelomic epithelium gives rise to so-called supporting cell progenitors, which enter the medulla. This key cell lineage generates Sertoli cells in the testis and pre-granulosa cells in the ovary. In both sexes, the supporting cells are thought to direct other uncommitted progenitor cells to the testicular or ovarian pathways, including the germline (Piprek et al., 2017; Rotgers et al., 2018). Germ cells are specified in the epiblast very early in development, and they migrate into the undifferentiated gonads (via the hindgut in mammals, via the bloodstream in birds) (Tagami et al., 2017). The germ cells of both sexes populate the gonad but are uncommitted to either the spermatogenesis or oogenesis pathway until somatic gonadal cells send inductive cues. Germ cell fate is therefore closely linked to somatic development of the gonad. In mouse, after the germ cells have settled in the gonads, the somatic supporting cell lineage begins to differentiate. In female mammals, somatic, and intrinsic signals induce germ cells to express *Stra8* and enter meiosis during embryogenesis. A large body of evidence previously pointed to retinoic acid (RA) as the somatic indicative signal triggering meiosis in females (Bowles et al., 2006; Koubova et al., 2006). However, surprisingly, recent data has shown that compound mutant mouse ovaries lacking all retinoic acid receptors or all three RALDH2 enzymes that synthesize RA can still initiate meiosis (Chassot et al., 2020; Vernet et al., 2020). The exact gonadal somatic signal for female germ cell sexual development is therefore again open to investigation. In male mammal gonads, the germ cells do not enter meiosis during embryogenesis. Instead, they lose pluripotency and enter mitotic arrest (Spiller et al., 2017). These sexually dimorphic germ cell fates are intimately linked to the development of the gonadal somatic cells. In males, this lineage gives rise to pre-Sertoli cells and, in females, pre-granulosa cells (Stevant and Nef, 2019). Signals such as Fgf9 sent from the Sertoli cells act with intrinsic factors, such as Nanos2, to antagonize meiosis and instead direct the germ cells down the male pathway, toward spermatogenesis (Suzuki and Saga, 2008; Bowles et al., 2010). The supporting cell lineage also sends inductive signals to the presumptive steroidogenic lineage, directing their differentiation into Leydig cells (in the testis) or thecal cells (in the ovary) (Yao et al., 2002; Rebourcet et al., 2014). In the developing mammalian ovary, proper follicle formation requires cross-talk between the female somatic and germ cell populations (Liu et al., 2010; Baillet and Mandon-Pepin, 2012). Hence, the sexual fate of the gonadal soma and the germ cells hinges upon the key supporting cell lineage.

In the mouse, the key supporting cell lineage derives from the coelomic epithelium via asymmetric cell division and egression into the underlying gonadal mesenchyme (Piprek et al., 2016; Lin et al., 2017; Stevant and Nef, 2019). Surprisingly, recent research has shown that, in contrast to mammals, the coelomic epithelium in the chicken embryo does not generate the supporting cell lineage (Sertoli or pre-granulosa cells). Rather, it gives rise to a non-steroidogenic interstitial cell population (Estermann et al., 2020). In chicken, the supporting cells develop from a mesenchymal source present in the gonad during early development (Sekido and Lovell-Badge, 2007; Estermann et al., 2020). These cells have a specific molecular signature, expressing the transcription factors *PAX2, DMRT1* and *OSR1*, and the signaling molecule, *WNT4*. The finding that supporting cells in chicken derive form a different source to those in mouse was surprising, given the conservation of overall gonadal morphogenesis among vertebrate embryos (DeFalco and Capel, 2009). However, a major difference between birds and mammals is the genetic gonadal sex-determining trigger. In mouse and other mammals, the Y chromosome-linked *SRY* gene operates as the master sex switch, initiating Sertoli cell differentiation in male embryos (Koopman et al., 1990, 1991; Sinclair et al., 1990; Goodfellow and Lovell-Badge, 1993). *SRY* is absent outside the mammalian clade, and in fact, birds have a different sex chromosome system. Birds have ZZ/ZW sex chromosomes, in which male (ZZ) is the homogametic sex and female (ZW) is heterogametic (Marshall Graves, 2008). The Z linked gene, *DMRT1* operates as the testis determining factor via a dosage mechanisms (Smith et al., 2009; Lambeth et al., 2014; Ioannidis et al., 2021). Due to the lack of Z sex chromosome compensation, male supporting cells have double the dose of *DMRT1* compared to females (Raymond et al., 1999; Smith et al., 2003; Ayers et al., 2015). *DMRT1* knockdown or knock out results in feminization of the gonad. Moreover, over-expression of this gene causes gonadal masculinization, indicating that *DMRT1* is the sex-determining gene in chicken, and presumably in all birds (Smith et al., 2009; Lambeth et al., 2014; Ioannidis et al., 2021). This would be consistent with the deep evolutionary conservation of the Z sex chromosome in birds, across some 60 million years (Handley et al., 2004; Zhou et al., 2014; Xu et al., 2019). In the male chicken embryo, DMRT1 is known to activate *SOX9* expression, which is crucial in Sertoli differentiation, and AMH, which is important for Müllerian duct regression (Lambeth et al., 2014). In females (ZW), due to the lower levels of *DMRT1* expression, supporting cells differentiate toward pre-granulosa cells by upregulating FOXL2 and Aromatase (Lambeth et al., 2013; Major et al., 2019). We previously characterized cell lineage specification during chicken gonadal sex differentiation and identified *PAX2* as a novel marker of the early supporting cell lineage (Estermann et al., 2020). During the process of gonadal sex differentiation, *PAX2* expression is down-regulated in chicken gonads (Estermann et al., 2020). This suggests that PAX2 down-regulation could be used to predict the onset of gonadal sex differentiation in chicken. However, the conservation of both the mesenchymal origin of gonadal cells and the role of PAX2 in birds beyond the chicken have not been previously explored.

Modern birds are classified into two main groups, the Palaeognathe, (the flightless ratites and volant tinamous) and

Neognathae (all other birds). The Neognathae is divided into two clades, the Galloanserae (chickens, quails, and ducks et al.) and Neoaves, the perching birds (around 95% of all extant avian species) (Cracraft, 2001; Hackett et al., 2008). Most research on avian gonadal development has focused on the chicken, or related members of the Galloanserae clade, such as quail and duck (Takada et al., 2006; Smith et al., 2009; Ayers et al., 2015; Bai et al., 2020; Okuno et al., 2020). Additionally, these studies have focused mainly on the conservation of mammalian genes involved in gonadal sex differentiation. There is very little information regarding gonadal sex differentiation among the other major avian clades (Hirst et al., 2017a). Comparative analysis in birds is required to fully understand the mechanism of avian sex determination and gonadal sex differentiation.

Historically, gonadal sex differentiation has been characterized on the basis of morphology, whereby the condensation of Sertoli cells marks the onset of testis formation and organization of pre-follicular cells marks the onset of ovary formation (Wilhelm et al., 2007). In the chicken embryo, the first morphological sign of testis formation, as in mammals, is the appearance of Sertoli cells and their coalescence in the medullary cords of the gonad. In the female chicken embryo, the first overt morphological sign of sex differentiation is a thickening of the outer coelomic epithelium into a cortex and fragmentation of the underling medulla (Carlon and Stahl, 1985). However, histology alone has proven to be inconsistent and inaccurate to determine the precise time of gonadal sex differentiation onset. A clear example is studies on Japanese quail embryos (*Coturnix japonica*). Several histological hematoxylin-eosin based analyses determined that quail gonads were sexually differentiated at embryonic day 6 (E6) (stage 30), E7 (stage 32) or E8 (stage 35) (Kannankeril and Domm, 1968; Intarapat and Satayalai, 2014; Mohamed et al., 2017). However, sexual differentiation is likely to be triggered at the genetic level prior to overt histological differentiation. In the quail, the Sertoli cell marker *SOX9* is detectable at E5 (stage 27) (Takada et al., 2006), indicating that sexual differentiation begins at the molecular level distinctly prior to morphological differentiation. The development of more accurate molecular methods to determine sexual differentiation is required to improve knowledge of avian sex determination and for informing methodologies targeting species conservation.

Here we report the first comparative molecular characterization of gonadal sex differentiation in birds from each of the three main clades, Galloanserae (chicken and quail), Palaeognathe (emu), and Neoaves (zebra finch). Our analysis demonstrates a conservation of the $PAX2^{+}$ mesenchymal origin of supporting cells in all analyzed birds. In addition, PAX2 down-regulation immediately precedes up-regulation of male and female supporting cell markers, and the morphological onset of sexual differentiation. PAX2 gonadal down-regulation precisely predicted the onset of sex differentiation in each avian clade, more accurately than previous histological analysis. Altogether these results indicate that the process of gonadal sex differentiation is conserved among the major bird clades. This research proposes PAX2 immunodetection as a new methodology to evaluate gonadal differentiation in birds.

MATERIALS AND METHODS

Eggs

Fertilized HyLine Brown chicken eggs (*Gallus gallus domesticus*) were obtained from Research Poultry Farm (Victoria, Australia). Wild type Japanese quail eggs (*Coturnix japonica*) were provided by the Monash transgenic quail facility. Fertilized emu (*Dromaius novaehollandiae*) eggs were purchased from Emu Logic (Toorahweenah, NSW). Zebra finch (*Taeniopygia guttata*) embryos were obtained from wild-derived birds. The zebra finch colony is a captive population derived from wild caught birds under Deakin University Animal Ethics #G23-2018. The birds used in this study were several generation-captive birds derived from this initial population. Fresh eggs were collected in nests in outdoor aviaries and artificially incubated at Deakin University (Geelong, Australia). Eggs were incubated under humid conditions at 37.5°C until collection and staged (Hamburger and Hamilton, 1951; Ainsworth et al., 2010; Nagai et al., 2011; Murray et al., 2013).

Sexing PCR

A small piece of limb tissue was digested in 30 μl of PCR compatible digestion buffer (10 mM Tris-HCL (pH8.3); 50 mM KCl; 0.1 mg/mL gelatin; 0.45% NP-40; 0.45% Tween-20 containing Proteinase K at 200 μg/mL) and incubated for 20 min at 55°C followed by 6 min at 95°C and hold at 4°C (Clinton et al., 2001). Chicken sexing PCR was performed as previously described (Clinton et al., 2001; Hirst et al., 2017a).

The quail PCR sexing protocol is a modification of a previously described method (Dickens et al., 2012). This method relies upon specific amplification of a female (W) restricted sequence called *WPKCI*. The reaction was performed in a final volume of 10μL containing 1x Go-Taq buffer (Promega), 1.5 mM MgCl2, 0.2 mM dNTP's, 0.5 μM of each *18S* rRNA primers (forward: 5′-*AGCTCTTTCTCGATTCCGTG*-3′; reverse: 5′-*GGGTAGACACAAGCTGAGCC*-3′) 1μM of each *qWPKCI* primers (forward: 5′-*TTGGGCATTTGAAGATTGTC*-3′; reverse: 5′-*GTCTGAAGGGTCTGAGGGT*-3′), 0.5U Go Taq polymerase (Promega) and 1 μL of the tissue digestion. The PCR program consisted of denaturation for 2 min at 94°C followed by 25 cycles of incubation at 94°C × 10 s; 56°C × 10 s; 72°C × 10 s and final extension at 72°C for 5 min, followed by 4°C hold.

Emu sexing PCR protocol is a modification of a previously described method (Huynen et al., 2002). This method relies upon sex-specific amplification of a W-linked (female) DNA fragment. The sexing reaction was performed in a final volume of 20 μL containing 1x Go-Taq buffer (Promega), 1.5 mM MgCl2, 0.2 mM dNTP's, 0.5 μM of each sexing primers (forward: 5′-*CCTTTAAACAAGCTRTTAAAGCA*-3′; reverse: 5′-*TCTCTTTTGTTCTAGACAMCCTGA*-3′), 0.5U Go Taq polymerase (Promega) and 1 μL of the tissue digestion. The PCR program consisted of denaturation for 2 min at 95°C followed by 10 cycles of incubation at 95°C × 15 s; 55°C × 20 s; 72°C × 20 s, 25 cycles of incubation at 95°C × 15 s; 47°C × 20 s; 72°C × 20 s and final extension at 72°C for 7 min, followed by 4°C hold.

Zebra finch sexing PCR protocol is a modification of a previously described method (Soderstrom et al., 2007). This method relies upon specific amplification of a fragment of the *CDH* gene located on the W chromosome. As an internal control, a fragment of the *CHD* gene located in the Z chromosome was amplified. The reaction was performed in a final volume of 11 μL. W1 (5′-*GGGTTTTGACTGACTAACTGAT*T-3′), W2 (5′-*GTTCAAAGCTACATGAATAAACA*-3′), Z1 (5′-*GTGTAGTCCGCTGCTTTTGG*-3′) and Z2 (5′-*GTTCGTGGTCTTCCACGTTT*-3′) primers used at a final concentration of 0.1 μM each. 1 μL of digestion buffer was used with 10 μL of the sexing mix. The PCR program consisted of denaturation for 2 min at 94°C followed by 30 cycles of incubation at 94°C × 30 s; 56°C × 45 s; 72°C × 45 s and final extension at 72°C for 5 min, followed by 4°C hold. PCR products and molecular ladder (1 kb plus, Invitrogen) were run on a 2% agarose gel for 30 min at 130 V and visualized with gel red (Biotium).

Immunofluorescence

Whole embryos or urogenital systems were collected, briefly fixed in 4% PFA/PBS for 15 min, cryo-protected in 30% sucrose overnight and blocked in OCT embedding compound for sectioning. Immunofluorescence was carried out as described previously (Estermann et al., 2020). Briefly, 10 μm frozen sections were cut and antigen retrieval was performed for DMRT1 and PAX2 protein immunofluorescence using the Dako PT Link automated system. Sections were then permeabilized in 1% Triton X-100 in PBS for 10 min at room temperature and washed 3 times in PBS. All sections were blocked in 2% BSA in PBS for 1 h at room temperature followed by primary antibody incubation overnight at 4°C in 1% BSA in PBS. The following primary antibodies were used: rabbit anti-PAX2 (Biolegend 901001, 1;500), rabbit anti-DMRT1 (in house antibody; 1:2000), rabbit anti-AMH (Abexa ABX132175; 1:1000), rabbit anti-Aromatase (in house antibody; 1:4000), rabbit anti-FOXL2 (in house antibody; 1:2000), and rabbit anti-SOX9 (Millipore AB5535, 1:4000). After overnight incubation with primary antibody, sections were then washed 3 times in PBS and incubated for 1 h at room temperature with Alexa Fluor 488 donkey anti-Rabbit (1:1000) and Alexa Fluor 594 donkey anti-Mouse (1:1000) in 1% BSA in PBS. Sections were counterstained in DAPI/PBS and mounted in Fluorsave (Millipore). Images were collected on a Zeiss Axiocam MRC5 microscope using the same exposure time between males and females for expression comparisons.

For double immunofluorescence using two primary antibodies raised in the same species (rabbit anti-PAX2 and rabbit anti-DMRT1), the iterative indirect immunofluorescence imaging (4i) protocol was used on paraffin sections (Gut et al., 2018). Dissected gonads were fixed overnight in 4% paraformaldehyde at 4°C, paraffin-embedded and sectioned in the transverse plane at 5μm. After deparaffinisation, antigen retrieval was carried out using TE buffer (Moreau et al., 2019). Sections were incubated with anti-DMRT1 antibody (1:2000, in house) and anti-cytokeratin antibody (1:200, Novus Bio NBP2-29429) overnight at 4°C. Sections were then washed with 1X PBS and incubated with Donkey anti-Rabbit Alexa Fluor® Plus 647 (1:2000, Invitrogen) and Donkey anti-mouse Alexa Fluor® Plus 488 (1:2000, Invitrogen) together with DAPI for 2 h at room temperature, after which the tissue was washed with 1X PBS. Slides were mounted in imaging buffer (Gut et al., 2018) and images were captured using a 3i Marianas spinning disk confocal at low laser power. Sections were washed in 1X PBS and antibodies were eluted following the 4i protocol. After elution, sections were imaged again with the same parameters to ensure that the first round of antibody labels were removed. Slides were then incubated with anti-PAX2 (1:400, Biolegend 901001) and anti-cytokeratin (1:200, Novus Bio NBP2-29429) in 5% BSA in 1X PBS overnight at 4°C with the same wash, secondary antibody incubation and imaging parameters from the first round of labeling. Brightness and contrast were equally altered across all images to improve data display using ImageJ (Schneider et al., 2012).

qRT-PCR

Gonadal pairs were collected in Trizol reagent (Sigma-Aldrich) homogenized and Phenol-Chloroform RNA extraction was performed as per the manufacturer's instructions (Trizol, Invitrogen). DNA-free™ DNA Removal Kit (Invitrogen) was used to remove genomic DNA. 100-500 ug of RNA was converted into cDNA using Promega Reverse Transcription System. QuantiNova SYBR® Green PCR Kit was used to perform qRT-PCR. PAX2 expression levels were quantified by Pfaffl method (Pfaffl, 2001) using β-actin as internal control. Data was analyzed using 2-way ANOVA. Statistical significance was determined by Tukey's post-test. *PAX2* Fw: 5′-*GGCGAGAAGAGGAAACGTGA*-3′, *PAX2* Rv: 5′-*GAAGGTGCTTCCGCAAACTG-3′*, β-*actin Fw*: 5′-*CTCTGACTGACCGCGTTACT-3′* and β-*actin* Rv: 5′-*TACCAACCATCACACCCTGAT-3′*.

RESULTS

Chicken

Previous chicken single-cell RNA-seq identified the gonadal supporting cell precursors as a mesenchymal population expressing the transcription factors *PAX2, DMRT1, OSR1* and the signaling molecule, *WNT4* (Estermann et al., 2020). PAX2 and DMRT1 immunofluorescence was performed to evaluate PAX2 expression pattern before, during and after gonadal differentiation (**Figure 1** and **Supplementary Figure 1**). At E4.5 (HH24) and E5.0 (HH26), PAX2 positive cells were detected in the gonadal medulla in both sexes (**Figure 1A**). In males, from E5.5 (HH28) to E6.0 (HH29), PAX2 expression continued to be present in the basal region of the gonad but was absent in the most apical (**Figure 1A**). In females, a similar pattern occurred at E6.0 (**Figure 1A**). This data suggests that PAX2 is down-regulated at the onset of gonadal sex differentiation.

We previously found that *PAX2* mRNA was co-expressed with DMRT1 protein in gonadal sections (Estermann et al., 2020), but the co-localization of PAX2 and DMRT1 proteins in the same cells/nucleus was not assessed, because both primary antibodies were raised in rabbit. Iterative indirect immunofluorescence imaging (4i) (Gut et al., 2018) was used here to detect DMRT1

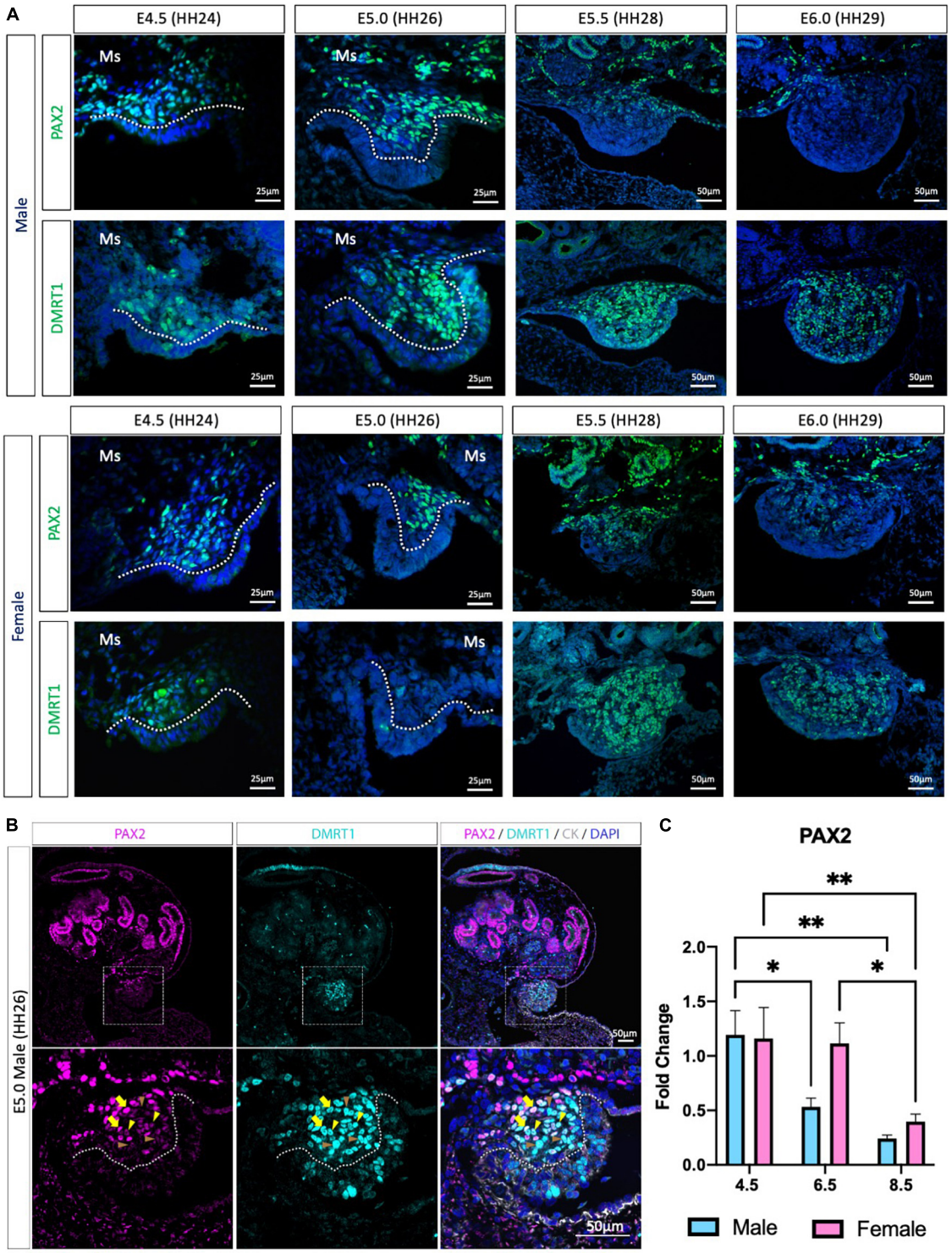

FIGURE 1 | PAX2 expression in bipotential supporting cells before sex differentiation. **(A)** PAX2 and DMRT1 protein expression in E4.5, E5.0, E5.5, and E6.0 male and female chicken gonads. Dotted white line denotes the gonadal mesenchyme versus epithelium. Ms indicates the mesonephros. **(B)** PAX2 (magenta), DMRT1 (cyan), and cytokeratin (CK, white) immunofluorescence in E5.0 chicken urogenital system. Dashed white box indicates the magnification area; dotted white line denotes the gonadal mesenchyme versus epithelium. Yellow arrows show cells expressing both DMRT1 and PAX2 at high levels; yellow arrowheads indicate DMRT1^{+} cells expressing low levels of PAX2; brown arrowheads indicate DMRT1 positive PAX2 negative cells. **(C)** Decline in *PAX2* mRNA expression during gonadal sex differentiation. *PAX2* mRNA expression by qRT-PCR in E4.5, E6.5, and E8.5 male and female gonads. Expression level is relative to β-actin and normalized to E4.5 male. Bars represent Mean ± SEM. * and ** = adjusted p value < 0.05 and <0.01, respectively. 2-way ANOVA and Tukey's post-test.

and PAX2 proteins in the same undifferentiated chicken gonad just prior to sexual differentiation at E5.0 (HH26) (**Figure 1B** and **Supplementary Figure 1A**). PAX2 positive cells in the gonadal mesenchyme were also DMRT1 positive. Interestingly, a gradient of PAX2 expression was noted; high in some cells (basal), lower in others (apical). This presumably reflects the gene being down-regulated among cells. Additionally, some DMRT1 positive cells were negative for PAX2, as expected, due to DMRT1 being expressed in the left coelomic epithelium and in the germ cells.

To evaluate the expression pattern of PAX2 in differentiating embryonic chicken gonads, immunofluorescence was performed on E6.5 (HH30) and E8.5 (HH34) male and female gonads (**Supplementary Figures 1B–D**). PAX2 was not expressed in E6.5 testis (**Supplementary Figure 1B**), consistent with previous reports of PAX2 down-regulation upon sexual differentiation (Estermann et al., 2020). DMRT1, AMH, and SOX9 immunofluorescence confirmed that these gonads were presumptive testes (**Supplementary Figure 1B**). In females, PAX2 expression was absent from the apical region of the gonad, whereas it was still expressed in the basal region of the gonad at E6.5 (**Supplementary Figure 1C**). This expression pattern was complementary to FOXL2 expression pattern, more strongly expressed in the gonadal apical than the basal region (**Supplementary Figure 1C**). Only few aromatase positive cells were detected in the gonad at this stage, suggesting that the gonadal differentiation had just commenced. As for the male, the female gonad also showed PAX2 being down-regulated after sex differentiation, on a cell-to-cell basis. By E8.5, PAX2 expression was excluded from the gonad in both sexes (**Supplementary Figure 1D**). To quantify these changes in *PAX2* expression, qRT-PCR was performed in male and female gonads at E4.5 (HH24), E6.5 (HH30) and E8.5 (HH34). These time points correspond to the period before, at the onset and after the onset of morphological gonadal sex differentiation. Consistent with the immunofluorescence data, *PAX2* expression was significantly reduced after gonadal sex differentiation in both sexes (E6.5 and E8.5) (**Figure 1C**). In females, expression reduction was delayed, occurring by E8.5 (**Figure 1C**). This suggests that male gonad sex differentiation commences prior to female gonadal sex differentiation. In conclusion, PAX2 is expressed in chicken undifferentiated gonadal supporting cells, co-localizing with DMRT1 in the medulla, and its expression is down-regulated during sexual differentiation.

Quail

To evaluate if the PAX2$^+$ mesenchymal origin of gonadal supporting cells is conserved among birds or is specific to chicken, gonads were analyzed from all three main bird clades. The Japanese quail (*Coturnix japonica*) belongs to the Galloanserae clade, the same group as chicken. This means that gonadal differentiation is likely to be very conserved between the two species. All previous studies on quail gonadal sex differentiation have relied upon histology to define the onset of sexual differentiation. Consequently, the timing of gonadal sex differentiation in this species has been variably reported, from between E6 (Kannankeril and Domm, 1968), E7 (Mohamed et al., 2017), and E8 (Intarapat and Satayalai, 2014). Quail gonadal sex differentiation was analyzed by immunofluorescence from E3.5 (stage 21) to E6.0 (stage 30), in half day incubation intervals (**Figure 2**). PAX2 was used as a (presumed) undifferentiated supporting cell precursor marker. Meanwhile, DMRT1, SOX9 and AMH were used as Sertoli cell markers in the testis and aromatase as pre-granulosa cell marker in developing ovary. Consistent with the chicken data, PAX2 positive cells started colonizing the region underlying the coelomic epithelium in both sexes of quail gonads at E3.5 (stage 21) and E4.0 (stage 24) (**Figure 2**). Unlike in chicken, DMRT1 was not detected in the undifferentiated quail gonads. Instead, by E4.0, DMRT1 expression was first detected and already sexually dimorphic, showing higher intensity levels in males than females (**Figures 2A,B**). By E4.5, PAX2 expression was turned off in the gonadal cells and its expression was excluded from the gonad during subsequent time points, when DMRT1 and other markers of sexual differentiation were activated (**Figure 2**). Some PAX2 positive cells were still visible in the basal region of the gonad, adjacent to the mesonephros (**Figure 2**). In addition, higher DMRT1 expression in males also suggests that the supporting cells commenced differentiation into Sertoli cells (**Figure 2A**). Some AMH positive cells were observed in the gonadal mesenchyme at E4.5 and E5.0 (stage 27) in both male and female gonads, but no SOX9 (Sertoli cell marker) (**Figure 2A**) or aromatase (pre-granulosa cell marker) (**Figure 2B**). The latter two were detected from E5.5 (stage 28). This quail data indicates that the PAX2$^+$ mesenchymal origin of supporting cells observed in chicken is conserved among Galliformes. In addition, PAX2 down-regulation indicates that gonads commence gonadal sex differentiating at E4.5 in quail, much earlier than reported. This indicates that gene expression is a better predictor than morphological markers in defining the precise onset of gonadal sex determination.

Zebra Finch

The other major clade of the Neoganthae is the Neoaves (perching birds). This group contains almost 95% of all living modern birds and is the result of early and rapid diversification around the Cretaceous mass extinction event (Claramunt and Cracraft, 2015; Prum et al., 2015). One of the most widely studied models in this clade is the zebra finch (*Taeniopygia guttata*), primarily in the field of neurobiology. Due to its popularity, the zebra finch genome was the second avian genome to be sequenced (Warren et al., 2010; Mak et al., 2015; Patterson and Fee, 2015). In addition, embryonic gonadal sex differentiation and primordial germ cell colonization have been studied in zebra finch, showing some differences between previous chicken reports (Hirst et al., 2017a; Jung et al., 2019). Zebra finch gonads have been reported to be sexually differentiated at E6.5, evidenced by *SOX9* and *FOXL2* mRNA expression in males and females, respectively (Hirst et al., 2017a). At E4.5 these markers are not expressed, suggesting an undifferentiated state (Hirst et al., 2017a). To evaluate if PAX2$^+$ mesenchymal origin of supporting cells is conserved in Neoaves, PAX2, DMRT1, FOXL2, and AMH immunofluorescence was performed in male and female zebra finch gonads at E4.5 (stage 24), E5.5 (stage 28) and E6.5 (stage 31). PAX2 positive mesenchymal cells were

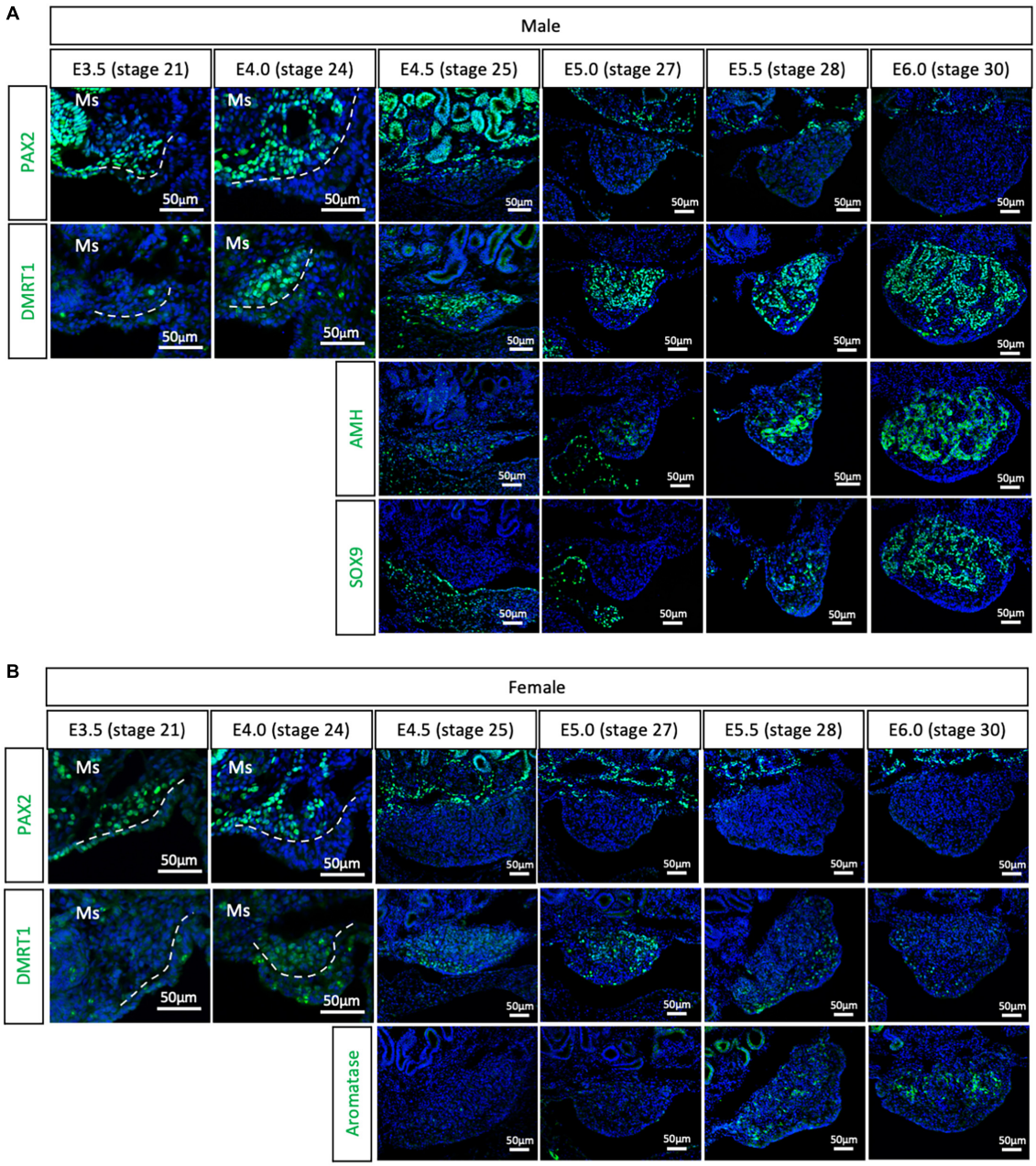

FIGURE 2 | PAX2^{+} mesenchymal origin of supporting cells is conserved in quails. **(A)** PAX2, DMRT1, AMH, and SOX9 protein expression in E3.5, E4.0, E4.5, E5.0, E5.5, and E6.0 male quail gonads. **(B)** PAX2, DMRT1, and Aromatase protein expression in E3.5, E4.0, E4.5, E5.0, E5.5, and E6.0 female quail gonads. Dashed white line denotes the gonadal epithelial versus medullary mesenchyme. Ms indicates the mesonephros. DAPI was used as counterstain.

detected in both male and female gonads at E4.5 (**Figure 3**). DMRT1, AMH and FOXL2 were not detected in the gonads at this stage. Altogether, this suggests that the zebra finch gonads are undifferentiated at E4.5. This is consistent with previous reports (Hirst et al., 2017a).

By E5.5, PAX2 expression was extinguished from both male (**Figure 3A**) and female (**Figure 3B**) gonads. DMRT1 and AMH positive Sertoli cells were identified in the male testicular medulla at E5.5 (**Figure 3A**). The downregulation of PAX2 and up-regulation of supporting cell markers indicates that gonadal sex differentiation in zebra finches commences at E5.5. By E6.5, FOXL2 expression was detected in the ovarian medulla (**Figure 3B**). In males, DMRT1 and AMH positive testicular cords were evident in the gonadal medulla (**Figure 3A**). Altogether, this data confirms the conservation of PAX2^{+} mesenchymal cell origin of supporting cells in Neoaves, and in particular in zebra finch. In addition, using PAX2 as a predictor of sex differentiation we were able to

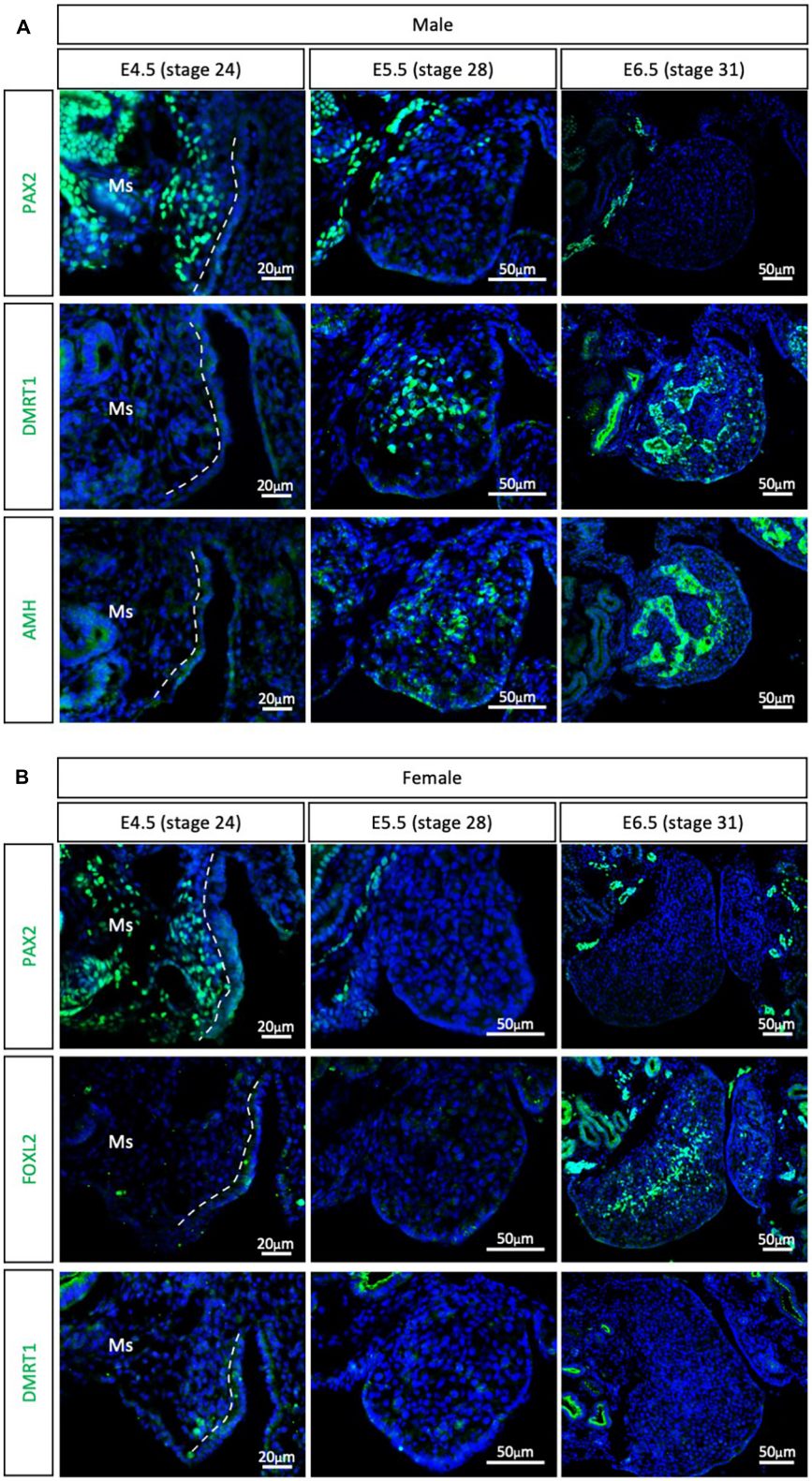

FIGURE 3 | PAX2^{+} mesenchymal origin of supporting cells is conserved in Neoaves (zebra finch). **(A)** PAX2, DMRT1, and AMH protein expression E4.5, E5.5, and E6.5 male zebra finch gonads. **(B)** PAX2, FOXL2, and DMRT1 protein expression in E4.5, E5.0, E5.5, and E6.5 female zebra finch gonads. Dashed white line indicates the gonadal epithelial and mesenchyme limit. Ms indicates the mesonephros. DAPI was used as counterstain.

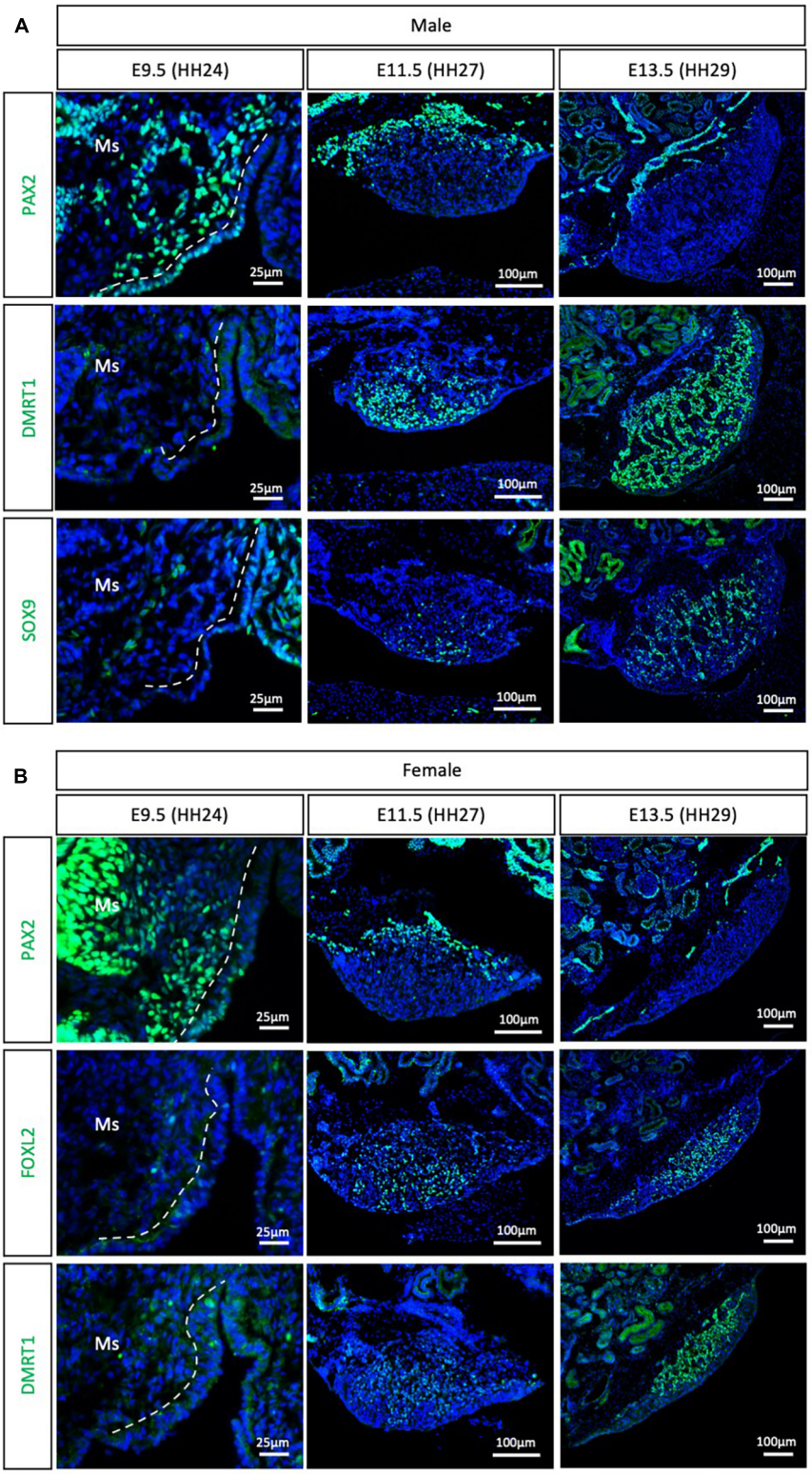

FIGURE 4 | PAX2^{+} mesenchymal origin of supporting cells is conserved in ratites (emu). **(A)** PAX2, DMRT1, and SOX9 protein expression in E9.5, E11.5, and E13.5 male emu gonads. **(B)** PAX2, FOXL2, and DMRT1 protein expression in E9.5, E11.5, and E13.5 female emu gonads. Dashed white line indicates the gonadal epithelium vs. medullary mesenchyme. Ms indicates the mesonephros. DAPI was used as counterstain.

determine that zebra finch gonadal sex differentiation begins at E5.5 (stage 28).

Emu

The Palaeognathae superorder includes the flightless ratites and the volant neotropical tinamou. Among the ratites, gonadal sex differentiation has only been described in the emu (*Dromaius novaehollandiae*) (Hirst et al., 2017a). Previous histological data suggested that emu gonadal differentiation commences at E16, evidenced by the presence of seminiferous cords in male gonads, containing DMRT1^{+} Sertoli cells (Hirst et al., 2017a). As noted previously, histological analysis is not the best methodology for defining the onset of sex differentiation. To gain insight into the specific timeframe of gonadal sex differentiation in emu and assess if PAX2 mesenchymal origin of supporting cells is conserved in ratites, gonadal immunofluorescence was performed at E9.5 (HH24), E11.5 (HH27) and E13.5 (HH29). PAX2 positive cells were detected at E9.5 in the medullary mesenchyme of both male and female emu gonads (**Figure 4**). This expression pattern is similar to the previous data shown for chicken, quail and zebra finch. FOXL2, SOX9 and DMRT1 were not expressed at E9.5 (HH24) (**Figure 4**), indicating that the gonads were undifferentiated and bipotential. By E11.5 (HH27), PAX2 expression was extinguished from the gonad in both sexes. In males DMRT1 and, to a lesser extent, SOX9, were expressed in the E11.5 (HH27) testis, indicating activation of the testicular differentiation pathway (**Figure 4A**). Similarly, in females, FOXL2 expression was up-regulated, indicating that the ovarian differentiation program had commenced (**Figure 4B**). By E13.5, in males, DMRT1^{+}/SOX9^{+} testicular cords were identified in the gonadal medulla (**Figure 4A**). In females, FOXL2 was expressed in pre-granulosa cells in the ovarian medulla (**Figure 4B**). This data indicates that emu gonadal sex differentiation commences at E11.5 (HH27), earlier than previous reports based on histology. In addition, a PAX2 + mesenchymal origin of supporting cells is also conserved in the Palaeognathae clade.

DISCUSSION

The data presented here support a conserved origin of gonadal supporting cells in birds, distinct from that reported in the mouse. In the mouse model, the supporting cell lineage derives from the coelomic epithelium (Stevant et al., 2018, 2019). The gonadal supporting cells in birds do not derive from the coelomic epithelium but rather from a *DMRT1* and *PAX2* positive mesenchymal population. In this study, we show that PAX2 is expressed in the bipotential supporting cells of the gonadal mesenchyme in members of the Galloanserae (chicken and quail), Neoaves (zebra finch) and Paleognathae (emu), suggesting a conserved mechanism among all birds. In addition, this is the first systematic evaluation of gonadal sex differentiation in quail, emu and zebra finch using expression of gonadal marker proteins.

Previous reports based in histological and morphological analysis of the quail gonad have not consistently determined an embryonic stage of gonadal sex differentiation. Previous estimates of gonadal sex differentiation onset ranged from E5.5 to E8.0 (Kannankeril and Domm, 1968; Intarapat and Satayalai, 2014; Mohamed et al., 2017). The results reported here indicate that quail gonad sex differentiation commences at E4.5, earlier than previously suggested. This is shown by down-regulation of the undifferentiated supporting cell marker PAX2 and the up-regulation of DMRT1 in male gonads (**Figure 2**). These results show that gene expression analysis is more accurate than morphological and histological analysis in determining the onset of gonadal sex differentiation. Similarly, previous histological analysis of emu gonads suggested that sex differentiation commences at E16 (Hirst et al., 2017a). The data presented here indicates that emu gonadal sex determination commences at E11.5 (**Figure 4**), earlier than previous histological data suggests. In zebra finch, previous reports suggested the onset of sex differentiation occurs between E4.5 (undifferentiated) and E6.5 (differentiated). Our results agree with this data, showing that zebra finch gonadal sex differentiation commences at E5.5 (**Figure 3**). Down-regulation of PAX2 expression precisely predicted the onset of sexual differentiation in the three avian clades, more accurately than previous histological analysis. This research identifies PAX2 as a new marker for evaluating gonadal differentiation in birds.

In female chicken embryos, FOXL2 and aromatase proteins were expressed in the apical supporting cells at E6.5 (HH 30) (**Supplementary Figure 1C**), suggesting that those are the first supporting cells to differentiate. This apical-basal wave of differentiation is consistent with the concentration of PAX2 positive cells in the basal region of the gonad (**Figures 1A–C**). A similar pattern was observed in male quail gonads. At E5.5 (stage 28), SOX9 and AMH proteins were expressed in the apical testicular cords of the quail, suggesting that those are the first supporting cells to differentiate, and by E6.0 all Sertoli cells were SOX9, AMH and DMRT1 positive (**Figure 2A**). Recently, two transcriptionally distinctive Sertoli cell populations in E10.5 chicken testis were identified. One expressed lower levels of *SOX9* and *DMRT1* and higher levels of *CBR4* and *GSTA2* and was located in the peripheral testicular cords. The second population was located in the basal region, expressing higher levels of *SOX9* and *DMRT1* but no *GSTA2* (Estermann et al., 2020). This suggests that there may be two distinctive stages of Sertoli cell maturation, inner immature and outer mature populations. Mouse *Sry* is expressed as a wave across the male gonad (Larney et al., 2014), starting from the central region of the genital ridges, and then extending to cranial and caudal poles (Polanco and Koopman, 2007). 3D imaging approaches would be crucial to be understand how supporting cell differentiation occurs in birds and to understand if gonadal development also follows a longitudinal wave of differentiation, as in mouse.

Despite conservation of cell types, recent single-cell RNA-seq data from embryonic chicken gonads has shown that cell

lineage specification in the gonad may also vary substantially between birds and mammals (Estermann et al., 2020). This research has shown that there are two main sources of gonadal cells; the coelomic epithelium and the mesonephric mesenchyme (Sekido and Lovell-Badge, 2007; Estermann et al., 2020). The current study confirms that this is the case for members of all three major bird clades. It is unclear why birds exhibit this different developmental origin of the key supporting cell lineage. A mesenchymal origin of supporting cells could be an ancestral feature, lost in mammals, or a feature acquired by the avian lineage. Further research is required to evaluate if the mesenchymal origin of supporting cells also occurs among reptiles, amphibians or fish. A key difference between placental mammals and birds is the genetic sex-determination system (XY vs. ZW). It would be interesting to evaluate if the supporting cell origin is correlated with the genetic sex-determination system (XY vs. ZW), sex determining genes (Sry vs. DMRT1 vs. others) and if it is also present in environmental sex determining species. Reptiles have diverse sex determining systems, ranging from pure GSD with either XX/XY or ZZ/ZW sex chromosome systems, to GSD modifiable by egg temperature, through to complete temperature dependent sex determination (TSD) (Warner, 2011; Ge et al., 2017; Whiteley et al., 2021). In at least one turtle species with TSD, the supporting cell lineage has been shown to derive form the coelomic epithelium (Yao et al., 2004). At present, there is not observable correlation between the type of sex determining system and the sources of gonadal supporting cells. Gonadal epithelium lineage tracing by GFP electroporation is feasible in oviparous reptiles, which would shed light on the origin of gonadal cell lineages in these groups (Hirst et al., 2017b). Among reptiles, crocodilians are the closest living clade to birds (Green et al., 2014), making them an ideal model to test the possible synapomorphy of gonadal PAX2 in birds and to study the evolution of the mesenchymal epithelial supporting cell origin. A previous ultrastructural study suggested that the supporting cell lineage in the American alligator (*Alligator mississippiensis*) may be of coelomic epithelial origin (Smith and Joss, 1993).

In summary, this study demonstrates a conserved gonadal PAX2 positive mesenchymal expression pattern in representatives of all three bird clades. Analysis should be expanded to other avian species to evaluate the degree of conservation among birds more broadly. Among the Galloanserae, only Galliformes have been studied in any detail (chicken and quail). Anseriformes (ducks, geese, and swans) could be examined. In addition, among the Neovaes, only the zebra finch has been studied in any detail. During the rapid diversification that characterize the Neoaves, birds could exhibit other mechanisms of gonadal formation, diverging from the $PAX2^{+}$ mesenchymal origin. It would be interesting to expand this study to more members of this diverse clade. Given the monophyly of birds and their conserved ZZ/ZW sex determining system, we postulate that the gonadal PAX2 mesenchymal expression pattern is prevalent among avians.

DATA AVAILABILITY STATEMENT

The original contributions presented in the study are included in the article/**Supplementary Material**, further inquiries can be directed to the corresponding author.

ETHICS STATEMENT

The animal study was reviewed and approved by Animal Ethics Office, Monash University (AEC approval not required for avian embryos less than mid embryogenesis as per state legislation). The zebra finch colony is a captive population derived from wild caught birds under Deakin University Animal Ethics # G23-2018. The birds used in this study were several generation-captive birds derived from this initial population. As for emu, quail, and chicken, animal ethics was not required for the finch embryos, as they were harvested less than mid-gestation (permitted by Australian law).

AUTHOR CONTRIBUTIONS

ME designed and performed most of the experiments and analyzed the results. MM and JM contributed with additional experiments and analysis. AC and CS supervised the work. ME and CS wrote the manuscript. All authors read and approved the final manuscript.

FUNDING

This research was funded by Australian Research Council (ARC) Discovery Project # 200100709, awarded to CS.

ACKNOWLEDGMENTS

We thank Dr. Olivier Serralbo and Monash Transgenic Quail Facility for facilitating the fertile wild type quail eggs. We acknowledge use of the facilities and technical assistance of Monash Histology Platform, Department of Anatomy and Developmental Biology, Monash University. We also acknowledge the facilities and technical assistance of Monash Micro Imaging.

SUPPLEMENTARY MATERIAL

The Supplementary Material for this article can be found online at: https://www.frontiersin.org/articles/10.3389/fcell.2021.735203/full#supplementary-material

REFERENCES

Ainsworth, S. J., Stanley, R. L., and Evans, D. J. (2010). Developmental stages of the Japanese quail. *J. Anat.* 216, 3–15. doi: 10.1111/j.1469-7580.2009.01173.x

Ayers, K. L., Lambeth, L. S., Davidson, N. M., Sinclair, A. H., Oshlack, A., and Smith, C. A. (2015). Identification of candidate gonadal sex differentiation genes in the chicken embryo using RNA-seq. *BMC Genomics* 16:704. doi: 10.1186/s12864-015-1886-5

Bai, D. P., Chen, Y., Hu, Y. Q., He, W. F., Shi, Y. Z., Fan, Q. M., et al. (2020). Transcriptome analysis of genes related to gonad differentiation and development in Muscovy ducks. *BMC Genomics* 21:438. doi: 10.1186/s12864-020-06852-z

Baillet, A., and Mandon-Pepin, B. (2012). Mammalian ovary differentiation - a focus on female meiosis. *Mol. Cell. Endocrinol.* 356, 13–23. doi: 10.1016/j.mce.2011.09.029

Bowles, J., Feng, C. W., Spiller, C., Davidson, T. L., Jackson, A., and Koopman, P. (2010). FGF9 suppresses meiosis and promotes male germ cell fate in mice. *Dev. Cell* 19, 440–449. doi: 10.1016/j.devcel.2010.08.010

Bowles, J., Knight, D., Smith, C., Wilhelm, D., Richman, J., Mamiya, S., et al. (2006). Retinoid signaling determines germ cell fate in mice. *Science* 312, 596–600. doi: 10.1126/science.1125691

Carlon, N., and Stahl, A. (1985). Origin of the somatic components in chick embryonic gonads. *Arch. Anat. Microsc. Morphol. Exp.* 74, 52–59. doi: 10.1007/bf00341521

Chassot, A. A., Le Rolle, M., Jolivet, G., Stevant, I., Guigonis, J. M., Da Silva, F., et al. (2020). Retinoic acid synthesis by ALDH1A proteins is dispensable for meiosis initiation in the mouse fetal ovary. *Sci. Adv.* 6:eaaz1261. doi: 10.1126/sciadv.aaz1261

Claramunt, S., and Cracraft, J. (2015). A new time tree reveals Earth history's imprint on the evolution of modern birds. *Sci. Adv.* 1:e1501005. doi: 10.1126/sciadv.1501005

Clinton, M., Haines, L., Belloir, B., and Mcbride, D. (2001). Sexing chick embryos: a rapid and simple protocol. *Br. Poult. Sci.* 42, 134–138. doi: 10.1080/713655025

Cracraft, J. (2001). Avian evolution. Gondwana biogeography and the Cretaceous-Tertiary mass extinction event. *Proc. Biol. Sci.* 268, 459–469. doi: 10.1098/rspb.2000.1368

DeFalco, T., and Capel, B. (2009). Gonad morphogenesis in vertebrates: divergent means to a convergent end. *Annu. Rev. Cell Dev. Biol.* 25, 457–482. doi: 10.1146/annurev.cellbio.042308.13350

Dickens, M. J., Balthazart, J., and Cornil, C. A. (2012). Brain aromatase and circulating corticosterone are rapidly regulated by combined acute stress and sexual interaction in a sex-specific manner. *J. Neuroendocrinol.* 24, 1322–1334. doi: 10.1111/j.1365-2826.2012.02340.x

Eggers, S., Ohnesorg, T., and Sinclair, A. (2014). Genetic regulation of mammalian gonad development. *Nat. Rev. Endocrinol.* 10, 673–683. doi: 10.1038/nrendo.2014.163

Estermann, M. A., Williams, S., Hirst, C. E., Roly, Z. Y., Serralbo, O., Adhikari, D., et al. (2020). Insights into gonadal sex differentiation provided by single-cell transcriptomics in the chicken embryo. *Cell Rep.* 31:107491. doi: 10.1016/j.celrep.2020.03.055

Ge, C., Ye, J., Zhang, H., Zhang, Y., Sun, W., Sang, Y., et al. (2017). Dmrt1 induces the male pathway in a turtle species with temperature-dependent sex determination. *Development* 144, 2222–2233.

Goodfellow, P. N., and Lovell-Badge, R. (1993). SRY and sex determination in mammals. *Annu. Rev. Genet.* 27, 71–92. doi: 10.1146/annurev.ge.27.120193.000443

Green, R. E., Braun, E. L., Armstrong, J., Earl, D., Nguyen, N., Hickey, G., et al. (2014). Three crocodilian genomes reveal ancestral patterns of evolution among archosaurs. *Science* 346:1254449.

Gut, G., Herrmann, M. D., and Pelkmans, L. (2018). Multiplexed protein maps link subcellular organization to cellular states. *Science* 361:eaar7042. doi: 10.1126/science.aar7042

Hackett, S. J., Kimball, R. T., Reddy, S., Bowie, R. C., Braun, E. L., Braun, M. J., et al. (2008). A phylogenomic study of birds reveals their evolutionary history. *Science* 320, 1763–1768. doi: 10.1126/science.1157704

Hamburger, V., and Hamilton, H. L. (1951). A series of normal stages in the development of the chick embryo. *J. Morphol.* 88, 49–92. doi: 10.1002/jmor.1050880104

Handley, L. J., Ceplitis, H., and Ellegren, H. (2004). Evolutionary strata on the chicken Z chromosome: implications for sex chromosome evolution. *Genetics* 167, 367–376. doi: 10.1534/genetics.167.1.367

Hirst, C. E., Major, A. T., Ayers, K. L., Brown, R. J., Mariette, M., Sackton, T. B., et al. (2017a). Sex reversal and comparative data undermine the W chromosome and support Z-linked DMRT1 as the regulator of gonadal sex differentiation in birds. *Endocrinology* 158, 2970–2987. doi: 10.1210/en.2017-00316

Hirst, C. E., Serralbo, O., Ayers, K. L., Roeszler, K. N., and Smith, C. A. (2017b). "Genetic manipulation of the avian urogenital system using in ovo electroporation," in *Avian and Reptilian Developmental Biology: Methods and Protocols*, ed. G. Sheng (New York, NY: Springer New York).

Huynen, L., Millar, C. D., and Lambert, D. M. (2002). A DNA test to sex ratite birds. *Mol. Ecol.* 11, 851–856. doi: 10.1046/j.1365-294x.2002.01483.x

Intarapat, S., and Satayalai, O. (2014). Microanatomical study of embryonic gonadal development in Japanese quail (*Coturnix japonica*). *Anat. Res. Int.* 2014:168614.

Ioannidis, J., Taylor, G., Zhao, D., Liu, L., Idoko-Akoh, A., Gong, D., et al. (2021). Primary sex determination in birds depends on DMRT1 dosage, but gonadal sex does not determine adult secondary sex characteristics. *Proc. Natl. Acad. Sci. U. S. A.* 118:e2020909118. doi: 10.1073/pnas.2020909118

Jung, K. M., Kim, Y. M., Keyte, A. L., Biegler, M. T., Rengaraj, D., Lee, H. J., et al. (2019). Identification and characterization of primordial germ cells in a vocal learning Neoaves species, the zebra finch. *FASEB J.* 33, 13825–13836. doi: 10.1096/fj.201900760rr

Kannankeril, J. V., and Domm, L. V. (1968). Development of the gonads in the female Japanese quail. *Am. J. Anat.* 123, 131–146. doi: 10.1002/aja.1001230106

Koopman, P., Gubbay, J., Vivian, N., Goodfellow, P., and Lovell-Badge, R. (1991). Male development of chromosomally female mice transgenic for Sry. *Nature* 351, 117–121. doi: 10.1038/351117a0

Koopman, P., Munsterberg, A., Capel, B., Vivian, N., and Lovell-Badge, R. (1990). Expression of a candidate sex-determining gene during mouse testis differentiation. *Nature* 348, 450–452. doi: 10.1038/348450a0

Koubova, J., Menke, D. B., Zhou, Q., Capel, B., Griswold, M. D., and Page, D. C. (2006). Retinoic acid regulates sex-specific timing of meiotic initiation in mice. *Proc. Natl. Acad. Sci. U. S. A.* 103, 2474–2479. doi: 10.1073/pnas.0510813103

Lambeth, L. S., Cummins, D. M., Doran, T. J., Sinclair, A. H., and Smith, C. A. (2013). Overexpression of aromatase alone is sufficient for ovarian development in genetically male chicken embryos. *PloS One* 8:e68362. doi: 10.1371/journal.pone.0068362

Lambeth, L. S., Raymond, C. S., Roeszler, K. N., Kuroiwa, A., Nakata, T., Zarkower, D., et al. (2014). Over-expression of DMRT1 induces the male pathway in embryonic chicken gonads. *Dev. Biol.* 389, 160–172. doi: 10.1016/j.ydbio.2014.02.012

Larney, C., Bailey, T. L., and Koopman, P. (2014). Switching on sex: transcriptional regulation of the testis-determining gene *Sry*. *Development* 141, 2195–2205. doi: 10.1242/dev.107052

Lawson, K. A. (1999). Fate mapping the mouse embryo. *Int. J. Dev. Biol.* 43, 773–775.

Lin, Y. T., Barske, L., Defalco, T., and Capel, B. (2017). Numb regulates somatic cell lineage commitment during early gonadogenesis in mice. *Development* 144, 1607–1618.

Liu, C. F., Liu, C., and Yao, H. H. (2010). Building pathways for ovary organogenesis in the mouse embryo. *Curr. Top. Dev. Biol.* 90, 263–290. doi: 10.1016/s0070-2153(10)90007-0

Liu, C., Rodriguez, K., and Yao, H. H. (2016). Mapping lineage progression of somatic progenitor cells in the mouse fetal testis. *Development* 143, 3700–3710.

Major, A. T., Ayers, K., Chue, J., Roeszler, K., and Smith, C. (2019). FOXL2 antagonises the male developmental pathway in embryonic chicken gonads. *J. Endocrinol.* doi: 10.1530/JOE-19-0277 [Epub ahead of print].

Mak, S. S., Wrabel, A., Nagai, H., Ladher, R. K., and Sheng, G. (2015). Zebra finch as a developmental model. *Genesis* 53, 669–677. doi: 10.1002/dvg.22900

Marshall Graves, J. A. (2008). Weird animal genomes and the evolution of vertebrate sex and sex chromosomes. *Annu. Rev. Genet.* 42, 565–586. doi: 10.1146/annurev.genet.42.110807.091714

Mohamed, G., Selim, A., Abd-Elhafeez, H., and Mohamed, M. (2017). Histomorphological developmental studies of the left ovary in the Japanese quail (*Coturnix Coturnix Japonica*). *Mathews J. Cytol. Histol.* 1:002.

Moreau, J. L. M., Kesteven, S., Martin, E., Lau, K. S., Yam, M. X., O'reilly, V. C., et al. (2019). Gene-environment interaction impacts on heart development and embryo survival. *Development* 146:dev172957. doi: 10.1242/dev.172957

Murray, J. R., Varian-Ramos, C. W., Welch, Z. S., and Saha, M. S. (2013). Embryological staging of the Zebra Finch, *Taeniopygia guttata*. *J. Morphol.* 274, 1090–1110. doi: 10.1002/jmor.20165

Nagai, H., Mak, S. S., Weng, W., Nakaya, Y., Ladher, R., and Sheng, G. (2011). Embryonic development of the emu, *Dromaius novaehollandiae*. *Dev. Dyn.* 240, 162–175. doi: 10.1002/dvdy.22520

Nef, S., Stevant, I., and Greenfield, A. (2019). Characterizing the bipotential mammalian gonad. *Curr. Top. Dev. Biol.* 134, 167–194. doi: 10.1016/bs.ctdb.2019.01.002

Okuno, M., Miyamoto, S., Itoh, T., Seki, M., Suzuki, Y., Mizushima, S., et al. (2020). Expression profiling of sexually dimorphic genes in the Japanese quail, *Coturnix japonica*. *Sci. Rep.* 10:20073.

Patterson, M. M., and Fee, M. S. (2015). "Zebra finches in biomedical research," in *Laboratory Animal Medicine*, eds J. G. Fox, L. C. Anderson, G. M. Otto, K. R. Pritchett-Corning, and M. T. Whary (Boston: Academic Press). doi: 10.1016/B978-0-12-409527-4.00023-7

Pfaffl, M. W. (2001). A new mathematical model for relative quantification in real-time RT-PCR. *Nucleic Acids. Res.* 29:e45. doi: 10.1093/nar/29.9.e45

Piprek, R. P., Kloc, M., and Kubiak, J. Z. (2016). "Early development of the gonads: origin and differentiation of the somatic cells of the genital ridges," in *Molecular Mechanisms of Cell Differentiation in Gonad Development*, ed. R. P. Piprek (Cham: Springer International Publishing). doi: 10.1007/978-3-319-31973-5_1

Piprek, R. P., Kolasa, M., Podkowa, D., Kloc, M., and Kubiak, J. Z. (2017). Cell adhesion molecules expression pattern indicates that somatic cells arbitrate gonadal sex of differentiating bipotential fetal mouse gonad. *Mech. Dev.* 147, 17–27. doi: 10.1016/j.mod.2017.07.001

Polanco, J. C., and Koopman, P. (2007). *Sry* and the hesitant beginnings of male development. *Dev. Biol.* 302, 13–24. doi: 10.1016/j.ydbio.2006.08.049

Prum, R. O., Berv, J. S., Dornburg, A., Field, D. J., Townsend, J. P., Lemmon, E. M., et al. (2015). A comprehensive phylogeny of birds (Aves) using targeted next-generation DNA sequencing. *Nature* 526, 569–573.

Raymond, C. S., Kettlewell, J. R., Hirsch, B., Bardwell, V. J., and Zarkower, D. (1999). Expression of Dmrt1 in the genital ridge of mouse and chicken embryos suggests a role in vertebrate sexual development. *Dev. Biol.* 215, 208–220. doi: 10.1006/dbio.1999.9461

Rebourcet, D., O'shaughnessy, P. J., Pitetti, J. L., Monteiro, A., O'hara, L., Milne, L., et al. (2014). Sertoli cells control peritubular myoid cell fate and support adult Leydig cell development in the prepubertal testis. *Development* 141, 2139–2149. doi: 10.1242/dev.107029

Rotgers, E., Jorgensen, A., and Yao, H. H. (2018). At the crossroads of fate-somatic cell lineage specification in the fetal gonad. *Endocr. Rev.* 39, 739–759. doi: 10.1210/er.2018-00010

Schneider, C. A., Rasband, W. S., and Eliceiri, K. W. (2012). NIH Image to ImageJ: 25 years of image analysis. *Nat. Methods* 9, 671–675.

Sekido, R., and Lovell-Badge, R. (2007). Mechanisms of gonadal morphogenesis are not conserved between chick and mouse. *Dev. Biol.* 302, 132–142.

Sinclair, A. H., Berta, P., Palmer, M. S., Hawkins, J. R., Griffiths, B. L., Smith, M. J., et al. (1990). A gene from the human sex-determining region encodes a protein with homology to a conserved DNA-binding motif. *Nature* 346, 240–244. doi: 10.1038/nmeth.2089

Smith, C. A., and Joss, J. M. P. (1993). Gonadal sex differentiation in *Alligator mississippiensis*, a species with temperature-dependent sex determination. *Cell Tissue Res.* 273, 149–162. doi: 10.1186/s12864-016-2396-9

Smith, C. A., and Sinclair, A. H. (2004). Sex determination: insights from the chicken. *Bioessays* 26, 120–132. doi: 10.1002/bies.10400

Smith, C. A., Katz, M., and Sinclair, A. H. (2003). DMRT1 is upregulated in the gonads during female-to-male sex reversal in Zw chicken embryos. *Biol. Reprod.* 68, 560–570. doi: 10.1095/biolreprod.102.007294

Smith, C. A., Roeszler, K. N., Ohnesorg, T., Cummins, D. M., Farlie, P. G., Doran, T. J., et al. (2009). The avian Z-linked gene DMRT1 is required for male sex determination in the chicken. *Nature* 461, 267–271. doi: 10.1038/nature08298

Soderstrom, K., Qin, W., and Leggett, M. H. (2007). A minimally invasive procedure for sexing young zebra finches. *J. Neurosci. Methods* 164, 116–119. doi: 10.1016/j.jneumeth.2007.04.007

Spiller, C., Koopman, P., and Bowles, J. (2017). Sex determination in the mammalian germline. *Annu. Rev. Genet.* 51, 265–285. doi: 10.1146/annurev-genet-120215-035449

Stevant, I., and Nef, S. (2019). Genetic control of gonadal sex determination and development. *Trends Genet.* 35, 346–358. doi: 10.1016/j.tig.2019.02.004

Stevant, I., Kuhne, F., Greenfield, A., Chaboissier, M. C., Dermitzakis, E. T., and Nef, S. (2019). Dissecting cell lineage specification and sex fate determination in gonadal somatic cells using single-cell transcriptomics. *Cell Rep.* 2, 3272–3283.e3. doi: 10.1016/j.celrep.2019.02.069

Stevant, I., Neirijnck, Y., Borel, C., Escoffier, J., Smith, L. B., Antonarakis, S. E., et al. (2018). Deciphering cell lineage specification during male sex determination with single-cell RNA sequencing. *Cell Rep.* 22, 1589–1599. doi: 10.1016/j.celrep.2018.01.043

Suzuki, A., and Saga, Y. (2008). Nanos2 suppresses meiosis and promotes male germ cell differentiation. *Genes Dev.* 22, 430–435.

Tagami, T., Miyahara, D., and Nakamura, Y. (2017). Avian primordial germ cells. *Adv. Exp. Med. Biol.* 1001, 1–18. doi: 10.1016/j.celrep.2018.01.043

Takada, S., Ota, J., Kansaku, N., Yamashita, H., Izumi, T., Ishikawa, M., et al. (2006). Nucleotide sequence and embryonic expression of quail and duck Sox9 genes. *Gen. Comp. Endocrinol.* 145, 208–213. doi: 10.1016/j.ygcen.2005.08.009

Vernet, N., Condrea, D., Mayere, C., Feret, B., Klopfenstein, M., Magnant, W., et al. (2020). Meiosis occurs normally in the fetal ovary of mice lacking all retinoic acid receptors. *Sci. Adv.* 6:eaaz1139.

Warner, D. A. (2011). "Chapter 1 - Sex determination in reptiles," in *Hormones and Reproduction of Vertebrates*, eds D. O. Norris and K. H. Lopez (London: Academic Press).

Warren, W. C., Clayton, D. F., Ellegren, H., Arnold, A. P., Hillier, L. W., Kunstner, A., et al. (2010). The genome of a songbird. *Nature* 464, 757–762.

Whiteley, S. L., Holleley, C. E., Wagner, S., Blackburn, J., Deveson, I. W., Marshall Graves, J. A., et al. (2021). Two transcriptionally distinct pathways drive female development in a reptile with both genetic and temperature dependent sex determination. *PLoS Genet.* 17:e1009465. doi: 10.1371/journal.pgen.1009465

Wilhelm, D., Palmer, S., and Koopman, P. (2007). Sex determination and gonadal development in mammals. *Physiol. Rev.* 87, 1–28.

Xu, L., Auer, G., Peona, V., Suh, A., Deng, Y., Feng, S., et al. (2019). Dynamic evolutionary history and gene content of sex chromosomes across diverse songbirds. *Nat. Ecol. Evol.* 3, 834–844.

Yang, Y., Workman, S., and Wilson, M. (2018). The molecular pathways underlying early gonadal development. *J. Mol. Endocrinol.* doi: 10.1530/JME-17-0314 [Epub ahead of print].

Yao, H. H., Dinapoli, L., and Capel, B. (2004). Cellular mechanisms of sex determination in the red-eared slider turtle, *Trachemys scripta*. *Mech Dev* 121, 1393–1401.

Yao, H. H., Whoriskey, W., and Capel, B. (2002). Desert Hedgehog/Patched 1 signaling specifies fetal Leydig cell fate in testis organogenesis. *Genes Dev.* 16, 1433–1440.

Zhou, Q., Zhang, J., Bachtrog, D., An, N., Huang, Q., Jarvis, E. D., et al. (2014). Complex evolutionary trajectories of sex chromosomes across bird taxa. *Science* 346:1246338.

Conflict of Interest: The authors declare that the research was conducted in the absence of any commercial or financial relationships that could be construed as a potential conflict of interest.

frontiers in Cell and Developmental Biology

ORIGINAL RESEARCH
published: 21 September 2021
doi: 10.3389/fcell.2021.715868

SALL1 Modulates CBX4 Stability, Nuclear Bodies, and Regulation of Target Genes

Immacolata Giordano[1†], Lucia Pirone[1†‡], Veronica Muratore[1], Eukene Landaluze[1], Coralia Pérez[1], Valerie Lang[2], Elisa Garde-Lapido[1], Monika Gonzalez-Lopez[1], Orhi Barroso-Gomila[1], Alfred C. O. Vertegaal[3], Ana M. Aransay[1,4], Jose Antonio Rodriguez[5], Manuel S. Rodriguez[6], James D. Sutherland[1] and Rosa Barrio[1]**

[1] Center for Cooperative Research in Biosciences (CIC bioGUNE), Basque Research and Technology Alliance, Derio, Spain, [2] Viralgen Vector Core, Parque Científico y Tecnológico de Guipúzcoa, San Sebastián, Spain, [3] Department of Cell and Chemical Biology, Leiden University Medical Center, Leiden, Netherlands, [4] Centro de Investigación Biomédica en Red. Enfermedades Hepáticas y Digestivas (CIBERehd), Instituto de Salud Carlos III, Madrid, Spain, [5] Department of Genetics, Physical Anthropology and Animal Physiology, University of the Basque Country, Leioa, Spain, [6] Laboratoire de Chimie de Coordination-CNRS, Paul Sabatier: Université Toulouse III, Toulouse, France

Development is orchestrated through a complex interplay of multiple transcription factors. The comprehension of this interplay will help us to understand developmental processes. Here we analyze the relationship between two key transcription factors: CBX4, a member of the Polycomb Repressive Complex 1 (PRC1), and SALL1, a member of the Spalt-like family with important roles in embryogenesis and limb development. Both proteins localize to nuclear bodies and are modified by the small ubiquitin-like modifier (SUMO). Our results show that CBX4 and SALL1 interact in the nucleoplasm and that increased SALL1 expression reduces ubiquitination of CBX4, enhancing its stability. This is accompanied by an increase in the number and size of CBX4-containing Polycomb bodies, and by a greater repression of CBX4 target genes. Thus, our findings uncover a new way of SALL1-mediated regulation of Polycomb bodies through modulation of CBX4 stability, with consequences in the regulation of its target genes, which could have an impact in cell differentiation and development.

Keywords: CBX4, SALL1, nuclear bodies, SUMO, ubiquitin

OPEN ACCESS

Edited by:
Juan Jose Sanz-Ezquerro, Centro Nacional de Biotecnología, Consejo Superior de Investigaciones Científicas (CSIC), Spain

Reviewed by:
Ana Carmena, Institute of Neurosciences of Alicante (IN), Spain
Smita Misra, Meharry Medical College, United States
Stefan Müller, Goethe University Frankfurt, Germany

***Correspondence:**
James D. Sutherland
jsutherland@cicbiogune.es
orcid.org/0000-0003-3229-793X
Rosa Barrio
rbarrio@cicbiogune.es
orcid.org/0000-0002-9663-0669

†These authors share first authorship

‡Present address:
Lucia Pirone, Council for Agricultural Research and Economics, Research Centre for Plant Protection and Certification, Rome, Italy

Specialty section:
This article was submitted to Signaling, a section of the journal Frontiers in Cell and Developmental Biology

Received: *27 May 2021*
Accepted: *30 August 2021*
Published: *21 September 2021*

Citation:
Giordano I, Pirone L, Muratore V, Landaluze E, Pérez C, Lang V, Garde-Lapido E, Gonzalez-Lopez M, Barroso-Gomila O, Vertegaal ACO, Aransay AM, Rodriguez JA, Rodriguez MS, Sutherland JD and Barrio R (2021) SALL1 Modulates CBX4 Stability, Nuclear Bodies, and Regulation of Target Genes. Front. Cell Dev. Biol. 9:715868. doi: 10.3389/fcell.2021.715868

INTRODUCTION

Development of higher organisms is orchestrated by a complex interplay of regulatory networks involving multiple signaling pathways and transcriptional regulatory factors. Two key families of transcriptional repressor proteins involved in development are the Polycomb Group (PcG) and the Spalt-like (SALL) proteins.

Polycomb Group proteins are involved in epigenetic regulation and control cell fate during embryonic development. These proteins accumulate in nuclear foci called Polycomb (Pc) bodies, which are involved in transcriptional repression (Saurin et al., 1998; Cheutin and Cavalli, 2012; Entrevan et al., 2016; Schuettengruber et al., 2017) and form two distinct complexes: Polycomb Repressive Complex 1 and 2 (PRC1 and PRC2), conserved from flies to human. A crucial component of the PRC1 complex is CBX4. CBX4 is required to maintain the transcriptionally repressive state of HOX genes during development, and has an important role in several essential

pathways. Thus, it has been described to facilitate differentiation of hematopoietic stem cells (Klauke et al., 2013), counteracting cellular senescence (Ren et al., 2019) and maintaining the epithelial lineage identity *via* repression of non-epidermal lineage and cell cycle inhibitor genes (Mardaryev et al., 2016). Moreover, CBX4 is recruited rapidly to sites of DNA damage (Ismail et al., 2012) and has emerged as a critical component of the DNA end resection machinery (Soria-Bretones et al., 2017).

Spalt-like family members (SALL1 to SALL4), on the other hand, are important regulators of animal development, being crucial for the formation of the limbs, kidneys, and the central and peripheral nervous systems, among other organs (de Celis and Barrio, 2009). SALL proteins are characterized by the presence of several precisely spaced copies of the zinc finger domain (de Celis and Barrio, 2009). They also contain a N-terminal glutamine-rich region, which could have a role in dimerization or protein–protein interactions (Kohlhase et al., 1998; Buck et al., 2000; Sweetman et al., 2003; Borozdin et al., 2006), and a conserved N-terminal motif that mediates its interaction with one of the major corepressor complexes in mammalian cells, the nucleosome remodeling deacetylase (NuRD) complex (Kiefer et al., 2002; Lauberth and Rauchman, 2006). Like the PcG proteins, SALL1 and its homologs localize in nuclear bodies, as it has been reported in cultured cells and *in vivo* (Netzer et al., 2001; Kiefer et al., 2002; Sánchez et al., 2010; Abedin et al., 2011). However, the nature and function of these bodies have not been explored.

CBX4 and SALL1 play important roles in different aspects of human health. Dysregulation of CBX4 contributes to the occurrence and progression of human tumors, in which it can act as either oncogene or tumor suppressor, depending on the cellular context (Wang et al., 2016). Mutations in *SALL1*, on the other hand cause Townes–Brocks Syndrome (TBS), an autosomal dominant syndrome characterized by renal anomalies, hearing loss, congenital heart defects, and eye anomalies among other symptoms (Kohlhase, 1993). TBS-causing mutations produce truncated SALL1 proteins lacking most of the zinc finger pairs, which aberrantly localize to the cytoplasm and interfere with centrosomal components, resulting in the formation of longer and more abundant primary cilia in patient-derived cells (Bozal-Basterra et al., 2018, 2020).

As described for many other transcriptional regulatory factors, the localization and activity of CBX4 and SALL1 can be modulated by post-translational modifications, including conjugation to ubiquitin or ubiquitin-like (UbL) proteins, such as small ubiquitin-like modifier (SUMO). Thus, CBX4 is SUMOylated and it is a substrate of the SUMO-deconjugating enzyme SENP2 (Wotton and Merrill, 2007; Kang et al., 2010). In addition, it was identified as a SUMO substrate in different proteomic analyses (Golebiowski et al., 2009; Galisson et al., 2011; Hendriks et al., 2014, 2015; Lamoliatte et al., 2014; Tammsalu et al., 2014; Xiao et al., 2015; Hendriks and Vertegaal, 2016). Interestingly, CBX4 itself is proposed to be a SUMO E3 ligase, and is involved in SUMOylation of the transcriptional corepressor C-terminal-binding protein (CtBP) (Kagey et al., 2003), the nucleocytoplasmic shuttling protein hnRNP (Pelisch et al., 2012), the transcriptional co-activator Prdm16 (Chen et al., 2018), and other chromatin-associated factors including CTCF, Dnmt3a, or Bm1 (Li et al., 2007; MacPherson et al., 2009; Ismail et al., 2012). CBX4 has also been found ubiquitinated and its polyubiquitination influences the dynamics of the PRC1 at the chromatin and the regulation of downstream genes (Povlsen et al., 2012; Mertins et al., 2013; Udeshi et al., 2013; Ning et al., 2017; Akimov et al., 2018; Wang et al., 2020).

In the case of SALL1, interaction with SUMO1 and the SUMO E2 conjugase UBC9 has been reported using yeast two-hybrid and *in vitro* assays, with SUMOylation mapped to lysine 1086 (Netzer et al., 2002). Subsequently, SALL1 as well as other SALL proteins, have been confirmed as targets of SUMOylation by proteomics analyses (Golebiowski et al., 2009; Galisson et al., 2011; Hendriks et al., 2014, 2015; Schimmel et al., 2014; Xiao et al., 2015; Hendriks and Vertegaal, 2016). In *Drosophila*, SUMOylation of SALL homologs influences their role in vein pattern formation in the wing and their transcriptional repressor activity (Sánchez et al., 2010, 2011).

Remarkably, although different functional aspects of CBX4 and SALL1 have been addressed in previous studies, a regulatory interplay between these proteins has not been described so far. Interestingly, we identified CBX4, as well as other PcG proteins, as a possible interactor of SALL1 by proximity proteomics (Bozal-Basterra et al., 2018). In addition, *sall* genes and *Pc* interact genetically in *Drosophila*, as mutations in the homolog *spalt-major* enhanced the phenotypical effects of Pc group mutations during embryogenesis (Casanova, 1989; Landecker et al., 1994). These findings, together with the localization of both proteins to nuclear bodies, as well as the regulation by SUMO of both proteins, prompted us to further investigate a potential functional or regulatory interplay between SALL1 and CBX4. We report here a novel interaction between these two transcriptional regulators in the nucleoplasm. Interestingly, SALL1 influences the stability of CBX4 by modulating its ubiquitination, which might be related to changes in the regulatory capacity of CBX4 over HOX genes. Overall, we present here a novel mechanism of regulation of a crucial factor in development, which has consequences for the regulation of its target genes.

MATERIALS AND METHODS

Cell Culture and Cell Transfection

Human U2OS (ATCC HTB-96) and HEK 293FT (Invitrogen) cells, as well as derived cell lines, were cultured at 37°C with 5% of CO2 in DMEM (Dulbecco's modified Eagle's medium; Gibco) supplemented with 10% FBS and 1% penicillin/streptomycin (Gibco). HEK 293FT cells were transiently transfected using calcium phosphate in 10 cm dishes with 3–10 μg of DNA using different sets of plasmids according to each experiment. Briefly, DNA was mixed with 500 μl of 2.5 M $CaCl_2$ and H_2O (1:10). The was added drop by drop to the same volume of HBS (NaCl 280 mM, KCl 10 mM, Na2HPO4 1.5 mM, glucose 12 mM, HEPES 50 mM), incubated for 10–15 min, and added to the cells. U2OS cells were transiently transfected using PEI

(Sigma Aldrich #408727), or Effectene (Qiagen) according to the manufacturers' instructions.

Generation of Plasmids

The following plasmids were used in this study (**Table 1**). DNA fragments were amplified from the indicated plasmids by high-fidelity PCR Platinum SuperFi (Thermo). PCR products were purified using mi-Gel Extraction kit (Metabion), digested if necessary using the restriction enzymes (Fermentas; NEB) and assembled by ligation or using NEBuilder HiFi Master Mix (NEB). All resulting plasmids were checked by sequencing. Cloning details are available upon request.

Lentiviral Transduction

Lentiviral expression constructs were packaged using psPAX2 and pMD2.G in HEK 293FT cells, and cell culture supernatants were used to transduce HEK 293FT cells to generate stable cell populations expressing SALL1 (constitutive: LL-GFS-SALL1-IRES-puro; or inducible: TripZ-SALL1-2xHA-puro). Selection was performed using 1 μg/ml of puromycin.

Bioinformatics Analyses

SUMOylation sites and SUMO-interacting motif (SIM) predictions were searched using SUMOplot,[1] GPS-SUMO[2] (Zhao et al., 2014), and JASSA programs (Beauclair et al., 2015). Sequence search and comparison was performed using BLAST.[3] Alignments were performed using Clustal.[4]

SUMOylation and Ubiquitination Assays in Cultured Cells

For the isolation of SUMOylated SALL1, one 10 cm dish of HEK 293FT cells was transfected with 7 μg of *CMV-SALL1-2xHA*, *CMV-SALL1ΔSUMO-2xHA*, and 3 μg of *CAG-bioSUMO3-T2A-BirA^{opt}-T2A-GFPpuro* or *CAG-BirA^{opt}-T2A-GFPpuro* as control. Isolation of SUMOylated protein was done according to previously reported methodology (Pirone et al., 2016, 2017).

[1]http://www.abgent.com/sumoplot
[2]http://sumosp.biocuckoo.org
[3]http://blast.ncbi.nlm.nih.gov/Blast.cgi/
[4]https://www.ebi.ac.uk/Tools/msa/clustalo/

TABLE 1 | Plasmids used in the study.

Name of the vector	References	Parental vectors	Cloning sites/notes
CAG-bioSUMO3-T2A-BirA^{opt}-T2A-GFPpuro	Pirone et al., 2017	–	–
CMV-CBX4-YFP	This work	*pEYFP-N1*	*Eco*RI-*Sal*I (KAN); CBX4 generated by high-fidelity PCR
CMV-SALL1-YFP	Pirone et al., 2017	*pEYFP-N1*	*Eco*RI-*Sal*I (KAN); SALL1 generated by high-fidelity PCR
CMV-SALL1ΔSUMO-YFP	This work	*CMV-SALL1-YFP*	*Eco*RI-*Sal*I; mutants introduced by overlap extension PCR (KAN); K571R; K592R; K982R; K1086R
CMV-SALL1ΔSIM-YFP	This work	*CMV-SALL1-YFP*	*Eco*RI-*Sal*I; mutants introduced by overlap extension PCR (KAN); predicted SIMs mutated to AAAA; SIM71: VLIV; SIM195: VIIE; SIM254: ILLL; SIM1252: ISVI
CMV-SALL1-2xHA	This work	*CMV-SALL1-YFP*	EYFP exchanged for 2xHA using *Sal*I-*Not*I (KAN)
CMV-SALL1^{826}-2xHA	This work	*CMV-SALL1(826)-YFP*	EYFP exchanged for 2xHA using *Sal*I-*Not*I (KAN)
CB6-HA-N	M. Way lab (CRUK, London)	*CB6*	CB6 has CMV promoter and confers neo selection; contains N-terminal HA epitope and MCS (AMP)
CMV-EGFP-β-galactosidase	This work	*pEGFP-N1*	LacZ subcloned from pIND/lacZ (Invitrogen)
CB6-HA-SALL1	This work	*CB6-HA-N*	*SALL1* from *CMV-SALL1-YFP*
CB6-HA-SALL1ΔSUMO	This work	*CB6-HA-N*	*SALL1* from *CMV-SALL1 ΔSUMO-YFP*
CB6-HA-CBX4	This work	*CB6-HA-N*	CBX4 from CMV-CBX4-YFP
*CMV-SALL1-BirA**	This work	*CMV-SALL1-YFP*	*Exchanged YFP for BirA*(BioID) by Sal1-Not1*
*CMV-Pc-BirA**	This work	*CMV-SALL1-BirA**	*Drosophila Pc* (PCR amplified) exchanged for SALL1 using *Eco*R1-*Sal*1 (KAN); Pc source: Addgene #1927
*CMV-CBX4-BirA**	This work	*CMV-SALL1-BirA**	*CBX4* (PCR amplified) exchanged for *SALL1* using *Eco*R1-*Sal*1 (KAN)
CMV-BirAopt-2A-puro	Pirone et al., 2017	–	–
CMV-bioUB-2A-BirAopt-2A-puro	Pirone et al., 2017	–	–
LL-CMV-GFS-SALL1-IRES-puro	This work	LL-CMV-GFS-IRES-puro	SALL1 inserted into modified version of Lentilox3.7; expresses N-terminal GFP-FLAG-STREP tag
TripZ-SALL1-2xHA-puro	This work	*CMV-SALL1-2xHA; TRIPZ*	Inserted SALL1-2xHA amplicon into BshT1-Mlu1TRIPZ (Dharmacon)
pcDNA3	Invitrogen	–	–
Lenti-Cas9-blast vector	Addgene #52962	–	–
psPAX2	Addgene #12260	–	–
pMD2.G (VSV-G envelope)	Addgene #12259	–	–
pEYFP-N1, pEYFP-C	Clontech	–	–

KAN or AMP indicate the antibiotic resistant cassette (kanamycin or ampicillin, respectively) in the vector for bacterial transformation.

For the ubiquitination assay of CBX4, one 10 cm dish was transfected with 5 μg of *CMV-SALL1-YFP*, *CMV-SALL1ΔSUMO-YFP*, *CMV-GFP-β-galactosidase*, *CMV-BirA-2A-puro*, *CMV-bioUB-2A-BirA-2A-puro*, or *CB6-HA-CBX4*. After transfection, medium was supplemented with biotin at 50 μM. Twenty-four hours after transfection, plates were treated with MG132 (10 μM, 12 h; Calbiochem). Transfected cells were collected after 48–72 h, washed three times with phosphate buffered saline (PBS) and resuspended in lysis buffer [0.5 ml/10 cm dish; 8 M urea, 1% SDS, 50 mM *N*-ethylmaleimide, 1× protease inhibitor cocktail (Roche) in 1× PBS]. Sonication was performed to reduce sample viscosity and samples were cleared by centrifugation at room temperature (RT). High-capacity NeutrAvidin-agarose beads (Thermo Scientific) were equilibrated and 30–60 μl suspension was used for incubation with extracts (12–18 h; RT; gentle agitation). Beads were subjected to stringent washes using the following washing buffers all prepared in 1× PBS (Franco et al., 2011): WB1 (8 M urea, 0.25% SDS); WB2 (6 M Guanidine-HCl); WB3 (6.4 M urea, 1 M NaCl, 0.2% SDS), WB4 (4 M urea, 1 M NaCl, 10% isopropanol, 10% ethanol, and 0.2% SDS); WB5 (8 M urea, 1% SDS); and WB6 (2% SDS). Samples were eluted in 50 μl of Elution Buffer (4× Laemmli sample buffer, 100 mM DTT) by two cycles of heating (5 min; 99°C), with vortexing in between. Beads were separated by centrifugation (18,000 × *g*, 5 min).

For the isolation of ubiquitinated endogenous CBX4 from cells lysates, 10 cm dishes were transfected with 5 μg of *CMV-SALL1-2xHA* plasmid or with pcDNA3 plasmid as control. After 48 h, cells were washed three times with 1× PBS and lysed in 500 μl of tandem ubiquitin binding entities (TUBEs) buffer [20 mM Phosphate buffer, pH 7.5 (Sigma), 2 mM EDTA (Sigma), 50 mM sodium fluoride (Sigma), 5 mM tetra-sodium pyrophosphate (Sigma), and 10 mM β-glycerol 2-phosphate (Sigma)]. The buffer was filtered through a 0.22 μm membrane and stored at 4°C. Eighty microliters of the lysate were taken as input. Ubiquitinated material was isolated using TUBEs based on RAD23 Homolog A (RAD23A) ubiquitin binding domains fused to GST and expressed in bacteria (Hjerpe et al., 2009; Aillet et al., 2012). To eliminate proteins with binding affinity for the beads (Glutathione Sepharose 4B, GE Healthcare), lysates were incubated with 125 μg of GST bound to glutathione-agarose beads for 1 h at 4°C and centrifugated for 2 min at 1000 rpm. After washing GST-TUBES beads with cold 1× PBS twice, supernatants were added, incubated for 1 h at 4°C and centrifugated for 2 min at 1000 rpm. The supernatants were then removed and beads were washed three times with TUBEs buffer. The beads were washed three times with PBS-Tween 0.5% and twice with TUBEs buffer containing NaCl (0.5 M). Finally, the beads were resuspended in 50 μl of Boiling buffer (50 mM Tris–HCl pH 6.8, 10% glycerol, 2% SDS, Bromophenol Blue, 10% β-mercaptoethanol) warmed at 60°C before use.

In vitro SUMOylation

Using PCR templates with incorporated 5′ T7 priming site +/− 3′ epitope-tags, SALL1-2xHA and CBX4 were transcribed/translated *in vitro* using the TNT® Quick Coupled Transcription/Translation System (Promega) according to the manufacturer's instruction and were then incubated in a buffer containing an ATP regenerating system [(50 mM Tris pH 7.5, 10 mM MgCl2, 2 mM ATP, 10 mM creatine phosphate (Sigma), 3.5 U/ml of creatine kinase (Sigma), and 0.6 U/ml of inorganic pyrophosphatase (Sigma)], 10 μg of SUMO1 or a combination of 5 μg of SUMO2 and SUMO3, 0.325 μg UBC9 and 0.8 μg of purified SAE1/2 (ENZO Life Sciences). SALL1 SUMOylation was checked adding 0.5–2 μl of *in vitro* transcribed/translated protein in the SUMOylation assay. Reactions were incubated at 30°C for 2 h and stopped by addition of SDS sample buffer.

GFP-Trap Co-pulldown

HEK 293FT cells were plated at 25–30% confluence. Transient transfections were performed using calcium phosphate in a 10 cm dish with 5 μg of *CMV-CBX4-YFP*, *CMV-SALL1-YFP*, *CMV-SALL1ΔSUMO-YFP*, *CMV-SALL1ΔSIM-YFP*, *CMV-YFP*, *CMV-SALL1-2xHA*, *CMV-SALL1-826-2xHA*, *CB6-HA*, *CB6-HA-SALL1*, *CB6-HA-SALL1ΔSUMO* or *CB6-HA-CBX4* in complete medium. All steps after transfection were performed at 4°C. Two days after transfection, cells were washed three times with cold 1× PBS and detached from the dish with a scraper. Cells of 10 cm dishes were lysed by adding 1 ml of Lysis Buffer [25 mM Tris–HCl pH 7.5, 150 mM NaCl, 1 mM EDTA, 1% NP-40, 0.5% Triton X-100, 5% glycerol, protease inhibitors (Roche)] followed by incubation on a rotating wheel for 30 min at 4°C. Lysates were sonicated and spun down at 25,000 × *g* for 20 min. After saving 40 μl of supernatant (input), the rest of the lysate was incubated overnight with 30 μl of equilibrated GFP-Trap resin (Chromotek) in a rotating wheel. Beads were washed five times for 5 min each with washing buffer (25 mM Tris–HCl pH 7.5, 300 mM NaCl, 1 mM EDTA, 1% NP-40, 0.5% Triton X-100, 5% glycerol). Beads were centrifuged at 2000 × *g* for 2 min after each wash. For elution, samples were boiled for 5 min at 95°C in 2× Laemmli buffer.

BioID Analysis of Interactions

Proximity interaction between CBX4 or Pc proteins to SALL1 was verified by the BioID method (Roux et al., 2013), consistent on fusing them to a promiscuous form of the enzyme BirA (BirA*) and to isolate the biotinylated material by streptavidin−beads pulldowns. HEK 293FT cells were transfected with 5 μg of CMV-CBX4-BirA* or CMV-Pc-BirA* in combination with *CMV-SALL1-2xHA* or *CMV-SALL1826-2xHA*. After 24 h, the medium was supplemented with 50 mM of biotin. At 48 h, cells were washed three times in cold 1× PBS and collected in 1 ml of lysis buffer [8 M urea, 1% SDS, protease inhibitor cocktail (Roche) in 1× PBS]. Lysates were sonicated and cleared by centrifugation, incubated overnight with 40 μl of equilibrated NeutrAvidin-agarose beads (Thermo Scientific) and washed with WB1–6 as indicated in the ubiquitination protocol above. Elution was done as previously described using 50 μl of Elution Buffer (4× Laemmli sample buffer, 100 mM DTT) by two cycles of heating (5 min, 99°C), with vortexing in between. Beads were separated by centrifugation (18,000 × *g*, 5 min).

Cycloheximide Assay

3×10^5 HEK 293FT cells per well were plated in six-well plates. Four hours later, cells were transfected with 2 μg of *CMV-SALL1-YFP*, *CMV-SALL1ΔSUMO-YFP*, or *CMV-GFP-β-galactosidase* plasmid per well using the calcium phosphate method. Twenty-four hours after transfection, cells were treated with 50 μg of cycloheximide (CHX, 50 μg/ml) in combination or not with MG132 (10 μM) for different time points (0, 4, 8, or 16 h). Cells were lysed in RIPA buffer [150 mM NaCl, 1.0% NP-40, 0.5% sodium deoxycholate, 0.1% SDS, 50 mM Tris, pH 8.0, protease inhibitors (Roche)] and analyzed by Western blot.

Western Blot

Samples were boiled at 95° for 5 min. Proteins were separated by SDS-PAGE (BioRad) and blotted using wet transfer to nitrocellulose membranes (0.45 μm pore; Cytiva). Membranes were blocked in 1× PBS with 0.1% Tween-20 (PBS-T) and 5% non-fat dry milk (blocking buffer) for 1 h and, for biotin detection, Casein Blocking Buffer 1× (Sigma #B6429). After that, membranes were incubated in blocking buffer for 1 h at RT or overnight at 4°C with the following primary antibodies: mouse monoclonal anti-HA (Sigma, 1:1000, #H3663), mouse monoclonal anti-β-Actin (Sigma, 1:1000, #A2228), mouse monoclonal anti-GFP (Roche, 1:1000, #11814460001), mouse monoclonal anti-SALL1 (R&D, 1:1000, #PP-K9814-00), rabbit polyclonal anti-CBX4 (Proteintech, 1:1000, #18544-1-AP), rabbit polyclonal anti-Avitag (GeneScript, 1:1000, #A00674), or rabbit monoclonal Vinculin (Cell Signaling, 1:1000, #13901S).

After three washes with PBS-T, the blots were incubated for 1 h with secondary antibodies: HRP-conjugated anti-mouse or anti-rabbit (1:5000, Jackson ImmunoResearch #115-035-062 or #111-035-045, respectively), HRP-conjugated anti-biotin (1:1000, Cell Signaling Technology #7075), HRP-conjugated anti-tubulin (1:5000, Proteintech #66031), or HRP-conjugated anti-GAPDH (1:5000, Proteintech #60004). Membranes were washed three times in PBS-T, developed using Clarity Western ECL substrate (Biorad) or Super Signal West Femto (Pierce), and chemiluminescent signals detected using a ChemiDoc camera system (Biorad). Quantification of bands was performed using Fiji software and normalized to Actin, GAPDH, or Vinculin levels, unless otherwise indicated. At least three independent blots were quantified per experiment.

Immunostaining and Microscopy Analysis

For immunostaining and microscopy analysis, 50,000 cells per well were seeded in a 24 well-plate on 12 mm diameter round acid-washed sterile coverslips. U2OS cells were transfected with 2 μg of *CMV-SALL1-YFP*, *CMV-SALL1ΔSUMO-YFP*, or *pEYFP-C1*, 1.5 μg of *CMV-SALL1-YFP* or HEK 293FT_TripZ-SALL1-2xHA were used.

After 2 days cells were washed three times with cold 1× PBS, fixed in 4% paraformaldehyde (Santa Cruz) supplemented with 0.1% Triton X-100 in 1× PBS for 20 min at RT. Then, coverslips were washed three times with 1× PBS to remove the fixative. Blocking was performed in blocking buffer (1% BSA, 0.3% Triton X-100, 25 mM NaCl in 1× PBS) for 1 h at RT. Incubation with primary antibodies diluted in blocking solution was performed during 1 h at 37°C in a humidity chamber or overnight at 4°C. The following primary antibodies were used: rabbit polyclonal anti-SALL1 (1:200, Abcam #31905), mouse monoclonal anti-GFP (1:500, Roche #11814460001), mouse monoclonal anti-PML (Promyelocytic Leukemia Protein) (1:100, Santacruz #sc-966), mouse monoclonal anti-SC35 (Splicing Component, 35 KDa, also known as Serine and Arginine Rich Splicing Factor 2) (1:200, BD Pharmingen #556363), rabbit polyclonal anti-CBX4 (1:100, Proteintech #18544-1-AP), rabbit polyclonal anti-SUMO2/3 (1:100, Eurogentec #AV-SM23-0100), mouse monoclonal anti SUMO1 (1:100, Developmental Studies Hybridoma Bank, DSHB, #21C7), or mouse monoclonal anti-SUMO2 (1:100, DSHB #8A2). Endogenous SALL1 or SALL1-2xHA in HEK 293FT_TripZ-SALL1-2xHA cells were stained by a primary antibody against SALL1 (R&D, 1:100, #PP-K9814-00).

After incubation with the primary antibody, cells were gently washed three times with 1× PBS and then incubated with the secondary antibody in the dark for 1 h at RT. The secondary antibodies conjugated to fluorophores used were donkey anti-mouse or anti-rabbit Alexa Fluor 488, Alexa Fluor 568, or Alexa Fluor 647 (1:200, Molecular Probes). To visualize the nuclei, we incubated the cells with DAPI (1:15,000, Roche #10236276001) for 5 min at RT. Another three washes were performed to remove unbound secondary antibody. Finally, coverslips were mounted using Prolong Gold antifade reagent (Molecular Probes #P36930) and stored in the dark at 4°C.

Stained cells were visualized using an Upright Fluorescent Microscope Axioimager D1 or a Leica SP2 or SP8 confocal microscope with 63× objective. For the quantification of Pc bodies, Fiji software was used.

Proximity Ligation Assays

U2OS cells were plated and transfected by PEI in six-well plates with 2 μg of *CMV-SALL1-2xHA* or *pcDNA3*. After 2 days, cells were transferred to an eight-well chamber slide (LabTek #177410) and allowed to attach for 12 h. Proximity ligation assay (PLA) was performed using the Duolink *In Situ* Red kit (Olink Bioscience; Gullberg et al., 2004; Söderberg et al., 2006) according to the manufacturer's instructions. Primary antibodies used: mouse monoclonal anti-SALL1 (1:250, R&D Systems #PP-K9814-00); rabbit polyclonal anti CBX4 (1:100, Proteintech #18544-1-AP). Images were recorded on a Leica SP8 confocal microscope system using 488 and 561 nm wavelengths for excitation and a 63× lens for magnification, and were analyzed with the Leica confocal software, Adobe Photoshop, and ImageJ softwares.

Reverse Transcription-Quantitative PCR Analysis

HEK 293FT cells transfected with 5 μg of *CMV-SALL1-YPF*, *CMV-SALL1ΔSUMO-YFP* or *CMV-GFP-β-galactosidase* plasmids, or HEK 293-TripZ-SALL1-2xHA_puro cells induced with different concentrations of doxycycline (dox), were used for reverse transcription-quantitative PCR (RT-qPCR) analysis.

Forty-eight hours after transfection, or 72 h after induction, total RNA was obtained by using EZNA Total RNA Kit (Omega) and quantified using a NanoDrop spectrophotometry. cDNAs were prepared using the SuperScript III First-Strand Synthesis System (Invitrogen) using 1 mg of total RNA in 20 μl volume per reaction. qPCR was done using PerfeCTa SYBR Green SuperMix Low Rox (Quantabio). Reactions were performed in 20 μl, adding 5 μl of cDNA and 0.5 μl of each primer (10 μM), in a CFX96 thermocycler (BioRad) using the following protocol: 95°C for 5 min and 40 cycles of 95°C for 15 s, 56 or 62°C for 30 s and 72°C 20 s. Melting curve analysis was performed for each pair of primers between 65 and 95°C, with 0.5°C temperature increments every 5 s. Relative gene expression data were analyzed using the ΔΔCt method (Livak and Schmittgen, 2001). Reactions were carried out in duplicate and results were derived from at least three independent experiments, normalized to GAPDH and presented as relative expression levels. Primer sequences are listed in **Table 2**.

Statistical Analysis

Statistical analysis was performed using GraphPad 7.0 software. Data were analyzed by Shapiro-Wilk normality test and Levene's test of variance. We used Mann–Whitney-*U* test or Unpaired *T*-test for comparing two groups and one-way ANOVA for more than two groups. *P*-values were represented by asterisks as follows: **P*-value < 0.05; ***P*-value < 0.01; ****P*-value < 0.001; *****P*-value < 0.0001. Differences were considered significant when $P < 0.05$.

TABLE 2 | Oligonucleotide sequences used for RT-qPCR.

Name	Sequence
hHoxa11_for	5′-AACGGGAGTTCTTCTTCAGCGTCT-3′
hHoxa11_rev	5′-ACTTGACGATCAGTGAGGTTGAGC-3′
hHoxb4_for	5′-AGGTCTTGGAGCTGGAGAAGGAAT-3′
hHoxb4_rev	5′-GGTGTTGGGCAACTTGTGGTCTTT-3′
hHoxb7_for	5′-AGACCCTGGAGCTGGAGAAAGAAT-3′
hHoxb7_rev	5′-ATGCGCCGGTTCTGAAACCAAATC-3′
hHoxb13_for	5′-TACGCTGATGCCTGCTGTCAACTA-3′
hHoxb13_rev	5′-AGTACCCGCCTCCAAAGTAACCAT-3′
hHoxc6_for	5′-AGGACCAGAAAGCCAGTATCCAGA-3′
hHoxc6_rev	5′-ATTCCTTCTCCAGTTCCAGGGTCT-3′
hHoxc10_for	5′-TGAAATCAAGACGGAGCAGAGCCT-3′
hHoxc10_rev	5′-TTGCTGTCAGCCAATTTCCTGTGG-3′
hHoxc12_for	5′-AGGGAACTCTCAGACCGCTTGAAT-3′
hHoxc12_rev	5′-AGAGCTTGCTCCCTCAACAGAAGT-3′
hHoxd13_for	5′-ATGTGGCTCTAAATCAGCCGGACA-3′
hHoxd13_rev	5′-AGATAGGTTCGTAGCAGCCGAGAT-3′
hGata4_for	5′-TCTCAGAAGGCAGAGAGTGTGTCA-3′
hGata4_rev	5′-GGTTGATGCCGTTCATCTTGTGGT-3′
hGAPDH_for	5′-CATGTTCGTCATGGGTGTGAACCA-3′
hGAPDH_rev	5′-AGTGATGGCATGGACTGTGGTCAT-3′
hSALL1_for	5′-GCTTGCACTATTTGTGGAAGAGC-3′
hSALL1_rev	5′-GAACTTGACGGGATTGCCTCCT-3′
hCBX4_for	5′-CATCGAGAAGAAGCGGATCCGCAAG-3′
hCBX4_rev	5′-CTGTTCTGGAAGGCGATCAGCAGCC-3′

RESULTS

SALL1 Does Not Colocalize With CBX4 in Nuclear Bodies

In agreement with previous reports (Netzer et al., 2001; Kiefer et al., 2002; Sánchez et al., 2010; Abedin et al., 2011), we detected endogenous SALL1 in discrete domains in the nucleus of U2OS human osteosarcoma cells (**Supplementary Figure 1A**). Similar results were obtained in U2OS cells transfected with human SALL1-YFP (**Supplementary Figures 1B,C**). These SALL1 foci were reminiscent of Pc bodies, where PRC proteins, such as CBX4 accumulate. Thus, we hypothesized that SALL1 and CBX4 could colocalize in nuclear bodies.

To test this hypothesis, *SALL1-YFP* plasmid was transfected into U2OS cells, where endogenous CBX4 was visualized by immunofluorescence using anti-CBX4 specific antibodies. However, SALL1 and CBX4 were found to localize to different subsets of nuclear bodies (**Figure 1A**).

In order to further characterize the nature of CBX4 and SALL1 bodies, we explored their possible colocalization with SUMO. We transfected U2OS cells with SALL1-YFP and examined its localization, and that of endogenous CBX4, with SUMO using immunofluorescence. While CBX4 did not colocalize with SUMO1 or SUMO2/3 (**Supplementary Figures 2A,B**), a partial colocalization between SALL1 and SUMO proteins was observed: some of the SALL1 bodies clearly colocalized with SUMO1 and SUMO2/3, while other SALL1 bodies did not (**Figure 1** and **Supplementary Figure 2E**). Conversely, some SUMO1 and SUMO2/3 bodies colocalized with SALL1, while others did not. These results fit with the well-known heterogenic nature of nuclear bodies (Zidovska, 2020). Neither CBX4, nor SALL1 colocalize with other nuclear factors, such as PML (**Supplementary Figures 2C,H**) or SC35 (**Supplementary Figures 2D,I**).

As shown previously, SALL1 undergoes SUMOylation in cells (Pirone et al., 2017), which might modulate its localization. To test this possibility, we generated a SALL1 SUMO mutant (SALL1ΔSUMO) by mutating four lysine residues (K571, K592, K982, and K1086) to arginine (**Supplementary Figure 3A**). These residues correspond to the four SUMOylation motifs conserved in vertebrates, predicted by SUMOplot and GPS-SUMO programs with highest scores (**Supplementary Figures 3C,D**) and the motif IKED (K982) being previously identified by proteomic analysis (Xiao et al., 2015; Hendriks and Vertegaal, 2016). As predicted, the SALL1ΔSUMO mutant lost the capacity to be SUMOylated in cells (**Supplementary Figure 3B**). Therefore, we considered SALL1ΔSUMO a SUMO-deficient mutant of SALL1. Interestingly, neither the lack of colocalization with CBX4, nor the partial colocalization with endogenous SUMO1 and SUMO2/3 were visibly altered when SALL1ΔSUMO-YFP was analyzed (**Figures 1B,E** and **Supplementary Figure 2F**). These results, indicating that the localization of SALL1 to a subset of SUMO bodies does not depend on its SUMOylation status, raised the possibility that SALL1 localization to these foci might be mediated by the presence of SIMs in this protein.

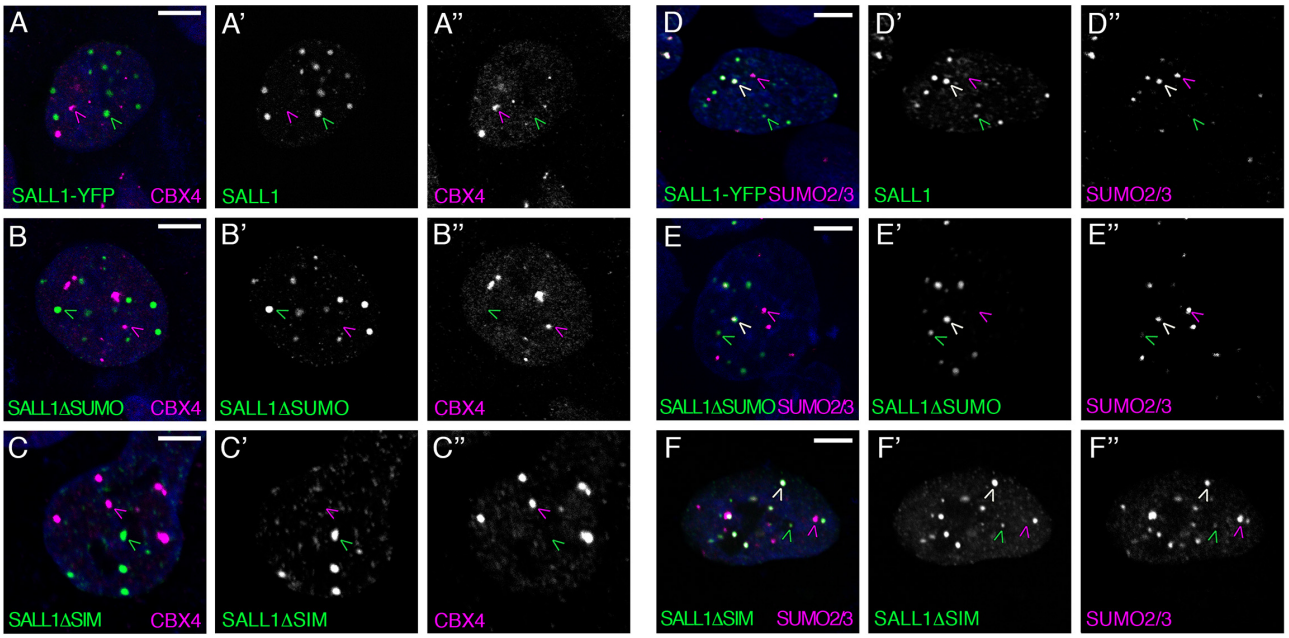

FIGURE 1 | SALL1 and CBX4 do not colocalize in nuclear bodies. **(A–F)** Confocal images of U2OS cells showing expression of SALL1-YFP, SALL1ΔSUMO-YFP, or SALL1ΔSIM-YFP (green), and endogenous CBX4 (magenta in **A–C**) or endogenous SUMO2/3 (magenta in **D–F**). Nuclei were stained with DAPI. Black and white pictures show single green or magenta channels. Green arrowheads indicate SALL1 bodies, magenta arrowheads indicate Pc bodies **(A–C)**, or SUMO bodies **(D–F)** and white arrowheads indicate colocalization of SALL1 and SUMO2/3 **(D–F)**. Pictures were taken with a Leica DM IRE2 confocal microscope using a 63× objective. Scale bars indicate 5 μm.

By analyzing the amino acid sequence of SALL1, we noted the presence of four high-scored SIMs (**Supplementary Figures 3A,D**). To investigate the role of these putative SIMs, we generated a SALL1ΔSIM version in which the four motifs were mutated to alanines. Remarkably, localization of SALL1 was unaffected by these mutations. Thus, SALL1ΔSIM-YFP readily localized to nuclear bodies, and partially colocalized with SUMO1 and SUMO2/3, but not with CBX4 (**Figures 1C,F** and **Supplementary Figure 2G**). The lack of colocalization between these two proteins in nuclear bodies prompted us to re-examine the interaction results obtained previously by mass spectrometry (MS).

SALL1 Interacts With CBX4 in a SUMOylation-Independent Manner

Previous MS results suggested that CBX4 could interact with full length SALL1 (Bozal-Basterra et al., 2018). We checked whether we could detect the CBX4-SALL1 interaction using CBX4-BioID. HEK 293FT cells were transfected with CBX4 fused to a promiscuous variant of the BirA biotin ligase (CBX4-BirA*) together with either full length SALL1-2xHA or the truncated form of SALL1^{826}-2xHA, causative of TBS. After pulldown using NeutrAvidin beads, the eluates were analyzed by Western blot. As shown in **Figure 2A**, CBX4 was in close proximity to both the full length and the truncated SALL1 forms (elution panel, lanes 1 and 2). *Drosophila* Pc (DmPc-BirA, the fly CBX4 homolog; lane 3) is also able to interact with full-length SALL1-HA.

We further confirmed the interaction between SALL1 and CBX4 by using pulldown experiments. CBX4-YFP was transiently overexpressed in HEK 293FT together with SALL1-2xHA or SALL1^{826}-2xHA, and GFP-Trap-based pulldown assays were carried out. SALL1-YFP was used as a positive control, since it is known to bind to the truncated mutant. As shown in **Figure 2B**, CBX4-YFP interacted both with full length and truncated SALL1 (elution panel, lanes 1 and 2).

SALL1 post-translational modifications could affect its interaction with other proteins. In this regard, SALL1 SUMOylation might be particularly relevant for its interaction with CBX4, which contain SIM domains (Merrill et al., 2010). In order to test whether SUMOylation could have a role in SALL1 binding to CBX4, we analyzed the SALL1ΔSUMO capability to interact with CBX4 (**Figure 2C**). WT SALL1-YFP and SALL1ΔSUMO-YFP were transiently transfected in HEK 293FT cells together with CBX4-HA (lanes 4 and 5, respectively). A GFP-Trap pulldown was performed and analyzed by Western blot. Our results show that the SUMOylation-deficient SALL1 mutant was still able to interact with CBX4 (elution panel, compare lanes 4 and 5). No appreciable differences were noted between WT SALL1 and SALL1ΔSUMO in their ability to interact with CBX4.

On the other hand, since CBX4 is known to be SUMOylated *in vitro* (Kagey et al., 2003; Merrill et al., 2010), we tested whether the predicted SIMs in SALL1 could have a role in its interaction with CBX4. As shown in **Figure 2C** (elution panel, compare lanes 4 and 6) SALL1 WT and SALL1ΔSIM showed similar capacity to

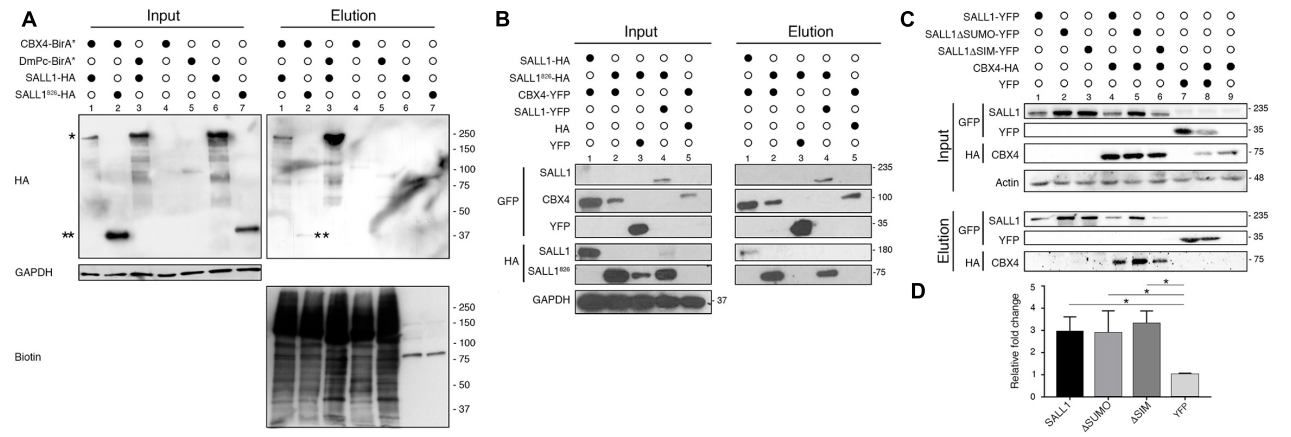

FIGURE 2 | SALL1 interacts with CBX4 in a SUMOylation-independent manner. **(A)** Validation of the interaction between human SALL1 and human CBX4 or *Drosophila melanogaster* Pc proteins using BioID-based biotin pulldown in transfected HEK 293FT cells. In the Input panel, the relative expression of the HA-tagged SALL1 proteins (the full-length protein or a TBS-related truncation mutant) is shown. One asterisk indicates SALL1-HA, while two asterisks indicate SALL1^{826}-HA. Negative controls (single expression of each individual protein) are shown in lanes 4–7. Anti-GAPDH was used as loading control. As shown in the Elution panel, CBX4-BirA* interact preferentially with full-length SALL1-HA (lane 1). Anti-biotin blot shows the efficiency of the different pulldowns. **(B)** Validation of the interaction between SALL1 and CBX4 using GFP-Trap. The Input panel shows the expression of epitope-tagged SALL1 and CBX4 proteins in transfected HEK 293FT cells. YFP alone and HA empty vector were used as controls. Lanes 1 and 2 of the Elution panel, show that CBX4 interacts with SALL1 full length and the truncated form. **(C)** SUMO-related SALL1 mutants interact with CBX4. Western blot analysis of proteins extracted from HEK 293FT cells transfected with the indicated plasmids. Pulldowns were performed using GFP-Trap. As shown in the Elution panel (lanes 4, 5, and 6), interaction between CBX4 and WT SALL1 or SALL1 mutants was readily detected in all blot images. **(D)** Graph showing that CBX4 levels increase when co-expressed with WT SALL1-YFP, SALL1ΔSUMO-YFP, or SALL1ΔSIM-YFP. The intensity of CBX4 bands in blots was quantified using ImageJ, normalized to b-Actin and reported as fold change relative to the YFP alone control. The mean plus SEM of three independent experiments is plotted. *P*-values were calculated using Mann–Whitney test. **P*-value < 0.05. **(A–C)** Antibodies used are indicated to the left. Molecular weight markers are indicated to the right in KDa.

bind CBX4. While differences in the intensity of CBX4 signals between SALL1 WT, SALL1ΔSUMO and SALL1ΔSIM can be observed, these differences were mostly due to the expression levels of the YFP-tagged SALL1 proteins. For example, the higher expression levels of SALL1ΔSUMO compared to SALL1 WT are most likely directly related to the higher levels of CBX4-HA detected in the pulldown.

In summary, these results confirm SALL1/CBX4 interaction, and show that neither SALL1 SUMOylation, nor its predicted SIM motifs are necessary for binding to CBX4 in our experimental setting.

SALL1 and CBX4 Interact in the Nucleoplasm

Both proteins localize to the nucleus, with non-overlapping enrichment in nuclear bodies, so we thought that the SALL1-CBX4 interaction might occur in the nucleoplasm where weaker immunofluorescence signals can be observed (**Supplementary Figure 4**). In order to explore this possibility, we decided to apply the PLA, a technique that allows the detection of protein–protein interactions *in situ*.

U2OS cells were transfected with *CMV-SALL1-2xHA* or with an empty *pcDNA3* vector as negative control, and anti-SALL1 and anti-CBX4 antibodies were used to perform PLA (**Figures 3A–E**; Söderberg et al., 2006; Matic et al., 2010). The signal from each detected pair of PLA probes is visualized as a fluorescent spot. Our analysis of the number of spots revealed an interaction between SALL1 and CBX4 in the nucleus (**Figures 3A,E**). Combined with the SALL1/CBX4 localization analyses described above, these results suggest that the interaction between SALL1 and CBX4 takes place most probably in the nucleoplasm instead of in nuclear bodies.

SALL1 Post-transcriptionally Increases the Levels of CBX4

Considering previous evidence that SALL1 can be SUMOylated and that CBX4 can act as an E3 ligase to increase SUMOylation of several substrates (Kagey et al., 2003; Li et al., 2007; MacPherson et al., 2009; Ismail et al., 2012; Pelisch et al., 2012; Chen et al., 2018), we hypothesized that the SALL1/CBX4 interaction could drive SALL1 SUMOylation. However, our *in vitro* SUMOylation assays in the presence of SUMO1 or SUMO2/3 showed that the SUMOylated form of SALL1 did not vary in a statistically significant manner when different amounts of CBX4 were added to the reaction (**Supplementary Figure 5**).

These results suggested that CBX4 does not function as a SUMO E3 ligase for SALL1 in this experimental settings, leaving the question of what could be the biological outcome of the interaction between these proteins unanswered. Intriguingly, while performing the experiments to validate the SALL1-CBX4 interaction, we had noticed that the levels of CBX4 were higher in cells co-transfected with SALL1 proteins (SALL1 WT, SALL1ΔSUMO, or SALL1ΔSIM) than in control cells co-expressing YFP (**Figure 2B**, lanes 1 vs. 5; **Figure 2C**, lanes 4, 5, and 6 vs. 8 and 9). This observation was supported by a quantitative analysis of the immunoblot results (**Figure 2D**),

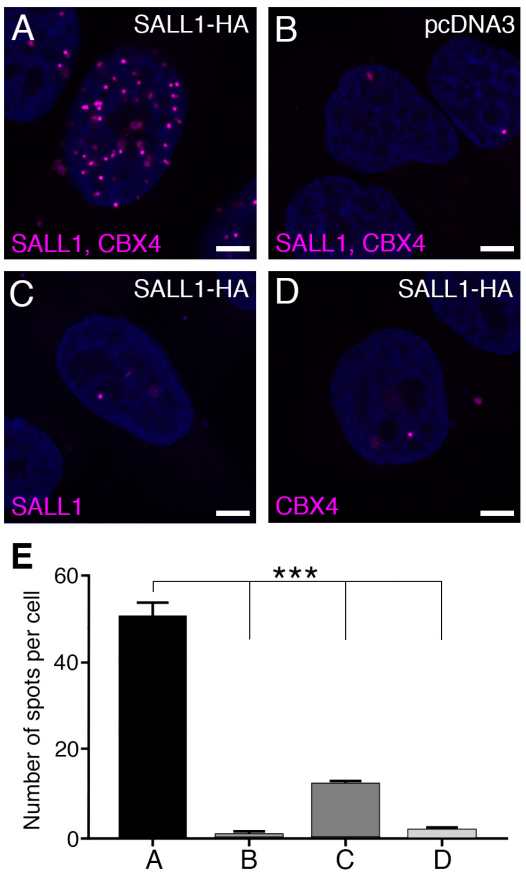

FIGURE 3 | SALL1 and CBX4 interact in the nucleoplasm. **(A–D)** Confocal pictures of a proximity ligation assay (PLA) showing *in situ* interaction of SALL1 and CBX4 in the nucleus of U2OS cells, visualized as magenta spots. Cells were transfected with SALL1-HA or with the empty pcDNA3 vector as negative control. Antibodies used in the assay are indicated in magenta. Panel **A** shows SALL1 and CBX4 interaction, while panels **B–D** are negative controls. **(E)** Quantification of PLA signals per cell as in **A–D**. Bars represent mean plus SEM of three independent experiments. *P*-values were calculated using one-way ANOVA test. ****P*-value < 0.001.

and was further confirmed using a transient co-expression experiment in HEK 293FT cells. In this experiment, Western blot analysis revealed higher levels of CBX4-HA in cells co-expressing SALL1-YFP than in cells co-expressing YFP alone (**Figure 4A**).

In order to discard any potential artifact due to the transient overexpression conditions, we generated two HEK 293FT-derived cell lines stably expressing SALL1. On one hand, we generated a HEK 293FT cell line constitutively expressing a GFS (GFP-Flag-Strep)-tagged version of SALL1 at levels moderately increased over the endogenous SALL1. Western blot analysis showed increased levels of endogenous CBX4 in HEK 293FT_GFS-SALL1 cells compared with parental HEK 293FT cells (**Figure 4B**). On the other hand, we used the inducible lentiviral vector TripZ to generate the HEK 293FT_TripZ-SALL1-2xHA cell line (see section "Materials and Methods"). This vector, based on the Tet-On system, allowed us to induce the expression of SALL1-2xHA in a doxycycline dependent manner, while preserving the expression of endogenous SALL1. As verified by immunofluorescence analysis (**Figure 4C**), increasing concentrations of doxycycline (1 ng/ml, 10 ng/ml, 0.1 μg/ml, or 1 μg/ml), lead to a progressive increment of the SALL1 expression in HEK 293FT_TripZ-SALL1-2xHA cells. The levels of endogenous CBX4 protein were analyzed in these cells using Western blot (**Figures 4D,E**). Quantification of three independent experiments showed that CBX4 levels were significantly increased when the cells were treated with 1 μg/ml of doxycycline compared to untreated cells (**Figure 4E**).

Since SALL1 is a transcription factor, we wondered whether the increased CBX4 levels described above could be due to SALL1-mediated transcriptional activation of CBX4 expression, potentially in an indirect way, as SALL1 is mostly described as a transcriptional repressor. We tested this possibility using the inducible HEK 293FT_TripZ-SALL1-2xHA cell model. SALL1 and CBX4 mRNA expression was analyzed by RT-qPCR) in control or doxycycline-treated cells. As expected, SALL1 mRNA expression increased in a doxycycline-dependent manner (**Figure 4F**). However, CBX4 mRNA expression levels did not vary significantly.

Altogether these results demonstrate that increasing levels of SALL1 are correlated with increasing CBX4 protein levels and, importantly, that this effect occurs at a post-transcriptional level.

SALL1 Stabilizes CBX4 Avoiding Its Degradation *via* the Proteasome

Different mechanisms may contribute to increase the levels of a given protein, including changes in subcellular localization, solubility, or alteration in protein stability due to reduced degradation. The results described above led us to test the hypothesis that SALL1 could stabilize CBX4.

To this end, we analyzed the half-life of CBX4 by using a time-course experiment with CHX. HEK 293FT cells were transfected with WT SALL1-YFP, SALL1ΔSUMO-YFP, or GFP-β-gal and treated with 50 μg/ml of CHX in presence or absence of 10 μM of the proteasome inhibitor MG132. Cells were collected at different time points (0, 4, 8, and 16 h after initiation of treatment) and the levels of endogenous CBX4 were analyzed by Western blot.

As shown **Figure 5A**, the levels of CBX4 began to decrease after 4 h of CHX treatment in cells expressing GFP-β-gal. However, in SALL1 WT or SALL1ΔSUMO-transfected cells the reduction in CBX4 levels was slower than in control cells. Quantification of six independent experiments is shown in **Figure 5B**. When cells were co-treated with CHX and MG132 (**Figure 5C**), proteasome degradation was inhibited and CBX4 levels did not decline at 4 h. Consequently, as shown in the Western blot quantification, no significant differences in the CBX4 levels were observed between cells transfected with SALL1, SALL1ΔSUMO, or control (**Figure 5D**). Overall, these results show that CBX4 protein is more stable in presence of SALL1 or SALL1ΔSUMO, and that degradation of CBX4 occurs through the ubiquitin proteasome system (UPS). Therefore, we concluded that SALL1 stabilizes CBX4 protein slowing down its degradation *via* the proteasome, and that SUMOylation of SALL1 seems not to be essential for CBX4 stabilization.

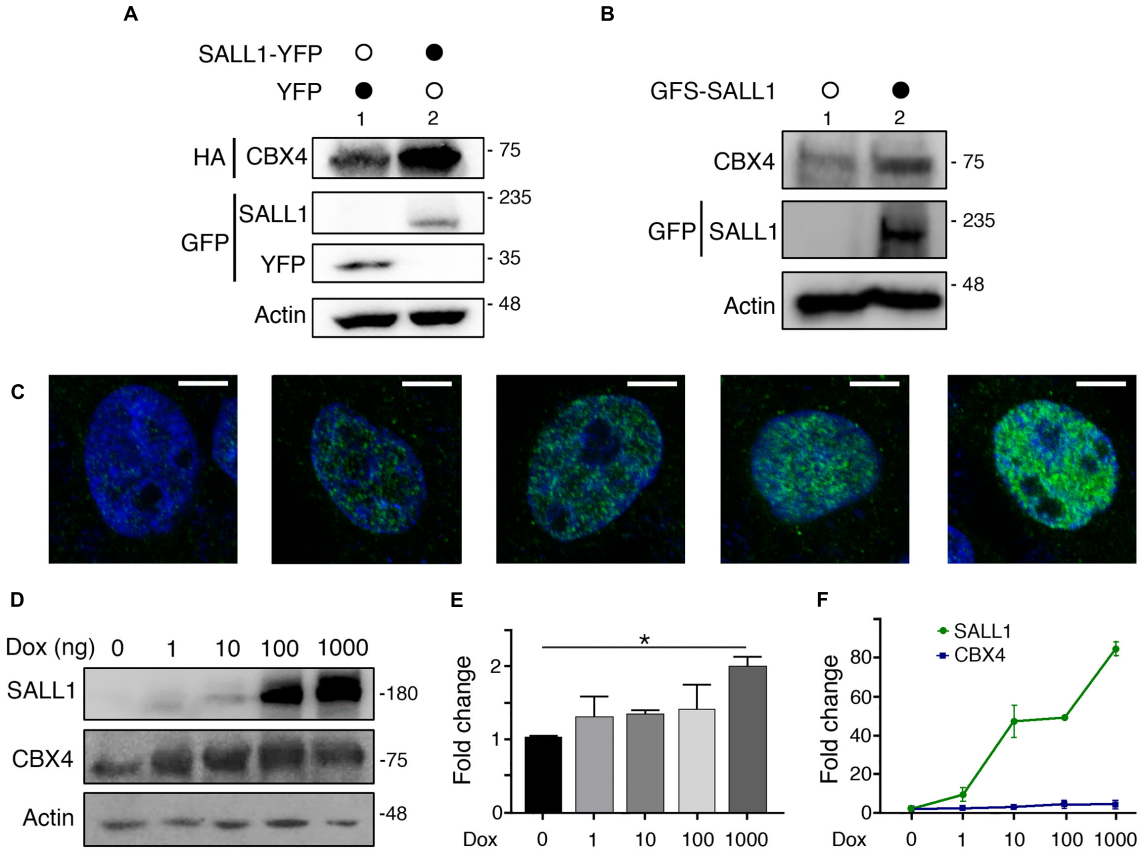

FIGURE 4 | SALL1 influences the levels of CBX4. **(A)** Western blot showing protein levels of CBX4-HA when co-expressed with SALL1-YFP or YFP alone in HEK 293FT cells. Actin expression was used as loading control. **(B)** Western blot showing expression levels of endogenous CBX4 protein in parental HEK 293FT cells (lane 1) or in HEK 293FT cells stably expressing GFS-SALL1 (lane 2). **(C)** Confocal microscopy images showing inducible expression SALL1-2xHA in HEK 293FT_TripZ-SALL1-2xHA cells. Cells were treated with different concentrations of doxycycline (Dox) to induce SALL1 expression as indicated. SALL1-2xHA was detected using anti-SALL1 primary antibody (green). Cell nuclei were stained with DAPI (blue). **(D)** Western blot analysis showing expression levels of endogenous CBX4 in HEK 293FT_TripZ-SALL1-2xHA cells treated with increasing concentrations of Dox. **(E)** Quantification of the expression levels of endogenous CBX4 in HEK 293FT_TripZ-SALL1-2xHA cells treated with increasing concentrations of Dox. Three independent experiments as the one shown in **D** were performed. The intensity of CBX4 bands was quantified using ImageJ, and the values were normalized to the levels of Actin. *P*-value was calculated using one-way ANOVA test. **P*-value < 0.05. **(F)** RT-qPCR analysis of *SALL1* and *CBX4* mRNA expression in HEK 293FT_TripZ-SALL1-2xHA cells treated with increasing concentrations of Dox. SALL1 and CBX4 expression were normalized using *GAPDH* expression and shown as fold change relative to untreated control. **(A,B,D)** Molecular weight markers are shown to the right in KDa. Antibodies were used as indicated to the left. **(E,F)** The mean plus SEM of at least three independent experiments is shown.

SALL1 Influences CBX4 Ubiquitination

Previous reports have shown that CBX4 is ubiquitinated to mediate its degradation through the proteasome (Ning et al., 2017). To investigate a potential relationship between SALL1 expression and CBX4 ubiquitination, we used the bioUb system (Pirone et al., 2017). First, we tested the efficiency of this system to detect the ubiquitinated fraction of CBX4. We transiently transfected HEK 293FT cells with CBX4-HA together with BirA-2A-bioUb or BirA as control. Cells were treated with biotin in presence or absence of the proteasome inhibitor MG132. Protein lysates were processed for bioUb assay (see section "Materials and Methods") and results were analyzed by Western blot (**Figure 6A**). Ubiquitinated CBX4 is shown in the elution panel. A band above 100 KDa and a high molecular weight smear, both consistent with ubiquitinated forms of CBX4, are visible. As expected, the levels of ubiquitinated CBX4 increased in presence of the proteasome inhibitor MG132. Anti-Avitag antibodies detecting bioUb also showed an increase in the general ubiquitination levels in presence of MG132, as shown in the elution panel. These results confirmed the modification of CBX4 by ubiquitination and its degradation *via* UPS.

Next, to test whether SALL1 could increase CBX4 stability by impairing its ubiquitination and subsequent proteasomal degradation, we studied CBX4 ubiquitination in the inducible HEK 293FT_TripZ-SALL1-2xHA cells. These cells were transiently transfected with *CBX4-YFP* together with *BirA-2A-bioUb* or *BirA* as control. The cells were treated or not with 1 μg/ml of doxycycline to induce SALL1 expression, in the presence or absence of 10 μM MG132. Protein lysates were processed for bioUb assay, and the results were analyzed by Western blot (**Figure 6B**). A statistically significant reduction of CBX4 ubiquitination was observed in presence of high

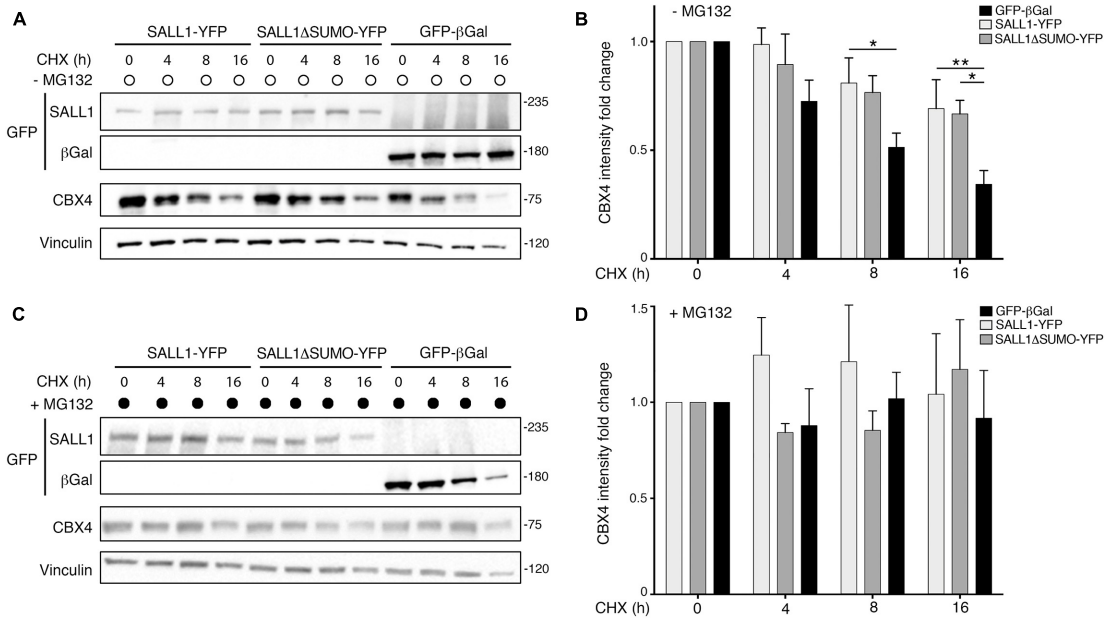

FIGURE 5 | SALL1 stabilizes CBX4 protein. **(A,C)** Western blot analysis of cycloheximide (CHX) chase experiments performed in HEK 293FT cells transfected with *SALL1-YFP*, *SALL1*Δ*SUMO-YFP*, or *GFP-β-gal*. Cells were treated with 50 μg/ml of CHX in the absence **(A)** or presence **(C)** of 10 μM of the proteasome inhibitor MG132. Cells were collected at different time points (0, 4, 8, and 16 h after initiation of treatment) and endogenous CBX4 levels were analyzed by Western blot. Vinculin was used as loading control. Molecular weight markers are shown to the right in KDa. Antibodies were used as indicated to the left. **(B,D)** CBX4 levels were quantified after CHX treatment alone **(B)** or in combination with MG132 **(D)**, normalized to Vinculin, and data from six different independent experiments were pooled together. Graphs show mean plus SEM. *P*-values were calculated using one-way ANOVA test. **P*-value < 0.05; ***P*-value < 0.01.

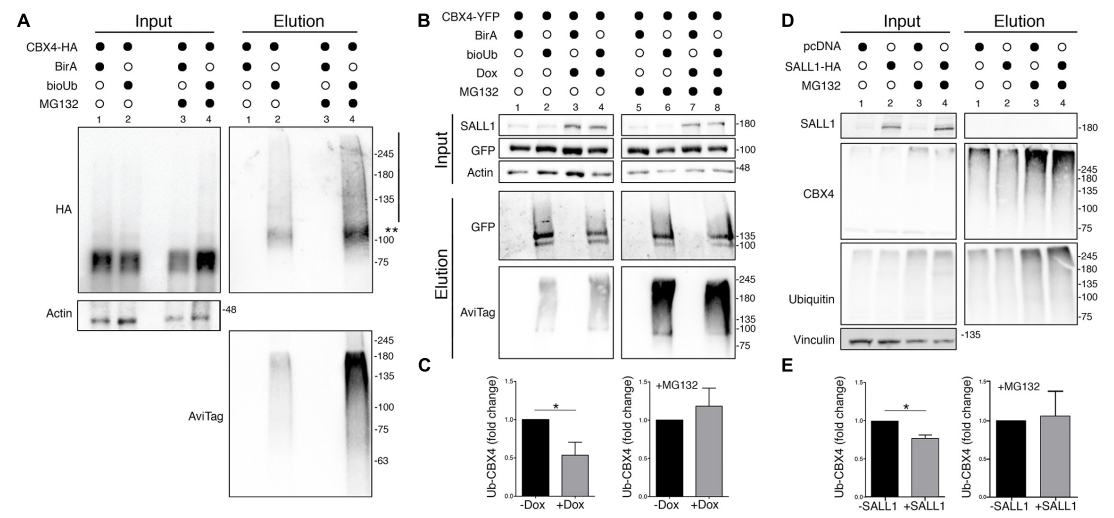

FIGURE 6 | CBX4 ubiquitination is reduced in presence of SALL1. **(A)** Western blot analysis of HEK 293FT cells transfected with *CBX4-HA* together with *CMV-BirA-2A-bioUb* or *BirA* as a negative control. Cells were treated with 50 μM of biotin in the presence or absence of 10 μM MG132. Protein lysates were subjected to pulldown with streptavidin beads and the results were analyzed by Western blot. Two asterisks indicate monoubiquitinated CBX4-HA protein and the vertical line indicates the polyubiquitination smear. **(B)** Western blot analysis of HEK 293FT_TripZ-SALL1-2xHA cells transiently transfected with *CBX4-YFP* together with *BirA-2A-bioUb* or *BirA* as control. The cells were treated or not with 1 μg/ml of doxycycline (Dox), in presence or absence of 10 μM of MG132. Protein lysates were incubated with streptavidin beads to isolate bioUb conjugated proteins and results were analyzed by Western blot. β-Actin was used as loading control. **(C)** The levels of ubiquitinated CBX4-YFP in Dox induced and not induced cells, in presence (right panel) or absence (left panel) of MG132, were quantified and normalized to the CBX4 levels in the input. **(D)** Western blot analysis of endogenous CBX4 in HEK 293FT cells transfected with *CMV-SALL1-2xHA* (lanes 2 and 4) or with pcDNA3 control plasmid (lanes 1 and 3), in presence (lanes 3 and 4) or absence (lanes 1 and 2) of 10 μM MG132. **(E)** Quantification of ubiquitinated CBX4 in the elution panel normalized to the CBX4 levels in the input, in cells expressing or not SALL1-HA, in presence (right panel) or absence (left panel) of MG132. **(A,B,D)** Molecular weight markers are shown to the right in KDa. Antibodies were used as indicated to the left. **(C,E)** Graphs represent mean plus SEM. *P*-values were calculated on $n = 4$ using Mann–Whitney test. **P*-value < 0.05.

levels of SALL1 (**Figures 6B,C**, in the elution panel compare lane 4 with lane 2). However, in the presence of MG132, no significant differences were appreciated between induced and not induced cells (**Figure 6C**, in the elution panel compare lanes 6 and 8).

To further analyze the ubiquitination of endogenous CBX4, we transiently expressed SALL1-2xHA or pcDNA3 as a control in HEK 293FT cells. After lysis, total ubiquitinated material was isolated from the cells by pulldown using TUBES (see section "Materials and Methods"), and analyzed by Western blot (**Figures 6D,E**). In presence of SALL1, the levels of ubiquitinated CBX4 were reduced when compared with cells transfected with the control plasmid (elution panel, compare lanes 1 and 2). No significant differences were appreciated when cells were treated with MG132 (elution panel, lane 4 vs. lane 3). Quantification of ubiquitinated CBX4 in relation to the CBX4 input in shown in **Figure 6E**. Taken together, these results indicated that SALL1 is able to stabilize CBX4 protein by reducing its ubiquitination and subsequent degradation *via* the UPS.

SALL1 Modulates the Number and Size of CBX4-Containing Pc Bodies, as Well as the Expression of CBX4 Target Genes

Although SALL1 does not colocalize with CBX4 in Pc bodies, the finding that SALL1 modulates CBX4 protein levels prompted us to investigate a potential effect of SALL1 expression on CBX4-containing Pc bodies. We transiently transfected SALL1-YFP or its mutant SALL1ΔSUMO-YFP in U2OS cells. GFP-β-gal was transfected as control. Transfected cells were stained with a specific CBX4 primary antibody and the number and area of CBX4-containing Pc bodies were examined in more than 100 cells per condition (**Supplementary Figure 6**). Using confocal microscopy and image analysis with Fiji software (**Figures 7A,B**),

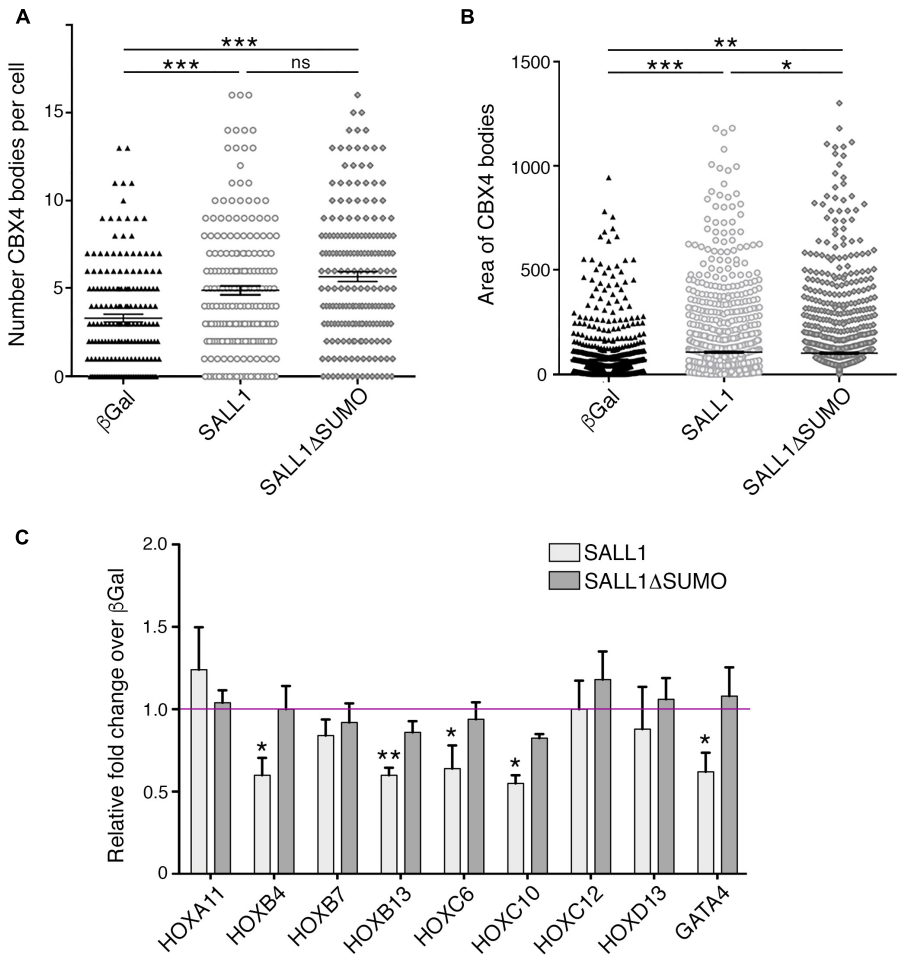

FIGURE 7 | SALL1 expression increases the number and size of CBX4-containing Pc bodies and enhances downregulation of CBX4 targets. **(A,B)** Graphs represent the number of CBX4-containing Pc bodies **(A)** and their mean area in pixels quantified using Fiji software **(B)** in U2OS cells expressing SALL1-YFP, SALL1ΔSUMO-YFP, or GFP-β-gal as a negative control. **(C)** Graph showing the mRNA expression levels of several CBX4 target genes in HEK 293FT cells expressing SALL1-YFP, SALL1ΔSUMO-YFP, or GFP-β-gal as control. Data shown correspond to the mean plus SEM of at least five independent RT-qPCR experiments. Gene expression data were normalized to *GAPDH* and are shown as relative fold change over β-Gal expressing cells (magenta line). *P*-values were calculated using one-way ANOVA test. **P*-value < 0.05; ***P*-value < 0.01; ****P*-value < 0.001.

we observed that Pc bodies were significantly larger and more abundant in cells expressing SALL1 or SALL1ΔSUMO than in cells expressing β-Gal. No significant differences in the number of bodies were observed between cells expressing SALL1 and SALL1ΔSUMO. However, the area of the Pc bodies was significantly smaller in SALL1ΔSUMO compared to SALL1 transfected cells. These results revealed that SALL1 SUMOylation status does not influence the increase in the number of Pc bodies, but it may influence their size.

Finally, since SALL1 increases CBX4 protein levels, as well as the size and number of Pc bodies, and increased formation of Pc bodies may lead to stronger transcriptional repression of several PRC1 target genes (Gonzalez et al., 2014; Soshnikova, 2014; Cheutin and Cavalli, 2018), we hypothesized that SALL1 overexpression could lead to a stronger transcriptional repression of CBX4 targets, including HOX genes.

To test this possibility, HEK 293FT cells were transiently transfected with SALL1-YFP, SALL1ΔSUMO-YFP, or GFP-β-gal as control, and the expression levels of several direct CBX4 target genes (*HOXA11*, *HOXB4*, *HOXB7*, *HOXB13*, *HOXC6*, *HOXC10*, *HOXC12*, *HOXD13*, and *GATA4*) were analyzed by RT-qPCR. Significant differences in the expression of *HOXB4*, *HOXB13*, *HOXC6*, *HOXC10*, and *GATA4* were observed between wild-type SALL1 and β-Gal expressing control cells (**Figure 7C**). However, no significant differences were observed between SALL1ΔSUMO-transfected cells and control cells.

Taken together, these results indicate that high SALL1 levels modulate the transcriptional repression capacity of CBX4 on some of its target genes. Interestingly, SUMOylation of SALL1 seemed to be necessary for this transcriptional effect.

DISCUSSION

In this work, we have confirmed that SALL1 and CBX4 proteins interact with each other. Although both proteins can be SUMOylated and contain validated [CBX4 (Merrill et al., 2010)] or predicted (SALL1) SIM motifs, our results suggest that the SALL1/CBX4 interaction does not depend on the SUMOylation status of SALL1, nor the mutation of its putative SIMs. We note the possible contribution of the endogenous SALL1 to the interaction, as dimers with the endogenous WT SALL1 and exogenous mutants could be formed, bridging the interaction of mutant SALL1 with CBX4.

Neither SALL1 WT nor the SALL1ΔSUMO or SALL1ΔSIM mutant forms showed colocalization with CBX4 in Pc bodies, a subset of nuclear bodies that have been defined as centers of chromatin regulation for transcriptional repression of target genes (Entrevan et al., 2016). This observation indicates that the SALL1-CBX4 interaction does not occur in this specific cellular compartment. Despite this, we demonstrate that SALL1, as well as its SUMOylation-deficient mutant form, increase the number and size of CBX4-containing Pc bodies. We

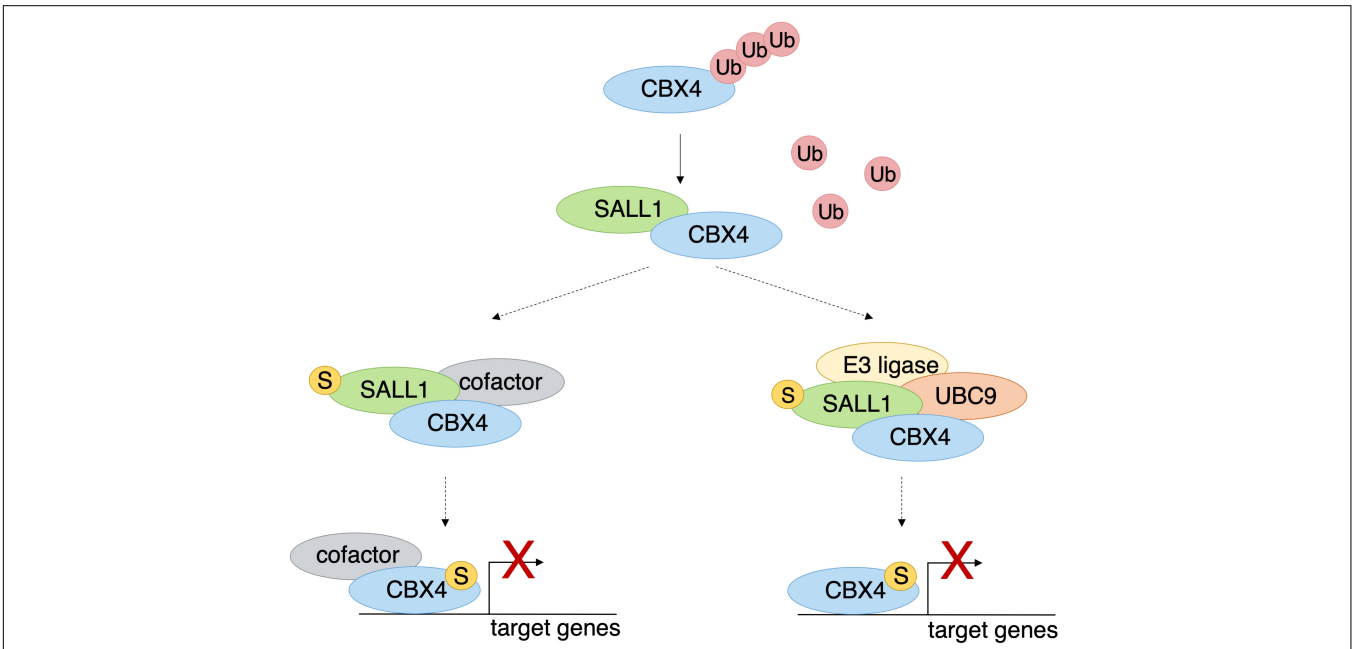

FIGURE 8 | SALL1 influences regulation of CBX4 target genes. Hypothetical model showing speculative scenarios whereby SALL1 could influence CBX4-mediated regulation of target genes. Binding to SALL1 (SUMOylated or non-SUMOylated) could stabilize CBX4 by interfering with its ubiquitination and its consequent degradation by the proteasome. CBX4 stabilization entails an increment of its protein levels and its accumulation in Pc bodies. Binding to SUMOylated SALL1 increases CBX4-mediated transcriptional repression of its target genes. At least two non-exclusive hypothetical mechanisms might underlie this effect. Under one hypothetical scenario (left side), it could be due to the concurrent recruitment of other essential cofactors. In another hypothetical scenario (right side), SUMOylated SALL1 could increase CBX4 transcriptional repression by facilitating its SUMOylation through recruitment of SUMOylation machinery components. Discontinuous arrows indicate speculative events that have not been proven experimentally.

speculate that a dynamic and transitory interaction with SALL1 in the nucleoplasm may indirectly influence Pc body formation by altering CBX4 levels. In fact, we demonstrated that SALL1 stabilizes and increases CBX4 protein levels in a post-translational manner, reducing its ubiquitination with subsequent reduction of its degradation *via* the proteasome.

Different hypothetical scenarios could explain the SALL1-mediated stabilization of CBX4. As a transcriptional repressor, SALL1 could inhibit the transcription of ubiquitin E3 ligase(s) involved in CBX4 modification or could facilitate the binding and/or the recognition of CBX4 by DUBs (Ning et al., 2017). Interestingly, SALL1 was found to interact with members of the UPS, which might disrupt CBX4 homeostasis (Bozal-Basterra et al., 2018). Importantly, we show that high SALL1 levels increase CBX4-mediated transcriptional repression of some of its target genes. Although SUMOylation of SALL1 does not seem to affect its ability to regulate CBX4 protein levels, it seems to be important for SALL1 to modulate CBX4 transcriptional repression activity: only when SALL1 is SUMOylated, the recruitment of CBX4 on the chromatin results in a functional effect. In a speculative scenario, one possible explanation of these results could be the involvement of a third component. For instance, SUMOylation of SALL1 could facilitate the simultaneous interaction with other members of the PRC1, such as RING1 or PHC1. Interestingly, those factors were also found as possible SALL1 interactors in the proximity proteomics analysis that hinted initially to a possible SALL1/CBX4 interaction (Bozal-Basterra et al., 2018). Otherwise, SUMOylation of SALL1 could facilitate the interaction of CBX4 with co-factors required for gene repression (Cheng et al., 2014).

These highly speculative hypotheses can be summarized into the model shown in **Figure 8**. SALL1 (in its unmodified or SUMOylated form) would interact with CBX4. This interaction would result in less ubiquitination of CBX4 with its consequent stabilization (**Figure 8**). Thus, CBX4 would be recruited on chromatin, where it would act as a transcriptional repressor of its target genes. In its SUMOylated form, SALL1 could interact, not only with CBX4, but also with repression cofactors or other components of PRC1, which could be recruited on chromatin along with CBX4 (**Figure 8**, left). The recruitment of transcriptional cofactor(s), or various components of PRC1, would result in the activation of the multiprotein complex with consequent repression of the target genes.

In an alternative hypothesis, SUMOylated SALL1 could enhance CBX4 repression capacity by facilitating its SUMOylation. The SUMOylation of CBX4 is known to be necessary for its repression activity on the chromatin (Kang et al., 2010). We observed that, in the presence of high levels of SALL1, the SUMOylation of CBX4 increased (data not shown). However, this was probably the result of increasing the total levels of the protein. In addition, SALL1 was demonstrated to interact with UBC9 and SUMO1 in a yeast two-hybrid system (Netzer et al., 2002). Interestingly, some members of the SUMOylation pathway were also found in the proximity proteomics analysis of SALL1 (Bozal-Basterra et al., 2018). In this alternative hypothetical scenario, once SUMOylated SALL1 promotes CBX4 stabilization impairing its ubiquitination, it would be able also to promote CBX4 SUMOylation by recruiting an E3 SUMO ligase or other components of the SUMOylation machinery (**Figure 8**, right). In this regard, the K224 residue involved in CBX4 SUMOylation, and the adjacent K209 and K247 residues were predicted as putative ubiquitination sites by UbPred.[5] This raises the interesting possibility that modification of CBX4 by ubiquitin and SUMO would be mutually exclusive events. Whether this is the case, and whether SALL1 is involved in this regulation, would require further investigation.

Additional experiments are necessary to further test the non-mutually exclusive hypotheses for SALL1-mediated regulation of CBX4. Our results suggest that SALL1 plays an important role in the control of the expression of key developmental genes through the post-transcriptional regulation of CBX4. Where and when this regulation takes place *in vivo* during development deserves further investigation.

DATA AVAILABILITY STATEMENT

The original contributions presented in the study are included in the article/**Supplementary Material**, further inquiries can be directed to the corresponding author/s.

AUTHOR CONTRIBUTIONS

IG, LP, JS, and RB designed the experiments and analyzed the data. IG, LP, JR, JS, and RB wrote the manuscript. IG, LP, VM, EL, CP, VL, EG-L, MG-L, and OB-G developed the experimental protocols, performed the experiments, and analyzed the data. ACOV, AA, JR, and MSR provided the scientific resources. All authors contributed to the article and approved the submitted version.

FUNDING

RB, MSR, ACOV, JS, and OB-G acknowledged funding by the grant 765445-EU (UbiCODE Program). RB acknowledged funding by grants BFU2017-84653-P (MINECO/FEDER, EU), SEV-2016-0644 (Severo Ochoa Excellence Program), SAF2017-90900-REDT (UBIRed Program), and IT1165-19 (Basque Country Government). Additional support was provided by the Department of Industry, Tourism, and Trade of the Basque Country Government (Elkartek Research Programs) and by the Innovation Technology Department of the Bizkaia County. AA acknowledged Centro de Investigación Biomédica en Red. Enfermedades Hepáticas y Digestivas (CIBERehd). RB, LP, ACOV, MSR and JS thank the UPStream consortium (ITN program PITN-GA-2011-290257, EU).

ACKNOWLEDGMENTS

We thank Laura Bozal-Basterra and Arkaitz Carracedo (CIC bioGUNE) for their help in data analysis.

[5]http://www.ubpred.org/

SUPPLEMENTARY MATERIAL

The Supplementary Material for this article can be found online at: https://www.frontiersin.org/articles/10.3389/fcell.2021.715868/full#supplementary-material

Supplementary Figure 1 | SALL1 localizes to nuclear bodies. Endogenous SALL1 **(A)** and transiently expressed SALL1-YFP **(B)** localize to nuclear bodies in U2OS cells. In contrast, YFP alone, used as a control, shows a homogenous distribution in the nucleus and cytoplasm **(C)**. Pictures were taken with an AxioD Fluorescent microscope using 100× objective. Scale bars indicate 5 μm.

Supplementary Figure 2 | Characterization of CBX4 and SALL1 nuclear bodies. **(A–D)** Endogenous CBX4 (green) does not colocalize with SUM2/3, SUMO1, nor PML bodies or with SC35 (magenta) in U2OS cells. **(E–I)** SALL1-YFP (green) partially colocalizes with endogenous SUMO1 (magenta) in U2OS cells **(E)**. Similar results were obtained for the SALL1ΔSUMO and SALL1DSIM mutants **(F,G)**. SALL1 does not colocalize with PML **(H)** nor with SC35 **(I)**. Green and magenta channels are shown independently in black and white. Nuclei were stained with DAPI (blue). White arrowheads indicate colocalization, green arrowheads indicate domains where mainly CBX4 **(A–D)** or SALL1 **(E–I)** proteins are present, magenta arrowheads indicate domains where mainly SUMO2 **(A)**, SUMO1 **(B,E–G)**, PML **(C,H)**, or SC35 **(D,I)** are present. Pictures were taken using a Leica DM IRE2 confocal microscope with a 63× objective, except for pictures in C that were taken using an AxioD Fluorescent microscope and objective 40×. Scale bars indicate 5 μm.

Supplementary Figure 3 | SALL1 SUMOylation sites and SIMs are conserved throughout evolution. **(A)** SALL1 schematic representation. Ovals represent the zinc fingers (ZF) distributed along the protein. Blue rectangle represents the poly-glutamine (PQ) domain. In magenta, SUMO consensus sites mutated in SALL1ΔSUMO and, in blue, predicted SIMs mutated in SALL1ΔSIM. **(B)** SALL1 fused to HA tag was SUMOylated in the presence (black circles) of bioSUMO3, transiently transfected in HEK 293FT cells. Asterisks indicate the modified SALL1 (SUMO-SALL1) that is shifted if compared with the size of non-modified SALL1 (arrowhead). Anti-tubulin staining was used as a loading control. Molecular weight markers are shown to the right in KDa. SALL1ΔSUMO fused to HA tag is not SUMOylated in presence of bioSUMO3. In the input the expression of WT and SUMO mutant of SALL1 are shown. **(C)** In magenta, SUMO consensus sites in SALL1 that were mutated in SALL1ΔSUMO and, in blue, the predicted SIMs of SALL1, mutated in SALL1ΔSIM mutant. **(D)** Evolutionary conservation of the SUMOylation and SIM sites in SALL1 homologs in the indicated species. Asterisks indicate identical residues; colons and semicolons indicate conservative and semi-conservative changes, respectively.

Supplementary Figure 4 | CBX4 and SALL1 localize to the nucleoplasm. Endogenous CBX4 **(A)** and endogenous SALL1 **(B)** shown in green localize to nuclear bodies in U2OS cells **(A′,B′)**. Increasing the intensity reveals the localization of both proteins in the nucleoplasm **(A″,B″)**. Single green channels are shown in black and white. Pictures were taken using a Leica DM IRE2 confocal microscope with a 63× objective.

Supplementary Figure 5 | SALL1 SUMOylation is independent of CBX4. *In vitro* SUMOylation of SALL1 with SUMO1 or SUMO2/3 in the presence of growing quantities of CBX4 (in μl). Wheat germ was added as negative control. The vertical bar indicates the SUMOylated forms of SALL1, the empty arrowhead indicates the unmodified SALL1. Molecular weight markers are shown to the right in KDa.

Supplementary Figure 6 | Variation of Polycomb bodies upon SALL1 expression. Representative composition of independent U2OS cells transfected with equal amounts of SALL1-YFP, SALL1ΔSUMO-YFP, or GFP-β-gal plasmids, stained for endogenous CBX4. Nuclei were labeled with DAPI (not shown). Pictures were taken using a Leica DM IRE2 confocal microscope with a 63× objective, using the same settings for all the conditions.

REFERENCES

Abedin, M. J., Imai, N., Rosenberg, M. E., and Gupta, S. (2011). Identification and characterization of Sall1-expressing cells present in the adult mouse kidney. *Nephron Exp. Nephrol.* 119, e75–e82. doi: 10.1159/000328925

Aillet, F., Lopitz-Otsoa, F., Hjerpe, R., Torres-Ramos, M., Lang, V., and Rodriguez, M. S. (2012). Isolation of ubiquitylated proteins using tandem ubiquitin-binding entities. *Methods Mol. Biol.* 832, 173–183. doi: 10.1007/978-1-61779-474-2_12

Akimov, V., Barrio-Hernandez, I., Hansen, S. V. F., Hallenborg, P., Pedersen, A. K., Bekker-Jensen, D. B., et al. (2018). UbiSite approach for comprehensive mapping of lysine and N-terminal ubiquitination sites. *Nat. Struct. Mol. Biol.* 25, 631–640. doi: 10.1038/s41594-018-0084-y

Beauclair, G., Bridier-Nahmias, A., Zagury, J. F., Saib, A., and Zamborlini, A. (2015). JASSA: a comprehensive tool for prediction of SUMOylation sites and SIMs. *Bioinformatics* 31, 3483–3491. doi: 10.1093/bioinformatics/btv403

Borozdin, W., Steinmann, K., Albrecht, B., Bottani, A., Devriendt, K., Leipoldt, M., et al. (2006). Detection of heterozygousSALL1 deletions by quantitative real time PCR proves the contribution of aSALL1 dosage effect in the pathogenesis of Townes-Brocks syndrome. *Hum. Mutat.* 27, 211–212. doi: 10.1002/humu.9396

Bozal-Basterra, L., Gonzalez-Santamarta, M., Muratore, V., Bermejo-Arteagabeitia, A., Da Fonseca, C., Barroso-Gomila, O., et al. (2020). LUZP1, a novel regulator of primary cilia and the actin cytoskeleton, is a contributing factor in Townes-Brocks syndrome. *eLife* 9:e55957. doi: 10.7554/eLife.55957

Bozal-Basterra, L., Martín-Ruíz, I., Pirone, L., Liang, Y., Sigurðsson, J. O., Gonzalez-Santamarta, M., et al. (2018). Truncated SALL1 impedes primary cilia function in Townes-Brocks syndrome. *Am. J. Hum. Genet.* 102, 249–265. doi: 10.1016/j.ajhg.2017.12.017

Buck, A., Archangelo, L., Dixkens, C., and Kohlhase, J. (2000). Molecular cloning, chromosomal localization, and expression of the murine SALL1 ortholog Sall1. *Cytogenet. Genome Res.* 89, 150–153. doi: 10.1159/000015598

Casanova, J. (1989). Mutations in the *spalt* gene of *Drosophila* cause ectopic expression of Ultrabithorax and Sex combs reduced. *Rouxs Arch. Dev. Biol.* 198, 137–140. doi: 10.1007/BF02438938

Chen, Q., Huang, L., Pan, D., Zhu, L. J., and Wang, Y.-X. (2018). Cbx4 sumoylates Prdm16 to regulate adipose tissue thermogenesis. *Cell Rep.* 22, 2860–2872. doi: 10.1016/j.celrep.2018.02.057

Cheng, B., Ren, X., and Kerppola, T. K. (2014). KAP1 represses differentiation-inducible genes in embryonic stem cells through cooperative binding with PRC1 and derepresses pluripotency-associated genes. *Mol. Cell. Biol.* 34, 2075–2091. doi: 10.1128/MCB.01729-13

Cheutin, T., and Cavalli, G. (2012). Progressive polycomb assembly on H3K27me3 compartments generates polycomb bodies with developmentally regulated motion. *PLoS Genet.* 8:e1002465. doi: 10.1371/journal.pgen.1002465

Cheutin, T., and Cavalli, G. (2018). Loss of PRC1 induces higher-order opening of Hox loci independently of transcription during *Drosophila* embryogenesis. *Nat. Commun.* 9:3898. doi: 10.1038/s41467-018-05945-4

de Celis, J. F., and Barrio, R. (2009). Regulation and function of *spalt* proteins during animal development. *Int. J. Dev. Biol.* 53, 1385–1398. doi: 10.1387/ijdb.072408jd

Entrevan, M., Schuettengruber, B., and Cavalli, G. (2016). Regulation of genome architecture and function by polycomb proteins. *Trends Cell Biol.* 26, 511–525. doi: 10.1016/j.tcb.2016.04.009

Franco, M., Seyfried, N. T., Brand, A. H., Peng, J., and Mayor, U. (2011). A novel strategy to isolate ubiquitin conjugates reveals wide role for ubiquitination during neural development. *Mol. Cell. Proteomics* 10:M110.002188. doi: 10.1074/mcp.M110.002188

Galisson, F., Mahrouche, L., Courcelles, M., Bonneil, E., Meloche, S., Chelbi-Alix, M. K., et al. (2011). A novel proteomics approach to identify SUMOylated proteins and their modification sites in human cells. *Mol. Cell. Proteomics* 10:M110.004796. doi: 10.1074/mcp.M110.004796

Golebiowski, F., Matic, I., Tatham, M. H., Cole, C., Yin, Y., Nakamura, A., et al. (2009). System-wide changes to SUMO modifications in response to heat shock. *Sci. Signal.* 2:ra24. doi: 10.1126/scisignal.2000282

Gonzalez, I., Mateos-Langerak, J., Thomas, A., Cheutin, T., and Cavalli, G. (2014). Identification of regulators of the three-dimensional polycomb organization by a microscopy-based genome-wide RNAi screen. *Mol. Cell* 54, 485–499. doi: 10.1016/j.molcel.2014.03.004

Gullberg, M., Gustafsdottir, S. M., Schallmeiner, E., Jarvius, J., Bjarnegard, M., Betsholtz, C., et al. (2004). Cytokine detection by antibody-based proximity ligation. *Proc. Natl. Acad. Sci. U.S.A.* 101, 8420–8424. doi: 10.1073/pnas.0400552101

Hendriks, I. A., D'Souza, R. C., Chang, J.-G., Mann, M., and Vertegaal, A. C. O. (2015). System-wide identification of wild-type SUMO-2 conjugation sites. *Nat. Commun.* 6:7289. doi: 10.1038/ncomms8289

Hendriks, I. A., D'Souza, R. C. J., Yang, B., Verlaan-de Vries, M., Mann, M., and Vertegaal, A. C. O. (2014). Uncovering global SUMOylation signaling networks in a site-specific manner. *Nat. Struct. Mol. Biol.* 21, 927–936. doi: 10.1038/nsmb.2890

Hendriks, I. A., and Vertegaal, A. C. (2016). A comprehensive compilation of SUMO proteomics. *Nat. Rev. Mol. Cell Biol.* 17, 581–595. doi: 10.1038/nrm.2016.81

Hjerpe, R., Aillet, F., Lopitz-Otsoa, F., Lang, V., England, P., and Rodriguez, M. S. (2009). Efficient protection and isolation of ubiquitylated proteins using tandem ubiquitin-binding entities. *EMBO Rep.* 10, 1250–1258. doi: 10.1038/embor.2009.192

Ismail, I. H., Gagné, J.-P., Caron, M.-C., McDonald, D., Xu, Z., Masson, J.-Y., et al. (2012). CBX4-mediated SUMO modification regulates BMI1 recruitment at sites of DNA damage. *Nucleic Acids Res.* 40, 5497–5510. doi: 10.1093/nar/gks222

Kagey, M. H., Melhuish, T. A., and Wotton, D. (2003). The polycomb protein Pc2 is a SUMO E3. *Cell* 113, 127–137. doi: 10.1016/s0092-8674(03)00159-4

Kang, X., Qi, Y., Zuo, Y., Wang, Q., Zou, Y., Schwartz, R. J., et al. (2010). SUMO-specific protease 2 is essential for suppression of polycomb group protein-mediated gene silencing during embryonic development. *Mol. Cell* 38, 191–201. doi: 10.1016/j.molcel.2010.03.005

Kiefer, S. M., McDill, B. W., Yang, J., and Rauchman, M. (2002). Murine Sall1 represses transcription by recruiting a histone deacetylase complex. *J. Biol. Chem.* 277, 14869–14876. doi: 10.1074/jbc.M200052200

Klauke, K., Radulovic, V., Broekhuis, M., Weersing, E., Zwart, E., Olthof, S., et al. (2013). Polycomb Cbx family members mediate the balance between haematopoietic stem cell self-renewal and differentiation. *Nat. Cell Biol.* 15, 353–362. doi: 10.1038/ncb2701

Kohlhase, J. (1993). "Townes-Brocks syndrome," in *GeneReviews((R))*, eds M. P. Adam, H. H. Ardinger, R. A. Pagon, S. E. Wallace, L. J. H. Bean, G. Mirzaa, et al. (Seattle, WA: University of Washington).

Kohlhase, J., Wischermann, A., Reichenbach, H., Froster, U., and Engel, W. (1998). Mutations in the SALL1 putative transcription factor gene cause Townes-Brocks syndrome. *Nat. Genet.* 18, 81–83. doi: 10.1038/ng0198-81

Lamoliatte, F., Caron, D., Durette, C., Mahrouche, L., Maroui, M. A., Caron-Lizotte, O., et al. (2014). Large-scale analysis of lysine SUMOylation by SUMO remnant immunoaffinity profiling. *Nat. Commun.* 5:5409. doi: 10.1038/ncomms6409

Landecker, H. L., Sinclair, D. A., and Brock, H. W. (1994). Screen for enhancers of Polycomb and Polycomblike in *Drosophila melanogaster*. *Dev. Genet.* 15, 425–434. doi: 10.1002/dvg.1020150505

Lauberth, S. M., and Rauchman, M. (2006). A conserved 12-amino acid motif in Sall1 recruits the nucleosome remodeling and deacetylase corepressor complex. *J. Biol. Chem.* 281, 23922–23931. doi: 10.1074/jbc.M513461200

Li, B., Zhou, J., Liu, P., Hu, J., Jin, H., Shimono, Y., et al. (2007). Polycomb protein Cbx4 promotes SUMO modification of de novo DNA methyltransferase Dnmt3a. *Biochem. J.* 405, 369–378. doi: 10.1042/BJ20061873

Livak, K. J., and Schmittgen, T. D. (2001). Analysis of relative gene expression data using real-time quantitative PCR and the 2(-Delta Delta C(T)) method. *Methods* 25, 402–408. doi: 10.1006/meth.2001.1262

MacPherson, M. J., Beatty, L. G., Zhou, W., Du, M., and Sadowski, P. D. (2009). The CTCF insulator protein is posttranslationally modified by SUMO. *Mol. Cell. Biol.* 29, 714–725. doi: 10.1128/MCB.00825-08

Mardaryev, A. N., Liu, B., Rapisarda, V., Poterlowicz, K., Malashchuk, I., Rudolf, J., et al. (2016). Cbx4 maintains the epithelial lineage identity and cell proliferation in the developing stratified epithelium. *J. Cell Biol.* 212, 77–89. doi: 10.1083/jcb.201506065

Matic, I., Schimmel, J., Hendriks, I. A., van Santen, M. A., van de Rijke, F., van Dam, H., et al. (2010). Site-specific identification of SUMO-2 targets in cells reveals an inverted SUMOylation motif and a hydrophobic cluster SUMOylation motif. *Mol. Cell* 39, 641–652. doi: 10.1016/j.molcel.2010.07.026

Merrill, J. C., Melhuish, T. A., Kagey, M. H., Yang, S.-H., Sharrocks, A. D., and Wotton, D. (2010). A role for non-covalent SUMO interaction motifs in Pc2/CBX4 E3 activity. *PLoS One* 5:e8794. doi: 10.1371/journal.pone.0008794

Mertins, P., Qiao, J. W., Patel, J., Udeshi, N. D., Clauser, K. R., Mani, D. R., et al. (2013). Integrated proteomic analysis of post-translational modifications by serial enrichment. *Nat. Methods* 10, 634–637. doi: 10.1038/nmeth.2518

Netzer, C., Bohlander, S. K., Rieger, L., Müller, S., and Kohlhase, J. (2002). Interaction of the developmental regulator SALL1 with UBE2I and SUMO-1. *Biochem. Biophys. Res. Commun.* 296, 870–876. doi: 10.1016/s0006-291x(02)02003-x

Netzer, C., Rieger, L., Brero, A., Zhang, C. D., Hinzke, M., Kohlhase, J., et al. (2001). SALL1, the gene mutated in Townes-Brocks syndrome, encodes a transcriptional repressor which interacts with TRF1/PIN2 and localizes to pericentromeric heterochromatin. *Hum. Mol. Genet.* 10, 3017–3024. doi: 10.1093/hmg/10.26.3017

Ning, B., Zhao, W., Qian, C., Liu, P., Li, Q., Li, W., et al. (2017). USP26 functions as a negative regulator of cellular reprogramming by stabilising PRC1 complex components. *Nat. Commun.* 8:349. doi: 10.1038/s41467-017-00301-4

Pelisch, F., Pozzi, B., Risso, G., Muñoz, M. J., and Srebrow, A. (2012). DNA damage-induced heterogeneous nuclear ribonucleoprotein K SUMOylation regulates p53 transcriptional activation. *J. Biol. Chem.* 287, 30789–30799. doi: 10.1074/jbc.M112.390120

Pirone, L., Xolalpa, W., Mayor, U., Barrio, R., and Sutherland, J. D. (2016). Analysis of SUMOylated proteins in cells and in vivo using the bioSUMO strategy. *Methods Mol. Biol.* 1475, 161–169. doi: 10.1007/978-1-4939-6358-4_12

Pirone, L., Xolalpa, W., Sigurðsson, J. O., Ramirez, J., Pérez, C., González, M., et al. (2017). A comprehensive platform for the analysis of ubiquitin-like protein modifications using in vivo biotinylation. *Sci. Rep.* 7:40756. doi: 10.1038/srep40756

Povlsen, L. K., Beli, P., Wagner, S. A., Poulsen, S. L., Sylvestersen, K. B., Poulsen, J. W., et al. (2012). Systems-wide analysis of ubiquitylation dynamics reveals a key role for PAF15 ubiquitylation in DNA-damage bypass. *Nat. Cell Biol.* 14, 1089–1098. doi: 10.1038/ncb2579

Ren, X., Hu, B., Song, M., Ding, Z., Dang, Y., Liu, Z., et al. (2019). Maintenance of nucleolar homeostasis by CBX4 alleviates senescence and osteoarthritis. *Cell Rep.* 26, 3643–3656.e7. doi: 10.1016/j.celrep.2019.02.088

Roux, K. J., Kim, D. I., and Burke, B. (2013). BioID: a screen for protein-protein interactions. *Curr. Protoc. Protein Sci.* 74, 19.23.1–19.23.14. doi: 10.1002/0471140864.ps1923s74

Sánchez, J., Talamillo, A., González, M., Sánchez-Pulido, L., Jiménez, S., Pirone, L., et al. (2011). *Drosophila* Sal and Salr are transcriptional repressors. *Biochem. J.* 438, 437–445. doi: 10.1042/BJ20110229

Sánchez, J., Talamillo, A., Lopitz-Otsoa, F., Pérez, C., Hjerpe, R., Sutherland, J. D., et al. (2010). Sumoylation modulates the activity of *spalt*-like proteins during wing development in *Drosophila*. *J. Biol. Chem.* 285, 25841–25849. doi: 10.1074/jbc.M110.124024

Saurin, A. J., Shiels, C., Williamson, J., Satijn, D. P., Otte, A. P., Sheer, D., et al. (1998). The human polycomb group complex associates with pericentromeric heterochromatin to form a novel nuclear domain. *J. Cell Biol.* 142, 887–898. doi: 10.1083/jcb.142.4.887

Schimmel, J., Eifler, K., Sigurðsson, J. O., Cuijpers, S. A. G., Hendriks, I. A., Verlaan-de Vries, M., et al. (2014). Uncovering SUMOylation dynamics during cell-cycle progression reveals FoxM1 as a key mitotic SUMO target protein. *Mol. Cell* 53, 1053–1066. doi: 10.1016/j.molcel.2014.02.001

Schuettengruber, B., Bourbon, H.-M., Di Croce, L., and Cavalli, G. (2017). Genome regulation by polycomb and trithorax: 70 years and counting. *Cell* 171, 34–57. doi: 10.1016/j.cell.2017.08.002

Söderberg, O., Gullberg, M., Jarvius, M., Ridderstråle, K., Leuchowius, K.-J., Jarvius, J., et al. (2006). Direct observation of individual endogenous protein complexes in situ by proximity ligation. *Nat. Methods* 3, 995–1000. doi: 10.1038/nmeth947

Soria-Bretones, I., Cepeda-García, C., Checa-Rodriguez, C., Heyer, V., Reina-San-Martin, B., Soutoglou, E., et al. (2017). DNA end resection requires constitutive

sumoylation of CtIP by CBX4. *Nat. Commun.* 8:113. doi: 10.1038/s41467-017-00183-6

Soshnikova, N. (2014). Hox genes regulation in vertebrates. *Dev. Dyn.* 243, 49–58. doi: 10.1002/dvdy.24014

Sweetman, D., Smith, T., Farrell, E. R., Chantry, A., and Munsterberg, A. (2003). The conserved glutamine-rich region of chick Csal1 and Csal3 mediates protein interactions with other spalt family members. Implications for Townes-Brocks syndrome. *J. Biol. Chem.* 278, 6560–6566. doi: 10.1074/jbc.M209066200

Tammsalu, T., Matic, I., Jaffray, E. G., Ibrahim, A. F. M., Tatham, M. H., and Hay, R. T. (2014). Proteome-wide identification of SUMO2 modification sites. *Sci. Signal.* 7:rs2. doi: 10.1126/scisignal.2005146

Udeshi, N. D., Svinkina, T., Mertins, P., Kuhn, E., Mani, D. R., Qiao, J. W., et al. (2013). Refined preparation and use of anti-diglycine remnant (K-epsilon-GG) antibody enables routine quantification of 10,000s of ubiquitination sites in single proteomics experiments. *Mol. Cell. Proteomics* 12, 825–831. doi: 10.1074/mcp.O112.027094

Wang, X., Li, L., Wu, Y., Zhang, R., Zhang, M., Liao, D., et al. (2016). CBX4 suppresses metastasis via recruitment of HDAC3 to the Runx2 promoter in colorectal carcinoma. *Cancer Res.* 76, 7277–7289. doi: 10.1158/0008-5472.CAN-16-2100

Wang, X., Qin, G., Liang, X., Wang, W., Wang, Z., Liao, D., et al. (2020). Targeting the CK1α/CBX4 axis for metastasis in osteosarcoma. *Nat. Commun.* 11:1141. doi: 10.1038/s41467-020-14870-4

Wotton, D., and Merrill, J. C. (2007). Pc2 and SUMOylation. *Biochem. Soc. Trans.* 35(Pt 6), 1401–1404. doi: 10.1042/BST0351401

Xiao, Z., Chang, J.-G., Hendriks, I. A., Sigurðsson, J. O., Olsen, J. V., and Vertegaal, A. C. O. (2015). System-wide analysis of SUMOylation dynamics in response to replication stress reveals novel small ubiquitin-like modified target proteins and acceptor lysines relevant for genome stability. *Mol. Cell. Proteomics* 14, 1419–1434. doi: 10.1074/mcp.O114.044792

Zhao, Q., Xie, Y., Zheng, Y., Jiang, S., Liu, W., Mu, W., et al. (2014). GPS-SUMO: a tool for the prediction of sumoylation sites and SUMO-interaction motifs. *Nucleic Acids Res.* 42, W325–W330. doi: 10.1093/nar/gku383

Zidovska, A. (2020). The rich inner life of the cell nucleus: dynamic organization, active flows, and emergent rheology. *Biophys. Rev.* 12, 1093–1106. doi: 10.1007/s12551-020-00761-x

Conflict of Interest: VL is employed by the company Viralgen Vector Core.

The remaining authors declare that the research was conducted in the absence of any commercial or financial relationships that could be construed as a potential conflict of interest.

Publisher's Note: All claims expressed in this article are solely those of the authors and do not necessarily represent those of their affiliated organizations, or those of the publisher, the editors and the reviewers. Any product that may be evaluated in this article, or claim that may be made by its manufacturer, is not guaranteed or endorsed by the publisher.

frontiers in Cell and Developmental Biology

REVIEW
published: 15 October 2021
doi: 10.3389/fcell.2021.750534

Muscle Satellite Cell Heterogeneity: Does Embryonic Origin Matter?

*Lara Rodriguez-Outeiriño[1,2], Francisco Hernandez-Torres[2,3], F. Ramírez-de Acuña[1,2], Lidia Matías-Valiente[1,2], Cristina Sanchez-Fernandez[1,2], Diego Franco[1,2] and Amelia Eva Aranega[1,2]**

[1] Department of Experimental Biology, Faculty of Experimental Sciences, University of Jaén, Jaén, Spain, [2] Medina Foundation, Technology Park of Health Sciences, Granada, Spain, [3] Department of Biochemistry and Molecular Biology III and Immunology, Faculty of Medicine, University of Granada, Granada, Spain

Muscle regeneration is an important homeostatic process of adult skeletal muscle that recapitulates many aspects of embryonic myogenesis. Satellite cells (SCs) are the main muscle stem cells responsible for skeletal muscle regeneration. SCs reside between the myofiber basal lamina and the sarcolemma of the muscle fiber in a quiescent state. However, in response to physiological stimuli or muscle trauma, activated SCs transiently re-enter the cell cycle to proliferate and subsequently exit the cell cycle to differentiate or self-renew. Recent evidence has stated that SCs display functional heterogeneity linked to regenerative capability with an undifferentiated subgroup that is more prone to self-renewal, as well as committed progenitor cells ready for myogenic differentiation. Several lineage tracing studies suggest that such SC heterogeneity could be associated with different embryonic origins. Although it has been established that SCs are derived from the central dermomyotome, how a small subpopulation of the SCs progeny maintain their stem cell identity while most progress through the myogenic program to construct myofibers is not well understood. In this review, we synthesize the works supporting the different developmental origins of SCs as the genesis of their functional heterogeneity.

Keywords: myogenic precursor cells, embryonic myogenesis, adult myogenesis, satellite cell heterogeneity, muscle regeneration

OPEN ACCESS

Edited by:
Sofia J. Araújo, University of Barcelona, Spain

Reviewed by:
So-ichiro Fukada, Osaka University, Japan
Atsushi Asakura, University of Minnesota Twin Cities, United States

****Correspondence:***
Amelia Eva Aranega
aaranega@ujaen.es

Specialty section:
This article was submitted to Morphogenesis and Patterning, a section of the journal Frontiers in Cell and Developmental Biology

Received: *30 July 2021*
Accepted: *27 September 2021*
Published: *15 October 2021*

Citation:
Rodriguez-Outeiriño L, Hernandez-Torres F, Ramírez-de Acuña F, Matías-Valiente L, Sanchez-Fernandez C, Franco D and Aranega AE (2021) Muscle Satellite Cell Heterogeneity: Does Embryonic Origin Matter? Front. Cell Dev. Biol. 9:750534. doi: 10.3389/fcell.2021.750534

INTRODUCTION

Muscle repair and homeostasis are mediated by resident stem cells, also called SCs. Anatomically, SCs are located between the myofiber basal lamina and the sarcolemma of the muscle fiber and functionally are quiescent cells. Quiescent SCs are characterized by the expression of the transcription factor Pax7 but, upon acute injury, pathological conditions or muscle homeostasis, they become activated and give rise to myogenic progenitors that massively proliferate, start to express the myogenic regulatory factors (MRFs) Myf5, Myod1, Myf6 (also known as MRF4), and Myog, differentiate and fuse to form new myofibers and restore the muscle tissue. Classically, SCs have been considered a homogeneous population of muscle stem cells. However, a deeper molecular characterization together with grafting experiments have revealed a certain level of SCs heterogeneity in terms of the expression of specific markers and cellular functionality that determine their regenerative potential. It is well known that SCs and developmental myogenic progenitors share the transcriptional program that drives myogenic differentiation and muscle

genesis. Several lineage tracing studies have established that SCs originate from myogenic precursors in the dermomyotome. Nevertheless, behavioral heterogeneity has also been observed in myogenic precursors during development, given the differences in proliferative rate observed in dermomyotome-derived progenitors during embryonic myogenesis and MRF expression patterns in fetal and perinatal stages, despite their functional redundancy (Gros et al., 2005; Kassar-Duchossoy et al., 2005; Picard and Marcelle, 2013). Therefore, developmental myogenesis could provide us with an appropriate scenario to better understand satellite heterogeneity.

In this review, we summarize the latest research evidence on SC functional heterogeneity and examine the principles that sustain myogenic progenitor pool diversity of SCs of somitic origin and the implications for the emergence of SC heterogeneity.

SATELLITE CELLS IN THE CONTEXT OF ADULT MYOGENESIS

Skeletal muscle is a heterogeneous tissue that represents one-third of human body mass with a high capability of regeneration throughout life (Janssen et al., 2000). This ability resides mainly in *bona fide* muscle stem cells, SCs, described by electron microscopy in Mauro (1961). The SC population represents a quiescent cell population between the basal lamina and the myofiber plasma membrane and is characterized by the expression of the paired box transcription factor Pax7 (Seale et al., 2000). Although SCs uniformly express Pax7, the role of this gene in the context of muscle stem cell biology has been largely controversial (Oustanina et al., 2004). Therefore, research by Lepper et al. (2009) that conditionally inactivates Pax7 gene expression in adult SCs in the mouse shows that Pax7 could be dispensable for proper muscle stem cell function and muscle regeneration in adult skeletal muscle and is only required for myogenic function during the perinatal period. In contrast, subsequent studies, carried out by using similar mouse models, have demonstrated that Pax7 plays an essential role in regulating the myogenic potential and function of satellite cells in both neonatal and adult skeletal muscle, challenged the efficiency for Pax7 deletion in Lepper's study (Günther et al., 2013; von Maltzahn et al., 2013). Nonetheless, full ablation of Pax7 positive cells in adult mice confirmed that Pax7-expressing cells are essential for acute injury-induced muscle regeneration (Lepper et al., 2011; Sambasivan et al., 2011). In addition, more recent studies have highlighted that SCs are the main stem cell source for muscle regeneration (von Maltzahn et al., 2013).

Upon muscle injury, disease, or adult skeletal muscle homeostasis, SCs are activated to achieve appropriate muscle repair. During this process, an embryonic myogenic transcriptional program is recapitulated (Hernandez-Torres et al., 2017). Pax7 is downregulated and the Myogenic Regulatory Factors (MRFs), members of the basic-helix-loop-helix family, are sequentially upregulated to directly activate SCs toward the myogenic differentiation program and eventual fusion to existing myofibers or to form new myofibers (Weintraub et al., 1991). Myf5 is the first MRF that becomes upregulated in SCs, followed by Myod1, which indicates the myogenic commitment to myoblasts (Rudnicki et al., 1992, 1993). The terminal differentiation to myocyte is regulated by the expression of MRF Myog (Venuti et al., 1995). Along with this myogenic specification, reciprocal inhibition between Pax7 and the MRFs' Myod1 and Myog is required for an accurate differentiation (Olguin et al., 2007).

In the framework of SC activation, it is interesting to note that cell proliferation takes place through symmetric or asymmetric division. In symmetric division, two identical daughter cells (Pax7 +) are formed, maintaining the SC pool in adult skeletal muscle. Meanwhile, asymmetric division gives rise to both committed (Pax7 + /Myf5 + /Myod1 +) and stem cell (Pax7+) progeny. Committed SC Pax7−/Myf5 + /Myod1 + can also undergo symmetrical division to increase the number of myogenic precursors during muscle regeneration (Motohashi and Asakura, 2014; Feige et al., 2018). A correct balance between symmetric and asymmetric SC division is needed to keep the SC pool together and successfully complete muscle repair throughout life. In some muscle disorders such as Duchenne Muscle Dystrophy (DMD), a decreased asymmetric division leads to a lack of myogenic progenitors and, therefore, to inappropriate muscle homeostasis and flawed regeneration (Dumont et al., 2015). A full understanding of the regulation of the different pathways of SC activation and the mechanism underlying muscle stem cell division decisions helps us to better understand SC biology and function in the context of muscle repair and disease.

BEHAVIORAL HETEROGENEITY IN THE SATELLITE CELL POPULATION

The process by which SCs emerge from their quiescent status and enter the myogenic program is well established; however, several studies have highlighted the existence of different SC responses related to their performance during the muscle repair process (Tierney and Sacco, 2016; Cornelison, 2018). In this section, we examine the different behaviors of SCs and identify different SC subpopulations during their activation and myogenic differentiation in the course of regeneration.

Different responses associated with their proliferative capabilities have been identified in the onset of SC activation. An initial study to analyze the cycle time for SCs *in vivo*, revealed that SCs are a mixture of cell populations comprising 80% fast-dividing cells, mainly responsible for providing myonuclei to growing fibers, and 20% slow-dividing cells (**Figure 1**). The slowest proliferative subpopulation was designed as "reserve cells" as they are likely to undergo asymmetric division and thus produce stem-like cells that maintain the SC pool (Schultz, 1996). According to these observations, a study of *in vitro* myogenic differentiation of fresh isolated SCs performed by Ono et al. (2012) also discriminated a minor subpopulation of activated and undifferentiated SCs from fast-dividing cells that divides more slowly and displays a long-term self-renewal ability, after their passage tended to immediately differentiate

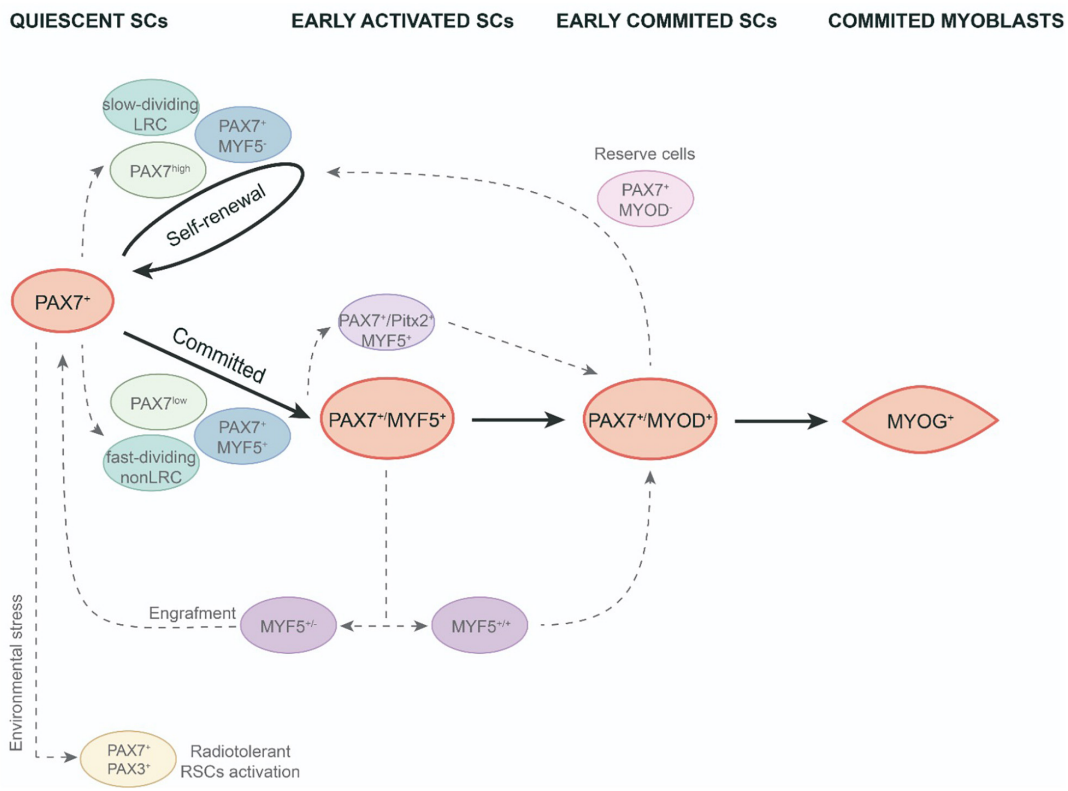

FIGURE 1 | Functional heterogeneity in adult satellite cell population. SCs activation and myogenic differentiation during adult muscle regeneration (black arrows). SC heterogeneity in the course of quiescence, early activation and early commitment of adult SCs (discontinued gray arrows). LRC, label-retaining cells; non-LRC, non-label-retaining cells; RSCs, reserve stem cells; SCs, satellite cells.

without producing any additional proliferative progeny. The undifferentiated very slow-dividing SC subpopulation was characterized by a higher expression of Id1 protein, an inhibitor of myogenic differentiation (Ono et al., 2012). Interestingly, when slow-dividing SCs were transplanted, they also produced regenerating myofibers *in vivo* (Ono et al., 2012). These authors interpreted that, in a regenerative scenario, slow-dividing cells have a preferential effect for engraftment.

As observed above, asymmetric division allows to preserve the pool of SCs for any required future regeneration as one of the two daughter cells maintains its stem cell status. In this context, Shinin et al. (2006) revealed a non-random process of DNA segregation during asymmetric division, in which the cell that retains the old DNA template expresses the quiescent SC marker Pax7. This observation connects with the hypothesis of the immortal DNA strand proposed by Cairns et al., which supports stem cells that segregate the original DNA and reduces accumulated DNA replication errors in the tissue (Cairns, 1975). Thus, non-random DNA segregation of some SCs could give rise to a subpopulation with a robust stem-cell status. Regarding these findings, using transgenic Tg:Pax7-nGFP mice, Rocheteau et al. (2012) showed that quiescent SCs display different levels of Pax7 expression linked to different stemness properties. Thus, the Pax7^{high} subpopulation is more prone to asymmetric DNA segregation, retaining the old DNA strand, and exhibiting a low metabolic status as dormant adult SCs (Rocheteau et al., 2012). Nevertheless, this dormant state is reversible as, after several transplantations, the Pax7^{high} subpopulation was able to give rise to both Pax7^{high} and Pax7^{low} SCs and thus allow proper muscle repair (Rocheteau et al., 2012; **Figure 1**).

To study these different SC proliferative dynamics, Chakkalakal et al. (2014) used a TetO-H2B-GFP reporter. They found that approx. 30% of SCs retained the H2B-GFP label (LRCs), whereas the vast majority lost it (non-LRCs). Both cell populations are formed at birth and during the juvenile period they set up as different populations with divergent behaviors that will persist throughout adult life. LRCs were less differentiated and, when transplanted, showed similar properties to stem cells, generating self-renewal and differentiated cells. Meanwhile, non-LRCs only undergo myogenic differentiation (**Figure 1**). They found that the CIP/KIP family members p21cip1 (Cdkn1a) and p27kip1 (Cdkn1b) were responsible for maintaining these LRCs at the stemness stage (Chakkalakal et al., 2014). Together, these findings indicate the existence of a less common subpopulation of SCs with a greater stem-cell status. These cells are preferably in a dormant status, less prone to proliferate but, once activated, they undergo asymmetric division with non-random DNA strand segregation. So, after cell transplantation, they can produce both progenies, the stem cells and the myogenic committed cells. Consequently, it has been postulated that this subpopulation

could be the true muscle stem cells responsible for maintaining SC populations long-term throughout life.

To elucidate the mechanism underlying the diverse pattern of activations in different SC populations, using an Myf5$^{nlacZ/+}$ mouse line, Zammit et al. identified the main SC subpopulation expressing both the stem cell marker CD34 and also the Myf5 transcription factor, thus revealing that quiescent SCs are committed to myogenesis. Yet, a minor subpopulation CD34-/Myf5- maintains the committed-lineage population (Beauchamp et al., 2000). To investigate the impact of Myf5 expression on different SC populations, Gayraud-Morel et al. (2012) studied the transcriptome and functional behavior of SC heterozygous for Myf5 in mice. They showed that Myf5 ± SCs were transcriptionally committed to myogenic differentiation, as demonstrated by the higher expression levels for some differentiation genes such as Myod1, Myog, and/or contractile protein genes. Interestingly, this heterozygous Myf5 SC population displays a high Tie2 expression, a marker for SC self-renewal. In addition, when they analyzed the functional behavior of this SC population, they found that Myf5 ± similarly contributes to muscle regeneration after an injury compared to wild type. Moreover, Myf5 ± cells more efficiently replenish the SC niche and, after a second injury, were capable of contributing to new myofiber formation (Gayraud-Morel et al., 2012; **Figure 1**). These findings highlight the relevance of Myf5 expression levels in functional heterogeneity in early committed SCs.

Satellite cell heterogeneous behavior has been also observed during the early *in vitro* differentiation process of activated SCs. *In vitro* experiments in the C2C12 cell line and freshly isolated myofibers from EDL found an SC subpopulation of reserve-like cells in activated progenitors that also expressed MRF Myod1 (Yoshida et al., 1998; Zammit et al., 2004). When kept in culture, Pax7 + /Myod1 + cells mostly downregulate Pax7 and differentiate into myotubes, however, a minor subset of this cell population downregulated Myod1 and remained in cell culture as Pax7 + /Myod1- reserve cells (**Figure 1**). This subpopulation can re-enter the cell cycle, upregulate Myod1 and give rise to either myogenic committed cells (Myod1 + /Myog +) or new reserve cells (Pax7 + /Myod1-) (Yoshida et al., 1998; Zammit et al., 2004). These research studies highlight the fact that a subpopulation of committed progenitors can revert to quiescence to maintain self-renewal of the muscle stem cell pool. Besides, it has been shown that satellite cell–derived myoblasts isolated from adult mice lacking the *MyoD* gene (*MyoD*$^{-/-}$) exhibit a high resistance to apoptosis through microRNA (miRNA)-mediated down-regulation of Pax3; as well as a significantly higher engraftment rate after intramuscular transplantation (Asakura et al., 2007; Hirai et al., 2010). In addition, a subset of SCs in the adult muscle also express the transcription factor Pitx2 and *in vitro* gain and loss of function experiments indicate that Pitx2 has an effect expanding SC-derived myogenic committed population (Vallejo et al., 2018; **Figure 1**). Finally, it is interesting to note that proximity to the blood vessels it has been associated with SC self-renewal (Verma et al., 2018).

In terms of the gene expression profile, intriguingly, another subset of SCs also expresses Pax3 (a paralog of Pax7) in some muscles (Relaix et al., 2006). Importantly, it has recently been stated that Pax3 + /Pax7 + SCs can play specific roles under environmental stimulus. Hence, Pax7 + /Pax3 + SC subpopulations demonstrate different behaviors when submitted to radiation stress or environmental pollutants (der Vartanian et al., 2019; Scaramozza et al., 2019). By utilizing Mx1-Cre transgenic reporter mice, which allow to trace resident stem cells in most adult tissues, Scaramozza et al. (2019) showed that freshly isolated Mx1 + SCs and Mx1 − SCs exhibited similar Pax7 expression levels but only Mx1 + SCs were enriched for Pax3. The Mx1 + /Pax7 + /Pax3 + SCs displayed reduced levels of reactive oxygen species (ROS) in both basal conditions and after irradiation. Due to their relatively low abundance and consistent with reserve stem cell (RSC) characteristics, these cells possess important stem cell activity upon transplantation but only make a slight contribution to muscle repair. Conversely, an extensive clonal expansion of Mx1 + /Pax7 + /Pax3 + SCs allows extensive muscle repair as well as niche repopulations upon selective pressure of radiation stress. However, the lack of Pax3 in these cells increased ROS components and diminished cell survival and stress tolerance. These findings show that a discrete subpopulation of radiotolerant RSCs of SCs undergo clonal expansion under severe stress (Scaramozza et al., 2019; **Figure 1**). In the same line, der Vartanian et al. (2019) have shown a bimodal response to environmental stress for SC subpopulations. Therefore, the exposure to a ubiquitous and highly toxic pollutant (2,3,7,8-tetrachlorodibenzo-p-dioxin; TCDD) leads to a specific loss of PAX3- MuSCs in adult skeletal muscle, whereas PAX3 + MuSCs are preserved. Nevertheless, PAX3-positive MuSCs become sensitized to environmental stress when the PAX3 function is lost and PAX3-mediated induction of mTORC1 is required for protection (der Vartanian et al., 2019). All these data highlight a functional heterogeneity of SCs related to their response to environmental stress controlled by PAX3.

It is interesting to note that, since SC functional heterogeneity in adult muscles is substantively based on the variability of their cell proliferation and the expression of different myogenic specification and/or determination genes, developmental myogenesis could offer the potential to understand this diversification behavior in the SC compartment.

EMBRYONIC MYOGENESIS OVERVIEW: PROGENITOR AND MYOBLAST POPULATIONS

Primary and Secondary Myogenesis

In vertebrates, prenatal skeletal muscle development takes place through two rounds of myogenesis. Between embryonic day E9.5 and E14.5 in mice, a primary round (also termed embryonic myogenesis) takes place to give rise to primary muscle fibers. This is followed by a secondary round of myogenesis (also termed fetal myogenesis), which gives rise to the majority of skeletal-muscle fibers present at birth (Biressi et al., 2007a; Tajbakhsh, 2009; Deries and Thorsteinsdóttir, 2016). Each round of myogenesis requires the proliferation, determination, and commitment of

progenitors to myoblasts, differentiation of myocytes, and fusion of myocytes toward multinucleate myofibers.

All muscles in the trunk and limbs derive from myogenic precursor cells (MPCs), which are present in somites, transient structures that form pairwise on either side of the neural tube. The somites are initially a spherical accumulation of cells but they soon subdivide into two compartments, the ventral mesenchymal sclerotome (ST) and the dorsal epithelial dermomyotome (DMT) (Hernandez-Torres et al., 2017, 2018; **Figure 2**). ST contains precursor cells that will give rise to the axial skeleton and ribs (Hernandez-Torres et al., 2017, 2018). DMT encloses proliferating progenitors of all skeletal muscles of the trunk, brown fat, endothelial cells, and dorsal dermis. MPCs from the dorsomedial (DML), ventrolateral (VLL) (**Figure 2**), rostral (ROL), and caudal lips (CAL) of the epithelial DMT undergo an epithelial–mesenchymal transition (EMT) and accumulate underneath, where they differentiate to form the myotome (MT) (**Figure 2**), the first muscle fibers of the embryo (Buckingham and Relaix, 2015; Deries and Thorsteinsdóttir, 2016; Hernandez-Torres et al., 2017, 2018). Later, MPCs from the central portion of the remaining DMT also reach the MT and thus contribute to its growth. The epaxial MT (located in the dorsomedial position) gives rise to the deep back muscles and the hypaxial DMT (located in the ventrolateral position) will form the body wall muscles, the diaphragm, and the intercostal muscles (Buckingham and Relaix, 2015; Deries and Thorsteinsdóttir, 2016; Hernandez-Torres et al., 2017, 2018). At the limb level, MPCs from the hypaxial DMT undergo an EMT and migrate toward the fore and hind limbs to form dorsal and ventral muscle masses in the limb bud mesenchyme (Biressi et al., 2007a; Deries and Thorsteinsdóttir, 2016; Hernandez-Torres et al., 2017, 2018). After MPCs reach their anatomical goals, they begin to differentiate to form primary muscle fibers that express a specific set of proteins such as the slow MyHC and myosin light chain 1 (MyLC1, Myl1) (Kelly et al., 1997).

During a later fetal or secondary phase (E14.5–17.5 in mouse) characterized by growth and maturation of each muscle anlagen, a group of remaining MPCs either fuse with each other or with the primary fibers and give rise to secondary or fetal fibers that express specific markers such as β-enolase, Nfix, or MyLC3 (Myl3) (Keller et al., 1992; Kelly et al., 1997; Fougerousse et al., 2001; Messina et al., 2010). At this time, the fibers also start to express fast MyHC isoforms (van Horn and Crow, 1989). Throughout secondary myogenesis, muscle growth is performed essentially by cell fusion and the addition of myonuclei from proliferating progenitors (White et al., 2010). During this phase, a subset of MPCs will also form the pool of adult muscle stem cells—the SCs (Gros et al., 2005; Kassar-Duchossoy et al., 2005; Relaix et al., 2005). Therefore, secondary myofibers form the majority of muscle and this process is complete after birth in mice (Relaix et al., 2005). Importantly, after birth (0–21 days postnatally), neonatal myogenesis is necessary for proper muscle growth and myofiber growth takes place with the rapid increase of myonuclear cell numbers, while some neonatal progenitors reach a unique anatomical position and locate between the plasmalemma and basement membrane of the adult myofibers. Thus, they are called SCs (Mauro, 1961).

In the gene regulatory cascade that regulates embryonic myogenesis, Pax3 and Pax7 genes are indispensable upstream regulators for specification and migration of MPCs in the trunk (Buckingham and Relaix, 2007; Lagha et al., 2009; Buckingham and Rigby, 2014; Mayeuf-Louchart et al., 2014, 2016). Pax3 is already expressed in presomitic mesoderm, maintaining its expression in the epithelial somite (Tajbakhsh and Cossu, 1997). With further development, Pax3 expression is progressively restricted to the dermomyotome and later to the DML and VLL of the DMT. Pax3 is also expressed in the hypaxial DMT-derived cells during E10.5–E13.5. Pax7 expression begins later and is restricted to the central portion of the DMT. In the limbs, Pax7 expression begins at E11.5 in hypaxial DMT-derived

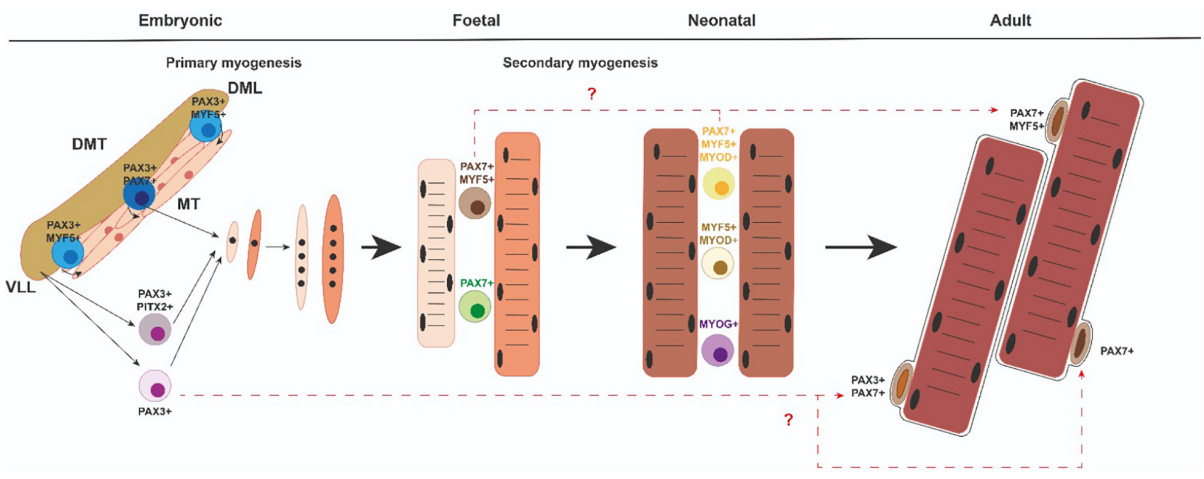

FIGURE 2 | Myogenic progenitors and satellite cells. Diverse myogenic cell populations emerging in the course of developmental and neonatal myogenesis could give rise to different subsets of SC within adult muscle. DMT, dermomyotome; MT, myotome; DML dorsomedial lip of the dermomyotome; VLL, ventrolateral lip of the dermomyotome.

cells. Pax7 expression is maintained during fetal and neonatal myogenesis as well as in adult SCs (**Figure 2**). Pax3 is not generally expressed in muscle after E13.5. However, a few adult SCs also are Pax3 + (Relaix et al., 2006; **Figure 2**). It is of note that Pitx2 transcription factor is also present in some of the myogenic cell progenitors in the VLL of the DMT as well as in migrating muscle precursor cells toward the limb buds (Hernandez-Torres et al., 2017). From a functional point of view, Pax3 is necessary for somite segmentation and formation of the dermomyotome lips (Schubert et al., 2001; Relaix et al., 2004). Although primary myotome is present in Pax3 mutant mice, limb muscles are absent, mainly due to defective pre-myoblast cell migration (Relaix et al., 2004; Messina and Cossu, 2009). However, Pax7 mutant mice show no defects in embryonic or fetal myogenesis but Pax7 is required to maintain adult SCs and make them function (Seale et al., 2000; Oustanina et al., 2004; Kuang et al., 2006; Relaix et al., 2006; von Maltzahn et al., 2013). In addition, Pax7 is sufficient to lead to myogenic specification *in vitro* (Seale et al., 2004). Interestingly, Pax3/Pax7 double mutant mice do not give rise to any limb muscle but neither does the primary myotome initially form (Relaix et al., 2005). Overall, all these data indicate that the gradual expression of Pax3 or Pax7 is critical for initiating the generation and survival of embryonic, fetal, neonatal, and adult muscle progenitors.

Myogenic determination and differentiation of all MPCs are controlled by the myogenic regulatory factor (MRF) family: Myf5, Myod1, Myf6, and Myog (Buckingham and Rigby, 2014). Myf5, Myod1, and Myf6 have traditionally been classified as determining factors that regulate cell fate and lineage progression from MPCs to myoblasts. Myog later acts to regulate myoblast terminal differentiation, myofiber maturation, and size (Zammit, 2017). Thus, the MRFs are expressed in myoblasts, myocytes, and myofibers at different stages of myogenesis (Buckingham and Rigby, 2014; Comai and Tajbakhsh, 2014).

During somite maturation, Myf5 expression is activated in the epaxial and hypaxial domains of the DM. Shortly after, the Myf5 expressing cells move beneath the DM to form the primary myotome (Relaix and Marcelle, 2009; Nitzan and Kalcheim, 2013). Myod1 is also present in these DM domains (Ott et al., 1991; Tajbakhsh et al., 1997; Venters et al., 1999; Cinnamon et al., 2001; Kablar et al., 2003; Kassar-Duchossoy et al., 2004; Buckingham and Rigby, 2014). At the same time, Myf6 expression is initiated in the DM and MT but is downregulated at E12.5 in mice, suggesting that Myf6 could have a function in MPC determination (Summerbell et al., 2002; Kassar-Duchossoy et al., 2004). Curiously, around fetal day E14.5 in mice, Myf6 transcription is reactivated in all skeletal muscles (Bober et al., 1991; Hinterberger et al., 1991; Summerbell et al., 2002). This first wave of Pax3 + MPCs that progressively express Myf5, Myod1, and Myf6 rapidly gives rise to DESMIN + myoblasts that form the MT (Kassar-Duchossoy et al., 2005; Comai and Tajbakhsh, 2014; **Figure 2**). Soon after, a second wave of Pax3/Pax7-expressing MPCs is displaced from the central DM toward MT, activates Myf5 and Myod1, and differentiates (Relaix et al., 2005; Buckingham and Relaix, 2007; **Figure 2**). A subset of this second wave of MPCs does not activate Myf5 and Myod1 but retains a proliferative status, thus forming a reserve of MPCs for later embryonic and fetal development (Relaix et al., 2005; Buckingham and Relaix, 2007). It is interesting to highlight that the Pax3 positive MPCs from the hypaxial DM that exit their epithelial structure, begin a long-range migration to the limbs, retain their proliferative status and avoid MRF expression (Vasyutina and Birchmeier, 2006; **Figure 2**). These migrating MPCs begin to express Myod1 and Myog after reaching the limbs buds, form ventral and dorsal cell masses, and start to differentiate into myoblast, myocytes, and muscle fibers (Lee et al., 2013).

Different Progenitors and Myoblast Populations

As a result of the multiple rounds of skeletal myogenesis, embryonic and fetal myoblasts emerge as different cell populations. It has been shown that these distinct groups of myoblasts display distinctive *in vitro* characteristics such as different morphologies, culture media conditions, and drug responses and give rise to myofibers with distinct morphologies. Therefore, embryonic myoblasts are elongated cells in culture and differentiate into mononucleated or oligonucleated myotubes, with the highest tendency to differentiate and give rise to smaller colonies when cultured *in vitro,* while fetal myoblasts exhibit a more triangular shape (Biressi et al., 2007a). Moreover, embryonic myoblast differentiation is not affected by molecules such as TGFβ, BMP-4, or phorbol esters and present a different sensitivity to merocyanine 540 (Nameroff and Rhodes, 1989). However, fetal myoblasts proliferate to a limited extent in response to growth factors, differentiate into large multinucleated myotubes, and their differentiation is inhibited by TGFβ, BMP-4, and phorbol esters. Moreover, genetic analyses of Pax3/7 and Myf5/Myod1/Mrf4 transcription factors and genome-wide expression analysis have revealed that embryonic and fetal myoblasts are specified by different transcription factor cocktails and express different genes (Kassar-Duchossoy et al., 2004, 2005; Relaix et al., 2006; Biressi et al., 2007b).

An intriguing issue in the field is whether embryonic, fetal, and adult myoblasts derive from common or different progenitor populations. In this sense, genetic labeling and ablation of myogenic progenitors have revealed that Pax3 + and Pax7 + cells contribute differentially to embryonic and fetal limb myogenesis. Consequently, Pax3 + /Pax7 + cells contribute to muscle and endothelium, are required for embryonic myogenesis, and generate Pax7 + cells. Later, Pax7 + cells produce fetal myogenesis (Hutcheson et al., 2009; **Figure 2**). Moreover, these two embryonic and fetal limb myogenic populations have autonomous genetic requirements. In the somite, Beta-Catenin is necessary for proper dermomyotome and myotome formation and limb progenitor delamination. However, Beta-catenin is not required for embryonic myoblast specification or differentiation in limbs but is important for determining fetal progenitor number and myofiber number and type (Hutcheson et al., 2009). On the other hand, from E5 to E17 in chicks and E12 to E15 in mice, different myogenic progenitors have been identified, depending on their proliferative capabilities, as a minor Pax7 + slow-cycling less-differentiated population and a

major Pax7 + /Myf5 + highly proliferative pool of cells further engaged in the myogenic program (Picard and Marcelle, 2013; **Figure 2**). These results add levels of complexity to cellular heterogeneity during vertebrate skeletal muscle development. Besides, another intriguing topic in the field is whether myoblast diversity is due to different intrinsic changes or whether changes in myogenic cells occur as a consequence of the extrinsic environment (Murphy and Kardon, 2011).

DOES THE EMBRYONIC ORIGIN OF SATELLITE CELLS UNDERLIE FUNCTIONAL HETEROGENEITY?

Although it is well accepted that SCs arise from Pax3/Pax7-expressing DMT-cells (Gros et al., 2005; Relaix et al., 2005; Schienda et al., 2006; Hutcheson et al., 2009; Lepper and Fan, 2010) the embryonic origin of SCs is still an open issue. In this sense, a seminal lineage tracing study using a Myf5-Cre-stop-flox-YFP reporter mouse line demonstrated the existence of a small subpopulation of ∼10% of SCs that had never previously expressed Myf5 (Kuang et al., 2007). These Myf5-YFP-reporter-negative cells were more prone to divide in an asymmetrical apical–basal manner, generating a more committed YFP-reporter-positive cell and a negative cell that self-renewed. Moreover, this subset of Myf5-YFP-reporter-negative cells had a much higher capacity to repopulate the SC niche (compared to Myf5-YFP-reporter-positive SCs) when transplanted into PAX7-null animals, indicating that these cells could retain more robust self-renewal capabilities. Conversely, non-*Myf5* expression SCs were more prone to myogenic differentiation in *in vivo* engraftment assays (Kuang et al., 2007; **Figure 1**). However, other Cre/lox lineage analyses revealed that essentially all adult SCs associated with limb and body wall musculature and the diaphragm and extraocular muscles originate from Myod1 + progenitors (Kanisicak et al., 2009). These data have highlighted some still unsolved questions about the embryonic origin of SCs. For example, can SC progenitors also constitute a heterogeneous cell pool? In other words, can SCs originate from different dermomyotome/embryonic and/or fetal progenitors that give rise to functionally-diverse populations of SCs?

It is very well accepted that SCs derive from the same embryonic "founder" cells as the muscle in which they reside. In this context, it is interesting to highlight that during the multiple growth phases during myogenesis, SCs arise from stem and progenitor cells that resist differentiation throughout life and eventually arrive at the SC compartment. To further distinguish myogenic progenitors that form the muscle prenatally from the juvenile and adult SC population, different rounds of founder stem cells have been termed FSC1, FSC2, and FSC3 (Tajbakhsh, 2009). FSC1 has been defined as cells that express Pax3 and form the myotome; FSC2 as progenitors released from the central dermomyotome that express Pax3/Pax7, and FSC3 as progenitors that migrate from the ventral dermomyotome to form the skeletal muscles in the limbs, diaphragm, and tongue. FSC3 cells also express Pax3 but start to express Myf5/Myod1/(Mrf4) once they reach their destination (Tajbakhsh, 2009). In this regard, it has been proposed that FCS1 is exhausted early in the embryo but FSC2 and FSC3 remain and contribute to the majority of SCs (Tajbakhsh, 2009). On the other hand, juvenile SCs, located beneath the basement membrane, emerge from about 2 days before birth in mice but continue to proliferate until about 12 days postnatally. Then, at around 2 weeks, quiescent "adult" SCs can definitely be identified (Tajbakhsh, 2009). It has been assumed in the field that the founder stem cells that establish the muscles before birth give rise to juvenile SCs at postnatal stages that encourage muscle growth and regeneration (Sambasivan and Tajbakhsh, 2007). However, mononuclear "juvenile SCs" are heterogeneous as they include: (1) Pax7 + /(Myf5 + /Myod1 +) identified as future SCs; (2) myoblasts that upregulate or downregulate Pax7 but express Myf5 and Myod1 and can give rise to future SCs or differentiate, and (3) differentiated Pax7-/Myog + (Kassar-Duchossoy et al., 2005; Sambasivan and Tajbakhsh, 2007; **Figure 2**). All these "juvenile" cells must be distinguished from those in G0 and emerge from approx. 2–3 weeks after birth as adult quiescent SCs (Shinin et al., 2006). In this scenario, several questions need to be addressed: How can "satellite" cells be differentiated from fetal and/or juvenile myoblast precursors? Could the heterogeneous cell populations emerging at the fetal and/or juvenile stages give rise to functionally different populations with different quiescent properties and functions? Future works in this area could help to advance the characterization of the embryonic origin of "different" adult SC populations.

At this point, it is interesting to recall that approx. 90% of quiescent SCs also express Myf5 despite Pax7 expression being present in all SCs in the adult muscle. Further analysis of the developmental stage at which the precursors of SCs first express muscle determination genes using the Tamoxifen-inducible $Myf5^{CreER}$ mouse line revealed that a significant number of SCs develop from cells that expressed Myf5 for the first time at the fetal stage (∼E15) in the mouse (Biressi et al., 2013). Nevertheless, it has also been taken into account that Pax3 is present in some SCs in several skeletal muscles (Relaix et al., 2006) and that they retain long-term self-renewal and proliferation as well as a better response to stress and/or environmental injuries (Yang et al., 2016; der Vartanian et al., 2019; Scaramozza et al., 2019). These data generate new questions about links between SC functional heterogeneity in adults and their embryonic/fetal origin. For example, do Pax7 + /Myf5 + and Pax7 + /Pax3 + SC populations in adult muscle share common fetal myogenic progenitors that eventually downregulate Pax3 and upregulate MRFs in some of their daughter cells? Alternatively, do Pax7 + /Myf5 + SC populations originate from fetal progenitors while Pax3 + /Pax7 + SCs derive from Pax3 + embryonic progenitors that remain in fetal, juvenile, and adult muscle as Myf5 negative cells? An additional question arises as to whether different cell populations emerge due to intrinsic changes or extrinsic environmental factors possibly regulating such differences. A deeper analysis of the molecular signals that differentially regulate the different phases of myogenesis will help us to better address these questions.

DISCUSSION/CONCLUDING REMARKS

Muscle regeneration is mediated by SCs that lie in close proximity to the muscle fibers. Stem cell heterogeneity is recognized as functionally relevant for tissue homeostasis and repair. Muscle SCs are a heterogeneous population regarding cell cycle progression, lineage commitment, ability to self-renew and repopulate the niche, and response to environmental stress. To sustain proper muscle regeneration, quiescent SCs activate, proliferate, and recapitulate the embryonic myogenic program to differentiate and form new myoblasts that give rise to muscle fibers and/or fuse with pre-existing fibers. In this scenario, it is interesting to note that these different SC behaviors are mainly supported by diverse cell subpopulations with different myogenic determination gene expression profiles and proliferative capabilities. Although it is very well accepted that SCs originate from dermomyotome progenitors, the developmental origin of muscle stem cells has not been fully clarified. As several previous studies have indicated that diverse myogenic precursors emerge that also display differences in proliferation rates and myogenic gene expression during embryonic, fetal, and neonatal myogenesis, developmental myogenesis could be an excellent platform to better understand SC behavior in adult muscles. In this regard, further analysis of the molecular mechanisms underlying the emergence of different myoblast populations during the different rounds of embryonic, fetal, and neonatal myogenesis could enable us to decipher whether diverse muscle stem cell populations could arise from those diverse cell populations. Finally, another critical point that needs to be addressed is how a subset of myogenic progenitors leave the cell cycle, resist myogenic differentiation throughout development, and give rise to quiescent SCs.

AUTHOR CONTRIBUTIONS

LR-O and AA conceived the structure and content. FH-T, LR-O, and AA designed and produced the figures. FH-T, FR, LM-V, CS-F, and DF revised the manuscript critically for important intellectual content. AA corrected, edited, and approved the final version of the document to be published. All authors contributed to the article and approved the submitted version.

FUNDING

This work was partially supported by grants PID2019-10 7492GB-I00 (Ministerio de Ciencia e Innovación, Spain) and 06030050P1 PROY I + D + I. FEDER ANDALUCIA (Junta de Andalucía, Spain). LR-O is recipient of a FPU grant (FPU17/03843).

REFERENCES

Asakura, A., Hirai, H., Kablar, B., Morita, S., Ishibashi, J., Piras, B. A., et al. (2007). Increased survival of muscle stem cells lacking the MyoD gene after transplantation into regenerating skeletal muscle. *Proc. Natl. Acad. Sci. U.S.A.* 104, 16552–16557. doi: 10.1073/PNAS.0708145104

Beauchamp, J. R., Heslop, L., Yu, D. S. W., Tajbakhsh, S., Kelly, R. G., Wernig, A., et al. (2000). Expression of CD34 and Myf5 defines the majority of quiescent adult skeletal muscle satellite cells. *J. Cell Biol.* 151, 1221–1233. doi: 10.1083/jcb.151.6.1221

Biressi, S., Bjornson, C. R. R., Carlig, P. M. M., Nishijo, K., Keller, C., and Rando, T. A. (2013). Myf5 expression during fetal myogenesis defines the developmental progenitors of adult satellite cells. *Dev. Biol.* 379, 195–207. doi: 10.1016/J.YDBIO.2013.04.021

Biressi, S., Molinaro, M., and Cossu, G. (2007a). Cellular heterogeneity during vertebrate skeletal muscle development. *Dev. Biol.* 308, 281–293. doi: 10.1016/j.ydbio.2007.06.006

Biressi, S., Tagliafico, E., Lamorte, G., Monteverde, S., Tenedini, E., Roncaglia, E., et al. (2007b). Intrinsic phenotypic diversity of embryonic and fetal myoblasts is revealed by genome-wide gene expression analysis on purified cells. *Dev. Biol.* 304, 633–651. doi: 10.1016/J.YDBIO.2007.01.016

Bober, E., Lyons, G. E., Braun, T., Cossu, G., Buckingham, M., and Arnold, H. H. (1991). The muscle regulatory gene, Myf-6, has a biphasic pattern of expression during early mouse development. *J. Cell Biol.* 113, 1255–1265. doi: 10.1083/jcb.113.6.1255

Buckingham, M., and Relaix, F. (2007). The role of PAX genes in the development of tissues and organs: Pax3 and Pax7 regulate muscle progenitor cell functions. *Annu. Rev. Cell Dev. Biol.* 23, 645–673. doi: 10.1146/annurev.cellbio.23.090506.123438

Buckingham, M., and Relaix, F. (2015). PAX3 and PAX7 as upstream regulators of myogenesis. *Semin. Cell Dev. Biol.* 44, 115–125. doi: 10.1016/j.semcdb.2015.09.017

Buckingham, M., and Rigby, P. W. J. (2014). gene regulatory networks and transcriptional mechanisms that control myogenesis. *Dev. Cell* 28, 225–238. doi: 10.1016/j.devcel.2013.12.020

Cairns, J. (1975). Mutation selection and the natural history of cancer. *Nature* 255, 197–200. doi: 10.1038/255197A0

Chakkalakal, J. V., Christensen, J., Xiang, W., Tierney, M. T., Boscolo, F. S., Sacco, A., et al. (2014). Early forming label-retaining muscle stem cells require p27kip1 for maintenance of the primitive state. *Development* 141, 1649–1659. doi: 10.1242/DEV.100842

Cinnamon, Y., Kahane, N., Bachelet, I., and Kalcheim, C. (2001). The sub-lip domain–a distinct pathway for myotome precursors that demonstrate rostral-caudal migration. *Development* 128, 341–351.

Comai, G., and Tajbakhsh, S. (2014). Molecular and cellular regulation of skeletal myogenesis. *Curr. Top. Dev. Biol.* 110, 1–73. doi: 10.1016/B978-0-12-405943-6.00001-4

Cornelison, D. D. W. (2018). "Known unknowns": current questions in muscle satellite cell biology. *Curr. Top. Dev. Biol.* 126, 205–233. doi: 10.1016/BS.CTDB.2017.08.006

der Vartanian, A., Quétin, M., Michineau, S., Auradé, F., Hayashi, S., Dubois, C., et al. (2019). PAX3 confers functional heterogeneity in skeletal muscle stem cell responses to environmental stress. *Cell Stem Cell* 24, 958–973. doi: 10.1016/J.STEM.2019.03.019

Deries, M., and Thorsteinsdóttir, S. (2016). Axial and limb muscle development: dialogue with the neighbourhood. *Cell. Mol. Life Sci.* 73, 4415–4431. doi: 10.1007/s00018-016-2298-7

Dumont, N. A., Wang, Y. X., von Maltzahn, J., Pasut, A., Bentzinger, C. F., Brun, C. E., et al. (2015). Dystrophin expression in muscle stem cells regulates their polarity and asymmetric division. *Nat. Med.* 21, 1455–1463. doi: 10.1038/nm.3990

Feige, P., Brun, C. E., Ritso, M., and Rudnicki, M. A. (2018). Orienting muscle stem cells for regeneration in homeostasis, aging, and disease. *Cell Stem Cell* 23, 653–664. doi: 10.1016/j.stem.2018.10.006

Fougerousse, F., Edom-Vovard, F., Merkulova, T., Ott, M. O., Durand, M., Butler-Browne, G., et al. (2001). The muscle-specific enolase is an early marker of human myogenesis. *J. Muscle Res. Cell Motil.* 22, 535–544. doi: 10.1023/A:1015008208007

Gayraud-Morel, B., Chrétien, F., Jory, A., Sambasivan, R., Negroni, E., Flamant, P., et al. (2012). Myf5 haploinsufficiency reveals distinct cell fate potentials for

adult skeletal muscle stem cells. *J. Cell Sci.* 125, 1738–1749. doi: 10.1242/jcs.097006

Gros, J., Manceau, M., Thomé, V., and Marcelle, C. (2005). A common somitic origin for embryonic muscle progenitors and satellite cells. *Nature* 435, 954–958. doi: 10.1038/nature03572

Günther, S., Kim, J., Kostin, S., Lepper, C., Fan, C.-M., and Braun, T. (2013). Myf5-positive satellite cells contribute to Pax7-dependent long-term maintenance of adult muscle stem cells. *Cell Stem Cell* 13, 590–601. doi: 10.1016/J.STEM.2013.07.016

Hernandez-Torres, F., Lozano-Velasco, E., Vallejo-Pulido, D., Aranega, A., and Franco, D. (2018). "Skeletal muscle progenitor specification during development," in *Reference Module in Biomedical Sciences*, eds B. Brand-Saberi and M. Saberi (Amsterdam: Elsevier), 1–11.

Hernandez-Torres, F., Rodríguez-Outeiriño, L., Franco, D., and Aranega, A. E. (2017). Pitx2 in embryonic and adult myogenesis. *Front. Cell Dev. Biol.* 5:46. doi: 10.3389/fcell.2017.00046

Hinterberger, T. J., Sassoon, D. A., Rhodes, S. J., and Konieczny, S. F. (1991). Expression of the muscle regulatory factor MRF4 during somite and skeletal myofiber development. *Dev. Biol.* 147, 144–156. doi: 10.1016/S0012-1606(05)80014-4

Hirai, H., Verma, M., Watanabe, S., Tastad, C., Asakura, Y., and Asakura, A. (2010). MyoD regulates apoptosis of myoblasts through microRNA-mediated down-regulation of Pax3. *J. Cell Biol.* 191, 347–365. doi: 10.1083/JCB.201006025

Hutcheson, D. A., Zhao, J., Merrell, A., Haldar, M., and Kardon, G. (2009). Embryonic and fetal limb myogenic cells are derived from developmentally distinct progenitors and have different requirements for β-catenin. *Genes Dev.* 23, 997–1013. doi: 10.1101/GAD.1769009

Janssen, I., Heymsfield, S. B., Wang, Z. M., and Ross, R. (2000). Skeletal muscle mass and distribution in 468 men and women aged 18-88 yr. *J. Appl. Physiol.* 89, 81–88. doi: 10.1152/jappl.2000.89.1.81

Kablar, B., Krastel, K., Tajbakhsh, S., and Rudnicki, M. A. (2003). Myf5 and MyoD activation define independent myogenic compartments during embryonic development. *Dev. Biol.* 258, 307–318. doi: 10.1016/S0012-1606(03)00139-8

Kanisicak, O., Mendez, J. J., Yamamoto, S., Yamamoto, M., and Goldhamer, D. J. (2009). Progenitors of skeletal muscle satellite cells express the muscle determination gene, MyoD. *Dev. Biol.* 332, 131–141. doi: 10.1016/J.YDBIO.2009.05.554

Kassar-Duchossoy, L., Gayraud-Morel, B., Gomès, D., Rocancourt, D., Buckingham, M., Shinin, V., et al. (2004). Mrf4 determines skeletal muscle identity in Myf5:myod double-mutant mice. *Nature* 431, 466–471. doi: 10.1038/nature02876

Kassar-Duchossoy, L., Giacone, E., Gayraud-Morel, B., Jory, A., Gomès, D., and Tajbakhsh, S. (2005). Pax3/Pax7 mark a novel population of primitive myogenic cells during development. *Genes Dev.* 19, 1426–1431. doi: 10.1101/gad.345505

Keller, A., Ott, M. O., Lamandé, N., Lucas, M., Gros, F., Buckingham, M., et al. (1992). Activation of the gene encoding the glycolytic enzyme β-enolase during early myogenesis precedes an increased expression during fetal muscle development. *Mech. Dev.* 38, 41–54. doi: 10.1016/0925-4773(92)90037-K

Kelly, R. G., Zammit, P. S., Schneider, A., Alonso, S., Biben, C., and Buckingham, M. E. (1997). Embryonic and fetal myogenic programs act through separate enhancers at the MLC1F/3F Locus. *Dev. Biol.* 187, 183–199. doi: 10.1006/DBIO.1997.8577

Kuang, S., Chargé, S. B., Seale, P., Huh, M., and Rudnicki, M. A. (2006). Distinct roles for Pax7 and Pax3 in adult regenerative myogenesis. *J. Cell Biol.* 172, 103–113. doi: 10.1083/JCB.200508001

Kuang, S., Kuroda, K., Le Grand, F., and Rudnicki, M. A. A. (2007). Asymmetric self-renewal and commitment of satellite stem cells in muscle. *Cell* 129, 999–1010. doi: 10.1016/j.cell.2007.03.044

Lagha, M., Brunelli, S., Messina, G., Cumano, A., Kume, T., Relaix, F., et al. (2009). Pax3:foxc2 reciprocal repression in the somite modulates muscular versus vascular cell fate choice in multipotent progenitors. *Dev. Cell* 17, 892–899. doi: 10.1016/J.DEVCEL.2009.10.021

Lee, A. S. J., Harris, J., Bate, M., Vijayraghavan, K., Fisher, L., Tajbakhsh, S., et al. (2013). Initiation of primary myogenesis in amniote limb muscles. *Dev. Dyn.* 242, 1043–1055. doi: 10.1002/dvdy.23998

Lepper, C., Conway, S. J., and Fan, C.-M. (2009). Adult satellite cells and embryonic muscle progenitors have distinct genetic requirements. *Nature* 460, 627–631. doi: 10.1038/nature08209

Lepper, C., and Fan, C. M. (2010). Inducible lineage tracing of Pax7-descendant cells reveals embryonic origin of adult satellite cells. *Genesis* 48, 424–436. doi: 10.1002/DVG.20630

Lepper, C., Partridge, T. A., and Fan, C. M. (2011). An absolute requirement for pax7-positive satellite cells in acute injury-induced skeletal muscle regeneration. *Development* 138, 3639–3646. doi: 10.1242/dev.067595

Mauro, A. (1961). Satellite cell of skeletal muscle fibers. *J. Biophys. Biochem. Cytol.* 9, 493–495. doi: 10.1083/jcb.9.2.493

Mayeuf-Louchart, A., Lagha, M., Danckaert, A., Rocancourt, D., Relaix, F., Vincent, S. D., et al. (2014). Notch regulation of myogenic versus endothelial fates of cells that migrate from the somite to the limb. *Proc. Natl. Acad. Sci. U.S.A.* 111, 8844–8849. doi: 10.1073/PNAS.1407606111

Mayeuf-Louchart, A., Montarras, D., Bodin, C., Kume, T., Vincent, S. D., and Buckingham, M. (2016). Endothelial cell specification in the somite is compromised in Pax3-positive progenitors of Foxc1/2 conditional mutants, with loss of forelimb myogenesis. *Development* 143, 872–879. doi: 10.1242/DEV.128017

Messina, G., Biressi, S., Monteverde, S., Magli, A., Cassano, M., Perani, L., et al. (2010). Nfix regulates fetal-specific transcription in developing skeletal muscle. *Cell* 140, 554–566. doi: 10.1016/J.CELL.2010.01.027

Messina, G., and Cossu, G. (2009). The origin of embryonic and fetal myoblasts: a role of Pax3 and Pax7. *Genes Dev.* 23, 902–905. doi: 10.1101/GAD.1797009

Motohashi, N., and Asakura, A. (2014). Muscle satellite cell heterogeneity and self-renewal. *Front. Cell Dev. Biol.* 2:1. doi: 10.3389/FCELL.2014.00001

Murphy, M., and Kardon, G. (2011). "Origin of vertebrate limb muscle," in *Current Topics in Developmental Biology*, ed. G. K. Pavlath (San Diego, CA: Elsevier), 1–32.

Nameroff, M., and Rhodes, L. D. (1989). Differential response among cells in the chick embryo myogenic lineage to photosensitization by merocyanine 540. *J. Cell. Physiol.* 141, 475–482. doi: 10.1002/JCP.1041410305

Nitzan, E., and Kalcheim, C. (2013). Neural crest and somitic mesoderm as paradigms to investigate cell fate decisions during development. *Dev. Growth Differ.* 55, 60–78. doi: 10.1111/DGD.12004

Olguin, H. C., Yang, Z., Tapscott, S. J., and Olwin, B. B. (2007). Reciprocal inhibition between Pax7 and muscle regulatory factors modulates myogenic cell fate determination. *J. Cell Biol.* 177, 769–779. doi: 10.1083/JCB.200608122

Ono, Y., Masuda, S., Nam, H. S., Benezra, R., Miyagoe-Suzuki, Y., and Takeda, S. (2012). Slow-dividing satellite cells retain long-term self-renewal ability in adult muscle. *J. Cell Sci.* 125, 1309–1317. doi: 10.1242/JCS.096198

Ott, M. O., Bober, E., Lyons, G., Arnold, H., and Buckingham, M. (1991). Early expression of the myogenic regulatory gene, myf-5, in precursor cells of skeletal muscle in the mouse embryo. *Development* 111, 1097–1107.

Oustanina, S., Hause, G., and Braun, T. (2004). Pax7 directs postnatal renewal and propagation of myogenic satellite cells but not their specification. *EMBO J.* 23, 3430–3439. doi: 10.1038/SJ.EMBOJ.7600346

Picard, C. A., and Marcelle, C. (2013). Two distinct muscle progenitor populations coexist throughout amniote development. *Dev. Biol.* 373, 141–148. doi: 10.1016/J.YDBIO.2012.10.018

Relaix, F., and Marcelle, C. (2009). Muscle stem cells. *Curr. Opin. Cell Biol.* 21, 748–753. doi: 10.1016/J.CEB.2009.10.002

Relaix, F., Montarras, D., Zaffran, S., Gayraud-Morel, B., Rocancourt, D., Tajbakhsh, S., et al. (2006). Pax3 and Pax7 have distinct and overlapping functions in adult muscle progenitor cells. *J. Cell Biol.* 172, 91–102. doi: 10.1083/jcb.200508044

Relaix, F., Rocancourt, D., Mansouri, A., and Buckingham, M. (2004). Divergent functions of murine Pax3 and Pax7 in limb muscle development. *Genes Dev.* 18, 1088–1105. doi: 10.1101/GAD.301004

Relaix, F., Rocancourt, D., Mansouri, A., and Buckingham, M. (2005). A Pax3/Pax7-dependent population of skeletal muscle progenitor cells. *Nature* 435, 948–953. doi: 10.1038/nature03594

Rocheteau, P., Gayraud-Morel, B., Siegl-Cachedenier, I., Blasco, M. A., and Tajbakhsh, S. (2012). A subpopulation of adult skeletal muscle stem cells retains all template DNA strands after cell division. *Cell* 148, 112–125. doi: 10.1016/J.CELL.2011.11.049

Rudnicki, M. A., Braun, T., Hinuma, S., and Jaenisch, R. (1992). Inactivation of MyoD in mice leads to up-regulation of the myogenic HLH gene Myf-5 and results in apparently normal muscle development. *Cell* 71, 383–390. doi: 10.1016/0092-8674(92)90508-A

Rudnicki, M. A., Schnegelsberg, P. N. J., Stead, R. H., Braun, T., Arnold, H. H., and Jaenisch, R. (1993). MyoD or Myf-5 is required for the formation of skeletal muscle. *Cell* 75, 1351–1359. doi: 10.1016/0092-8674(93)90621-V

Sambasivan, R., and Tajbakhsh, S. (2007). Skeletal muscle stem cell birth and properties. *Semin. Cell Dev. Biol.* 18, 870–882. doi: 10.1016/j.semcdb.2007.09.013

Sambasivan, R., Yao, R., Kissenpfennig, A., van Wittenberghe, L., Paldi, A., Gayraud-Morel, B., et al. (2011). Pax7-expressing satellite cells are indispensable for adult skeletal muscle regeneration. *Development* 138, 3647–3656. doi: 10.1242/dev.067587

Scaramozza, A., Park, D., Kollu, S., Beerman, I., Sun, X., Rossi, D. J., et al. (2019). Lineage tracing reveals a subset of reserve muscle stem cells capable of clonal expansion under stress. *Cell Stem Cell* 24, 944–957. doi: 10.1016/J.STEM.2019.03.020

Schienda, J., Engleka, K. A., Jun, S., Hansen, M. S., Epstein, J. A., Tabin, C. J., et al. (2006). Somitic origin of limb muscle satellite and side population cells. *Proc. Natl. Acad. Sci. U.S.A.* 103, 945–950. doi: 10.1073/pnas.0510164103

Schubert, F. R., Tremblay, P., Mansouri, A., Faisst, A. M., Kammandel, B., Lumsden, A., et al. (2001). Early mesodermal phenotypes in splotch suggest a role for Pax3 in the formation of epithelial somites. *Dev. Dyn.* 222, 506–521. doi: 10.1002/DVDY.1211

Schultz, E. (1996). Satellite cell proliferative compartments in growing skeletal muscles. *Dev. Biol.* 175, 84–94.

Seale, P., Ishibashi, J., Scimè, A., and Rudnicki, M. A. (2004). Pax7 is necessary and sufficient for the myogenic specification of CD45+:Sca1+ stem cells from injured muscle. *PLoS Biol.* 2:E130. doi: 10.1371/JOURNAL.PBIO.0020130

Seale, P., Sabourin, L. A., Girgis-Gabardo, A., Mansouri, A., Gruss, P., and Rudnicki, M. A. (2000). Pax7 is required for the specification of myogenic satellite cells. *Cell* 102, 777–786. doi: 10.1016/S0092-8674(00)00066-0

Shinin, V., Gayraud-Morel, B., Gomès, D., and Tajbakhsh, S. (2006). Asymmetric division and cosegregation of template DNA strands in adult muscle satellite cells. *Nat. Cell Biol.* 8, 677–682. doi: 10.1038/NCB1425

Summerbell, D., Halai, C., and Rigby, P. W. J. (2002). Expression of the myogenic regulatory factor Mrf4 precedes or is contemporaneous with that of Myf5 in the somitic bud. *Mech. Dev.* 117, 331–335. doi: 10.1016/S0925-4773(02)00208-3

Tajbakhsh, S. (2009). Skeletal muscle stem cells in developmental versus regenerative myogenesis. *J. Inter. Med.* 266, 372–389. doi: 10.1111/j.1365-2796.2009.02158.x

Tajbakhsh, S., and Cossu, G. (1997). Establishing myogenic identity during somitogenesis. *Curr. Opin. Genet. Dev.* 7, 634–641. doi: 10.1016/S0959-437X(97)80011-1

Tajbakhsh, S., Rocancourt, D., Cossu, G., and Buckingham, M. (1997). Redefining the genetic hierarchies controlling skeletal myogenesis: Pax-3 and Myf-5 act upstream of MyoD. *Cell* 89, 127–138. doi: 10.1016/S0092-8674(00)80189-0

Tierney, M. T., and Sacco, A. (2016). Satellite cell heterogeneity in skeletal muscle homeostasis. *Trends Cell Biol.* 26, 434–444. doi: 10.1016/j.tcb.2016.02.004

Vallejo, D., Hernández-Torres, F., Lozano-Velasco, E., Rodriguez-Outeiriño, L., Carvajal, A., Creus, C., et al. (2018). PITX2 enhances the regenerative potential of dystrophic skeletal muscle stem cells. *Stem Cell Rep.* 10, 1398–1411. doi: 10.1016/j.stemcr.2018.03.009

van Horn, R., and Crow, M. T. (1989). Fast myosin heavy chain expression during the early and late embryonic stages of chicken skeletal muscle development. *Dev. Biol.* 134, 279–288. doi: 10.1016/0012-1606(89)90100-0

Vasyutina, E., and Birchmeier, C. (2006). The development of migrating muscle precursor cells. *Brain Struct. Funct.* 211, 37–41. doi: 10.1007/s00429-006-0118-9

Venters, S. J., Thorsteinsdottir, S., and Duxson, M. J. (1999). Early development of the myotome in the mouse. *Dev. Dyn.* 216, 219–232. doi: 10.1002/(SICI)1097-0177(199911)216:3<219::AID-DVDY1<3.0.CO;2-J

Venuti, J. M., Morris, J. H., Vivian, J. L., Olson, E. N., and Klein, W. H. (1995). Myogenin is required for late but not early aspects of myogenesis during mouse development. *J. Cell Biol.* 128, 563–576.

Verma, M., Asakura, Y., Murakonda, B. S. R., Pengo, T., Latroche, C., Chazaud, B., et al. (2018). Muscle satellite cell cross-talk with a vascular niche maintains quiescence via VEGF and notch signaling. *Cell Stem Cell* 23, 530–543. doi: 10.1016/J.STEM.2018.09.007

von Maltzahn, J., Jones, A. E., Parks, R. J., and Rudnicki, M. A. (2013). Pax7 is critical for the normal function of satellite cells in adult skeletal muscle. *Proc. Natl. Acad. Sci. U.S.A.* 110, 16474–16479. doi: 10.1073/PNAS.1307680110

Weintraub, H., Davis, R., Tapscott, S., Thayer, M., Krause, M., Benezra, R., et al. (1991). The myoD gene family: nodal point during specification of the muscle cell lineage. *Science* 251, 761–766. doi: 10.1126/SCIENCE.1846704

White, R. B., Biérinx, A.-S., Gnocchi, V. F., and Zammit, P. S. (2010). Dynamics of muscle fibre growth during postnatal mouse development. *BMC Dev. Biol.* 10:21. doi: 10.1186/1471-213X-10-21

Yang, Q., Yu, J., Yu, B., Huang, Z., Zhang, K., Wu, D., et al. (2016). PAX3+ skeletal muscle satellite cells retain long-term self-renewal and proliferation. *Muscle Nerve* 54, 943–951. doi: 10.1002/MUS.25117

Yoshida, N., Yoshida, S., Koishi, K., Masuda, K., and Nabeshima, Y. (1998). Cell heterogeneity upon myogenic differentiation: down-regulation of MyoD and Myf-5 generates 'reserve cells.'. *J. Cell Sci.* 111, 769–779. doi: 10.1242/JCS.111.6.769

Zammit, P. S. (2017). Function of the myogenic regulatory factors Myf5, MyoD, Myogenin and MRF4 in skeletal muscle, satellite cells and regenerative myogenesis. *Semin. Cell Dev. Biol.* 72, 19–32. doi: 10.1016/J.SEMCDB.2017.11.011

Zammit, P. S., Golding, J. P., Nagata, Y., Hudon, V., Partridge, T. A., and Beauchamp, J. R. (2004). Muscle satellite cells adopt divergent fates: a mechanism for self-renewal? *J. Cell Biol.* 166, 347–357. doi: 10.1083/JCB.200312007

Conflict of Interest: The authors declare that the research was conducted in the absence of any commercial or financial relationships that could be construed as a potential conflict of interest.

Publisher's Note: All claims expressed in this article are solely those of the authors and do not necessarily represent those of their affiliated organizations, or those of the publisher, the editors and the reviewers. Any product that may be evaluated in this article, or claim that may be made by its manufacturer, is not guaranteed or endorsed by the publisher.

frontiers in Cell and Developmental Biology

BRIEF RESEARCH REPORT
published: 22 October 2021
doi: 10.3389/fcell.2021.767048

Mosmo Is Required for Zebrafish Craniofacial Formation

Carlos Camacho-Macorra[1,2†], Marcos Sintes[1†], Noemí Tabanera[1,2], Irene Grasa[1], Paola Bovolenta[1,2‡] and Marcos J. Cardozo[1,2*‡]*

[1] Centro de Biología Molecular Severo Ochoa, Consejo Superior de Investigaciones Científicas, Universidad Autónoma de Madrid, Madrid, Spain, [2] Centro de Investigación Biomédica en Red de Enfermedades Raras, Instituto de Salud Carlos III, Madrid, Spain

OPEN ACCESS

Edited by:
Rosa Barrio,
CIC bioGUNE, Spain

Reviewed by:
Laura Anne Lowery,
Boston University, United States
Santhosh Girirajan,
The Pennsylvania State University, United States

***Correspondence:**
Paola Bovolenta
pbovolenta@cbm.csic.es
Marcos J. Cardozo
mcardozo@cbm.csic.es

[†] These authors have contributed equally to this work and share first authorship

[‡] These authors have contributed equally to this work and share senior authorship

Specialty section:
This article was submitted to Signaling, a section of the journal Frontiers in Cell and Developmental Biology

Received: 30 August 2021
Accepted: 05 October 2021
Published: 22 October 2021

Citation:
Camacho-Macorra C, Sintes M, Tabanera N, Grasa I, Bovolenta P and Cardozo MJ (2021) Mosmo Is Required for Zebrafish Craniofacial Formation. Front. Cell Dev. Biol. 9:767048. doi: 10.3389/fcell.2021.767048

Hedgehog (Hh) signaling is a highly regulated molecular pathway implicated in many developmental and homeostatic events. Mutations in genes encoding primary components or regulators of the pathway cause an array of congenital malformations or postnatal pathologies, the extent of which is not yet fully defined. Mosmo (Modulator of Smoothened) is a modulator of the Hh pathway, which encodes a membrane tetraspan protein. Studies in cell lines have shown that Mosmo promotes the internalization and degradation of the Hh signaling transducer Smoothened (Smo), thereby down-modulating pathway activation. Whether this modulation is essential for vertebrate embryonic development remains poorly explored. Here, we have addressed this question and show that in zebrafish embryos, the two *mosmo* paralogs, *mosmoa* and *mosmob*, are expressed in the head mesenchyme and along the entire ventral neural tube. At the cellular level, Mosmoa localizes at the plasma membrane, cytoplasmic vesicles and primary cilium in both zebrafish and chick embryos. CRISPR/Cas9 mediated inactivation of both *mosmoa* and *mosmob* in zebrafish causes frontonasal hypoplasia and craniofacial skeleton defects, which become evident in the adult fish. We thus suggest that *MOSMO* is a candidate to explain uncharacterized forms of human congenital craniofacial malformations, such as those present in the 16p12.1 chromosomal deletion syndrome encompassing the *MOSMO* locus.

Keywords: hedgehog signaling (Hh), Smoothened (Smo), tetraspan transmembrane protein, craniofacial abnormalities, Mosmo

INTRODUCTION

Communication among cells is a fundamental mechanism for the development of multicellular organisms. This communication is mostly mediated by elaborated signaling mechanisms, among which the Hedgehog (Hh) pathway represents a prototypical example. This pathway is evolutionary conserved and pleiotropically used among species (Ingham et al., 2011). Indeed, its function has been involved in a wide variety of developmental events including cell specification, proliferation, differentiation, migration, and axon guidance as well as in adult tissues' homeostasis and regeneration (Sánchez-Camacho and Bovolenta, 2009; Briscoe and Thérond, 2013; Petrova and Joyner, 2014). These functions are exerted in different tissues and organs: among others, the central nervous system (CNS), the limbs, the vascular system, and the craniofacial structures (Abramyan, 2019; Sasai et al., 2019).

Hedgehog signaling relies on the widespread participation of core components of the pathway such as the transmembrane proteins Patched (Ptc) and Smoothened (Smo). By default, Ptc blocks the function of Smo that remains localized in endosomes. Upon Hh ligand binding, Ptc releases Smo inhibition, enabling Smo localization at the primary cilium of the targeted cell, thereby initiating the activation of specific intracellular cascades (Murone et al., 1999). The diversification and specificity of the signaling outputs is instead fostered by the participation of other components that have more restricted spatio-temporal distributions and/or can modify intracellular signaling in a context dependent manner. These include, for example, the ligands themselves [i.e., Sonic (Shh), Indian (Ihh), and Desert (Dhh) hedgehog], a number of Hh binding proteins such as Boc, Cdon, and Gas1 that can act both as positive (Cole and Krauss, 2003; Allen et al., 2007, 2011) or negative signaling regulators (Bergeron et al., 2011; Cardozo et al., 2014; Echevarría-Andino and Allen, 2020) and transcriptional or non-transcriptional effectors of the pathway (e.g., Gli1, Gli2, Gli3, PKA, and Src) (Jia et al., 2004; Sánchez-Camacho and Bovolenta, 2009; Yam et al., 2009; Hui and Angers, 2011). This diversity also explains the broad spectrum of congenital malformations (e.g., holoprosencephaly, ciliopathies, skeletal, and craniofacial defects) associated with mutations in gene encoding components of the Hh pathway (Sasai et al., 2019) or its defective postnatal function, which has been associated with a large number of cancer types (Jeng et al., 2020).

Whether we have unveiled the full extent of the Hh pathway complexity and of the pathologies associated to its dysfunction is still undetermined. Indeed, a recent genome-wide screen aimed at identifying novel modulators of Hh signaling using CRISPR/Cas9 technology in the NIH-3T3 mouse cell line, uncovered the existence of new pathway regulators, including an unannotated gene, now known as *MOSMO* (MOdulator of SMOothened) (Pusapati et al., 2018). In the same study, *Mosmo* was demonstrated to encode a membrane tetraspan protein, which promoted the endocytosis of the Hh transducer Smo, thereby lowering its levels at the cell plasma membrane (Pusapati et al., 2018). To what extent Mosmo participates in Hh signaling regulation *in vivo,* however, it is just beginning to be elucidated (Lasser et al., 2020; Kong et al., 2021; Pizzo et al., 2021).

Here, we have addressed this question and report that in zebrafish the two *mosmo* paralogs (*mosmoa* and *mosmob*) have an overlapping distribution in embryonic ventral neural tube and then in the larva head mesenchyme. Consistent with the latter distribution genetic inactivation of both paralogs causes frontonasal hypoplasia and craniofacial skeleton defects, suggesting that *MOSMO* is a candidate to explain uncharacterized forms of these type of human congenital malformations.

METHODS

Fish Lines and Husbandry

AB/Tübingen (AB/Tue) zebrafish were maintained at 28°C on 14/10 h light/dark cycle. Embryos were raised at 28°C, collected and maintained in E3 medium (5 mM NaCl, 0.17 mM KCl, 0.33 mM CaCl, 0.33 mM MgSO4, 10^{-5}% Methylene Blue). All used procedures were approved by the ethical committees for animal experimentation of the Consejo Superior de Investigaciones Científicas (CSIC) and Comunidad Autónoma de Madrid.

Chick Embryos Maintenance

Fertilized chick embryos (Santa Isabel Farm, Cordoba, Spain) were incubated at 38°C in a humidified incubator until the desired stage, determined according to Hamburger and Hamilton (1992).

Whole Mount *in situ* Hybridization

Total mRNA from AB/Tue zebrafish embryos was extracted using RNeasy Mini kit (Qiagen) according to manufacturer instructions. cDNA was synthesized using Super Script kit (Roche) following manufacturer instructions. PCR products, obtained from cDNA amplification using specific primers (**Supplementary Table 1**), were cloned in PCSA plasmid (Agilent Technologies), as described by the manufacturer. Plasmid DNA preparations were obtained using Genopure Plasmid Midi kit (Roche) following kit instructions. Digoxigenin-UTP-labeled antisense probes for *in situ* hybridization (ISH) were synthesized and purified using Super Script kit (Roche) following the manufacturer instructions. ISH was performed by standard procedures and visualized with NBT/BCIP (dark blue).

Cloning Procedures

The PCSA-mosmoa_p1 plasmid was used as a template to amplify by PCR *mosmoa* and further add an hemagglutinin tag (HA) and restriction sites with the following primers: Fw 5′-aatCTCGAGCCTGAGATGGATAAACTC-3′. Rv 5′-ttaGAA TTCTCAAGCGTAATCTGGAACATCGTATGGGTAGCCAGG AAGACACACTTC-3′. The PCR product was cloned in PCSA plasmid (Agilent Technologies) as described by the manufacturer. The mosmoa-HA fragment was then excised with restriction enzymes and cloned in the pCIG vector (Megason and McMahon, 2002) for chick embryo electroporation and in pCS2 for cell transfection and synthesis of mRNA to be injected in zebrafish embryos.

Chick Embryo Electroporation

The pCIG Mosmoa-HA plasmid (1 μg/μl) was co-injected with a pCAG-2A-Arl13b-tRFP [Arl13b-tRFP construct generated by Schmitz et al. (2017)] (1 μg/μl) into the neural tube ventricle of HH10 chick embryos followed by *in ovo* electroporation as previously described (Cardozo et al., 2014).

Cell Transfection, Tissue Processing, and Immunochemistry

Human embryonic kidney (HEK) cells were cultured on glass coverslips in DMEM supplemented with 10% fetal calf serum and glutamine (2 mM). The pCS2-*mosmoa*-HA construct was transfected using lipotransfectin (Solmeglas) following the manufacture instructions. Cells were fixed with 4% paraformaldehyde in 0.1 M phosphate buffer pH 7.2 (wt/vol)

at 37°C and then washed in PBS containing 0.5% Triton-X-100. Chick embryos were fixed by immersion in 4% cold PFA overnight at 4°C, washed, incubated in a 15% sucrose-PBS solution (wt/vol), embedded and frozen in a 7.5% gelatine in 15% sucrose solution (wt/vol). Cryostat sections, whole embryos or cells samples were stained with Hoechst and α-HA antibody produced in rabbit (1:250. Sigma, H-6908) and Donkey anti-Rabbit Alexa Fluor 488 secondary antibody (Invitrogen, A-21206), following standard procedures.

Zebrafish Mutant Generation

Single guide RNAs (sgRNAs) targeting coding regions of *mosmoa* and *mosmob* for CRISPR/Cas9 deletion were designed using the tools provided by CHOPCHOP online service[1] searching for potential disruption of restriction enzyme sites (Labun et al., 2019). Oligos were designed as described in Varshney et al. (2016) and their sequence is reported in **Supplementary Table 1**. sgRNAs were transcribed and purified using Maxi Script T7 (NEB) following the manufacturer's instructions. sgRNAs were microinjected together with Cas9 protein (300 ng/μL; EnGen® Spy Cas9 NLS, New England Biolabs) in 1 to 2 cell stage AB/Tue using a Narishige microinjector. F0 embryos were let grown and outcrossed with wt AB/Tue fish. Genomic DNA from tail clips of F1 zebrafish embryos was amplified by PCR and digested to identify disruption of selected restriction sites. DNA from potential mutants were sequenced, those with a disrupted and truncated reading frame were selected to generate the fish lines.

Genotyping

DNA from embryos or adult fish was amplified by PCR using the primers listed in **Supplementary Table 1**. PCR products were digested with selected enzymes at 37°C for 2 h to distinguish among wt, heterozygous, and mutant *mosmoa* and/or *mosmob* fish.

Bone and Cartilage Staining

Cartilage staining of zebrafish larvae and adult fish bones was performed with Alcian Blue and Alizarin Red, as, respectively described in Schilling et al. (1996), Sakata-Haga et al. (2018).

Imaging and Data Processing

Embryos were immersed in 75% glycerol and whole-body images were obtained using a Leica CTR5000 stereomicroscope connected to a Leica DFC500 digital camera operated by Leica software. The adult fish stained with the Alizarin Red chromogen, which also emits red fluorescence, were photographed under fluorescent light stimulation using a Leica CTR5000 stereomicroscope connected to a Leica DFC350 FX digital camera operated by Leica software. The drawings in **Figure 4G** were traced in Adobe Illustrator using representative photographs of wt and *mosmoa*$^{-/-}$;*mosmob*$^{-/-}$ adult mutants. LSM710 confocal laser scanning coupled to an AxioObserver inverted microscope (Zeiss) was used to obtain digital images of cryostat sections or cells samples. ImageJ (Fiji) software was used to process and analyze images.

[1]http://chopchop.cbu.uib.no

Statistical Analyses

The ImageJ (Fiji) software was employed to obtain quantifications reported in **Figure 3**. Adult fish were anesthetized with tricaine and photographed in lateral views and the distance from the eye to the tip of the preorbital region was measured and normalized to the eye size in each one of the analyzed genotypes. Data were analyzed using GraphPad Prism 7 statistic software. One-way ANOVA test was used owing to the parametric distribution of the data, followed by Tukey's multiple comparisons test to determine differences among groups.

RESULTS

Mosmo Paralogs Show a Largely Overlapping Distribution in the Developing Zebrafish

The zebrafish genome carries two different paralogs of the *mosmo* gene: *mosmoa* and *mosmob* (ZFIN:ZDB-GENE-101203-6; ZFIN:ZDB-GENE-060929-1030). To determine their expression pattern during embryonic and larval development, we generated two different specific ISH probes for each one of the two paralogs (**Figure 1A**). Both *mosmoa* and *mosmob* were detected at gastrulation and bud stages as well as during somitogenesis (**Figures 1H,I,O,P**). At this stage *shha*, one of the ligands of the pathway, is expressed along the midline of the entire ventral neural tube (**Figures 1B,C**), from which it diffuses to pattern the adjacent cells with a mechanism highly conserved across vertebrates (Martí et al., 1995; Roelink et al., 1995). During somitogenesis, *mosmoa* and *mosmob* were also found localized along the length of the ventral neural tube (**Figures 1J,Q**) with an overlapping distribution that, however, was more dorsally extended than that of *shha* (**Figures 1C–G**). Specific expression was also observed in the mesenchyme surrounding the neural tube (**Figures 1D–G**) and in the optic vesicles (**Figures 1K,R**). At 2 dpf and larval stages, *mosmoa* and *mosmob* were no longer detected in the neural tube but strongly localized in the head mesenchyme (**Figures 1L,M,S,T**), surrounding, among others, the ethmoid plate (**Figures 1N,N′,U,U′**).

The reported patterns were consistently observed with both of the probes generated for each one of the paralogs (**Figure 1**), validating the reported distribution.

*M*osmoa Localizes at the Plasma Membrane, Endosomes, and Primary Cilia

Attempts to determine the subcellular localization of the protein showed that, at least in NIH-3T3 cells, Mosmo localizes at the plasma membrane and endosome (Pusapati et al., 2018). To verify if this is the subcellular distribution in the developing embryo, we generated a human influenza hemagglutinin (HA) tagged version of *mosmoa* (*mosmoa-HA*). We focused on this paralog because its amino acid (aa) sequence is 100% identical to that of its human ortholog, whereas mosmob aa sequence has a lower homology (89.8% identity). We first verified the efficiency of our construct by transfecting HEK cells with the

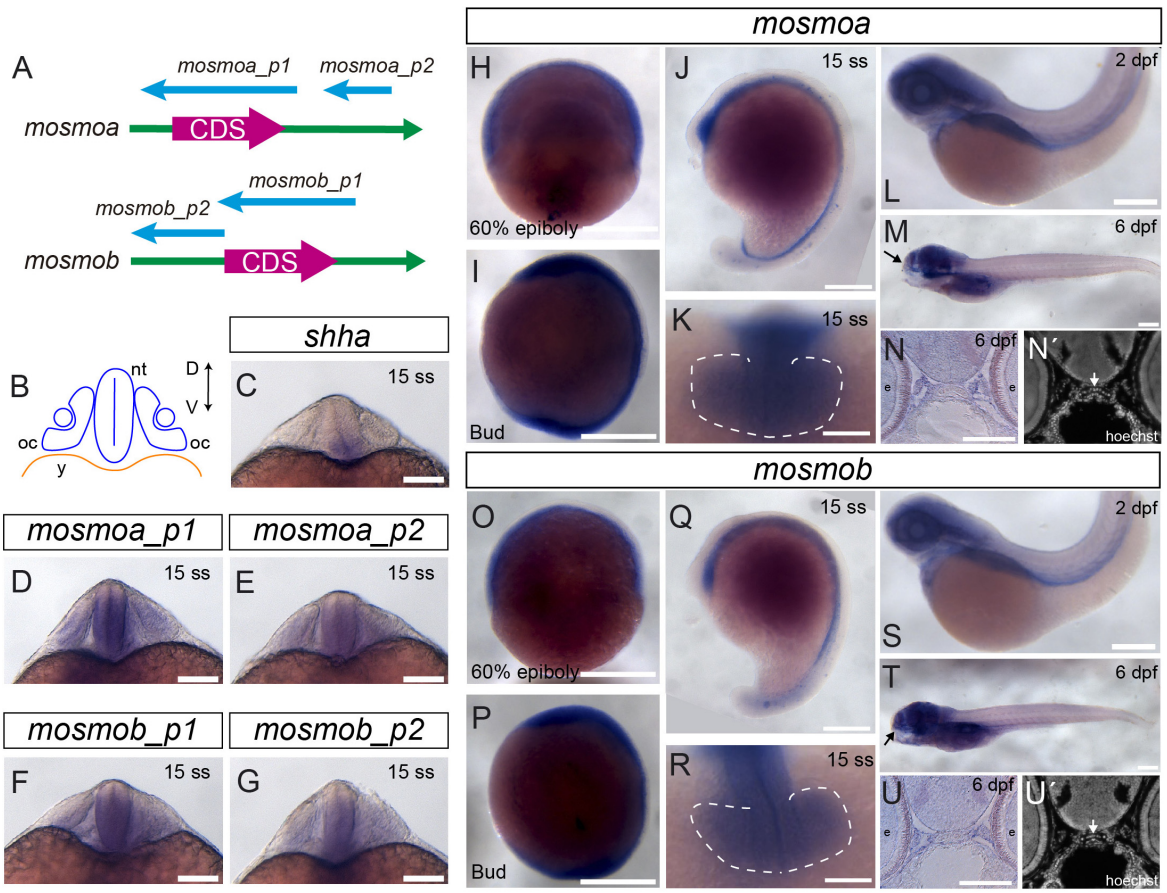

FIGURE 1 | Mosmo paralogs show a largely overlapping distribution in zebrafish. **(A)** Schematic representation of *mosmoa* and *mosmob* mRNAs and probes used for *in situ* hybridization (ISH). p1, probe #1. p2, probe #2. **(B)** Schematic representation of a frontal section of a zebrafish embryo at 20 hpf at the level of the optic cup. Expression pattern of *shha* **(C)**, *mosmoa* **(D,E)** and *mosmob* **(F,G)** at 20 hpf. Note that the two probes for *mosmoa* and *mosmob* show an identical distribution. Note also that both paralogs have an overlapping distribution in the ventral neural tube but more dorsally extended than that of *shha*. **(H,U)** Expression pattern of embryos hybridized with *mosmoa* and *mosmob* at 60% epiboly **(H,O)**, bud **(I,P)** and 15 ss stage **(J,K,Q,R)**, 2 dpf **(L,S)** as well as at 6 dpf **(M,T)**. Note that at 60% epiboly and bud stage the expression of both genes is localized along the ventral anterior-posterior axis of the embryos. At 15 ss, a low level expression of both *mosmoa* and *mosmob* is detected in the optic vesicles (**K,R,** dashed line) and along the ventral neural tube from the diencephalon to the tail bud **(J,Q)**. At 2 and 6 dpf, the expression of both genes localizes to the head region. The eyes were removed in panels **(M,T)**. Frontal sections of 6 dpf embryos hybridized *in toto* for *mosmoa* **(N)** or *mosmob* **(U)** and counterstained with Hoechst **(N′,U′)**. ISH signal for both paralogs localizes around the ethmoid cartilage **(N,N′,U,U′** white arrows). D, dorsal; V, ventral; oc, optic cup; nt, neural tube; and y, yolk. Scale bars: 200 μM.

mosmoa-HA containing plasmid followed by immunostaining for HA. As reported for NIH-3T3 cells (Pusapati et al., 2018), the tagged protein was detected at the plasma membrane and endosomes (**Figure 2A**). When *mosmoa-HA* mRNA was injected in zebrafish, HA immunosignal was similarly localized at the blastomers' plasma membrane and endosomes (**Figure 2B**).

When Hh signaling is active, Smo localizes at the primary cilium of the targeted cells. Notably, Mosmo was also observed in the primary cilia of NIH-3T3 cells (Pusapati et al., 2018). We thus asked if this localization could be observed also *in vivo*. The primary cilium can be easily detected in the chick neural tube as this organelle protrudes in the rather wide ventricle of chicken embryos. We thus co-electroporated two plasmids carrying *mosmoa-HA* and *arl13b-RFP*, respectively. The latter is a primary cilium specific protein, widely used to visualize this structure (Schmitz et al., 2017). Indeed, 24 h after electroporation, at HH14, HA, and RFP fluorescent signals co-localized in the cilium of a subset of the electroporated cells (**Figures 2C–D′**).

Taken together these data indicate that *in vivo* Mosmoa localizes at the plasma membrane, endosomes, and the primary cilia, suggesting that it may favors Smo translocation to this organelle, thus influencing signaling activation.

Mosmo Paralogs Are Required for Zebrafish Craniofacial Formation

To explore the possible roles of *mosmoa* and *mosmob*, we inactivated the two genes using CRISPR-Cas9 technology. We selected founders at the F1 generation that carried frameshift mutations in either *mosmoa* or *mosmob* gene and generated stable *mosmoa*$^{-/-}$ and *mosmob*$^{-/-}$ mutant lines (**Figure 3A**). *Mosmoa*$^{-/-}$ and *mosmob*$^{-/-}$ mutant embryos show no gross

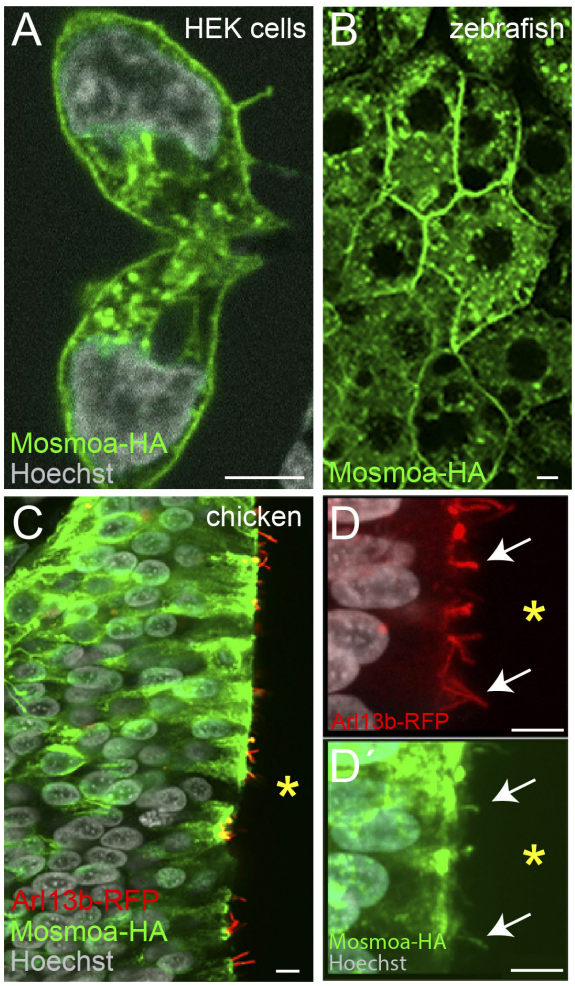

FIGURE 2 | *Mosmoa* localizes at the plasma membrane, endosomes, and primary cilia. **(A)** Example of human embryonic kidney (HEK) cells transfected with *mosmoa-HA*, immunostained for α-HA (green), and counterstained with Hoechst (white). **(B)** Dorsal view of a zebrafish gastrula (7 hpf) injected with *mosmoa-HA* mRNA and immunostained for α-HA (green). **(C–D′)** Transversal sections of chick embryo neural tubes co-electroporated with *mosmoa-HA* and the cilia marker *arl13b-RFP*. In both HEK cells and zebrafish EVL cells Mosmoa-HA signal localizes at the plasma membrane and in endo-vesicles. In HH14 chick embryos, neural tube Mosmoa-HA is also observed in the in the *Arl13b*-positive cilia (white arrows) **(D,D′)**. Yellow asterisk marks the neural tube ventricle **(C–D′)**. Scale bars: 5 μm.

morphological defects and grew to adulthood without evident defects. This was perhaps not surprising given that both genes share expression pattern and their respective proteins present a high degree of sequence homology, suggesting that the two paralogs may compensate each other activity. To overcome this possible compensatory effect, we intercrossed the *mosmoa*$^{-/-}$ and *mosmob*$^{-/-}$ mutant lines obtaining a *mosmoa*$^{-/-}$;*mosmob*$^{-/-}$ double mutant fish. At first glance, double mutant embryos showed no major gross alterations or histological defects along the neural tube and their size was similar to that of their sibling (not shown).

Other than in the neural tube, the two *mosmo* paralogs are expressed with a largely overlapping pattern also in different regions of the larva head. We thus used Alcian blue staining to label the cranio-facial cartilage of the larva. There were no obvious differences in the cartilaginous elements when wt, *mosmoa*$^{-/-}$;*mosmob*$^{-/+}$ and *mosmoa*$^{-/-}$;*mosmob*$^{-/-}$ were compared (**Figures 3B–G**), although the rostral tip of the head appeared flatter at least in part of the double mutants (**Figure 3F**, arrowhead). To determine if this abnormality was only transient, we analyzed the morphology of the head in the adult fish. *Mosmoa*$^{-/-}$;*mosmob*$^{-/-}$ double mutants consistently exhibited a significantly shorter frontonasal region (**Figures 3H,I**), which was not observed in their sibling of other genotypes (**Figure 3J**). Furthermore, the operculum was reduced in size, leaving the gills exposed (**Figure 3I**).

Hedgehog signaling is essential for the development of the anterior neurocranium (Wada et al., 2005) and disruption of *smo* activity in zebrafish affects the craniofacial skeleton (Eberhart et al., 2006; Swartz et al., 2012). Thus, the frontonasal hypoplasia observed in the double mutants could be the consequence of alterations in the osseous components of the craniofacial skeleton. To determine this possibility, we stained the skeleton of wt, *mosmoa*$^{\pm}$;*mosmob*$^{\pm}$ and *mosmoa*$^{-/-}$;*mosmob*$^{-/-}$ adult fish with Alizarin red (**Figures 4A–F**). The bones of the frontonasal region, especially the maxillary and premaxillary bones of *mosmoa*$^{-/-}$;*mosmob*$^{-/-}$ double mutants were altered as compared to those of wt or heterozygous fish (**Figures 4A–F**) as highlighted in the schematic drawings reporting the phenotypes (**Figure 4G**).

Taken together these data indicate that *mosmoa* and *mosmob* have an overlapping function, which is required for the acquisition of a proper craniofacial structure in zebrafish.

DISCUSSION

Modulators of Hh signaling play crucial roles in diversifying the output of Hh signaling (Gallardo and Bovolenta, 2018). The present study reinforces this idea and shows that in zebrafish the combined activity of the two *mosmo* paralogs, *mosmoa* and *mosmob*, are required for the proper craniofacial formation in zebrafish.

This apparently restricted effect is somewhat surprising as both *mosmoa* and *mosmob* are expressed with an overlapping pattern not only in the craniofacial mesenchyme of the larvae but also along the ventral region of the embryonic neural tube. The latter distribution overlaps with that of a number of Hh signaling components, including the ligand *shha*, *shhb* (Ekker et al., 1995), or the receptor *ptch2* (Concordet et al., 1996), and the transducer *smo* (Varga et al., 2001). In line with the idea that Mosmo acts on Smo promoting its endocytosis (Pusapati et al., 2018), we found Mosmoa localized in endocytic vesicles and the plasma membrane as well as the primary cilium, where Smo translocate when Hh signaling is activated. Thus and as previously proposed (Pusapati et al., 2018), the combined activity of the two *mosmo* paralogs could modulate Hh signaling activation in different contexts during development. However,

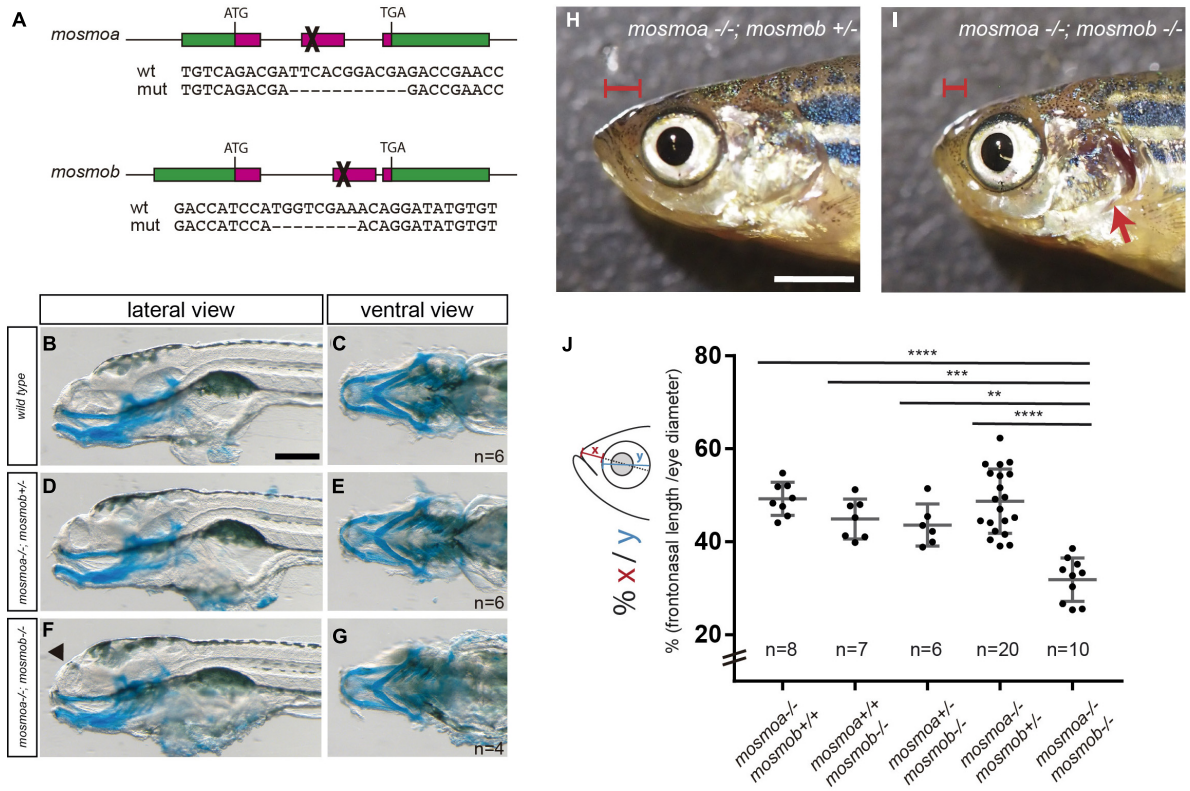

FIGURE 3 | *mosmoa*$^{-/-}$;*mosmob*$^{-/-}$ double mutants display facial abnormalities. **(A)** Schematic representation of the strategy used to inactivate *mosmoa* and *mosmob* zebrafish genes using CRISPR-Cas9 technology and sequence of the selected mutants. **(B–G)** Lateral and ventral views of 5 dpf wild type **(B,C)**, *mosmoa*$^{-/-}$;*mosmob*$^{\pm}$ **(D,E)** and *mosmoa*$^{-/-}$;*mosmob*$^{-/-}$ **(F,G)** zebrafish larvae stained with Alcian Blue to detect cartilage head organization. The rostral tip of the head appeared flatter in some of the double mutants (**F**, arrowhead). Eyes were removed for better staining visualization. The number of animals analyzed for each genotype is indicated in the right bottom corner in panels **(C,E,G)**. Scale bar 150 μm. **(H,I)** Lateral view of adult *mosmoa*$^{-/-}$;*mosmob*$^{\pm}$ **(H)** and *mosmoa*$^{-/-}$;*mosmob*$^{-/-}$ double mutants **(I)**. Note that in double mutants the head is flatter and shorter (**I**, red brackets) than in *mosmoa*$^{-/-}$;*mosmob*$^{\pm}$ fish and the operculum is abnormal exposing the gills (**I**, red arrow). **(J)** Quantification of the distance from the eye to the tip of the preorbital region (x) in relation to the eye size (y) in adult fish of different genotypes. *mosmoa*$^{-/-}$;*mosmob*$^{-/-}$ double mutants show a shorter fronto-nasal length than their siblings. One-way ANOVA followed by Tukey's multiple comparison tests to analyze differences among groups. $^{**}P < 0.01$, $^{***}P < 0.001$, and $^{****}P < 0.0001$. Scale bar 20 mm.

loss of *mosmo* function in zebrafish seems to be mostly linked to the formation of the cranio-facial skeleton, with an evident head hypoplasia in the adult mutant fish but no other obvious defects. Indeed, *Mosmo* double mutants grow to adulthood and do not seem to have obvious behavioral problems, supporting a non-essential role of *mosmo* paralogs for zebrafish growth, survival, and reproduction. Consistent with this idea, we have not observed neural tube defects or gross abnormalities in other organs of the mutants at least upon histological analysis. Nevertheless, we cannot rule out the possibility that subtle defects may be found with a more in-depth analysis. Indeed, a recent study shows that, in mouse, *Mosmo* contributes to embryonic development and its loss of function causes skeletal, heart, and lung anomalies leading to embryonic lethality (Kong et al., 2021). However, coinciding with our observations, no defects in neural tube patterning were, however, found (Kong et al., 2021). Knock-down of *mosmo* in *Xenopus* instead shows a craniofacial phenotype in which both craniofacial and cartilage development appears affected, in association with alteration of neural crest cell proliferation and migration (Lasser et al., 2020). Interestingly, the coexistence of neurodevelopmental and craniofacial defects were observed in experiments performed in both *Drosophila* and *Xenopus* aimed at testing the importance of "a two-hit model" as trigger of neurodevelopmental disorders (Pizzo et al., 2021). Notably the study demonstrated a synergistic interaction between mutated *mosmo* and *setd5* (Pizzo et al., 2021), a gene encoding a histone methyltransferase, which has been associated with intellectual disability (Grozeva et al., 2014). This functional interaction observed in both *Drosophila* and *Xenopus* seems to be present also in humans (Pizzo et al., 2021). In this respect the *mosmoa*$^{-/-}$;*mosmob*$^{-/-}$ double mutants, could be an additional model in which to explore how *setd5* and *mosmo* synergize causing more severe congenital malformations.

The Hh ligands Shh and Ihh are osteogenic regulators and both are expressed in craniofacial elements (Chiang et al., 1996; Pan et al., 2013). In both mouse and zebrafish, Ihh secreted by chondrocytes stimulates the ossification of the perichondrial cell layer that surrounds the developing cartilage (St-Jacques et al., 1999; Hammond and Schulte-Merker, 2009). In mice, conditional inactivation of *ihh* in cranial neural crest cells

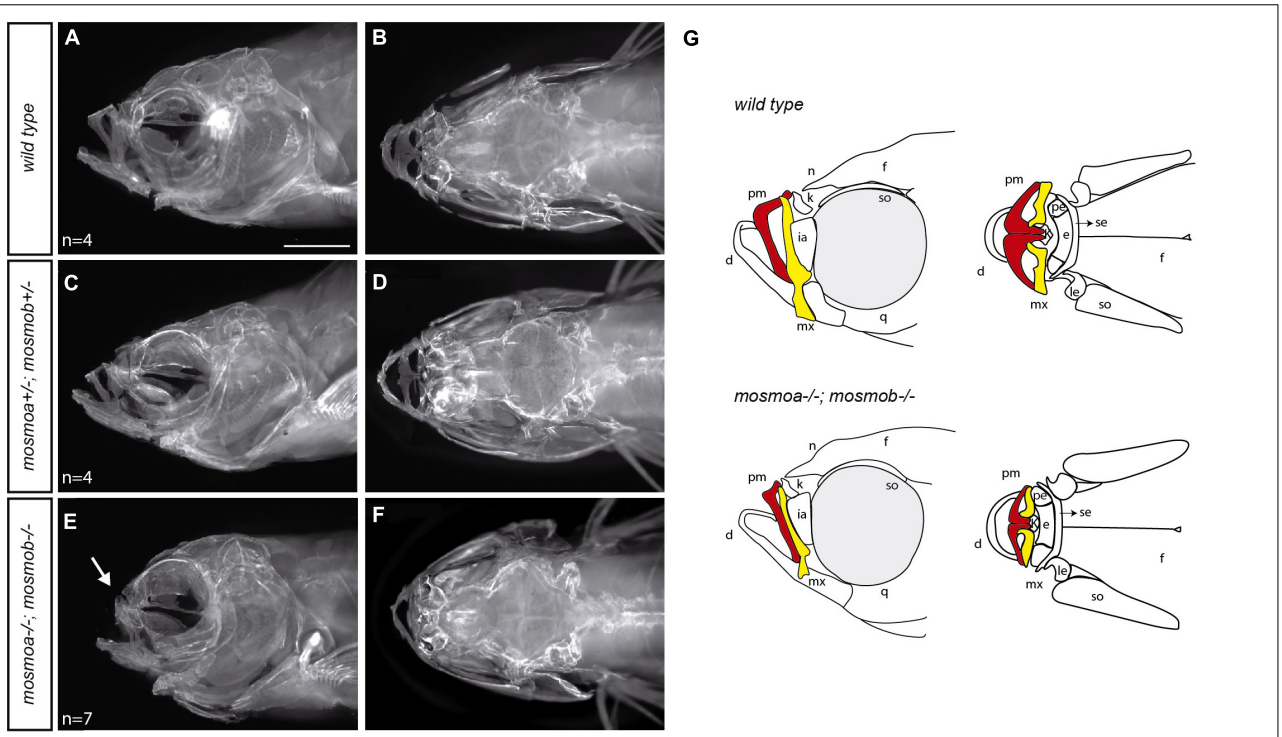

FIGURE 4 | Mosmo paralogs are required for head bone formation in zebrafish. **(A–F)** Lateral **(A,C,E)** and dorsal **(B,D,F)** views of the head of wt **(A,B)**, *mosmoa*$^{\pm}$;*mosmob*$^{\pm}$ **(C,D)** and *mosmoa*$^{-/-}$;*mosmob*$^{-/-}$ **(E,F)** adult zebrafish stained with alizarin red to label bone tissue. Note the bone malformation in the frontonasal region of *mosmoa*$^{-/-}$;*mosmob*$^{-/-}$ double mutants (**E**, arrow) in comparison to heterozygous and wt fish **(A,C)**. **(G)** Cartoons of the craniofacial appearance of wt and *mosmoa*$^{-/-}$;*mosmob*$^{-/-}$ adult mutants, from lateral and dorsal views, highlighting the maxillary (yellow) and premaxillary (red) bones. The number of animals analyzed for each genotype is indicated in the left bottom corner in panels **(A,C,E)**. d, dentary; e, ethmoid; f, frontal; ia, infraorbital; k, kinethmoid; le, lateral ethmoid; mx, maxillary; n, nasal; pe, pre-ethmoid; pm, premaxillary; q, quadrate; se, supraethmoid; and so, supraorbital. Scale bar, 2 mm.

causes skeletal malformations, including a markedly hypoplastic nasomaxillary complex (Amano et al., 2020). Furthermore, zebrafish mutants lacking enzymes involved in proteoglycans synthesis (*fam20b*$^{-/-}$ and *xylt1*$^{-/-}$) exhibit an accelerated *ihh* expression and premature bone formation, resulting in an adult fish with midface hypoplasia among other malformations (Eames et al., 2011). These features resemble those we observe in the *mosmoa*$^{-/-}$; *mosmob*$^{-/-}$ double mutants. Thus, it is tempting to speculate that *mosmo* paralogs may participate in signaling response triggered by *ihh* during osteogenesis, perhaps with an accelerated bone formation in the absence of Mosmo activity.

Intraflagellar proteins (IFTs) in the primary cilia, such as IFT80, affect Hh signaling and are required for osteoblast differentiation (Yuan et al., 2016). The craniofacial/skeletal abnormalities linked to Mosmo function in *Xenopus* (Lasser et al., 2020; Pizzo et al., 2021), mouse (Kong et al., 2021), and zebrafish (this study) together with MOSMO protein subcellular localization, suggest that *MOSMO* homologs could be key controllers of SMO translocation to the primary cilia during osteogenesis, thereby modulating signal transduction. Although worthwhile testing, this possibility remains at the moment a speculation, given the lack appropriate genetic tools that enable following protein movements within the cilium.

Independently of the precise pathway components with which Mosmo may function, the coincidence of some phenotypic features observed upon inactivation of *Mosmo* in *Xenopus* (Lasser et al., 2020; Pizzo et al., 2021), mouse (Kong et al., 2021), and zebrafish (this study) suggests that defective function of the human *MOSMO* may have similar consequences. Notably, a deletion in chromosome 16, encompassing the human *MOSMO* among others genes, causes a rare disease known as recurrent 16p12.1 deletion syndrome. Patients present developmental delay, intellectual disability, and other anomalies which may vary from individual to individual. Among these anomalies, craniofacial and skeletal are among the most frequently found defects (Girirajan et al., 2010), including microcephaly and flat face (Ballif et al., 2007; Girirajan et al., 2010), resembling, at some point, the phenotype observed in adult *mosmoa*$^{-/-}$;*mosmob*$^{-/-}$ mutants.

CONCLUSION

In conclusion, our study shows a restricted and overlapping distribution of *mosmo* genes in zebrafish revealing the subcellular localization of the Mosmoa protein during development in endosomes, plasma membrane, and primary cilia. More importantly, the generation of *mosmoa*$^{-/-}$;*mosmob*$^{-/-}$ zebrafish mutants provides support for the idea that the human *MOSMO* might be a candidate gene underlying uncharacterized

forms of rare congenital craniofacial malformations. The double mutants further provide the opportunity to dissect the contribution of *MOSMO* to the phenotype associated with the human 16p12.1 deletion syndrome.

DATA AVAILABILITY STATEMENT

The original contributions presented in the study are included in the article/**Supplementary Material**, further inquiries can be directed to the corresponding authors.

ETHICS STATEMENT

The animal study was reviewed and approved by the Consejo Superior de Investigaciones Científicas (CSIC) and Comunidad Autónoma de Madrid.

AUTHOR CONTRIBUTIONS

MC and PB conceptualized and designed the research study and wrote the manuscript. MS and CC-M performed the ISH analysis and mutant generation and characterization. NT and MC generated data reported in **Figures 2**, **3** and IG in **Figure 4**. PB obtained the financial support. All authors read and approved the manuscript.

FUNDING

This work was supported by grants from the Spanish MINECO (BFU2016-75412-R with FEDER funds); AEI (PID2019-104186RB-I00 and RED2018-102553-T) and a grant from the Fundación Ramon Areces to PB. CC-M and MC are supported by predoctoral contract from the CIBERER and a Juan de la Cierva postdoctoral contract from the AEI (IJCI-2016-27683), respectively. IG is supported by a contract (CAM20_CBM_AI_06) from the 2020 program "Garantía Juvenil" of the Comunidad Autónoma de Madrid. A CBM Institutional grant from the Fundación Ramon Areces is also acknowledged.

ACKNOWLEDGMENTS

We acknowledged the excellent technical assistance of Alfonso Gutierrez Garcia in the fish facilities and the staff of the CBMSO Image analysis facility. We also acknowledged Elisa Martí for the pCAG-2A-Arl13b-tRFP vector.

SUPPLEMENTARY MATERIAL

The Supplementary Material for this article can be found online at: https://www.frontiersin.org/articles/10.3389/fcell.2021.767048/full#supplementary-material

REFERENCES

Abramyan, J. (2019). Hedgehog signaling and embryonic craniofacial disorders. *J. Dev. Biol.* 7:9. doi: 10.3390/jdb7020009

Allen, B. L., Song, J. Y., Izzi, L., Althaus, I. W., Kang, J.-S., Charron, F., et al. (2011). Overlapping roles and collective requirement for the coreceptors GAS1, CDO, and BOC in SHH pathway function. *Dev. Cell* 20, 775–787. doi: 10.1016/j.devcel.2011.04.018

Allen, B. L., Tenzen, T., and McMahon, A. P. (2007). The Hedgehog-binding proteins Gas1 and Cdo cooperate to positively regulate Shh signaling during mouse development. *Genes Dev.* 21, 1244–1257. doi: 10.1101/gad.1543607

Amano, K., Okuzaki, D., Aikawa, T., and Kogo, M. (2020). Indian hedgehog in craniofacial neural crest cells links to skeletal malocclusion by regulating associated cartilage formation and gene expression. *FASEB J.* 34, 6791–6807. doi: 10.1096/fj.201903269R

Ballif, B. C., Hornor, S. A., Jenkins, E., Madan-Khetarpal, S., Surti, U., Jackson, K. E., et al. (2007). Discovery of a previously unrecognized microdeletion syndrome of 16p11.2–p12.2. *Nat. Genet.* 39, 1071–1073. doi: 10.1038/ng2107

Bergeron, S. A., Tyurina, O. V., Miller, E., Bagas, A., and Karlstrom, R. O. (2011). brother of cdo (umleitung) is cell-autonomously required for Hedgehog-mediated ventral CNS patterning in the zebrafish. *Development* 138, 75–85. doi: 10.1242/dev.057950

Briscoe, J., and Thérond, P. P. (2013). The mechanisms of Hedgehog signalling and its roles in development and disease. *Nat. Rev. Mol. Cell Biol.* 14, 416–429. doi: 10.1038/nrm3598

Cardozo, M. J., Sánchez-Arrones, L., Sandonis, Á, Sánchez-Camacho, C., Gestri, G., Wilson, S. W., et al. (2014). Cdon acts as a Hedgehog decoy receptor during proximal-distal patterning of the optic vesicle. *Nat. Commun.* 5:4272. doi: 10.1038/ncomms5272

Chiang, C., Litingtung, Y., Lee, E., Young, K. E., Corden, J. L., Westphal, H., et al. (1996). Cyclopia and defective axial patterning in mice lacking Sonic hedgehog gene function. *Nature* 383, 407–413. doi: 10.1038/383407a0

Cole, F., and Krauss, R. S. (2003). Microform holoprosencephaly in mice that lack the Ig superfamily member Cdon. *Curr. Biol.* 13, 411–415. doi: 10.1016/s0960-9822(03)00088-5

Concordet, J. P., Lewis, K. E., Moore, J. W., Goodrich, L. V., Johnson, R. L., Scott, M. P., et al. (1996). Spatial regulation of a zebrafish patched homologue reflects the roles of sonic hedgehog and protein kinase A in neural tube and somite patterning. *Development* 122, 2835–2846.

Eames, B. F., Yan, Y.-L., Swartz, M. E., Levic, D. S., Knapik, E. W., Postlethwait, J. H., et al. (2011). Mutations in fam20b and xylt1 reveal that cartilage matrix controls timing of endochondral ossification by inhibiting chondrocyte maturation. *PLoS Genet.* 7:e1002246. doi: 10.1371/journal.pgen.1002246

Eberhart, J. K., Swartz, M. E., Crump, J. G., and Kimmel, C. B. (2006). Early hedgehog signaling from neural to oral epithelium organizes anterior craniofacial development. *Development* 133, 1069–1077. doi: 10.1242/dev.02281

Echevarría-Andino, M. L., and Allen, B. L. (2020). The hedgehog co-receptor BOC differentially regulates SHH signaling during craniofacial development. *Development* 147:dev.189076. doi: 10.1242/dev.189076

Ekker, S. C., Ungar, A. R., Greenstein, P., von Kessler, D. P., Porter, J. A., Moon, R. T., et al. (1995). Patterning activities of vertebrate hedgehog proteins in the developing eye and brain. *Curr. Biol.* 5, 944–955. doi: 10.1016/S0960-9822(95)00185-0

Gallardo, V., and Bovolenta, P. (2018). Positive and negative regulation of Shh signalling in vertebrate retinal development. *F1000Res* 7:F1000 Faculty Rev-1934.

Girirajan, S., Rosenfeld, J. A., Cooper, G. M., Antonacci, F., Siswara, P., Itsara, A., et al. (2010). A recurrent 16p12.1 microdeletion supports a two-hit model for severe developmental delay. *Nat. Genet.* 42, 203–209. doi: 10.1038/ng.534

Grozeva, D., Carss, K., Spasic-Boskovic, O., Parker, M. J., Archer, H., Firth, H. V., et al. (2014). De Novo loss-of-function mutations in SETD5, encoding a methyltransferase in a 3p25 microdeletion syndrome critical region, cause

intellectual disability. *Am. J. Hum. Genet.* 94, 618–624. doi: 10.1016/j.ajhg.2014.03.006

Hamburger, V., and Hamilton, H. L. (1992). A series of normal stages in the development of the chick embryo. *Dev. Dyn.* 195, 231–272. doi: 10.1002/aja.1001950404

Hammond, C. L., and Schulte-Merker, S. (2009). Two populations of endochondral osteoblasts with differential sensitivity to Hedgehog signalling. *Development* 136, 3991–4000. doi: 10.1242/dev.042150

Hui, C.-C., and Angers, S. (2011). Gli proteins in development and disease. *Annu. Rev. Cell Dev. Biol.* 27, 513–537. doi: 10.1146/annurev-cellbio-092910-154048

Ingham, P. W., Nakano, Y., and Seger, C. (2011). Mechanisms and functions of Hedgehog signalling across the metazoa. *Nat. Rev. Genet.* 12, 393–406. doi: 10.1038/nrg2984

Jeng, K.-S., Chang, C.-F., and Lin, S.-S. (2020). Sonic hedgehog signaling in organogenesis, tumors, and tumor microenvironments. *Int. J. Mol. Sci.* 21:758. doi: 10.3390/ijms21030758

Jia, J., Tong, C., Wang, B., Luo, L., and Jiang, J. (2004). Hedgehog signalling activity of Smoothened requires phosphorylation by protein kinase A and casein kinase I. *Nature* 432, 1045–1050. doi: 10.1038/nature03179

Kong, J. H., Young, C. B., Pusapati, G. V., Espinoza, F. H., Patel, C. B., Beckert, F., et al. (2021). Gene-teratogen interactions influence the penetrance of birth defects by altering Hedgehog signaling strength. *Development* 148. doi: 10.1242/dev.199867

Labun, K., Montague, T. G., Krause, M., Torres Cleuren, Y. N., Tjeldnes, H., and Valen, E. (2019). CHOPCHOP v3: expanding the CRISPR web toolbox beyond genome editing. *Nucleic Acids Res.* 47, W171–W174. doi: 10.1093/nar/gkz365

Lasser, M., Bolduc, J., Murphy, L., O'Brien, C., Lee, S., Girirajan, S., et al. (2020). 16p12.1 deletion orthologs are expressed in motile neural crest cells and are important for regulating craniofacial development in *Xenopus laevis*. *bioRxiv* [Preprint]. doi: 10.1101/2020.12.11.421347

Martí, E., Takada, R., Bumcrot, D. A., Sasaki, H., and McMahon, A. P. (1995). Distribution of Sonic hedgehog peptides in the developing chick and mouse embryo. *Development* 121, 2537–2547.

Megason, S. G., and McMahon, A. P. (2002). A mitogen gradient of dorsal midline Wnts organizes growth in the CNS. *Development* 129, 2087–2098. doi: 10.1242/dev.129.9.2087

Murone, M., Rosenthal, A., and de Sauvage, F. J. (1999). Sonic hedgehog signaling by the Patched–Smoothened receptor complex. *Curr. Biol.* 9, 76–84. doi: 10.1016/S0960-9822(99)80018-9

Pan, A., Chang, L., Nguyen, A., and James, A. W. (2013). A review of hedgehog signaling in cranial bone development. *Front. Physiol.* 4:61. doi: 10.3389/fphys.2013.00061

Petrova, R., and Joyner, A. L. (2014). Roles for Hedgehog signaling in adult organ homeostasis and repair. *Development* 141, 3445–3457. doi: 10.1242/dev.083691

Pizzo, L., Lasser, M., Yusuff, T., Jensen, M., Ingraham, P., Huber, E., et al. (2021). Functional assessment of the "two-hit" model for neurodevelopmental defects in *Drosophila* and *X. laevis*. *PLoS Genet.* 17:e1009112. doi: 10.1371/journal.pgen.1009112

Pusapati, G. V., Kong, J. H., Patel, B. B., Krishnan, A., Sagner, A., Kinnebrew, M., et al. (2018). CRISPR screens uncover genes that regulate target cell sensitivity to the morphogen sonic hedgehog. *Dev. Cell* 44:271. doi: 10.1016/j.devcel.2018.01.002

Roelink, H., Porter, J. A., Chiang, C., Tanabe, Y., Chang, D. T., Beachy, P. A., et al. (1995). Floor plate and motor neuron induction by different concentrations of the amino-terminal cleavage product of sonic hedgehog autoproteolysis. *Cell* 81, 445–455. doi: 10.1016/0092-8674(95)90397-6

Sakata-Haga, H., Uchishiba, M., Shimada, H., Tsukada, T., Mitani, M., Arikawa, T., et al. (2018). A rapid and nondestructive protocol for whole-mount bone staining of small fish and *Xenopus*. *Sci. Rep.* 8:7453. doi: 10.1038/s41598-018-25836-4

Sánchez-Camacho, C., and Bovolenta, P. (2009). Emerging mechanisms in morphogen-mediated axon guidance. *BioEssays* 31, 1013–1025. doi: 10.1002/bies.200900063

Sasai, N., Toriyama, M., and Kondo, T. (2019). Hedgehog signal and genetic disorders. *Front. Genet.* 10:1103. doi: 10.3389/fgene.2019.01103

Schilling, T. F., Piotrowski, T., Grandel, H., Brand, M., Heisenberg, C. P., Jiang, Y. J., et al. (1996). Jaw and branchial arch mutants in zebrafish I: branchial arches. *Development* 123, 329–344.

Schmitz, F., Burtscher, I., Stauber, M., Gossler, A., and Lickert, H. (2017). A novel Cre-inducible knock-in ARL13B-tRFP fusion cilium reporter. *Genesis* 55:e23073. doi: 10.1002/dvg.23073

St-Jacques, B., Hammerschmidt, M., and McMahon, A. P. (1999). Indian hedgehog signaling regulates proliferation and differentiation of chondrocytes and is essential for bone formation. *Genes Dev.* 13, 2072–2086.

Swartz, M. E., Nguyen, V., McCarthy, N. Q., and Eberhart, J. K. (2012). Hh signaling regulates patterning and morphogenesis of the pharyngeal arch-derived skeleton. *Dev. Biol.* 369, 65–75. doi: 10.1016/j.ydbio.2012.05.032

Varga, Z. M., Amores, A., Lewis, K. E., Yan, Y.-L., Postlethwait, J. H., Eisen, J. S., et al. (2001). Zebrafish smoothened functions in ventral neural tube specification and axon tract formation. *Development* 128, 3497–3509. doi: 10.1242/dev.128.18.3497

Varshney, G. K., Carrington, B., Pei, W., Bishop, K., Chen, Z., Fan, C., et al. (2016). A high-throughput functional genomics workflow based on CRISPR/Cas9-mediated targeted mutagenesis in zebrafish. *Nat. Protoc.* 11, 2357–2375. doi: 10.1038/nprot.2016.141

Wada, N., Javidan, Y., Nelson, S., Carney, T. J., Kelsh, R. N., and Schilling, T. F. (2005). Hedgehog signaling is required for cranial neural crest morphogenesis and chondrogenesis at the midline in the zebrafish skull. *Development* 132, 3977–3988. doi: 10.1242/dev.01943

Yam, P. T., Langlois, S. D., Morin, S., and Charron, F. (2009). Sonic hedgehog guides axons through a noncanonical, Src-family-kinase-dependent signaling pathway. *Neuron* 62, 349–362. doi: 10.1016/j.neuron.2009.03.022

Yuan, X., Cao, J., He, X., Serra, R., Qu, J., Cao, X., et al. (2016). Ciliary IFT80 balances canonical versus non-canonical hedgehog signalling for osteoblast differentiation. *Nat. Commun.* 7:11024. doi: 10.1038/ncomms11024

Conflict of Interest: The authors declare that the research was conducted in the absence of any commercial or financial relationships that could be construed as a potential conflict of interest.

Publisher's Note: All claims expressed in this article are solely those of the authors and do not necessarily represent those of their affiliated organizations, or those of the publisher, the editors and the reviewers. Any product that may be evaluated in this article, or claim that may be made by its manufacturer, is not guaranteed or endorsed by the publisher.

frontiers in Cell and Developmental Biology

ORIGINAL RESEARCH
published: 10 December 2021
doi: 10.3389/fcell.2021.770458

Developmental Disruption of *Erbb4* in *Pet1*+ Neurons Impairs Serotonergic Sub-System Connectivity and Memory Formation

*Candela Barettino[1†], Álvaro Ballesteros-Gonzalez[1†], Andrés Aylón[1], Xavier Soler-Sanchis[1], Leticia Ortí[1], Selene Díaz[1], Isabel Reillo[2], Francisco García-García[3], Francisco José Iborra[1], Cary Lai[4], Nathalie Dehorter[5], Xavier Leinekugel[6], Nuria Flames[2] and Isabel Del Pino[1]**

[1]Neural Plasticity Laboratory, Príncipe Felipe Research Center, Valencia, Spain, [2]Developmental Neurobiology Unit, Instituto de Biomedicina de Valencia, IBV-CSIC, Valencia, Spain, [3]Bioinformatics and Biostatistics Unit, Príncipe Felipe Research Center (CIPF), Valencia, Spain, [4]Department of Psychological and Brain Sciences, Indiana University, Bloomington, IN, United States, [5]INMED, INSERM, Aix Marseille University, Marseille, France, [6]Institut de Neurobiology de la Méditerranée (INMED, UMR1249), INSERM, Marseille, France

OPEN ACCESS

Edited by:
Sofia J. Araújo,
University of Barcelona, Spain

Reviewed by:
Sara Migliarini,
University of Pisa, Italy
Mariano Soiza-Reilly,
CONICET Institute of Physiology, Molecular Biology and Neurosciences (IFIBYNE), Argentina

***Correspondence:**
Isabel Del Pino
idelpino@cipf.es

†These authors have contributed equally to this work and share first authorship

Specialty section:
This article was submitted to Signaling, a section of the journal Frontiers in Cell and Developmental Biology

Received: 03 September 2021
Accepted: 19 November 2021
Published: 10 December 2021

Citation:
Barettino C, Ballesteros-Gonzalez Á, Aylón A, Soler-Sanchis X, Ortí L, Díaz S, Reillo I, García-García F, Iborra FJ, Lai C, Dehorter N, Leinekugel X, Flames N and Del Pino I (2021) Developmental Disruption of Erbb4 *in* Pet1+ *Neurons Impairs Serotonergic Sub-System Connectivity and Memory Formation. Front. Cell Dev. Biol. 9:770458. doi: 10.3389/fcell.2021.770458*

The serotonergic system of mammals innervates virtually all the central nervous system and regulates a broad spectrum of behavioral and physiological functions. In mammals, serotonergic neurons located in the rostral raphe nuclei encompass diverse sub-systems characterized by specific circuitry and functional features. Substantial evidence suggest that functional diversity of serotonergic circuits has a molecular and connectivity basis. However, the landscape of intrinsic developmental mechanisms guiding the formation of serotonergic sub-systems is unclear. Here, we employed developmental disruption of gene expression specific to serotonergic subsets to probe the contribution of the tyrosine kinase receptor ErbB4 to serotonergic circuit formation and function. Through an *in vivo* loss-of-function approach, we found that ErbB4 expression occurring in a subset of serotonergic neurons, is necessary for axonal arborization of defined long-range projections to the forebrain but is dispensable for the innervation of other targets of the serotonergic system. We also found that *Erbb4*-deletion does not change the global excitability or the number of neurons with serotonin content in the dorsal raphe nuclei. In addition, ErbB4-deficiency in serotonergic neurons leads to specific behavioral deficits in memory processing that involve aversive or social components. Altogether, our work unveils a developmental mechanism intrinsically acting through ErbB4 in subsets of serotonergic neurons to orchestrate a precise long-range circuit and ultimately involved in the formation of emotional and social memories.

Keywords: serotonin, ErbB4, NRG, memory, neuromodulation, neurodevelopmental disorders

1 INTRODUCTION

Serotonin (also known as 5-hydroxytryptamine (5HT)) is a phylogenetically conserved signaling molecule (Hay-Schmidt, 2000) regulating diverse emotional, cognitive and neurovegetative functions. In mammals, serotonergic neurons distributed in the raphe nuclei of the brainstem are clustered in different groups topographically classified as B1–B9 (Dahlstrom and Fuxe, 1964).

The largest group of serotonergic neurons allocate within the dorsal (B7 and B6) and median raphe (B8) nuclei (DRN and MRN, respectively) and develop exuberant axonal projections targeting almost every brain region.

A functionally diverse competence of DRN and MRN serotonergic circuits is thought to result from the development of extensive axonal projections reaching multiple brain targets. DRN and MRN serotonergic circuit formation is guided by intrinsic and extrinsic factors. For instance, general transcriptional mechanisms involved in serotonergic fate specification, i.e. *Lmx1b*, act at subsequent developmental stages to promote axon outgrowth from most serotonergic neurons (Donovan et al., 2019). Additional findings suggest that cell adhesion molecules (Cadherin 13) molecules and guidance cues (Eph5/ephrinA5) are involved in the negative regulation of axon outgrowth and/or pathfinding in addition to neuron proliferation of serotonergic neurons (Forero et al., 2017; Teng et al., 2017). In particular, high levels of ephrinA5 receptor expression in DRN has been described to repel axon growth in the hypothalamus and regulate proper arborization of serotonergic fibers in the olfactory bulb through repulsion by ephrinA5 (Teng et al., 2017).

Recent findings from multiscale analysis support the idea of a molecular, circuit and functional heterogeneity even within the DRN and MRN neurons. Electrophysiological, neuroanatomical and transcriptomic profiling suggest that DRN and MRN serotonergic neurons are highly heterogeneous (Okaty et al., 2015; Ren et al., 2019; Okaty et al., 2020; Senft et al., 2021). For example, neurons within the DRN have been described to segregate between circuits expressing the vesicular glutamate transporter 3 (Vglut3) preferentially innervating cortical areas and circuits expressing thyrotropin-releasing hormone (Trh) preferentially innervating subcortical nuclei (Ren et al., 2019) and regulating different behavioral demands (Ren et al., 2018). Additional studies showed restricted expression of the neuropeptide galanin in serotonergic neurons innervating the medial prefrontal cortex (Fernandez et al., 2016). However, although these findings were fundamental to parse out molecular profiles and assign them to projection-specificity, serotonergic neurons expressing Vglut3, Trh and/or galanin do not account for all DRN serotonergic circuits projecting to the forebrain. Thus, the molecular profiles of projection-defined serotonergic sub-systems targeting specific forebrain regions such as the thalamic sub-areas remain unresolved (Ren et al., 2019). Moreover, specific molecular mechanisms underlying sub-circuit development within the DRN or MRN are largely unknown.

NRG/ErbB4 signaling pathway has been thoroughly studied for its influence on the development of cortical GABAergic (Flames et al., 2004; Fazzari et al., 2010; Ting et al., 2011; Del Pino et al., 2013; Batista-Brito et al., 2017; Del Pino et al., 2017) and thalamocortical circuits (Lopez-Bendito et al., 2006) as well as in dopaminergic circuit function (Skirzewski et al., 2018). Genetic targeting previously revealed that ErbB4 is also expressed in subsets of serotonergic neurons (Bean et al., 2014). Nevertheless, whether ErbB4 is an intrinsic factor contributing to projection-defined serotonergic circuit development is unclear. Therefore, to gain a better understanding of the mechanisms underlying serotonergic circuit organization, we interrogate the functional relevance of *Erbb4*-expression for serotonergic circuit development and function. Here, we show that ErbB4 is co-expressed in subsets of adult 5HT neurons expressing the transcription factor *Pet1* required for serotonergic fate. We further demonstrate that ErbB4 is required for the axonal arborization of serotonergic projections in specific postsynaptic targets while dispensable for 5HT expression and global excitability in the DRN. Finally, we revealed that developmental deficiency of ErbB4 in serotonergic circuits impairs cognitive function related to specific types of memory in adult mice without affecting other emotional behaviors such as anxiety or coping behavior. Altogether, our findings link, for the first time, the NRG/ErbB4 signaling pathway with the organization of serotonergic sub-systems and unveils the specific role of this link in memory formation.

2 MATERIALS AND METHODS

2.1 Animals

Erbb4$^{f/f;Pet1\text{-}Cre;Ai9f/+}$ were generated by breeding *Pet1-Cre* (Fev-Cre) lines (JAX stock #012712; RRID:MGI:3696982) (Scott et al., 2005) with mice carrying the loxP-flanked (f) *Erbb4* alleles (Golub et al., 2004) and *Ai9/tdTomato* lines (JAX stock #007909; RRID: MGI:J:155793) (Madisen et al., 2010). Control mice included mice carrying *Pet1-Cre* or *Erbb4*$^{f/f}$ alleles. All animal procedures were approved by the Ethics Committee (CIPF, Spain) and complied with the Spanish and European regulations for the use of laboratory animals.

2.2 Immunohistochemistry and Imaging Analysis

Mice (postnatal day P60–90) were transcardially perfused with 4% PFA, post-fixed for 2 h and sectioned with a freezing microtome. Immunohistochemistry for 5HT, ErbB4 and tdTomato was performed in 40 µm-thick sections using the following primary antibodies: rabbit anti-ErbB4 (0618 produced by Cary Lai), goat anti-5HT (Abcam 66047 (1: 1,000), rabbit anti-5HT (1:5,000, Sigma #S5545, RRID:AB_ 477522) and rabbit anti-RFP (1:2,000, Rockland Cat# 600-401-379, RRID:AB_2209751). Secondary antibodies and Alexa555-conjugated streptavidin were purchased from Molecular Probes. Subsequently, sections were counterstained with DAPI and mounted with Mowiol. For the reconstruction of biocytin-filled neurons during *ex vivo* electrophysiology, 300 µm-thick brain sections were fixed overnight in 4% PFA at 4°C and incubated with Alexa488-conjugated streptavidin (1:500, Thermo Fisher Scientific Cat# S11223, RRID:AB_2336881).

Imaging of fluorescently labelled axonal arbors in target regions of the serotonergic system was performed with 20X 0.80NA objective in an Aperio Versa slide scanner (Leica Biosystems) or with the DMI-4 SP8 confocal microscope (Leica Biosystems). Following the neuroanatomical features (Franklin and Paxinos, 2008) in DAPI counterstained brain sections, images of 1,500 × 1,500 pixels (for the lateral hypothalamus, periventricular nucleus of the thalamus or

corpus callosum) or manually delimited brain regions (for the dentate gyrus, CA3 and CA1) were extracted from two single z-planes per area and from 3 areas per mouse in ImageScope (Leica Biosystems). The percentage of area occupied by fluorescent signal was performed in Fiji/ImageJ (RRID:SCR_002285) applying the same threshold over the background for all genotypes. For analysis of relative density of fluorescently labeled fibers, a threshold of 30 and 50 arbitrary units of intensity over the background was applied in images acquired with AperioVersa and with the confocal microscope, respectively. Background signal was quantified from 3 different regions of the field of view without tdTomato+ neuropil labelling. For cell counting, colocalization analysis and morphological reconstruction of biocytin-filled neurons, images were acquired with a 20X 0.75NA objective in a DMI-4 SP8 confocal microscope (Leica Biosystems). Colocalization was quantified from two different optical planes per section. For analysis of fluorescence intensity, images were acquired at 16bit depth. For neural tracing and morphological reconstruction, stacks were acquired at 1 µm step size and the SNT 3.1.109 tool of Fiji/ImageJ was employed (Arshadi et al., 2021).

2.3 *Ex Vivo* Electrophysiology

Erbb4$^{+/+;Pet1\text{-}Cre;Ai9f/+}$ and *Erbb4*$^{f/f;Pet1\text{-}Cre;Ai9f/+}$ male mice (12–13 weeks-old) were used. First, mice were anaesthetized with isoflurane and perfused with ice-cold artificial cerebrospinal fluid (aCSF) medium containing (in mM): 87 NaCl, 25 $NaHCO_3$, 5 D-(+)-glucose, 65 sucrose, 2.5 KCl, 1.25 NaH_2PO4, 0.5 $CaCl_2$, 7 $MgCl_2$, 5 ascorbic acid and 3.1 pyruvic acid saturated with 95% CO_2 and 5% O_2(pH 7.4). Then, mice were decapitated and brain was removed and placed in oxygenated aCSF. 300-µm coronal slices were obtained with a vibratome (Microm HM 650 V) and transferred to a chamber with aCSF solution consisting of: 125 NaCl, 25 $NaHCO_3$, 25 D-(+)-glucose, 2.5 KCl, 1.25 NaH_2PO_4, 2 $CaCl_2$, 1 $MgCl_2$, 1 ascorbic acid and 4 pyruvic acid saturated with 95% CO_2 and 5% O_2 (pH 7.4). Slices were allowed to recover at 35°C for 30 min. Patch clamp recordings in whole-cell configuration were performed at 25°C using a potassium gluconate-based intracellular solution containing (in mM): 135 K-gluconate, 10 HEPES, 10 Na-phosphocreatinine, 4 KCl, 4 MgATP, 0.3 NaGTP and adjusted to 290mosmol/l and pH7.2–7.4. Biocytin was added to the internal solution at a concentration of 1.5–2.5 mg/ml for *post hoc* immunohistochemistry. tdTomato expressing neurons were visualized with an upright microscope (Olympus BX51WI; RRID:SCR_018949) equipped with an ORCA-ER CCD Camera (Hamamatsu), a 40X/0.8 nA water-immersion objective (Olympus), a X-Cite 120Q fluorescence lamp and infrared-differential interference optics contrast for bright field imaging. Micro-pipettes of 10–12 MΩ were pulled from borosilicate glass using a vertical P-10 puller (Narishige). Data was acquired and sampled at 20 kHz using a MultiClamp 700B (Molecular Devices, RRID:SCR_018455), a digitizer Digidata 1440A (Molecular Devices, RRID:SCR_021038) and pClamp software (Molecular Devices, RRID:SCR_011323).

Intrinsic electrophysiological properties were calculated using different current-clamp protocols. Resting Membrane Potential (V_{rest}) was measured after breaking into the cell. Input Resistance (R_{in}) was obtained using 500 ms hyperpolarizing current steps of Δ5 pA from −20 to 0 pA. Rheobase, action potential kinetics and input-output function were measured by applying 500 ms depolarizing current steps of Δ 10 pA from 0 to +180 pA in neurons held at −70 mV. EasyElectrophysiology software (EasyElectrophysiology Ltd., RRID:SCR_021190) (Garcia et al., 2014) was used for the analysis of electrophysiological properties. Threshold potential was defined as dV/dt = 10 mV/ms using first derivative method. AP threshold was defined in a region of 10 ms before peak. Rise and decay time were determined in a minimum-maximum cutoff percentage of 10–90%. Half-width is calculated as the time between rise and decay at half amplitude. fAHP was detected in a search region of 0–9 ms after peak and mAHP in a region of 30–70 ms. Both values were calculated as baseline minus the minimum value within each region. Rheobase was defined as the minimum current injected to obtain the first AP from neurons held at −70 mV. Maximum firing frequency was obtained from spike frequency discharge upon +190 pA current injected. Inter-spike interval (ISI) was calculated as the difference between first and second AP at first step with ≥2AP. Spike frequency adaptation was obtained by dividing the first ISI by the final ISI of the trace with ≥4AP. Input-output curve was plotted averaging the number of AP detected for each neuron at each current step.

2.4 Mouse Behavioral Analysis

Adult *Erbb4*$^{f/f}$ and *Erbb4*$^{f/f;Pet1\text{-}Cre}$ male and female littermates (P60) were used for behavioral tests. Mice were maintained under standard housing conditions in 12 h dark/light cycles with food and water *ad libitum*. All different tests were implemented during the light phase blind to the genotype. Mice were handled and habituated to the experimenter for 3 days before the behavioral assays. All behavioral tests were separated at least by 24 h. The order of tests was as follows: open field, habituation to open field, Y-maze, sociability test, elevated plus maze (EPM), dark-light box and nest building test. Contextual fear conditioning, prepulse inhibition of the startle response (PPI), forced swimming and tail suspension test were performed in separated batches of animals. Testing apparatuses were cleaned with a solution of 70% ethanol in water after each trial to avoid olfactory cues. Behavioral tasks were recorded with a Logitech C270 webcam HD camera and analysed using Ethovision® XT software (Noldus, RRID:SCR_000441) unless otherwise stated.

2.4.1 Open Field

Spontaneous locomotor activity was measured in an open field apparatus. It consisted of a rectangular chamber of 48 × 48 × 48 cm that was made of plastic under uniform light conditions (70 lux). Mice were allowed to explore the arena for 10 min. The arena was delimited for analysis into two different regions: centre (square area of 30 × 30 cm equidistant from the walls) and the remaining borders. The time spent, velocity, distance as well as transitions between the zones were calculated with Ethovision® XT. Habituation to the open field was performed 1 day after first

exposure to the arena in the same conditions as previously described.

2.4.2 Spontaneous Alternation Task in the Y-Maze

Spontaneous alternation task was performed in a transparent Y-maze (50 × 8 cm each arm). Mice were placed into the centre of the maze and allowed to freely explore for 8 min. The exploration was recorded and the sequence of mouse entries in each arm was analysed *post hoc*. The spontaneous alternation behavior was calculated as the number of triads containing entries into all three arms divided by the maximum possible alternations as follows:

$$I_{alternation} = \frac{total\ alternations}{(total\ entries\ -2)} \times 100$$

2.4.3 Sociability and Preference for Social Novelty Test

Sociability and preference for social novelty was assessed in a three chambered arena (50 × 25 × 25 cm) with one cylinder in each side chamber. The cylinders (wire cup-like containers) allowed auditory, visual and olfactory interaction between mice. This paradigm consisted of three phases: habituation, sociability phase (S1) and social novelty (S2). During habituation, mice are allowed to explore the arena with the cylinders empty for 5 min. We routinely control that animals do not have a preference for any context by measuring the time spent in the lateral chambers during the habituation phase. In the S1 phase mice are allowed to explore the arena for 10 min with an unfamiliar male mouse and an object randomly allocated inside each side chamber´s cylinder. In the S2 phase, a new non-familiar mouse is placed instead of the object and the test mouse is allowed to explore both subjects for additional 10 min. The chamber in which the S1 or S2 mice were placed was counterbalanced between trials, to avoid spontaneous preference.

To assess time sniffing the social and non-social cylinders or familiar versus novel subject, a circular area of 15 cm diameter encompassing each cylinder was set in Ethovision® XT and exploration time was defined as the time during which the mouse nose is inside the area (sniffing zone). A preference index (I_p) was calculated for each phase by subtracting the time sniffing the non-social area from the time sniffing the social area. For S2 the I_p was calculated by subtracting the time sniffing the area of the unfamiliar subject from the time sniffing the area with the familiar subject.

$$I_p = \frac{t_{unfamiliar\ area} - t_{familiar\ area}}{t_{unfamiliar\ area} + t_{familiar\ area}}$$

A positive score in the preference index indicates a preference for the social stimuli in S1 phase or for the novel (unfamiliar) subject in the S2 phase, and a negative score indicates a preference for the non-social stimuli in the S1 phase or a deficit in social memory in the S2 phase.

2.4.4 Elevated Plus Maze

The elevated plus maze consisted of four arms (50 × 10 cm) elevated 50 cm above the floor. The plus maze had two closed arms with black acrylic glass walls (30 cm high) and two open (wall-free) arms connected by a central platform. Indirect illumination provided 100 lux to the open arms and 15 lux to the closed arms. Mice were gently placed in the centre of the maze and their behavior was recorded for 5 min. Time spent and the number of entries in each arm was quantified *post hoc* with Ethovision® XT.

2.4.5 Dark-Light Box

This test is based on the innate aversion of rodents to avoid open and strong illuminated zones. The test apparatus consisted of two boxes (25 × 25 cm each) connected by a small aperture: the light box, (open box with direct illumination of 450 lux) and the dark box (opaque). Mice were placed facing the dark box and their behavior was recorded for 5 min. Mice were video-tracked in the light box post hoc with Ethovision®XT software. Time spent in the light box as well as the number of transitions between the boxes were quantified, and a ratio of time in dark box over time in light box was calculated. A transition is considered when the head of the mouse enters the other zone.

2.4.6 Prepulse Inhibition Test

Response and inhibition of animals after non-startling pulse (prepulse) were recorded in a restrictive acoustic startle response system (The StartFear Combined System; Panlab, Spain). All mice were habituated to the testing chamber without background noise 2 days before the PPI test. For each test session, mice were placed in the cage for 5 min in order to acclimatize to a background noise of 70 dB. After that, three 20 ms pulse stimuli were delivered at 120 dB to define the basal level of the startle reaction for each mouse. Then, mice received blocks of 4 different trials presented pseudo-randomly. Each of them consisted on four trial types: a first acoustic pulse of 120 dB followed of three different 20 ms prepulse trials of 80, 85, and 90 dB each. The maximum startle amplitude of response to acoustic pulses for each mouse were used for the calculation of the percentage of PPI, divided by the average amplitude of startle response for each different trial, as follows:

$$\%\ PPI = \frac{(startle\ amplitude\ in\ the\ startle\ trial - startle\ amplitude\ in\ the\ prepulse\ trial)}{startle\ amplitude\ in\ the\ startle\ trial} \times 100$$

2.4.7 Nesting Behavior

To study the ability of mice to build the nest, two pieces of nesting material made of cotton fibber (3 × 1 cm each) were introduced in the cage in which the mouse was individually housed. Nest quality was imaged at 1, 2, and 3 h after placement of the nesting material. The unused pieces of nesting material were weighted at each timepoint (t). The percentage of unused cotton was calculated to measure organizational behavior at different timepoints as follows:

$$\%\ \text{Unshredded cotton} = \frac{weight_{nesting\ material\ at\ t(x)}}{weight_{nesting\ material\ at\ t(0)}} \times 100$$

2.4.8 Contextual Fear Conditioning

Fear memory was tested using the Fear Conditioning system (Maze Engineers, Boston, USA) in an acrylic plastic cage of 17 ×

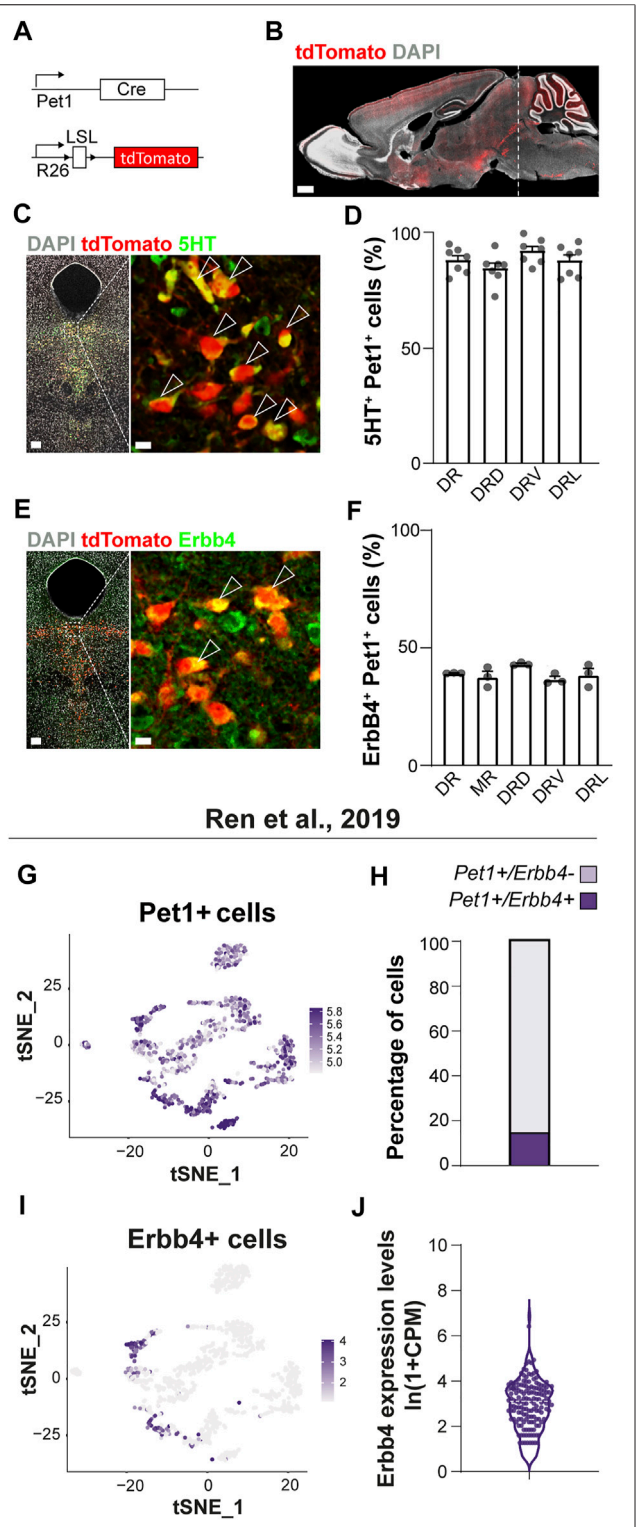

FIGURE 1 | *Erbb4* expression in serotonergic neurons of the dorsal raphe labelled in *Pet1*-reporter mice. **(A)** Genetic strategy to generate *Pet1*-reporter mice. LSL: loxP-STOP-loxP. **(B)** Sagittal brain section of an adult *Pet1*-reporter mouse showing tdTomato-labelled projections and 5HT neurons located in the raphe nuclei (dashed line). **(C)** Confocal images of 5HT immunohistochemistry and *Pet1*-tdTomato+ neurons in the dorsal raphe (*Continued*)

FIGURE 1 | nucleus (DR). **(D)** Quantification of percentage of colocalization of 5HT+ among *Pet1*-tdTomato+ cells in the DR and in each DR subregion ($n = 7$ brains from 4 different litters) **(E)** Confocal image of ErbB4 immunolabelling with *Pet1*-tdTomato+ neurons in the DR. **(F)** Quantification of percentage of colocalization of ErbB4+ cells among *Pet1*-tdTomato+ cells in the MR, DR and in each DR subregion ($n = 3$ brains from 3 different litters). **(G)** tSNE plot showing *Pet1* transcripts in the different clusters from the scRNA-seq dataset of Ren et al. (2019). Cells are colored according to log-normalized *Pet1* transcripts. Color legend reflects expression values of *Pet1* ln (CPM+1). **(H)** Percentage of cells *Pet1*+ from the Ren et al. (2019) study presenting *Erbb4* transcripts. (15.41% of total *Pet1*+ cells display *Erbb4* transcripts, i.e. 153 *Erbb4*+ cells from 999 *Pet1*+ cells). **(I)** tSNE plot showing *Erbb4* transcripts in the different clusters from the original dataset. Cells are colored according to log-normalized *Erbb4* transcripts. Color legend reflects expression values of *Erbb4* in ln (CPM+1). **(J)** Violin plot representing the cell distribution according to number of *Erbb4* transcripts (ln (CPM+1)) within *Pet1*+/ErbB4+ cells (average from 153 *Erbb4*+ cells: 2.82 ± 0.09 reads (mean ± SEM)). DRD: dorsal region or the DR, DRV: ventral region of the DR, DRL: lateral region of the DR. Scale bars in (**B**): 1000 µm and in **(C,E)**: 100 and 10 µm. Data are represented as mean ± SEM.

17 × 25 cm placed over a shock generator grid. During contextual fear conditioning test (CFC), mice were first allowed to explore the context (conditioned-stimulus) consisting of the transparent chamber, distal visual cues and olfactory cues (ethanol 70%) during 3 min. This was followed by three 0.7 mA foot-shocks (unconditioned stimulus, US) of 1 s given with a 30 s inter-stimulus interval. Memory retrieval was tested 1 day after conditioning, placing mice in the same context without the US during 5 min. Memory performance was defined as the percentage of immobility over total time. Immobility was manually quantified and quantifications were validated with Ethovision® XT.

2.4.9 Forced Swimming Test

Mice were placed in a transparent cylindrical tank (12 cm of diameter) made of glass filled with water at room temperature. The height of the tank was 23.5 cm to prevent the mice from scaping. The tank was illuminated with 56 lux. Then, mice were gently and slowly placed in the water and their escape related mobility was recorded with a video camera for 6 min. Percentage of immobility over the total time was hand-measured by two different researchers blind to genotype.

2.4.10 Tail Suspension Test

Tail suspension test was carried out to assess depression-like behavior. Mice were suspended by their tails with tape in a position that prevented them from escaping. Escape-oriented behavior was recorded during 6 min. Percentage of immobility over the total time was hand-measured by two different researchers blind to genotype.

2.5 Analysis of Published Single-Cell RNAsequencing Data and Visualization

Dataset were downloaded from NCBI database (GSE135132) from Ren et al. (2019) article. RStudio (R version 4.0.2, RRID: SCR_001905) software was used for assessing scRNAseq analysis. *Seurat* package (version 4.0.1, RRID:SCR_016341) was used for

performing filtering, highly-variable gene-selection, dimensionality reduction and clustering. Cells with fewer than 300 detected genes and genes detected in fewer than 3 cells were removed from original datasets for following analysis. *SCTransform* function was used for normalization, scale and detection of variable genes. Counts were log-normalized using the natural logarithm of 1 + counts per million [ln (CPM+1)]. PCA, tSNE and UMAP dimensional reductions were performed considering significant dimensions. Clusters were defined based on shared nearest neighbor (SNN) using *FindClusters* function considering PCA dimensional reduction. *Pet1 (Fev)* and *Erbb4* transcripts in the datasets were visualized using *FeaturePlot* function of tSNE reduction. The percentage of *Pet1* cells expressing *Erbb4* was determined used custom function. *Erbb4* transcripts in *Pet1* cells was plotted using *VlnPlot* function.

2.6 Statistics

Statistical analyses were carried out with the GraphPad Prism 9 software (RRID:SCR_002798) and with R programming. The study of the coordinates (Euclidean distance and nearest neighbor distance) and principal component analysis were performed with R. All data are presented as mean ± SEM. Biological replicas (N values) are different animals (behavior and immunohistochemistry) or cells from >3 different brains (electrophysiology) derived from >3 different litters. Statistical methods were used to predetermine the sample size. Randomization was not used. Experiments and analyses were performed blind to genotype by two different experimentalists. Differences were considered significant when $p < 0.05$ (*), $p < 0.01$ (**) or $p < 0.001$ (***). The data were analyzed with parametric tests (Student's t test or ANOVA), when the datasets fulfilled the assumptions of normality (Kolmogorov-Smirnov test) and homoscedasticity (Levene's test). Non-parametric tests for independent groups or Mann-Whitney test were applied when normality was not reached and Kolmogorov-Smirnov test was used when comparing probability distributions. Statistical analysis of the majority of experiments included the sex perspective except when appropriately indicated. For this purpose: animals of both sexes were included in the samples of each experiment. Pooled analysis for both sexes was carried out after performing stratified analysis by sex and validating that the patterns of data distribution were common in males and females.

3 RESULTS

3.1 ErbB4 Is Expressed in Molecularly Defined Subsets of +*Pet1*+ Neurons of the Dorsal Raphe Nuclei

To understand whether ErbB4 is involved in serotonergic circuit development, we employed mouse genetics to label serotonergic neurons with a fluorescent protein tdTomato reporter controlled by a Cre recombinase driven by *Pet1* promoter (*tdTomato*$^{f/+;Pet1\text{-Cre mice}}$, hereafter named *Pet1*-reporter mice) (**Figure 1A**), a determinant of serotonergic fate (Hendricks et al., 1999). *Pet1*-reporter mice allow the specific genetic targeting of a major population of serotonergic neurons within the raphe nuclei (**Figure 1B**) as shown by colocalization analysis between tdTomato and 5HT in the dorsal raphe nucleus (DRN) (86 ± 2% 5HT+ among *Pet1*+tdTomato+ cells) (**Figures 1C,D**) (77 ± 3% of *Pet1*+tdTomato+ among 5HT+ cells) (data not shown).

We then evaluated whether serotonergic neurons from the *Pet1* lineage express ErbB4. *Erbb4:CreERT2* reporter mice suggest ErbB4 expression in approximately 20% of 5HT neurons in the DR (Bean et al., 2014; Zhang et al., 2020). To validate this finding *in situ* at protein level, we employed immunohistochemistry with a previously validated anti- ErbB4 antibody (Zhu et al., 1995; Del Pino et al., 2013) in *Pet1*-reporter mice (**Figure 1E**). Quantification of percentage of ErbB4-expressing neurons within the *Pet1*+tdTomato+ cells showed that a subset of *Pet1*+ cells colocalized with ErbB4 in the DRN (39%) and similar percentages of colocalization were observed in each of the DRN subregions (DRD: 43%; DRV: 37%; DRL: 38%) and in the MRN (B8) (37%) (**Figure 1F**). In addition, to elucidate whether *Pet1*+ErbB4+ are serotonergic, we performed immunohistochemistry for 5HT as well as ErbB4 onto *Pet1*-reporter mice (**Supplementary Figure S1**). Quantifications *Pet1*+/ErbB4+/5HT+ and *Pet1*+/ErbB4+/5HT- neurons revealed that 95 ± 2% and 85 ± 5% of *Pet1*+ErbB4+ cells are serotonergic in the DRN and MRN respectively (**Supplemetary Figure S1**). These data suggested that ErbB4 is present in the DRN/MRN and marks a subpopulation of *Pet1*+ serotonergic neurons. Notably, ErbB4 neurons that are *Pet1*-negative and express 5HT can be found intermingled with *Pet1*-positive neurons (data not shown), suggesting that *Pet1*+ErbB4+ cells represent a subset of ErbB4-expressing serotonergic population.

Next, we aimed to better characterize the molecular identity of adult ErbB4+ serotonergic neurons taking advantage of transcriptomic data from recent single cell RNAseq of adult Sert and/or *Pet1*-expressing serotonergic neurons (Okaty et al., 2020; Ren et al., 2019). From 999 to 2,350 sequenced cells expressing *Sert* and/or *Pet1* in the Ren et al., 2019 (Ren et al., 2019) and Okaty et al., 2020 studies, respectively, *Erbb4* transcripts where detected in 15 and 37% of all cells (**Figure 1**; **Supplementary Figure S2**). Importantly, cells displaying *Erbb4* transcripts are not randomly distributed in the tSNE representation but locate mostly in four out of 13 clusters from the Ren et al., 2019 dataset (**Figures 1G–J**) and eight out of 14 clusters from the Okaty et al., 2020 dataset (**Supplementary Figure S2**). In addition, a close inspection of the molecular identity of *Pet1*-expressing neurons clustered by scRNAseq of the Ren et al., 2019 study (Ren et al., 2019) (**Supplementary Figure S3**), suggests that ErbB4-expressing neurons belong to clusters mapping to both the DRN as well as MRN. Specifically, *Erbb4* transcripts are present in cells from the cluster expressing the Iruquois Homeobox 2 (*Irx2*) and Tachykinin3 receptor (*Tacr3*) which was mapped to MRN in the original study (Ren et al., 2019) (**Supplementary Figure S3A**). In agreement with this, we performed a colocalization analysis between *Pet1*+tomato+ and ErbB4 immunolabelled neurons and found that 22 ± 4% *Pet1*+ were ErbB4+ in the MRN (data not shown). These data strongly suggest that ErbB4 expression, despite being anatomically distributed throughout the

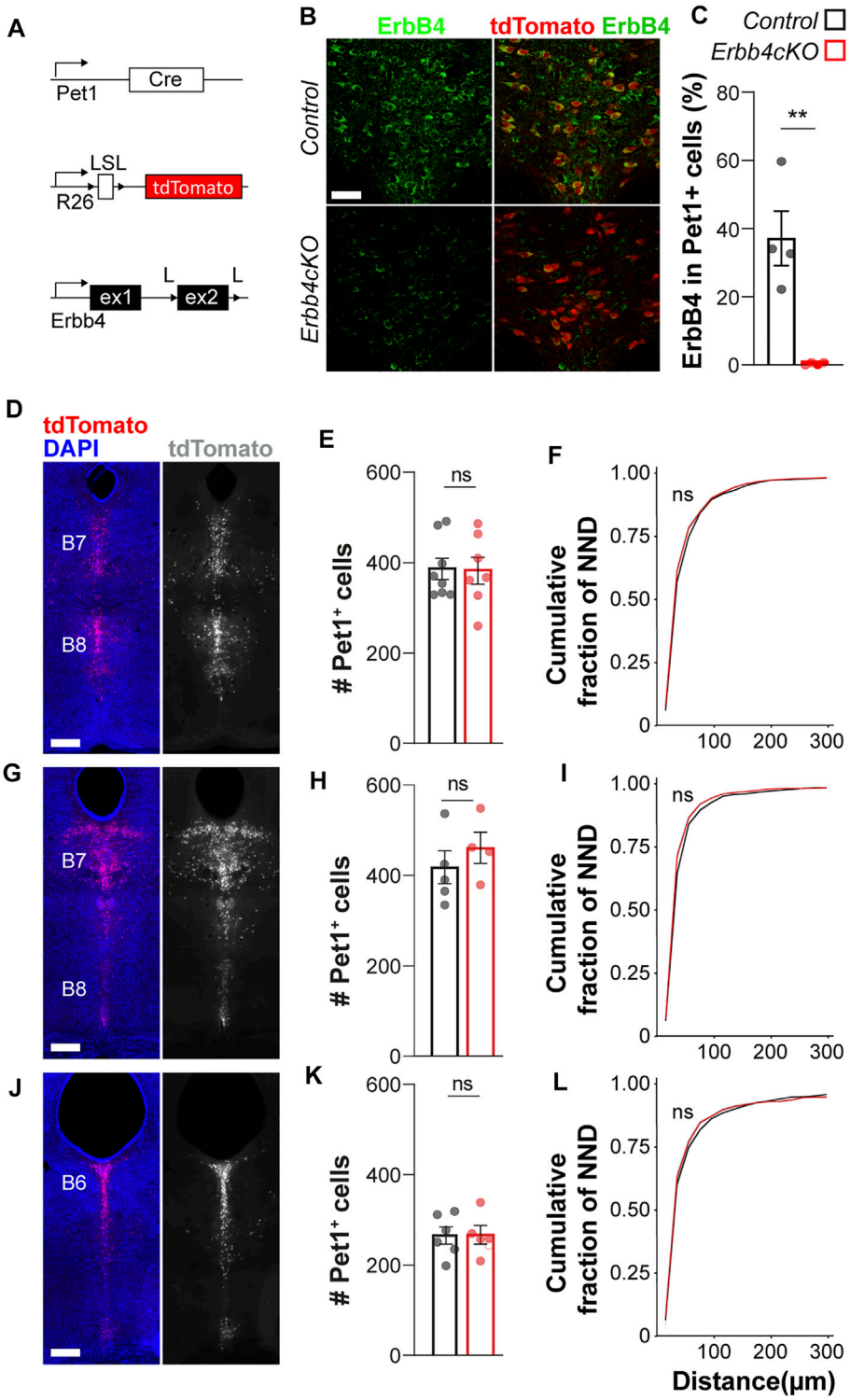

FIGURE 2 | ErbB4 is not required for *Pet1*+ serotonergic neuronal migration. **(A)** Genetic strategy to generate *Erbb4cKO* mice. L: loxP, LSL: loxP-STOP-loxP site. **(B)** Confocal images of ErbB4-expressing and *Pet1*-driven tdTomato-expressing neurons in the dorsal raphe of control and *Erbb4cKO* mice. (n = 4 brains in control and n = 4 in *Erbb4cKO* mice from 3 different litters) **(C)** Quantification of percentage of colocalization of ErbB4+ and tdTomato+ neurons shows a significant reduction of colocalizing cells in *Erbb4cKO* mice when compared to control mice. **(D–L)** Distribution of *Pet1*-tdtomato+ neurons in the dorsal raphe nucleus (DRN). Coronal brain sections showing distribution of tdTomato+ neurons assessed at different levels of the DRN: Bregma –4.48 mm and **(D)** Bregma –4.72 mm **(G)** corresponding to B7/B8 nuclei as well as Bregma –5.02 mm **(J)** corresponding to B6. **(E, H, K)** Quantification of total tdTomato+ neurons found at each coordinate as depicted in **(D, G, J)** in the DRN of control and *Erbb4cKO* mice shows non-significant differences (n = 5–8 control and n = 4–7 mutant brains from 3 different litters). **(F, I, L)** Cumulative fraction of NNDs measured at each coordinate in the DRN shows non-significant differences in cell distribution (n = 5–8 control and n = 4–7 mutant brains from 3 different litters). Scale bars in **(B)**: 50 μm and in **(D, G, J)**: 500 μm. Data are represented as mean ± SEM. ns: not significant differences; **: $p < 0.01$. t-test or Kolmogorov-Smirnov test.

different regions of the DRN and MRN, correspond to specific 5HT molecular subtypes of neurons.

3.2 *Erbb4* Deletion From *Pet1*+ Neurons Does Not Affect Serotonergic Neuron Migration

Having identified that ErbB4 is expressed in a subset of adult DRN *Pet1*+ neurons, we examined whether ErbB4 is involved in serotonergic circuit development. To address the contribution of ErbB4 to serotonergic system formation, we generated ErbB4$^{f/f;\ \text{Pet1-}Cre;Ai9f/+}$ mice (hereafter named ErbB4cKO mice) in which the exon 2 of the *Erbb4* gene, is excised in serotonergic neurons since early fate specification using the *Pet1*-Cre-recombinase (**Figure 2A**). By performing immunohistochemistry against ErbB4 and quantifying the colocalization between *Pet1*+tdTomato+ cells and ErbB4 expressing cells, we observed a robust reduction in the percentage of *Pet1*+tdTomato+ neurons displaying high immunofluorescent signal for ErbB4 in the adult DRN in *Erbb4cKO* mice when compared to controls (*Erbb4*$^{+/+;\ \text{Pet1-}Cre;Ai9f/+}$ mice) (control: 37 ± 8%; *Erbb4cKO:* 1 ± 0.2% ErbB4+ among tdTomato+ cells; $p = 0.003$) (**Figures 2B,C**), showing that *in vivo* Erbb4-deficiency in serotonergic neurons can be efficiently achieved with this genetic strategy.

The ligands of ErbB4, Neuregulin 1 (*Nrg1*) and Neuregulin 3 (*Nrg3*), mediate long and short-range attraction of migrating GABAergic interneurons expressing ErbB4 in the forebrain (Zhang et al., 1997; Flames et al., 2004; Bartolini et al., 2017). Recent studies suggest that *Nrg3* is expressed in the roof plate early during morphogenesis E9–E11 (La Manno et al., 2021). At E9–E11, serotonergic neurons migrate from the ventricular zone close to the floor plate to the medial hindbrain (Hawthorne et al., 2010). Thus, we asked whether NRG/ErbB4 signaling would be involved in the migration and final cellular allocation of serotonergic neurons within the raphe nuclei. To tackle this question, we quantified the total number of *Pet1*-driven tdTomato+ cells in three different coordinates across the dorsal-caudal axis of the DRN corresponding to two different rostro-caudal levels of the B7 nucleus and the rostral B6 and MRN (B8). We observed that the total number of tdTomato+ neurons was not significantly different between control and *Erbb4cKO* mice at any of the neuroanatomical coordinates ($p > 0.05$, *t-test*) (**Figures 2D,E,G,H,J,K**; **Supplementary Figure S4**), indicating that migration and survival of serotonergic neurons is not affected by loss of ErbB4. In addition, cellular distribution of *Pet1*+ serotonergic neurons in the DRN and MRN was assessed by obtaining the spatial coordinates of each tdTomato+ cell within the DRN and MRN, respectively and calculating the distance from each tdTomato+ cells to its nearest neighbor (nearest neighbor distance or NND) at each coordinate. Spatial distributions were compared in cumulative fractions of NND for each population and did not reveal significant differences for any of the three neuroanatomical coordinates analyzed between control and *Erbb4cKO* mice ($p > 0.05$, *Kolmogorov-Smirnov test*) (**Figures 2F,I,L**) (**Supplementary Figure S4**). Altogether these data suggested that ErbB4 is dispensable for *Pet1*+ serotonergic neurons to migrate and allocate in the DRN and MRN (B8).

3.3 *Erbb4*-Loss in *Pet1*+ Neurons Impairs the Long-Range Connectivity of Serotonergic Sub-Systems

In addition to migration, NRG/ErbB4 signaling participates in axon navigation and synaptogenesis during embryonic and postnatal development in local and long-range projecting neural circuits within the forebrain (Lopez-Bendito et al., 2006; Fazzari et al., 2010; Del Pino et al., 2013; Del Pino et al., 2017). Therefore, we hypothesized that ErbB4 might be necessary for the development of long-range efferent serotonergic connectivity. To test this hypothesis, we monitored in adult control and *Erbb4cKO* the serotonergic axon arborization across different postsynaptic targets of the serotonergic system: the retrosplenial granular cortex (RSGc), the hippocampus (DG, CA1, and CA3), the posterior periventricular nucleus of the thalamus (PVT) and the lateral hypothalamus (LH) (**Figures 3A,B**). We observed that serotonergic axons labelled with tdTomato were present in all regions (RSGc, DG, CA3, CA1, PVT, and LH) in control as well as *Erbb4cKO* mice (**Figures 3C–J**; **Supplementary Figure S5**). To assess the density of terminal arborization from serotonergic connectivity, we quantified the area occupied by tdTomato+ signal normalized to a field of view/total area in each brain region (**Figure 3C**). Non-significant differences in axonal density were observed between control and *Erbb4cKO* in RSGs (control: 1.43 ± 0.31%; *Erbb4cKO:* 1.15 ± 0.20%; $p = 0.446$) (**Figures 3D,E**), hippocampus (control DG: 19.92 ± 1.74%; *Erbb4cKO* DG*:* 12.32 ± 1.44%; $p = 0.630$; control CA3: 1.8 ± 0.2%; *Erbb4cKO* CA3*:* 2.3 ± 0.4%; $p = 0.509$; control CA1: 1.2 ± 0.2%; *Erbb4cKO* CA1*:* 1.3 ± 0.2%; $p = 0.28$; (**Figures 3F,G**; **Supplementary Figure S5**); and LH (control: 30.26 ± 3.29%; *Erbb4cKO:* 33.14 ± 3.71%; $p = 0.568$) (**Figures 3J,K**). In contrast, *Erbb4cKO* mice displayed significantly reduced axonal density in the PVT region when compared to controls (control: 7.8 ± 1.0%; *Erbb4cKO:* 7.1 ± 1.0%; $p = 0.0025$) (**Figures 3H,I**). These results obtained with epifluorescence imaging were reproduced in the PVT using confocal microscopy (**Supplementary Figure S6**) (control: 13.5 ± 1.0%; *Erbb4cKO:* 7.5 ± 0.7%; $p = 0.0002$). Thus, our data suggest that, while global serotonergic connectivity arriving to the LH or to other cortical targets (i.e. hippocampus and RSGc) is not dependent on ErbB4 expression, ErbB4 is required for the axonal arborization of a subpopulation of *Pet1*+ serotonergic projections reaching the PVT area.

3.4 *Pet1*+ Neurons Lacking Erbb4 Do Not Cause Local Defects in the DRN

Since serotonergic branching is regulated by serotonin levels during brain development (Migliarini et al., 2013) we investigated whether the serotonergic connectivity deficits observed in the PVT region in *Erbb4cKO* mice could arise from changes in 5HT expression within the DRN. Immunohistochemistry against 5HT and colocalization

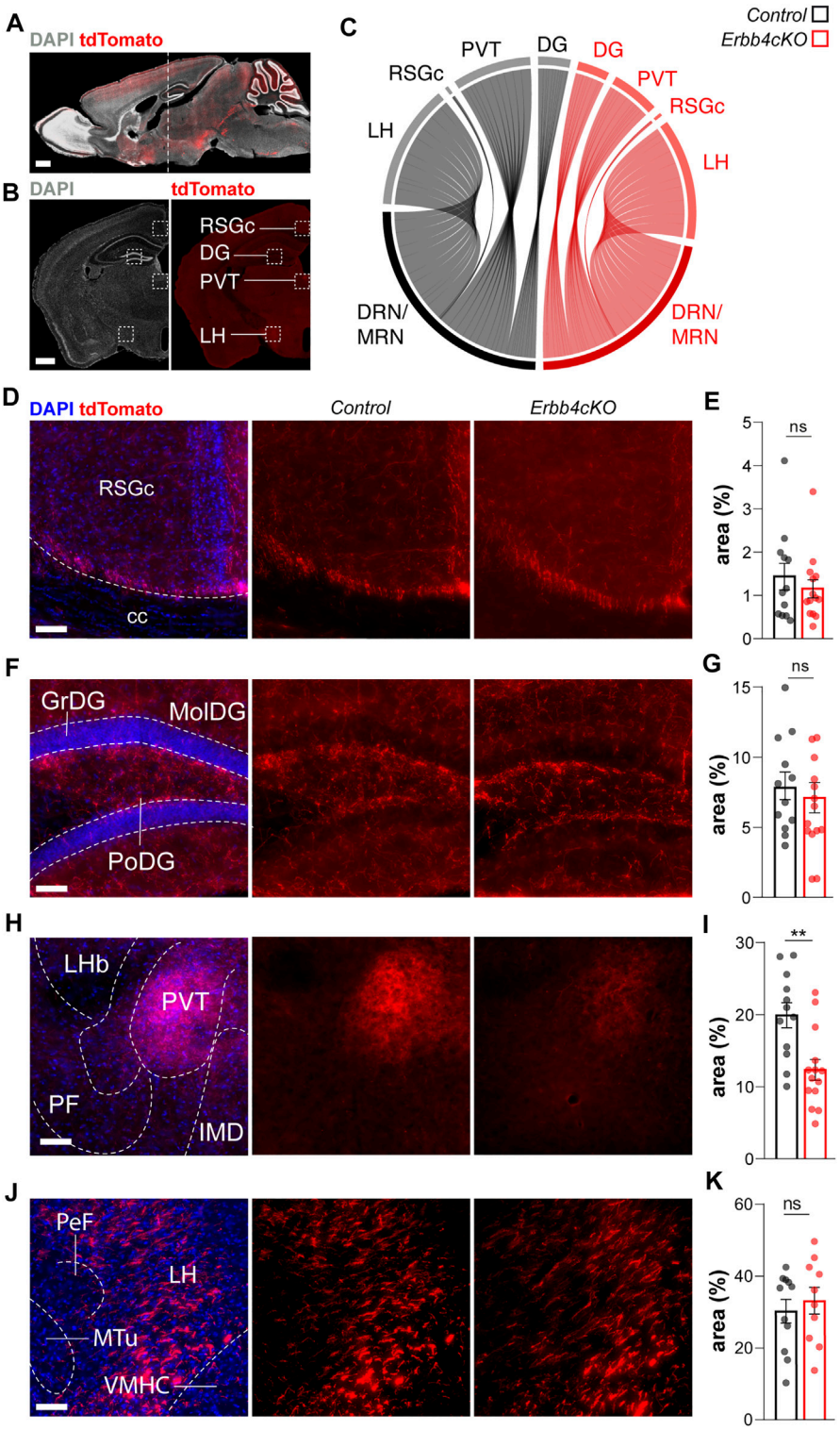

FIGURE 3 | Long-range connectivity deficits in ErbB4-deficient *Pet1*+ neurons of male and female mice. **(A)** *Pet1*+tdTomato+ cells in a sagittal section of a mouse brain. Dashed line indicates the location of the brain regions analysed in coronal sections. **(B)** Coronal section of an adult *Pet1*-reporter mouse showing tdTomato-labelled projections. Dashed squares indicate the location of the brain areas analyzed. **(C)** Circular plot representing relative connectivity to different brain areas from raphe nucleus (RN) in control (black) and *Erbb4cKO* (red) mice. **(D, F, H, J)** Confocal images of *Pet1*+ tdTomato+ connectivity from raphe nucleus to different brain areas for control and *Erbb4cKO* mice. **(E, G, I, K)** Quantification of connectivity area normalized to the field of view are presented as percentage of area occupied by tdTomato signal (area%) (*n* = 11–12 control and *n* = 10–15 mutant from 3 different litters). RSGc: retrosplenial granular cortex c region; cc: corpus callosum; GrDG:

(*Continued*)

FIGURE 3 | granular dentate gyrus; MolDG: molecular dentate gyrus; PoDG: polymorph layer of the dentate gyrus; LHb: lateral habenular nucleus; PVT: periventricular thalamus; PF: parafascicular thalamic nucleus; IMD: intermediodorsal thalamic nucleus; PeF: perifornical nucleus; LH: lateral hypothalamic area; Mtu: medial tuberal nucleus; VMHC: ventromedial hypothalamic nucleus central part. Scales bars in **(A,B)**: 1000 μm and in **(D, F, H, J)**: 100 μm. Data are represented as mean ± SEM. ns: not significant differences; **: $p < 0.01$; t-test or Mann-Whitney non-parametric test.

analysis between 5HT+ and tdTomato+ cells did not reveal significant differences between the number of *Pet1*+ neurons expressing 5HT in controls and *Erbb4cKO* mice (control: 88.29 ± 3.90%; *Erbb4cKO:* 81.55 ± 2.11; $p = 0.155$) (**Figures 4A–C**). Quantification of 5HT signal intensity measured within *Pet1*+ neurons followed a similar distribution in controls and *Erbb4cKO* mice ($p > 0.05$; *Kolmogorov-Smirnov test*) (**Figure 4D**), indicating that ErbB4 deletion does not affect global 5HT content in the DRN.

To further understand whether developmental deletion of ErbB4 in serotonergic cells alters the excitability of the DRN, we probed the intrinsic electrophysiological properties of tdTomato+ neurons in acute brain slices of controls and *Erbb4cKO* mice. Through whole-cell patch-clamp recordings performed in adult tdTomato+ neurons within the DRN (**Figure 4E**), we observed that the majority of neurons exhibited spike frequency adaptation (73% in control [11 of 15 recorded cells]; 84% in mutant [16 of 19 recorded cells]). For comparison of intrinsic properties, we explored whether neurons recorded belonged to a similar neural subtype. We examined the morphology of neurons recorded by performing *post hoc* histochemistry against biocytin-filled tdTomato+ neurons. Sholl analysis of neuronal morphology did not reveal significant differences between control and *Erbb4cKO* mice ($p > 0.05$; *two-way ANOVA test*) (**Figures 4F,G**), indicating that recorded neurons with adapting firing profile displayed similar dendrite complexity and suggesting that they belonged to an electrophysiologically and morphologically similar *Pet1*-expressing neuronal subtype. Next, our analysis of multiple electrophysiological properties as well as the input/output relationship did not reveal significant differences in most of the passive and active intrinsic properties between neurons from control and *Erbb4cKO* mice ($p > 0.05$; *two-way ANOVA test*) (**Figure 4H**; **Table 1**). A significantly reduced medium after hyperpolarization was observed in *Erbb4cKO* mice when compared to control (**Table 1**), indicating that ErbB4 deficiency in serotonergic neuron has an effect on specific membrane properties without causing a prominent change in global excitability. Altogether, our findings suggest that ErbB4 dysfunction in the DRN does not lead to a local phenotype in DRN neither at the intrinsic excitability level nor in serotonergic tone of *Pet1*+ neurons.

3.5 ErbB4 Deficiency in *Pet1*+ Serotonergic Neurons Cause Specific Behavioral Impairments in Social and Fear Memory

To evaluate whether the connectivity deficits observed upon ErbB4-deficiency in *Pet1*+ serotonergic neurons impact on brain function, we tested control ($Erbb4^{f/f}$) and *Erbb4cKO* littermates in behavioral assays. Spontaneous locomotor activity was evaluated using the open field and the Y-maze, respectively. Controls and *Erbb4cKO* mice travelled similar distances (control: 49.63 ± 2.22 m; *Erbb4cKO:* 54.77 ± 301 m; $p = 0.254$) with a comparable velocity in the open field (control: 5.52 ± 0.24 cm/s; *Erbb4cKO:* 6.09 ± 0.33 cm/s; $p = 0.255$) (**Figures 5A,B**). In addition, we did not find differences in other parameters indicative of anxiety such as the time spent in the center *vs* borders in the open field between control and mutant mice (Centre: control: 17.81 ± 1.24%; *Erbb4cKO:* 18.36 ± 1.207%; $p > 0{,}9999$; Borders: control: 82.19 ± 1.24%; *Erbb4cKO:* 81.64 ± 1.21%; $p > 0.9999$) (**Figure 5C**). Spontaneous alternation was also evaluated in the Y-maze (**Figures 5D–F**). Similar number of entries (control: 32.00 ± 1.55; *Erbb4cKO:* 32.54 ± 1.30; $p = 0.792$) (**Figure 5E**) as well as percent of alternations were observed between control and *Erbb4cKO* mice (control: 51.40 ± 2.19%; *Erbb4cKO:* 47.25 ± 2.71; $p = 0.242$) (**Figure 5F**), indicating that ErbB4-dysfunction in the serotonergic systems does not affect locomotor activity or working memory.

To test sociability and social memory we employed the three-chamber test that consisted of three sessions: habituation (empty cylinders), sociability (conspecific mouse "stranger 1" or "S1" and object) and preference for social novelty (familiar mouse "S1" and new-conspecific "stranger 2" or "S2") (**Figure 5G**). In the habituation phase, mice explored similarly the lateral chambers of the 3-chamber test (**Figure 5H**), indicating no contextual preference. During the sociability phase, we observed no differences between control and *Erbb4cKO* mice in distance travelled (data not shown), in agreement with a lack of locomotion phenotype in the open field. Both genotypes showed preference for mouse S1 over the object (control: 0.23 ± 0.040; *Erbb4cKO:* 0.22 ± 0.04; $p = 0.8353$) (**Figure 5I**). However, when animals were exposed to the preference for social novelty test, we observed that *Erbb4cKO* mice spent less time exploring the novel mouse S2 and displayed a significantly reduced preference index for the novel S2 conspecific over the previously known S1 mouse when compared to controls (control: 0.26 ± 0.04; *Erbb4cKO:* 0.10 ± 0.06; $p = 0.036$) (**Figure 5J**). Together, the lack of sociability phenotype and the reduced preference for social novelty that we observed suggest that social memory could be impaired in *Erbb4cKO* mice.

To elucidate whether alterations found in social memory might be influenced by anxiety, control and *Erbb4cKO* animals were tested for anxiety-like behavior using the elevated plus maze and the dark-light box test. In agreement with a lack of anxiety-like behavior in the open field (**Figure 5C**), we did not find significant differences between control and mutant mice in the percentage of time spent in the different zones of the elevated plus maze (**Figure 6A**), or in the ratio of time spent in open vs close arms of the elevated plus maze (control: 4.48 ± 0.534; *Erbb4cKO:* 4.20 ± 0.59; $p = 0.729$) (**Figure 6B**). In addition, we did not observe significant differences in the number of transitions

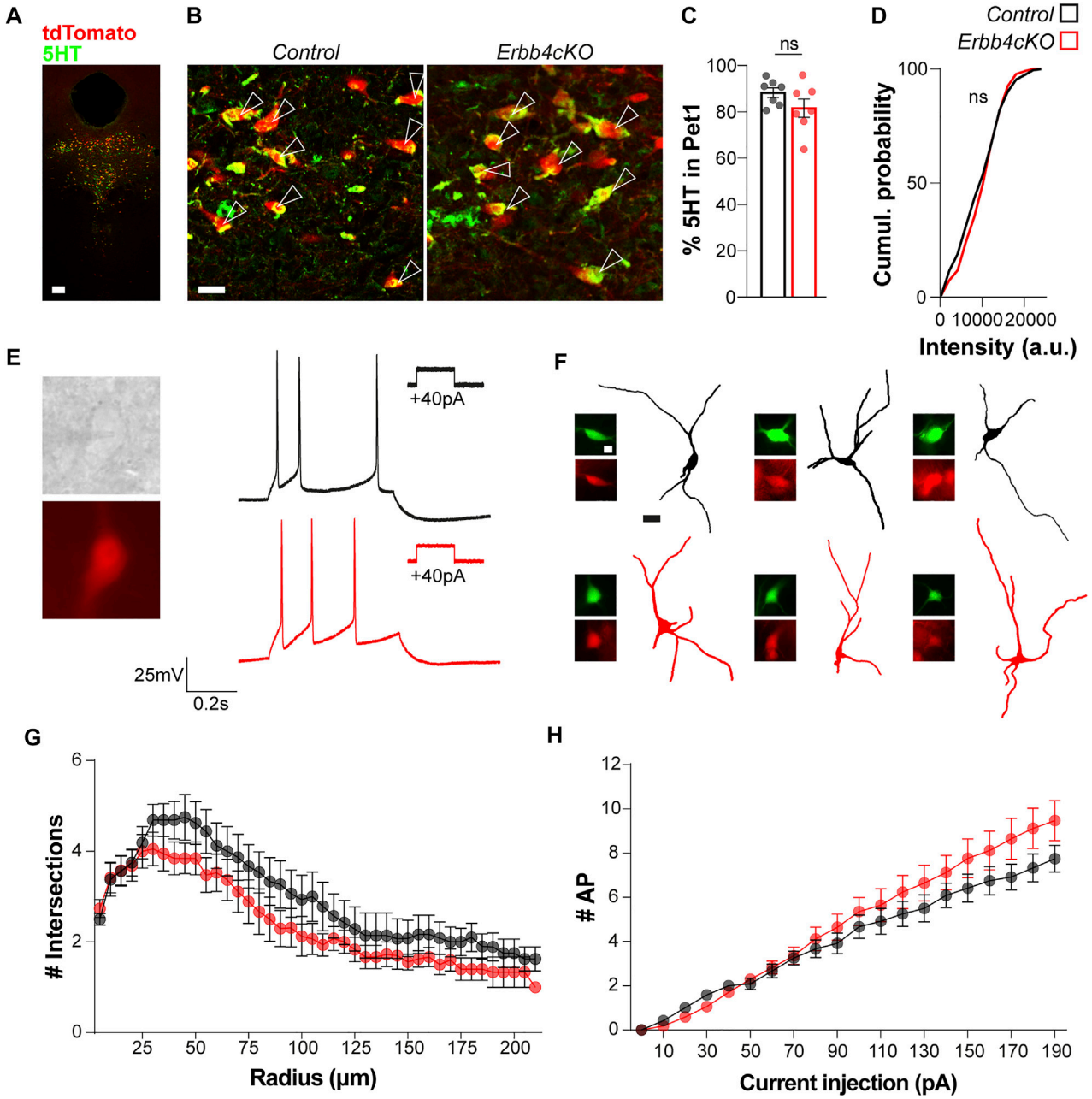

FIGURE 4 | ErbB4 deficiency in Pet + neurons does not lead to changes in global excitability or serotonin content in the DRN in male mice. **(A)** Colocalization of *Pet1*-tdTomato and 5HT in the raphe nucleus. **(B)** Magnifications for the colocalization of *Pet1*-tdTomato and 5HT in control and *Erbb4cKO* mice. Arrow heads point to double positive cells for *Pet1* and 5HT. **(C)** Quantification of the percentage of *Pet1*+ cells expressing 5HT ($n = 7$ control and $n = 7$ mutant mice from 4 different litters). **(D)** Cumulative probability of 5HT intensity for control and *Erbb4cKO* cells expressed as arbitrary units (n = 5 control and $n = 5$ mutant mice from 3 different litters). **(E)** Representative images and traces of *Pet1*+ tdTomato-expressing neurons recorded in current clamp mode in control (black) and *Erbb4cKO* (red) mice. **(F)** Reconstructions of *Pet1*+ cells recorded. Images of streptavidin-Alexa488 (green) and tdTomato (red) for each cell. **(G)** Sholl analysis of *Pet1*+ tdTomato+ cells recorded for control and *Erbb4cKO* mice. Intersections are quantified per radius of 5 µm of difference from soma ($n = 11$ neurons from 3 different control mice and $n = 16$ neurons from 3 different mutant mice). **(H)** Input-output plot showing number of spikes as a function of injected current displayed by *Pet1*+ tdTomato+ neurons in control ($n = 11$ neurons from 3 different control mice) and *Erbb4cKO* mice ($n = 16$ neurons from 3 different mutant mice). Scale bars in **(A)**: 100 and 20 µm and **(F)** 10 and 25 µm. Data are represented as mean ± SEM. ns: not significant differences. t-test, Kolmogorov-Smirnov test or two-way ANOVA with Bonferroni correction for multiple comparisons.

TABLE 1 | Global intrinsic excitability of *Pet1*+tdTomato+ neurons in the dorsal raphe is not affected by ErbB4-deficiency in serotonergic neurons. Intrinsic electrophysiological properties of *Pet1*+ tdTomato-expressing neurons in the dorsal raphe nucleus of control and *Erbb4cKO* mice. V_{rest}: resting membrane potential; R_{in}: input resistance; AHP: afterhyperpolatization; FS latency: latency to first spike at rheobase; MFF: maximum firing frequency. Data are represented as mean ± SEM.

	Ctrl	*Erbb4cKO*	*p-value*	Test
RMP	–67.21 ± 2.104	–63.02 ± 1.546	0.1133	t-test
R*in* (MΩ)	1,053 ± 125.2	1,189 ± 108.7	0.4237	t-test
Amplitude (mV)	71.79 ± 1.480	67.66 ± 2.718	0.5437	Mann-Whitney
Threshold (mV)	–29.45 ± 1.2460	–30.83 ± 1.846	0.5811	t-test
Rise Time (ms)	0.8264 ± 0.03684	1.130 ± 0.3047	0.6709	Mann-Whitney
Decay Time (ms)	3.601 ± 0.2138	3.224 ± 0.1676	0.1691	t-test
Half-width (ms)	2.990 ± 0.1995	2.636 ± 01532	0.1646	t-test
fAHP (ms)	–19.13 ± 1.221	–21.10 ± 1.153	0.2626	t-test
mAHP (ms)	–21.32 ± 1.085	–17.49 ± 1.308	0.0486(*)	t-test
Rheobase (pA)	17.27 ± 2.727	25.00 ± 2.739	0.0664	Mann-Whitney
FS latency (ms)	193.4 ± 19.70	182.9 ± 22.09	0.7414	t-test
Inter-spike interval (ms)	289.2 ± 28.29	236.0 ± 23.00	0.1555	t-test
Spike Frequency Accommodation	0.29 ± 0.02	0.42 ± 0.75	0.1635	t-test
MFF (Hz)	4.00 ± 0.30	4.78 ± 0.48	0.2275	t-test

(control: 6.0 ± 0.27; *Erbb4cKO*: 6.30 ± 0.26; $p = 0.448$) (**Figure 6C**) and ratio of time spent in the dark over the brightly illuminated area (control: 1.60 ± 0.21; *Erbb4cKO:* 1.77 ± 0.32; $p = 0.660$) in the dark-light box test (**Figure 6D**), indicating that Erbb4 deficiency in *Pet1*+ serotonergic circuits have no effect on anxiety levels.

To further elucidate whether behavioral deficits could involve abnormal attentional levels, control and *Erbb4cKO* animals were tested in the prepulse inhibition of the startle reflex (PPI) test. Both genotypes display startle reflex to a 120dB sound (control: 56.64 ± 6.81%; *Erbb4cKO*: 48.89 ± 7.45%; $p = 0.457$) (**Figure 6E**). Inhibition of startle reflex by the presentation of a prepulse of 80, 85 or 90 dB was not significantly different between controls and *Erbb4cKO* animals (80dB: control: 18.67 ± 5.46%; *Erbb4cKO*: 22.95 ± 5.72%; $p > 0.999$; 85dB: control: 29.43 ± 5.07%; *Erbb4cKO*: 32.37 ± 6.09%; $p > 0.999$; 90 dB: control: 34.97 ± 4.49%; *Erbb4cKO*: 33.04 ± 5.71%; $p > 0.999$) (**Figure 6F**), suggesting that *Erbb4cKO* do not have attentional deficits.

We also monitored nesting behavior in the home cage to determine the species-typical behavior of *Erbb4cKO* animals (**Figure 6G**). We did not observe significant differences in the ability of animals to build a nest between controls and *Erbb4cKO* mice, suggesting that serotonergic deficits observed in *Erbb4cKO* mice are not relevant for the innate organized behavior ($p > 0.05$; *two-way ANOVA*) (**Figure 6H**).

In light of the deficits observed in social memory in *Erbb4cKO* animals, we evaluated whether other types of memory could be affected by Erbb4 deficiency in *Pet1*+ serotonergic circuits with the contextual fear conditioning paradigm (**Figure 6I**). While *Erbb4cKO* and control mice displayed similar levels of freezing upon presentation of the unconditional stimulus (electric shock), freezing displayed 24 h after fear conditioning during fear memory retrieval was significantly reduced in *Erbb4cKO* mice when compared to controls (control: 57.37 ± 2.49; *Erbb4cKO:* 48.28 ± 2.54; $p = 0.013$) (**Figure 6J**). These data indicated that fear memory retrieval is impaired in *Erbb4cKO* mice.

Finally, to assess whether Erbb4-deficiency in *Pet1*+ neurons is affecting parallel serotonergic sub-systems described to regulate coping behavior in face of challenge (Ren et al., 2018), mice performed the forced swimming and tail suspension tasks. In both tasks, *Erbb4cKO* mutants and control mice presented similar levels of immobility (FS: control: 23.57 ± 1.64s; *Erbb4cKO:* 20.66 ± 1.95s; $p = 0.263$; TS: control: 38.03 ± 2.37s; *Erbb4cKO:* 34.75 ± 2.66s; $p = 0.361$) (**Figures 6K–L**) indicative of normal coping behavior in *Erbb4cKO* mutants.

Altogether our data suggest that developmental deficiency of *Erbb4* in *Pet1*+ serotonergic circuits leads to the abnormal processing of specific types of memory that contain a social or aversive components, but does not have an effect on locomotion, emotional, attentional or organizational behaviors.

4 DISCUSSION

Here, we provide evidence for a new role of ErbB4 in the development of serotonergic sub-systems. In particular, we found that long-range connectivity taking place between *Pet1*-expressing subpopulations and the PVT area requires ErbB4. In addition, our behavioral characterization revealed that the developmental disruption of ErbB4 in discrete serotonergic neurons has selective functional consequences on the processing of specific types of memory associated with an emotional or social component, such as fear and social memory.

The formation of serotonergic axons takes place over a protracted period during brain development spanning embryonic to postnatal stages. In rodents, axon growth begins early after serotonergic neuron migration reaching target areas by birth (Bang et al., 2012). Subsequently, terminal arborization sprouting and refinement takes place during the postnatal period (Lidov and Molliver, 1982; Maddaloni et al., 2017). Here we show that NRG/ErbB4 signaling is necessary for the proper arborization of serotonergic axons reaching the PVT, but is dispensable for the innervation of other targets of the serotonergic system (lateral hypothalamus, hippocampus and retrosplenial cortex). Previous work demonstrates that more than one subgroup of serotonergic subpopulations from different rhombomeric segments innervates an

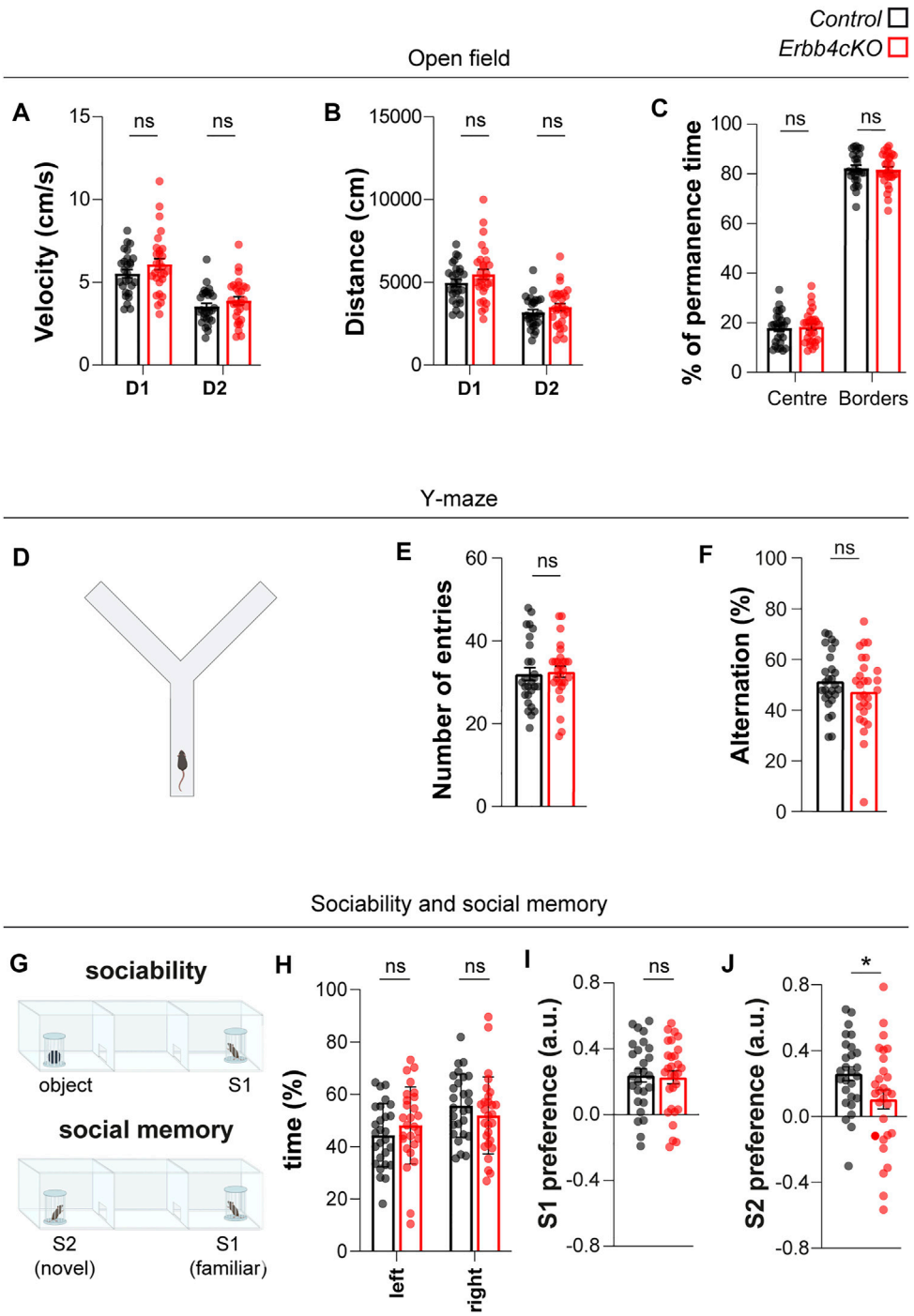

FIGURE 5 | Mice with Erbb4 deletion in *Pet1+* neurons display social memory deficits but no phenotypes on sociability, locomotor activity or attentional levels. **(A–C)** Locomotor activity in the open field during day 1 (D1) and day 2 (D2) of control and *Erbb4cKO* mice is represented as velocity **(A)** and distance travelled **(B)**. **(C)** Percentage of permanence time in the centre and borders of the open field. **(D,E)** Locomotor activity was measured in the Y-maze as total number of entries. **(F)** Working memory measured as percentage of spontaneous alternations during Y-maze test. **(G)** Schematic of the sociability test and social novelty test. **(H)** Percentage of time spent in the lateral chambers during the habituation phase to the 3-chamber test. **(I)** Index of preference of S1 versus object during sociability phase. **(J)** Index of preference of S2 versus S1 during social memory phase. In the statistical analysis of all experiments described in this figure, the sex perspective has been included. Animals of both sexes were included in the samples of each experiment. After checking that patterns of data distribution were common in males and females via a stratified analysis by sex, pooled analysis was carried out. For all these behavioral tests, $n = 27$ (11 females, 16 males) control and $n = 29$ (12 females, 17 males) mutant from 7 different litters. Data are represented as mean ± SEM. ns: not significant differences; *: $p < 0.05$. t-test, Mann-Whitney or two-way ANOVA with Bonferroni correction for multiple comparisons.

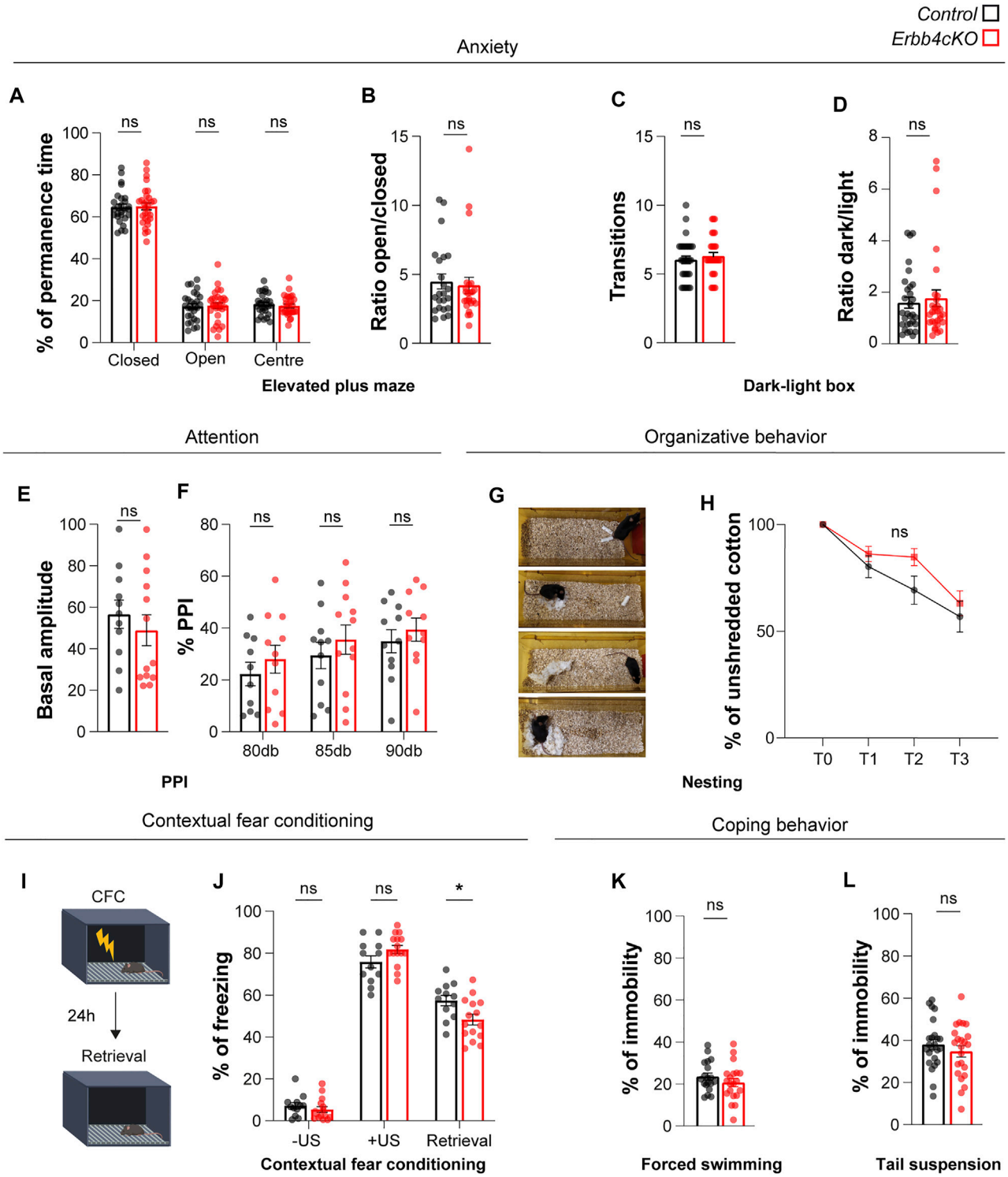

FIGURE 6 | Mice with Erbb4 deletion in *Pet1+* neurons display fear memory deficits but do not show abnormalities in anxiety or organizational behavior. **(A)** Percentage of permanence time the closed arms, open arms and centre of the elevated plus maze test. **(B)** Ratio of permanence time in the open arms over the closed arms during the elevated plus maze test. **(C)** Number of transitions between lighted and dark areas in the light-dark box test **(D)** Ratio between dark and light permanence time in light-dark box test. **(E)** Basal amplitude of startle reflex for control and *Erbb4cKO* mice. **(F)** Percentage of prepulse inhibition (PPI) of startle response for control and *Erbb4cKO* mice. **(G)** Sample images of four different time points during the nest building test. **(H)** Percentage of unshredded cotton used by mice for building a nest at 0, 1, 2, and 3 h after providing them with new material. **(I)** Diagram of contextual fear conditioning (CFC) test (mofidied from Biorender.com). Retrieval test was performed 24 h after CFC by placing the mouse in the same context. **(J)** Percentage of freezing for each phase of the CFC learning and retrieval. -US:

(*Continued*)

FIGURE 6 | before unconditioned stimulus; +US: after unconditioned stimulus; Retrieval: 1 day after CFC. **(K)** Percentage of immobility for the forced swimming test. **(L)** Percentage of immobility in the tail suspension test. In the statistical analysis of all experiments described in this figure, the sex perspective has been included. Animals of both sexes were included in the samples of each experiment. After checking that patterns of data distribution were common in males and females via a stratified analysis by sex, pooled analysis was carried out. For all behavioral tests except PPI, CFC, forced swimming and tail suspension, $n = 27$ (11 females, 16 males) control and $n = 29$ (12 females, 17 males) mutant mice from 8 different litters. For PPI test, $n = 11$ (6 females, 5 males) control and $n = 13$ (8 females, 5 males) mutant mice from 4 different litters. For CFC test, $n = 12$ (7 females, 5 males) control and $n = 15$ (9 females, 6 males) mutant from 4 different litters. For forced swimming, $n = 19$ (7 females, 12 males) control and $n = 20$ (7 females, 13 males) mutant mice. For tail suspension, $n = 24$ (13 females, 11 males) and $n = 23$ (13 females, 10 males). Data are represented as mean ± SEM. ns: not significant differences; *: $p < 0.05$. t-test, Mann-Whitney or two-way ANOVA with Bonferroni correction for multiple comparisons.

individual target area (Bang et al., 2012). In particular, it was reported that the PVT is innervated by Pet1-expressing serotonergic neurons originating from rhombomere (r)1 — populating the DRN, MRN and B9 groups — and from r2 — populating the MRN exclusively — (Jensen et al., 2008; Bang et al., 2012; Senft et al., 2021), but we can not exclude that other raphe nuclei also project to the PVT region. It remains to be determined whether our *Erbb4cKO* approach disrupts axon arborization from ErbB4 expressing neurons that are both in the DRN and MRN. Our results demonstrate that serotonergic circuit formation of long-range projections targeting the PVT is regulated by NRG/ErbB4 signaling. However, we can not exclude that: 1) the PVT could be also innervated by ErbB4-negative serotonergic neurons and 2) that disruption of ErbB4 in serotonergic circuits affects axon development in other postsynaptic targets not visited in this study. While it is reasonable to consider that serotonergic circuit wiring relies on the combination of guidance and signaling molecules as well as environmental factors during development, our findings reinforce the notion that intrinsic signaling pathways regulated by ErbB4, act as organizers of specific serotonergic sub-systems during brain development.

The developmental disruption of ErbB4 in serotonergic circuits has a very specific impact on the behavioral performance of mice. The specific behavioral phenotypes restricted to fear and social memory deficits observed in $Erbb4^{f/f;Pet1\text{-}Cre;Ai9f/+}$ mice are in line with the participation of NRG/ErbB4 signaling in the development of discrete serotonergic circuits. The notion that serotonergic circuits are organized into segregated sub-systems regulating specific behaviors (Abrams et al., 2004) is supported by functional manipulations of projection-defined serotonergic circuits. For example, studies show that specific long-range efferent projections from the DRN play a role in anxiety [DRN → bed nucleus of the stria terminalis (Marcinkiewcz et al., 2016), DRN → central amygdala (Ren et al., 2018)], coping behavior [DRN → orbitofrontal cortex (Ren et al., 2018)], sociability [DRN → anterior cingulate cortex (Li et al., 2021)] and fear memory [DRN → bed nucleus of the stria terminalis (Marcinkiewcz et al., 2016)]. Other excellent studies inform about serotonergic sub-systems characterized by dopamine receptor expression modulating aggressive behavior through multiple postsynaptic targets (Niederkofler et al., 2016). Our findings disclose a serotonergic sub-system that relies on ErbB4 for proper regulation of at least two types of memory: associative fear memory and social memory. Interestingly, several studies link the function of PVT to fear memory processing in rodents (Padilla-Coreano et al., 2012; Li et al., 2014; Do-Monte et al., 2015; Penzo et al., 2015; Choi and McNally, 2017; Chen and Bi, 2019) and sociability (Yamamuro et al., 2020). Although different types of neurons within the PVT have been shown to regulate emotional and motivated behaviors, our study is the first to report the association between circuits integrating the PVT and the formation of social memories.

Recently, a study showed that downregulation of ErbB4 in adult mice results in hyperexcitability of serotonergic neurons and anxiogenic behavior (Zhang et al., 2020). In contrast, we show that the developmental disruption of ErbB4 does not cause an anxiogenic response in mice nor it leads to prominent changes in global excitability of serotonergic neurons. Hence, the functional implications of acute downregulation of *Erbb4* in the adult brain are very different from the ErbB4-deficiency in serotonergic circuits during its development. We deduce this could be due to unknown developmental plasticity rules in the serotonergic system, that are absent in the adult brain. Furthermore, the different outcomes obtained from adult and developmental *Erbb4* disruption might result from the genetic targeting of different serotonergic subsets, since the study of Zhang et al. (2020) employed the *Sert-Cre* mice to target *Erbb4* expression in the adult brain and our data suggests that subsets of 5HT+ErbB4+ neurons are *Pet1*-negative in the DRN and MRN.

Finally, substantial evidence associate Nrg/Erbb4 signaling to neurodevelopmental disorders (reviewed in(Mei and Nave, 2014)) such as schizophrenia (Norton et al., 2006; Silberberg et al., 2006; Walsh et al., 2008; Mostaid et al., 2017). Most of our knowledge on cognitive dysfunction in NRG/ErbB4-deficiency disorders stems from studies focusing on cortical GABAergic interneurons, which are the most numerous neuronal subtype expressing ErbB4 in the brain (Fazzari et al., 2010) (reviewed in (Rico and Marin, 2011)). Our findings reveal novel neural circuit basis (i.e. DRN/MRN → PVT) of cognitive dysfunction in NRG/ErbB4-deficiency disorders involving GABAergic and non-GABAergic neurons in the raphe nuclei. In addition to the already known defects in cortical inhibitory/excitatory balance (Del Pino et al., 2013; Del Pino et al., 2017; Wang et al., 2018) and in the dopaminergic system (Skirzewski et al., 2018), our results on DRN → PVT circuit dysfunction contribute to better understand the pathophysiology of ErbB4-deficiency disorders.

Altogether, we disclose ErbB4 as new intrinsic factor of serotonergic subpopulations that acts as organizer of 5HT long-range sub-circuits regulating the formation of emotional and social memories.

DATA AVAILABILITY STATEMENT

The original contributions presented in the study are included in the article/**Supplementary Material**, further inquiries can be directed to the corresponding author.

ETHICS STATEMENT

The animal study was reviewed and approved by the Ethics Committee of the Fundación Centro de Investigación Príncipe Felipe and complied with the Spanish and European regulations for the use of laboratory animals.

AUTHOR CONTRIBUTIONS

Conceptualization: IP. Methodology: CB, AB-G, AA, XS, LO, SD, IR, XL, and IP. Formal analysis: CB, AB-G, AA, XS, IR, and IP. Interpretation: CB, AB-G, XL, ND, NF, and IP. Data curation: AB-G and FG-G. Writing—original-draft: CB, AB-G, and IP. Writing—review and editing: CB, AB-G, XS, IR, FG-G, FI, CL, ND, XL, NF, and IP. Visualization: CB, AB-G, and IP. Supervision: IP. Resources: CL, XL, NF, and IP. Project administration: IP. Funding acquisition: IP.

FUNDING

This work was supported by the CIDEGenT excellence research program of the Valencian government (CIDEGENT/2019/044) and by the Spanish Ministry of Science, Innovation and Universities (RTI 2018-100872-J-I00) as well as by the Young IBRO Regions Connecting Award to IDP and the ERC Consolidator Grant 101002203 to NF. Part of the equipment employed in this work has been funded by Generalitat Valenciana and co-financed with ERDF funds (OP ERDF of Comunitat Valenciana 2014-2020).

ACKNOWLEDGMENTS

We would like to thank K. Lloyd (UC Davis), B. Rico (King´s College London) and O. Marín (King´s College London) for the Erbb4 and Ai9 mouse strains. We thank V. Ramos as well as A. Teruel for general laboratory support. We are very grateful to K. Kass-Youssef, A. Busquets-García and members of the Di Cristo, Dehorter, Flames and Del Pino laboratories for stimulating discussions and ideas.

SUPPLEMENTARY MATERIAL

The Supplementary Material for this article can be found online at: https://www.frontiersin.org/articles/10.3389/fcell.2021.770458/full#supplementary-material

REFERENCES

Abrams, J. K., Johnson, P. L., Hollis, J. H., and Lowry, C. A. (2004). Anatomic and Functional Topography of the Dorsal Raphe Nucleus. *Ann. N Y Acad. Sci.* 1018, 46–57. doi:10.1196/annals.1296.005

Arshadi, C., Günther, U., Eddison, M., Harrington, K. I. S., and Ferreira, T. A. (2021). SNT: a Unifying Toolbox for Quantification of Neuronal Anatomy. *Nat. Methods* 18, 374–377. doi:10.1038/s41592-021-01105-7

Bang, S. J., Jensen, P., Dymecki, S. M., and Commons, K. G. (2012). Projections and Interconnections of Genetically Defined Serotonin Neurons in Mice. *Eur. J. Neurosci.* 35, 85–96. doi:10.1111/j.1460-9568.2011.07936.x

Bartolini, G., Sánchez-Alcañiz, J. A., Osório, C., Valiente, M., García-Frigola, C., and Marín, O. (2017). Neuregulin 3 Mediates Cortical Plate Invasion and Laminar Allocation of GABAergic Interneurons. *Cel Rep.* 18, 1157–1170. doi:10.1016/j.celrep.2016.12.089

Batista-Brito, R., Vinck, M., Ferguson, K. A., Chang, J. T., Laubender, D., Lur, G., et al. (2017). Developmental Dysfunction of VIP Interneurons Impairs Cortical Circuits. *Neuron* 95, 884–895. doi:10.1016/j.neuron.2017.07.034

Bean, J. C., Lin, T. W., Sathyamurthy, A., Liu, F., Yin, D.-M., Xiong, W.-C., et al. (2014). Genetic Labeling Reveals Novel Cellular Targets of Schizophrenia Susceptibility Gene: Distribution of GABA and Non-GABA ErbB4-Positive Cells in Adult Mouse Brain. *J. Neurosci.* 34, 13549–13566. doi:10.1523/JNEUROSCI.2021-14.2014

Chen, M., and Bi, L.-l. (2019). Optogenetic Long-Term Depression Induction in the PVT-CeL Circuitry Mediates Decreased Fear Memory. *Mol. Neurobiol.* 56, 4855–4865. doi:10.1007/s12035-018-1407-z

Choi, E. A., and McNally, G. P. (2017). Paraventricular Thalamus Balances Danger and Reward. *J. Neurosci.* 37, 3018–3029. doi:10.1523/JNEUROSCI.3320-16.2017

Dahlström, A., and Fuxe, K. (1964). Localization of Monoamines in the Lower Brain Stem. *Experientia* 20, 398–399. doi:10.1007/BF02147990

Del Pino, I., Brotons-Mas, J. R., Marques-Smith, A., Marighetto, A., Frick, A., Marín, O., et al. (2017). Abnormal Wiring of CCK+ Basket Cells Disrupts Spatial Information Coding. *Nat. Neurosci.* 20, 784–792. doi:10.1038/nn.4544

del Pino, I., García-Frigola, C., Dehorter, N., Brotons-Mas, J. R., Alvarez-Salvado, E., Martínez de Lagrán, M., et al. (2013). Erbb4 Deletion from Fast-Spiking Interneurons Causes Schizophrenia-like Phenotypes. *Neuron* 79, 1152–1168. doi:10.1016/j.neuron.2013.07.010

Do-Monte, F. H., Quiñones-Laracuente, K., and Quirk, G. J. (2015). A Temporal Shift in the Circuits Mediating Retrieval of Fear Memory. *Nature* 519, 460–463. doi:10.1038/nature14030

Donovan, L. J., Spencer, W. C., Kitt, M. M., Eastman, B. A., Lobur, K. J., Jiao, K., et al. (2019). Lmx1b Is Required at Multiple Stages to Build Expansive Serotonergic Axon Architectures. *Elife* 8, 1. doi:10.7554/eLife.48788

Fazzari, P., Paternain, A. V., Valiente, M., Pla, R., Luján, R., Lloyd, K., et al. (2010). Control of Cortical GABA Circuitry Development by Nrg1 and ErbB4 Signalling. *Nature* 464, 1376–1380. doi:10.1038/nature08928

Fernandez, S. P., Cauli, B., Cabezas, C., Muzerelle, A., Poncer, J.-C., and Gaspar, P. (2016). Multiscale Single-Cell Analysis Reveals Unique Phenotypes of Raphe 5-HT Neurons Projecting to the Forebrain. *Brain Struct. Funct.* 221, 4007–4025. doi:10.1007/s00429-015-1142-4

Flames, N., Long, J. E., Garratt, A. N., Fischer, T. M., Gassmann, M., Birchmeier, C., et al. (2004). Short- and Long-Range Attraction of Cortical GABAergic Interneurons by Neuregulin-1. *Neuron* 44, 251–261. doi:10.1016/j.neuron.2004.09.028

Forero, A., Rivero, O., Wäldchen, S., Ku, H.-P., Kiser, D. P., Gärtner, Y., et al. (2017). Cadherin-13 Deficiency Increases Dorsal Raphe 5-HT Neuron Density and Prefrontal Cortex Innervation in the Mouse Brain. *Front. Cel. Neurosci.* 11, 307. doi:10.3389/fncel.2017.00307

Franklin, K. B. J., and Paxinos, G. (2008). *The Mouse Brain in Stereotaxic Coordinates, Compact*. 3rd ed.. USA: Elsevier Academic Press.

Garcia, S., Guarino, D., Jaillet, F., Jennings, T., Pröpper, R., Rautenberg, P. L., et al. (2014). Neo: an Object Model for Handling Electrophysiology Data in Multiple Formats. *Front. Neuroinform.* 8, 10. doi:10.3389/fninf.2014.00010

Golub, M. S., Germann, S. L., and Lloyd, K. C. K. (2004). Behavioral Characteristics of a Nervous System-specific erbB4 Knock-Out Mouse. *Behav. Brain Res.* 153, 159–170. doi:10.1016/j.bbr.2003.11.010

Hawthorne, A. L., Wylie, C. J., Landmesser, L. T., Deneris, E. S., and Silver, J. (2010). Serotonergic Neurons Migrate Radially through the Neuroepithelium by Dynamin-Mediated Somal Translocation. *J. Neurosci.* 30, 420–430. doi:10.1523/JNEUROSCI.2333-09.2010

Hay-Schmidt, A. (2000). The Evolution of the Serotonergic Nervous System. *Proc. R. Soc. Lond. B* 267, 1071–1079. doi:10.1098/rspb.2000.1111

Hendricks, T., Francis, N., Fyodorov, D., and Deneris, E. S. (1999). The ETS Domain Factor Pet-1 Is an Early and Precise Marker of central Serotonin Neurons and Interacts with a Conserved Element in Serotonergic Genes. *J. Neurosci.* 19, 10348–10356. doi:10.1523/jneurosci.19-23-10348.1999

Jensen, P., Farago, A. F., Awatramani, R. B., Scott, M. M., Deneris, E. S., and Dymecki, S. M. (2008). Redefining the Serotonergic System by Genetic Lineage. *Nat. Neurosci.* 11, 417–419. doi:10.1038/nn2050

La Manno, G., Siletti, K., Furlan, A., Gyllborg, D., Vinsland, E., Mossi Albiach, A., et al. (2021). Molecular Architecture of the Developing Mouse Brain. *Nature* 596, 92–96. doi:10.1038/s41586-021-03775-x

Li, L., Zhang, L.-Z., He, Z.-X., Ma, H., Zhang, Y.-T., Xun, Y.-F., et al. (2021). Dorsal Raphe Nucleus to Anterior Cingulate Cortex 5-HTergic Neural Circuit Modulates Consolation and Sociability. *Elife* 10, 1. doi:10.7554/eLife.67638

Li, Y., Dong, X., Li, S., and Kirouac, G. J. (2014). Lesions of the Posterior Paraventricular Nucleus of the Thalamus Attenuate Fear Expression. *Front. Behav. Neurosci.* 8, 94. doi:10.3389/fnbeh.2014.00094

Lidov, H. G. W., and Molliver, M. E. (1982). An Immunohistochemical Study of Serotonin Neuron Development in the Rat: Ascending Pathways and Terminal fields. *Brain Res. Bull.* 8, 389–430. doi:10.1016/0361-9230(82)90077-6

López-Bendito, G., Cautinat, A., Sánchez, J. A., Bielle, F., Flames, N., Garratt, A. N., et al. (2006). Tangential Neuronal Migration Controls Axon Guidance: a Role for Neuregulin-1 in Thalamocortical Axon Navigation. *Cell* 125, 127–142. doi:10.1016/j.cell.2006.01.042

Maddaloni, G., Bertero, A., Pratelli, M., Barsotti, N., Boonstra, A., Giorgi, A., et al. (2017). Development of Serotonergic Fibers in the Post-Natal Mouse Brain. *Front. Cel. Neurosci.* 11, 202. doi:10.3389/fncel.2017.00202

Madisen, L., Zwingman, T. A., Sunkin, S. M., Oh, S. W., Zariwala, H. A., Gu, H., et al. (2010). A Robust and High-Throughput Cre Reporting and Characterization System for the Whole Mouse Brain. *Nat. Neurosci.* 13, 133–140. doi:10.1038/nn.2467

Marcinkiewcz, C. A., Mazzone, C. M., D'Agostino, G., Halladay, L. R., Hardaway, J. A., DiBerto, J. F., et al. (2016). Serotonin Engages an Anxiety and Fear-Promoting Circuit in the Extended Amygdala. *Nature* 537, 97–101. doi:10.1038/nature19318

Mei, L., and Nave, K.-A. (2014). Neuregulin-ERBB Signaling in the Nervous System and Neuropsychiatric Diseases. *Neuron* 83, 27–49. doi:10.1016/j.neuron.2014.06.007

Migliarini, S., Pacini, G., Pelosi, B., Lunardi, G., and Pasqualetti, M. (2013). Lack of Brain Serotonin Affects Postnatal Development and Serotonergic Neuronal Circuitry Formation. *Mol. Psychiatry* 18, 1106–1118. doi:10.1038/mp.2012.128

Mostaid, M. S., Mancuso, S. G., Liu, C., Sundram, S., Pantelis, C., Everall, I. P., et al. (2017). Meta-analysis Reveals Associations between Genetic Variation in the 5′ and 3′ Regions of Neuregulin-1 and Schizophrenia. *Transl Psychiatry* 7, e1004. doi:10.1038/tp.2016.279

Niederkofler, V., Asher, T. E., Okaty, B. W., Rood, B. D., Narayan, A., Hwa, L. S., et al. (2016). Identification of Serotonergic Neuronal Modules that Affect Aggressive Behavior. *Cel Rep.* 17, 1934–1949. doi:10.1016/j.celrep.2016.10.063

Norton, N., Moskvina, V., Morris, D. W., Bray, N. J., Zammit, S., Williams, N. M., et al. (2006). Evidence that Interaction between Neuregulin 1 and its Receptor erbB4 Increases Susceptibility to Schizophrenia. *Am. J. Med. Genet.* 141B, 96–101. doi:10.1002/ajmg.b.30236

Okaty, B. W., Freret, M. E., Rood, B. D., Brust, R. D., Hennessy, M. L., deBairos, D., et al. (2015). Multi-Scale Molecular Deconstruction of the Serotonin Neuron System. *Neuron* 88, 774–791. doi:10.1016/j.neuron.2015.10.007

Okaty, B. W., Sturrock, N., Escobedo Lozoya, Y., Chang, Y., Senft, R. A., Lyon, K. A., et al. (2020). A Single-Cell Transcriptomic and Anatomic Atlas of Mouse Dorsal Raphe *Pet1* Neurons. *Elife* 9, 1. doi:10.7554/eLife.55523

Padilla-Coreano, N., Do-Monte, F. H., and Quirk, G. J. (2012). A Time-dependent Role of Midline Thalamic Nuclei in the Retrieval of Fear Memory. *Neuropharmacology* 62, 457–463. doi:10.1016/j.neuropharm.2011.08.037

Penzo, M. A., Robert, V., Tucciarone, J., De Bundel, D., Wang, M., Van Aelst, L., et al. (2015). The Paraventricular Thalamus Controls a central Amygdala Fear Circuit. *Nature* 519, 455–459. doi:10.1038/nature13978

Ren, J., Friedmann, D., Xiong, J., Liu, C. D., Ferguson, B. R., Weerakkody, T., et al. (2018). Anatomically Defined and Functionally Distinct Dorsal Raphe Serotonin Sub-systems. *Cell* 175, 472–487. e420. doi:10.1016/j.cell.2018.07.043

Ren, J., Isakova, A., Friedmann, D., Zeng, J., Grutzner, S. M., Pun, A., et al. (2019). Single-cell Transcriptomes and Whole-Brain Projections of Serotonin Neurons in the Mouse Dorsal and Median Raphe Nuclei. *Elife* 8, 1. doi:10.7554/eLife.49424

Rico, B., and Marín, O. (2011). Neuregulin Signaling, Cortical Circuitry Development and Schizophrenia. *Curr. Opin. Genet. Dev.* 21, 262–270. doi:10.1016/j.gde.2010.12.010

Scott, M. M., Wylie, C. J., Lerch, J. K., Murphy, R., Lobur, K., Herlitze, S., et al. (2005). A Genetic Approach to Access Serotonin Neurons for *In Vivo* and *In Vitro* Studies. *Proc. Natl. Acad. Sci.* 102, 16472–16477. doi:10.1073/pnas.0504510102

Senft, R. A., Freret, M. E., Sturrock, N., and Dymecki, S. M. (2021). Neurochemically and Hodologically Distinct Ascending VGLUT3 versus Serotonin Subsystems Comprise the R2-*Pet1* Median Raphe. *J. Neurosci.* 41, 2581–2600. doi:10.1523/JNEUROSCI.1667-20.2021

Silberberg, G., Darvasi, A., Pinkas-Kramarski, R., and Navon, R. (2006). The Involvement ofErbB4 with Schizophrenia: Association and Expression Studies. *Am. J. Med. Genet.* 141B, 142–148. doi:10.1002/ajmg.b.30275

Skirzewski, M., Karavanova, I., Shamir, A., Erben, L., Garcia-Olivares, J., Shin, J. H., et al. (2018). ErbB4 Signaling in Dopaminergic Axonal Projections Increases Extracellular Dopamine Levels and Regulates Spatial/working Memory Behaviors. *Mol. Psychiatry* 23, 2227–2237. doi:10.1038/mp.2017.132

Teng, T., Gaillard, A., Muzerelle, A., and Gaspar, P. (2017). EphrinA5 Signaling Is Required for the Distinctive Targeting of Raphe Serotonin Neurons in the Forebrain. *eNeuro* 4, 0327-16. doi:10.1523/ENEURO.0327-16.2017

Ting, A. K., Chen, Y., Wen, L., Yin, D.-M., Shen, C., Tao, Y., et al. (2011). Neuregulin 1 Promotes Excitatory Synapse Development and Function in GABAergic Interneurons. *J. Neurosci.* 31, 15–25. doi:10.1523/JNEUROSCI.2538-10.2011

Walsh, T., McClellan, J. M., McCarthy, S. E., Addington, A. M., Pierce, S. B., Cooper, G. M., et al. (2008). Rare Structural Variants Disrupt Multiple Genes in Neurodevelopmental Pathways in Schizophrenia. *Science* 320, 539–543. doi:10.1126/science.1155174

Wang, H., Liu, F., Chen, W., Sun, X., Cui, W., Dong, Z., et al. (2018). Genetic Recovery of ErbB4 in Adulthood Partially Restores Brain Functions in Null Mice. *Proc. Natl. Acad. Sci. USA* 115, 13105–13110. doi:10.1073/pnas.1811287115

Yamamuro, K., Bicks, L. K., Leventhal, M. B., Kato, D., Im, S., Flanigan, M. E., et al. (2020). A Prefrontal-Paraventricular Thalamus Circuit Requires Juvenile Social Experience to Regulate Adult Sociability in Mice. *Nat. Neurosci.* 23, 1240–1252. doi:10.1038/s41593-020-0695-6

Zhang, D., Sliwkowski, M. X., Mark, M., Frantz, G., Akita, R., Sun, Y., et al. (1997). Neuregulin-3 (NRG3): a Novel Neural Tissue-Enriched Protein that Binds and Activates ErbB4. *Proc. Natl. Acad. Sci.* 94, 9562–9567. doi:10.1073/pnas.94.18.9562

Zhang, S.-R., Wu, J.-L., Chen, H., Luo, R., Chen, W.-J., Tang, L.-J., et al. (2020). ErbB4 Knockdown in Serotonergic Neurons in the Dorsal Raphe Induces Anxiety-like Behaviors. *Neuropsychopharmacol.* 45, 1698–1706. doi:10.1038/s41386-020-0601-7

Zhu, X., Lai, C., Thomas, S., and Burden, S. J. (1995). Neuregulin Receptors, erbB3 and erbB4, Are Localized at Neuromuscular Synapses. *EMBO J.* 14, 5842–5848. doi:10.1002/j.1460-2075.1995.tb00272.x

Conflict of Interest: The authors declare that the research was conducted in the absence of any commercial or financial relationships that could be construed as a potential conflict of interest.

Publisher's Note: All claims expressed in this article are solely those of the authors and do not necessarily represent those of their affiliated organizations, or those of the publisher, the editors and the reviewers. Any product that may be evaluated in this article, or claim that may be made by its manufacturer, is not guaranteed or endorsed by the publisher.

frontiers in Cell and Developmental Biology

REVIEW
published: 21 December 2021
doi: 10.3389/fcell.2021.786129

Origin and Development of the Adipose Tissue, a Key Organ in Physiology and Disease

Esmeralda Parra-Peralbo[1]*, *Ana Talamillo*[2]* and *Rosa Barrio*[2]

[1]Faculty of Biomedical and Health Sciences, European University, Villaviciosa de Odón, Spain, [2]Center for Cooperative Research in Biosciences (CIC BioGUNE), Basque Research and Technology Alliance (BRTA), Derio, Spain

Adipose tissue is a dynamic organ, well known for its function in energy storage and mobilization according to nutrient availability and body needs, in charge of keeping the energetic balance of the organism. During the last decades, adipose tissue has emerged as the largest endocrine organ in the human body, being able to secrete hormones as well as inflammatory molecules and having an important impact in multiple processes such as adipogenesis, metabolism and chronic inflammation. However, the cellular progenitors, development, homeostasis and metabolism of the different types of adipose tissue are not fully known. During the last decade, *Drosophila melanogaster* has demonstrated to be an excellent model to tackle some of the open questions in the field of metabolism and development of endocrine/metabolic organs. Discoveries ranged from new hormones regulating obesity to subcellular mechanisms that regulate lipogenesis and lipolysis. Here, we review the available evidences on the development, types and functions of adipose tissue in *Drosophila* and identify some gaps for future research. This may help to understand the cellular and molecular mechanism underlying the pathophysiology of this fascinating key tissue, contributing to establish this organ as a therapeutic target.

Keywords: WAT, BAT, beige adipocytes, adipose tissue, adipose stem cells, drosophila, fat body development, adepithelial cells

OPEN ACCESS

Edited by:
Juan Jose Sanz-Ezquerro, National Center for Biotechnology (CSIC), Spain

Reviewed by:
Tamás Röszer, University of Ulm, Germany
Julien Colombani, University of Copenhagen, Denmark
Rénald Delanoue, INSERM U1091 Institut de biologie de Valrose, France

***Correspondence:**
Esmeralda Parra-Peralbo
esmeralda.parra@universidadeuropea.es
Ana Talamillo
atalamillo@cicbiogune.es

Specialty section:
This article was submitted to Signaling, a section of the journal Frontiers in Cell and Developmental Biology

Received: *29 September 2021*
Accepted: *01 December 2021*
Published: *21 December 2021*

Citation:
Parra-Peralbo E, Talamillo A and Barrio R (2021) Origin and Development of the Adipose Tissue, a Key Organ in Physiology and Disease. Front. Cell Dev. Biol. 9:786129. doi: 10.3389/fcell.2021.786129

INTRODUCTION

In this manuscript we review the past and recent literature on the origin, development, types and function of mammalian adipose tissue and put it in relation to physiological and disease conditions such as obesity, diabetes, lipodystrophies or cancer-associated cachexia. We identify the gaps that need to be addressed regarding the origin and development of this tissue and propose *Drosophila* as a suitable model organism to explore those open questions. We review the existing evidences on the origin, development and function of the adipose tissue (AT) of this organism, making a clear distinction between the embryonic and larval stages and the adulthood, when the developmental programmes are finished. As we considered there are two different scenarios where play different actors and also where same actors could play different roles. We also review the available studies in *Drosophila* on the above-mentioned metabolic diseases.

MAMMALIAN ADIPOSE TISSUE AND ASSOCIATED DISEASES

The lifestyle of developed countries, where population have an easy access to high caloric food and decreased physical exercise, has played important roles into the rise of obesity and Type 2 Diabetes

Mellitus (T2DM) to the category of pandemics (Doria et al., 2008; Guilherme et al., 2008; Saltiel, 2012). Global prevalence of overweight and obesity combined has risen by 27.5% for adults and 47.1% for children between 1980 and 2013 (Ng et al., 2014). Furthermore, excess body weight is one of the major risk factors contributing to the global incidence of disease worldwide. According to the International Diabetes Federation (IDF), more than 371 million people across the globe have diabetes and this number is predicted to rise to over 550 million by 2030. Adipose tissue (AT) plays also important roles in other diseases. For instance, lipid storages at AT are susceptible to be wasted by tumour-secreted molecules, a fact known as cancer-associated cachexia (Rydén and Arner, 2007; Tsoli et al., 2016). This process is featured by increased systemic inflammation, general metabolic dysfunction, and elevated resting energy expenditure (Fearon et al., 2011). Cachexia affects 50–80% of cancer patients and accounts for up to 20% of cancer deaths. It is estimated that death normally ensues when weight loss exceeds 30–40% (Arthur et al., 2014). In this scenario, the understanding of adipocytes' development will improve our knowledge on metabolic diseases such as obesity and T2DM, as well as on anomalous metabolic states that lead to chronic inflammation. (Stephens, 2012; Wu et al., 2013; Hotamisligil, 2017). Understanding in deep the biology of the AT will allow the development of potential therapies targeting thermogenesis as a means of increasing energy expenditure.

The Adipose Tissue as a Regulator of Energy Homeostasis in Mammals

Energy is fundamental for life. Therefore, storage and homeostasis of energy are key processes for any organism. In the mammalian body, including that of humans, the energy that is neither consumed nor converted into glycogen is stored in form of neutral lipids in the adipocytes of the AT, more specifically in the lipid droplets (LDs). The LDs are key organelles controlling fat storage and mobilization (Olofsson et al., 2008; Beller et al., 2010). They consist of a core of neutral lipids (triglyceride and cholesterol esters) surrounded by a monolayer of phospholipid and cholesterol in which several proteins are embedded (Thiam and Beller, 2017).

Importantly, the AT is a plastic organ able to adapt to different physiological circumstances to ensure energy distribution among the different needs: metabolism, thermogenesis and lactation (Cinti, 2018). AT can grow by either increasing the number of adipocytes, which depends on adipocyte stem cells (ASC) or increasing the LDs size. In fat oxidizing tissues, LDs expansion is supported by specific mitochondria, known as peridroplet mitochondria. Those remain bound to the LD even after the homogenization the tissue and show specific features such as enhanced bioenergetic capacity, reduced β-oxidation capacity, supported LD expansion by providing ATP for triacylglycerides (TAG) synthesis, and maintenance of a distinct protein composition due to low fusion-fission dynamics (Benador et al., 2018).

In mammals there are different types of ATs: white AT (WAT), designed for energy storage, and brown AT (BAT), intended to dissipate energy and generate heat (Berry et al., 2013; Gupta, 2014). WAT is classified in subcutaneous or visceral WAT, depending on its anatomical location (Cleal et al., 2017). The two types of WATs have distinct developmental timing, microscopic appearance, molecular signature and certainly biological function. Subcutaneous WAT may protect against certain aspects of metabolic dysfunction (Snijder et al., 2003a; Snijder et al., 2003b). Visceral WAT is associated with metabolic complications and appears to increase the risk of T2DM, hyperlipidemia and cardiovascular disease (Grauer et al., 1984). Increasing number of evidences converge on to the idea that within mammalian bodies there are different AT depots, which present a vast heterogeneity among them, and contain the ASC that support their homeostasis (Cleal et al., 2017).

TABLE 1 | Factors expressed in differentiated adipocytes.

Marker	Adipocyte type
LEP, ASC1	White
TEMEM26, HOXC9, TBX1	Beige
UCP1, PRDM16, P2RX5	Beige and brown
ZIC1, LHX8	Brown
ADIPQ	White, beige and brown

Abbreviations: ADIPQ, adiponectin; ASC1, asc-type amino acid transporter 1; HOXC9, homeobox C9; LEP, leptine; LHX8, LIM homeobox 8; P2RX5, purinergic Receptor P2X, ligand-gated ion channel 5; PRDM16, PR domain containing 16; TEMEM26, transmembrane protein 26; TBX1, t-box 1; UCP1, uncoupling protein 1; ZIC1, zinc finger protein of the cerebellum 1.

Until recently, the functions of the BAT were associated to the neonatal period (Novak et al., 1971) and the scientific community thought that this type of fat was not present during the adulthood. A bit more a decade ago, BAT was identified in adult humans and it was found to be reduced, on mass and activity, in obese and diabetic patients (Cypess et al., 2009; Cypess et al., 2013; Lidell et al., 2013; Alcalá et al., 2019). This finding pointed out to the idea of enhancement of BAT preadipocyte differentiation and proliferation as a therapeutic strategy to fight obesity (Alcalá et al., 2019). Later evidences converged on to the idea that adult human BAT shares molecular characteristics with murine "beige" cells rather than classical brown cells (Wu et al., 2012; Cannon et al., 2020).

"Beige" or "brite" adipocytes, also known as Beige Adipose Tissue (BeAT), are energy-burning adipocytes, with "brown-like' features, such as increased mitochondrial content, multilocular storing of LDs, and the ability to burn off lipids as heat (Ikeda et al., 2018). BeAT is found in different spots of the adult body within the WAT (Cypess et al., 2009; Cypess et al., 2013; Lidell et al., 2013; Wu et al., 2012; Whittle et al., 2011). Although beige adipocytes share some markers with brown adipocytes, they also show specific markers different from those of both brown and white adipocytes (**Table 1**) (Sharp et al., 2012; Waldén et al., 2012; Ussar et al., 2014).

In spite of their distinct functions, WAT and "Beige AT" (BeAT) share the ability for reciprocal, reversible transdifferentiation to tackle special physiologic needs. Thus, chronic need for thermogenesis induces browning and chronic

TABLE 2 | Mammalian AT secreted molecules.

	–	–
Adipokines	Leptin	LEP
	Adiponectin[a]	ADIPOQ
	Resistin	RETN
	Fibrillin 1 (aprosin)[a]	FBN1
	Serpin family E member 1 (plasminogen activator inhibitor)	SERPINE1 (PAI-1)
	Apelin[a]	APLN
	Intelectin 1 (omentin)	ITLN1
	Retinol-binding protein 4	RPB4
	Nicotinamide phosphoribosyltransferase (visfatin)	NAMPT
	Nucleobindin 2 (nesfatin 1)	NUCB2
	Dipeptidyl peptidase IV	DPP-4
	Endocannabinoids	
Alternate complement system	Complement C3	C3
	Complement factor B	CFB
	Complement factor D (adipsin)[a]	CFD
Growth factors	Fibroblast growth factor-21	FGF21
	Bone morphogenetic protein	BMP
Vasculotrophic factors	Vascular endothelial growth factor	VEGFA
	NO	
	CO	
	Angiotensin II	AGT
Neurotrophic factors	Nerve growth factor	NGF
	Semaphorin 3 and 6	SEMA3A/SEMA6A
	Neuregulin 4	NRG4
Inflammatory cytokines	Tumor necrosis factor α	TNFα
	Interleukin 6	IL6
	Interleukin 33	IL33
	Interleukin 1B	IL1B
	C-C Motif chemokine ligand 5	CCL5 (RANTES)
	Interleukin 8	IL8
	C-X-C Motif chemokine ligand 12 (stromal cell-derived factor 1)	CXCL12 (SDF1)
	Macrophage migration inhibitory factor	MIF
	C-C Motif chemokine ligand 2 (Monocyte chemoattractant protein-1)	CCL2 (MCP1)
Lipid metabolism	Lipoprotein lipase	LPL
	Cholesteryl ester transfer protein	CETP
BAT-adipokines	Peptidase M20 domain containing 1	PM20D1

[a]*Secreted also by skeletal muscles. In parenthesis, other used names for the same factor. NO, nitric oxide; CO, carbon monoxide.*

positive energy balance induces whitening (Cohen and Spiegelman, 2016; Cinti, 2018). Different signals, after birth and adult state, will determine BeAT differentiation. While Platelet activating factor and Interleukin 6 (IL-6) are determining factors in BeAT development after birth, β-adrenergic stimulation and IL-4 are active during adulthood (Chung et al., 2017; Finlin et al., 2017; Babaei et al., 2018; Yu et al., 2019; Hoang et al., 2021). Interestingly, a switch from BeAT to WAT underlies cancer-associated cachexia, triggered by the parathyroid-hormone-related protein (Kir et al., 2014; Petruzzelli and Wagner, 2016).

The Adipose Tissue in Signalling and Inflammation in Mammals

AT is a large endocrine organ, insulin sensitive, that secretes around 600 different adipokines, the hormones that act on distant organs **(Table 2)** (Lehr et al., 2012a; Cinti, 2018) as well as a vast diversity of other signalling molecules, such as metabolites, lipids, non-coding RNAs or extracellular vesicles (Funcke and Scherer, 2019). Leptin and adiponectin are well known hormones secreted by adipocytes (Cinti, 2018). Leptin inhibits appetite, stimulate thermogenesis, enhance fatty acid oxidation, decrease glucose, and reduce body weight and fat. Adiponectin mediates the insulin-sensitizing effect (Yadav et al., 2013). Omentin, secreted by non-adipocyte cells in the AT, acts as insulin-sensitizing factor and it has been reported to have anti-inflammatory, anti-atherogenic and anti-cardiovascular disease properties (Tan et al., 2010). Dipeptidyl peptidase IV, secreted by visceral white adipocytes from obese individuals, seems to be associated to insulin-resistance development (Lamers et al., 2011; Lehr et al., 2012b).

AT is not only composed by adipocytes but also comprises as well other cell types such as preadipocytes, fibroblasts, stromal cells, T-cells, granulocytes, macrophages and monocytes (Hotamisligil, 2017). During the last years, several adipokines and cytokines secreted by AT and also other molecules of signalling pathways linking AT metabolism and immune system, have been identified. For example resistin, a hormone secreted by macrophages M1, pro-inflammatory phenotype, that infiltrate obese adipoctyes, produces a notable effect on systemic metabolism by acting as a crosstalk between obesity-

inflammation and metabolic diseases (Schwartz and Lazar, 2011). Likewise, the dysfunction of AT is associated with the secretion of multiple molecules that mediate the inflammatory response. In fact, stressed adipocytes from obese ATs activate the inflammasome system, which could induce a chronic low-grade inflammation. Inflammation appears in other tissues besides AT, including brain, liver, airways and pancreatic islets. This inflammatory state is known as "metaflammation" because it contributes to several immunometabolic diseases, including T2DM, cardiovascular disease, asthma, neurodegenerative disease, cancer and lipodystrophies (Hotamisligil, 2017; Cinti, 2018).

The Origin and Development of the Mammalian Adipose Tissue

A great number of studies, most of them carried out *in vitro*, shed light on the factors involved in differentiation of white, brown and beige adipocytes, such as peroxisome proliferator-activated receptor gamma (PPARγ), CCAAT/enhancer binding proteins (C/EPB), krupper-like factors (KLFs), peroxisome proliferator-activated receptor gamma coactivator-1 alpha (PGC1a) or nuclear factor I A (NFIA) (reviewed at (Hiraike et al., 2017; Cinti, 2018; Hiraike et al., 2020). However, the initial commitment of mesenchymal progenitors to the adipocyte lineage remains less explored (Billon et al., 2007).

A comprehensive understanding of the origin of white/brown/beige adipocytes differentiation is of upmost interest given the potential to induce browning AT in obese patients (Cypess and Kahn, 2010). It is accepted that animals with more BAT are more resistant not only to obesity but also to T2DM (Kopecký et al., 1996; Collins et al., 1997; Guerra et al., 1998; Almind et al., 2007). Conversely, animals without functional BAT are prone to obesity and T2DM (Lowell et al., 1993; Bachman et al., 2002; Feldmann et al., 2009). Attempts to block lipid storage or inhibiting WAT development failed, as several studies have shown that this strategy drives fat accumulation in organs not specialized for fat storage. This condition is known as "ectopic lipid" and has been associated with insulin resistance and the development of T2DM (Gastaldelli, 2011).

BAT, WAT and BeAT can develop from both neural crest and mesoderm, specifically BAT develops from paraxial mesoderm and WAT and Beige AT does from lateral plate mesoderm (Billon et al., 2007). Periaortic arch adipose tissue (PAAT), which is composed of both BAT and WAT, is derived from multiple cell lines, being neural crest cells the main contributors (Fu et al., 2019). Furthermore, brown adipocytes could arise from Myogenic Factor 5 (MYF5)-expressing myogenic precursor cells by the action of PRDM16 (PRD1-BF1-RIZ1 homologous domain containing 16). PRDM16 controls a bidirectional cell fate switch between skeletal myoblasts and BeAT cells and it is also responsible for beige cells found within WAT depots (Seale et al., 2008; Enerbäck, 2009; Lshibashi and Seale, 2010; Petrovic et al., 2010; Seale et al., 2011). PRDM16 gene expression is downregulated by miR-149-3p during fasting conditions allowing the switch from subcutaneous to visceral AT (Ding et al., 2016).

The specific origin of the beige adipocytes remains to be clarified. Some evidences support the idea that they arise from unique precursor cells (Wu et al., 2012), but others suggest that they may arise from white adipocytes in a process referred to as transdifferentiation (Cinti, 2012; Cinti, 2018).

Moreover, developed spots of both BAT and WAT present a remarkable adipocytes' heterogeneity. Low- and high-thermogenic brown adipocytes with distinct features and functions coexist in BAT. Low-thermogenic brown adipocytes, unlike the high-thermogenic ones, show low *Ucp1* and *Adipoq* expression, larger lipid droplets, lower mitochondrial content and are functionally specialized in fatty acid uptake (Song et al., 2020). Similarly, functional heterogeneity is found when comparing subcutaneous and omental preadipocytes, which show distinct capacities for replication, adipogenesis and apoptosis (Tchkonia et al., 2005).

To study in deep all aspects of adipocyte biology is required to know the molecular properties of adipose precursor cells and the ontogeny of fat cells *in vivo* (Gupta, 2014). Understanding the origin and differentiation of the different types of adipocytes might pave the way for future therapies for obesity, T2DM, cancer-associate cachexia and immunometabolic diseases (Stephens, 2012; Jung et al., 2019).

OPEN QUESTIONS ON THE ORIGIN AND FUNCTION OF THE ADIPOSE TISSUE

One of the most important open questions is the origin of the AT: which factor(s) are required for the specification of the AT primordium, how proliferation of ASC is regulated and how ASC differentiate into adipocytes. The identification and characterization of the ASC population is fundamental to understand AT development, formation and maintenance.

Equally important is to study how the ASC contribute to the homeostasis and maintenance of the AT under both normal energy intake and excess nutrient load. In the same way, it would be critical to know the growth factors and developmental signalling pathways altering ASC behaviour and adipocyte formation. Furthermore, although some factors determining fat cells fate has been described, most of these studies have been carried out *in vitro* and their role *in vivo* has not been explored (Berry et al., 2013; Gupta, 2014; Jung et al., 2019).

Last but not least, the growing number of functions in which the mammalian AT is involved require further studies, being the use of model systems an important tool to be exploited (Hotamisligil, 2017).

DROSOPHILA AS A MODEL TO STUDY ADIPOSE TISSUE

The ability to store nutrients, mainly in form of TAG, is conserved from yeast to human (Kadereit et al., 2008) (**Figure 1**). Even though a better knowledge on AT from an evolutionary perspective could improve our understanding on the development, function and dysfunction of this organ, this theme

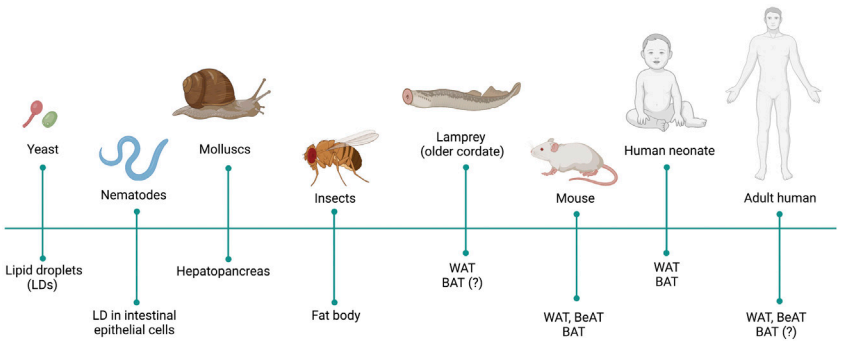

FIGURE 1 | Evolution of the adipose tissue (AT). Presence of fat cells, fat organs and proper AT is indicated in different phyla and species throughout evolution.

remain as a neglected enigma (Ottaviani et al., 2011). TAG synthesis and lipolysis related genes are already present in unicellular organisms such as *Saccharomyces cerevisiae* or *Candida parapsilosis* (Zweytick et al., 2000; Neugnot et al., 2002; Daum et al., 2007). *Caenorhabiditis elegans* also stores TAG in form of LDs in the intestinal epithelial cells (Watts, 2009).

The ability to, not only store fat, but also to secrete endocrine factors is already present in molluscs. *Haliotis fulgens* or *Helix aspersa* store TAG in the midintestinal gland known as hepatopancreas. This also secretes a glucose lowering level hormone, Phe-Met-Arg-Phe-amide (FMRFa), belonging to the evolutionarily conserved RF-amide neuropeptide family (Rőszer and Kiss-Tóth, 2014). Neuropeptide FF (NPFF) an anorexigenic peptide, also member of this family, is critical to keep a basal NPY gene expression at arcuate nucleus and promote diet-induced thermogenesis, coupling energy homeostasis with energy partitioning to AT and bone tissue (Zhang et al., 2018). Moreover, NPFF is able to promote macrophage M2, anti-inflammatory phenotype, activation and increase the proliferation of murine and human adipose tissue macrophages (Waqas et al., 2017). Latter in evolution, the AT, in addition to serve as a fat storage and endocrine tissue, is also involved in immunity, as is the case of insects. The lipid storage tissue in insects is known as fat body (FB), which is an endocrine-secreting organ involved in nutrient sensing, development, metabolism, immunity and reproduction (Doane, 1960; Dean et al., 1985; Charroux and Royet, 2010).

WAT is present in most of vertebrate taxa, including fish, amphibian, reptiles and mammals (Gesta et al., 2007; Todorčević et al., 2009; Imrie and Sadler, 2010). Lampreys, at the base of vertebrates' evolution, present fat cells with similar morphological characteristic to white and brown adipocytes (Müller, 1968), which is in conflict with the generally accepted idea about BAT is not present in cold-blooded vertebrates.

BAT is larger in small mammals, such as mouse, than in human. A recent debate points out to mice BAT, rather than the human adult BAT, as a classic defined BAT and, therefore, considers mouse the best model to study the development of this tissue (Cannon et al., 2020).

However, considering the complexity of the AT in mammals, a simpler model than mouse is required to study the development and determination of this tissue. A model organism that allows performing genetics analysis *in vivo* would be suitable to address those open questions. In this regard, *Drosophila* represents a good model for the study of AT based on its genetics accessibility, the lower complexity of the AT and the functional conservation of this tissue along evolution.

Drosophila melanogaster has been used for more than 100 years to study conserved biological processes and decipher the molecular and genetic basis of multicellular organisms, as well as a vast number of human diseases (Yamaguchi and Yoshida, 2018). Several studies have established *Drosophila* as a model to study obesity and metabolic diseases [reviewed at (Musselman and Kühnlein, 2018)]. Importantly, molecules and signalling pathways involved in the regulation of metabolism and physiology of the AT in mammals are conserved in *Drosophila*. For instance, *Drosophila* insulin/insulin like growth factor signalling (IIS) acts as a conserved satiety pathway promoting glucose uptake by peripheral tissues (Saltiel and Kahn, 2001) and sustaining sugar and lipid anabolic processes (Kim and Rulifson, 2004; Buch et al., 2008). Glucagon-like peptide adipokinetic hormone (Akh) signalling, conversely, is activated in response to reduced nutrient availability and promotes mobilization of energy reserves (Kim and Rulifson, 2004; Lee and Park, 2004; Bharucha et al., 2008). Short neuropeptide F (sNPF) is a functional homolog of mammalian orexigenic Neuropeptide Y (Nässel and Wegener, 2011), and its overexpression in sNPF-producing neurons causes hyperphagia and body fat accumulation in flies (Baumbach et al., 2014). Conversely, downregulation of this gene in sNPF-positive neurons reduces food intake (Lee et al., 2004). More recently, *Drosophila* has been demonstrated to be a good model to study T2DM. Flies fed on high sugar diet (HSD) develop diabetes showing increased levels of glucose in their hemolymph (blood-like system), insulin resistance and heart dysfunction (Palanker Musselman et al., 2011; Pasco and Léopold, 2012; Na et al., 2013). *Drosophila* has also been used as a model to identify new regulators of mammalian glucose metabolism (Ugrankar et al., 2015) and has made important contributions

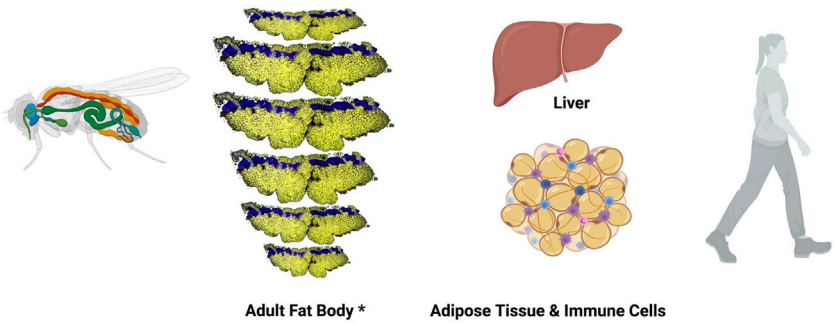

FIGURE 2 | *Drosophila melanogaster* fat body and mammalian functional orthologous organs. Left, schematic representation of *Drosophila melanogaster* adult animal. Fat body is in orange, heat in red and digestive system in green. *Adult *Drosophila* FB is represented here using a composition made by repeating a confocal image of a single panicle of one the dorsal abdominal segments from an adult female fly. Confocal image shows adipocytes in yellow (Nile Red staining) and oenocyte nuclei in blue (DAPI staining). Right, illustrations show mammalian liver and adipose tissue (cells in orange) infiltrated with immune cells (blue and purple cells).

to understand the main components of signalling pathways involved in tumour development, including the cancer associated cachexia (Figueroa-Clarevega and Bilder, 2015; Enomoto et al., 2018; Saavedra and Perrimon, 2019).

Studies to fully understand the regulation of lipid metabolism in *Drosophila* are ongoing. It is well known that lipids are taken by adipocytes from the hemolymph, and are esterified and stored as TAGs and cholesterol esters. Moreover, the *Drosophila* FB, functionally equivalent to mammalian AT and liver, carries out glycolysis and lipogenesis using carbohydrates (**Figure 2**) [reviewed at (Arrese and Soulages, 2010)]. Also, cellular lipid uptake as well as lipid transport and lipoprotein metabolism has been well studied in *Drosophila* (Parra-Peralbo and Culi, 2011; Palm et al., 2012; Rodríguez-Vázquez et al., 2015; Yin et al., 2021). Furthermore, fly mutants in Lipin, a phosphatidate phosphatase required for normal insulin pathway signalling that plays a central role in FB function and energy metabolism, Seipin, a transmembrane protein with roles in ER calcium homeostasis and lipid storage, or Sik3 (Salt-inducible kinase 3), a kinase involved in lipid catabolism by regulating *bmm* gene expression show reduced lipid content and lipodystrophy (Li et al., 2019). All together make this model organism suitable to study different types of lipodystrophies.

As Edward O. Wilson said in "Letters to a young Scientist" for, each biological question there is a suitable system for discovering the answer (Wilson, 2013). In that case, we, as Azeez and collaborators, think that *Drosophila melanogaster* is a suitable system to identify the primordium of AT and the population of ASCs in adults, as well as to characterize the adult AT in order to understand the adipocyte biology (Azeez et al., 2014). As a proof of principle, Pospisilik *et al* (Pospisilik et al., 2010) found Hedgehog as a determinant of Brown versus White adipose cell fate, using *Drosophila* as a model system. In addition, a well-established cell linage tracing system, G-TRACE, has been a key tool for exploring origin, development and differentiation of tissues in *Drosophila* (Evans et al., 2009), only very recently available in mammalian model systems (Berry et al., 2013; Jung et al., 2019).

ORIGIN AND DEVELOPMENT OF EMBRYONIC FAT BODY PRECURSORS

The *Drosophila* FB arises from the embryonic mesoderm (Hartenstein and Jan 1992). At stage 11, the progenitor fat cells arise from nine bilateral clusters of cells in the inner mesodermal layer that span the parasegments 4 through 12 and the mesoderm separates in the splanchnopleure and somatopleure. The somatopleure will give rise to the FB, somatic musculature and other cell types (Campos-Ortega and Hartenstein, 1985). FB cells' lineage can be traced by analyzing the expression patterns of the genes *Alcohol dehydrogenase* (*Adh*), *Collagen type IV alpha 1* (*Col4a1*), the steroid hormone receptor *seven up* (*svp*) and *serpent* (*srp*), as well as the enhancer-trap line *29D* that exhibits an expression pattern restricted to developing embryonic fat cells (Hoshizaki et al., 1994) **(Tables 3, 4)**. This enhancer-trap line allowed tracing the fat-cell lineage to nine bilateral cluster of cells within the emerging mesoderm, representing the progenitor fat cells. The *svp*-positive cells at stage 12 identified early precursor fat cells, and the expression of *Adh* and *Col4a1* was used to identify the terminal fat cell differentiation at stage 15. By late stage 15/16 embryo, mature fat cells coalesce into a single cell thick FB layer throughout the abdomen and form three domains: the lateral FB, the dorsal fat cell projection, and the ventral collar (Miller et al., 2002). Finally, the expression of the GATA-like transcription factor Srp is a marker for the early stages of fat cell development (Sam et al., 1996). Other enhancer traps-lines that drive expression in fat cells at larval and adult stages are *3-76a*, *X8-157a,* and *l(3)2E2*. Interestingly, *l(3)2E2* regulates *svp* gene expression (Hoshizaki et al., 1995). Therefore, *svp* and the gene(s) near to the enhancer trap *29D* were suggested to be key factors for determination and differentiation of embryonic FB (**Tables 3, 4**) (Hoshizaki et al., 1994).

The development of the FB requires the GATA-like transcription factor Srp, necessary and sufficient for the progression through the early stages and development of fat cells (Saltiel and Kahn, 2001; Buch et al., 2008; Musselman and Kühnlein, 2018). In fact, FB and gonads derive from

TABLE 3 | Factors and signalling pathways playing a role in fat body development or function.

Factor/pathway	Abbreviation	Human homolog	Stage	Function	References
Adipokinetic hormone (Akh)/Akh receptor signalling	Akh/AkhR	Functional homolog to glucagon	L, A	Carbohydrate and lipid mobilization	Fu et al., (2019), Seale et al., (2008), Enerbäck (2009), Daum et al. (2007), TM. (1978), Butterworth et al., (1988), Britton and Edgar. (1998), Guarner et al., (2017), Britton et al. (2002), Hoshizaki. (1994)
Alcohol dehydrogenase	Adh	15-hydroxyprostaglandin dehydrogenase	E	Fat metabolism	Todorčević et al. (2009)
Bigmax	Bigmax	Max-like protein X	L	Sugar sensing and lipogenesis	Arrese and Soulages, (2010)
Brummer lipase	Bmm	Adipose triglyceride lipase, ATGL	L, A	Lipolysis independent of Akh	Yamada et al. (2018)
Cabut	Cbt	Kruppel-like factors 10 and 11	L	Transcriptional repression upon sugar sensing	Arrese and Soulages, (2010)
cAMP-responsive element binding protein B	dCREB2	CREB/CREM	A	Akh target. TAG storage modulation	(Seale et al., 2008; Ren et al., 2015)
CCHamide-2[a]	CCHa2	Neuropeptide	L	Ilp2 and 5 expression and secretion	Ugrankar et al., (2019), Ugrankar et al. (2011)
Dawdle[a]	Daw	Activin	L	DILPs secretion, inhibition of carbohydrase and lipase at intestine	Bi et al. (2012), Beller et al. (2006)
Dorsal	Dl	RELA proto-oncogene	L	Toll target, induced by fungi and Gram-positive bacteria	Grönke et al. (2010)
Dorsal-related immunity factor	Dif	RELA proto-oncogene	L	Toll target, induced by fungi and Gram-positive bacteria	Grönke et al. (2010)
DP Transcription Factor	DP	Transcription Factor Dp-1, TFDP1	L	Endoreplication	Baumbach et al. (2014)
Drosophila insulin/insulin like growth factor (IGF) signalling	ISS	Insulin like signalling	L	Coordination of nutritional status, endoreplicating tissue metabolism and growth. Determination of final body size. Inhibition of immune gene expression	Feldmann et al., (2009), Gastaldelli, (2011), Baumbach et al. (2014), Fu et al., (2019), Lee et al., (2004), TM. (1978), Palanker et al., (2009), Reis et al., (2010), Bartok et al. (2015), Palu and Thummel (2016)
E2F Transcription Factor1, 2	E2f1, E2f2	E2F Transcription Factor 1-6	L	Endoreplication	Baumbach et al. (2014)
Ecdysone signalling	Ec	NF	L	Antagonist to ISS, systemic growth inhibition	Walther and Farese, (2012)
Eiger[a]	Egr	Tumor necrosis factor alpha, TNFalpha	L	Activation of JNK-dependent inhibition of Ilps production	Pancreatic Hormones (1990)
Endoplasmic reticulum degradation enhancing α-mannosidase-like protein 1	Edem1	ER degradation enhancing alpha-mannosidase like protein 2	L	Systemic insulin signaling maintenance	Isabel et al. (2005)
Extracellularly regulated kinase 7	Erk7	Mitogen-activated protein kinase 15	L	Growth, lipid storage and adaptation to nutrient shortage	Riechmann and Rehorn, (1998)
Forkhead box, sub-group O	Foxo	FOXO3	L, A	Inhibition of Daw expression. Increased lifespan	Werthebach et al. (2019)
Glass bottom boat	Gbb	Bone morphogenetic protein 7	L	FB development and metabolic homeostasis	Moore et al. (1998)
Growth blocking peptide 1[a]	GBP1	Epidermal growth factors, EGF	L	Induction of Ilp secretion	Hasygar et al. (2021)
Growth blocking peptide 2[a]	GBP2	Epidermal growth factors, EGF	L	Induction of Ilp secretion	Hasygar et al. (2021)
Hepatocyte nuclear factor 4	Hnf4	Hepatocyte nuclear factor 4 gamma	L	Carbohydrate metabolism	Palm et al. (2012), Rodríguez-Vázquez et al., (2015)
Histone deacetylase 4	HDAC4	HDAC	A	Akh target under short fasting condition. Lipolysis	Delanoue et al. (2016), Koyama and Mirth. (2016)
Imaginal morphogenesis protein-late 2[a]	ImpL2	Insulin-Like Growth Factor Binding Protein 7, IGFBP7	L, A	Binds DILPs extracellularly and inhibits ISS, tumour-mediated FB wasting	Kadereit et al., (2008), Schaffer et al., (1990)
Immune deficiency signalling	Imd	NF	L	Immunity, inhibition of growth, reduction of ISS/TOR signalling and TAG storage	Grönke et al., (2010), Post et al., (2018)
Insulin like peptide 2	Ilp2	Insulin	L	Regulate glycogen synthesis	Fu et al. (2019)
Insulin like peptide 3	Ilp3	Insulin	L	Synthesis and release of trehalose into hemolymph	Butterworth et al. (1988)
Insulin like peptide 5	Ilp5	Insulin	L	Regulate glycogen synthesis	Fu et al. (2019)

(Continued on following page)

TABLE 3 | (*Continued*) Factors and signalling pathways playing a role in fat body development or function.

Factor/pathway	Abbreviation	Human homolog	Stage	Function	References
Insulin like peptide 6[a]	Ilp6	Insulin	L	Toll pathway target, repression of DILP2, lifespan extension	Zimmermann et al., (2004), Heine et al., (2018), DiAngelo and Birnbaum, (2009)
Insulin like peptide 7	Ilp7	Insulin	L	Regulation of TAG synthesis	Palu and Thummel, (2016)
Kruppel	Kr	BCL6 transcription repressor	L	Fat determination/differentiation (?)	Todorčević et al., (2009), Palanker Musselman et al., (2011)
Lipid storage droplet-1	Lsd-1	Perilipin 2	L	Lipolysis	Evans et al. (2009), Campos-Ortega and Hartenstein. (1985)
Lipid storage droplet-2	Lsd-2	Perilipin 2	L	Involved in TAG storage	(Hartenstein and Jan 1992, Campos-Ortega and Hartenstein, (1985)
Lipin	Lpin	Lipin 3	L	FB development and TAG storage	Hoshizaki et al. (1995)
Liver kinase B1	Lkb1	Liver kinase B1	A	Akh/AkhR signalling target under short fasting condition. Lipolysis	Delanoue et al., (2016), Koyama and Mirth, (2016)
mir-8 stem loop	miR-8	microRNA 200a	L	Ec signalling target, growth regulation	Schaffer et al., (1990), Hughson et al. (2021), Young and Zechner. (2013)
Mondo	Mondo	MLX interacting protein	L	Sugar sensing and lipogenesis	Enomoto et al., (2018), Saavedra and Perrimon, (2019), Arrese and Soulages, (2010)
Myc	Myc	MYC proto-oncogene	L	Ec signalling target, control of glucose and lipid metabolism, Ilp2 secretion	Schaffer et al., (1990), Arrese et al., (2006), Gáliková et al., (2015)
NAD + dependentdeacetylase Sirtuin 1	Sirt1	Sirtuin 1	L	Inhibition of TAG storage	Yin et al. (2021)
NAD + dependent deacetylase Sirtuin 2	Sirt2	Sirtuin 2	L, A	Glucose homeostasis and peripheral insulin sensitivity. Increased lifespan	Rodríguez-Vázquez et al. (2015)
No child left behind	Nclb	PWP1 homolog	L	ERK7 target, growth-promoting downstream effector of mTOR	Riechmann and Rehorn, (1998)
PDGF- and VEGF-related factor 1	Pvf1	Platelet derived growth factor	A	Repression of lipid synthesis by activating TOR signaling at oenocytes at the end of AT development. Tumour-mediated FB wasting	Luong et al., (2006), Sousa-Nunes et al., (2011)
protein 53	p53	protein 53	L	Sensing nutrient stress and metabolic homeostasis, AMPK target	Grönke et al. (2003)
Relish	Rel	Nuclear factor kappa B subunit 1	L	Imd target, induced by Gram-negative bacteria	Grönke et al. (2010)
Salt-inducible kinase 3	Sik3	SIK family kinase 3	A	Akh/AkhR signalling target under short fasting conditions. Insulin target feeding conditions. Lipolysis	Delanoue et al., 2016, Koyama and Mirth, 2016)
Serpent	Srp	GATA binding protein 1	E	Fat determination/differentiation	Todorčević et al., (2009), Saltiel and Kahn, (2001), Buch et al., (2008), Musselman and Kühnlein, (2018)
Seven up	Svp	Nuclear receptor subfamily 2 group F member 2	E, L, A	Fat determination. Immunity and xenobiotic response	Todorčević et al. (2009)
Slimfast	Slif	Solute carrier family 7 member 1	L	Amino acid sensing	Cermelli et al. (2006)
Snazarus	Snz	Sorting nexin 25	L	Activation of TAG storage a t peripheral LD	Sam et al. (1996)
Stearoyl-CoA desaturase	Desat1	Stearoyl-CoA desaturase 5	L	Fatty acids and lipid biosynthesis	Arrese et al. (2006)
Store-operated calcium entry	SOCE	Store-operated calcium entry	A	Akh/AkhR signalling target. TAG storage modulation	Petrovic et al. (2010)
Stunted[a]	Sun	ATP synthase F1 subunit epsilon	L	TOR signalling target, Ilp secretion	Ballard et al. (2010)
Sturkopf	Sturkopf	Lipid droplet associated hydrolase	L	Endocrine physiology regulation (ISS and JH pathway)	Miller et al. (2002)
Sugarbabe	Sug	Gli-similar transcription factor	L	ERK7 target, lipogenic TF	Enomoto et al., (2018), Riechmann and Rehorn (1998)
Target Of Rapamycine signalling	TOR	mTOR signalling	L	Cellular nutrient sensing	Cermelli et al., (2006), Krahmer et al. (2013), Grönke et al. (2003), Ballard et al. (2010)
Telomere fusion	Tefu	ATM serine/threonine kinase	L		Lee et al. (2004)

(Continued on following page)

TABLE 3 | (*Continued*) Factors and signalling pathways playing a role in fat body development or function.

Factor/pathway	Abbreviation	Human homolog	Stage	Function	References
				E2F/DP target, inhibition of DNA damage response	
Triglyceride Lipase	TGL	Lipase A, lysosomal acid type	L	Lsd-1 target. Lypolisis	Britton et al. (2002)
Toll signalling	Toll	Toll-like receptor family signalling	L	Immunity, inhibition of growth, reduction of ISS signalling and TAG storage	Palanker et al., (2009), DiAngelo and Birnbaum, (2009), Okamoto et al. (2009), Slaidina et al. (2009), Grönke et al. (2010)
Type IV collagen	Col4a1	Collagen type IV alpha 1 chain	E	Fat metabolism	Todorčević et al. (2009)
Uncouple protein 4C	Ucp4C	Uncouple protein 1	A	Dissipation of energy in the mitochondria	Rajan and Perrimon, (2012), Ingaramo et al., (2020)
Unpaired 2[a]	Upd2	JAKSTAT ligand, functional homolog to leptin	L	p53 target, DILPs secretion	Teixeira et al., (2003), Grönke et al. (2003)

[a]*FB-secreted factors. Abbreviation: NF, not found; E, embryo; L, larvae; A, adult.*

TABLE 4 | Enhancer trap lines.

Enhacer trap	Cells	Cytological location
29D	EFC	58DE
l (3)2E2	EFC, LFC, AFC	87B (*seven up*)
3-76a	EFC, LFC, AFC, ADEC	5CD
X8-157a	EFC, LFC, AFC, ADEC	19D
RD721	LFC, AFC	58C
RD1937	LFC, AFC	3CD
l (2)0734	LFC, AFC	Chr 2
l (2)895	LFC, AFC	60F (*kruppel*)
l (2)3552	LFC, AFC	Chr 2
l (2)10,435	LFC, AFC	Chr 2
l (3)4504	LFC, AFC	Chr 3
l (3)7842	LFC, AFC	Chr 3
S3358	LFC, AFC	26D
rP445	LFC, AFC	24A
AS3	LFC, AFC	25BC
RD1272	LFC, AFC	64B
RD61	AFC	54BC

Abbreviations: EFC, embryonic fat cells; L, larvae fat cells; A, adult fat cells; ADEC, adepithelial cells. In parenthesis, genes probably regulated by those enhancers.

mesoderm and abdA allows gonadal mesoderm to develop by repressing Srp function in this region (Moore et al., 1998).

ORIGIN AND DEVELOPMENT OF THE LARVAL FAT BODY

The larval FB is a single cell layer that spreads along the larval body cavity, surrounding the gut and reproductive organs and being exposed to the hemolymph (TM. (1978); Dean et al., 1985). Larval FB contains 2200 cells, a number that remains constant throughout FB development. At larval stages, the FB growth is achieved by increasing cell size through endoreplication cycles, with successive rounds of DNA synthesis without mitosis (Butterworth et al., 1988; Britton and Edgar, 1998). Cell size changes are associated with the accumulation of LDs, glycogen deposits and protein granules. The endocycling progression in the FB cells requires the heteromeric transcription factor complex E2f1/E2f2/DP to repress *telomere fusion (tefu)* and suppress DNA damage responses (Guarner et al., 2017). In addition, endoreplication in the FB cells is tightly regulated in response to nutrition and depends on IIS (Britton et al., 2002).

Evidences suggest that the development of larval FB might require the expression of various unidentified genes, revealed by the expression of a number of enhancer traps (**Table 4**) including *3-76a*, *X8-157a, l(3)2E2*. Specifically, the last one regulates the gene expression of *svp*, suggesting that Svp activity might be involved in that process. *kruppel* (*kr*) expression is not detected in fat cells during embryogenesis, nor during the first- and second-instar stages. However, Kr is expressed in fat cells at the stage previous to metamorphosis and in adults **(Table 4)**. It is possible that Kr serves as a transcriptional regulator in the FB in this last larval instar (**Table 3**) (Hoshizaki, 1994; Hoshizaki et al., 1994). According to that, it has been found that Kruppel-like factor 11 (KLF11) is a novel browning transcription factor in human adipocytes (Loft et al., 2015).

At the end of the larval development, the FB undergoes a remodelling process with massive autophagy that initiates the pupal transition. The larval FB decreases gradually throughout metamorphosis, and during the first 3 days of adulthood, until no more cells can be observed.

ROLES OF THE LARVAL FAT BODY

The *Drosophila* larval FB is involved in multiple functions that allow the coordination of the metabolic homeostasis. Larval FB extends as a longitudinal fat sheet at each larval body side. Salivary glands present also an associated-FB whose function is unknown. The most important functions of this tissue include the storage and release of energy, the nutrient sensing function, and the role in the systemic immunity (**Figure 3**). These functions are regulated by hormones and require the crosstalk of the FB with other tissues. The pathways that adjust the growth rate to the nutritional conditions are the IIS and the target of rapamycin (TOR) pathways, and those involved in the systemic immunity are the Toll and Immune deficiency (Imd) pathways. In the next sections, we review the current knowledge about the role of these signalling pathways and the main factors involved in the different

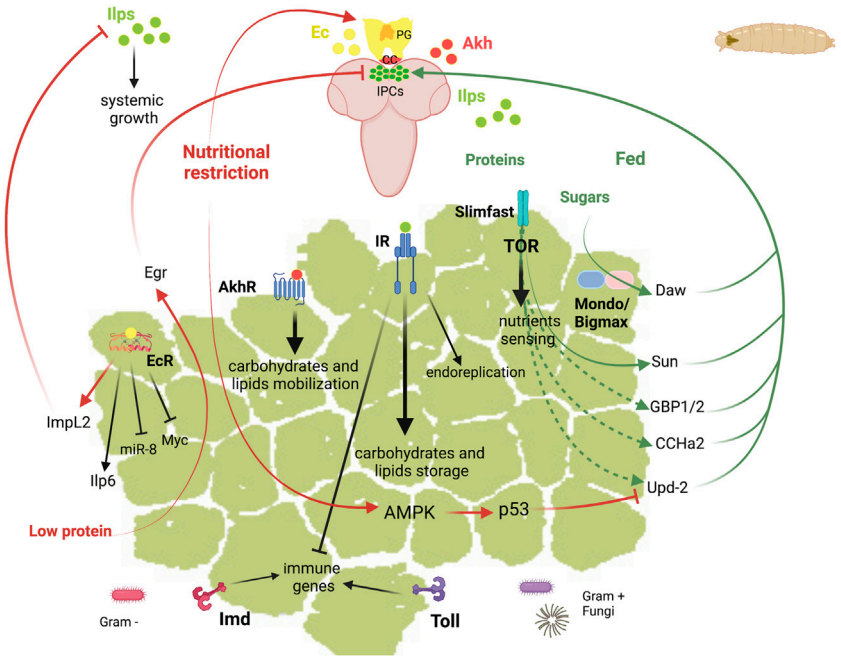

FIGURE 3 | Schematic representation of the diverse functions of *Drosophila* fat body in larvae. Top, larvae brain represented in soft purple. Abbreviations: Akh Adipokinetic hormone; AkhR, Akh receptor; AMPK, AMP-activated protein kinase; CC, corpora cardiaca; CCHa2, CCHamide-2; Daw, Dawdle; Ec, ecdysone; EcR, ecdysone receptor; Egr, Eiger; GBP1/2, Growth blocking peptide 1/2; ImpL2, Imaginal morphogenesis protein-late 2; Imd, Immune deficiency; Ilps, insulin-like peptides; Ilp6, Insulin-like peptide 6; IPC, insulin producing cells; IR, insulin receptor; miR-8, mir-8 stem loop; PG, prothoracic gland; Sun, Stunted; Svp, Seven up; TOR, target of rapamycin; Upd2, Unpaired 2.

functions of the larval FB and in its communication with other tissues.

Store and Release of Energy Reserves

Similar to the mammalian WAT, the *Drosophila* larval FB stores and releases energy in response to the organism energetic demands. The energy is stored mainly in the form of glycogen and of TAGs, the lipolysis products of those being transported to other tissues to support growth and survival.

Carbohydrates

In *Drosophila*, glycogen is the main storage form of carbohydrates and is found in the body wall muscles and in the FB in late larval stages (Baker and Thummel, 2007; Garrido et al., 2015). In addition to glycogen, trehalose is synthesized in the FB and released into the hemolymph. Upon starvation, glycogen is mobilized to maintain the circulating sugar levels (Mattila et al., 2015; Yamada et al., 2018). In mammals, the sensing of sugar at intracellular levels is mediated by the heterodimer formed by the conserved bHLH-Zip transcription factors ChREBP (Carbohydrate Response Element Binding Protein) and MondoA, together with their common partner Mlx (Max-like protein X), which are activated by sugars and promote the conversion of sugars to lipids. They control most of the sugar-responsive genes as well as carbohydrate, amino acid and lipid metabolism (Havula and Hietakangas, 2012; Mattila et al., 2015). In *Drosophila,* the single orthologs of ChREBP/Mondo and Mlx are Mondo and Bigmax, respectively, and this transcriptional network is essential for sugar tolerance also in this organism. Accordingly, the Mondo-Bigmax deficient *Drosophila* larvae presents lethality on any diet containing high levels of sucrose, glucose or fructose (Havula et al., 2013). In addition to the regulation of metabolic genes, Mondo-Bigmax regulate the expression of the TGFβ/Activin ligand Dawdle (Daw), the Gli-similar transcription factor Sugarbabe and the orthologue of mammalian Kruppel-like factors 10 and 11, Cabut (Bartok et al., 2015; Mattila et al., 2015). As detailed in next sections, the intracellular glucose sensing by Mondo-Bigmax is coupled to systemic growth through Daw. Other nutrient sensors involved in sugar tolerance are the nuclear receptor Hnf4 (Hepatocyte nuclear factor 4) and the NAD^+-dependent deacetylase Sirtuin 1 and 2 (Sirt1, Sirt2). Hnf4 plays a critical role in carbohydrate metabolism as shown by the *Hnf4* mutant larvae, which display highly elevated circulating glucose and trehalose levels and defects in lipid homeostasis (Palanker et al., 2009; Palu and Thummel, 2016). Sirt2, is required in the FB to maintain glucose homeostasis and peripheral insulin sensitivity by deacetylating and stabilizing Hnf4 through protein interactions (Palu and Thummel, 2016). Moreover, Sirt1 negatively regulates TAG accumulation in the larval FB (Reis et al., 2010).

Lipids

TAG is the main lipid form in the FB, which is synthesized from dietary carbohydrates, fatty acids or proteins and is stored in intracellular LDs. Similarly to mammals, LDs of different sizes belong to distinct functional classes, which

differ in their properties owing to differential association with particular sets of LD-associated proteins (Wilfling et al., 2013). Characterization of the LD proteome at different stages uncovered that LD-associated proteins are different according to the functional complexity among LDs (Cermelli et al., 2006; Beller et al., 2010; Walther and Farese, 2012; Krahmer et al., 2013). The best characterized LD proteins in the FB during the larval life are Lsd-1 and Lsd-2 (Lipid storage droplet-1 and -2), homologous to the mammalian PAT domain protein family (Perilipin, ADRP, and TIP47) (Grönke et al., 2003; Teixeira et al., 2003). Lsd-2 is required for storage of TAG, whereas Lsd-1 stimulates TAG hydrolysis (Bi et al., 2012). The subproteome analysis of LDs of *Drosophila* FB identified 248 proteins (Beller et al., 2006). Most of them were involved in cellular metabolism but proteins have been identified with diverse biological functions, including intracellular transport, cell organization and cell biogenesis. For instance, the droplet-associated protein Sturkopf has a role in endocrine physiology regulation (Werthebach et al., 2019). The *sturkopf* mutant adults show a mild decrease in TAG storage levels. However, they fail to adjust their developmental rate to dietary yeast-to-sugar ratio changes, suggesting a function in insulin and juvenile hormone signalling activities. Moreover, distinct spatially LD populations have been described in *Drosophila* FB: the peripheral LDs, in contact with the plasma membrane, and the larger cytoplasmic medial LDs. The peripheral LD homeostasis is regulated by Snazarus (Snz), which binds to LDs and promotes TAG storage (Ugrankar et al., 2019).

Interestingly, the regulation of lipid homeostasis is coupled to FB development and growth. For example, Lipin, which converts phosphatidate to diacylglycerol, is required for normal FB development and TAG storage (Ugrankar et al., 2011). Loss of *Lipin* in *Drosophila* leads to severe defects in the development of the FB with changes in cell nucleus, mitochondria, autophagosome formation and size of LDs. Similarly, the *Drosophila* BMP-5,7 orthologue, glass bottom boat (gbb), is also required for the development of the larval FB and for maintaining proper metabolism. *gbb* mutants exhibit developmental delay and altered FB morphology with reduced total lipid, glucose and trehalose levels (Ballard et al., 2010). A recent study shows that the FB expression of the atypical MAP kinase, Erk7 (Extracellularly regulated kinase 7), inhibits cell autonomous and systemic growth and lipid storage. *Erk7* expression is upregulated by fasting and, therefore, contributes to the adaptation to nutrient shortage. Erk7 regulates the subcellular localization of the chromatin binding protein No child left behind (Nclb), a growth-promoting downstream effector of mTOR, and inhibits the expression of the lipogenic transcription factor gene *sugarbabe* (Hasygar et al., 2021).

The Insulin/Glucagon Axis

The energy storage in the FB during the larval development is required during low nutrient conditions and for the survival during the non-feeding periods, such as before and during metamorphosis and during the early stages of adulthood. The maintenance of the metabolic homeostasis requires the communication between the nutrient-storing FB and the consuming tissues.

In mammals, the main hormones that regulate the mobilization of fat and glucose are insulin and glucagon (Freychet P. 1990). Insulin is secreted by pancreatic β cells in response to high blood sugar levels, which triggers glycogen synthesis. Under low sugar levels pancreatic α cells release glucagon and triggers the breakdown of glycogen. Glucagon is also a lipolytic hormone that regulates fatty acids, ketone bodies and TAG.

In *Drosophila*, the insulin/glucagon axis is well conserved and involves the insulin-like peptides (Ilps) and the glucagon-like peptide Akh (Schaffer et al., 1990; Semaniuk et al., 2021). The mobilization of carbohydrate and lipid energy reserves from the FB in response to starvation is regulated by Akh/AkhR, which is produced by the neurosecretory cells of the corpora cardiaca (Kim and Rulifson, 2004; Lee and Park, 2004; Isabel et al., 2005). For carbohydrate mobilization, Akh/AkhR stimulates, through glycogen phosphorylase, the conversion of stored glycogen to hemolymph trehalose, which is important during the nonfeeding periods and during adult flight. The lipid mobilization through the action of Akh/AkhR, led to the phosphorylation of Lsd-1, which activates the Triglyceride Lipase (TGL) (Arrese et al., 2006; Arrese and Soulages, 2010). However, the role of Akh/AkhR is not completely elucidated as some reports suggest that Akh/AkhR is dispensable for lipid homeostasis in third instar larvae (Lee and Park, 2004; Gáliková et al., 2015). A recent report shows that, although in nutrient abundant conditions Akh/AkhR is dispensable during larval development, in low nutrient stress conditions Akh/AkhR signalling alters larval development and the adult metabolism and behaviour (Hughson et al., 2021).

In mammals, the mobilization of fatty acids from TAG storage is coordinated by the hormone-sensitive lipase (HSL) and the Patatin Like phospholipase Domain Containing 2 (PNPLA2, also known as ATGL) (Zimmermann et al., 2004; Young and Zechner, 2013). Interestingly, ATGL-dependent lipolysis of WAT triggers a systemic insulin release, which is essential for the replenishment of BAT energy storage in mice (Heine et al., 2018). In *Drosophila*, independently of Akh/AkhR signalling, the Brummer (Bmm) lipase, homolog of mammalian ATGL, converts the accumulated TAG to fatty acids (Grönke et al., 2005).

Nutrient Sensor and Systemic Growth

The FB acts as a sensing organ that coordinates the metabolic and physiological responses to the nutrient status of the organism. The FB relays the nutrient information through the secretion of humoral factors to the insulin-producing cells (IPCs), which secrete Ilps to control the systemic ISS.

Signalling Pathways in the Fat Body Regulating Body Growth

In *Drosophila* FB, the IIS and the TOR pathways regulate nutrient uptake, storage and metabolism. In addition, there is a crosstalk between the steroid hormone 20-hydroxyecdysone (ecdysone) and those pathways. Furthermore, the FB is the main sensor of internal oxygen levels that control organismal growth.

The *Drosophila* genome encodes eight Ilps (Grönke et al., 2010): Ilp, 2, 3 and 5 are produced by IPCs in the brain and are functionally comparable to insulin; Ilp6, produced by the FB, is related to mammalian Insulin Growth Factors, IGFs (Okamoto et al., 2009; Slaidina et al., 2009); Ilp7 and Ilp8 are relaxin-like peptides (Grönke et al., 2010). Similar to mammalian insulin, Ilps are able to regulate circulating levels of carbohydrates in the hemolymph. Insulin is a positive regulator of fat cell mass, acting through changes in both cell number and lipid storage (DiAngelo and Birnbaum, 2009). Ilp2 and Ilp5 regulate glycogen deposition, Ilp3 is responsible for the synthesis and release of trehalose into hemolymph and Ilp5 and Ilp7 regulate the synthesis of TAG (Kim and Rulifson, 2004; Post et al., 2018; Semaniuk et al., 2021). In addition, IIS/PI3K (Phosphatidylinositol 3-kinase) signalling coordinates nutritional status with endoreplicating tissues metabolism and growth (Britton et al., 2002). Thus, insulin regulates the critical weight, a checkpoint that occurs early in third instar larvae that determines the final body size (Mirth and Riddiford, 2007).

Mammals and *Drosophila* use the TOR pathway for cellular nutrient sensing, playing an important role in the balance of energy storage. The TOR kinase activity depends on amino acid availability and mediates protein synthesis, amino acid import, ribosome biogenesis and autophagy (Saxton and Sabatini, 2017). Consequently, *Tor* mutant larvae show reduced size and glucose and lipid storage levels, larvae showing a transparent phenotype (Colombani et al., 2003; Luong et al., 2006).

In addition, there is crosstalk between IIS and ecdysone. Ecdysone signalling in the FB antagonizes IIS and promotes autophagy (Rusten et al., 2004; Colombani et al., 2005). Furthermore, ecdysone modulates organismal growth through a FB relay that attenuates systemic insulin signalling (Colombani et al., 2005; Arquier et al., 2008; Honegger et al., 2008; Jin et al., 2012; Lee et al., 2018).

Humoral Fat Body Derived Signals

In *Drosophila* and other animals, the organisms require sensing the levels of oxygen to adapt their systemic growth to the environmental conditions. A central regulator for the maintenance of oxygen homeostasis is the hypoxia-inducible factor 1 (HIF-1), a heterodimeric transcription factor composed of the oxygen regulated HIF-1α and the constitutively expressed HIF-1β. In presence of oxygen, HIF-1α is hydroxylated by HIF prolyl hydroxylase (Hph), targeting it for ubiquitin-dependent proteasomal degradation. In hypoxia, HIF-1α is stabilized and induces the expression of target genes that regulate growth and metabolism (Semenza, 2014).

To link the organismal growth to the nutrient availability, the FB produces signalling molecules that promote or inhibit the insulin secretion from IPCs **(Figure 3** and **Table 3).** Some of these factors and neuropeptides are secreted in response to dietary fats and/or sugars such as Unpaired 2 (Upd2), Daw and CCHamide-2 (CCHa2).

Upd2, a JAK/STAT cytokine (Rajan and Perrimon, 2012), binds to its receptor Dome (Domeless) on GABAergic neurons, releases the inhibition of IPCs and promotes Ilp secretion. Recently, an essential role for adipose p53 in sensing nutrient stress and maintaining metabolic homeostasis has been reported (Ingaramo et al., 2020). Under nutrient deprivation and high-sugar diet, p53 is activated in the FB and represses the expression of Upd2. This AMP-activated protein kinase (AMPK)-dependent p53 activation leads to modulation of Ilp2 levels, systemic insulin/TOR signalling and autophagy induction (Ingaramo et al., 2020). Another response to the consumption of sugar is the release by the FB of the activin-like factor Daw, which promotes the secretion of Ilps through the TGF-β/activin receptor Baboon (Babo) (Ghosh and O'Connor, 2014). In addition, Daw released from the FB signals to the intestine where inhibits the expression of carbohydrases and lipases by enhancing Smad on X (Smox) levels (Chng et al., 2014). The sugar induced gene expression of Daw is mediated by Mondo-Bigmax, whereas Foxo (forkhead box, sub-group O) negatively regulates its expression (Bai et al., 2013; Mattila et al., 2015). A third mechanism by which carbohydrates promote Ilp expression and secretion is through CCHa2, a neuropeptide induced in the FB by proteins and sugars. When released, the CCHa2 peptide promotes the secretion of Ilp2 and Ilp5 via its receptor, CCHa2R, expressed in the IPCs (Ren et al., 2015; Sano et al., 2015).

TOR-dependent FB humoral signals couple Ilp2 and Ilp5 secretion from the IPCs with amino acid intake and some humoral factors are secreted in response to dietary amino acids such as Stunted (Sun), Eiger (Egr) and the Growth blocking peptides GBP1 and GBP2 (Colombani et al., 2003; Honegger et al., 2008; Géminard et al., 2009; Rajan and Perrimon, 2012; Ghosh and O'Connor, 2014; Sano et al., 2015; Agrawal et al., 2016; Delanoue et al., 2016; Koyama and Mirth, 2016). Interestingly, amino acid-dependent TOR signalling derived from the FB controls neural stem cell proliferation independent from IPCs-derived Ilps. In the developing central nervous system, embryonic and larval neuroblasts undergo proliferative phases, intercalated with periods of a quiescent state, that is reversible by dietary amino acids (Britton and Edgar, 1998). The TOR-mediated amino acid sensing induces a secreted FB signal that activates the expression of Ilps in glial cells. The local glial Ilps signal on adjacent neuroblasts via the IIS/PI3K/TOR pathway and control their reactivation (Chell and Brand, 2010; Sousa-Nunes et al., 2011).

Furthermore, ecdysone signalling in the FB modulates insulin dependent systemic growth through the regulation of Myc, microRNA miR-8 and ImpL2 (Ecdysone-inducible gene L2), a member of the immunoglobulin superfamily homolog to the Insulin-Like Growth Factor Binding Protein 7, IGFBP7 (Arquier et al., 2008; Honegger et al., 2008; Hyun et al., 2009; Delanoue et al., 2010; Jin et al., 2012; Lee et al., 2018).

The FB is a sensor tissue for amino acid levels and coordinates growth of peripheral tissues through a humoral mechanism (Colombani et al., 2003). Hence, the downregulation of the Slimfast (Slif) amino acid transporter within the FB is sufficient to induce a general reduction in the rate of larval growth (Colombani et al., 2003). In response to dietary amino acids, the peptide Sun is released from the FB (Delanoue et al., 2016). Sun binds to Methuselah (Mth), a secretin-incretin receptor on IPCs, and stimulates the secretion of Ilps. On the other hand, under

conditions of low amino-acid concentrations, Egr, a *Drosophila* tumor necrosis factor alpha (TNF-alpha) orthologue is released from the larval FB (Agrawal et al., 2016). This cytokine signals through its receptor Grindelwald (Grnd) on the larval IPCs to activate the JNK-dependent inhibition of Ilps production. The expression of the endoplasmic reticulum (ER) degradation enhancing α-mannosidase-like protein 1 (Edem1) in the FB is also crucial for maintaining systemic insulin signalling, since its down-regulation results in the accumulation of Ilp2 in the IPCs and reduced systemic insulin signalling. The reduction in Edem1 levels is crucial for survival during starvation as lowering *edem1* expression levels facilitates the activation Eiger on IPCs and the reduction in ISS. In addition, Edem1 regulates Upd2 to manage the metabolic status (Pathak and Varghese, 2021). Moreover, Growth-blocking peptides 1 and 2 (GBP1 and GBP2) are epidermal growth factors-like cytokines secreted by the FB upon availability of dietary amino acids (Koyama and Mirth, 2016). Recently, it was shown that these adipose tissue factors regulate Ilps secretion by silencing a pair of inhibitory neurons that synapse with IPCs (Meschi et al., 2019).

During late larval life, increased levels of ecdysone affect also systemic growth. Myc expression in the *Drosophila* FB triggers a cell autonomous mechanism that controls glucose and lipid metabolism to favour the storage of nutrients (Parisi et al., 2013). During the late third instar, ecdysone signalling represses Myc function inhibiting systemic growth. This suggests a humoral factor released downstream of Myc that relays information to control IIS (Delanoue et al., 2010). The ability of FB Myc activity to affect IPC Ilp2 secretion depends on stearoyl-CoA desaturase (Desat1) activity, an enzyme necessary for production of fatty acids and lipid biosynthesis (Parisi et al., 2013). The increased levels of ecdysone suppress the body growth also through the regulation of FB microRNA miR-8 (Hyun et al., 2009; Jin et al., 2012). Multiple peptide hormones regulated by miR-8 may contribute to *Drosophila* growth (Lee et al., 2015). Among them, the IGF-like factor Ilp6 and the Imaginal morphogenesis protein Late 2 (ImpL2) are upregulated in the FB of miR-8 null mutant larvae. Ilp6 expression from larval FB represses secretion of Ilp2 from IPCs and extends lifespan (Bai et al., 2012). Before and during pupariation or in response to starvation, Ilp6 communicates the FB with other organs. For example, it promotes the growth of imaginal discs, which gives rise to adult organs, and the lipid uptake in oenocytes, cell clusters of ectodermal origin that regulate lipid metabolism (Chatterjee et al., 2014). Nutritional restriction also increases the levels of ecdysone, which triggers the production of ImpL2 in the FB (Lee et al., 2018). In response to nutrient limitation, the FB nutrient sensor function, which restricts the growth of peripheral tissues, is complemented by the release of nutrients through autophagic degradation of the FB cytoplasm. This provides other tissues with a source of nutrients necessary for survival. Thus, under conditions of low TOR signalling, autophagy promotes normal cell function and survival (Scott et al., 2004).

To adapt the systemic growth to the environmental conditions, the FB integrates the oxygen and amino acids levels through the Hph/HIF-1α and Hph/TOR pathways. In hypoxia, the FB release HIF-1α-dependent humoral factors that inhibit Ilps expression and secretion from the IPCs, thereby restricting the systemic growth. Moreover, independently of HIF-1α, Hph is required for nutrient-dependent TOR activation (Texada et al., 2019). To allow adults viability in hypoxia, the larval FB inhibits TORC1 signalling and reorganizes the lipid storage (Lee et al., 2019). A recent study showed that FOXO is a hypoxia inducible factor that mediates tolerance to low oxygen by inducing immune-like responses in the FB (Barretto et al., 2020).

Systemic Immunity

The *Drosophila* FB coordinates not only the nutrient storage and the animal growth but also the humoral immune response. In *Drosophila*, the infection by microbes induces the secretion of antimicrobial peptides (AMP) by the FB, which are controlled by the Toll and Imd pathways (De Gregorio et al., 2002). The Toll-NF-kB signalling, which triggers the nuclear translocation of Dif (Dorsal-related immunity factor) and Dorsal, is induced by fungi and Gram-positive bacteria, whereas infection by Gram-negative bacteria leads to the processing and transport or Relish via the Imd pathway. To support the immune activation, the FB increases its volume, expands the ER and alters its metabolism, shifting from lipid metabolism to membrane phospholipid synthesis (Martínez et al., 2020). These changes, induced by Toll signalling to sustain AMP synthesis and secretion, may become detrimental if maintained over long periods due to insufficient nutrient storage. Thus, the expression of a constitutively active Toll receptor in the larval FB inhibits the whole organismal growth, disrupts the insulin signalling in the FB and reduces the TAG storage (DiAngelo and Birnbaum, 2009; Roth et al., 2018; Suzawa et al., 2019). Similarly, persistent activation of the Imd pathway in the larval FB diminished IIS/TOR activity, which resulted in decreased TAG levels and impaired whole animal growth (Davoodi et al., 2019). Moreover, increasing insulin signalling in the FB leads to decreased immune gene expression and, vice versa, decreasing insulin signalling leads to increased immune gene expression and increased resistance to infection (Musselman and Kühnlein, 2018). This supports a model in which insulin signalling and the immune response negatively regulate each other to maintain the energy balance.

ORIGIN AND DEVELOPMENT/ DIFFERENTIATION OF ADULT FAT BODY

The origin of the adult FB, in invertebrate, as in mammals, remains elusive and unexplored due to the difficulty in its manipulation (The mesoderm and its derivatives and BM, 1993; Hoshizaki et al., 1995; Berry et al., 2013). Although both larval and adult FBs play a role as energy storage organs and nutrient availability sensing, they show different features. For example, contrary to the larval FB, adult FB is able to expand by increasing the number of adipocytes. Moreover, they might not share a common origin: while larval FB derives from the nine embryonic bilateral primordia, the origin of the adult FB has not been identified (Hoshizaki et al., 1994; Hoshizaki et al., 1995; Aguila et al., 2007).

During metamorphosis, unlike most larval tissues that undergo histolysis, some of the larval FB cells persist and are found in the newly eclosed adult, free floating as single cells or small clusters. These larval fat cells are refractive to the autophagic cell death that

removes most of the larval cells during metamorphosis. It has been shown that these larval adipocytes, now dissociated, are a source of nutrients during the non-feeding stage of adulthood, approximately the first 3 days after eclosion (Aguila et al., 2007). Three to five days after eclosion these cells are replaced by the adult fat adipocytes (Johnson and Butterworth, 1985), which accumulate lipid reserves through feeding and *de novo* lipid synthesis during those days. The myokine Pvf1 (PDGF- and VEGF-related factor 1) represses lipid synthesis at the end of the adult FB lipid build-up phase by activating TOR pathway specifically in the oenocytes (Ghosh et al., 2020). Adult adipocytes must develop from some pupal progenitors, the specific cells that give rise to the adult fat cells have not been identified (The mesoderm and its derivatives and BM, 1993).

The development of adult FB might require the expression of genes driven by a number of enhancers that are identified through enhancer traps (**Table 4**). Most of them, except for 29D and *RD61*, drive the expression in larval FB as well as in adult one *3-76a*, *X8-157a* and *l(3)2E2* driving the expression in fat cells of all stages. As *l(3)2E2* is an enhancer of the *srp* gene, the activity of Srp might be also involved in fat cell decision or/and differentiation programmes at adult stage **(Tables 3**, **4)** (Hoshizaki et al., 1995).

Although the cells that give rise to the adult fat cells have not been identified, two fundamentally different mechanisms have been suggested to explain how the adult FB arises: 1) cell remodelling, a process in which larval FB tissue is dissociated into isolated cells that later associate to form the adult FB (Larsen, 1976), or 2) the complete destruction of larval FB and simultaneous synthesis of adult FB from undifferentiated ASC (Haunerland and Shirk, 1995).

Potential Adipose Stem Cell Population

It has been shown that adult FB derives from the mesoderm (Lawrence and Johnston, 1986). However, the ASC population that maintain the adult FB has not been identified. Hoshizaki *et al.* suggested that a subset of adepithelial cells, precursors of adult thoracic muscles, might be as well the precursors of adult adipocytes (Hoshizaki et al., 1995). Adepithelial cells are in fact a plausible source of ASCs, since two of the fat cells-specific enhancer traps mentioned above, *3-76a* and *X8-157a*, are also active in the adepithelial cells. This suggests a possible lineage connexion for fat cells from embryo to adult, including the adepithelial cells during larval stage. Furthermore, adepithelial cells are the precursors of adult muscles (Holz et al., 1997) and a subset of these cells expressing Breathless are the precursors of the adult tracheal air sacs (Sato and Kornberg, 2002). This might suggest that adepithelial cells could potentially be the pluripotent stem cell population in the adult stage.

ROLE OF ADULT FAT BODY

In spite of the fact that most of the functional studies in *Drosophila* are conducted at larval stages, there are enough evidences to ensure that the adult FB carries out liver, adipose, and immune functions (Hotamisligil, 2017; Arrese and Soulages, 2010). Oenocytes, specialized hepatocyte-like cells, are closely associated to adipocytes, specifically at the subcuticular FB (**Figure 2**) (Gutierrez et al., 2007). In fact, very recently, the role of oenocytes regulating lipid synthesis and content in the adipose tissue has been described, a role-played by hepatocytes in mammals. Furthermore, loss of function of TOR pathway in adult oenocytes leads to obesity (Ghosh et al., 2020).

Although further studies would be necessary to prove the equivalence of these organs, there is a subcuticular FB that is extended through the whole *Drosophila* adult body (**Figure 2**), and also a FB wrapping some organs such as the heart, intestine, spermatheca and brain, and these could be the equivalent to mammalian subcutaneous and visceral WAT, respectively.

There are not many evidences indicating the existence of a BAT or beige adipocytes tissue in *Drosophila*. However, a set of genes coding for Uncouple proteins, including UCP1 that is a marker for BAT in mammalian systems, are conserved in *Drosophila* (Harms and Seale, 2013). Similarly to UCP1, *Drosophila* Ucp4C has been involved into the dissipation of energy in the mitochondria (Cannon and Nedergaard, 2004; Da-Ré et al., 2014).

Metabolism

Adult FB has an important role in physiology, longevity as well as disease, e.g., cancer (**Figure 4**).

Metabolic Organ

Similarly to the larval one, the adult FB is the central metabolic organ involved in the accumulation of fat and glycogen from caloric overload and in the mobilization of the stored fat during starvation or egg production (Lee and Park, 2004; Parra-Peralbo and Culi, 2011; Musselman et al., 2013; Mattila and Hietakangas, 2017; Zhao and Karpac, 2017; Weaver and Drummond-Barbosa, 2019). Not surprisingly, in females the FB has higher proportion of lipids than that in males (Johnson and Butterworth, 1985). In contrast to larval FB there are evidences suggesting the ability of adult FB to grow in order to accumulate lipids, in obese flies (DiAngelo and Birnbaum, 2009).

In the adult FB, Akh/AkhR signalling activates cAMP-responsive element binding (CREB) transcription factor (Song et al., 2017). CREB downregulation was shown to promote overeating and obesity in adult flies (Iijima et al., 2009). In addition, Akh/AkhR signalling modulates TAG content in adult FB through the store-operated calcium entry (SOCE) (Baumbach et al., 2014). Under short-term fasting conditions, Akh/AkhR signalling promotes lipase *bmm* gene expression by reducing Lkb1-Sik3 (Salt-inducible kinase 3)-HDAC4 (Histone deacetylase 4) signalling axis, probably through Foxo (Wang et al., 2011; Choi et al., 2015). Under long-term fasting conditions, however, the reduction of the Lkb1-Sik3 pathway to induce the lipolytic response is independent of Akh/AkhR. Conversely, insulin pathway induces Sik3 activity under feeding conditions, independently of Lkb1 (Choi et al., 2015) (**Figure 4**).

Recently, Relish known to be part of Imd pathway, as mentioned above, has been identified as a repressor of *bmm* gene expression through FOXO, by fasting-dependent histone deacetylation, during metabolic adaptation to fasting (Molaei et al., 2019).

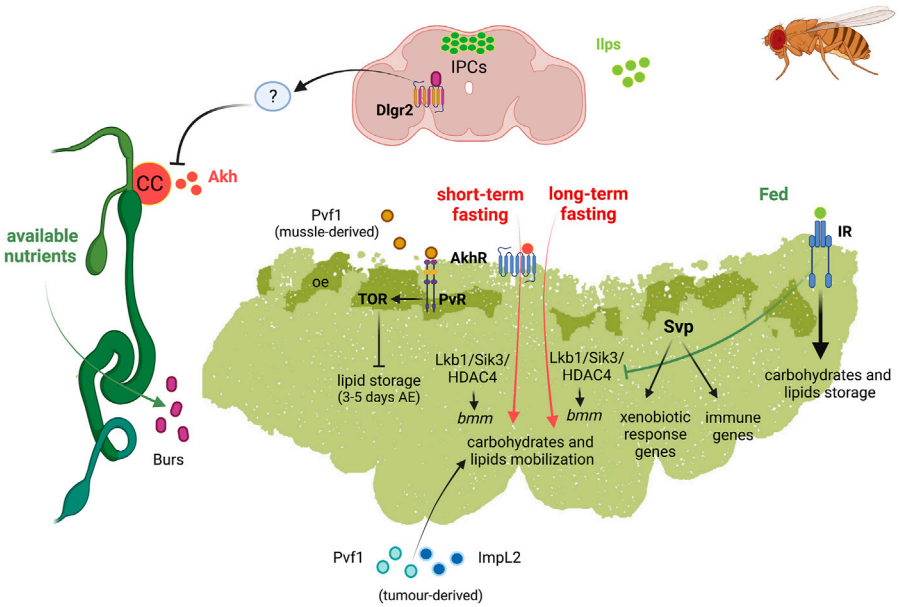

FIGURE 4 | Schematic representation of the diverse functions of *Drosophila* fat body in adult fly. Left, adult digestive system represented in green; top, adult brain represented in soft purpure. Abbreviations: Akh Adipokinetic hormone; AkhR, Akh receptor; bmm, brummer lipase gene; Burs, Bursicon receptor; CC, corpora cardiaca; Dlgr2, leucine rich repeat containing G protein-coupled receptor 2; HDAC4, Histone desacetylase 4; ImpL2, Imaginal morphogenesis protein-late 2; Ilps, insulin-like peptides; IPC, insulin producing cells; IR, insulin receptor; Lkb1, Liver kinase B1; oe, oenocytes; Pvf1, PDGF- and VEGF-related factor 1; PvR, Pvf1 receptor; Sik3, Salt-inducible kinase 3; Svp, Seven up; TOR, target of rapamycin.

Crosstalk in Inter-Organ Communication: Links to Fat Body

Recently, an intestinal/neuronal/FB inter-organ communication has been described in adults to preserve energy homeostasis. In response to nutrients, enteroendocrine cells secrete systemically the hormone Bursicon α (Bursα), which binds to its neural receptor DLgr2. Bursα/DLgr2 signalling regulates energy metabolism through a neuronal relay that repress AKH production and, therefore, the subsequent modulation of AKHR signalling within the FB. The reduction of systemic Bursα/DLgr2 signalling leads to exacerbated glucose oxidation, strong lipodystrophy and depletion of energy stores with the consequent reduced organismal resistance to nutrient deprivation conditions (Scopelliti et al., 2019). Therefore, Bursicon inhibits the mobilization of glycogen storage under nutrient availability (**Figure 4**).

Aging and Longevity

The overexpression in the adult FB of the gene *foxo*, encoding for the key target of the IIS pathway, leads to increased life span (Giannakou et al., 2004). Similarly, overexpression of the gene *Sirt2* in adult FB increases longevity in both sexes. It also modulates the composition of the LD proteome, a plausible mechanism underlying extended longevity by *Sirt2*, as LDs regulate aging processes (Goldberg et al., 2009; Hoffmann et al., 2013). All these evidences point to a role of the adult AT in controlling longevity.

Cancer-Associated Cachexia

Tumors and their microenvironment can produce different circulating factors that cause cachexia, the wasting syndrome observed in advance cancer patients which is characterized by a general metabolic dysfunction that includes systemic inflammation, increased catabolism and lipolysis or proteolysis in muscles and AT (Ebadi and Mazurak, 2014). In *Drosophila,* two main models of cachexia have been described which show similarities with human patients (Figueroa-Clarevega and Bilder, 2015; Kwon et al., 2015; Song et al., 2019). One of the models is induced by activation of Yorkie (Yki), the Yap1 oncogen ortholog, in intestine stem cells that secrete a PDGF-and VEGF-related factor 1 (PvF1) ligand. Pvf1 leads to the pathological activation of ERK/MAPK signalling in peripheral tissues and induce wasting of muscles and AT (Song et al., 2019). The other model consists of the transplantation, in adult flies, of clones of eye disc cells mutant for the polarity gene *scribble* and ectopically expressing an activated form of Ras $^{(V12)}$ (Ras^{V12}, $scrib^{-/-}$). Interestingly, both tumor models secrete high levels of ImpL2 (Figueroa-Clarevega and Bilder, 2015; Kwon et al., 2015). Increased levels of circulating ImpL2 reduce systemic insulin signalling, which leads to reduction of nutrients uptake by muscle and adipose tissue, driving organ wasting. The Ras^{V12}, $scrib^{-/-}$ tumors also induce a systemic autophagy stress response in muscles and AT that mediates organ wasting (Katheder et al., 2017; Khezri et al., 20215). Recently, another wasting model in *Drosophila*, relates the FB remodelling and muscle detachment to the tumor-secreted matrix metalloproteinase 1 (Mmp1). Mmp1 can modulate TGFβ signalling in the FB and disrupts the basement membrane/extracellular matrix in FB and muscle (Lodge et al., 2021). All theses studies show that the conservation of the signalling pathways and the existing

genetic tools, make of *Drosophila* an important model to study the process of organ wasting and to identify new molecular mechanisms involved in this process.

Immunity and Xenobiotic Response

The FB acts as a detoxifying tissue based on the expression of members of the Cytochrome P450 (Cyp450) superfamily of monooxygenases. These are enzymes involved in metabolizing foreign substances and drugs implicated in resistance to insecticides (Feyereisen, 1999; Chung et al., 20097; Terhzaz et al., 2015).

Recently, Weaver and Drummond-Barbosa showed that the nuclear receptor Svp regulates a number of factors involved in immunity and xenobiotic detoxification responses in adult female FB (Weaver and Drummond-Barbosa, 2020). Specifically, Svp would acts as the first line of defence against infections, regulating genes involved in the capture and elimination of foreign pathogens. Svp also regulates the expression of genes encoding members of the CYP450 family involved in the initiation of phase I of the xenobiotic detoxification response. Reduction of *svp* expression results in the upregulation of genes encoding Metallothionein A and B (*MtnA* and *MtnB*) (Weaver and Drummond-Barbosa, 2020). MtnA and B are enzymes involved in heavy metal detoxification and protection against free radicals and have been involved in the response to xenobiotic and immune stress (Bonneton et al., 1996). It has been suggested that a reduced activity of Svp could lead to a toxic scenario, which would need MtnA and B activity to eliminate this toxicity (Weaver and Drummond-Barbosa, 2020) (**Figure 4**).

CONCLUDING REMARKS AND FUTURE PERSPECTIVES

The AT is a central organ, which regulates metabolism and immune responses, as inflammation, so that it has a major impact on human physiology. AT dysfunction associates to metabolic diseases such as: obesity, diabetes, lipodystrophies and cancer-associated cachexia.

Despite of the advance in the knowledge in the last years, still there are many open questions that need to address about the functions and development of AT.

However, the knowledge at this moment can only be obtained through the studies of animal models. *Drosophila* can be a good model for the study of AT based on the possibility of the genetics analysis that can be performed *in vivo*, the lower complexity of the tissue and the functional conservation of this tissue along the evolution.

Further studies focused on tracing the cell lineages expressing the transcription factors Svp, Srp and Kr, involved in the determination and differentiation and maintenance of fat cells during embryonic and larval stages, would shed light on how those processes develop and what are the actors involved. Similarly, it would be very interesting to trace the cells showing expression driven by the enhancer traps *l(3)2E2*, *3-76a* and *X8-157*, which show expression in embryonic, larval and adult fat cells.

Adepithelial cells could potentially represent the ASC population of adult FB in *Drosophila*. Future characterization of the gene expression profile of this population will help to understand the origin and cellular differentiation of adult adipocytes. Also, it will reveal the mechanisms leading to the different adipocyte fates as well as putative fate-switching factors.

Most of the studies that shed light on the functions carried out by FB were conducted at larval stages. Therefore, further studies are needed to characterize and identify potentially new functions of the adult AT related to regulation of energy homeostasis and immunity that may be conserved in mammals. The identification of adult FB-secreted derived signals would drive to a comprehensive understanding of the roles that this organ is playing in inter-organ communication and in AT wasting, which would help to understand human cancer-associated cachexia and other diseases like obesity and DMT2.

AUTHOR CONTRIBUTIONS

EP-P conceived the idea, wrote the manuscript and elaborated the figures and tables. AT wrote the manuscript and reviewed the figures and tables. RB wrote/reviewed the manuscript, reviewed the figure and reviewed/elaborated the tables.

FUNDING

EP-P acknowledges the funding from European University to support this work. RB acknowledges funding by grants BFU 2017-84653-P and PID 2020-114178GB-I00 (MINECO/MICINN/FEDER, EU), SEV-2016-0644 (Severo Ochoa Excellence Program), SAF 2017-90900-REDT (UBIRed Program), 765445-EU (UbiCODE Program) and IT1165-19 (Basque Country Government). Additional support was provided by the Department of Industry, Tourism, and Trade of the Basque Country Government (Elkartek Research Programs) and by the Innovation Technology Department of the Bizkaia County.

ACKNOWLEDGMENTS

Authors would like to thank the reviewers for their thoughtful comments and efforts towards improving our manuscript.

REFERENCES

Agrawal, N., Delanoue, R., Mauri, A., Basco, D., Pasco, M., Thorens, B., et al. (2016). The Drosophila TNF Eiger Is an Adipokine that Acts on Insulin-Producing Cells to Mediate Nutrient Response. *Cell Metab* 23 (4), 675–684. doi:10.1016/j.cmet.2016.03.003

Aguila, J. R., Suszko, J., Gibbs, A. G., and Hoshizaki, D. K. (2007). The Role of Larval Fat Cells in Adult *Drosophila melanogaster*. *J. Exp. Biol.* 210 (6), 956–963. doi:10.1242/jeb.001586

Alcalá, M., Calderon-Dominguez, M., Serra, D., Herrero, L., and Viana, M. (2019). Mechanisms of Impaired Brown Adipose Tissue Recruitment in Obesity. *Front. Physiol.* Vol. 10.

Almind, K., Manieri, M., Sivitz, W. I., Cinti, S., and Kahn, C. R. (2007). Ectopic Brown Adipose Tissue in Muscle Provides a Mechanism for Differences in Risk of Metabolic Syndrome in Mice. *Proc. Natl. Acad. Sci.* 104 (7), 2366–2371. doi:10.1073/pnas.0610416104

Arquier, N., Géminard, C., Bourouis, M., Jarretou, G., Honegger, B., Paix, A., et al. (2008). Drosophila ALS Regulates Growth and Metabolism through Functional Interaction with Insulin-like Peptides. *Cel Metab* 7 (4), 333–338. doi:10.1016/j.cmet.2008.02.003

Arrese, E. L., Patel, R. T., and Soulages, J. L. (2006). The Main Triglyceride-Lipase from the Insect Fat Body Is an Active Phospholipase A1: Identification and Characterization. *J. Lipid Res.* 47 (12), 2656–2667. doi:10.1194/jlr.m600161-jlr200

Arrese, E. L., and Soulages, J. L. (2010). Insect Fat Body: Energy, Metabolism, and Regulation. *Annu. Rev. Entomol.* 55, 207–225. doi:10.1146/annurev-ento-112408-085356

Arthur, S. T., Noone, J. M., Van Doren, B. A., Roy, D., and Blanchette, C. M. (2014). One-year Prevalence, Comorbidities and Cost of Cachexia-Related Inpatient Admissions in the USA. *Drugs Context* 3, 212265. doi:10.7573/dic.212265

Azeez, O. I., Meintjes, R., and Chamunorwa, J. P. (2014). Fat Body, Fat Pad and Adipose Tissues in Invertebrates and Vertebrates: The Nexus. *Lipids Health Dis.* Vol. 13. doi:10.1186/1476-511x-13-71

Babaei, R., Schuster, M., Meln, I., Lerch, S., Ghandour, R. A., Pisani, D. F., et al. (2018). Jak-Tgfβ Cross-Talk Links Transient Adipose Tissue Inflammation to Beige Adipogenesis. *Sci. Signal.* 11 (527), 11. doi:10.1126/scisignal.aai7838

Bachman, E. S., Dhillon, H., Zhang, C. Y., Cinti, S., Bianco, A. C., Kobilka, B. K., et al. (2002). betaAR Signaling Required for Diet-Induced Thermogenesis and Obesity Resistance. *Science* 297 (5582), 843–845. doi:10.1126/science.1073160

Bai, H., Kang, P., Hernandez, A. M., and Tatar, M. (2013). Activin Signaling Targeted by Insulin/dFOXO Regulates Aging and Muscle Proteostasis in Drosophila. *Plos Genet.* 9 (11), e1003941. doi:10.1371/journal.pgen.1003941

Bai, H., Kang, P., and Tatar, M. (2012). Drosophila Insulin-like Peptide-6 (Dilp6) Expression from Fat Body Extends Lifespan and Represses Secretion of Drosophila Insulin-like Peptide-2 from the Brain. *Aging Cell* 11 (6), 978–985. doi:10.1111/acel.12000

Baker, K. D., and Thummel, C. S. (2007). Diabetic Larvae and Obese Flies-Emerging Studies of Metabolism in Drosophila. *Cel Metab.* Vol. 6, 257–266. doi:10.1016/j.cmet.2007.09.002

Ballard, S. L., Jarolimova, J., and Wharton, K. A. (2010). Gbb/BMP Signaling Is Required to Maintain Energy Homeostasis in Drosophila. *Dev. Biol.* 337 (2), 375–385. doi:10.1016/j.ydbio.2009.11.011

Barretto, E. C., Polan, D. M., Beevor-Potts, A. N., Lee, B., and Grewal, S. S. (2020). Tolerance to Hypoxia Is Promoted by FOXO Regulation of the Innate Immunity Transcription Factor NF-kB/relish in Drosophila. *Genetics* 215 (4), 1013–1025. doi:10.1534/genetics.120.303219

Bartok, O., Teesalu, M., Ashwall-Fluss, R., Pandey, V., Hanan, M., Rovenko, B. M., et al. (2015). The Transcription Factor Cabut Coordinates Energy Metabolism and the Circadian Clock in Response to Sugar Sensing. *EMBO J.* 34 (11), 1538–1553. doi:10.15252/embj.201591385

Baumbach, J., Hummel, P., Bickmeyer, I., Kowalczyk, K. M., Frank, M., Knorr, K., et al. (2014). A drosophila *In Vivo* Screen Identifies Store-Operated Calcium Entry as a Key Regulator of Adiposity. *Cel Metab.* 19 (2), 331–343. doi:10.1016/j.cmet.2013.12.004

Beller, M., Riedel, D., Jänsch, L., Dieterich, G., Wehland, J., Jäckle, H., et al. (2006). Characterization of the Drosophila Lipid Droplet Subproteome. *Mol. Cel Proteomics* 5 (6), 1082–1094. doi:10.1074/mcp.m600011-mcp200

Beller, M., Bulankina, A. V., Hsiao, H.-H., Urlaub, H., Jäckle, H., and Kühnlein, R. P. (2010). PERILIPIN-dependent Control of Lipid Droplet Structure and Fat Storage in Drosophila. *Cel Metab.* 12 (5), 521–532. doi:10.1016/j.cmet.2010.10.001

Benador, I. Y., Veliova, M., Mahdaviani, K., Petcherski, A., Wikstrom, J. D., Assali, E. A., et al. (2018). Mitochondria Bound to Lipid Droplets Have Unique Bioenergetics, Composition, and Dynamics that Support Lipid Droplet Expansion. *Cel Metab.* 27 (4), 869–885. e6. doi:10.1016/j.cmet.2018.03.003

Berry, D. C., Stenesen, D., Zeve, D., and Graff, J. M. (2013). *The Developmental Origins of Adipose Tissue*, 140. Cambridge): DevelopmentDevelopment, 3939–3949. doi:10.1242/dev.080549

Bharucha, K. N., Tarr, P., and Zipursky, S. L. (2008). A Glucagon-like Endocrine Pathway inDrosophilamodulates Both Lipid and Carbohydrate Homeostasis. *J. Exp. Biol.* 211 (19), 3103–3110. doi:10.1242/jeb.016451

Bi, J., Xiang, Y., Chen, H., Liu, Z., Grönke, S., Kühnlein, R. P., et al. (2012). Opposite and Redundant Roles of the Two Drosophila: Perilipins in Lipid Mobilization. *J. Cel Sci* 125 (15), 3568–3577. doi:10.1242/jcs.101329

Billon, N., Iannarelli, P., Monteiro, M. C., Glavieux-Pardanaud, C., Richardson, W. D., Kessaris, N., et al. (2007). The Generation of Adipocytes by the Neural Crest. *Development* 134 (12), 2283–2292. doi:10.1242/dev.002642

Bonneton, F., Théodore, L., Silar, P., Maroni, G., and Wegnez, M. (1996). Response of Drosophila Metallothionein Promoters to Metallic, Heat Shock and Oxidative Stresses. *FEBS Lett.* 380 (1–2), 33–38. doi:10.1016/0014-5793(95)01544-2

Britton, J. S., and Edgar, B. A. (1998). Environmental Control of the Cell Cycle in Drosophila: Nutrition Activates Mitotic and Endoreplicative Cells by Distinct Mechanisms. *Development* 125 (11), 2149–2158. doi:10.1242/dev.125.11.2149

Britton, J. S., Lockwood, W. K., Li, L., Cohen, S. M., and Edgar, B. A. (2002). Drosophila's insulin/PI3-Kinase Pathway Coordinates Cellular Metabolism with Nutritional Conditions. *Dev. Cel* 2 (2), 239–249. doi:10.1016/s1534-5807(02)00117-x

Buch, S., Melcher, C., Bauer, M., Katzenberger, J., and Pankratz, M. J. (2008). Opposing Effects of Dietary Protein and Sugar Regulate a Transcriptional Target of Drosophila Insulin-like Peptide Signaling. *Cel Metab.* 7 (4), 321–332. doi:10.1016/j.cmet.2008.02.012

Butterworth, F. M., Emerson, L., and Rasch, E. M. (1988). Maturation and Degeneration of the Fat Body in the Drosophila Larva and Pupa as Revealed by Morphometric Analysis. *Tissue Cell* 20 (2), 255–268. doi:10.1016/0040-8166(88)90047-x

Campos-Ortega, J. A., and Hartenstein, V. (1985). *The Embryonic Development of* Drosophila melanogaster. Springer Berlin Heidelberg.

Cannon, B., and Nedergaard, J. (2004). Brown Adipose Tissue: Function and Physiological Significance. *Physiol. Rev.* Vol. 84, 277–359. doi:10.1152/physrev.00015.2003

Cannon, B., Jong, J. M. A., Fischer, A. W., Nedergaard, J., and Petrovic, N. (2020). Human Brown Adipose Tissue: Classical Brown rather Than Brite/beige? *Exp. Physiol.* 105 (8), 1191–1200. doi:10.1113/ep087875

Cermelli, S., Guo, Y., Gross, S. P., and Welte, M. A. (2006). The Lipid-Droplet Proteome Reveals that Droplets Are a Protein-Storage Depot. *Curr. Biol.* 16 (18), 1783–1795. doi:10.1016/j.cub.2006.07.062

Charroux, B., and Royet, J. (2010). Drosophila Immune Response: From Systemic Antimicrobial Peptide Production in Fat Body Cells to Local Defense in the Intestinal Tract. *Fly* 4 (1), 40–47. doi:10.4161/fly.4.1.10810

Chatterjee, D., Katewa, S. D., Qi, Y., Jackson, S. A., Kapahi, P., and Jasper, H. (2014). Control of Metabolic Adaptation to Fasting by dILP6-Induced Insulin Signaling in Drosophila Oenocytes. *Proc. Natl. Acad. Sci. U S A.* 111 (50), 17959–17964. doi:10.1073/pnas.1409241111

Chell, J. M., and Brand, A. H. (2010). Nutrition-responsive Glia Control Exit of Neural Stem Cells from Quiescence. *Cell* 143 (7), 1161–1173. doi:10.1016/j.cell.2010.12.007

Chng, W. bin. A., Sleiman, M. S. B., Schüpfer, F., and Lemaitre, B. (2014). Transforming Growth Factor β/activin Signaling Functions as a Sugar-Sensing Feedback Loop to Regulate Digestive Enzyme Expression. *Cell Rep* 9 (1), 336–348. doi:10.1016/j.celrep.2014.08.064

Choi, S., Lim, D. S., and Chung, J. (2015). Feeding and Fasting Signals Converge on the LKB1-SIK3 Pathway to Regulate Lipid Metabolism in Drosophila. *Plos Genet.* 11 (5). doi:10.1371/journal.pgen.1005263

Chung, H., Sztal, T., Pasricha, S., Sridhar, M., Batterham, P., and Daborn, P. J. (2009). Characterization of *Drosophila melanogaster* Cytochrome P450 Genes. *Proc. Natl. Acad. Sci. U S A.* 106 (14), 5731–5736. doi:10.1073/pnas.0812141106

Chung, K.-J., Chatzigeorgiou, A., Economopoulou, M., Garcia-Martin, R., Alexaki, V. I., Mitroulis, I., et al. (2017). A Self-Sustained Loop of Inflammation-Driven Inhibition of Beige Adipogenesis in Obesity. *Nat. Immunol.* 18 (6), 654–664. doi:10.1038/ni.3728

Cinti, S. (2018). Adipose Organ Development and Remodeling. *Compr. Physiol.* Vol. 8, 1357–1431. doi:10.1002/cphy.c170042

Cinti, S. (2012). The Adipose Organ at a Glance. *Dis. Model. Mech.* 5, 588–594. doi:10.1242/dmm.009662

Cleal, L., Aldea, T., and Chau, Y.-Y. (2017). Fifty Shades of white: Understanding Heterogeneity in white Adipose Stem Cells. *Adipocyte* 6, 205–216. doi:10.1080/21623945.2017.1372871

Cohen, P., and Spiegelman, B. M. (2016). Cell Biology of Fat Storage. *MBoC* 27, 2523–2527. doi:10.1091/mbc.e15-10-0749

Collins, S., Daniel, K. W., Petro, A. E., and Surwit, R. S. (1997). Strain-Specific Response Toβ3-Adrenergic Receptor Agonist Treatment of Diet-Induced Obesity in Mice1. *Endocrinology* 138 (1), 405–413. doi:10.1210/endo.138.1.4829

Colombani, J., Bianchini, L., Layalle, S., Pondeville, E., Dauphin-Villemant, C., Antoniewski, C., et al. (2005). Antagonistic Actions of Ecdysone and Insulins Determine Final Size in Drosophila. *Science* 310 (5748), 667–670. doi:10.1126/science.1119432

Colombani, J., Raisin, S., Pantalacci, S., Radimerski, T., Montagne, J., and Léopold, P. (2003). A Nutrient Sensor Mechanism Controls Drosophila Growth. *Cell* 114 (6), 739–749. doi:10.1016/s0092-8674(03)00713-x

Cypess, A. M., and Kahn, C. R. (2010). Brown Fat as a Therapy for Obesity and Diabetes. *Curr. Opin. Endocrinol. Diabetes Obes.* 17, 143–149. doi:10.1097/med.0b013e328337a81f

Cypess, A. M., Lehman, S., Williams, G., Tal, I., Rodman, D., Goldfine, A. B., et al. (2009). Identification and Importance of Brown Adipose Tissue in Adult Humans. *N. Engl. J. Med.* 360 (15), 1509–1517. doi:10.1056/nejmoa0810780

Cypess, A. M., White, A. P., Vernochet, C., Schulz, T. J., Xue, R., Sass, C. A., et al. (2013). Anatomical Localization, Gene Expression Profiling and Functional Characterization of Adult Human Neck Brown Fat. *Nat. Med.* 19 (5), 635–639. doi:10.1038/nm.3112

Da-Ré, C., De Pittà, C., Zordan, M. A., Teza, G., Nestola, F., Zeviani, M., et al. (2014). UCP4C Mediates Uncoupled Respiration in Larvae of *Drosophila melanogaster*. *EMBO Rep.* 15 (5), 586–591.

Daum, G., Wagner, A., Czabany, T., and Athenstaedt, K. (2007). Dynamics of Neutral Lipid Storage and Mobilization in Yeast. *Biochimie* 89, 243–248. doi:10.1016/j.biochi.2006.06.018

Davoodi, S., Galenza, A., Panteluk, A., Deshpande, R., Ferguson, M., Grewal, S., et al. (2019). The Immune Deficiency Pathway Regulates Metabolic Homeostasis in Drosophila. *J. Immunol.* 202 (9), 2747–2759. doi:10.4049/jimmunol.1801632

De Gregorio, E., Spellman, P. T., Tzou, P., Rubin, G. M., and Lemaitre, B. (2002). The Toll and Imd Pathways Are the Major Regulators of the Immune Response in Drosophila. *EMBO J.* 21 (11), 2568–2579. doi:10.1093/emboj/21.11.2568

Dean, R. L., Locke, M., and Collins, J. V. (1985). "Structure of the Fat Body," in *Comprehensive Insect Physiology, Biochemistry, and Pharmacology*. Editors G. A. Kerkut and L. I. Gilbert (Oxford: Pergamon Press), Vol. 3, 155–210. doi:10.1016/b978-0-08-030804-3.50011-x

Delanoue, R., Meschi, E., Agrawal, N., Mauri, A., Tsatskis, Y., McNeill, H., et al. (2016). Drosophila Insulin Release Is Triggered by Adipose Stunted Ligand to Brain Methuselah Receptor. *Science* 353 (6307), 1553–1556. doi:10.1126/science.aaf8430

Delanoue, R., Slaidina, M., and Léopold, P. (2010). The Steroid Hormone Ecdysone Controls Systemic Growth by Repressing dMyc Function in drosophila Fat Cells. *Dev. Cel* 18 (6), 1012–1021. doi:10.1016/j.devcel.2010.05.007

DiAngelo, J. R., and Birnbaum, M. J. (2009). Regulation of Fat Cell Mass by Insulin in *Drosophila melanogaster*. *Mol. Cel Biol* 29 (24), 6341–6352. doi:10.1128/mcb.00675-09

Ding, H., Zheng, S., Garcia-Ruiz, D., Hou, D., Wei, Z., Liao, Z., et al. (2016). Fasting Induces a Subcutaneous-To-Visceral Fat Switch Mediated by microRNA-149-3p and Suppression of PRDM16. *Nat. Commun.* 7, 11533. doi:10.1038/ncomms11533

Doane, W. W. (1960). Developmental Physiology of the Mutantfemale Sterile(2) adipose ofDrosophila Melanogaster. I. Adult Morphology, Longevity, Egg Production, and Egg Lethality. *J. Exp. Zool.* 145 (1), 1–21. doi:10.1002/jez.1401450102

Doria, A., Patti, M.-E., and Kahn, C. R. (2008). The Emerging Genetic Architecture of Type 2 Diabetes. *Cel Metab.* 8, 186–200. doi:10.1016/j.cmet.2008.08.006

Ebadi, M., and Mazurak, V. C. (2014). Evidence and Mechanisms of Fat Depletion in Cancer. *Nutrients* Vol. 6, 5280–5297. doi:10.3390/nu6115280

Enerbäck, S. (2009). The Origins of Brown Adipose Tissue. *N. Engl. J. Med.* 360 (19), 2021–2023.

Enomoto, M., Siow, C., and Igaki, T. (2018). Drosophila as a Cancer Model. *Adv. Exp. Med. Biol.*, 173–194. doi:10.1007/978-981-13-0529-0_10

Evans, C. J., Olson, J. M., Ngo, K. T., Kim, E., Lee, N. E., Kuoy, E., et al. (2009). G-TRACE: Rapid Gal4-Based Cell Lineage Analysis in Drosophila. *Nat. Methods* 6 (8), 603–605. doi:10.1038/nmeth.1356

Fearon, K., Strasser, F., Anker, S. D., Bosaeus, I., Bruera, E., Fainsinger, R. L., et al. (2011). Definition and Classification of Cancer Cachexia: An International Consensus. *Lancet Oncol.* 12, 489–495. doi:10.1016/s1470-2045(10)70218-7

Feldmann, H. M., Golozoubova, V., Cannon, B., and Nedergaard, J. (2009). UCP1 Ablation Induces Obesity and Abolishes Diet-Induced Thermogenesis in Mice Exempt from Thermal Stress by Living at Thermoneutrality. *Cel Metab.* 9 (2), 203–209. doi:10.1016/j.cmet.2008.12.014

Feyereisen, R. (1999). Insect P450 Enzymes. *Annu. Rev. Entomol.* Vol. 44, 507–533. doi:10.1146/annurev.ento.44.1.507

Figueroa-Clarevega, A., and Bilder, D. (2015). Malignant drosophila Tumors Interrupt Insulin Signaling to Induce Cachexia-like Wasting. *Dev. Cel* 33 (1), 47–55. doi:10.1016/j.devcel.2015.03.001

Finlin, B. S., Zhu, B., Confides, A. L., Westgate, P. M., Harfmann, B. D., Dupont-Versteegden, E. E., et al. (2017). Mast Cells Promote Seasonal white Adipose Beiging in Humans. *Diabetes* 66 (5), 1237–1246. doi:10.2337/db16-1057

Freychet, P. (1990). *Pancreatic hormones. Hormones: from molecules to disease*. Editors E.-E. Baulieu and P. A. Kelly (Chapman and Hall: New York.

Fu, M., Xu, L., Chen, X., Han, W., Ruan, C., Li, J., et al. (2019). Neural Crest Cells Differentiate into Brown Adipocytes and Contribute to Periaortic Arch Adipose Tissue Formation. *Atvb* 39 (8), 1629–1644. doi:10.1161/atvbaha.119.312838

Funcke, J.-B., and Scherer, P. E. (2019). Beyond Adiponectin and Leptin: Adipose Tissue-Derived Mediators of Inter-organ Communication. *J. Lipid Res.* 60, 1648–1697. doi:10.1194/jlr.r094060

Gáliková, M., Diesner, M., Klepsatel, P., Hehlert, P., Xu, Y., Bickmeyer, I., et al. (2015). Energy Homeostasis Control in drosophila Adipokinetic Hormone Mutants. *Genetics* 201 (2), 665–683. doi:10.1534/genetics.115.178897

Garrido, D., Rubin, T., Poidevin, M., Maroni, B., Le Rouzic, A., Parvy, J. P., et al. (2015). Fatty Acid Synthase Cooperates with Glyoxalase 1 to Protect against Sugar Toxicity. *Plos Genet.* 11 (2), 1–26. doi:10.1371/journal.pgen.1004995

Gastaldelli, A. (2011). Role of Beta-Cell Dysfunction, Ectopic Fat Accumulation and Insulin Resistance in the Pathogenesis of Type 2 Diabetes Mellitus. *Diabetes Res. Clin. Pract.* 93 Suppl 1 (Suppl. 1), S60–S65. doi:10.1016/S0168-8227(11)70015-8

Géminard, C., Rulifson, E. J., and Léopold, P. (2009). Remote Control of Insulin Secretion by Fat Cells in Drosophila. *Cel Metab* 10 (3), 199–207.

Gesta, S., Tseng, Y.-H., and Kahn, C. R. (2007). Developmental Origin of Fat: Tracking Obesity to its Source. *Cell* 131, 242–256. doi:10.1016/j.cell.2007.10.004

Ghosh, A. C., and O'Connor, M. B. (2014). Systemic Activin Signaling Independently Regulates Sugar Homeostasis, Cellular Metabolism, and pH Balance in *Drosophila melanogaster*. *Proc. Natl. Acad. Sci. U S A.* 111 (15), 5729–5734. doi:10.1073/pnas.1319116111

Ghosh, A. C., Tattikota, S. G., Liu, Y., Comjean, A., Hu, Y., Barrera, V., et al. (2020). Drosophila Pdgf/vegf Signaling from Muscles to Hepatocyte-like Cells Protects against Obesity. *Elife* 9, 1–61. doi:10.7554/eLife.56969

Giannakou, M. E., Goss, M., Jünger, M. A., Hafen, E., Leevers, S. J., and Partridge, L. (2004). Long-lived Drosophila with Over-expressed dFOXO in Adult Fat Body. *Science* 305 (5682), 361. doi:10.1126/science.1098219

Goldberg, A. A., Bourque, S. D., Kyryakov, P., Boukh-Viner, T., Gregg, C., Beach, A., et al. (2009). A Novel Function of Lipid Droplets in Regulating Longevity. *Biochem. Soc. Trans.*, 1050. doi:10.1042/bst0371050

Grauer, W. O., Moss, A. A., Cann, C. E., and Goldberg, H. I. (1984). Quantification of Body Fat Distribution in the Abdomen Using Computed Tomography. *Am. J. Clin. Nutr.* 39 (4), 631–637. doi:10.1093/ajcn/39.4.631

Grönke, S., Beller, M., Fellert, S., Ramakrishnan, H., Jäckle, H., and Kühnlein, R. P. (2003). Control of Fat Storage by a Drosophila PAT Domain Protein. *Curr. Biol.* 13 (7), 603–606. doi:10.1016/s0960-9822(03)00175-1

Grönke, S., Clarke, D. F., Broughton, S., Andrews, T. D., and Partridge, L. (2010). Molecular Evolution and Functional Characterization of Drosophila Insulin-like Peptides. *Plos Genet.* 6 (2). doi:10.1371/journal.pgen.1000857

Grönke, S., Mildner, A., Fellert, S., Tennagels, N., Petry, S., Müller, G., et al. (2005). Brummer Lipase Is an Evolutionary Conserved Fat Storage Regulator in Drosophila. *Cel Metab* 1 (5), 323–330. doi:10.1016/j.cmet.2005.04.003

Guarner, A., Morris, R., Korenjak, M., Boukhali, M., Zappia, M. P., Van Rechem, C., et al. (2017). E2F/DP Prevents Cell-Cycle Progression in Endocycling Fat

Body Cells by Suppressing dATM Expression. *Dev. Cel* 43 (6), 689–703. doi:10.1016/j.devcel.2017.11.008

Guerra, C., Koza, R. A., Yamashita, H., Walsh, K., and Kozak, L. P. (1998). Emergence of Brown Adipocytes in white Fat in Mice Is under Genetic Control. Effects on Body Weight and Adiposity. *J. Clin. Invest.* 102 (2), 412–420. doi:10.1172/jci3155

Guilherme, A., Virbasius, J. V., Puri, V., and Czech, M. P. (2008). Adipocyte Dysfunctions Linking Obesity to Insulin Resistance and Type 2 Diabetes. *Nat. Rev. Mol. Cel Biol* 9, 367–377. doi:10.1038/nrm2391

Gupta, R. K. (2014). AdipocytesCurrent Biology. *Curr. Biol.* Vol. 24, R988. doi:10.1016/j.cub.2014.09.003

Gutierrez, E., Wiggins, D., Fielding, B., and Gould, A. P. (2007). Specialized Hepatocyte-like Cells Regulate Drosophila Lipid Metabolism. *Nature* 445 (7125), 275–280. doi:10.1038/nature05382

Harms, M., and Seale, P. (2013). Brown and Beige Fat: Development, Function and Therapeutic Potential. *Nat. Med.*, Vol. 19, 1252–1263. doi:10.1038/nm.3361

Hartenstein, V., and Jan, Y. N. (1992). Studying Drosophila Embryogenesis with P-lacZ Enhancer Trap Lines. *Roux's Arch. Dev. Biol.* 201 (4), 194–220. doi:10.1007/bf00188752

Hasygar, K., Deniz, O., Liu, Y., Gullmets, J., Hynynen, R., Ruhanen, H., et al. (2021). Coordinated Control of Adiposity and Growth by Anti-anabolic Kinase ERK7. *EMBO Rep.* 22 (2), 1–16. doi:10.15252/embr.201949602

Haunerland, N. H., and Shirk, P. D. (1995). Regional and Functional Differentiation in the Insect Fat Body. *Annu. Rev. Entomol.* 40 (1), 121–145. doi:10.1146/annurev.en.40.010195.001005

Havula, E., and Hietakangas, V. (2012). Glucose Sensing by ChREBP/MondoA-Mlx Transcription Factors. Vol. 23, Seminars in Cell and Developmental Biology. *Semin. Cel Dev Biol*, 640–647. doi:10.1016/j.semcdb.2012.02.007

Havula, E., Teesalu, M., Hyötyläinen, T., Seppälä, H., Hasygar, K., Auvinen, P., et al. (2013). Mondo/ChREBP-Mlx-Regulated Transcriptional Network Is Essential for Dietary Sugar Tolerance in Drosophila. *Plos Genet.* 9 (4). doi:10.1371/journal.pgen.1003438

Heine, M., Fischer, A. W., Schlein, C., Jung, C., Straub, L. G., Gottschling, K., et al. (2018). Lipolysis Triggers a Systemic Insulin Response Essential for Efficient Energy Replenishment of Activated Brown Adipose Tissue in Mice. *Cel Metab* 28 (4), 644–655. doi:10.1016/j.cmet.2018.06.020

Hiraike, Y., Waki, H., Miyake, K., Wada, T., Oguchi, M., Saito, K., et al. (2020). NFIA Differentially Controls Adipogenic and Myogenic Gene Program through Distinct Pathways to Ensure Brown and Beige Adipocyte Differentiation. *Plos Genet.* 16 (9), e1009044. doi:10.1371/journal.pgen.1009044

Hiraike, Y., Waki, H., Yu, J., Nakamura, M., Miyake, K., Nagano, G., et al. (2017). NFIA Co-localizes with PPARγ and Transcriptionally Controls the Brown Fat Gene Program. *Nat. Cel Biol* 19 (9), 1081–1092. doi:10.1038/ncb3590

Hoang, A. C., Yu, H., and Röszer, T. (2021). Transcriptional Landscaping Identifies a Beige Adipocyte Depot in the Newborn Mouse. *Cells* 10 (9). doi:10.3390/cells10092368

Hoffmann, J., Romey, R., Fink, C., Yong, L., and Roeder, T. (2013). Overexpression of Sir2 in the Adult Fat Body Is Sufficient to Extend Lifespan of Male and Female Drosophila. *Aging (Albany NY)* 5 (4), 315–327. doi:10.18632/aging.100553

Holz, A., Meise, M., and Janning, W. (1997). Adepithelial Cells in *Drosophila melanogaster*: Origin and Cell Lineage. *Mech. Dev.* 62 (1), 93–101. doi:10.1016/s0925-4773(97)00654-0

Honegger, B., Galic, M., Köhler, K., Wittwer, F., Brogiolo, W., Hafen, E., et al. (2008). Imp-L2, a Putative Homolog of Vertebrate IGF-Binding Protein 7, Counteracts Insulin Signaling in Drosophila and Is Essential for Starvation Resistance. *J. Biol.* 7 (3), 172. doi:10.1186/jbiol72

Hoshizaki, D. K. (1994). Krüppel Expression during Postembryonic Development of Drosophila. *Dev. Biol.* 163 (1), 133–140. doi:10.1006/dbio.1994.1129

Hoshizaki, D. K., Blackburn, T., Price, C., Ghosh, M., Miles, K., Ragucci, M., et al. (1994). Embryonic Fat-Cell Lineage in *Drosophila melanogaster*. *Development* 120 (9), 2489–2499. doi:10.1242/dev.120.9.2489

Hoshizaki, D. K., Lunz, R., Johnson, W., and Ghosh, M. (1995). Identification of Fat-Cell Enhancer Activity inDrosophila Melanogasterusing P-Element Enhancer Traps. *Genome* 38 (3), 497–506. doi:10.1139/g95-065

Hotamisligil, G. S. (2017). Inflammation, Metaflammation and Immunometabolic Disorders. *Nature* 542, 177–185. doi:10.1038/nature21363

Hughson, B. N., Shimell, M. J., and O'Connor, M. B. (2021). AKH Signaling in *D. melanogaster* Alters Larval Development in a Nutrient-dependent Manner that Influences Adult Metabolism. *Front. Physiol.*, 12. doi:10.3389/fphys.2021.619219

Hyun, S., Lee, J. H., Jin, H., Nam, J. W., Namkoong, B., Lee, G., et al. (2009). Conserved MicroRNA miR-8/miR-200 and its Target USH/FOG2 Control Growth by Regulating PI3K. *Cell* 139 (6), 1096–1108. doi:10.1016/j.cell.2009.11.020

Iijima, K., Zhao, L., Shenton, C., and Iijima-Ando, K. (2009). Regulation of Energy Stores and Feeding by Neuronal and Peripheral CREB Activity in Drosophila. *PLoS One* 4 (12). doi:10.1371/journal.pone.0008498

Ikeda, K., Maretich, P., and Kajimura, S. (2018). The Common and Distinct Features of Brown and Beige Adipocytes. *Trends Endocrinol Metab.* 29 (3), 191–200.

Imrie, D., and Sadler, K. C. (2010). White Adipose Tissue Development in Zebrafish Is Regulated by Both Developmental Time and Fish Size. *Dev. Dyn.* 239 (11), 3013–3023. doi:10.1002/dvdy.22443

Ingaramo, M. C., Sánchez, J. A., Perrimon, N., and Dekanty, A. (2020). Fat Body P53 Regulates Systemic Insulin Signaling and Autophagy under Nutrient Stress via Drosophila Upd2 Repression. *Cel Rep* 33 (4), 321. doi:10.1016/j.celrep.2020.108321

Isabel, G., Martin, J. R., Chidami, S., Veenstra, J. A., and Rosay, P. (2005). AKH-producing Neuroendocrine Cell Ablation Decreases Trehalose and Induces Behavioral Changes in Drosophila. *Am. J. Physiol. - Regul. Integr. Comp. Physiol.* 288 (2 57-2). 2004. doi:10.1152/ajpregu.00158.2004

Jin, H., Narry Kim, V., and Hyun, S. (2012). Conserved microRNA miR-8 Controls Body Size in Response to Steroid Signaling in Drosophila. *Genes Dev.* 26 (13), 1427–1432. doi:10.1101/gad.192872.112

Johnson, M. B., and Butterworth, F. M. (1985). Maturation and Aging of Adult Fat Body and Oenocytes in Drosophila as Revealed by Light Microscopic Morphometry. *J. Morphol.* 184 (1), 51–59. doi:10.1002/jmor.1051840106

Jung, S. M., Sanchez-Gurmaches, J., and Guertin, D. A. (2019). Brown Adipose Tissue Development and Metabolism. *Handb Exp. Pharmacol.* 251, 3–36. doi:10.1007/164_2018_168

Kadereit, B., Kumar, P., Wang, W.-J., Miranda, D., Snapp, E. L., Severina, N., et al. (2008). Evolutionarily Conserved Gene Family Important for Fat Storage. *Proc. Natl. Acad. Sci.* 105 (1), 94–99. doi:10.1073/pnas.0708579105

Katheder, N. S., Khezri, R., O'Farrell, F., Schultz, S. W., Jain, A., Schink, M. K. O., et al. (2017). Microenvironmental Autophagy Promotes Tumour Growth. *Nature* 541 (7637), 417–420. doi:10.1038/nature20815

Khezri, R., Holland, P., Schoborg, T. A., Abramovich, I., Takáts, S., Dillard, C., et al. (2021). Host Autophagy Mediates Organ Wasting and Nutrient Mobilization for Tumor Growth. *EMBO J.* 40 (18), e107336. doi:10.15252/embj.2020107336

Kim, S. K., and Rulifson, E. J. (20041670). Conserved Mechanisms of Glucose Sensing and Regulation by Drosophila Corpora Cardiaca Cells. *Nature* 431, 431316–431320. doi:10.1038/nature02897

Kir, S., White, J. P., Kleiner, S., Kazak, L., Cohen, P., Baracos, V. E., et al. (2014). Tumour-derived PTH-Related Protein Triggers Adipose Tissue browning and Cancer Cachexia. *Nature* 513 (7516), 100–104. doi:10.1038/nature13528

Kopecký, J., Hodný, Z., Rossmeisl, M., Syrový, I., and Kozak, L. P. (1996). Reduction of Dietary Obesity in aP2-Ucp Transgenic Mice: Physiology and Adipose Tissue Distribution. *Am. J. Physiol. - Endocrinol. Metab.* 270 (5 33-5).

Koyama, T., and Mirth, C. K. (2016). Growth-Blocking Peptides as Nutrition-Sensitive Signals for Insulin Secretion and Body Size Regulation. *Plos Biol.* 14 (2). doi:10.1371/journal.pbio.1002392

Krahmer, N., Hilger, M., Kory, N., Wilfling, F., Stoehr, G., Mann, M., et al. (2013). Protein Correlation Profiles Identify Lipid Droplet Proteins with High Confidence. *Mol. Cel Proteomics* 12 (5), 1115–1126. doi:10.1074/mcp.m112.020230

Kwon, H. J., Waghmare, I., Verghese, S., Singh, A., Singh, A., and Kango-Singh, M. (2015). Drosophila C-Terminal Src Kinase Regulates Growth via the Hippo Signaling Pathway. *Dev. Biol.* 397 (1), 67–76. doi:10.1016/j.ydbio.2014.10.010

Lamers, D., Famulla, S., Wronkowitz, N., Hartwig, S., Lehr, S., Ouwens, D. M., et al. (2011). Dipeptidyl Peptidase 4 Is a Novel Adipokine Potentially Linking Obesity to the Metabolic Syndrome. *Diabetes* 60 (7), 1917–1925. doi:10.2337/db10-1707

Larsen, W. J. (1976). Cell Remodeling in the Fat Body of an Insect. *Tissue Cell* 8 (1), 73–92. doi:10.1016/0040-8166(76)90021-5

Lawrence, P. A., and Johnston, P. (1986). Observations on Cell Lineage of Internal Organs of Drosophila. *J. Embryol. Exp. Morphol.* 91, 251–266. doi:10.1242/dev.91.1.251

Lee, B., Barretto, E. C., and Grewal, S. S. (2019). TORC1 Modulation in Adipose Tissue Is Required for Organismal Adaptation to Hypoxia in Drosophila. *Nat. Commun.* 10 (1). doi:10.1038/s41467-019-09643-7

Lee, G. J., Han, G., Yun, H. M., Lim, J. J., Noh, S., Lee, J., et al. (2018). Steroid Signaling Mediates Nutritional Regulation of Juvenile Body Growth via IGF-Binding Protein in Drosophila. *Proc. Natl. Acad. Sci. U S A.* 115 (23), 5992–5997. doi:10.1073/pnas.1718834115

Lee, G. J., Jun, J. W., and Hyun, S. (2015). MicroRNA miR-8 Regulates Multiple Growth Factor Hormones Produced from Drosophila Fat Cells. *Insect Mol. Biol.* 24 (3), 311–318. doi:10.1111/imb.12156

Lee, G., and Park, J. H. (2004). Hemolymph Sugar Homeostasis and Starvation-Induced Hyperactivity Affected by Genetic Manipulations of the Adipokinetic Hormone-Encoding Gene in *Drosophila melanogaster*. *Genetics* 167 (1), 311–323. doi:10.1534/genetics.167.1.311

Lee, K.-S., You, K.-H., Choo, J.-K., Han, Y.-M., and Yu, K. (2004). Drosophila Short Neuropeptide F Regulates Food Intake and Body Size. *J. Biol. Chem.* 279 (49), 50781–50789. doi:10.1074/jbc.m407842200

Lehr, S., Hartwig, S., Lamers, D., Famulla, S., Müller, S., Hanisch, F. G., et al. (2012). Identification and Validation of Novel Adipokines Released from Primary Human Adipocytes. *Mol. Cel Proteomics* 11 (1), M111–M010504. doi:10.1074/mcp.M111.010504

Lehr, S., Hartwig, S., and Sell, H. (2012). Adipokines: A Treasure Trove for the Discovery of Biomarkers for Metabolic Disorders. *Prot. Clin. Appl.* 6, 91–101. doi:10.1002/prca.201100052

Li, S., Yu, X., and Feng, Q. (2019). Fat Body Biology in the Last Decade. *Annu. Rev. Entomol.* 64, 315–333. doi:10.1146/annurev-ento-011118-112007

Lidell, M. E., Betz, M. J., Leinhard, O. D., Heglind, M., Elander, L., Slawik, M., et al. (2013). Evidence for Two Types of Brown Adipose Tissue in Humans. *Nat. Med.* 19 (5), 631–634. doi:10.1038/nm.3017

Lodge, W., Zavortink, M., Golenkina, S., Froldi, F., Dark, C., Cheung, S., et al. (2021). Tumor-derived MMPs Regulate Cachexia in a Drosophila Cancer Model. *Dev. Cel* 56 (18), 2664–2680. doi:10.1016/j.devcel.2021.08.008

Loft, A., Forss, I., Siersbæk, M. S., Schmidt, S. F., Larsen, A. S. B., Madsen, J. G. S., et al. (2015). Browning of Human Adipocytes Requires KLF11 and Reprogramming of PPARγ Superenhancers. *Genes Dev.* 29 (1), 7–22. doi:10.1101/gad.250829.114

Lowell, B. B., S-Susulic, V., Hamann, A., Lawitts, J. A., Himms-Hagen, J., Boyer, B. B., et al. (1993). Development of Obesity in Transgenic Mice after Genetic Ablation of Brown Adipose Tissue. *Nature* 366 (6457), 740–742. doi:10.1038/366740a0

Lshibashi, J., and Seale, P. (2010). Beige Can Be Slimming. *Sci. Sci.* Vol. 328, 1113–1114. doi:10.1126/science.1190816

Luong, N., Davies, C. R., Wessells, R. J., Graham, S. M., King, M. T., Veech, R., et al. (2006). Activated FOXO-Mediated Insulin Resistance Is Blocked by Reduction of TOR Activity. *Cel Metab* 4 (2), 133–142. doi:10.1016/j.cmet.2006.05.013

Martínez, B. A., Hoyle, R. G., Yeudall, S., Granade, M. E., Harris, T. E., David Castle, J., et al. (2020). Innate Immune Signaling in Drosophila Shifts Anabolic Lipid Metabolism from Triglyceride Storage to Phospholipid Synthesis to Support Immune Function. *Plos Genet.* (11), 16. doi:10.1371/journal.pgen.1009192

Mattila, J., Havula, E., Suominen, E., Teesalu, M., Surakka, I., Hynynen, R., et al. (2015). Mondo-Mlx Mediates Organismal Sugar Sensing through the Gli-Similar Transcription Factor Sugarbabe. *Cel Rep* 13 (2), 350–364. doi:10.1016/j.celrep.2015.08.081

Mattila, J., and Hietakangas, V. (2017). Regulation of Carbohydrate Energy Metabolism in *Drosophila melanogaster*. *Genetics* 207 (4), 1231–1253. doi:10.1534/genetics.117.199885

Meschi, E., Léopold, P., and Delanoue, R. (2019). An EGF-Responsive Neural Circuit Couples Insulin Secretion with Nutrition in Drosophila. *Dev. Cel* 48 (1), 76–86. doi:10.1016/j.devcel.2018.11.029

Miller, J. M., Oligino, T., Pazdera, M., López, A. J., and Hoshizaki, D. K. (2002). Identification of Fat-Cell Enhancer Regions inDrosophila Melanogaster. *Insect Mol. Biol.* 11 (1), 67–77. doi:10.1046/j.0962-1075.2001.00310.x

Mirth, C. K., and Riddiford, L. M. (2007). Size Assessment and Growth Control: How Adult Size Is Determined in Insects. *BioEssays* Vol. 29, 344–355. doi:10.1002/bies.20552

Molaei, M., Vandehoef, C., and Karpac, J. (2019). NF-κB Shapes Metabolic Adaptation by Attenuating Foxo-Mediated Lipolysis in Drosophila. *Dev. Cel* 49 (5), 802–810.e6. doi:10.1016/j.devcel.2019.04.009

Moore, L. A., Broihier, H. T., Van Doren, M., and Lehmann, R. (1998). Gonadal Mesoderm and Fat Body Initially Follow a Common Developmental Path in Drosophila. *Development* 125 (5), 837–844. doi:10.1242/dev.125.5.837

Müller, H. (1968). Fine Structure and Lipid Formation in Fat Cells of the Perimeningeal Tissue of Lampreys under normal and Experimental Conditions. *Z. Zellforsch Mikrosk Anat.* 84 (4), 585–608.

Musselman, L. P., Fink, J. L., Ramachandran, P. V., Patterson, B. W., Okunade, A. L., Maier, E., et al. (2013). Role of Fat Body Lipogenesis in protection against the Effects of Caloric Overload in drosophila. *J. Biol. Chem.* 288 (12), 8028–8042. doi:10.1074/jbc.m112.371047

Musselman, L. P., and Kühnlein, R. P. (2018). Drosophila as a Model to Study Obesity and Metabolic Disease. Vol. 121. *J. Exp. BiologyJ Exp Biol.*

Na, J., Musselman, L. P., Pendse, J., Baranski, T. J., Bodmer, R., Ocorr, K., et al. (2013). A Drosophila Model of High Sugar Diet-Induced Cardiomyopathy. *Plos Genet.* 9 (1), e1003175. doi:10.1371/journal.pgen.1003175

Nässel, D. R., and Wegener, C. (2011). A Comparative Review of Short and Long Neuropeptide F Signaling in Invertebrates: Any Similarities to Vertebrate Neuropeptide Y Signaling. *Peptides* 32, 1335–1355. doi:10.1016/j.peptides.2011.03.013

Neugnot, V., Moulin, G., Dubreucq, E., and Bigey, F. (2002). The Lipase/acyltransferase fromCandida Parapsilosis. *Eur. J. Biochem.* 269 (6), 1734–1745. doi:10.1046/j.1432-1327.2002.02828.x

Ng, M., Fleming, T., Robinson, M., Thomson, B., Graetz, N., Margono, C., et al. (2014). Global, Regional, and National Prevalence of Overweight and Obesity in Children and Adults during 1980-2013: A Systematic Analysis for the Global Burden of Disease Study 2013. *Lancet* 384 (9945), 766–781. doi:10.1016/S0140-6736(14)60460-8

Novak, M., Monkus, E., and Pardo, V. (1971). Human Neonatal Subcutaneous Adipose Tissue. Function and Ultrastructure. *Biol. Neonate* 19 (4–6), 306–321. doi:10.1159/000240425

Okamoto, N., Yamanaka, N., Yagi, Y., Nishida, Y., Kataoka, H., O'Connor, M. B., et al. (2009). A Fat Body-Derived IGF-like Peptide Regulates Postfeeding Growth in Drosophila. *Dev. Cel* 17 (6), 885–891. doi:10.1016/j.devcel.2009.10.008

Olofsson, S.-O., Boström, P., Andersson, L., Rutberg, M., Levin, M., Perman, J., et al. (2008). Triglyceride Containing Lipid Droplets and Lipid Droplet-Associated Proteins. *Curr. Opin. Lipidol.* 19, 441–447. doi:10.1097/mol.0b013e32830dd09b

Ottaviani, E., Malagoli, D., and Franceschi, C. (2011). The Evolution of the Adipose Tissue: A Neglected enigma. *Gen. Comp. Endocrinol.* 174, 1–4. doi:10.1016/j.ygcen.2011.06.018

Palanker, L., Tennessen, J. M., Lam, G., and Thummel, C. S. (2009). Drosophila HNF4 Regulates Lipid Mobilization and β-Oxidation. *Cel Metab* 9 (3), 228–239. doi:10.1016/j.cmet.2009.01.009

Palanker Musselman, L., Fink, J. L., Narzinski, K., Ramachandran, P. V., Sukumar Hathiramani, S., Cagan, R. L., et al. (2011). A High-Sugar Diet Produces Obesity and Insulin Resistance in Wild-type Drosophila. *DMM Dis. Model. Mech.* 4 (6), 842–849. doi:10.1242/dmm.007948

Palm, W., Sampaio, J. L., Brankatschk, M., Carvalho, M., Mahmoud, A., Shevchenko, A., et al. (2012). Lipoproteins in Drosophila Melanogaster-Aassembly, Function, and Influence on Tissue Lipid Composition. *Plos Genet.* 8 (7), e1002828. doi:10.1371/journal.pgen.1002828

Palu, R. A. S., and Thummel, C. S. (2016). Sir2 Acts through Hepatocyte Nuclear Factor 4 to Maintain Insulin Signaling and Metabolic Homeostasis in Drosophila. *Plos Genet.* 12 (4). doi:10.1371/journal.pgen.1005978

Parisi, F., Riccardo, S., Zola, S., Lora, C., Grifoni, D., Brown, L. M., et al. (2013). DMyc Expression in the Fat Body Affects DILP2 Release and Increases the Expression of the Fat Desaturase Desat1 Resulting in Organismal Growth. *Dev. Biol.* 379 (1), 64–75. doi:10.1016/j.ydbio.2013.04.008

Parra-Peralbo, E., and Culi, J. (2011). Drosophila Lipophorin Receptors Mediate the Uptake of Neutral Lipids in Oocytes and Imaginal Disc Cells by an Endocytosis-independent Mechanism. *Plos Genet.* 7 (2), e1001297. doi:10.1371/journal.pgen.1001297

Pasco, M. Y., and Léopold, P. (2012). High Sugar-Induced Insulin Resistance in Drosophila Relies on the Lipocalin Neural Lazarillo. *PLoS One* 7 (5), e36583. doi:10.1371/journal.pone.0036583

Pathak, H., and Varghese, J. (2021). Edem1 Activity in the Fat Body Regulates Insulin Signalling and Metabolic Homeostasis in Drosophila. *Life Sci. Alliance* 4 (8), 1079. doi:10.26508/lsa.202101079

Petrovic, N., Walden, T. B., Shabalina, I. G., Timmons, J. A., Cannon, B., and Nedergaard, J. (2010). Chronic Peroxisome Proliferator-Activated Receptor γ (PPARγ) Activation of Epididymally Derived White Adipocyte Cultures Reveals a Population of Thermogenically Competent, UCP1-Containing Adipocytes Molecularly Distinct from Classic Brown Adipocytes. *J. Biol. Chem.* 285 (10), 7153–7164. doi:10.1074/jbc.m109.053942

Petruzzelli, M., and Wagner, E. F. (2016). Mechanisms of Metabolic Dysfunction in Cancer-Associated Cachexia. *Genes Dev.* 30, 489–501. doi:10.1101/gad.276733.115

Pospisilik, J. A., Schramek, D., Schnidar, H., Cronin, S. J. F., Nehme, N. T., Zhang, X., et al. (2010). Drosophila Genome-wide Obesity Screen Reveals Hedgehog as a Determinant of Brown versus White Adipose Cell Fate. *Cell* 140 (1), 148–160. doi:10.1016/j.cell.2009.12.027

Post, S., Karashchuk, G., Wade, J. D., Sajid, W., De Meyts, P., and Tatar, M. (2018). Drosophila Insulin-like Peptides DILP2 and DILP5 Differentially Stimulate Cell Signaling and Glycogen Phosphorylase to Regulate Longevity. *Front. Endocrinol. (Lausanne)* 9 (MAY). 245. doi:10.3389/fendo.2018.00245

Rajan, A., and Perrimon, N. (2012). Drosophila Cytokine Unpaired 2 Regulates Physiological Homeostasis by Remotely Controlling Insulin Secretion. *Cell* 151 (1), 123–137. doi:10.1016/j.cell.2012.08.019

Reis, T., van Gilst, M. R., and Hariharan, I. K. (2010). A Buoyancy-Based Screen of drosophila Larvae for Fat- Storage Mutants Reveals a Role for Sir2 in Coupling Fat Storage to Nutrient Availability. *Plos Genet.* 6 (11), 206. doi:10.1371/journal.pgen.1001206

Ren, G. R., Hauser, F., Rewitz, K. F., Kondo, S., Engelbrecht, A. F., Didriksen, A. K., et al. (2015). CCHamide-2 Is an Orexigenic Brain-Gut Peptide in Drosophila. *PLoS One* 10 (7). doi:10.1371/journal.pone.0133017

Riechmann, V., and Rehorn, K. P. (1998). The Genetic Control of the Distinction between Fat Body and Gonadal Mesoderm in Drosophila. *Development* 125(4): 713–723.

Rodríguez-Vázquez, M., Vaquero, D., Parra-Peralbo, E., Mejía-Morales, J. E., and Culi, J. (2015). Drosophila Lipophorin Receptors Recruit the Lipoprotein LTP to the Plasma Membrane to Mediate Lipid Uptake. *Plos Genet.* 11 (6). doi:10.1371/journal.pgen.1005356

Rőszer, T., and Kiss-Tóth, É. D. (2014). FMRF-amide Is a Glucose-Lowering Hormone in the Snail Helix Aspersa. *Cell Tissue Res* 358 (2), 371–383. doi:10.1007/s00441-014-1966-x

Roth, S. W., Bitterman, M. D., Birnbaum, M. J., and Bland, M. L. (2018). Innate Immune Signaling in Drosophila Blocks Insulin Signaling by Uncoupling PI(3,4,5)P 3 Production and Akt Activation. *Cel Rep* 22 (10), 2550–2556. doi:10.1016/j.celrep.2018.02.033

Rusten, T. E., Lindmo, K., Juhász, G., Sass, M., Seglen, P. O., Brech, A., et al. (2004). Programmed Autophagy in the Drosophila Fat Body Is Induced by Ecdysone through Regulation of the PI3K Pathway. *Dev. Cel* 7 (2), 179–192. doi:10.1016/j.devcel.2004.07.005

Rydén, M., and Arner, P. (2007). Fat Loss in Cachexia-Is There a Role for Adipocyte Lipolysis? *Clin. Nutr.* Vol. 26, 1–6.

Saavedra, P., and Perrimon, N. (2019). Drosophila as a Model for Tumor-Induced Organ Wasting. *Adv. Exp. Med. Biol.*, 191–205. doi:10.1007/978-3-030-23629-8_11

Saltiel, A. R. (2012). Insulin Resistance in the Defense against Obesity. *Cel Metab.* 15, 798–804. doi:10.1016/j.cmet.2012.03.001

Saltiel, A. R., and Kahn, C. R. (2001). Insulin Signalling and the Regulation of Glucose and Lipid Metabolism. *Nature* 414, 799–806. doi:10.1038/414799a

Sam, S., Leise, W., and Keiko Hoshizaki, D. (1996). The Serpent Gene Is Necessary for Progression through the Early Stages of Fat-Body Development. *Mech. Dev.* 60 (2), 197–205. doi:10.1016/s0925-4773(96)00615-6

Sano, H., Nakamura, A., Texada, M. J., Truman, J. W., Ishimoto, H., Kamikouchi, A., et al. (2015). The Nutrient-Responsive Hormone CCHamide-2 Controls Growth by Regulating Insulin-like Peptides in the Brain of *Drosophila melanogaster*. *Plos Genet.* 11 (5). doi:10.1371/journal.pgen.1005209

Sato, M., and Kornberg, T. B. (2002). FGF Is an Essential Mitogen and Chemoattractant for the Air Sacs of the Drosophila Tracheal System. *Dev. Cel* 3 (2), 195–207. doi:10.1016/s1534-5807(02)00202-2

Saxton, R. A., and Sabatini, D. M. (2017). mTOR Signaling in Growth, Metabolism, and Disease. *Cell* Vol. 168, 960–976. doi:10.1016/j.cell.2017.02.004

Schaffer, M. H., Noyes, B. E., Slaughter, C. A., Thorne, G. C., and Gaskell, S. J. (1990). The Fruitfly *Drosophila melanogaster* Contains a Novel Charged Adipokinetic-Hormone-Family Peptide. *Biochem. J.* 269 (2), 315–320. doi:10.1042/bj2690315

Schwartz, D. R., and Lazar, M. A. (2011). Human Resistin: Found in Translation from Mouse to Man. *Trends Endocrinol. Metab.* 22, 259–265. doi:10.1016/j.tem.2011.03.005

Scopelliti, A., Bauer, C., Yu, Y., Zhang, T., Kruspig, B., Murphy, D. J., et al. (2019). A Neuronal Relay Mediates a Nutrient Responsive Gut/Fat Body Axis Regulating Energy Homeostasis in Adult Drosophila. *Cel Metab* 29 (2), 269–284. doi:10.1016/j.cmet.2018.09.021

Scott, R. C., Schuldiner, O., and Neufeld, T. P. (2004). Role and Regulation of Starvation-Induced Autophagy in the Drosophila Fat Body. *Dev. Cel* 7 (2), 167–178. doi:10.1016/j.devcel.2004.07.009

Seale, P., Bjork, B., Yang, W., Kajimura, S., Chin, S., Kuang, S., et al. (2008). PRDM16 Controls a Brown Fat/skeletal Muscle Switch. *Nature* 454 (7207), 961–967. doi:10.1038/nature07182

Seale, P., Conroe, H. M., Estall, J., Kajimura, S., Frontini, A., Ishibashi, J., et al. (2011). Prdm16 Determines the Thermogenic Program of Subcutaneous white Adipose Tissue in Mice. *J. Clin. Invest.* 121 (1), 96–105. doi:10.1172/jci44271

Semaniuk, U., Piskovatska, V., Strilbytska, O., Strutynska, T., Burdyliuk, N., Vaiserman, A., et al. (2021). *Drosophila Insulin-like Peptides: From Expression to Functions – a Review Entomologia Experimentalis et Applicata* (John Wiley & Sons), Vol. 169, 195–208. doi:10.1111/eea.12981

Semenza, G. L. (2014). Oxygen Sensing, Hypoxia-Inducible Factors, and Disease Pathophysiology. *Annu. Rev. Pathol. Mech. Dis.* 9, 47–71. doi:10.1146/annurev-pathol-012513-104720

Sharp, L. Z., Shinoda, K., Ohno, H., Scheel, D. W., Tomoda, E., Ruiz, L., et al. (2012). Human BAT Possesses Molecular Signatures that Resemble Beige/Brite Cells. *PLoS One* 7 (11), e49452. doi:10.1371/journal.pone.0049452

Slaidina, M., Delanoue, R., Gronke, S., Partridge, L., and Léopold, P. (2009). A Drosophila Insulin-like Peptide Promotes Growth during Nonfeeding States. *Dev. Cel* 17 (6), 874–884. doi:10.1016/j.devcel.2009.10.009

Snijder, M. B., Dekker, J. M., Visser, M., Bouter, L. M., Stehouwer, C. D., Kostense, P. J., et al. (2003). Associations of Hip and Thigh Circumferences Independent of Waist Circumference with the Incidence of Type 2 Diabetes: The Hoorn Study. *Am. J. Clin. Nutr.* 77 (5), 1192–1197. doi:10.1093/ajcn/77.5.1192

Snijder, M. B., Dekker, J. M., Visser, M., Yudkin, J. S., Stehouwer, C. D. A., Bouter, L. M., et al. (2003). Larger Thigh and Hip Circumferences Are Associated with Better Glucose Tolerance: The Hoorn Study. *Obes. Res.* 11 (1), 104–111. doi:10.1038/oby.2003.18

Song, A., Dai, W., Jang, M. J., Medrano, L., Li, Z., Zhao, H., et al. (2020). Low- and High-Thermogenic Brown Adipocyte Subpopulations Coexist in Murine Adipose Tissue. *J. Clin. Invest.* 130 (1), 247–257. doi:10.1172/JCI129167

Song, W., Cheng, D., Hong, S., Sappe, B., Hu, Y., Wei, N., et al. (2017). Midgut-Derived Activin Regulates Glucagon-like Action in the Fat Body and Glycemic Control. *Cel Metab* 25 (2), 386–399. doi:10.1016/j.cmet.2017.01.002

Song, W., Kir, S., Hong, S., Hu, Y., Wang, X., Binari, R., et al. (2019). Tumor-Derived Ligands Trigger Tumor Growth and Host Wasting via Differential MEK Activation. *Dev. Cel* 48 (2), 277–286. doi:10.1016/j.devcel.2018.12.003

Sousa-Nunes, R., Yee, L. L., and Gould, A. P. (2011). Fat Cells Reactivate Quiescent Neuroblasts via TOR and Glial Insulin Relays in Drosophila. *Nature* 471 (7339), 508–513. doi:10.1038/nature09867

Stephens, J. M. (2012). The Fat Controller: Adipocyte Development. *Plos Biol.* 10 (11), e1001436. doi:10.1371/journal.pbio.1001436

Suzawa, M., Muhammad, N. M., Joseph, B. S., and Bland, M. L. (2019). The Toll Signaling Pathway Targets the Insulin-like Peptide Dilp6 to Inhibit Growth in Drosophila. *Cel Rep* 28 (6), 1439–1446. doi:10.1016/j.celrep.2019.07.015

Tan, B. K., Adya, R., and Randeva, H. S. (2010). Omentin: A Novel Link between Inflammation, Diabesity, and Cardiovascular Disease. *Trends Cardiovasc. Med.* 20, 143–148. doi:10.1016/j.tcm.2010.12.002

Tchkonia, T., Tchoukalova, Y. D., Giorgadze, N., Pirtskhalava, T., Karagiannides, I., Forse, R. A., et al. (2005). Abundance of Two Human Preadipocyte Subtypes

with Distinct Capacities for Replication, Adipogenesis, and Apoptosis Varies Among Fat Depots. *Am. J. Physiol. Endocrinol. Metab.* 288 (1 51-1), E267–E277. doi:10.1152/ajpendo.00265.2004

Teixeira, L., Rabouille, C., Rørth, P., Ephrussi, A., and Vanzo, N. F. (2003). Drosophila Perilipin/ADRP Homologue Lsd2 Regulates Lipid Metabolism. *Mech. Dev.* 120 (9), 1071–1081. doi:10.1016/s0925-4773(03)00158-8

Terhzaz, S., Cabrero, P., Brinzer, R. A., Halberg, K. A., Dow, J. A. T., and Davies, S. A. (2015). A novel role of Drosophila cytochrome P450-4e3 in permethrin insecticide tolerance. *Insect Biochem. Mol. Biol.* 67, 38–46. doi:10.1016/j.ibmb.2015.06.002

Texada, M. J., Jørgensen, A. F., Christensen, C. F., Koyama, T., Malita, A., Smith, D. K., et al. (2019). A Fat-Tissue Sensor Couples Growth to Oxygen Availability by Remotely Controlling Insulin Secretion. *Nat. Commun.* 10 (1), 1–16. doi:10.1038/s41467-019-09943-y

The mesoderm and its derivatives (1993). in *The Development of Drosophila melanogasterCold Spring Harbor*. Editors A. BM (New York: Cold Spring Harbor Laboratory Press).

Thiam, A. R., and Beller, M. (2017). The Why, when and How of Lipid Droplet Diversity, *J. Cel Sci*, 130. 315–324. doi:10.1242/jcs.192021

TM, R. (1978). "Fat Body," in *The Genetics and Biology of Drosophila*. Editors M. Ashburner and T. R. F. Wright (London: Academic Press), 561–601.

Todorčević, M., Kjær, M. A., Djaković, N., Vegusdal, A., Torstensen, B. E., and Ruyter, B. (2009). N-3 HUFAs Affect Fat Deposition, Susceptibility to Oxidative Stress, and Apoptosis in Atlantic salmon Visceral Adipose Tissue. *Comp. Biochem. Physiol. - B Biochem. Mol. Biol.* 152 (2), 135–143.

Tsoli, M., Swarbrick, M. M., and Robertson, G. R. (2016). Lipolytic and Thermogenic Depletion of Adipose Tissue in Cancer Cachexia. *Semin. Cel Dev. Biol.* 54, 68–81. doi:10.1016/j.semcdb.2015.10.039

Ugrankar, R., Berglund, E., Akdemir, F., Tran, C., Kim, M. S., Noh, J., et al. (2015). Drosophila Glucome Screening Identifies Ck1alpha as a Regulator of Mammalian Glucose Metabolism. *Nat. Commun.* 6, 7102. doi:10.1038/ncomms8102

Ugrankar, R., Bowerman, J., Hariri, H., Chandra, M., Chen, K., Bossanyi, M. F., et al. (2019). Drosophila Snazarus Regulates a Lipid Droplet Population at Plasma Membrane-Droplet Contacts in Adipocytes. *Dev. Cel* 50 (5), 557–572. doi:10.1016/j.devcel.2019.07.021

Ugrankar, R., Liu, Y., Provaznik, J., Schmitt, S., and Lehmann, M. (2011). Lipin Is a Central Regulator of Adipose Tissue Development and Function in *Drosophila melanogaster*. *Mol. Cel Biol* 31 (8), 1646–1656. doi:10.1128/mcb.01335-10

Ussar, S., Lee, K. Y., Dankel, S. N., Boucher, J., Haering, M. F., Kleinridders, A., et al. (2014). ASC-1, PAT2, and P2RX5 Are Cell Surface Markers for white, Beige, and Brown Adipocytes. *Sci. Transl Med.* 6 (247), 247ra103. doi:10.1126/scitranslmed.3008490

Waldén, T. B., Hansen, I. R., Timmons, J. A., Cannon, B., and Nedergaard, J. (2012). Recruited vs. Nonrecruited Molecular Signatures of Brown, "brite," and white Adipose Tissues. *Am. J. Physiol. Endocrinol. Metab.* 302 (1), E19–E31. doi:10.1152/ajpendo.00249.2011

Walther, T. C., and Farese, R. V. (2012). Lipid Droplets and Cellular Lipid Metabolism. *Annu. Rev. Biochem.* 81, 687–714. doi:10.1146/annurev-biochem-061009-102430

Wang, B., Moya, N., Niessen, S., Hoover, H., Mihaylova, M. M., Shaw, R. J., et al. (2011). A Hormone-dependent Module Regulating Energy Balance. *Cell* 145 (4), 596–606. doi:10.1016/j.cell.2011.04.013

Waqas, S. F. H., Hoang, A. C., Lin, Y.-T., Ampem, G., Azegrouz, H., Balogh, L., et al. (2017). Neuropeptide FF Increases M2 Activation and Self-Renewal of Adipose Tissue Macrophages. *J. Clin. Invest.* 127 (7), 2842–2854. doi:10.1172/jci90152

Watts, J. L. (2009). Fat Synthesis and Adiposity Regulation in *Caenorhabditis elegans*. *Trends Endocrinol. Metab.* 20, 58–65. doi:10.1016/j.tem.2008.11.002

Weaver, L. N., and Drummond-Barbosa, D. (2019). The Nuclear Receptor Seven up Functions in Adipocytes and Oenocytes to Control Distinct Steps of Drosophila Oogenesis. *Dev. Biol.* 456 (2), 179–189. doi:10.1016/j.ydbio.2019.08.015

Weaver, L. N., and Drummond-Barbosa, D. (2020). The Nuclear Receptor Seven up Regulates Genes Involved in Immunity and Xenobiotic Response in the Adult drosophila Female Fat Body. *G3 Genes, Genomes, Genet.* 10 (12), 4625–4635. doi:10.1534/g3.120.401745

Werthebach, M., Stewart, F. A., Gahlen, A., Mettler-Altmann, T., Akhtar, I., Maas-Enriquez, K., et al. (2019). Control of Drosophila Growth and Survival by the Lipid Droplet-Associated Protein CG9186/Sturkopf. *Cel Rep* 26 (13), 3726–3740.doi:10.1016/j.celrep.2019.02.110

Whittle, A. J., López, M., and Vidal-Puig, A. (2011). Using Brown Adipose Tissue to Treat Obesity - the central Issue. *Trends Mol. Med.* 17, 405–411. doi:10.1016/j.molmed.2011.04.001

Wilfling, F., Wang, H., Haas, J. T., Krahmer, N., Gould, T. J., Uchida, A., et al. (2013). Triacylglycerol Synthesis Enzymes Mediate Lipid Droplet Growth by Relocalizing from the ER to Lipid Droplets. *Dev. Cel* 24 (4), 384–399. doi:10.1016/j.devcel.2013.01.013

Wilson, E. O. (2013). *Letter to a Young Scientist*. 18th ed. Harvard: Liveright.

Wu, J., Boström, P., Sparks, L. M., Ye, L., Choi, J. H., Giang, A.-H., et al. (2012). Beige Adipocytes Are a Distinct Type of Thermogenic Fat Cell in Mouse and Human. *Cell* 150 (2), 366–376. doi:10.1016/j.cell.2012.05.016

Wu, J., Cohen, P., and Spiegelman, B. M. (2013). Adaptive Thermogenesis in Adipocytes: Is Beige the New Brown? *Genes Dev.* 27, 234–250. doi:10.1101/gad.211649.112

Yadav, A., Kataria, M. A., Saini, V., and Yadav, A. (2013). Role of Leptin and Adiponectin in Insulin Resistance. *Clinica Chim. Acta* 417, 80–84. doi:10.1016/j.cca.2012.12.007

Yamada, T., Habara, O., Kubo, H., and Nishimura, T. (2018). Fat Body Glycogen Serves as a Metabolic Safeguard for the Maintenance of Sugar Levels in drosophila. *Dev* 145 (6), 65. doi:10.1242/dev.158865

Yamaguchi, M., and Yoshida, H. (2018). Drosophila as a Model Organism. *Adv. Exp. Med. Biol.*. 1076, 1–10. doi:10.1007/978-981-13-0529-0_1

Yin, J., Spillman, E., Cheng, E. S., Short, J., Chen, Y., Lei, J., et al. (2021). Brain-specific Lipoprotein Receptors Interact with Astrocyte Derived Apolipoprotein and Mediate Neuron-Glia Lipid Shuttling. *Nat. Commun.* 12 (1), 7. doi:10.1038/s41467-021-22751-7

Young, S. G., and Zechner, R. (2013). Biochemistry and Pathophysiology of Intravascular and Intracellular Lipolysis. *Genes Develop. Genes Dev* Vol. 27, 459–484. doi:10.1101/gad.209296.112

Yu, H., Dilbaz, S., Coßmann, J., Hoang, A. C., Diedrich, V., Herwig, A., et al. (2019). Breast Milk Alkylglycerols Sustain Beige Adipocytes through Adipose Tissue Macrophages. *J. Clin. Invest.* 129 (6), 2485–2499. doi:10.1172/jci125646

Zhang, L., Ip, C. K., Lee, I. J., Qi, Y., Reed, F., Karl, T., et al. (2018). Diet-induced Adaptive Thermogenesis Requires Neuropeptide FF Receptor-2 Signalling. *Nat. Commun.* 9 (1), 4722. doi:10.1038/s41467-018-06462-0

Zhao, X., and Karpac, J. (2017). Muscle Directs Diurnal Energy Homeostasis through a Myokine-dependent Hormone Module in Drosophila. *Curr. Biol.* 27 (13), 1941–1955.e6. doi:10.1016/j.cub.2017.06.004

Zimmermann, R., Strauss, J. G., Haemmerle, G., Schoiswohl, G., Birner-Gruenberger, R., Riederer, M., et al. (2004). Fat Mobilization in Adipose Tissue Is Promoted by Adipose Triglyceride Lipase. *Science* 306 (5700), 1383–1386. doi:10.1126/science.1100747

Zweytick, D., Athenstaedt, K., and Daum, G. (2000). Intracellular Lipid Particles of Eukaryotic Cells. *Biochim. Biophys. Acta (Bba) - Rev. Biomembranes* 1469, 101–120. doi:10.1016/s0005-2736(00)00294-7

Conflict of Interest: The authors declare that the research was conducted in the absence of any commercial or financial relationships that could be construed as a potential conflict of interest.

Publisher's Note: All claims expressed in this article are solely those of the authors and do not necessarily represent those of their affiliated organizations, or those of the publisher, the editors, and the reviewers. Any product that may be evaluated in this article, or claim that may be made by its manufacturer, is not guaranteed or endorsed by the publisher.

frontiers in Cell and Developmental Biology

ORIGINAL RESEARCH
published: 04 January 2022
doi: 10.3389/fcell.2021.757781

The Role of Bmp- and Fgf Signaling Modulating Mouse Proepicardium Cell Fate

Carlos Garcia-Padilla[1,2], *Francisco Hernandez-Torres*[1,3,4], *Estefania Lozano-Velasco*[1,3], *Angel Dueñas*[1], *Maria del Mar Muñoz-Gallardo*[1], *Isabel S. Garcia-Valencia*[1], *Lledó Palencia-Vincent*[1], *Amelia Aranega*[1,3] *and Diego Franco*[1,3]*

[1]*Cardiovascular Development Group, Department of Experimental Biology, University of Jaen, Jaen, Spain,* [2]*Department of Anatomy, Embryology and Zoology, School of Medicine, University of Extremadura, Badajoz, Spain,* [3]*Fundación Medina, Granada, Spain,* [4]*Department of Biochemistry and Molecular Biology, School of Medicine, University of Granada, Granada, Spain*

OPEN ACCESS

Edited by:
Rosa Barrio, CIC BioGUNE, Spain

Reviewed by:
Katherine Yutzey, Cincinnati Children's Hospital Medical Center, United States
Christos G. Zervas, Biomedical Research Foundation of the Academy of Athens (BRFAA), Greece

***Correspondence:**
Diego Franco
dfranco@ujaen.es

Specialty section:
This article was submitted to Signaling, a section of the journal Frontiers in Cell and Developmental Biology

Received: *12 August 2021*
Accepted: *06 December 2021*
Published: *04 January 2022*

Citation:
Garcia-Padilla C, Hernandez-Torres F, Lozano-Velasco E, Dueñas A, Muñoz-Gallardo MdM, Garcia-Valencia IS, Palencia-Vincent L, Aranega A and Franco D (2022) The Role of Bmp- and Fgf Signaling Modulating Mouse Proepicardium Cell Fate. Front. Cell Dev. Biol. 9:757781. doi: 10.3389/fcell.2021.757781

Bmp and Fgf signaling are widely involved in multiple aspects of embryonic development. More recently non coding RNAs, such as microRNAs have also been reported to play essential roles during embryonic development. We have previously demonstrated that microRNAs, i.e., miR-130, play an essential role modulating Bmp and Fgf signaling during early stages of cardiomyogenesis. More recently, we have also demonstrated that microRNAs are capable of modulating cell fate decision during proepicardial/septum transversum (PE/ST) development, since over-expression of miR-23 blocked while miR-125, miR-146, miR-223 and miR-195 enhanced PE/ST-derived cardiomyogenesis, respectively. Importantly, regulation of these microRNAs is distinct modulated by Bmp2 and Fgf2 administration in chicken. In this study, we aim to dissect the functional role of Bmp and Fgf signaling during mouse PE/ST development, their implication regulating post-transcriptional modulators such as microRNAs and their impact on lineage determination. Mouse PE/ST explants and epicardial/endocardial cell cultures were distinctly administrated Bmp and Fgf family members. qPCR analyses of distinct microRNAs, cardiomyogenic, fibrogenic differentiation markers as well as key elements directly epithelial to mesenchymal transition were evaluated. Our data demonstrate that neither Bmp2/Bmp4 nor Fgf2/Fgf8 signaling is capable of inducing cardiomyogenesis, fibrogenesis or inducing EMT in mouse PE/ST explants, yet deregulation of several microRNAs is observed, in contrast to previous findings in chicken PE/ST. RNAseq analyses in mouse PE/ST and embryonic epicardium identified novel Bmp and Fgf family members that might be involved in such cell fate differences, however, their implication on EMT induction and cardiomyogenic and/or fibrogenic differentiation is limited. Thus our data support the notion of species-specific differences regulating PE/ST cardiomyogenic lineage commitment.

Keywords: Bmp, Fgf, proepicardium, cell fate, heart development

INTRODUCTION

Bmp and Fgf signaling are widely involved in multiple aspects of embryonic development (Ornitz and Itoh, 2015; Ornitz and Marie, 2015; Wu et al., 2016; Graf et al., 2016; Salazar et al., 2016; Zinski et al., 2018; Xie et al., 2020; Mossahebi-Mohammadi et al., 2020). Within the developing cardiovascular system, Bmp and Fgf signaling plays essential roles in the determination and specification of the cardiogenic progenitors (Cohen et al., 2007; Hutson et al., 2010; Tirosh-Finkel et al., 2010; Razy-Krajka et al., 2018) as well as in other cardiovascular morphogenetic events such as valve development (Zhao B. et al., 2007; Cushing et al., 2008; Zhang et al., 2010; Zhang et al., 2012). In particular, the role of Bmp and Fgf has also been reported during the formation of the proepicardium/septum transversum (PE/ST) (Torlopp et al., 2010), providing signaling cues to direct the pericardial mesoderm to either proepicardial or myocardial fate (Kruithof et al., 2006; van Wijk et al., 2009). In this context, Bmp2 stimulates cardiomyocyte formation while Fgf2 stimulates epicardial differentiation in chicken embryos. Importantly, there are several discrepancies as whether the PE/ST is capable of giving rise to myocardial cells in mice (Cai et al., 2008; Zhou et al., 2008) as well as whether proepicardial cells are already committed to give rise to distinct cell types such as fibroblasts, endothelial and/or smooth muscle cells at this early developmental stage (Merki et al., 2005; Cai et al., 2008; Zhou et al., 2008; Red-Horse et al., 2010).

Bmp and Fgf signaling have been reported to be modulated by microRNAs (Wang et al., 2010; Icli et al., 2013; Lu et al., 2013; Gan et al., 2016; Pravoverov et al., 2019). In particular, during early cardiac progenitor differentiation, miR-130 has been reported to modulate Fgf8-Bmp2 signaling (Lopez-Sanchez et al., 2015a), providing an intricate regulatory feedback mechanism between with these growth factors and miR-130 that defines the temporal and spatial cues of cardiomyogenic lineage differentiation. More recently we have reported that over-expression of distinct microRNAs in chicken PE/ST, particularly miR-195 and miR-223, influenced cell fate determination of the PE cells, leading to increased formation of myocardial cells, a process that is dependent of Smurf1 and Smad3 (Dueñas et al., 2020). Importantly, miR-195 is distinctly modulated by Bmp and Fgf signaling, supporting a role of this microRNA in the Bmp- and Fgf-directed PE cell specification (Dueñas et al., 2020).

However, scarce evidences are reported as whether Bmp and Fgf signaling plays a role in PE development in mice (Li et al., 2017; Shah et al., 2017). In this context, it is important to highlight that mouse and chicken morphogenesis displayed substantial differences. In mice, two bilateral PE anlage are formed that subsequently fused in the embryonic midline to provide a single PE (Torlopp et al., 2010) while in chicken two anlagen are also formed but only the right-sided one is finally fully developed (Schlueter et al., 2006; Schulte et al., 2007; Schlueter and Brand, 2009; Schlueter and Brand, 2013). While the signalling pathways driving PE development have been substantially characterized (Schlueter et al., 2006; Schulte et al., 2007; Schlueter and Brand, 2009; Schlueter and Brand, 2013), our current understanding of the molecular mechanisms directing murine PE development is still incipient. In addition, epicardial colonization of the embryonic myocardium is also distinctly achieved between chicken and mice (Perez-Pomares et al., 1998; Vrancken Peeters et al., 1999; Manner et al., 2001; Perez-Pomares et al., 2002; Hirose et al., 2006). Furthermore, to date, no evidence of the functional role of discrete microRNAs have been reported regarding the development of the PE in mice, yet deletion of the *Dicer* processing enzyme highlighted their importance (Singh et al., 2011).

In this study, we dissected the functional role of Bmp and Fgf signaling during mouse PE/ST development, their implication regulating post-transcriptional modulators such as microRNAs and their impact on lineage determination. Mouse PE/ST explants, epicardial and endocardial cell cultures were distinctly administrated Bmp and Fgf family members. qPCR analyses demonstrates that Bmp and Fgf family members distinctly regulate microRNAs with potential to inhibit or to enhance PE/ST-derived cardiomyogenic differentiation. Surprisingly, neither those microRNAs with inducing capacity nor the cardiomyogenic inducing capacity previously documented in chicken PE/ST explants was recapitulated in mouse PE/ST explants, supporting the notion of specific-specific differences in PE/ST mouse and chicken development and lineage commitment response.

MATERIALS AND METHODS

Isolation of Proepicardium/Septum Transversum Explants

Experimental protocols were performed in agreement with the Spanish law in application of EU Guidelines for animal research. These protocols conformed to the Guide for Care and Use of Laboratory Animals, published by the US National Institutes of Health (NIH publication no. 85–23). Approved consent of the Ethic Committee of the University of Jaen was obtained prior to the initiation of the study. CD1 pregnant female mice were obtained at embryonic day (ED) 9.5. Embryos were removed from the uterus using iredectomy scissors and placing them into Earle's balanced salt solution (EBSS) (Gibco). PE/ST were manually dissected and transferred to EBSS solution. Subsequently they were placed into DMEM culture medium, cultured in hanging drops until appropriately treated with different growth factors and/or transfection agents as detailed below.

EPIC and MEVEC Cell Cultures

Inmortalized embryonic endocardial MEVEC (D'Amato et al., 2016) and epicardial EPIC (Ruiz-Villalba et al., 2013) cells (6×10^5 cells per well) were cultured in DMEM medium supplemented with 10% fetal bovine serum, 100 U/mL penicillin, 100 µg/ml streptomycin and 200 nM of L-glutamine in 100 cm^2 culture disk at 37°C in a humidified atmosphere of 5% CO_2, respectively. Cells were

fed every 2–3 days. Sub-cultured cells were treated with different growth factors (50 ng/μL) as detailed below for 24 h.

Growth Factor Administration

PE/ST explants were treated for 24 h with Bmp2, Bmp4, Bmp6, Bmp7, Bmp10, Fgf2, Fgf5, Fgf7, Fgf8 and Fgf10 (Peprotech, East Brunswick, NJ, United States), respectively, as reported by Dueñas et al. (2020). Tissue explants were collected and processed according for qPCR and/or immunohistochemistry. Each experimental condition was carried out in isolated tissues from at least 20 embryos. In all cases, 3–5 independent biological replicates were analyzed.

MicroRNA Transfections

Mouse E9.5 PE explants were cultured on collagen gels for 24 h at 37°C in a cell culture incubator before pre-miRNAs (microRNA precursors) administration as previously reported (Bonet et al., 2015; Dueñas et al., 2020). Pre-miRNAs (Thermo-Fisher) transfections were carried out with Lipofectamine 2000 (Invitrogen), following the manufacturer's guidelines. Briefly, 85 nM of pre-miRNA were applied to the explants (3–5 explants per well) for 24 h. After incubation, explants were processed for immunohistochemical (IHC) analyses. Negative controls, i.e. E9.5 PE explants treated only with Lipofectamine, were run in parallel. To perform IHC analyses, the explants were fixed with 1% PFA for 2 h at 4°C, rinsed for three times in PBS during 10 min, and stored in PBS at 4°C. Each experimental condition was carried out in isolated tissues from at least 20 embryos. In all cases, 3–5 independent biological replicates were analyzed.

Immunofluorescence Analyses by Confocal Laser Scanning Microscopy

Immunofluorescence analyses were performed as previously reported (Bonet et al., 2015; Dueñas et al., 2020). Briefly, control and experimental mouse E9.5 PE explants were collected after the corresponding treatment, rinsed in PBS for 10 min at room temperature, and fixed with 1% PFA for 2 h at 4°C. After fixation, the samples were rinsed three times (10 min each) in PBS at room temperature and then permeabilized with 1% Triton X-100 in PBS for 30 min at room temperature. To block nonspecific binding sites, PBS containing 5% goat serum and 1% bovine serum albumin (Sigma) was applied to the explants overnight at 4°C. As primary antibody, a polyclonal goat anti-cardiac troponin I (Hytest) was used, diluted (1:200) in PBS, and applied to each culture overnight at 4°C. Subsequently, the samples were rinsed three times (for 1 h each) in PBS to remove excess primary antibody and incubated overnight at 4°C with Alexa-Fluor 546 anti-goat (1:100; Invitrogen) as secondary antibody. After incubation with the secondary antibody, the explants were rinsed as described above. Finally, the explants and/or epicardial cell cultures, respectively, were incubated with phalloidin (1:1,000; Thermo-Fisher) overnight, and DAPI (1:1,000; Sigma) for 7 min at room temperature and rinsed three times in PBS for 5 min each. Explants were stored in PBS in darkness at 4°C until analyzed using a Leica TCS SP5 II confocal scanning laser microscope.

RNA Isolation and qPCR Analyses

All RT-qPCR experiments followed MIQE guidelines (Bustin et al., 2001) and similarly as previously reported (Bonet et al., 2015; Lozano-Velasco et al., 2015; Dueñas et al., 2020). Briefly, RNA was extracted and purified by using Trizol reactive (Invitrogen) according to the manufacturer's instructions. For mRNA expression measurements, 1 μg of total RNA was used for retro-transcription with Maxima First Strand cDNA Synthesis Kit for RT-qPCR (Thermo Scientific). Real time PCR experiments were performed with 1 μL of cDNA, SsoFast EvaGreen mix and corresponding primer sets. For microRNA expression analyses, 20 ng of total RNA was used for retrotranscription with Universal cDNA Synthesis Kit II (Qiagen) and the resulting cDNA was diluted 1/80. Real time PCR experiments were performed with 1 μL of diluted cDNA, ExiLENT SYBR Green master mix (Qiagen) and corresponding primer sets. microRNA primers were purchased from ThermoFisher and mRNA primers were custom designed using Primer3 software (**Supplementary Table S1**). All qPCRs were performed using a CFX384TM thermocycler (Bio-Rad) following the manufacturer's recommendations. The relative level of expression of each gene was calculated as described by Livak and Schmittgen (2001) using *Gapdh* and *Gusb* as internal control for mRNA expression analyses and *5S* and *6U* for microRNA expression analyses, respectively. Each PCR reaction was carried out in triplicate and repeated in at least three distinct biological samples to obtain representative means.

Statistical Analyses

For statistical analyses of datasets, unpaired Student's t-tests were used, as previously reported (Bonet et al., 2015; Dueñas et al., 2020). Significance levels or p values are stated in each corresponding figure legend. $p < 0.05$ was considered statistically significant.

Mouse Lines and Tissue Collection

Previously described $Wt1^{GFP/+}$ mice used in this study (Cano et al. 2013). Pregnant $Wt1^{GFP/+}$ female mice were harvested to E9.5 and to E10.5, respectively. E9.5 PE were manually dissected, pooled and stored in liquid nitrogen until used. E10.5 EE was FACS-sorted as previously described, pooled and stored in liquid nitrogen until used. At least 3-5 litters were used on each developmental stage until sufficient tissues was collected that would guarantee optimal RNA isolation.

miRNAseq Library Preparation, Sequencing and Proccesing of FastQ Files

500 pg of total RNA were used to generate barcoded miRNA-seq libraries using the *Bioo NEXTflex Small RNA* (BiooScientific). Briefly, 3′ and 5′ SR adapters were first ligated to the RNA sample. Next, reverse transcription followed by PCR amplification was

used to enrich cDNA fragments with adapters at both ends. Adapter-ligated cDNA fragments from different samples were pooled and run in a 6% polyacrilamide gel. The 147 nt band, corresponding to the pooled miRNA libraries, was purified from the gel. Finally, the quantity and quality of the pooled miRNA libraries were determined using the Agilent 2100 Bioanalyzer High Sensitivity DNA chip. Libraries were sequenced on a HiSeq 2500 (Illumina) and processed with RTA v1.18.66.3. FastQ files for each sample were obtained using bcl2fastq v2.20.0.422 software (Illumina). Sequencing reads were aligned to the mouse reference genome (mm10) with HISAT2 v2.10.0 (Kim et al., 2015) and then extracted the miRNA counts with featureCounts (Liao et al., 2014) and miRBase (Kozomara and Griffiths-Jones 2014) GFF3 for mouse. Raw counts were normalized with TPM (Transcripts per Million) and TMM (Trimmed Mean of M-values) methods, transformed into log2 expression [log2 (rawCount+1)] and compared to calculate fold-change and corrected pValue. The limits for the differential expression were Log2FC > 0.584 (1.5x) and corrected p Value <0.05. Only miRNAs detected in the three replicates of any condition were use in the analysis. These data are uploaded into Gene Expresssion Onmibus platform with accession number GSE189344.

mRNAseq Library Preparation, Sequencing and Proccesing of FastQ Files

First 2.5 ng of total RNA were used to amplify the cDNA using the *SMART-Seq v4 Ultra Low Input RNA Kit* (Clontech-Takara). 1 ng of amplified cDNA was used to generate barcoded libraries using the *Nextera XT DNA library preparation kit* (Illumina). Basically, cDNA is fragmented and adapters are added in a single reaction followed by an amplification and clean up. The size of the libraries was checked using the Agilent 2100 Bioanalyzer High Sensitivity DNA chip and their concentration was determined using the Qubit® fluorometer (ThermoFisher Scientific). Libraries were sequenced on a HiSeq 2500 (Illumina) and processed with RTA v1.18.66.3. FastQ files for each sample were obtained using bcl2fastq v2.20.0.422 software (Illumina). Sequencing reads were aligned to the mouse reference transcriptome (mm10 v92) and quantified with RSem v1.3.1 (Li and Dewey 2011). Raw counts were normalized with TPM (Transcripts per Million) and TMM (Trimmed Mean of M-values) methods, transformed into log2 expression [log2 (rawCount+1)] and compared to calculate fold-change and corrected pValue. The limits for the differential expression were Log2FC > 0.584 (1.5x) and corrected pValue <0.05. Only mRNAs detected in three transcriptomes were use in the analysis. These data are uploaded into Gene Expresssion Onmibus platform with accession number GSE189344.

Heatmap Representation

Normalized RNAseq data were graphically plotted as heatmaps using Morpheus software (https://software.broadinstitute.org/morpheus/).

RESULTS

miR-195 and miR-223 Does Not Enhance Proepicardium-Derived Cardiogenesis in Mice

Previous reports in our laboratory demonstrated that ectopic administration of miR-195 and miR-223, respectively, enhanced cardiomyogenesis in PE/ST explants in chicken (Dueñas et al., 2020). We now tested whether this process is also occurring in mouse PE/ST explants. As depicted in **Figure 1A**, mouse PE/ST explants were dissected and treated with miR-195 and miR-223, respectively, for 24 h and subsequently fixed for confocal image analyses. Analyses of cardiomyocyte terminal differentiation marker cardiac troponin demonstrate that neither miR-195 nor miR-223 enhanced cardiomyogenesis in mouse PE/ST explants (**Figures 1B–E**).

Bmp and Fgf Signalling in Mouse PE E9.5 Explants

We have previously reported that Bmp and Fgf family members, can distinctly modulate the expression of microRNAs that can differently modulate PE/ST-derived cardiomyogenesis. Thus, we have administered Bmp2, Bmp4, Fgf2 and Fgf8 to mouse E9.5 PE explants and tested the expression of distinct microRNAs previously involved in PE cell determination in chicken. Bmp2 administration eliminated miR-100 expression, increased miR-195b expression while miR-23b, miR-27b, miR-125a, miR-125b, miR-146b, miR-195a and miR-223 displayed no significant differences (**Figure 2**). Bmp4 administration increased miR-23b, miR-27b, miR-100 and miR-195a, eliminated miR-223 while no significant differences were observed for miR125a, miR-125b and miR-195b (**Figure 2**). Of note, miR-125a miR-125b and miR-146b display an enhanced trend but reached no statistical significance. Fgf2 administration increased miR-23b, miR-27b, miR-146b, miR-195a and miR-195b, while no changes were observed for miR-100, miR-125a, miR-125b and miR-223 (**Figure 1**). Finally, Fgf8 administration leads to increase of miR-23b, miR-100, miR-146b, miR-195a, miR-195b and miR-223, but no significant differences on miR-27b, miR-125a and miR-125b expression (**Figure 2**). Overall, these data demonstrate that distinct Bmp and Fgf family members can differentially modulate those microRNAs that significantly enhanced cardiomyogenesis (miR-195a, miR-195b and miR-223), those that mildly enhanced it (miR-125a, miR-125b and miR-146b) and those that do not enhance or even inhibit it (miR-23b, miR-27b and miR-100). Surprisingly, enhanced miR-195a, miR-195b and/or miR-223 is similarly observed for Bmp2/Bmp4 *vs* Fgf2/Fgf8 in mouse PE/ST explants, in contrast to our previous findings in chicken PE/ST, suggesting clear species-specific differences.

We subsequently tested if these growth factors could influence the expression of molecular markers involved in early (Mef2c, Nkx2.5, Gata4, Srf) and terminal (Tnnt2) differentiation of cardiomyogenesis. Bmp2 administration significantly increased Mef2c and Gata4 expression, Nkx2.5 and Tnnt2 were decreased and Srf displayed no significant differences (**Figure 3A**). Bmp4

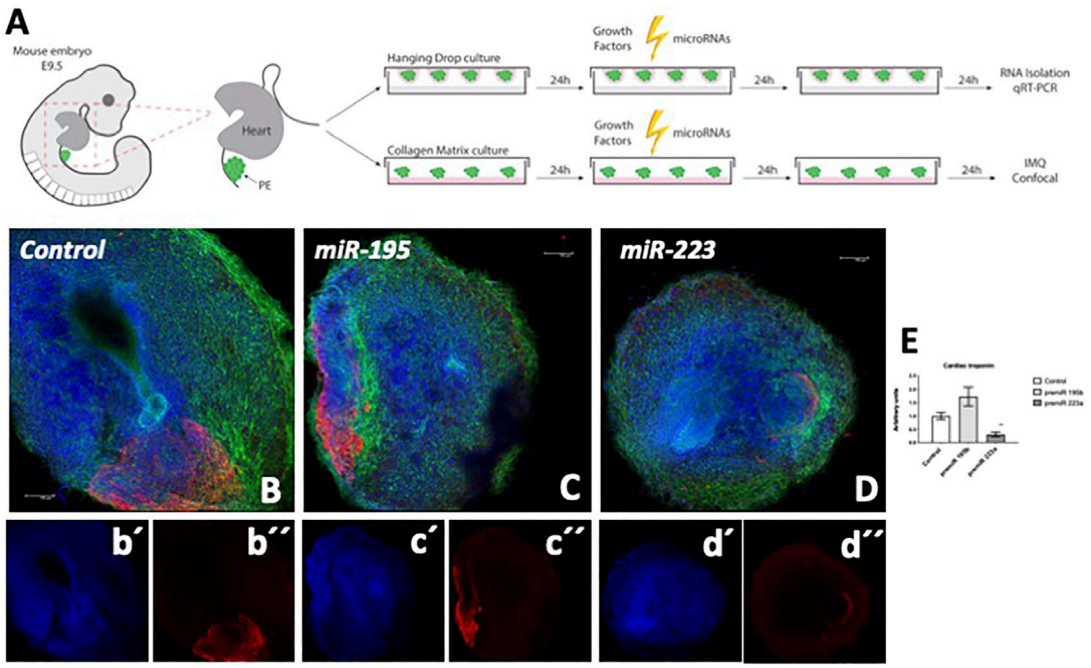

FIGURE 1 | Panel **(A)** Schematic representation of the experimental design of mouse PE/ST isolation, transfection with microRNAs or growth factor administration and subsequent analyses. Panels **(B–D)** Confocal microscopy analyses of cardiac troponin expression (red) in mouse E9.5 PE/ST explants treated with control **(B)** miR-195 mimics **(C)**, miR-223 mimics (D), respectively. Single channel confocal images of Dapi and cardiac troponin are depicted for control (b´, b´´), miR-195 (c´, c´´) and miR-233 (d´, d´´) treated explants, respectively. Panel **(E)** displays quantitation of mean cardiac troponin positive areas in each experimental condition ($n = 5$). Note that the cardiac troponin expression is similarly observed in miR-195 treated explants and controls, while a significant decreased in miR-223 treated explants is observed. Blue (DAPI), phalloidin (green).

and Fgf2 administration decreased Nkx2.5 and Tnnt2 while no significant differences were observed for the other markers analyzed (**Figure 3A**). Fgf8 administration did not modify any of the markers analyzed (**Figure 3A**). Importantly, analyses of fibrogenesis (Col1a1) and epithelial to mesenchymal transition (EMT) (Snail1, Snail2, Cdh5) markers were not significantly modulated by any of these growth factors, i.e. Bmp2, Bmp4, Fgf2, and Fgf8 (**Figure 3B**) while epicardial markers such as Wt1, Tcf21 and Tbx18 were either inhibited and/or not modified. Only Fgf8 administration significantly increased Tcf21 and Tbx18 expression (**Figure 3B**).

Differential Expression of Bmp and Fgf Family Members in Mouse PE/EE Transition

Given the fact that Bmp2, Bmp4, Fgf2 and Fgf8 distinct modulate microRNA expression and cardiomyogenic lineage determination in chicken and mouse PE/ST, and given the divergent morphogenetic events that occur between these two species, we took advantage of our recent performed comprehensive analysis of coding and non-coding RNA differential gene expression in mouse E9.5 proepicardium vs E10.5 embryonic epicardium to unravel the gene regulatory networks involved in PE to EE transition to search for novel Bmp and Fgf members that might be involved in this process (Franco et al., in preparation). Importantly, differential expression of growth factors during these developmental conditions have unraveled Bmp4, Bmp5, Bmp7, and Bmp10 are highly expressed in the PE at E9.5 while Bmp2, Bmp3 and Bmp6 display enhanced expression at E10.5 embryonic epicardium (**Figure 4**). In line with previous reports in chicken PE development, Bmp2 and Bmp4 are distinctly expressed during PE/EE development, but in addition novel Bmp members are also identified during mouse PE that were unnoticed during chicken development, such as Bmp5, Bmp7 and Bmp10 that might plays significant roles during PE/EE transition. Similarly, Fgf5, Fgf7, Fgf10, Fgf11 and Fgf12 are highly expressed in the PE at E9.5 while Fgf1, Fgf2, Fgf5, Fgf9 and Fgf18 display enhanced expression at E10.5 embryonic epicardium (**Figure 4**). Surprisingly, Fgf8 was not detected in our RNAseq analyses, pointing out to differential Fgf expression during PE/EE development in chicken and mice. Furthermore, our data also unraveled novel Fgf members that might be potentially involved in mouse PE/EE development, such as Fgf5, Fgf7, Fgf10, Fgf11 and Fgf12.

Novel Regulatory Roles of Bmp and Fgf Family Members During PE/ST Differentiation

To dissect the plausible signaling role these differentially expressed Bmp and Fgf family members during mouse PE/ST

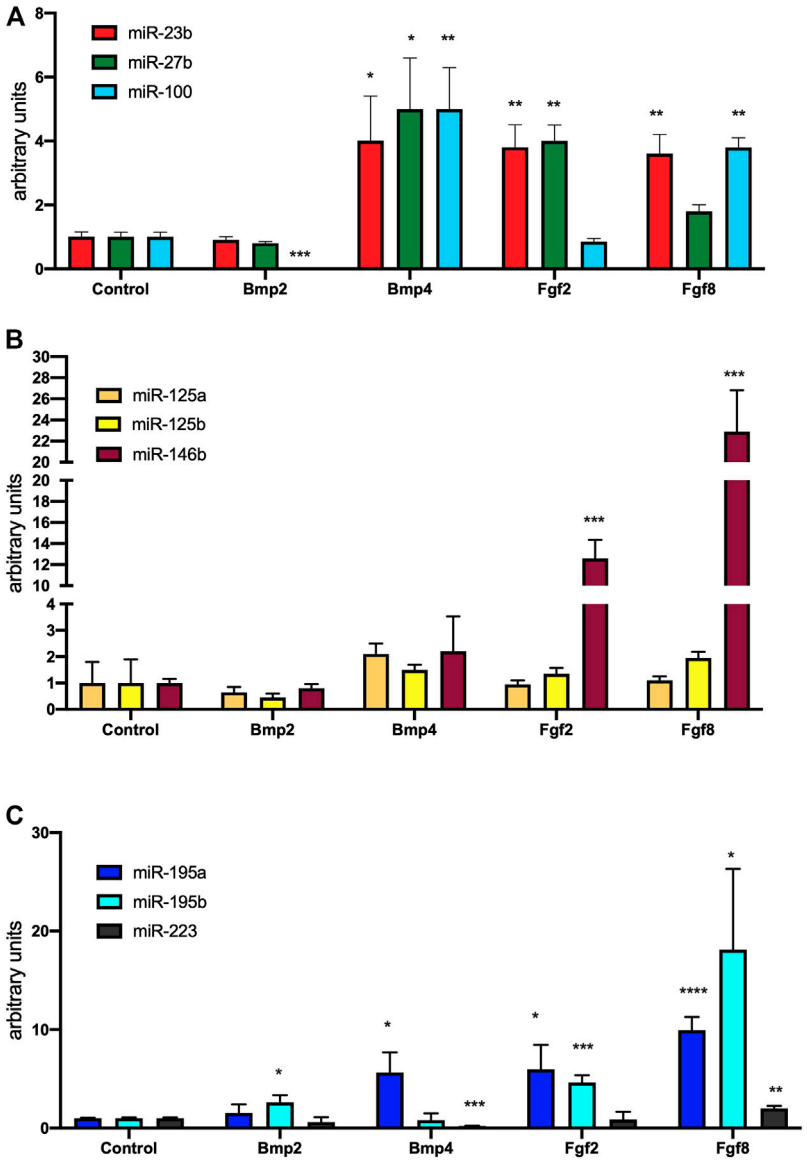

FIGURE 2 | Panel **(A)** RT-qPCR analyses of miR-23b, miR-27b and miR-100 expression after control, Bmp2, Bmp4, Fgf2 and Fgf8 treatments, respectively, to mouse E9.5 PE/ST explants. Panel **(B)** RT-qPCR analyses of miR-125a, miR-125b and miR-146b expression after control, Bmp2, Bmp4, Fgf2 and Fgf8 treatments, respectively, to mouse E9.5 PE/ST explants. Panel **(C)** RT-qPCR analyses of miR-195a, miR-195b and miR-223 expression after control, Bmp2, Bmp4, Fgf2 and Fgf8 treatments, respectively, to mouse E9.5 PE/ST explants. $^{*}p < 0.05$, $^{**}p < 0.01$, $^{***}p < 0.001$, $^{****}p < 0.0001$.

development, we administered Bmp6, Bmp7, Bmp10, Fgf5, Fgf7 and Fgf10 to mouse PE/ST explants and analyzed their role in microRNA and lineage specific expression. Bmp6 and Bmp7 administrated blunted expression of all microRNAs analyzed (miR-23b, miR-27b, miR-100, miR-125a, miR-125b, miR-146b, miR-195a, miR-195b and miR-223) (**Figure 5**). On the other hand, Bmp10 overexpression significantly enhanced miR-27b, miR-100, miR-125a, decreased miR-23b and while no differences were observed for the rest of microRNAs analyzed (miR-146b, miR-195a, miR-195b and miR-223) (**Figure 5**). Curiously, Fgf5 and Fgf7 administration also significantly decreased most of the microRNAs studied (miR-23b, miR-27b, miR-100, miR-146b, miR-195a, miR-195b and miR-223), while no significant differences were observed for miR-125a and miR-125b (**Figure 5**). On the other hand, Fgf10 administration, significantly decreased miR-23b, miR-27b, miR-100, miR-195a and miR-223, significantly enhanced miR-125a, miR-125b and miR-146b and displayed no significant differences for miR-195b (**Figure 5**). Overall, all these data demonstrate that only Fgf10 and Bmp10 are capable of significantly modulate microRNA expression in mouse PE/ST explants. Surprisingly, none of them is nonetheless capable of enhancing those microRNAs robustly enhance cardiomyogenesis (i.e. miR-195a, miR-195b and miR-223), but they are capable of modulating those that

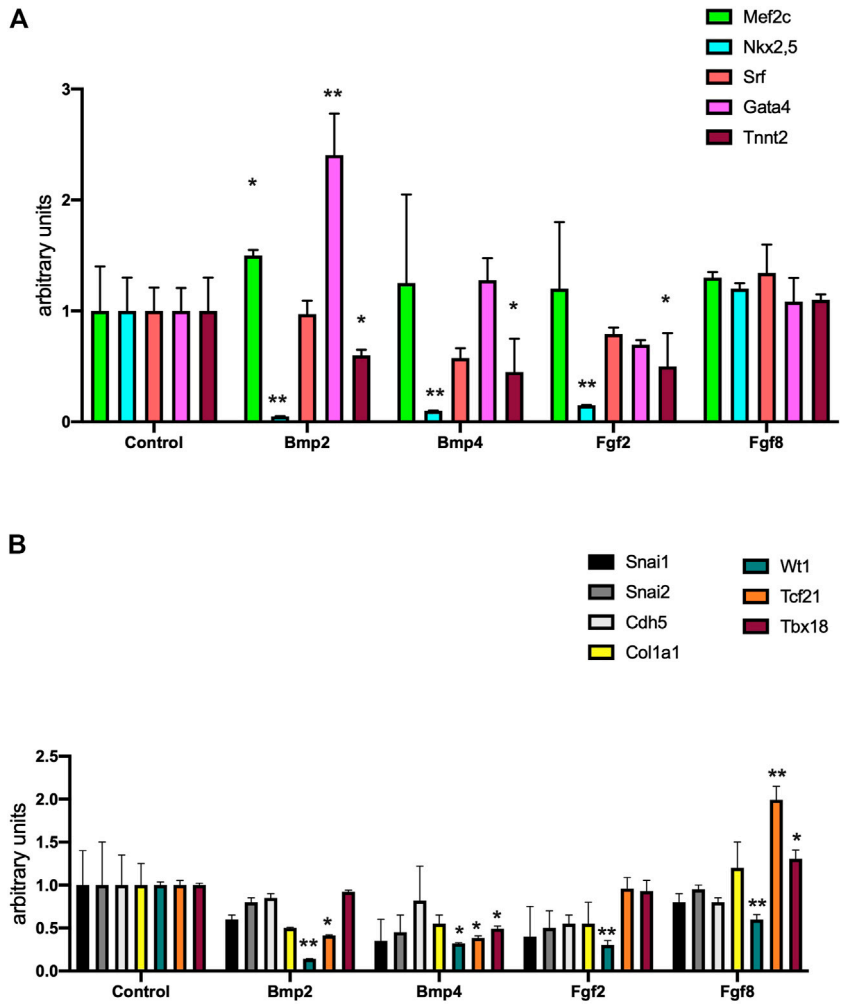

FIGURE 3 | Panel **(A)** RT-qPCR analyses of Mef2c, Nkx2.5, Srf, Gata4 and Tnnt2 expression after control, Bmp2, Bmp4, Fgf2 and Fgf8 treatments, respectively, to mouse E9.5 PE/ST explants. Panel **(B)** RT-qPCR analyses of Snai1, Sna2, Cdh5, Col1a1, Wt1, Tcf21 and Tbx18 expression after control, Bmp2, Bmp4, Fgf2 and Fgf8 treatments, respectively, to mouse E9.5 PE/ST explants. $^{*}p < 0.05$, $^{**}p < 0.01$, $^{***}p < 0.001$, $^{****}p < 0.0001$.

mildly enhance cardiomyogenesis (i.e., miR-125a and miR-125b). Importantly, Bmp10, but not Fgf10 also enhance microRNA expression that leads to consistent cardiomyogenic blockage (miR-27b, miR-100).

We subsequently tested whether these growth factors can influence cardiomyogenic lineage determination. Bmp6 and Bmp7 significantly decreased Nkx2.5 expression while *Mef2c, Srf* and Gata4 were not significantly decreased. *Tnnt2*, a marker of cardiac terminal differentiation was significantly decreased by Bmp6 but not by Bmp7 administration (**Figure 6A**). Bmp10 enhanced expression of all cardiomyogenic markers except *Nkx2.5* and *Tnnt2*. Fgf5 and Fgf7 exclusively increased *Srf* expression while the other tested markers were either decreased (Nkx2.5) or not significantly altered (Mef2c, Gata4 and Tnnt2) (**Figure 6A**). Fgf10 administration resulted in downregulation of Mef2c, Nkx2.5 and Tnnt2, while only Gata4 was up-regulated and Srf displayed no significant differences (**Figure 6A**). Overall, these data demonstrate that although several of these growth factors can promote upregulation of several early molecular markers of cardiogenesis, none of them is capable of inducing terminal cardiomyocyte differentiation.

We subsequently tested these growth factors can influence EMT and/or fibrogenesis. Bmp6 administration only enhance *Snai1* expression, while *Snai2*, Cdh5 and Col1a1 were not significantly altered (**Figure 6B**). Bmp7 only decreased Snai2, while Bmp10 only upregulated Snail1 and Col1a1. On the other hand, Fgf5, Fgf7 and Fgf10 significantly down-regulated Snail1, while Snail2 was also downregulated by Fgf7 and Fg10 administration (**Figure 6B**). In addition, Fgf5 upregulated Col1a1 and Fgf10 decreased Cdh5 expression (**Figure 6B**). Confocal imaging of mouse proepicardial explants treated with Fgf5, Fgf10, Bmp6 and Bmp10, respectively, demonstrate that such growth factors does not significantly promote EMT, in line with our qPCR data (**Figure 7**). In addition, we also demonstrated that epicardial markers such as Wt1, Tcf21 and Tbx18 were

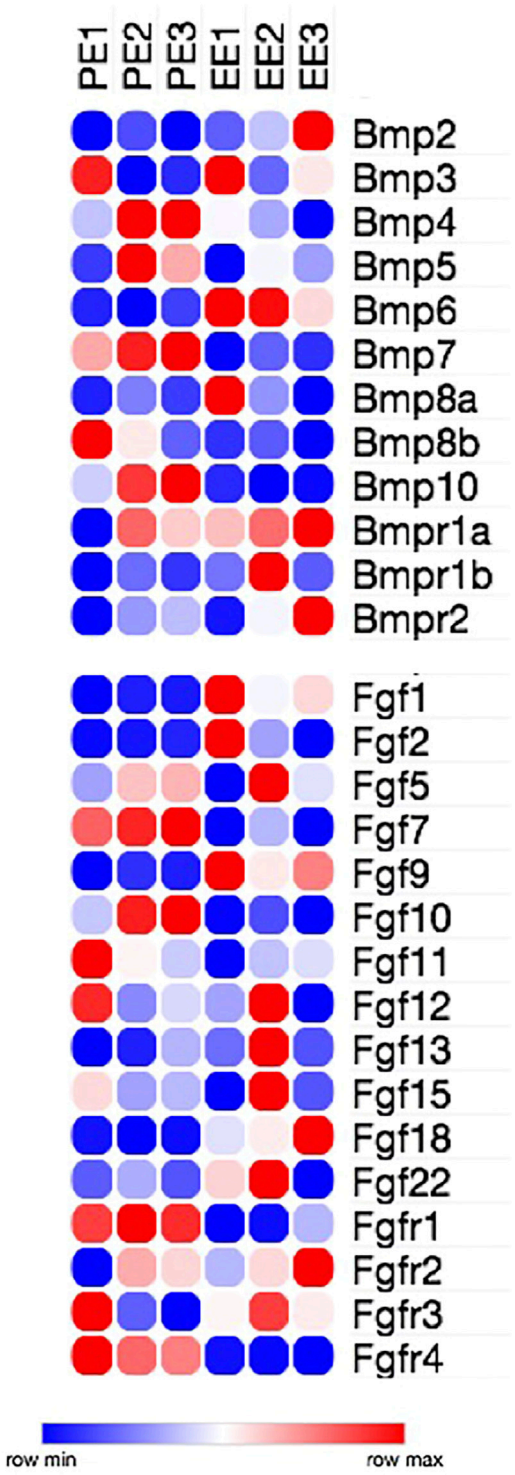

FIGURE 4 | Heatmap representation of Bmp and Fgf family members expression as revealed by RNAseq analyses in mouse E9.5 PE (PE1, PE2 and PE3) and E10.5 embryonic epicardium (EE1, EE2 and EE3).

significantly down-regulated, except for Bmp6 administration that significantly increased Tcf21 expression (**Figure 6B**). In summary, Bmp6 and Bmp10 might mildly enhanced EMT markers but Fgf5, Fgf7 and Fgf10 robustly inhibited them, while none of them effectively promote EMT in explant cultures. Furthermore, fibrogenesis was only up-regulated by Bmp10 and Fgf5.

Bmp and Fgf Signalling in Epicardial vs. Endocardial Cell Lineages

To further support the findings observed in *ex vivo* mouse PE/ST explants, we have administered Bmp2, Bmp4, Fgf2 and Fgf8 to two distinct cell lines, representing epicardial (EPIC; Ruiz-Villalba et al., 2013) and endocardial (MEVEC) cells and tested whether distinct microRNAs previously involved in PE cell determination are modulated by these growth factors. Bmp2 administration enhanced miR-27, miR-125a and miR-195b expression in both cell types, while display opposite regulation in endocardial vs epicardial cells for miR-23b, miR-125b, miR-146b, miR-195a and miR-223 (**Figure 8**). Bmp4 administration increased miR-27b, miR-125a, miR-125b, miR-195b, miR-223, decreased miR-23b while displayed opposite patterns of regulation for miR-146b, respectively (**Figure 8**). Fgf2 administration decreased miR-23b, miR-125a, miR-125b and miR-195a while displayed opposite patterns of regulation for miR-100, miR-185b and miR-223 in both cell types, respectively (**Figure 8**). Fgf8 increased miR-23b, decreased miR-27b and miR-125a in both cell types, while displayed opposite pattern for miR-100, miR-195a, miR-195b and miR-223 (**Figure 8**).

We subsequently monitored if these growth factors could influence the expression of molecular markers involved in early (Mef2c, Gata4, Srf, Nkx2.5) and terminal (Tnnt2) differentiation of cardiomyogenesis, fibrogenesis (Col1a1) and epithelial to mesenchymal transition (EMT) (Snai1, Snai2, Cdh5).

Bmp2 and Bmp4 administration did not modify the expression of any early and terminal differentiation markers in any of the 2 cell types analyzed, except for a significant downregulation of Nkx2.5 in EPIC cells (**Figure 9**). On the other hand, Fgf2 and Fgf8 significantly upregulated Mef2c and Tnnt2 expression in MEVEC, while only Fgf2 administration increased Mef2c but not Tnnt2 expression in EPIC cells (**Figure 9**). Furthermore, both growth factors, i.e. Fgf2 and Fgf8, decreased Nkx2.5 expression in MEVECs and Srf in EPIC while only Fgf2 administration resulted in down-regulation of Nkx2.5 and Tnnt2 in EPIC cells (**Figure 9**). Overall, these data demonstrate that only Fgf2 and Fgf8 are inducing terminal cardiomyocyte differentiation in MEVEC but not in EPIC cells.

Analyses of EMT inductors demonstrated that Bmp2 and Bmp4 can enhance the expression of Snai1 in MEVEC cells and Snai2 in EPIC cells, while Cdh5 expression is only downregulated in MEVEC cells by Bmp2 expression (**Figure 9**). On the other hand, Fgf2 and Fgf8 administration do not modify, or if any decreased, the expression of Snai1 and Snai2 in both cell types. Cdh5 expression is up-regulated by Fgf8 in MEVEC and by Fgf2 in EPIC cells. Fibrogenic marker Col1a1 is significantly upregulated in MEVEC but not in EPIC cells by Fgf2 and Fgf8, while Bmp2 and Bmp4 administrations does not

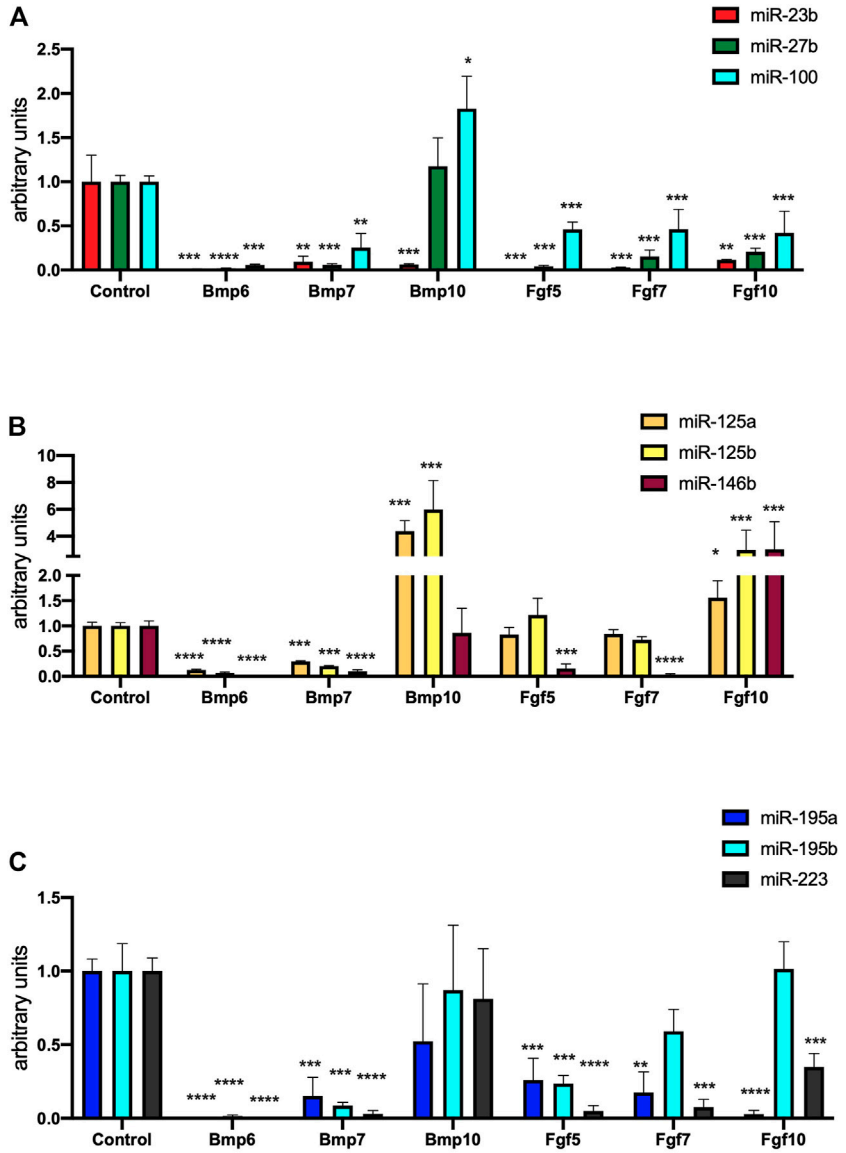

FIGURE 5 | Panel **(A)** RT-qPCR analyses of miR-23b, miR-27b and miR-100 expression after control, Bmp6, Bmp7, Bmp10, Fgf5, Fgf7 and Fgf10 treatments, respectively, to mouse E9.5 PE/ST explants. Panel **(B)** RT-qPCR analyses of miR-125a, miR-125b and miR-146b expression after control, Bmp6, Bmp7, Bmp10, Fgf5, Fgf7 and Fgf10 treatments, respectively, to mouse E9.5 PE/ST explants. Panel **(C)** RT-qPCR analyses of miR-195a, miR-195b and miR-223 expression after control, Bmp6, Bmp7, Bmp10, Fgf5, Fgf7 and Fgf10 treatments, respectively, to mouse E9.5 PE/ST explants. $^{*}p < 0.05$, $^{**}p < 0.01$, $^{***}p < 0.001$, $^{****}p < 0.0001$.

significantly alter its expression in any of the 2 cell types analyzed (**Figure 9**).

Overall, these data illustrate that these growth factors can distinctly modulate the expression of different microRNAs, previously reported to inhibit (miR-23b, miR-27b and miR-100), to mildly promote (miR-125a, miR-125b, miR-146b) or to substantially enhance (miR-195a, miR-195b, miR-223) cardiomyogenesis in chicken PE/ST. Surprisingly, none of tested growth factor distinctly enhanced or decreased the expression of these microRNAs, i.e. suggesting promotion or inhibition of cardiomyogenesis. Furthermore, Fgf2 and Fgf8, but not Bmp2 or Bmp4, can induced expression of cardiomyocyte terminal differentiation marker in endocardial but not in epicardial cells.

Additionally we also tested whether novel Bmp and Fgf family members with enhanced expression in PE/EE transition, might similarly modulate the expression of these microRNAs and/or distinct lineage markers. All growth factor tested significantly decreased the expression of miR-23b, miR-27b and miR-100 in MEVEC cells, except Bmp10 that enhanced expression of miR-100. Curiously, expression of these microRNAs is enhanced in EPIC cells for Fgf10, Bmp7 and Bmp10, except for miR-27b that is decreased by Bmp10 administration (**Figure 10A**). Similarly, all growth factor tested decreased the expression of miR-125a and

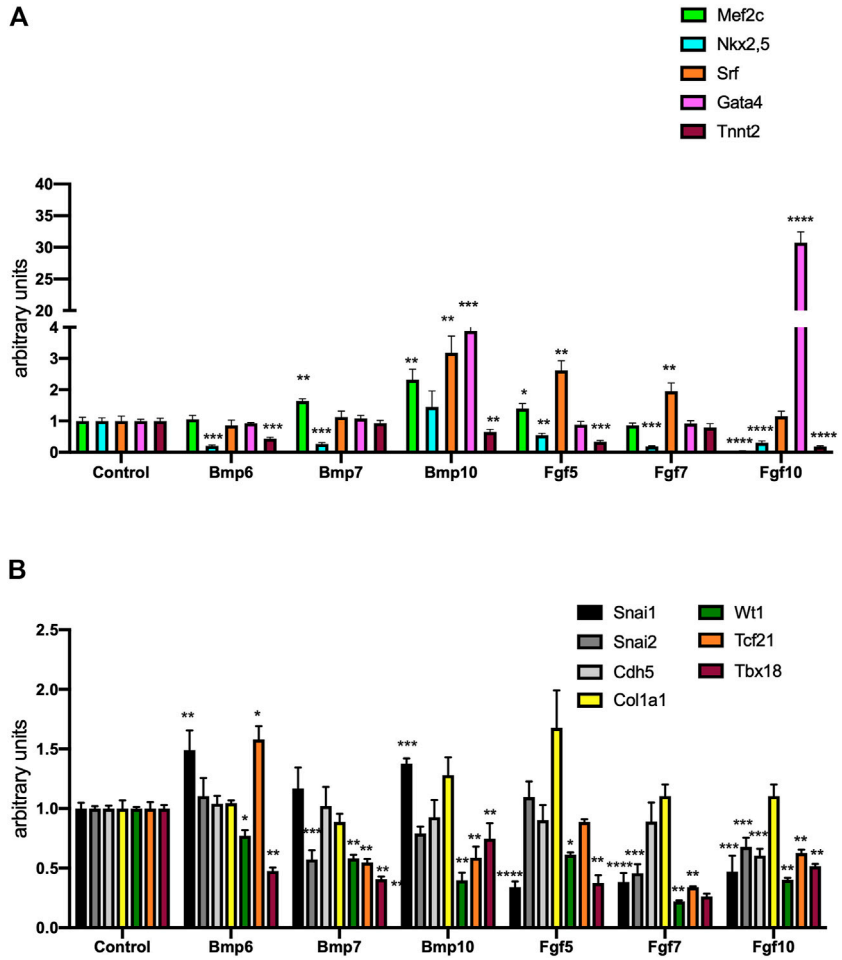

FIGURE 6 | Panel **(A)** RT-qPCR analyses of Mef2c, Nkx2.5, Srf, Gata4 and Tnnt2 expression after control, Bmp6, Bmp7, Bmp10, Fgf5, Fgf7 and Fgf10 treatments, respectively, to mouse E9.5 PE/ST explants. Panel **(B)** RT-qPCR analyses of Snai1, Sna2, Cdh5, Col1a1, Wt1, Tcf21 and Tbx18 expression after control, Bmp6, Bmp7, Bmp10, Fgf5, Fgf7 and Fgf10 treatments, respectively, to mouse E9.5 PE/ST explants. $*p < 0.05$, $**p < 0.01$, $***p < 0.001$, $****p < 0.0001$.

miR-125b in MEVEC cells or show no significant differences whereas Bmp7 and Bmp10 significantly up-regulated them in EPIC cells. In addition, Fgf10 also upregulates miR-125b in EPIC cells (**Figure 10B**). On the other hand, miR-195a and miR-195b are significantly downregulated by all growth factors tested in MEVEC except for Bmp10 does not alter miR-195a expression and increased miR-195b expression while miR-223 is significantly upregulated by Fgf5 and Bmp10 and down-regulated by Fgf10, Bmp6 and Bmp7 in MEVEC cells (**Figure 10C**). Importantly, Fgf10, Bmp7 and Bmp10 significantly upregulate miR-195a, miR-195b and miR-223 in EPIC cells, while the other growth factors tested decreased or did not modify their expression in this cell line (**Figure 10C**).

Lineage marker analyses after Bmp and Fgf administration showed that none of them is capable of enhancing early cardiomyogenic lineage markers in MEVEC cells, and most of them lead to significant downregulation, except for Bmp7 administration that resulted in significant upregulation of terminal cardiomyocyte differentiation marker Tnnt2 (**Figure 11A**). Within EPIC cells, only upregulation of early cardiomyocyte differentiation markers is observed, particularly Mef2c, but expression of Tnnt2 is either not altered or significantly downregulated by all growth factors tested.

Similarly, EMT instructive genes such as Snai1 and Snai2 are significantly down-regulated in MEVEC cells and EPIC cells, except for Bmp10 that enhanced Snai1 and Snai2 expression in EPIC cells. In line with this findings, Cdh5 is upregulated in all experimental conditions in both cell lines, particularly for Fgf10, Bmp6 and Bmp7 in MEVEC cells (**Figure 11B**) and Fgf7, Fgf10, Bmp6, Bmp7 and Bmp10 in EPIC cells. Fibrogenic marker analyses also demonstrate that all Bmp and Fgf treatments both cell types leads to downregulation of Col1a1 expression (**Figure 11B**). These data demonstrate that none of the Bmp and Fgf treatments reported herein lead to cardiomyocyte differentiation in epicardial cells and only Bmp7 is capable of inducing terminal differentiation in endocardial cells. In addition, EMT and fibrogenic differentiation are similarly halted in both cell lines by all growth factors analyzed.

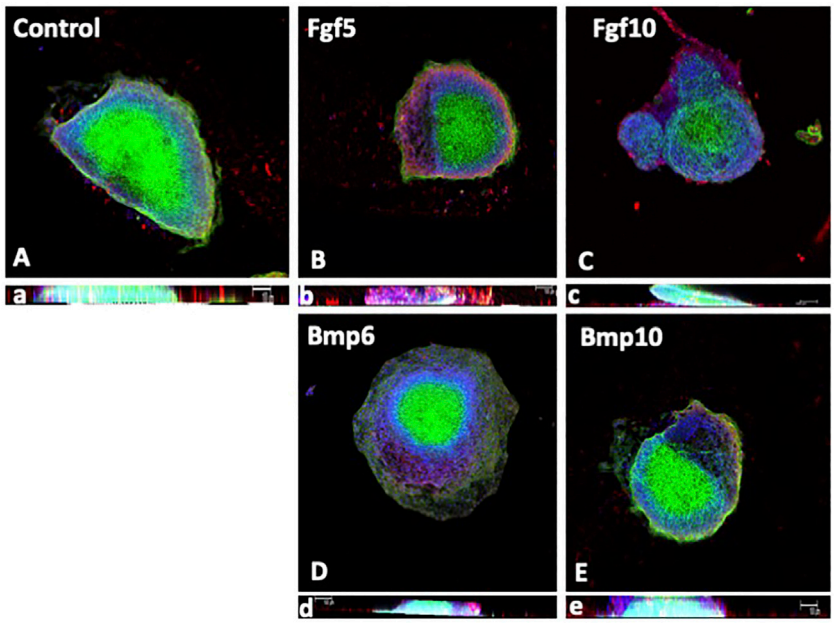

FIGURE 7 | Panels **(A–E)** Confocal images of mouse E9.5 PE/ST explants after control **(A)**, Fgf5 **(B)**, Fgf10 **(C)**, Bmp6 **(D)** and Bmp10 **(E)** treatments, respectively. Note that treatment with Fgf5, Fgf10 and Bmp10 displays limited migration, similar to controls, while Bmp6 is significantly increased. Panels a–e represent Z-stack confocal views, respectively, where it can be observed that none of them display signs of EMT.

DISCUSSION

The role distinct microRNAs during cardiovascular development has been widely demonstrated (Xin et al., 2013; Wojciechowska et al., 2017; Kalayinia et al., 2021). Conditional deletion of *Dicer* in the developing heart (Saxena and Tabin, 2010) or even specifically in the developing epicardium (Singh et al., 2011) leads to cardiovascular defects. Furthermore miR-1 mutants (Zhao Y. et al., 2007; Heidersbach et al., 2013) and miR-126 (Fish et al., 2008) are embryonic lethal due to cardiovascular alterations. Additional evidences on the role of distinct microRNAs during cardiogenesis have been reported for miR-130 in cardiomyogenic mesoderm determination (Lopez-Sanchez et al., 2015b), and for miR-23 and miR-199 in endocardial cushions formation (Lagendijk et al., 2011; Bonet et al., 2015). We have recently demonstrated that administration of miR-195 and/or miR-223 in enhances PE/ST-derived cardiomyogenesis in chicken (Dueñas et al., 2020). However, we demonstrated herein that such inductive roles are not conserved in mouse PE/ST explants. Such discrepancies might be related to the distinct morphogenetic events during PE development between mouse and chicken (Shulte et al., 2007) and thus that distinct signaling pathways that are involved (Shulte et al., 2007).

Bmp and Fgf have been reported to play essential roles in multiple aspects of embryogenesis (Ornitz and Itoh, 2015; Ornitz and Marie, 2015; Wu et al., 2016; Graf et al., 2016; Salazar et al., 2016; Zinski et al., 2018; Xie et al., 2020; Mossahebi-Mohammadi et al., 2020). In particular, during heart development, Bmp have been involved in early cardiogenic precursor determination (Lopez-Sanchez et al., 2002; López-Sánchez and García-Martínez, 2011) and also in later developmental states of myocardial growth and/or valvular development (Delot, 2003; Chen et al., 2004; Kruithof et al., 2012; Garside et al., 2013). Within the PE/ST development, distinct Bmp and Fgf have been reported during chicken development, demonstrating that Bmp2 and Bmp4 enhance cardiomyocyte commitment of precardiac mesoderm while Fgf2 and Fgf8 provide signaling cues to direct these cells into the PE lineage (Kruithof et al., 2006). We recently demonstrate that microRNAs involved in PE/ST-derived cardiomyogenesis are distinctly regulated by Bmp2/Bmp4, Fgf2/Fgf8 (Dueñas et al., 2020). Given the fact that miR-195 and miR-223 administration does not enhanced PE/ST cardiomyogenesis in mice, thus it might be plausible that such regulatory pathway is impaired in mice. Our data demonstrate primarily Fgf2 and Fgf8 enhanced expression of miR-195a, miR-195b and miR-223, while only Bmp2 enhanced miR-195b and Bmp4 enhanced miR195a, yet in any case early or terminal cardiomyocyte differentiation is increased in mouse PE/ST explants. Thus, these data suggest that alternative pathways might be involved regulating these PE/ST-derived cardiomyogenesis enhancing microRNAs. Curiously, neither Bmp2/Bmp4 and/or Fgf2/Fgf8 elicited modulation on EMT and fibrogenic markers, supporting a limited role of these growth factors directing key developmental processes during PE/ST development in mice.

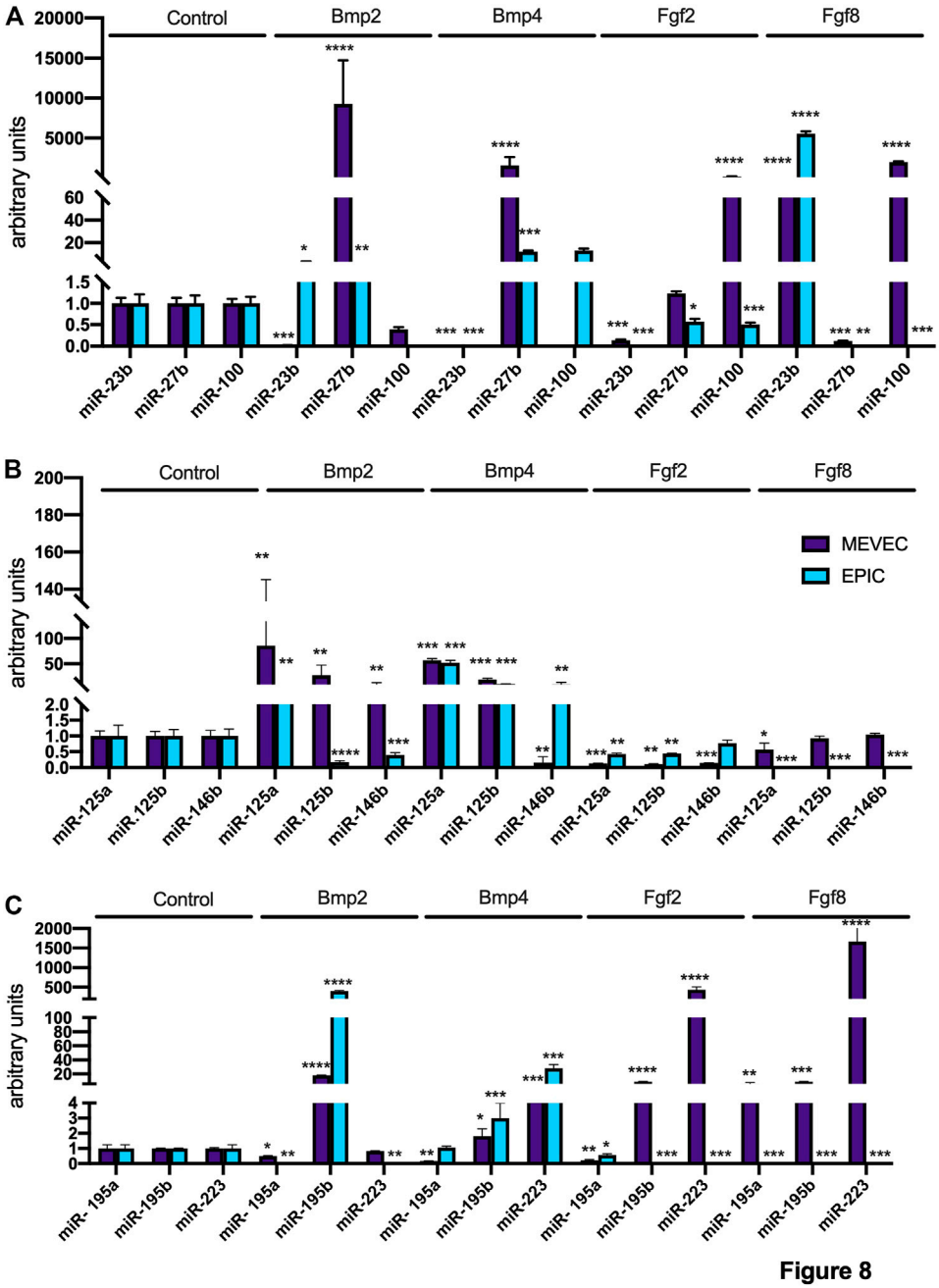

Figure 8

FIGURE 8 | Panel **(A)** RT-qPCR analyses of miR-23b, miR-27b and miR-100 expression after control, Bmp2, Bmp4, Fgf2 and Fgf8 treatments in MEVEC (endocardial) and EPIC (epicardial) cell lines, respectively. Panel **(B)** RT-qPCR analyses of miR-125a, miR-125b and miR-146b expression after control, Bmp2, Bmp4, Fgf2 and Fgf8 treatments in MEVEC (endocardial) and EPIC (epicardial) cell lines, respectively. Panel **(C)** RT-qPCR analyses of miR-195a, miR-195b and miR-223 expression after control, Bmp2, Bmp4, Fgf2 and Fgf8 treatments in MEVEC (endocardial) and EPIC (epicardial) cell lines, respectively. $^{*}p < 0.05$, $^{**}p < 0.01$, $^{***}p < 0.001$, $^{****}p < 0.0001$.

Distinct regulatory roles were observed in epicardial and endocardial cell lines. Bmp2/Bmp4 and Fgf2/Fgf8 distinctly modulate the expression of microRNAs that inhibit PE/ST-derived cardiomyogenesis (miR-23b, miR-27b and miR-100), preferentially up-regulating them in MEVEC cells while down-regulating them in EPIC cells. For those microRNAs that mildly enhance early cardiomyogenesis markers (miR-125a, miR-125b and miR-146b) Bmp2 leads to upregulation in MEVEC but not in EPIC cells while Bmp4 enhanced it in both cell lines. Surprisingly, those microRNAs that enhance cardiomyocyte terminal differentiation (miR-195a, miR-195b and miR-223) were similarly up-regulated in both cell lines by Bmp2 and Bmp4

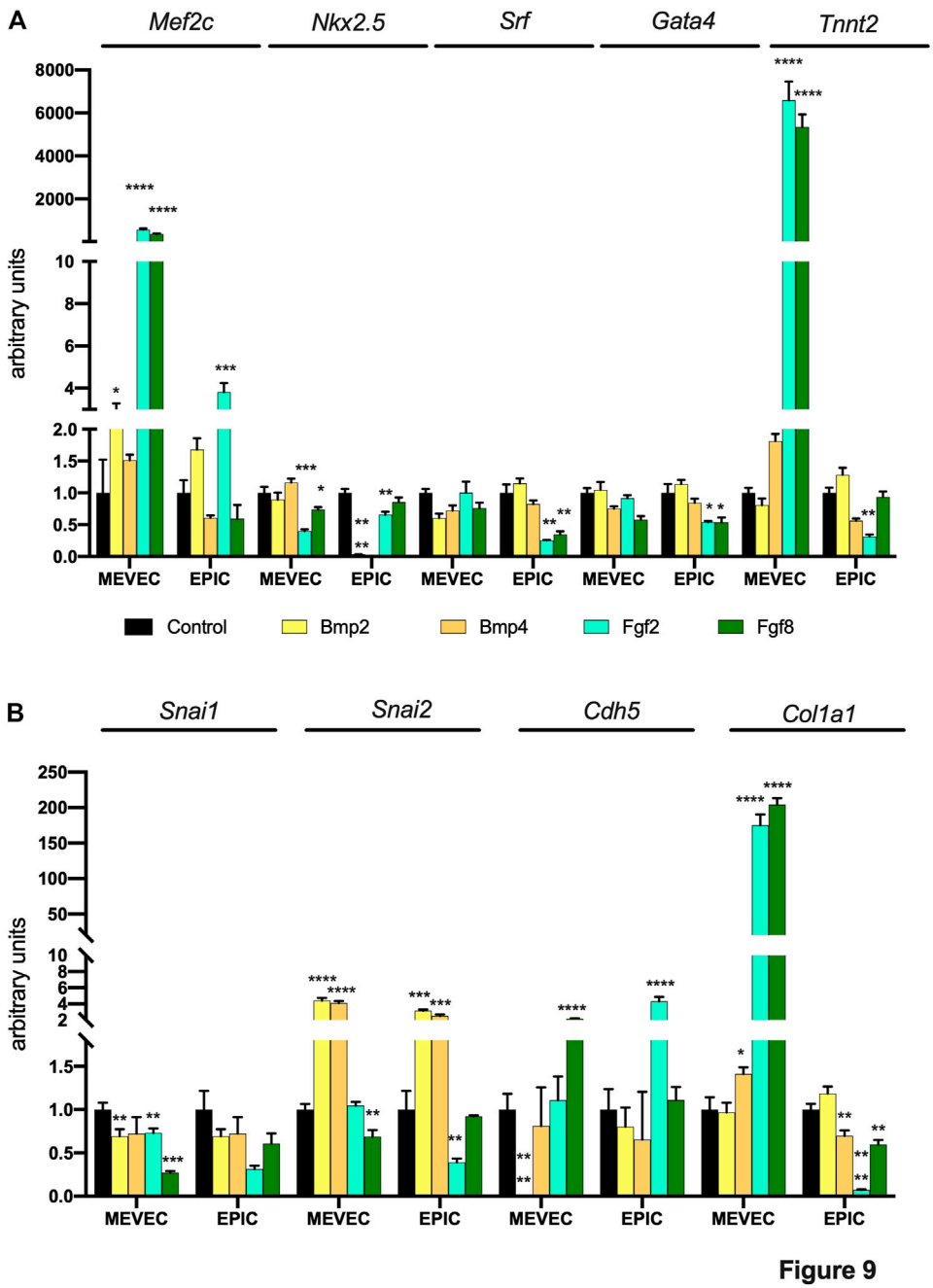

FIGURE 9 | Panel **(A)** RT-qPCR analyses of Mef2c, Nkx2.5, Srf, Gata4 and Tnnt2 expression after control, Bmp2, Bmp4, Fgf2 and Fgf8 treatments in MEVEC (endocardial) and EPIC (epicardial) cell lines, respectively. Panel **(B)** RT-qPCR analyses of Snai1, Snai2, Cdh5 and Col1a1 expression after control, Bmp2, Bmp4, Fgf2 and Fgf8 treatments in MEVEC (endocardial) and EPIC (epicardial) cell lines, respectively. *$p < 0.05$, **$p < 0.01$, ***$p < 0.001$, ****$p < 0.0001$.

but up-regulated only in endocardial cells by Fgf2 and Fgf8. In line with these findings, terminal cardiomyocyte differentiation is elicited exclusively in endocardial cells by Fgf2 and Fgf8. In addition EMT induction is similarly increased in both cells lines by Bmp2 and Bmp4, in line with previous findings in other embryonic contexts (Ma et al., 2005; Inai et al., 2008; Cai et al., 2011; Townsend et al., 2011; Inai et al., 2013; Richter et al., 2014), while fibrogenesis is exclusively increased by Fgf2 anf Fgf8 in endocardial but not in epicardial cells.

As revealed by RNAseq analyses during PE development in mice, several additional Bmp and Fgf family members (Bmp6, Bmp7, Bmp10, Fgf5, Fgf7 and Fgf10). are differentially expressed, suggesting a plausible role during PE development in mice. Curiously, Fgf8 expression was not detectable in PE/EE mouse

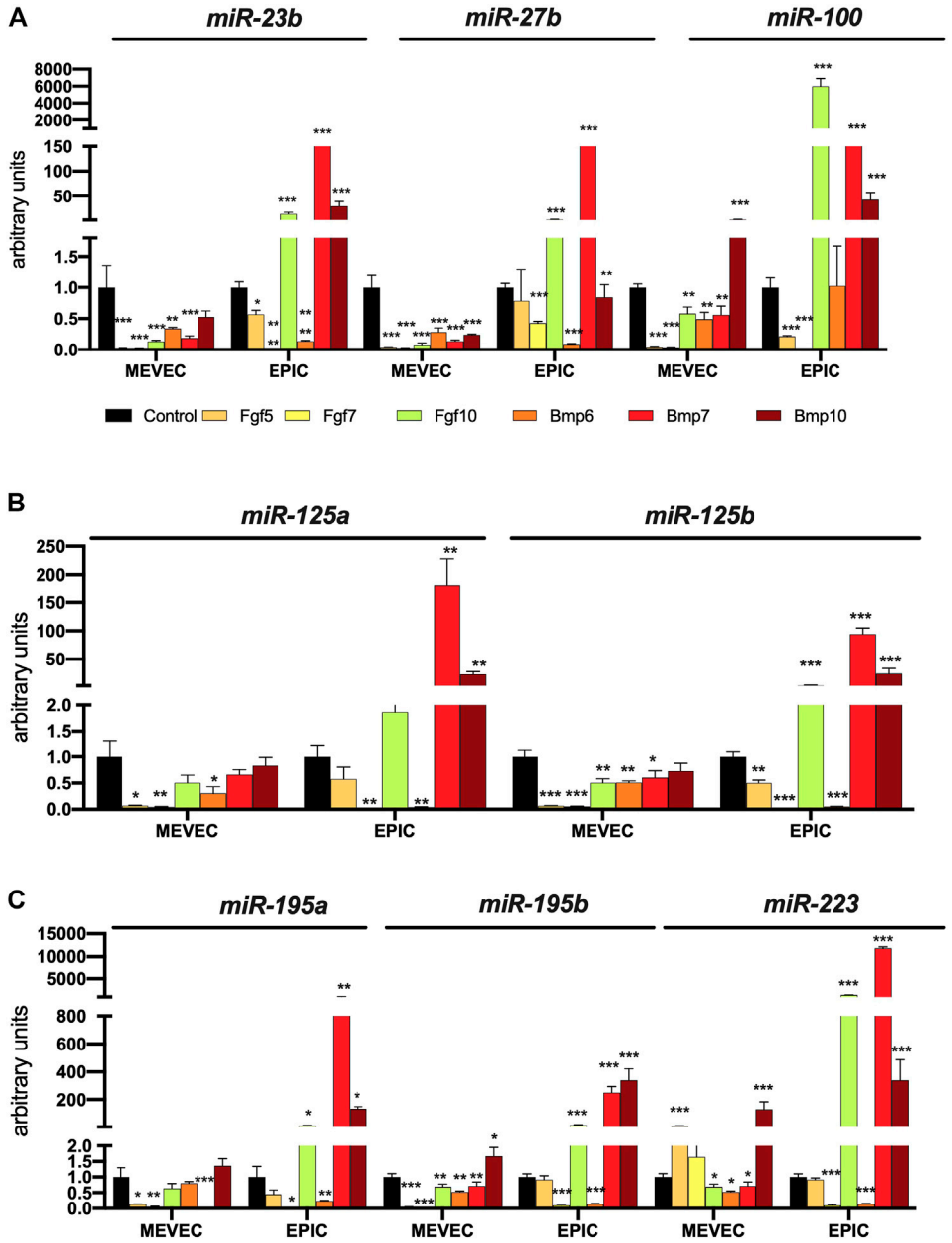

FIGURE 10 | Panel **(A)** RT-qPCR analyses of miR-23b, miR-27b and miR-100 expression after control, Bmp6, Bmp7, Bmp10, Fgf5, Fgf7 and Fgf10 treatments in MEVEC (endocardial) and EPIC (epicardial) cell lines, respectively. Panel **(B)** RT-qPCR analyses of miR-125a, miR-125b and miR-146b expression after control, Bmp6, Bmp7, Bmp10, Fgf5, Fgf7 and Fgf10 treatments in MEVEC (endocardial) and EPIC (epicardial) cell lines, respectively. Panel **(C)** RT-qPCR analyses of miR-195a, miR-195b and miR-223 expression after control, Bmp6, Bmp7, Bmp10, Fgf5, Fgf7 and Fgf10 treatments in MEVEC (endocardial) and EPIC (epicardial) cell lines, respectively. $^{*}p < 0.05$, $^{**}p < 0.01$, $^{***}p < 0.001$, $^{****}p < 0.0001$.

tissues, suggesting that it might not be relevant for mouse PE development, in line with our findings *in vitro*.

Bmp6 and Bmp7 are required for endocardial cushion formation during heart development (Kim et al., 2001), yet no evidences of their functional role and/or expression have been reported to date in the PE. The role of Bmp10 have been reported in different aspect of cardiac development (Neuhaus et al., 1999; Chen et al., 2004; Somi et al., 2004; Teichmann and Kessel, 2004; Huang et al., 2012; Capasso et al., 2020), yet no role in PE development is provided to date. While no evidences have been reported for Fgf5 and Fgf7 during heart development or PE development, Fgf10 have been implicated during both heart development (Kelly et al., 2001; Chan et al., 2010; Watanabe et al., 2010; Vega-Hernández et al., 2011; Rochais et al., 2014; Hubert et al., 2018) and PE formation (Torlopp et al., 2010). Thus, we

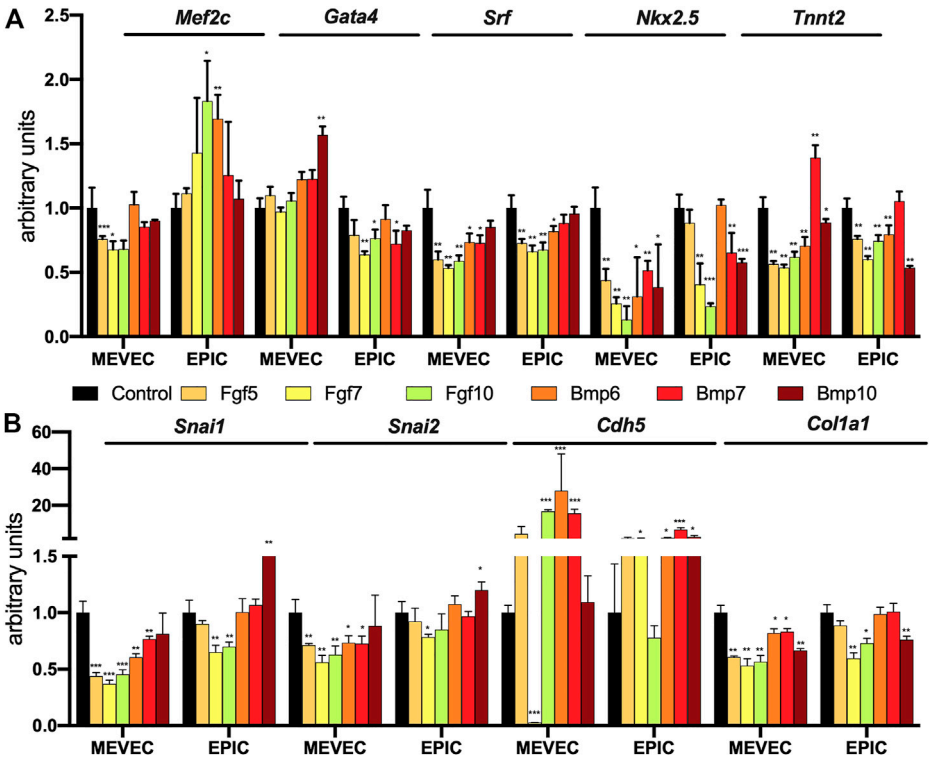

FIGURE 11 | Panel **(A)** RT-qPCR analyses of Mef2c, Nkx2.5, Srf, Gata4 and Tnnt2 expression after control, Bmp6, Bmp7, Bmp10, Fgf5, Fgf7 and Fgf10 treatments in MEVEC (endocardial) and EPIC (epicardial) cell lines, respectively. Panel **(B)** RT-qPCR analyses of Snai1, Snai2, Cdh5 and Col1a1 expression after control, Bmp6, Bmp7, Bmp10, Fgf5, Fgf7 and Fgf10 treatments in MEVEC (endocardial) and EPIC (epicardial) cell lines, respectively. $^{*}p < 0.05$, $^{**}p < 0.01$, $^{***}p < 0.001$, $^{****}p < 0.0001$.

identified herein novel Bmp and Fgf family members with potential implication in mouse PE/ST development.

Importantly, administration of different Fgf and Bmp growth factors to murine PE/ST explants distinctly modulate the expression of microRNAs that inhibit PE/ST-derived cardiomyogenesis (miR-23b, miR-27b and miR-100) as well as those that mildly enhance early cardiomyogenesis markers (miR-125a, miR-125b and miR-146b). However, none of them significantly up-regulate those microRNAs that enhance cardiomyocyte terminal differentiation (miR-195a, miR-195b and miR-223). In line with these results, no terminal differentiation up-regulation is observed in PE/ST explants. On the other hand, EMT induction is documented after Bmp6 and Bmp10 administration and severely blocked by Fgf5, Fgf7 and Fgf10. Overall, these data support the notion that these growth factors do not play a functional role enhancing cardiomyogenesis in the mouse PE and provide novel insights into the plausible role of Bmp10, Fgf5, Fgf7 and Fgf10 regulating cardiovascular EMT, as reported for, e.g. Fgf10, in other biological contexts (Abolhassani et al., 2014; Farajihaye Qazvini et al., 2019).

microRNA regulation by Fgf and Bmp family members is distinctly observed in epicardial and endocardial cell lines. Fgf10, Bmp7 and Bmp10 resulted in sustained upregulation of all cardiomyogenic inductive and inhibiting microRNAs in EPIC but not in MEVEC cells, supporting the notion of complex genetic post-transcriptional regulatory mechanisms driven by these growth factors. In this context, the end result is that neither early (with the exception of Mef2c) nor late cardiomyogenic terminal differentiation is achieved in any of the 2 cell types, except for Bmp7 in MEVEC cells. Thus, these data suggest that Bmp7 can be taken over the regulatory roles of other Bmp family members during PE/ST mouse development, yet it is highly intriguing that such effects are only observed in endocardial but not in epicardial cells. Additional experiments are required to fully understand these discrepancies.

Moreover, all Bmp and Fgf family members tested inhibited EMT, as Snai1 and Snai2 are preferentially downregulated and Cdh5 is upregulated, with the exception of Bmp10 in epicardial cells. Thus, these data further support the previous findings in PE/ST explants, highlight the plausible novel role of Fgf5, Fgf7, Fgf10, Bmp6, Bmp7 and Bmp10 in EMT regulation.

In summary, we demonstrated herein that PE/ST-derived cardiomyogenesis is distinctly regulated during chicken and mouse development. Distinct Bmp and Fgf family members play fundamental roles regulating miR-195/miR-223 expression in chicken PE/ST, that ultimately lead to enhanced cardiomyogenesis in chicken (Dueñas et al., 2020). However, such regulatory effects are not conserved in mouse PE/ST explants.

DATA AVAILABILITY STATEMENT

RNAseq data were uploaded into Gene Expresssion Onmibus platform with accession number GSE189344. https://www.ncbi.nlm.nih.gov/geo/query/acc.cgi?acc=GSE189344

ETHICS STATEMENT

The animal study was reviewed and approved by University of Jaen Ethics Committee.

AUTHOR CONTRIBUTIONS

CG-P, FH-T, EL-V, AD, MMM-G, IG-V, and LP-V contributed to data adquisition. DF designed experiments. DF draft manuscript, DF and AA revised experimental data and final manuscript writing.

SUPPLEMENTARY MATERIAL

The Supplementary Material for this article can be found online at: https://www.frontiersin.org/articles/10.3389/fcell.2021.757781/full#supplementary-material

REFERENCES

Abolhassani, A., Riazi, G. H., Azizi, E., Amanpour, S., Muhammadnejad, S., Haddadi, M., et al. (2014). FGF10: Type III Epithelial Mesenchymal Transition and Invasion in Breast Cancer Cell Lines. *J. Cancer* 5 (7), 537–547. doi:10.7150/jca.7797

Bonet, F., Dueñas, Á., López-Sánchez, C., García-Martínez, V., Aránega, A. E., and Franco, D. (2015). MiR-23b and miR-199a Impair Epithelial-To-Mesenchymal Transition during Atrioventricular Endocardial Cushion Formation. *Dev. Dyn.* 244 (10), 1259–1275. doi:10.1002/dvdy.24309

Bustin, S. A., Benes, V., Garson, J. A., Hellemans, J., Huggett, J., Kubista, M., et al. (2001). The MIQE Guidelines: Minimum Information for Publication of Quantitative Real-Time PCR Experiments. Clin C(T)) Method. *Methods* 25 (4), 402–408. doi:10.1373/clinchem.2008.112797

Cai, C.-L., Martin, J. C., Sun, Y., Cui, L., Wang, L., Ouyang, K., et al. (2008). A Myocardial Lineage Derives from Tbx18 Epicardial Cells. *Nature* 454 (7200), 104–108. doi:10.1038/nature06969

Cai, X., Nomura-Kitabayashi, A., Cai, W., Yan, J., Christoffels, V. M., and Cai, C.-L. (2011). Myocardial Tbx20 Regulates Early Atrioventricular Canal Formation and Endocardial Epithelial-Mesenchymal Transition via Bmp2. *Dev. Biol.* 360 (2), 381–390. doi:10.1016/j.ydbio.2011.09.023

Cano, E., Carmona, R., and Muñoz-Chápuli, R. (2013). Wt1-Expressing Progenitors Contribute to Multiple Tissues in the Developing Lung. *Am. J. Physiol. Lung Cell. Mol. Physiol.* 305 (4), L322–L332. doi:10.1152/ajplung.00424.2012

Capasso, T. L., Li, B., Volek, H. J., Khalid, W., Rochon, E. R., Anbalagan, A., et al. (2020). BMP10-mediated ALK1 Signaling Is Continuously Required for Vascular Development and Maintenance. *Angiogenesis* 23 (2), 203–220. doi:10.1007/s10456-019-09701-0

Chan, S. S.-K., Li, H.-J., Hsueh, Y.-C., Lee, D. S., Chen, J.-H., Hwang, S.-M., et al. (2010). Fibroblast Growth Factor-10 Promotes Cardiomyocyte Differentiation from Embryonic and Induced Pluripotent Stem Cells. *PLoS One* 5 (12), e14414. doi:10.1371/journal.pone.0014414

Chen, H., Shi, S., Acosta, L., Li, W., Lu, J., Bao, S., et al. (2004). BMP10 Is Essential for Maintaining Cardiac Growth during Murine Cardiogenesis. *Development* 131 (9), 2219–2231. doi:10.1242/dev.01094

Cohen, E. D., Wang, Z., Lepore, J. J., Lu, M. M., Taketo, M. M., Epstein, D. J., et al. (2007). Wnt/β-catenin Signaling Promotes Expansion of Isl-1-Positive Cardiac Progenitor Cells through Regulation of FGF Signaling. *J. Clin. Invest.* 117 (7), 1794–1804. doi:10.1172/jci31731

Cushing, M. C., Mariner, P. D., Liao, J. T., Sims, E. A., and Anseth, K. S. (2008). Fibroblast Growth Factor Represses Smad-mediated Myofibroblast Activation in Aortic Valvular Interstitial Cells. *FASEB j.* 22 (6), 1769–1777. doi:10.1096/fj.07-087627

D'Amato, G., Luxán, G., del Monte-Nieto, G., Martínez-Poveda, B., Torroja, C., Walter, W., et al. (2016). Sequential Notch Activation Regulates Ventricular Chamber Development. *Nat. Cel Biol* 18, 7–20. doi:10.1038/ncb3280

Delot, E. C. (2003). Control of Endocardial Cushion and Cardiac Valve Maturation by BMP Signaling Pathways. *Mol. Genet. Metab.* 80 (1-2), 27–35. doi:10.1016/j.ymgme.2003.07.004

Dueñas, A., Expósito, A., Muñoz, M. D. M., de Manuel, M. J., Cámara-Morales, A., Serrano-Osorio, F., et al. (2020). MiR-195 Enhances Cardiomyogenic Differentiation of the Proepicardium/septum Transversum by Smurf1 and Foxp1 Modulation. *Sci. Rep.* 10 (1), 9334. doi:10.1038/s41598-020-66325-x

Farajihaye Qazvini, F., Samadi, N., Saffari, M., Emami-Razavi, A. N., and Shirkoohi, R. (2019). Fibroblast Growth Factor-10 and Epithelial-Mesenchymal Transition in Colorectal Cancer. *EXCLI J.* 18, 530–539. doi:10.17179/excli2018-1784

Fish, J. E., Santoro, M. M., Morton, S. U., Yu, S., Yeh, R.-F., Wythe, J. D., et al. (2008). miR-126 Regulates Angiogenic Signaling and Vascular Integrity. *Dev. Cel* 15 (2), 272–284. doi:10.1016/j.devcel.2008.07.008

Gan, S., Huang, Z., Liu, N., Su, R., Xie, G., Zhong, B., et al. (2016). MicroRNA-140-5p Impairs Zebrafish Embryonic Bone Development via Targeting BMP-2. *FEBS Lett.* 590 (10), 1438–1446. doi:10.1002/1873-3468.12190

Garside, V. C., Chang, A. C., Karsan, A., and Hoodless, P. A. (2013). Co-ordinating Notch, BMP, and TGF-β Signaling during Heart Valve Development. *Cell. Mol. Life Sci.* 70 (16), 2899–2917. doi:10.1007/s00018-012-1197-9

Graf, D., Malik, Z., Hayano, S., and Mishina, Y. (2016). Common Mechanisms in Development and Disease: BMP Signaling in Craniofacial Development. *Cytokine Growth Factor. Rev.* 27, 129–139. doi:10.1016/j.cytogfr.2015.11.004

Heidersbach, A., Saxby, C., Carver-Moore, K., Huang, Y., Ang, Y. S., de Jong, P. J., et al. (2013). microRNA-1 Regulates Sarcomere Formation and Suppresses Smooth Muscle Gene Expression in the Mammalian Heart. *Elife* 2, e01323. doi:10.7554/eLife.01323

Hirose, T., Karasawa, M., Sugitani, Y., Fujisawa, M., Akimoto, K., Ohno, S., et al. (2006). PAR3 Is Essential for Cyst-Mediated Epicardial Development by Establishing Apical Cortical Domains. *Development* 133, 1389–1398. doi:10.1242/dev.02294

Huang, J., Elicker, J., Bowens, N., Liu, X., Cheng, L., Cappola, T. P., et al. (2012). Myocardin Regulates BMP10 Expression and Is Required for Heart Development. *J. Clin. Invest.* 122 (10), 3678–3691. doi:10.1172/jci63635

Hubert, F., Payan, S. M., and Rochais, F. (2018). FGF10 Signaling in Heart Development, Homeostasis, Disease and Repair. *Front. Genet.* 9, 599. doi:10.3389/fgene.2018.00599

Hutson, M. R., Zeng, X. L., Kim, A. J., Antoon, E., Harward, S., and Kirby, M. L. (2010). Arterial Pole Progenitors Interpret Opposing FGF/BMP Signals to Proliferate or Differentiate. *Development* 137 (18), 3001–3011. doi:10.1242/dev.051565

Icli, B., Wara, A. K. M., Moslehi, J., Sun, X., Plovie, E., Cahill, M., et al. (2013). MicroRNA-26a Regulates Pathological and Physiological Angiogenesis by Targeting BMP/SMAD1 Signaling. *Circ. Res.* 113 (11), 1231–1241. doi:10.1161/circresaha.113.301780

Inai, K., Burnside, J. L., Hoffman, S., Toole, B. P., and Sugi, Y. (2013). BMP-2 Induces Versican and Hyaluronan that Contribute to post-EMT AV Cushion Cell Migration. *PLoS One* 8 (10), e77593. doi:10.1371/journal.pone.0077593

Inai, K., Norris, R. A., Hoffman, S., Markwald, R. R., and Sugi, Y. (2008). BMP-2 Induces Cell Migration and Periostin Expression during Atrioventricular Valvulogenesis. *Dev. Biol.* 315 (2), 383–396. doi:10.1016/j.ydbio.2007.12.028

Kalayinia, S., Arjmand, F., Maleki, M., Malakootian, M., and Singh, C. P. (2021). MicroRNAs: Roles in Cardiovascular Development and Disease. *Cardiovasc. Pathol.* 50, 107296. doi:10.1016/j.carpath.2020.107296

Kelly, R. G., Brown, N. A., and Buckingham, M. E. (2001). The Arterial Pole of the Mouse Heart Forms from Fgf10-Expressing Cells in Pharyngeal Mesoderm. *Dev. Cel* 1 (3), 435–440. doi:10.1016/s1534-5807(01)00040-5

Kim, D., Langmead, B., and Salzberg, S. L. (2015). HISAT: a Fast Spliced Aligner with Low Memory Requirements. *Nat. Methods* 12 (4), 357–360. doi:10.1038/nmeth.3317

Kim, R. Y., Robertson, E. J., and Solloway, M. J. (2001). Bmp6 and Bmp7 Are Required for Cushion Formation and Septation in the Developing Mouse Heart. *Dev. Biol.* 235 (2), 449–466. doi:10.1006/dbio.2001.0284

Kozomara, A., and Griffiths-Jones, S. (2014). miRBase: Annotating High Confidence MicroRNAs Using Deep Sequencing Data. *Nucleic Acids Res.* 42, D68–D73. doi:10.1093/nar/gkt1181

Kruithof, B. P. T., Duim, S. N., Moerkamp, A. T., and Goumans, M.-J. (2012). TGFβ and BMP Signaling in Cardiac Cushion Formation: Lessons from Mice and Chicken. *Differentiation* 84 (1), 89–102. doi:10.1016/j.diff.2012.04.003

Kruithof, B. P. T., van Wijk, B., Somi, S., Kruithof-de Julio, M., Pérez Pomares, J. M., Weesie, F., et al. (2006). BMP and FGF Regulate the Differentiation of Multipotential Pericardial Mesoderm into the Myocardial or Epicardial Lineage. *Dev. Biol.* 295 (2), 507–522. doi:10.1016/j.ydbio.2006.03.033

Lagendijk, A. K., Goumans, M. J., Burkhard, S. B., and Bakkers, J. (2011). MicroRNA-23 Restricts Cardiac Valve Formation by Inhibiting Has2 and Extracellular Hyaluronic Acid Production. *Circ. Res.* 109 (6), 649–657. doi:10.1161/circresaha.111.247635

Liao, Y., Smyth, G. K., and Shi, W. (2014). FeatureCounts: An Efficient General Purpose Program for Assigning Sequence Reads to Genomic Features. *Bioinformatics* 30 (7), 923–930. doi:10.1093/bioinformatics/btt656

Li, B., and Dewey, C. N. (2011). RSEM: Accurate Transcript Quantification From RNA-Seq Data with or without a Reference Genome. *BMC Bioinformatics* 12, 323. doi:10.1186/1471-2105-12-323

Li, J., Miao, L., Zhao, C., Shaikh Qureshi, W. M., Shieh, D., Guo, H., et al. (2017). CDC42 Is Required for Epicardial and Pro-epicardial Development by Mediating FGF Receptor Trafficking to the Plasma Membrane. *Development* 144 (9), 1635–1647. doi:10.1242/dev.147173

Livak, K. J., and Schmittgen, T. D. (2001). Analysis of Relative Gene Expression Data Using Real-Time Quantitative PCR and the 2−ΔΔCT Method. *Methods* 25 (4), 402–408. doi:10.1006/meth.2001.1262

López-Sánchez, C., and García-Martínez, V. (2011). Molecular Determinants of Cardiac Specification. *Cardiovasc. Res.* 91 (2), 185–195. doi:10.1093/cvr/cvr127

Lopez-Sanchez, C., Climent, V., Schoenwolf, G., Alvarez, I., and Garcia-Martinez, V. (2002). Induction of Cardiogenesis by Hensen's Node and Fibroblast Growth Factors. *Cel Tissue Res.* 309 (2), 237–249. doi:10.1007/s00441-002-0567-2

Lopez-Sanchez, C., Franco, D., Bonet, F., Garcia-Lopez, V., Aranega, A., and Garcia-Martinez, V. (2015b). Negative Fgf8-Bmp2 Feed-Back Is Regulated by miR-130 during Early Cardiac Specification. *Dev. Biol.* 406 (1), 63–73. doi:10.1016/j.ydbio.2015.07.007

Lopez-Sanchez, C., Franco, D., Bonet, F., Garcia-Lopez, V., Aranega, A., and Garcia-Martinez, V. (2015a). Reciprocal Repression between Fgf8 and miR-133 Regulates Cardiac Induction through Bmp2 Signaling. *Data in Brief* 5, 59–64. doi:10.1016/j.dib.2015.08.009

Lozano-Velasco, E., Galiano-Torres, J., Jodar-Garcia, A., Aranega, A. E., and Franco, D. (2015). miR-27 and miR-125 Distinctly Regulate Muscle-Enriched Transcription Factors in Cardiac and Skeletal Myocytes. *Biomed. Res. Int.* 2015 (10), 391306. doi:10.1155/2015/391306

Lu, T.-Y., Lin, B., Li, Y., Arora, A., Han, L., Cui, C., et al. (2013). Overexpression of microRNA-1 Promotes Cardiomyocyte Commitment from Human Cardiovascular Progenitors via Suppressing WNT and FGF Signaling Pathways. *J. Mol. Cell Cardiol.* 63, 146–154. doi:10.1016/j.yjmcc.2013.07.019

Ma, L., Lu, M.-F., Schwartz, R. J., and Martin, J. F. (2005). Bmp2 Is Essential for Cardiac Cushion Epithelial-Mesenchymal Transition and Myocardial Patterning. *Development* 132 (24), 5601–5611. doi:10.1242/dev.02156

Männer, J., Pérez-Pomares, J. M., Macías, D., and Muñoz-Chápuli, R. (2001). The Origin, Formation and Developmental Significance of the Epicardium: a Review. *Cells Tissues Organs* 169, 89–103. doi:10.1159/000047867

Merki, E., Zamora, M., Raya, A., Kawakami, Y., Wang, J., Zhang, X., et al. (2005). Epicardial Retinoid X Receptor Is Required for Myocardial Growth and Coronary Artery Formation. *Proc. Natl. Acad. Sci.* 102 (51), 18455–18460. doi:10.1073/pnas.0504343102

Mossahebi-Mohammadi, M., Quan, M., Zhang, J.-S., and Li, X. (2020). FGF Signaling Pathway: A Key Regulator of Stem Cell Pluripotency. *Front. Cel Dev. Biol.* 8, 79. doi:10.3389/fcell.2020.00079

Neuhaus, H., Rosen, V., and Thies, R. S. (1999). Heart Specific Expression of Mouse BMP-10 a Novel Member of the TGF-β Superfamily. *Mech. Dev.* 80 (2), 181–184. doi:10.1016/s0925-4773(98)00221-4

Ornitz, D. M., and Itoh, N. (2015). The Fibroblast Growth Factor Signaling Pathway. *Wires Dev. Biol.* 4 (3), 215–266. doi:10.1002/wdev.176

Ornitz, D. M., and Marie, P. J. (2015). Fibroblast Growth Factor Signaling in Skeletal Development and Disease. *Genes Dev.* 29 (14), 1463–1486. doi:10.1101/gad.266551.115

Pérez-Pomares, J. M., Macías, D., García-Garrido, L., and Muñoz-Chápuli, R. (1998). The Origin of the Subepicardial Mesenchyme in the Avian Embryo: an Immunohistochemical and Quail-Chick Chimera Study. *Dev. Biol.* 200, 57–68. doi:10.1006/dbio.1998.8949

Pérez-Pomares, J. M., Phelps, A., Sedmerova, M., Carmona, R., González-Iriarte, M., Muñoz-Chápuli, R., et al. (2002). Experimental Studies on the Spatiotemporal Expression of WT1 and RALDH2 in the Embryonic Avian Heart: a Model for the Regulation of Myocardial and Valvuloseptal Development by Epicardially Derived Cells (EPDCs). *Dev. Biol.* 247, 307–326. doi:10.1006/dbio.2002.0706

Pravoverov, K., Whiting, K., Thapa, S., Bushong, T., Trang, K., Lein, P. J., et al. (2019). MicroRNAs Are Necessary for BMP-7-Induced Dendritic Growth in Cultured Rat Sympathetic Neurons. *Cell Mol Neurobiol* 39 (7), 917–934. doi:10.1007/s10571-019-00688-2

Razy-Krajka, F., Gravez, B., Kaplan, N., Racioppi, C., Wang, W., and Christiaen, L. (2018). An FGF-Driven Feed-Forward Circuit Patterns the Cardiopharyngeal Mesoderm in Space and Time. *Elife* 7, e29656. doi:10.7554/eLife.29656

Red-Horse, K., Ueno, H., Weissman, I. L., and Krasnow, M. A. (2010). Coronary Arteries Form by Developmental Reprogramming of Venous Cells. *Nature* 464 (7288), 549–553. doi:10.1038/nature08873

Richter, A., Valdimarsdottir, L., Hrafnkelsdottir, H. E., Runarsson, J. F., Omarsdottir, A. R., Oostwaard, D. W. v., et al. (2014). BMP4 Promotes EMT and Mesodermal Commitment in Human Embryonic Stem Cells via SLUG and MSX2. *Stem Cells* 32 (3), 636–648. doi:10.1002/stem.1592

Rochais, F., Sturny, R., Chao, C.-M., Mesbah, K., Bennett, M., Mohun, T. J., et al. (2014). FGF10 Promotes Regional Foetal Cardiomyocyte Proliferation and Adult Cardiomyocyte Cell-Cycle Re-entry. *Cardiovasc. Res.* 104 (3), 432–442. doi:10.1093/cvr/cvu232

Ruiz-Villalba, A., Ziogas, A., Ehrbar, M., and Pérez-Pomares, J. M. (2013). Characterization of Epicardial-Derived Cardiac Interstitial Cells: Differentiation and Mobilization of Heart Fibroblast Progenitors. *PLoS One* 8 (1), e53694. doi:10.1371/journal.pone.0053694

Salazar, V. S., Gamer, L. W., and Rosen, V. (2016). BMP Signalling in Skeletal Development, Disease and Repair. *Nat. Rev. Endocrinol.* 12 (4), 203–221. doi:10.1038/nrendo.2016.12

Saxena, A., and Tabin, C. J. (2010). miRNA-Processing Enzyme Dicer Is Necessary for Cardiac Outflow Tract Alignment and Chamber Septation. *Proc. Natl. Acad. Sci.* 107 (1), 87–91. doi:10.1073/pnas.0912870107

Schlueter, J., and Brand, T. (2009). A Right-Sided Pathway Involving FGF8/Snai1 Controls Asymmetric Development of the Proepicardium in the Chick Embryo. *Proc. Natl. Acad. Sci.* 106 (18), 7485–7490. doi:10.1073/pnas.0811944106

Schlueter, J., and Brand, T. (2013). Subpopulation of Proepicardial Cells Is Derived from the Somatic Mesoderm in the Chick Embryo. *Circ. Res.* 113 (10), 1128–1137. doi:10.1161/circresaha.113.301347

Schlueter, J., Männer, J., and Brand, T. (2006). BMP Is an Important Regulator of Proepicardial Identity in the Chick Embryo. *Dev. Biol.* 295 (2), 546–558. doi:10.1016/j.ydbio.2006.03.036

Schulte, I., Schlueter, J., Abu-Issa, R., Brand, T., and Männer, J. (2007). Morphological and Molecular Left-Right Asymmetries in the Development of the Proepicardium: a Comparative Analysis on Mouse and Chick Embryos. *Dev. Dyn.* 236 (3), 684–695. doi:10.1002/dvdy.21065

Shah, T. A., Zhu, Y., Shaikh, N. N., Harris, M. A., Harris, S. E., and Rogers, M. B. (2017). Characterization of New Bone Morphogenetic Protein (Bmp)-2 Regulatory Alleles. *Genesis* 55 (7), e23035. doi:10.1002/dvg.23035

Singh, M. K., Lu, M. M., Massera, D., and Epstein, J. A. (2011). MicroRNA-processing Enzyme Dicer Is Required in Epicardium for Coronary Vasculature

Development. *J. Biol. Chem.* 286 (47), 41036–41045. doi:10.1074/jbc.m111.268573

Somi, S., Buffing, A. A. M., Moorman, A. F. M., and Van Den Hoff, M. J. B. (2004). Expression of Bone Morphogenetic Protein-10 mRNA during Chicken Heart Development. *Anat. Rec.* 279A (1), 579–582. doi:10.1002/ar.a.20052

Teichmann, U., and Kessel, M. (2004). Highly Restricted BMP10 Expression in the Trabeculating Myocardium of the Chick Embryo. *Dev. Genes Evol.* 214 (2), 96–98. doi:10.1007/s00427-003-0380-2

Tirosh-Finkel, L., Zeisel, A., Brodt-Ivenshitz, M., Shamai, A., Yao, Z., Seger, R., et al. (2010). BMP-mediated Inhibition of FGF Signaling Promotes Cardiomyocyte Differentiation of Anterior Heart Field Progenitors. *Development* 137 (18), 2989–3000. doi:10.1242/dev.051649

Torlopp, A., Schlueter, J., and Brand, T. (2010). Role of Fibroblast Growth Factor Signaling during Proepicardium Formation in the Chick Embryo. *Dev. Dyn.* 239 (9), 2393–2403. doi:10.1002/dvdy.22384

Townsend, T. A., Robinson, J. Y., Deig, C. R., Hill, C. R., Misfeldt, A., Blobe, G. C., et al. (2011). BMP-2 and TGFβ2 Shared Pathways Regulate Endocardial Cell Transformation. *Cells Tissues Organs* 194 (1), 1–12. doi:10.1159/000322035

van Wijk, B., van den Berg, G., Abu-Issa, R., Barnett, P., van der Velden, S., Schmidt, M., et al. (2009). Epicardium and Myocardium Separate from a Common Precursor Pool by Crosstalk between Bone Morphogenetic Protein- and Fibroblast Growth Factor-Signaling Pathways. *Circ. Res.* 105 (5), 431–441. doi:10.1161/circresaha.109.203083

Vega-Hernández, M., Kovacs, A., De Langhe, S., and Ornitz, D. M. (2011). FGF10/FGFR2b Signaling Is Essential for Cardiac Fibroblast Development and Growth of the Myocardium. *Development* 138 (15), 3331–3340. doi:10.1242/dev.064410

Vrancken Peeters, M.-P. F. M., Gittenberger-de Groot, A. C., Mentink, M. M. T., and Poelmann, R. E. (1999). Smooth Muscle Cells and Fibroblasts of the Coronary Arteries Derive from Epithelial-Mesenchymal Transformation of the Epicardium. *Anat. Embryol.* 199, 367–378. doi:10.1007/s004290050235

Wang, J., Greene, S. B., Bonilla-Claudio, M., Tao, Y., Zhang, J., Bai, Y., et al. (2010). Bmp Signaling Regulates Myocardial Differentiation from Cardiac Progenitors through a MicroRNA-Mediated Mechanism. *Dev. Cel* 19 (6), 903–912. doi:10.1016/j.devcel.2010.10.022

Watanabe, Y., Miyagawa-Tomita, S., Vincent, S. D., Kelly, R. G., Moon, A. M., and Buckingham, M. E. (2010). Role of Mesodermal FGF8 and FGF10 Overlaps in the Development of the Arterial Pole of the Heart and Pharyngeal Arch Arteries. *Circ. Res.* 106 (3), 495–503. doi:10.1161/circresaha.109.201665

Wojciechowska, A., Braniewska, A., and Kozar-Kamińska, K. (2017). MicroRNA in Cardiovascular Biology and Disease. *Adv. Clin. Exp. Med.* 26 (5), 865–874. doi:10.17219/acem/62915

Wu, M., Chen, G., and Li, Y.-P. (2016). TGF-β and BMP Signaling in Osteoblast, Skeletal Development, and Bone Formation, Homeostasis and Disease. *Bone Res.* 4, 16009. doi:10.1038/boneres.2016.9

Xie, Y., Su, N., Yang, J., Tan, Q., Huang, S., Jin, M., et al. (2020). FGF/FGFR Signaling in Health and Disease. *Sig Transduct Target. Ther.* 5 (1), 181. doi:10.1038/s41392-020-00222-7

Xin, M., Olson, E. N., and Bassel-Duby, R. (2013). Mending Broken Hearts: Cardiac Development as a Basis for Adult Heart Regeneration and Repair. *Nat. Rev. Mol. Cel Biol* 14 (8), 529–541. doi:10.1038/nrm3619

Zhang, J., Chang, J. Y. F., Huang, Y., Lin, X., Luo, Y., Schwartz, R. J., et al. (2010). The FGF-BMP Signaling axis Regulates Outflow Tract Valve Primordium Formation by Promoting Cushion Neural Crest Cell Differentiation. *Circ. Res.* 107 (10), 1209–1219. doi:10.1161/circresaha.110.225318

Zhang, J., Liu, J., Liu, L., McKeehan, W. L., and Wang, F. (2012). The Fibroblast Growth Factor Signaling axis Controls Cardiac Stem Cell Differentiation through Regulating Autophagy. *Autophagy* 8 (4), 690–691. doi:10.4161/auto.19290

Zhao, B., Etter, L., Hinton, R. B., Jr, and Benson, D. W. (2007a). BMP and FGF Regulatory Pathways in Semilunar Valve Precursor Cells. *Dev. Dyn.* 236 (4), 971–980. doi:10.1002/dvdy.21097

Zhao, Y., Ransom, J. F., Li, A., Vedantham, V., von Drehle, M., Muth, A. N., et al. (2007b). Dysregulation of Cardiogenesis, Cardiac Conduction, and Cell Cycle in Mice Lacking miRNA-1-2. *Cell* 129 (2), 303–317. doi:10.1016/j.cell.2007.03.030

Zhou, B., Ma, Q., Rajagopal, S., Wu, S. M., Domian, I., Rivera-Feliciano, J., et al. (2008). Epicardial Progenitors Contribute to the Cardiomyocyte Lineage in the Developing Heart. *Nature* 454 (7200), 109–113. doi:10.1038/nature07060

Zinski, J., Tajer, B., and Mullins, M. C. (2018). TGF-β Family Signaling in Early Vertebrate Development. *Cold Spring Harb Perspect. Biol.* 10 (6), a033274. doi:10.1101/cshperspect.a033274

Conflict of Interest: The authors declare that the research was conducted in the absence of any commercial or financial relationships that could be construed as a potential conflict of interest.

Publisher's Note: All claims expressed in this article are solely those of the authors and do not necessarily represent those of their affiliated organizations, or those of the publisher, the editors, and the reviewers. Any product that may be evaluated in this article, or claim that may be made by its manufacturer, is not guaranteed or endorsed by the publisher.

frontiers in Cell and Developmental Biology

ORIGINAL RESEARCH
published: 11 January 2022
doi: 10.3389/fcell.2021.767954

Dynamic MicroRNA Expression Profiles During Embryonic Development Provide Novel Insights Into Cardiac *Sinus Venosus*/Inflow Tract Differentiation

Carlos Garcia-Padilla[1,2†], *Angel Dueñas*[1,2†], *Diego Franco*[2,3], *Virginio Garcia-Lopez*[1], *Amelia Aranega*[2,3], *Virginio Garcia-Martinez*[1] *and Carmen Lopez-Sanchez*[1]*

[1]Department of Human Anatomy and Embryology, Faculty of Medicine, Institute of Molecular Pathology Biomarkers, University of Extremadura, Badajoz, Spain, [2]Department of Experimental Biology, University of Jaen, Jaen, Spain, [3]Fundación Medina, Granada, Spain

OPEN ACCESS

Edited by:
Rosa Barrio,
CIC bioGUNE, Spain

Reviewed by:
Marina Campione,
National Research Council (CNR), Italy
Raquel P. Andrade,
Universidade do Algarve, Portugal

***Correspondence:**
Carmen Lopez-Sanchez
clopez@unex.es

[†]These authors have contributed equally to this work and share first authorship

Specialty section:
This article was submitted to Morphogenesis and Patterning, a section of the journal Frontiers in Cell and Developmental Biology

Received: 31 August 2021
Accepted: 16 December 2021
Published: 11 January 2022

Citation:
Garcia-Padilla C, Dueñas A, Franco D, Garcia-Lopez V, Aranega A, Garcia-Martinez V and Lopez-Sanchez C (2022) Dynamic MicroRNA Expression Profiles During Embryonic Development Provide Novel Insights Into Cardiac Sinus Venosus/Inflow Tract Differentiation. Front. Cell Dev. Biol. 9:767954. doi: 10.3389/fcell.2021.767954

MicroRNAs have been explored in different organisms and are involved as molecular switches modulating cellular specification and differentiation during the embryonic development, including the cardiovascular system. In this study, we analyze the expression profiles of different microRNAs during early cardiac development. By using whole mount *in situ* hybridization in developing chick embryos, with microRNA-specific LNA probes, we carried out a detailed study of miR-23b, miR-130a, miR-106a, and miR-100 expression during early stages of embryogenesis (HH3 to HH17). We also correlated those findings with putative microRNA target genes by means of mirWalk and TargetScan analyses. Our results demonstrate a dynamic expression pattern in cardiac precursor cells from the primitive streak to the cardiac looping stages for miR-23b, miR-130a, and miR-106a. Additionally, miR-100 is later detectable during cardiac looping stages (HH15-17). Interestingly, the *sinus venosus*/inflow tract was shown to be the most representative cardiac area for the convergent expression of the four microRNAs. Through *in silico* analysis we revealed that distinct Hox family members are predicted to be targeted by the above microRNAs. We also identified expression of several Hox genes in the *sinus venosus* at stages HH11 and HH15. In addition, by means of gain-of-function experiments both in cardiomyoblasts and *sinus venosus* explants, we demonstrated the modulation of the different Hox clusters, Hoxa, Hoxb, Hoxc, and Hoxd genes, by these microRNAs. Furthermore, we correlated the negative modulation of several Hox genes, such as Hoxa3, Hoxa4, Hoxa5, Hoxc6, or Hoxd4. Finally, we demonstrated through a dual luciferase assay that Hoxa1 is targeted by miR-130a and Hoxa4 is targeted by both miR-23b and miR-106a, supporting a possible role of these microRNAs in Hox gene modulation during differentiation and compartmentalization of the posterior structures of the developing venous pole of the heart.

Keywords: heart development, microRNAs, expression profiles, Hox genes, sinus venosus, inflow tract

INTRODUCTION

During chick gastrulation (stage HH3; Hamburger and Hamilton, 1951, 1992) the primitive streak precardiac cells invaginate and migrate anterolaterally to form the precardiac mesoderm, between the ectoderm and the inductive adjacent endoderm (Garcia-Martinez and Schoenwolf, 1993; Schultheiss et al., 1995; Garcia-Martinez et al., 1997; Redkar et al., 2001; Lopez-Sanchez et al., 2001, 2009, 2018), at both sides of the embryo (stages HH5-7), determining the first heart field (FHF; Harvey, 2002). Subsequently, this field will form the primitive endocardial tubes (stage HH8), which in the midline fuse into a single heart tube (stage HH10), structured into the endocardial and myocardial layers (Lopez-Sanchez and Garcia-Martinez 2011). Later on, a progenitor population originating from the adjacent pharyngeal mesoderm, the secondary heart field (SHF; Buckingham et al., 2005), will contribute to further cardiac development, giving rise to the dorsal *mesocardium*, as well as the posterior (venous) and anterior (arterial) heart poles, differentiating the inflow (IFT) and outflow tracts (OFT), respectively (Waldo et al., 2005; Abu-Issa and Kirby 2008; van den Berg et al., 2009; Camp et al., 2012; Zaffran and Kelly, 2012; De Bono et al., 2018a). The IFT, a relevant segment in the sinoatrial node formation, develops from a restricted set of cardiomyocytes located in the *sinus venosus* (SV). Furthermore, the outer surface of the SV gives rise to the proepicardium—epicardial primordium—development (Christoffels et al., 2006; van Wijk et al., 2009, 2018; Mommersteeg et al., 2010; Carmona et al., 2018).

A complex network of signaling pathways and transcriptional factors is required to regulate early cardiac development. In this sense, the FGF, TGF, and Wnt pathways, among others, have been widely involved in early cardiogenesis. In particular, within this signaling network, retinoic acid (RA) has been shown to pattern the SHF (Hochgreb et al., 2003; Stefanovic and Zaffran, 2017). RA signaling is required for SHF differentiation, modulating the expression of specific marker genes, including Fgf8, Fgf10, and Tbx1 (Ryckebusch et al., 2008; Sirbu et al., 2008; De Bono et al., 2018b). Previous genetic lineage analyses in mice have revealed that Homeobox (Hox) gene expressions—Hoxa1, Hoxa3, and Hoxb1—define distinct domains and sub-domains within the SHF (Bertrand et al., 2011). Thus, Hoxa1- and Hoxb1-expressing progenitor cells contribute to both cardiac poles' development, the IFT and the inferior wall of the OFT (Bertrand et al., 2011; Lescroart and Zaffran, 2018; Stefanovic et al., 2020).

Due to the fact that microRNAs represent a novel layer of complexity in the regulatory networks controlling gene expression, cell specification, and differentiation (Choi et al., 2013; Rajabi et al., 2020), this subclass of non-coding RNAs has been widely analyzed by its relevant role in cardiac development. Previous studies have provided evidence on the differential expression of several microRNAs contributing to cardiac fate specification and maintenance of cardiac progenitors during development (Chinchilla et al., 2011; Cao et al., 2012; Lopez-Sanchez et al., 2015a; Lopez-Sanchez et al., 2015b; Yan and Jiao 2016; Kalayinia et al., 2021). Some microRNA expressions, such as those of miR-125b, miR-142-3p, and miR-137, have also been referenced in the SV/IFT (Darnell et al., 2006).

In order to shed light on microRNAs and their role during early cardiac development, in this work, we analyze the expression pattern of miR-23b, miR-130a, miR-106a, and miR-100, from early stages of embryogenesis (HH3 to HH17). Although these microRNAs have been previously involved in cardiac structural and functional characteristics (Sucharov et al., 2008; Thum et al., 2008; Aguirre et al., 2014; Guan et al., 2016; Boureima Oumarou et al., 2019), their roles during cardiac development have still not been assessed. Our results show a common expression of these microRNAs in specific cardiac structures, the SV/IFT being the most representative cardiac area for their convergent expression. Also, we have correlated these findings with several Hox family members revealed as targets of these microRNAs by means of mirWalk and TargetScan analyses. Furthermore, we have identified that several Hox genes targeted by these microRNAs are expressed in the HH11 and HH15 *sinus venosus*. Finally, by using *in vitro* microRNA gain-of-function experiments on cardiomyoblasts derived from undifferentiated H9c2 cells, together with an analysis of chicken *sinus venosus* explants, we have shown in this study the specific relevance of distinct microRNAs in Hox gene modulation, suggesting a possible molecular role in the differentiation and/or compartmentalization of the developing venous pole of the heart.

RESULTS

Expression Profile of miR-23b, miR-130a, miR-106a, and miR-100 During Early Embryonic Development

In this work, we have analyzed the expression profile of miR-23b, miR-130a, miR-106a, and miR-100 during early chicken embryonic development (**Figures 1**, **2**), starting at early gastrulation stages through the formation of the early cardiac looped stages, from HH3 to HH17.

From early stages of development, miR-23b (**Figure 1A**) extends along the primitive streak (HH3). Later, this expression expands to the precardiac mesoderm and the underlying endoderm at both sides of the embryo and contributes to the formation of the first heart field (HH5), maintaining its expression in both primitive endocardial tubes (HH8). As shown in HH9-10, during cardiac tube formation, this expression is progressively restricted to the inflow tract. Noticeably, during early cardiac looping (HH11), miR-23b is expressed in both inflow and outflow tracts, subsequently being more evident on the dorsal surface of the cardiac *sinus venosus* and the dorsal mesocardium (HH14).

We have previously described that miR-130a starts expressing at the primitive streak stage (HH3), followed by an expansion toward both sides of the mesodermal and endodermal layers of the embryo (HH4). From stage HH5 onward, miR-130a is progressively restricted to the precardiac mesoderm and its

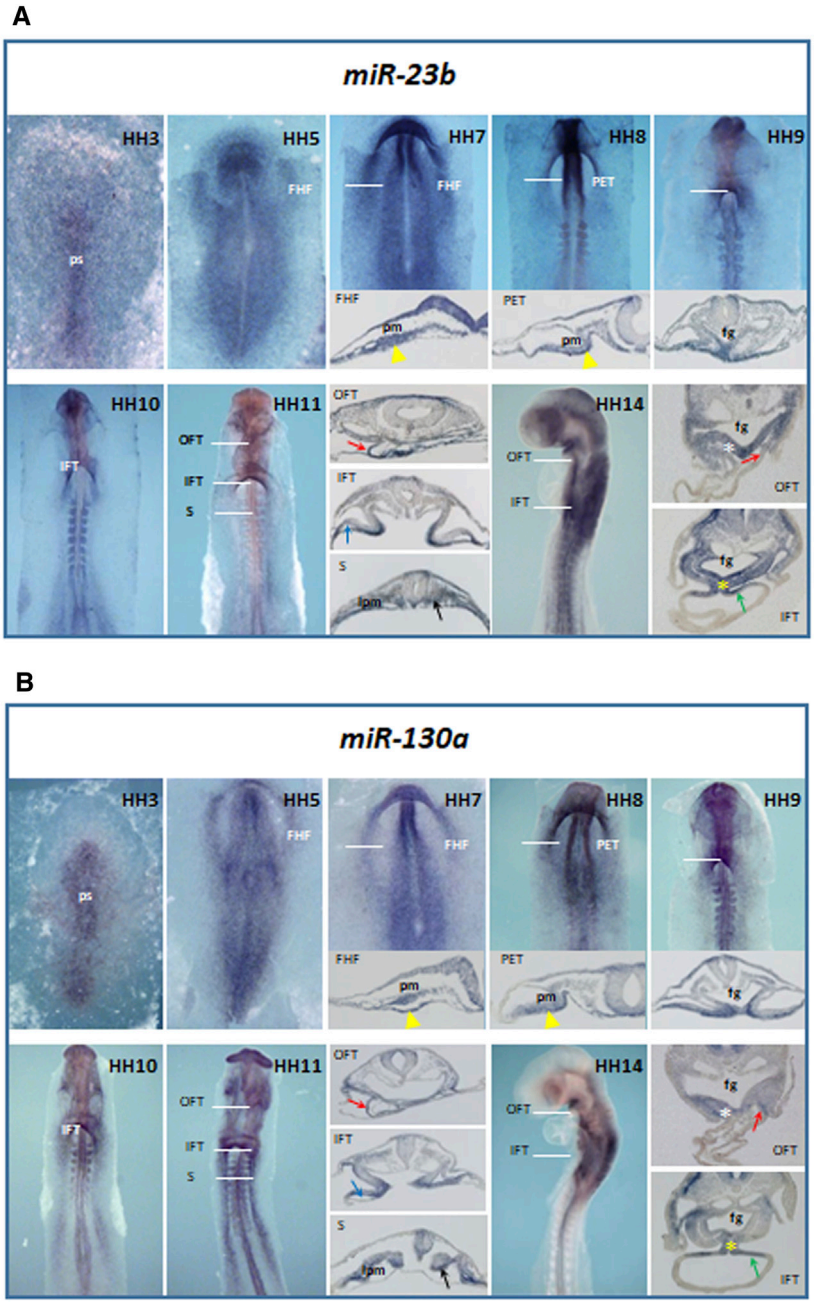

FIGURE 1 | Whole-mount ISH analysis of miR-23b **(A)**, miR-130a **(B)**, miR-106a **(C)**, and miR-100 **(D)** during chick embryo cardiac development, from HH3 through HH14. White lines indicate the transverse section levels of selected embryos: FHF, first heart field; PET, primitive endocardial tube; IFT, inflow tract; OFT, outflow tract and S, somite level. Note their expressions in the primitive streak (ps), precardiac mesoderm (pm), adjacent endoderm to precardiac mesoderm (yellow arrowhead), OFT (red arrow), dorsal surface of *sinus venosus* (green arrow), dorsal mesocardium (yellow asterisk), and vitelline vein (blue arrow); as well as in the foregut (fg), pharyngeal mesoderm (white asterisk), lateral plate mesoderm (lpm), and somites (black arrow) for miR-23b **(A)**, miR-130a **(B)**, and miR-106a **(C)**. Just from stage HH15 is observable miR-100 expression **(D)** in cardiac structures. V, ventricle.

underlying endoderm, subsequently expressing in both primitive endocardial tubes (Lopez-Sanchez et al., 2015a). One of the novelties of this study lies in the identification of miR-130a expression during primitive cardiac tube formation (**Figure 1B**), specifically in the dorsal mesocardium and the dorsal wall of the cardiac *sinus venosus* (HH9-14), as well as in the outflow tract.

During early stages of development, miR-106a (**Figure 1C**) shows a broad expression in the embryo, sharper in the primitive streak (HH3). Afterward, it expresses homogeneously throughout

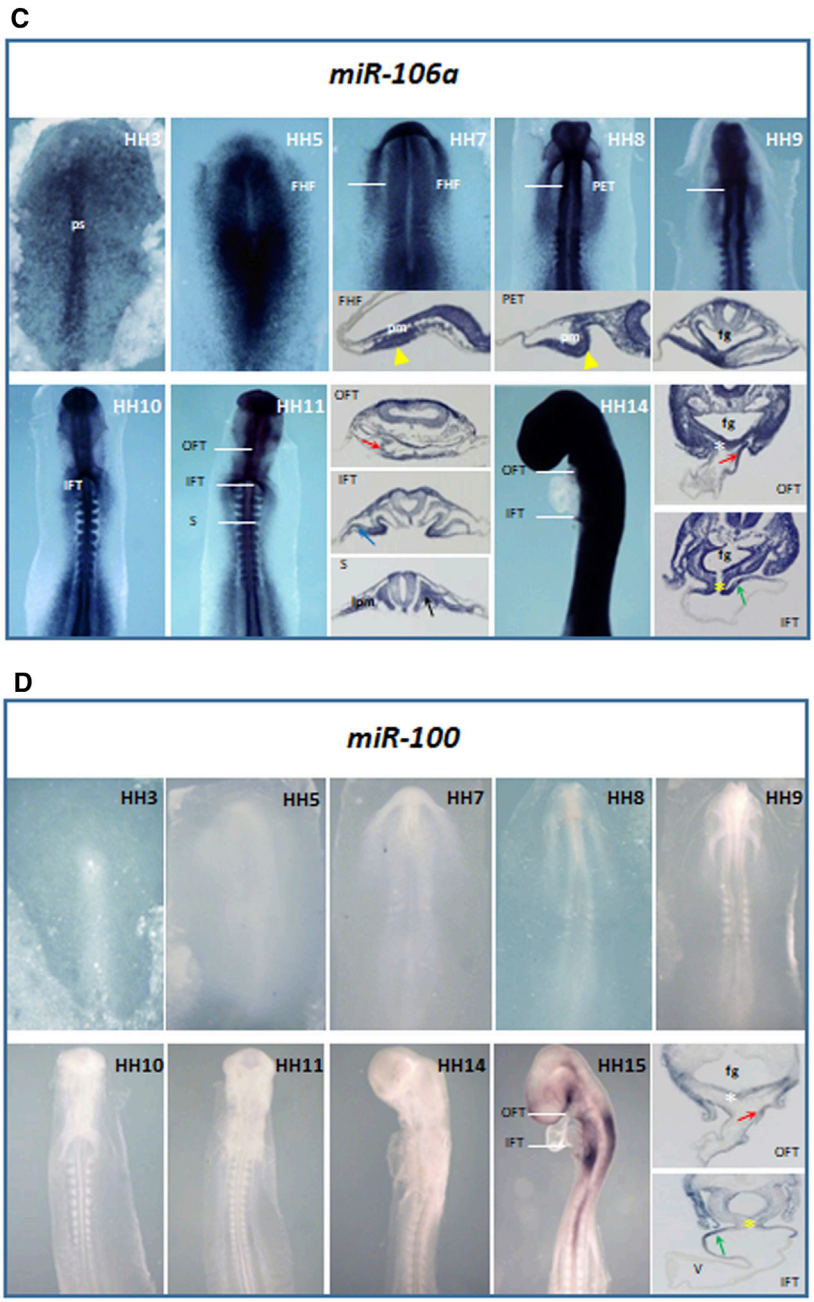

FIGURE 1 | (Continued).

the embryo (HH5-13), excluding the extraembryonic tissue. Although this expression covers all the heart regions and derivatives at early stages (HH8-11), it is restricted to the dorsal mesocardium and the inflow and outflow tracts at later stages (HH14). The signal stays homogeneously strong in the remaining embryo, except in the developing cardiac chambers.

Additionally, we have observed the expression of the microRNAs mentioned above in somites and the lateral plate mesoderm, among others (**Figures 1A–C**).

Unlike miR-23b, miR-130a, and miR-106a, the expression of miR-100 starts at the HH15 stage, being evident on the dorsal surface of the inflow tract and in the dorsal mesocardium and outflow tract (**Figure 1D**).

During cardiac looping stages (HH15–17), the four microRNAs analyzed (**Figure 2**) are expressed in the lateral–dorsal wall of the outflow tract and foregut, being evident in the dorsal wall of the inflow tract and the dorsal mesocardium. Interestingly, in these stages, all these microRNAs

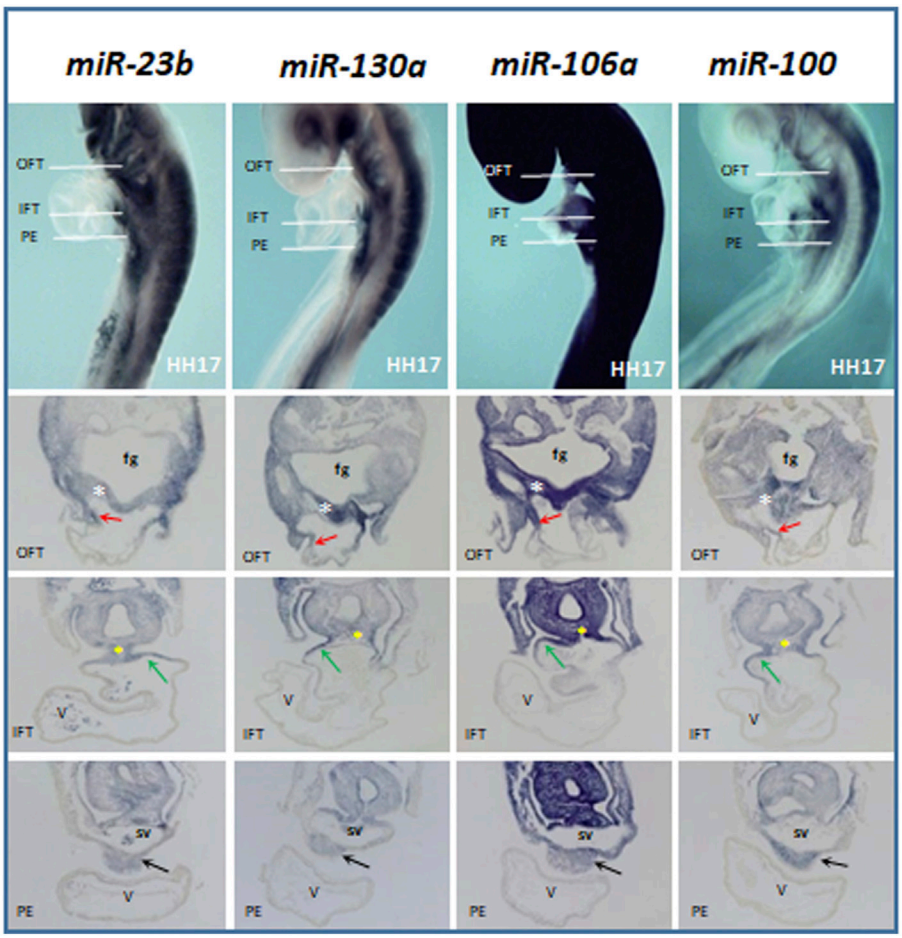

FIGURE 2 | Comparative whole-mount ISH analysis of miR-23b, miR-130a, miR-106a, and miR-100 expression profiles at stage HH17. The transverse section levels are indicated with white lines: OFT, outflow tract; IFT, inflow tract, and PE, proepicardium. Note their expressions in the lateral–dorsal wall of the OFT (red arrow), foregut (fg), dorsal wall of the IFT (green arrow), dorsal mesocardium (yellow asterisk), and proepicardium (black arrow). White asterisk, pharyngeal mesoderm; V, ventricle; sv, *sinus venosus*.

show a marked expression in the proepicardium, which is formed at the cardiac inflow region, both coming from a common progenitor pool (van Wijk et al., 2009, 2018).

Hox Cluster Family Members Are Differentially Modulated by miR-23b, miR-130a, miR-106a, and miR-100

Modulation by multiple microRNAs within the same pathway—and even common targets—has been widely reported (Wu et al., 2010; Shu et al., 2017). Since those microRNAs analyzed in this study are particularly expressed in the cardiac inflow tract at early developing stages, we have considered that they could recognize common targets likely involved in the differentiation processes of this segment. Several gene families and transcription factors are important to establish compartmentalization of the embryo, especially during early stages of development. In this sense, Hox gene families have gained pivotal relevance in the last 3 decades. Those genes are broadly conserved during evolution, and their roles to shape the body of the embryo have been widely described in multiple species (Roux and Zaffran, 2016; Lescroart and Zaffran, 2018). In addition, expression of Hox genes in the cardiovascular system is rather restricted, mostly confined to the posterior SHF-derived venous pole of the heart. We therefore explored the expression profile of all cranially expressed Hox genes, including all paralogues (Hoxa to Hoxd) from one to six in the chicken cardiac *sinus venosus* at stages HH11 and HH15 (**Figure 3**). From our data, most of these Hox genes were detected in the *sinus venosus* at stages HH11 and HH15, except for Hoxa1 (**Figure 3A**). In addition, we observed that Hoxa2, Hoxa4, and Hoxa5 (**Figure 3A**), Hoxb3 and Hoxb6 (**Figure 3B**), Hoxc4 and Hoxc6 (**Figure 3C**), and Hoxd1, Hoxd3, and Hoxd4 (**Figure 3D**) display well-marked expression at stage HH11 compared to HH15. On the other hand, Hoxa3 (**Figure 3A**), Hoxb1, Hoxb2, Hoxb4, and Hoxb5 (**Figure 3B**) showed an intense expression at HH15. Finally, Hoxa6 and Hoxc5 presented a similar expression at both stages (**Figures 3A,C**).

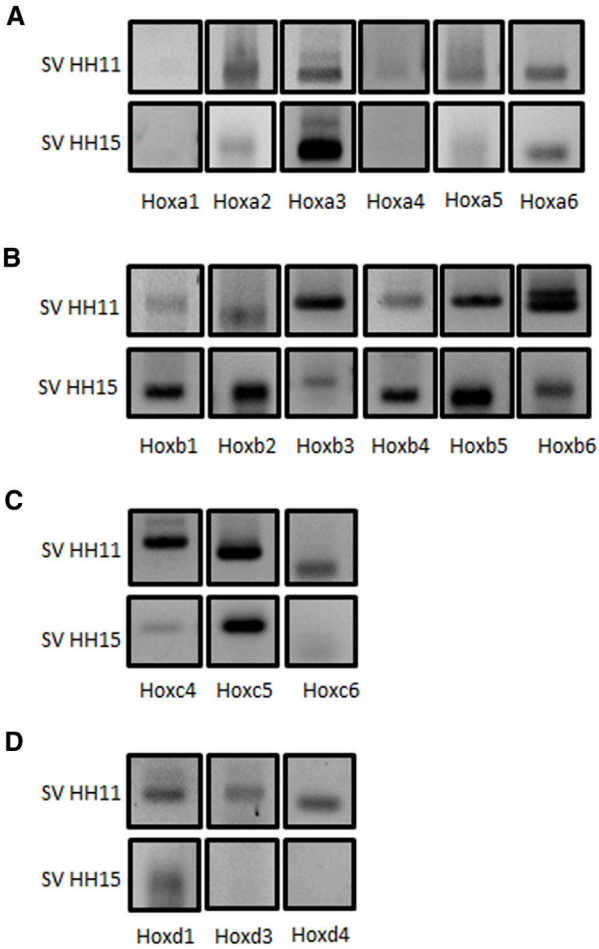

FIGURE 3 | Comparative analysis of Hox gene expression in the *sinus venosus* between stages HH11 and HH15. RT-PCR analyses of Hoxa (Panel **A**), Hoxb (Panel **B**), Hoxc (Panel **C**), and Hoxd (Panel **D**) cluster family members, as demonstrated by their amplified amplicons on agarose gel electrophoresis. Observe that most Hox genes analyzed, except Hoxa1, are detectable at HH11 and HH15 in the *sinus venosus*.

Since several Hox genes are expressed at stages HH11 and HH15, we considered in this study the possibility that microRNAs under analysis could be recognizing the 3′UTRs of the distinct Hox genes and thus modulating their expression. By using mirWalk (Sticht et al., 2018) and TargetScan softwares, we analyzed *in silico* those common targets shared by miR-23b, miR-130a, miR-106a, and miR-100. It is observed that these four microRNAs do not share any targets simultaneously, as shown in **Figure 4**. On the other hand, all Hox genes are recognized by at least one of these microRNAs, except Hoxa6 (**Supplementary Table S1**).

It is to note that H9c2 cardiomyoblasts can be differentiated into cardiomyocytes by administrating retinoic acid (RA) to the culture medium when cells reach a high degree of confluence (Branco et al., 2015). Our expression analyses of Nkx2.5—an early cardiogenic marker—and cardiac troponin T (cTnT)—a late differentiation marker—corroborated that there are differences between H9c2 cardiomyoblasts and cardiomyocytes (**Supplementary Figure S1**). To assess the possible role of these microRNAs as Hox gene modulators, we performed microRNA gain-of-function assays in cardiomyoblasts (**Supplementary Figure S2**). As observed in **Figure 5** and summarized in **Table 1**, after gain-of-function experiments in cardiomyoblasts, Hoxa1, Hoxa3, and Hoxa4 were repressed by the four microRNAs studied. Also, Hoxa2 and Hoxa5 were inhibited by miR-130a, and Hoxa6 was downregulated by miR-130a and miR-100. On the other hand, Hoxa5 was significantly upregulated by miR-23b and miR-106a administration. Hoxa6 was also upregulated by miR-23b (**Figure 5A**). With respect to the Hoxb cluster (**Figure 5B**, **Table 1**), different Hox genes were repressed by their respective microRNAs (Hoxb1/miR-130a; Hoxb5/miR-100 and Hoxb6 by mir-130a, miR-106a and miR-100). On the other hand, Hoxb1, Hoxb4, Hoxb5, and Hoxb6 were significantly upregulated by miR-23b. Hoxb5 was also upregulated by miR-130a and miR-106a. Hoxb2 and Hoxb3 were not detected in H9c2 cardiomyoblasts. Within the Hoxc cluster, only Hoxc6 expression was observed, showing a downregulation by miR-23b and miR-130a and upregulation by miR-106a and miR-100 (**Figure 5C**, **Table 1**). Finally, in reference to the Hoxd cluster (**Figure 5D**, **Table 1**), Hoxd3 and Hoxd4 were repressed by miR-23b and miR-100, and also, Hoxd3 was downregulated by miR-130a. In contrast, Hoxd3 and Hoxd4 were upregulated by miR-106a and miR-130a, respectively. Hoxd1 expression was not detected in H9c2 cardiomyoblasts.

Subsequently, in order to determine the modulation of Hox genes by these microRNAs in the developing venous pole of the heart, we performed gain-of-function experiments in *sinus*

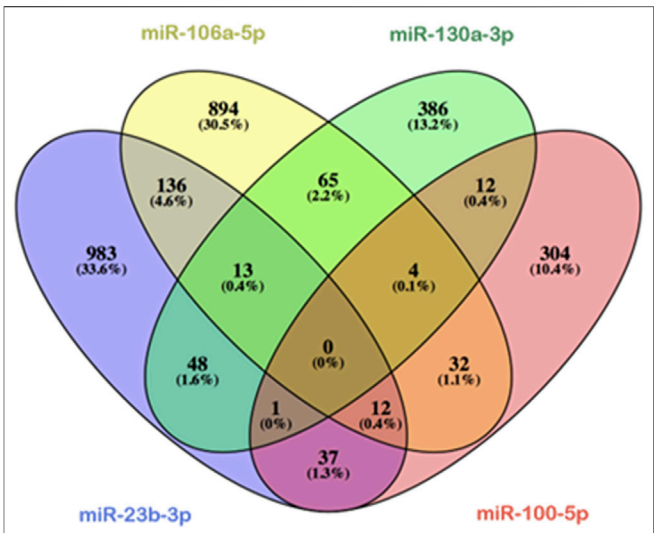

FIGURE 4 | Venn diagram shared potential targets of miR-23b-3p (blue ellipse), miR-130a-3p (green ellipse), miR-106-5p (yellow ellipse), and miR-100-5p (red ellipse), studied by means of mirWalk software analysis. Note *in silico* predictions that the four microRNAs studied have not shared any target, while a few numbers of common targets are recognized by three of the four microRNAs. Overlapping ellipses represent shared targets between these microRNAs.

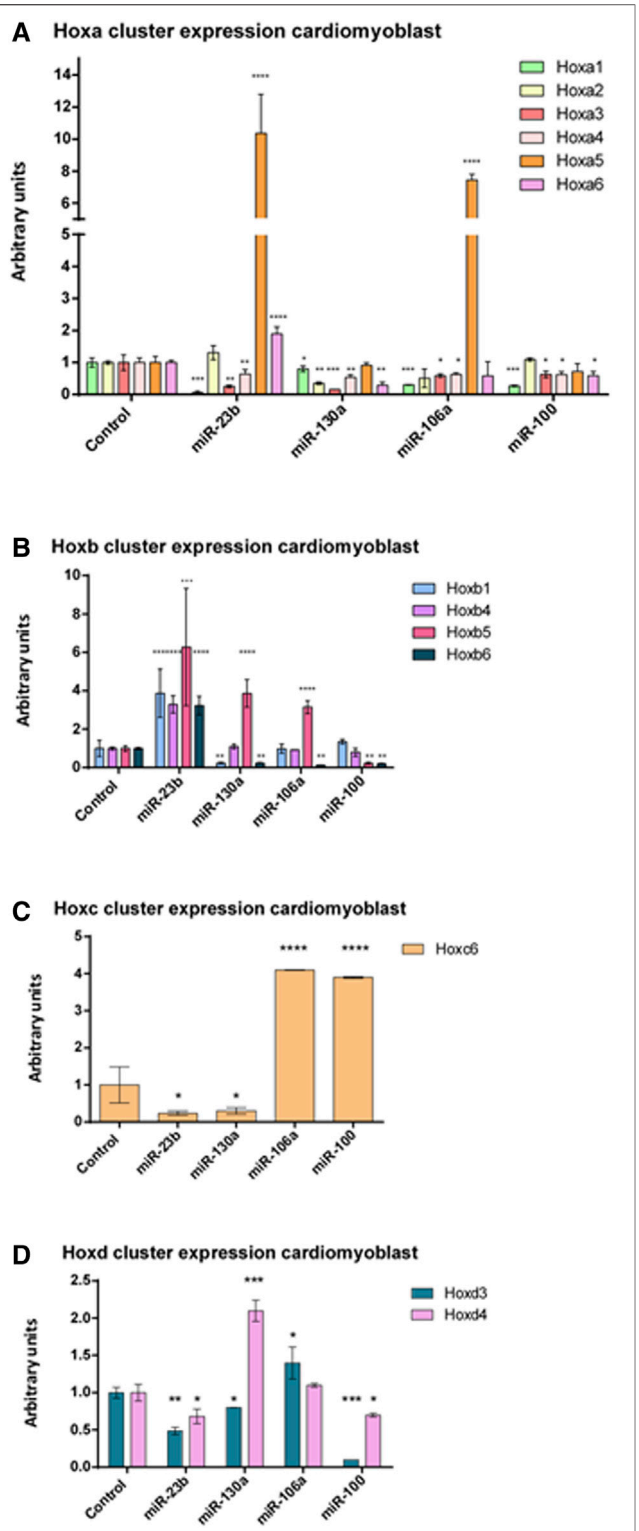

FIGURE 5 | qPCR analysis of Hoxa **(A)**, Hoxb **(B)**, Hoxc **(C)**, and Hoxd **(D)** clusters expression after miR-23b, miR-130a, miR-106a, and miR-100 gain-of-function assays in H9c2 cardiomyoblasts illustrating significant up- and downregulation of these Hox genes. Student's *t*-test: $*p < 0.05$, $**p < 0.01$, $***p < 0.005$, $****p < 0.001$.

venosus explants, at stages HH11 and HH15 (**Supplementary Figure S3**). **Figure 6** and **Tables 2**, **3** summarize our data, showing that Hoxa3 was downregulated by miR-23b, miR-106a, and miR-100 at stage HH11. Hoxa4 was downregulated by miR-130a and miR-100 at stage HH11 and by miR-23b, miR-106, and miR-100 at HH15 (**Figures 6A, B**). These data are in line with the results obtained in our gain-of-function experiments in cardiomyoblasts. Additionally, Hoxa5 was repressed by miR-23b, miR-106a, and miR-100 at stage HH11, while it was downregulated by miR-23b, miR-130a, and miR-106a at HH15. Also, Hoxa2 was repressed by miR-130a and miR-106a at HH15, suggesting their involvement in further stages of *sinus venosus* formation. On the other hand, the downregulation of Hoxb6 by miR-106a both in *sinus venosus* explants at HH11 and cardiomyoblasts would suggest a participation in early differentiation. As observed in **Figures 6C, D**, Hoxb1 and Hoxb4 were not detected in these experiments. Coinciding with the results obtained in cardiomyoblasts, Hoxc6 was downregulated by miR-23b and miR-130a at stage HH15 (**Figure 6F**) and Hoxd4 was repressed by miR-23b and miR-100 at HH11 (**Figure 6G**).

Since Hoxa1 and Hoxa4 expressions were modulated tnegatively by those microRNAs analyzed *in vitro* and given that their 3′UTR harbor multiple seed sequences for these microRNAs, we performed dual luciferase biochemical assays to determine whether miR-23b, miR-130a, miR-106a, and miR-100 could directly target either Hoxa4 or Hoxa1 3′UTRs (**Figure 7**). Our data demonstrated that miR-130a could not interact directly with Hoxa4 3′UTR (**Figure 7A**), which is in agreement with the fact that this microRNA is not predicted either by mirWalk or TargetScan. Interestingly, transfection with miR-106a and miR-23b significantly decreased Hox4 luciferase levels with respect to control samples (**Figures 7B, C**), in line with mirWalk predictions (**Supplementary Table S1**), thus proving a direct interaction between those two microRNAs and Hoxa4 3′UTR. As for Hoxa1 3′UTR (**Figures 7D–F**), only miR-130a reduced luciferase levels with respect to the control, thus suggesting an indirect repression exerted by miR-23b, miR-106a, and miR-100 on this gene.

DISCUSSION

Previous studies have demonstrated that a single microRNA may be a crucial regulator both in cardiac development and function. Imbalanced microRNA expression in the progenitor cells of the developing heart might cause congenital and/or structural defects, including altered cell migration and proliferation, as well as inappropriate cell type specification (Pang et al., 2019; Kalayinia et al., 2021). In particular, it has been reported that: 1) miR-23b is upregulated in cardiac hypertrophy, and its over-expression in cardiomyocytes *in vitro* is sufficient to promote hypertrophic growth (Thum et al., 2008; Boureima Oumarou et al., 2019); 2) miR-130a is required for adequate proliferation of cardiac progenitors (Kim et al., 2009), supported by gain-of-function murine experiments, leading to cardiomyocyte proliferation defects as ventricular hypoplasia; 3) miR-106a is

TABLE 1 | Hox genes modulated by microRNAs in cardiomyoblasts.

	Hoxa1	Hoxa2	Hoxa3	Hoxa4	Hoxa5	Hoxa6	Hoxb1	Hoxb4	Hoxb5	Hoxb6	Hoxc6	Hoxd3	Hoxd4
miR-23b	→	—	→	→	←	←	←	←	←	←	←	→	→
miR-130a	→	→	→	→	→	→	→	—	←	→	→	→	←
miR-106a	→	—	→	→	←	—	—	—	←	→	←	←	—
miR-100	→	—	→	→	—	→	—	—	→	→	←	→	→

Diagram illustrating Hox genes modulation exerted by miR-23b, miR-130a, miR-106a and miR-100 after gain-of-function assays in cardiomyoblast cell line (obtained from ***Figure 5****). Green arrows: upregulated. Red arrows: downregulated. Black lines: Do not regulate.*

significantly upregulated in cardiac hypertrophy, as demonstrated by *in vivo* and *in vitro* analyses (Guan et al., 2016); and 4) although miR-100 function is not relevant to hypertrophic gene expression, its role in cardiac regeneration has been widely demonstrated in zebrafish and mice, and it also plays specific roles in adult isoform cardiac gene regulation (Tarantino et al., 2010; Aguirre et al., 2014).

Since these microRNAs have proved significant in cardiac structural and functional features, we will proceed to discuss their relevance during cardiac development. Previously, the expression profile of miR-23b has been identified in the cardiac tissue of fetal mice from E12.5 to E18.5 (Cao et al., 2012). Also, miR-23b expression has been observed in developing chicks, although restricted to the atrium and the dorsal aorta, since stage HH22. On the other hand, a widespread expression of miR-130a, miR-106a, and miR-100 has been described (Darnell et al., 2006), although cardiac expression of these microRNAs has not been previously described. In our study, we carried out a detailed analysis of miR-23b, miR-130a, miR-106a, and miR-100 expression profiles, from early gastrulation stages to the formation of the early cardiac looping stage. Our results reveal miR-23b, miR-130a, and miR-106a expressions in the primitive streak and the first heart field, maintaining their expressions in both primitive endocardial tubes and cardiac tube formation. In addition, miR-100 expression is observed during cardiac looping stages. Subsequently, these four microRNAs show common expression in specific cardiac structures, including inflow and outflow tracts, as well as the dorsal mesocardium and the proepicardium. This is the first time that the cardiac expression profiles of these four microRNAs have been described, suggesting that they could play crucial roles in multiple cardiac development processes from early stages.

In our study, we show that numerous Hox genes are expressed in the *sinus venosus* at stages HH11 and HH15. These data are relevant since, to date, only the expression of a few Hox genes—Hoxa1, Hoxa3, Hoxa4, Hoxb1, and Hoxb4—has been demonstrated in different species (Searcy and Yutzey, 1998; Makki and Capecchi, 2010; Bertrand et al., 2011; Barak et al., 2012; Roux et al., 2015; Lescroart and Zaffran, 2018; Stefanovic et al., 2020). We have subsequently explored the possibility that those microRNAs studied by ISH, the expression of which is particularly observed in the *sinus venosus*, could recognize 3′UTRs regions of the Hox genes and modulate their expression. Based on *in silico* analysis, we observe that one or more of the microRNAs under study recognized all cranially expressed Hox genes, including all paralogues (Hoxa to Hoxd) from 1 to 6, except Hoxa6. The potential modulation of Hox gene expression is confirmed by the results we obtained from *in vitro* assays in cardiomyoblasts and *ex vivo* assays in *sinus venosus* explants.

The role of retinoic acid (RA) in differentiation and morphogenesis of structures derived from the posterior segment of the heart tube has been widely described (Bertrand et al., 2011; De Bono et al., 2018b). Deficient RA synthesis results in cellular hypoplasia and, consequently, in morphogenetic defects in both the atrium

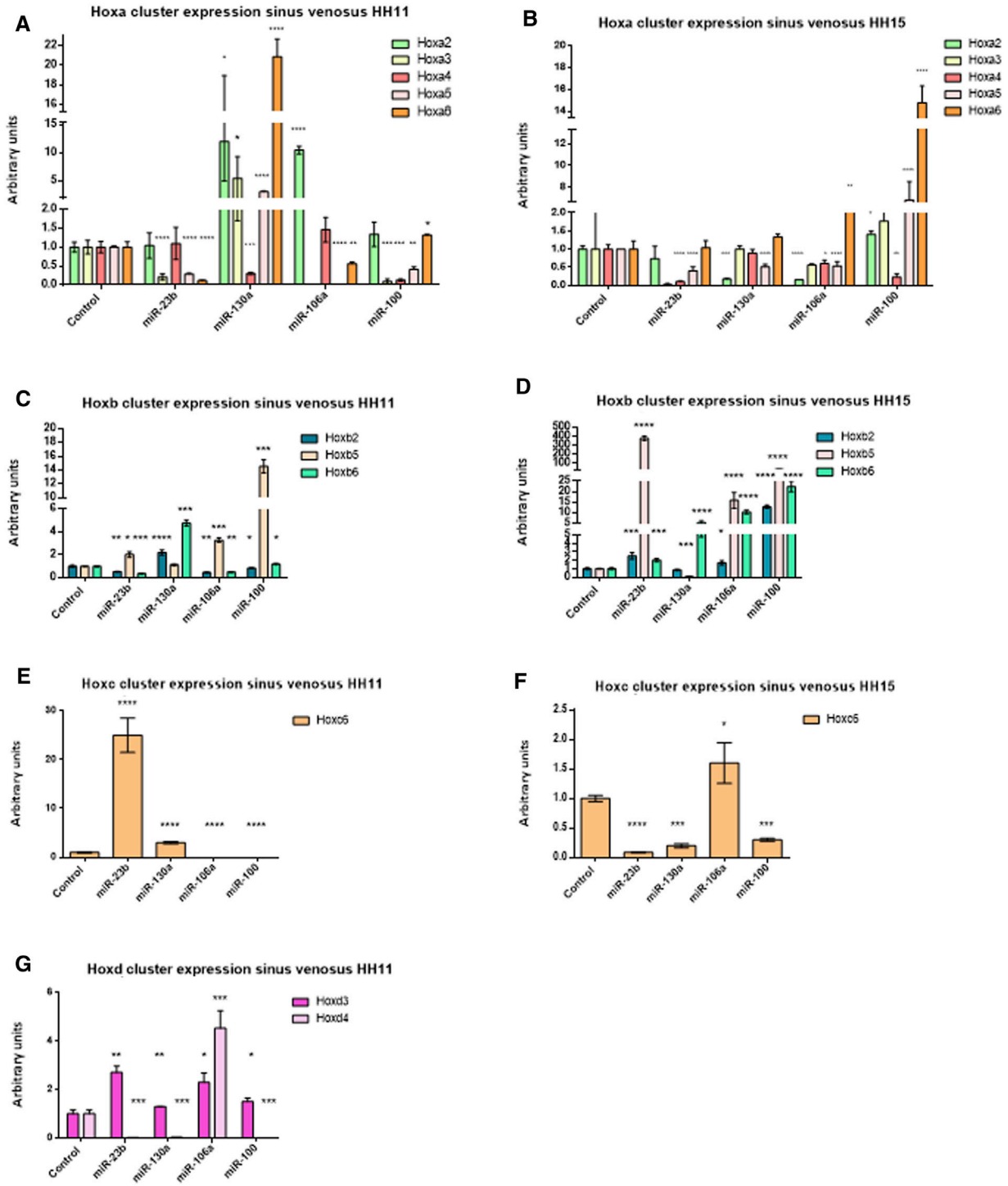

FIGURE 6 | qPCR analysis of the Hoxa cluster at stage HH11 **(A)** and HH15 **(B)**; Hoxb cluster at stage HH11 **(C)** and HH15 **(D)**; Hoxc cluster at stage HH11 **(E)** and HH15 **(F)**, and Hoxd cluster at stage HH11 **(G)** gene expression in *sinus venosus* explants after miR-23b, miR-130a, miR-106a, and miR-100 gain-of-function assays illustrating significant up- and downregulation of these Hox genes. Student's *t*-test: $*p < 0.05$, $**p < 0.01$, $***p < 0.005$, $****p < 0.001$.

TABLE 2 | Hox genes modulated by microRNAs in the *sinus venosus* at stage HH11.

	Hoxa2	Hoxa3	Hoxa4	Hoxa5	Hoxa6	Hoxb2	Hoxb5	Hoxb6	Hoxc6	Hoxd3	Hoxd4
miR-23b	—	↓	—	↓	↓	↓	↑	↓	↑	↑	↓
miR-130a	↑	↑	↓	↑	↑	↑	—	↑	↑	↑	↓
miR-106a	↑	↓	—	↓	↓	↓	↑	↓	↓	↑	↑
miR-100	—	↓	↓	↓	↑	↓	↑	↑	↓	↑	↓

Diagram illustrating Hox genes modulation exerted by miR-23b, miR-130a, miR-106a and miR-100 after gain-of-function assays in sinus venosus *explants at stage HH11 (obtained from* ***Figures 6A, C,E, G****). Green arrows: upregulated. Red arrows: downregulated. Black lines: Do not regulate.*

TABLE 3 | Hox genes modulated by microRNAs in the *sinus venosus* at stage HH15.

	Hoxa2	Hoxa3	Hoxa4	Hoxa5	Hoxa6	Hoxb2	Hoxb5	Hoxb6	Hoxc6	Hoxd3	Hoxd4
miR-23b	—	—	↓	↓	—	↑	↑	↑	↓	ND	ND
miR-130a	↓	—	—	↓	—	—	↓	↑	↓	ND	ND
miR-106a	↓	—	↓	↓	↑	↑	↑	↑	↑	ND	ND
miR-100	↑	—	↓	↑	↑	↑	↑	↑	↓	ND	ND

Diagram illustrating Hox genes modulation exerted by miR-23b, miR-130a, miR-106a and miR-100 after gain-of-function assays in sinus venosus *explants at stage HH15 (obtained from* ***Figures 6B, D, F****). Green arrows: upregulated. Red arrows: downregulated. Black lines: Do not regulate. ND: no detectable.*

and the *sinus venosus* (Niederreither et al., 1999, 2001). Interestingly, the administration of RA during mouse lung development is sufficient to induce Hoxa4 expression (Packer et al., 1998, 2000). Also, this gene has been recognized in many tissues as a potent inhibitor of cell mobility (Bhatlekar et al., 2017; Cheng et al., 2018). In our study, Hoxa4 provides an interesting example of a Hox gene downregulated by the microRNAs analyzed, as illustrated by both *in vitro* and *ex vivo* assays. In this context, it should be noted that the mobility of the cardiac progenitors is a dynamic and continuous determinant process during heart remodeling and conformation. Similarly, adequate cardiac physiological function requires certain cell subpopulation movement, not yet fully defined, from their origin to other cardiac regions. The repression of Hoxa4 that we observed in the *sinus venosus* at stages HH11 and HH15 reflects a much more complex mechanism, which may be responsible for cell mobility regulation of the different cardiac progenitors, likely involved in the developing venous pole of the heart. Although Hoxa4 modulation by means of microRNAs has not yet been described, some authors have demonstrated a negative modulation of Hoxa5 by miR-130a, after induction of Hoxa5 by RA (Yang et al., 2013). Supporting these data, our luciferase assays reveal that Hoxa4 is repressed by miR-23b and miR-106a, as the consequence of a direct physical interaction exerted between these microRNAs and its 3′UTR region.

On the other hand, we observe that Hoxd3 is upregulated both in the cardiomyoblasts and the *sinus venous* at stage HH11. Previous reports have pointed out that Hoxd3 is not expressed at later stages of cardiogenesis and also that treatment with RA is sufficient to repress its expression (Searcy and Yutzey, 1998), showing an opposite behavior to that of Hoxa4. In agreement with the above, in our study we observed that the expression of Hoxd3 is not detected in the *sinus venosus* at stage HH15. This fact could be a consequence of the specific restricted pattern of the microRNAs—miR23b, miR-130a, miR-106a, and miR-100-during this stage.

In summary, this study shows several novel findings in the field of cardiac development. Our data show a dynamic expression of miR-23b, miR-130a, miR-106a, and miR-100 from early stages of cardiogenesis. We also identify the expression of several Hox genes in the *sinus venosus* at stages HH11 and HH15. Noticeably, we observe that there

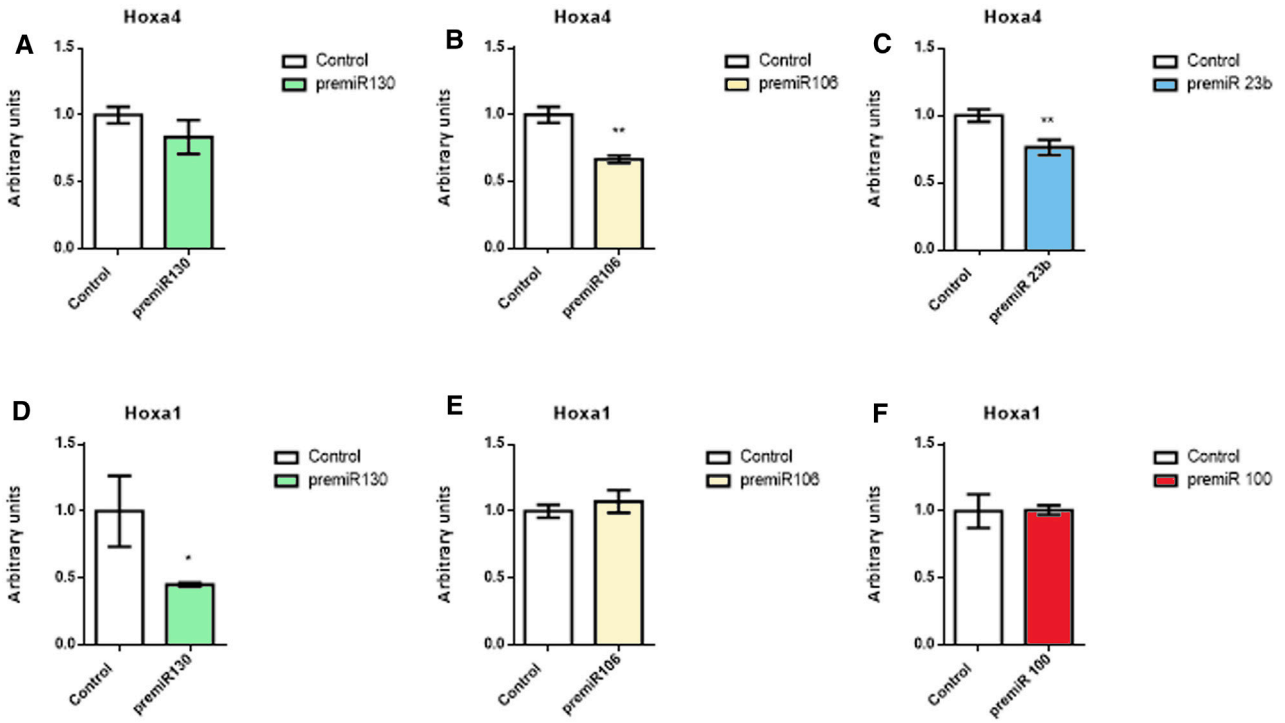

FIGURE 7 | Dual luciferase assays. Representative data of Hoxa4 **(A–C)** and Hoxa1 **(D–F)** 3′UTR luciferase assays after miR-130a, miR-106a, miR-23b, and miR-100 overexpression in 3T3 fibroblasts. Student's *t*-test: $*p < 0.05$, $**p < 0.01$, $***p < 0.005$, $****p < 0.001$.

is a negative modulation of several Hox genes by microRNAs, both in cardiomyoblasts and *sinus venosus*. Finally, the convergent expression of these microRNAs regulating Hox gene expressions in the *sinus venosus*/inflow tract supports the hypothesis of a potential role in differentiation and compartmentalization of the cardiac venous pole.

MATERIALS AND METHODS

Whole-Mount LNA *In Situ* Hybridization (ISH) and Sectioning

Fertilized eggs (Granja Santa Isabel, Córdoba, Spain) were incubated at 38°C in forced-draft, humidified incubators. Embryos were collected at stages HH3 to HH17 (Hamburger and Hamilton, 1951, 1992; Lopez-Sanchez et al., 2005) and fixed overnight at 4°C in 4% PFA, dehydrated in methanol, and stored at −20°C. Embryos were processed for LNA-ISH following our previous procedure (Lopez-Sanchez et al., 2015a) using miR-23b, miR-130a, miR-106a, and miR-100 LNA-labeled microRNA probes (miRCURY LNA™ Detection probe 5′-DIG and 3′-DIG labeled, Exiqon), respectively.

For histology, embryos were dehydrated with an ethanol series, cleared in isopropanol, and processed for paraplast embedding, obtaining 15-μm transverse serial sections.

H9c2 Cell Culture and microRNAs Transfections

The H9c2 cell line (kindly provided by Dr. Paulo J. Oliveira, Coimbra, Portugal) was cultured in DMEM medium supplemented with 10% foetal bovine serum, 100 U/mL penicillin, and 100 μg/ml streptomycin in 100-cm^2 culture disks at 37°C in a humidified atmosphere of 5% CO_2. Cells were fed every 2–3 days. Two sub-cultured condition transfections were performed. Myoblast H9c2 was sub-cultured at 50–60% confluence while induced-cardiomyocyte H9c2 reached 80–90% confluence. H9c2 cells (6×10^5 cells per well) were transfected with microRNA mimics for miR-23b, miR-130a, miR-106a, and miR-100 precursors (Thermo Fisher) as previously described (Branco et al., 2015).

Sinus Venosus Resection and microRNAs Transfections

Groups of embryos were collected at stages HH11 and HH15 and maintained in EBSS (Gibco) at low temperature until manipulation. The *sinus venosus* was resected from the embryos and transfected in hanging drops (Bonet et al., 2015; Dueñas et al., 2020) with microRNA mimics, including miR-23b, miR-130a, miR-106a, and miR-100 precursors, for 24 h at 37°C.

Pre-miRNAs transfection was carried out with Lipofectamine 2000 (Invitrogen) following the manufacturer's instructions. Negative control explants were treated only with Lipofectamine and were run in parallel.

RNA Isolation and qRT-PCR

Samples obtained from H9c2 cells and *sinus venosus* explants after microRNA transfections and control samples were subjected to qRT-PCR analysis following MIQE guidelines (Bustin et al., 2009; Bonet et al., 2015; Lozano-Velasco et al., 2015). RNA was extracted and purified by using a ReliaPrep RNA Cell Miniprep System Kit (Promega) according to the manufacturer's instructions. For mRNA expression measurements, 1 μg of total RNA was used for retro-transcription with a Maxima First Strand cDNA Synthesis Kit for qRT-PCR (Thermo Scientific). Real-time PCR experiments were performed with 2 μL of cDNA, Go Taq qPCR Master Mix (Promega), and corresponding primer sets (**Supplementary Table S2**). For microRNA expression analyses, 20 ng of total RNA was used for retro-transcription with a universal cDNA Synthesis Kit II (Exiqon), and the resulting cDNA was diluted 1/80. Real-time PCR experiments were performed with 1 μL of diluted cDNA and Go Taq qPCR Master Mix (Promega) as well. All qPCRs were performed using a CFX384TM thermocycler (Bio-Rad) following the manufacturer's recommendations. The relative expression of each gene was calculated by using Gusb and Gadph as internal controls for mRNA expression analyses and *5S* and *6U* for microRNA expression analyses, respectively (Livak and Schmittgen, 2001). Each PCR reaction was carried out in triplicate and repeated in at least three distinct biological samples to obtain representative means. qPCR data were analyzed using ΔDeltaCt (Deepak et al., 2007).

Amplification of Hox Genes From *Sinus Venosus* cDNA at Stages HH11–HH15

CDNA from the *sinus venosus* at stages HH11 and HH15 was obtained and processed as described above. For mRNA expression detection, Dream Taq polymerase (2x) and specific primers (**Supplementary Table S2**) were used, taking Gapdh as the internal loading control.

Luciferase Assays of 3′UTRs Hox Genes

Hoxa1 and Hoxa4 3′UTR constructs were PCR-amplified from chicken genomic DNA using primers bearing SpeI/HindIII restriction sites and cloned into the pGLuc-Basic vector (New England BioLabs). 3T3 fibroblasts (ATCC) were co-transfected with 100 ng of the Hoxa1 and Hoxa4 luciferase vector, 300 ng of pcLux vector control for internal normalization, and 20 nM of each microRNA. Luciferase activity was measured at 24 h after transfection (Pierce™ Gaussia Luciferase Flash Assay Kit) and normalized to the pcLux vector control (Pierce™ Cypridina Luciferase Flash Assay Kit). Luciferase activity was compared to non-transfected controls. Each luciferase assay was carried out in triplicate and repeated in at least three distinct biological samples to obtain representative assays.

Statistical Analysis

Student's *t*-test was used. Significance levels or *p*-values are stated in each corresponding figure, $p < 0.05$ being considered as statistically significant.

DATA AVAILABILITY STATEMENT

The original contributions presented in the study are included in the article/**Supplementary Materials**, further inquiries can be directed to the corresponding author.

ETHICS STATEMENT

Experimental protocols with animals were performed in agreement with the Spanish law in application of the EU Guidelines for animal research, and conformed to the Guide for the Care and Use of Laboratory Animals, published by the US National Institutes of Health (NIH Publication no.85-23). Approval by the University of Extremadura bioethics board was obtained prior to the initiation of the study.

AUTHOR CONTRIBUTIONS

The experimental study was designed and supervised by CL-S, DF, and VG-M, who also wrote the manuscript. CG-P, AD, and VG-L have contributed to the conception and design of the study, performed the experiments, and analyzed the data. All authors have contributed to the experimental work and analyzed and discussed the results. Also, all authors contributed to manuscript revision, and read and approved the submitted version.

FUNDING

This work has been financed with research grants IB18123 (to CL-S) and GR18185 (to VG-M, CTS005) from the Junta de Extremadura, with FEDER co-financing, and CTS-446 (to DF and AA) from the Junta de Andalucía Regional Council.

ACKNOWLEDGMENTS

We thank Laura Ortega Bermejo for her invaluable technical support with embryo handling and sample preparation for *in situ* hybridization.

SUPPLEMENTARY MATERIAL

The Supplementary Material for this article can be found online at: https://www.frontiersin.org/articles/10.3389/fcell.2021.767954/full#supplementary-material

REFERENCES

Abu-Issa, R., and Kirby, M. L. (2008). Patterning of the Heart Field in the Chick. *Developmental Biol.* 319, 223–233. doi:10.1016/j.ydbio.2008.04.014

Aguirre, A., Montserrat, N., Zacchigna, S., Nivet, E., Hishida, T., Krause, M. N., et al. (2014). *In Vivo* activation of a Conserved microRNA Program Induces Mammalian Heart Regeneration. *Cell Stem Cell* 15, 589–604. doi:10.1016/j.stem.2014.10.003

Barak, H., Preger-Ben Noon, E., and Reshef, R. (2012). Comparative Spatiotemporal Analysis ofHoxgene Expression in Early Stages of Intermediate Mesoderm Formation. *Dev. Dyn.* 241, 1637–1649. doi:10.1002/dvdy.23853

Bertrand, N., Roux, M., Ryckebüsch, L., Niederreither, K., Dollé, P., Moon, A., et al. (2011). Hox Genes Define Distinct Progenitor Sub-domains within the Second Heart Field. *Developmental Biol.* 353, 266–274. doi:10.1016/j.ydbio.2011.02.029

Bhatlekar, S., Viswanathan, V., Fields, J. Z., and Boman, B. M. (2017). Overexpression of HOXA4 and HOXA9 Genes Promotes Self-renewal and Contributes to colon Cancer Stem Cell Overpopulation. *J. Cel Physiol* 233, 727–735. doi:10.1002/jcp.25981

Bonet, F., Dueñas, Á., López-Sánchez, C., García-Martínez, V., Aránega, A. E., and Franco, D. (2015). MiR-23b and miR-199a Impair Epithelial-To-Mesenchymal Transition during Atrioventricular Endocardial Cushion Formation. *Dev. Dyn.* 244, 1259–1275. doi:10.1002/dvdy.24309

Boureima Oumarou, D., Ji, H., Xu, J., Li, S., Ruan, W., Xiao, F., et al. (2019). Involvement of microRNA-23b-5p in the Promotion of Cardiac Hypertrophy and Dysfunction via the HMGB2 Signaling Pathway. *Biomed. Pharmacother.* 116, 108977. doi:10.1016/j.biopha.2019.108977

Branco, A. F., Pereira, S. P., Gonzalez, S., Gusev, O., Rizvanov, A. A., and Oliveira, P. J. (2015). Gene Expression Profiling of H9c2 Myoblast Differentiation towards a Cardiac-like Phenotype. *PLoS One* 10, e0129303. doi:10.1371/journal.pone.0129303

Buckingham, M., Meilhac, S., and Zaffran, S. (2005). Building the Mammalian Heart from Two Sources of Myocardial Cells. *Nat. Rev. Genet.* 6, 826–835. doi:10.1038/nrg1710

Bustin, S. A., Benes, V., Garson, J. A., Hellemans, J., Huggett, J., Kubista, M., et al. (2009). The MIQE Guidelines: Minimum Information for Publication of Quantitative Real-Time PCR Experiments. *Clin. Chem.* 55, 611–622. doi:10.1373/clinchem.2008.112797

Camp, E., Dietrich, S., and Münsterberg, A. (2012). Fate Mapping Identifies the Origin of SHF/AHF Progenitors in the Chick Primitive Streak. *PLoS One* 7, e51948. doi:10.1371/journal.pone.0051948

Cao, L., Kong, L.-P., Yu, Z.-B., Han, S.-P., Bai, Y.-F., Zhu, J., et al. (2012). microRNA Expression Profiling of the Developing Mouse Heart. *Int. J. Mol. Med.* 30, 1095–1104. doi:10.3892/ijmm.2012.1092

Carmona, R., Ariza, L., Cañete, A., and Muñoz-Chápuli, R. (2018). Comparative Developmental Biology of the Cardiac Inflow Tract. *J. Mol. Cell Cardiol.* 116, 155–164. doi:10.1016/j.yjmcc.2018.02.004

Cheng, S., Qian, F., Huang, Q., Wei, L., Fu, Y., and Du, Y. (2018). HOXA4, Down-Regulated in Lung Cancer, Inhibits the Growth, Motility and Invasion of Lung Cancer Cells. *Cell Death Dis* 9, 465. doi:10.1038/s41419-018-0497-x

Chinchilla, A., Lozano, E., Daimi, H., Esteban, F. J., Crist, C., Aranega, A. E., et al. (2011). MicroRNA Profiling during Mouse Ventricular Maturation: a Role for miR-27 Modulating Mef2c Expression. *Cardiovasc. Res.* 89, 98–108. doi:10.1093/cvr/cvq264

Choi, E., Choi, E., and Hwang, K. C. (2013). MicroRNAs as Novel Regulators of Stem Cell Fate. *Wjsc* 5, 172–187. doi:10.4252/wjsc.v5.i4.172

Christoffels, V. M., Mommersteeg, M. T. M., Trowe, M.-O., Prall, O. W. J., de Gier-de Vries, C., Soufan, A. T., et al. (2006). Formation of the Venous Pole of the Heart from anNkx2-5-Negative Precursor Population RequiresTbx18. *Circ. Res.* 98, 1555–1563. doi:10.1161/01.RES.0000227571.84189.65

Darnell, D. K., Kaur, S., Stanislaw, S., Konieczka, J. K., Yatskievych, T. A., and Antin, P. B. (2006). MicroRNA Expression during Chick Embryo Development. *Dev. Dyn.* 235, 3156–3165. doi:10.1002/dvdy.20956

De Bono, C., Thellier, C., Bertrand, N., Sturny, R., Jullian, E., Cortes, C., et al. (2018b). T-box Genes and Retinoic Acid Signaling Regulate the Segregation of Arterial and Venous Pole Progenitor Cells in the Murine Second Heart Field. *Hum. Mol. Genet.* 27, 3747–3760. doi:10.1093/hmg/ddy266

De Bono, C., Théveniau-Ruissy, M., and Kelly, R. G. (2018a). Cardiac fields and Myocardial Cell Lineages. *Card. fields myocardial Cel. lineages* 4, 23–32. doi:10.1093/med/9780198757269.003.0004

Dueñas, A., Expósito, A., Muñoz, M. D. M., de Manuel, M. J., Cámara-Morales, A., Serrano-Osorio, F., et al. (2020). MiR-195 Enhances Cardiomyogenic Differentiation of the Proepicardium/septum Transversum by Smurf1 and Foxp1 Modulation. *Sci. Rep.* 10, 9334. doi:10.1038/s41598-020-66325-x

Garcia-Martinez, V., Darnell, D. K., Lopez-Sanchez, C., Sosic, D., Olson, E. N., and Schoenwolf, G. C. (1997). State of Commitment of Prospective Neural Plate and Prospective Mesoderm in Late Gastrula/early Neurula Stages of Avian Embryos. *Developmental Biol.* 181, 102–115. doi:10.1006/dbio.1996.8439

Garcia-Martinez, V., and Schoenwolf, G. C. (1993). Primitive-streak Origin of the Cardiovascular System in Avian Embryos. *Developmental Biol.* 159, 706–719. doi:10.1006/dbio.1993.1276

Guan, X., Wang, L., Liu, Z., Guo, X., Jiang, Y., Lu, Y., et al. (2016). miR-106a Promotes Cardiac Hypertrophy by Targeting Mitofusin 2. *J. Mol. Cell Cardiol.* 99, 207–217. doi:10.1016/j.yjmcc.2016.08.016

Hamburger, V., and Hamilton, H. L. (1951). A Series of normal Stages in the Development of the Chick Embryo. *J. Morphol.* 88, 49–92. doi:10.1002/jmor.1050880104

Hamburger, V., and Hamilton, H. L. (1992). A Series of normal Stages in the Development of the Chick Embryo. *Dev. Dyn.* 195, 231–272. doi:10.1002/aja.1001950404

Harvey, R. P. (2002). Patterning the Vertebrate Heart. *Nat. Rev. Genet.* 3, 544–556. doi:10.1038/nrg843

Hochgreb, T., Linhares, V. L., Menezes, D. C., Sampaio, A. C., Yan, C. Y. I., Cardoso, W. V., et al. (2003). A Caudorostral Wave of RALDH2 Conveys Anteroposterior Information to the Cardiac Field. *Development* 130, 5363–5374. doi:10.1242/dev.00750

Kalayinia, S., Arjmand, F., Maleki, M., Malakootian, M., and Singh, C. P. (2021). MicroRNAs: Roles in Cardiovascular Development and Disease. *Cardiovasc. Pathol.* 50, 107296. doi:10.1016/j.carpath.2020.107296

Kim, G. H., Samant, S. A., Earley, J. U., and Svensson, E. C. (2009). Translational Control of FOG-2 Expression in Cardiomyocytes by microRNA-130a. *PLoS One* 4, e6161. doi:10.1371/journal.pone.0006161

Lescroart, F., and Zaffran, S. (2018). Hox and Tale Transcription Factors in Heart Development and Disease. *Int. J. Dev. Biol.* 62, 837–846. doi:10.1387/ijdb.180192sz

Livak, K. J., and Schmittgen, T. D. (2001). Analysis of Relative Gene Expression Data Using Real-Time Quantitative PCR and the 2−ΔΔCT Method. *Methods* 25, 402–408. doi:10.1006/meth.2001.1262

Lopez-Sanchez, C., Franco, D., Bonet, F., Garcia-Lopez, V., Aranega, A., and Garcia-Martinez, V. (2015a). Negative Fgf8-Bmp2 Feed-Back Is Regulated by miR-130 during Early Cardiac Specification. *Developmental Biol.* 406, 63–73. doi:10.1016/j.ydbio.2015.07.007

Lopez-Sanchez, C., Franco, D., Bonet, F., Garcia-Lopez, V., Aranega, A., and Garcia-Martinez, V. (2015b). Reciprocal Repression between Fgf8 and miR-133 Regulates Cardiac Induction through Bmp2 Signaling. *Data in Brief* 5, 59–64. doi:10.1016/j.dib.2015.08.009

Lopez-Sanchez, C., Garcia-Lopez, V., Schoenwolf, G. C., and Garcia-Martinez, V. (2018). From Epiblast to Mesoderm: Elaboration of a Fate Map for Cardiovascular Progenitors. 3, 14–22. doi:10.1093/med/9780198757269.003.0003

Lopez-Sanchez, C., and Garcia-Martinez, V. (2011). Molecular Determinants of Cardiac Specification. *Cardiovasc. Res.* 91, 185–195. doi:10.1093/cvr/cvr127

Lopez-Sanchez, C., Garcia-Martinez, V., and Schoenwolf, G. C. (2001). Localization of Cells of the Prospective Neural Plate, Heart and Somites within the Primitive Streak and Epiblast of Avian Embryos at Intermediate Primitive-Streak Stages. *Cells Tissues Organs* 169, 334–346. doi:10.1159/000047900

Lopez-Sanchez, C., Garcia-Masa, N., Gañan, C. M., and Garcia-Martinez, V. (2009). Movement and Commitment of Primitive Streak Precardiac Cells during Cardiogenesis. *Int. J. Dev. Biol.* 53, 1445–1455. doi:10.1387/ijdb.072417cl

Lopez-Sanchez, C., Puelles, L., Garcia-Martinez, V., and Rodriguez-Gallardo, L. (2005). Morphological and Molecular Analysis of the Early Developing Chick Requires an Expanded Series of Primitive Streak Stages. *J. Morphol.* 264, 105–116. doi:10.1002/jmor.10323

Lozano-Velasco, E., Galiano-Torres, J., Jodar-Garcia, A., Aranega, A. E., and Franco, D. (2015). miR-27 and miR-125 Distinctly Regulate Muscle-Enriched Transcription Factors in Cardiac and Skeletal Myocytes. *Biomed. Res. Int.* 2015, 1–6. doi:10.1155/2015/391306

Makki, N., and Capecchi, M. R. (2010). Hoxa1 Lineage Tracing Indicates a Direct Role for Hoxa1 in the Development of the Inner Ear, the Heart, and the Third Rhombomere. *Developmental Biol.* 341, 499–509. doi:10.1016/j.ydbio.2010.02.014

Mommersteeg, M. T. M., Domínguez, J. N., Wiese, C., Norden, J., de Gier-de Vries, C., Burch, J. B. E., et al. (2010). The Sinus Venosus Progenitors Separate and Diversify from the First and Second Heart fields Early in Development. *Cardiovasc. Res.* 87, 92–101. doi:10.1093/cvr/cvq033

Niederreither, K., Subbarayan, V., Dollé, P., and Chambon, P. (1999). Embryonic Retinoic Acid Synthesis Is Essential for Early Mouse post-implantation Development. *Nat. Genet.* 21 (21), 444–448. doi:10.1038/7788

Niederreither, K., Vermot, J., Messaddeq, N., Schuhbaur, B., Chambon, P., and Dollé, P. (2001). Embryonic Retinoic Acid Synthesis Is Essential for Heart Morphogenesis in the Mouse. *Development* 128 (128), 1019–1031. doi:10.1242/dev.128.7.1019

Packer, A. I., Crotty, D. A., Elwell, V. A., and Wolgemuth, D. J. (1998). Expression of the Murine Hoxa4 Gene Requires Both Autoregulation and a Conserved Retinoic Acid Response Element. *Development* 125, 1991–1998. doi:10.1242/dev.125.11.1991

Packer, A. I., Mailutha, K. G., Ambrozewicz, L. A., and Wolgemuth, D. J. (2000). Regulation of the Hoxa4 and Hoxa5 Genes in the Embryonic Mouse Lung by Retinoic Acid and TGFbeta1: Implications for Lung Development and Patterning. *Dev. Dyn.* 217 (217), 62–74. doi:10.1002/(SICI)109710.1002/(SICI)1097-0177(200001)217:1<62:AID-DVDY6>3.0.CO;2-U

Pang, J. K. S., Phua, Q. H., and Soh, B.-S. (2019). Applications of miRNAs in Cardiac Development, Disease Progression and Regeneration. *Stem Cel Res. Ther.* 10, 336. doi:10.1186/s13287-019-1451-2

Rajabi, H., Aslani, S., Abhari, A., and Sanajou, D. (2020). Expression Profiles of microRNAs in Stem Cells Differentiation. *Cpb* 21, 906–918. doi:10.2174/1389201021666620021909252

Redkar, A., Montgomery, M., and Litvin, J. (2001). Fate Map of Early Avian Cardiac Progenitor Cells. *Development* 128, 2269–2279. doi:10.1242/dev.128.12.2269

Roux, M., Laforest, B., Capecchi, M., Bertrand, N., and Zaffran, S. (2015). Hoxb1 Regulates Proliferation and Differentiation of Second Heart Field Progenitors in Pharyngeal Mesoderm and Genetically Interacts with Hoxa1 during Cardiac Outflow Tract Development. *Developmental Biol.* 406, 247–258. doi:10.1016/j.ydbio.2015.08.015

Roux, M., and Zaffran, S. (2016). Hox Genes in Cardiovascular Development and Diseases. *Jdb* 4, 14. doi:10.3390/jdb4020014

Ryckebusch, L., Wang, Z., Bertrand, N., Lin, S.-C., Chi, X., Schwartz, R., et al. (2008). Retinoic Acid Deficiency Alters Second Heart Field Formation. *Proc. Natl. Acad. Sci.* 105, 2913–2918. doi:10.1073/pnas.0712344105

S.A. Deepak, S., K.R. Kottapalli, K., R. Rakwal, R., G. Oros, G., K.S. Rangappa, K., H. Iwahashi, H., et al. (2007). Real-Time PCR: Revolutionizing Detection and Expression Analysis of Genes. *Cg* 8 (4), 234–251. doi:10.2174/138920207781386960

Schultheiss, T. M., Xydas, S., and Lassar, A. B. (1995). Induction of Avian Cardiac Myogenesis by Anterior Endoderm. *Development* 121, 4203–4214. doi:10.1242/dev.121.12.4203

Searcy, R. D., and Yutzey, K. E. (1998). Analysis ofHox Gene Expression during Early Avian Heart Development. *Dev. Dyn.* 213, 82–91. doi:10.1002/(sici)1097-0177(199809)213:1<82:aid-aja8>3.0.co;2-u

Shu, J., Silva, B. V. R. e., Gao, T., Xu, Z., and Cui, J. (2017). Dynamic and Modularized microRNA Regulation and its Implication in Human Cancers. *Sci. Rep.* 7, 13356. doi:10.1038/s41598-017-13470-5

Sirbu, I. O., Zhao, X., and Duester, G. (2008). Retinoic Acid Controls Heart Anteroposterior Patterning by Down-regulatingIsl1 through theFgf8 Pathway. *Dev. Dyn.* 237, 1627–1635. doi:10.1002/dvdy.21570

Stefanovic, S., Laforest, B., Desvignes, J.-P., Lescroart, F., Argiro, L., Maurel-Zaffran, C., et al. (2020). Hox-dependent Coordination of Mouse Cardiac Progenitor Cell Patterning and Differentiation. *Elife* 9, e55124. doi:10.7554/eLife.55124

Stefanovic, S., and Zaffran, S. (2017). Mechanisms of Retinoic Acid Signaling during Cardiogenesis. *Mech. Development* 143, 9–19. doi:10.1016/j.mod.2016.12.002

Sticht, C., De La Torre, C., Parveen, A., and Gretz, N. (2018). miRWalk: An Online Resource for Prediction of microRNA Binding Sites. *PLoS One* 13 (10), e0206239. doi:10.1371/journal.pone.0206239

Sucharov, C., Bristow, M. R., and Port, J. D. (2008). miRNA Expression in the Failing Human Heart: Functional Correlates. *J. Mol. Cell Cardiol.* 45, 185–192. doi:10.1016/j.yjmcc.2008.04.014

Tarantino, C., Paolella, G., Cozzuto, L., Minopoli, G., Pastore, L., Parisi, S., et al. (2010). miRNA 34a, 100, and 137 Modulate Differentiation of Mouse Embryonic Stem Cells. *FASEB j.* 24, 3255–3263. doi:10.1096/fj.09-152207

Thum, T., Catalucci, D., and Bauersachs, J. (2008). MicroRNAs: Novel Regulators in Cardiac Development and Disease. *Cardiovasc. Res.* 79, 562–570. doi:10.1093/cvr/cvn137

van den Berg, G., Abu-Issa, R., de Boer, B. A., Hutson, M. R., de Boer, P. A. J., Soufan, A. T., et al. (2009). A Caudal Proliferating Growth center Contributes to Both Poles of the Forming Heart Tube. *Circ. Res.* 104, 179–188. doi:10.1161/CIRCRESAHA.108.185843

van Wijk, B., Barnett, P., and van den Hoff, M. J. B. (2018). The Developmental Origin of Myocardium at the Venous Pole of the Heart. 8, 64–74. doi:10.1093/med/9780198757269.003.0008

van Wijk, B., van den Berg, G., Abu-Issa, R., Barnett, P., van der Velden, S., Schmidt, M., et al. (2009). Epicardium and Myocardium Separate from a Common Precursor Pool by Crosstalk between Bone Morphogenetic Protein- and Fibroblast Growth Factor-Signaling Pathways. *Circ. Res.* 105, 431–441. doi:10.1161/CIRCRESAHA.109.203083

Waldo, K. L., Hutson, M. R., Ward, C. C., Zdanowicz, M., Stadt, H. A., Kumiski, D., et al. (2005). Secondary Heart Field Contributes Myocardium and Smooth Muscle to the Arterial Pole of the Developing Heart. *Developmental Biol.* 281, 78–90. doi:10.1016/j.ydbio.2005.02.012

Wu, S., Huang, S., Ding, J., Zhao, Y., Liang, L., Liu, T., et al. (2010). Multiple microRNAs Modulate p21Cip1/Waf1 Expression by Directly Targeting its 3′ Untranslated Region. *Oncogene* 29, 2302–2308. doi:10.1038/onc.2010.34

Yan, S., and Jiao, K. (2016). Functions of miRNAs during Mammalian Heart Development. *Ijms* 17, 789. doi:10.3390/ijms17050789

Yang, F., Miao, L., Mei, Y., and Wu, M. (2013). Retinoic Acid-Induced HOXA5 Expression Is Co-regulated by HuR and miR-130a. *Cell Signal.* 25 (25), 1476–1485. doi:10.1016/j.cellsig.2013.03.015

Zaffran, S., and Kelly, R. G. (2012). New Developments in the Second Heart Field. *Differentiation* 84, 17–24. doi:10.1016/j.diff.2012.03.003

Conflict of Interest: The authors declare that the research was conducted in the absence of any commercial or financial relationships that could be construed as a potential conflict of interest.

Publisher's Note: All claims expressed in this article are solely those of the authors and do not necessarily represent those of their affiliated organizations, or those of the publisher, the editors, and the reviewers. Any product that may be evaluated in this article, or claim that may be made by its manufacturer, is not guaranteed or endorsed by the publisher.

frontiers in Cell and Developmental Biology

MINI REVIEW
published: 21 February 2022
doi: 10.3389/fcell.2022.840005

Transcriptional Control of Axon Guidance at Midline Structures

*Eloísa Herrera and Augusto Escalante**

Instituto de Neurociencias, CSIC-UMH, Alicante, Spain

The development of the nervous system is a time-ordered and multi-stepped process that includes neurogenesis and neuronal specification, axonal navigation, and circuits assembly. During axonal navigation, the growth cone, a dynamic structure located at the tip of the axon, senses environmental signals that guide axons towards their final targets. The expression of a specific repertoire of receptors on the cell surface of the growth cone together with the activation of a set of intracellular transducing molecules, outlines the response of each axon to specific guidance cues. This collection of axon guidance molecules is defined by the transcriptome of the cell which, in turn, depends on transcriptional and epigenetic regulators that modify the structure and DNA accessibility to determine what genes will be expressed to elicit specific axonal behaviors. Studies focused on understanding how axons navigate intermediate targets, such as the floor plate of vertebrates or the mammalian optic chiasm, have largely contributed to our knowledge of how neurons wire together during development. In fact, investigations on axon navigation at these midline structures led to the identification of many of the currently known families of proteins that act as guidance cues and their corresponding receptors. Although the transcription factors and the regulatory mechanisms that control the expression of these molecules are not well understood, important advances have been made in recent years in this regard. Here we provide an updated overview on the current knowledge about the transcriptional control of axon guidance and the selection of trajectories at midline structures.

Keywords: neuron, growth cone, axon pathfinding, target, transcriptional regulation, circuits development

OPEN ACCESS

Edited by:
Rosa Barrio,
CIC bioGUNE, Spain

Reviewed by:
Takaaki Kuwajima,
University of Pittsburgh, United States
Avihu Klar,
Hebrew University Hadassah Medical School, Israel

****Correspondence:***
Augusto Escalante
aescalante@umh.es

Specialty section:
This article was submitted to Cell Adhesion and Migration, a section of the journal Frontiers in Cell and Developmental Biology

Received: *20 December 2021*
Accepted: *31 January 2022*
Published: *21 February 2022*

Citation:
Herrera E and Escalante A (2022) Transcriptional Control of Axon Guidance at Midline Structures. Front. Cell Dev. Biol. 10:840005. doi: 10.3389/fcell.2022.840005

INTRODUCTION

The survival of organisms relies on their ability to detect stimuli, process sensory information and generate adequate motor responses. These functions depend on the precise organization of neural networks that enable communication between cells in an efficient and accurate manner. These networks emerge during embryonic development when newly born neurons extend axons away from the cell body to navigate through the developing embryo in order to reach their final targets. The growth cone at the tip of the travelling axon is a specialized structure armed with a plethora of receptors that defines the response of the growing axon to the environmental cues and determines its direction. The existence of both commissural neurons that project to the opposite side of the brain and ipsilateral neurons that connect with targets in the same hemisphere, is essential for the distribution and integration of sensory information and the subsequent generation of coordinated motor responses in species with bilateral symmetry (Colamarino and Tessier-Lavigne, 1995). Intense research during the last few decades focused on how ipsilateral and contralateral axons behave at the midline in different species and contexts has

lead to the identification of many families of cues, receptors, and signaling cascades involved in axon pathfinding. Post-transcriptional mechanisms such as the microRNA-dependent regulation of guidance receptors (Yang et al., 2018), the regulation of local translation in axons (Zhuang et al., 2019; Corradi and Baudet, 2020), the role of lipids in axon guidance (Guy and Kamiguchi, 2021), novel ways of presenting guidance proteins (Dominici et al., 2017; Moreno-Bravo et al., 2017; Varadarajan et al., 2017; Wu et al., 2019; Dorskind and Kolodkin, 2021), interactions between different families of receptors (Zelina et al., 2014) or the targeted degradation of ligands or receptors (Gorla et al., 2019), all contribute to guarantee proper axon guidance progression and today we know that aberrant expression of axon guidance proteins or alterations in any of these mechanisms may result in a wide variety of neurodevelopmental diseases (Engle, 2010; Izzi and Charron, 2011; Nugent et al., 2012; Chédotal, 2014; Blockus and Chédotal, 2015; Van Battum et al., 2015; Roig-Puiggros et al., 2020). Despite these remarkable advances on the molecular mechanisms underlying axon guidance processes, current knowledge about the transcription factors (TFs) and the regulatory networks that orchestrate the expression of guidance molecules is still very limited (Butler and Tear, 2007). Here we provide an updated overview of the transcriptional mechanisms that control axonal trajectories during embryonic development paying particular attention to the navigation of neural axons at midline structures.

Identification of Regulatory Factors Controlling Axon Guidance

Pioneer work on *Drosophila* initially identified a number of TFs involved in controlling the trajectories of motoneurons (MNs) axons towards their corresponding muscles and, subsequent work in vertebrates, revealed some of the transcriptional regulators that define specific limb muscles innervation (Landgraf et al., 1999; Keleman and Dickson, 2001; Dasen et al., 2003; Fujioka et al., 2003; Broihier et al., 2004; Dasen et al., 2005; Labrador et al., 2005; Garces and Thor, 2006; Layden et al., 2006). Further studies in vertebrates proposed that combinatorial codes of LIM proteins specify different MN trajectories and these TFs control the expression of specific axon guidance receptors from the EphA family to define MN trajectories to the different limb regions (Tsuchida et al., 1994; Sharma et al., 1998; Thor et al., 1999; Kania et al., 2000; Kania and Jessell, 2003; Shirasaki et al., 2006). In addition, another member of the homeobox TF family, Nkx2.9, was described to control the expression of the Slit receptor Robo2 and promote dorsal axon exit from the spinal cord in vertebrate spinal accessory MNs (Dillon et al., 2005; Bravo-Ambrosio et al., 2012).

Subsequently, other families of TFs have been associated with determining axonal trajectories in different neural circuits. For instance, the POU-domain TF Acj6 (abnormal chemosensory jump) was described as essential for the targeting of olfactory projection neurons in *Drosophila* (Komiyama et al., 2003), and Pou4f2, another member of the POU-family (aka Brn3.2 or Brn3b), seems to play an important role in the specification and pathfinding of retinal ganglion cell (RGC) axons (Erkman et al., 2000; Wang et al., 2000). Also in the visual system, members of the FOX family (FoxG1 and FoxD1) regulate the expression of the ephrinA receptors to determine the termination of retinal projections along the anterior-posterior axis at the visual targets (Herrera, 2004; Carreres et al., 2011). In the mouse cortex, the zinc-finger TFs Fezf2 and Ctip2 direct the projections of layer 5 corticospinal axons towards subcortical regions (Arlotta et al., 2005; Bin Chen et al., 2005; Jie-Guang Chen et al., 2005; Molyneaux et al., 2005; Lodato et al., 2014) and Ctip2 together with Satb2 control the formation of the corpus callosum (Srivatsa et al., 2014). In both vertebrates and invertebrates the Run-containing domain TFs control specific axonal trajectories since missexpression of Runt in *Drosophila* photoreceptors results in axons targeting the medulla instead of the lamina (Kaminker et al., 2002) and alterations in the levels of Runx3 shift the laminar termination of somatosensory neuron axons along the dorsoventral axis of the mouse spinal cord (Chen et al., 2006).

In addition to the abovementioned examples, two neuronal populations have been particularly useful to study the molecular mechanisms underlying axon pathfinding: spinal neurons at the time their axons navigate the floor plate, and retinal ganglion cells when their axons traverse the optic chiasm. In the following sections we review recent findings on the transcriptional regulation of neuronal trajectories using these two classic midline axon guidance models.

Transcriptional Regulation of Axon Midline Crossing

The population of early born interneurons located in the most dorsal part of the spinal cord is known as dI1. As soon as dI1 neurons differentiate, they migrate ventrally to finally occupy the deep dorsal horns (Junge et al., 2016). A large number of reports studying this neuronal population have contributed to the current knowledge of how axons are attracted/repelled by guidance cues and their receptors [for recent reviews see (Chédotal, 2019; Comer et al., 2019)] and investigations on these neurons have also provided major insights into the regulatory mechanisms controlling axon guidance. There are two main subtypes of dI1 neurons: a population that occupies the medial intermediate spinal cord and project contralaterally (dI1c) and another cluster of cells that settle in the lateral intermediate spinal cord and avoid the floor plate to project ipsilaterally (dI1i). Both subtypes are derived from progenitor cells expressing the bHLH TF Atoh1 (Helms and Johnson, 1998, 2003; Lee et al., 1998; Helms et al., 2000; Gowan et al., 2001; Saba et al., 2005). Atoh1 induces the expression of the homeobox TFs Groucho co-repressors Barhl1 and Barhl2 (Bermingham et al., 2001; Saba et al., 2005; Reig et al., 2007) that are expressed in both dI1i and dI1c. Gain-of-function experiments showed that Barhl1 overexpression results in ectopic expression of Robo3, Nrp2 and DCC, and promotes midline crossing (Kawauchi et al., 2010). Using a similar approach, it was shown that Barhl2 also

promotes a commissural phenotype and that Barhl2 overexpression leads to the induction of the adhesion molecule Tag-1 (Saba et al., 2003).

On the other hand, it has been reported that Atoh1 induces the expression of the LIM homeodomain TFs Lhx2 and Lhx9, either directly or indirectly through Barhl TFs (Bermingham et al., 2001; Gowan et al., 2001; Nakada, 2004). Barhl2 mutant mice exhibited a shift in the position of dI1i neurons from lateral to medial regions concomitant with a dramatic loss of ipsilateral projections and an increased number of commissural axons, which agrees with the observed aberrant upregulation of the homeodomain TF Lhx2 in the dI1i neurons of these mice. *In vitro*, Barhl2 binds to the regulatory sequences of Lhx2 and represses its expression (Ding et al., 2012). Gain-of-function experiments have shown that this TF is able to induce Lhx2 and another member of the same family, Lhx9 in spinal neurons (Kawauchi et al., 2010). Together these results suggest that Barhl2 represses Lhx2 in dI1i neurons to block the commissural phenotype. Independent gain-of-function experiments in the chick spinal cord suggested a role for Lhx9 in dI1c axons after midline crossing in the control of rostral turning and the dorsoventral positioning of axons in the longitudinal plane (Avraham et al., 2009), but these two Lhx factors seem to contribute to the diversification of dI1c and dI1i subtypes at earlier stages of dl1 differentiation.

Both Lhx2 and Lhx9 are expressed in dI1c neurons whereas dI1i neurons express only Lhx9 (Wilson et al., 2008). Single Lhx2 or Lhx9 mutant mice do not exhibit guidance phenotypes in dI1 neurons but commissural axons do not cross the midline in double Lhx2/9 mutants, similarly to the phenotype observed in Robo3 mutants (Sabatier et al., 2004). This pointed at Robo3 as a downstream target of Lhx TFs (Wilson et al., 2008). Chromatin immunoprecipitation (ChIP) assays *in vitro* and *in vivo* revealed that Lhx2 binds the Robo3 promoter (Wilson et al., 2008; Marcos-Mondéjar et al., 2012) and gain-of-function experiments in the mouse spinal cord demonstrated that Lhx2 is capable of inducing Robo3 (Kawauchi et al., 2010). All these experiments suggested that the Lhx2/9-Robo3 cascade is the default program in dl1 neurons and this program needs to be repressed in order to generate ipsilateral neurons. Supporting this idea, it was shown that ectopic expression of Robo3 in dorsal spinal neurons redirects ipsilateral axons towards and across the floor plate (Escalante et al., 2013). Interestingily, another member of the Robo family, Robo2, is differentially expressed in the dl1 subpopulations and, while dI1c projections are not affected in Robo2 mutants, dl1i axons project aberrantly through the motor neuron pool closer to the midline (Wurmser et al., 2021). Additionally, different components of the Wnt signaling pathway, including β-catenin and several Wnt receptors seem to be also required for midline crossing in dl1c (Avilés and Stoeckli, 2016).

Despite all this progress, it is difficult to reconcile a simple linear cascade in the gene regulatory network (GRN) specifying a commissural versus ipsilateral choice in dI1 neurons given the complexity of the regulatory mechanisms linking Atoh1, Barhl1/2, Lhx2/9 and downstream targets. Together with a more precise definition of the GRN controlling the specification of dl1 subtypes, other questions such as whether Lhx TFs activate other guidance receptors such as DCC, Robo2 or members of the Wnt pathway, or whether Robo3 expression is regulated by other homeodomain TFs in different types of commissural interneurons remain to be answered.

In the mouse visual system, the majority of retinal ganglion cell axons cross the ventral diencephalon at the optic chiasm level (cRGCs) while a minority of these axons project to the ipsilateral hemisphere (iRGCs). In this model, also largely used to study axon guidance mechanisms, another member of the LIM homeodomain TF family, Islet2 (Isl2), is differentially expressed in the ipsi and the contralateral RGCs subpopulations (Pak et al., 2004). Isl2 mutant mice show an increased number of iRGCs at the expense of the cRGCs. However, this only affects the subgroup of cRGCs that are born in the ventrotemporal region of the retina at late developmental stages and the targets of Isl2 to control the projection of this late-born RGC population have not been identified. The TF Pou4f1 (aka Brn3a) is also expressed in cRGCs but not iRGCs (Quina et al., 2005) but its function in axon guidance at the midline is still a matter of investigation. Finally, other TFs implicated in the establishment of cRGCs identity are the members of the SoxC family, particularly Sox4, Sox11 and Sox12 (Kuwajima et al., 2017). SoxC proteins bind to the Hes5 promoter to repress Notch signaling and induce cRGCs differentiation. SoxC genes regulate the expression of Plexin-A1 and Nr-Cam, which are required in cRGCs for correct axonal decussation at the chiasm (Kuwajima et al., 2012). Also, an ectopic ipsilateral projection is apparent in Sox4/Sox11/Sox12 triple conditional mutant mice (Kuwajima et al., 2017), suggesting that these proteins may be repressing the differentiation of iRGCs.

Transcriptional Regulation of Axon Midline Avoidance

While the transcriptional regulation of midline crossing was originally described in dl1 spinal neurons, the regulation of axon midline avoidance was initially characterized in the visual system. The zinc finger TF Zic2, expressed in ipsilateral but not in contralateral RGCs, was reported as the main determinant of iRGC (Herrera et al., 2003). The expression of Zic2 and the generation of iRGCs in the ventrotemporal retina depends, at least partially, on the expression of CyclinD2 in a populatin of neural progenitors located at the ciliary margin zone of the embryonic retina (Marcucci et al., 2016). Functional experiments in mice initially demonstrated that Zic2 is necessary and sufficient to induce the expression of the tyrosine kinase receptor EphB1 that mediates axonal repulsion throught its ligand ephrinB2 expressed by midline cells (Williams et al., 2003; García-Frigola et al., 2008). The upregulation of EphB1 by Zic2 in iRGCs was later confirmed by chromatin immunoprecipitation assays followed by massive secuencing (ChIP-seq) which also identified other Zic2 targets including different members of the Wnt signaling pathway (Morenilla-Palao et al., 2020). In agreement with previous observations in spinal dl1c neurons (Avilés and Stoeckli, 2016), loss-of-function experiments in RGCs demonstrated that β-catenin is essential also

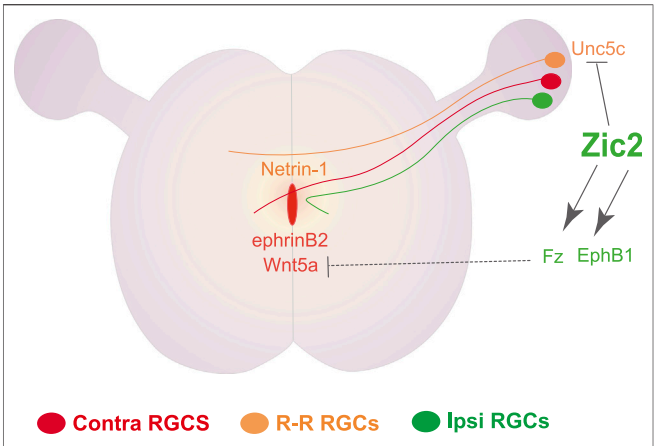

FIGURE 1 | Transcriptional control of ipsilateral trajectories in the visual system. The TF Zic2 controls the trajectory of ipsilateral RGC axons through the transcriptional upregulation of the tyrosine receptor EphB1, which in turn mediates repulsion from glial cells at the midline that express ephrinB2. Concomitantly, Zic2 induces the expression of several Wnt receptors and cytoplasmic proteins to inhibit the attractive response towards Wnt5a -also expressed at the midline-experienced by contralateral RGCs. Zic2 also represses the expression of the Netrin1 receptor Unc5c in iRGCs to allow axon growth through a Netrin1-expressing area at the chiasm.

for midline crossing in visual axons. Further functional experiments ruled out the canonical Wnt pathway as a regulator of axon guidance at the midline and demonstrated that, while contralateral axons enhance their growth upon Wnt5a exposure, ipsilateral axons collapse in response to Wnt5a, suggesting that a non-canonical Wnt signaling pathway mediates midline crossing. ChIP-Seq assays in RGCs also demonstrated that the differential response of ipsi- and contralateral visual axons to Wnt5a is regulated by binding of Zic2 to the regulatory regions of specific Wnt receptors and other Wnt signaling components such as Apc2. The induction of Zic2 results in the accumulation of β-catenin which is potentially phosphorylated by EphB1 at the growth cone after contact with ephrinB2 at the midline (Morenilla-Palao et al., 2020). Another component of the Zic2-controlled program is the Netrin receptor Unc5c. Unc5c is expressed in a subset of cRGCs that transiently project to the opposite retina during early postnatal stages. Netrin1 is expressed in the ventral diencephalon to impede the growth of these retino-retinal axons into the optic chiasm. In iRGCs, Zic2 binds to regulatory regions near the *Unc5c* locus and represses its expression in order to facilitate their growth into the diencephalic region (Murcia-Belmonte et al., 2019) (**Figure 1**). Thus, Zic2 binds to the regulatory regions of many genes, including EphB1, different components of the Wnt pathway and Unc5c, to specify iRGCs and regulate their guidance at the midline.

The positive correlation between the number of ipsilateral axons and the expression of Zic2 in the retina of different species pointed to this TF as a determinant of iRGCs identity across evolution. In addition to being expressed in the developing mouse retina, Zic2 is expressed in ferrets in a larger retinal area that coincides with the zone occupied by iRGCs in this species. In humans, Zic2 and EphB1 are both expressed in the temporal half of the retina also coinciding with the location of iRGCs and, in *Xenopus*, Zic2 is expressed in the retina during metamorphosis when a late-born ipsilateral projection is generated. However, in zebrafish and chicken Zic2 is not expressed in RGCs during development and accordingly these species lack an ipsilateral projection (Herrera et al., 2003; Lambot et al., 2005; Murcia-Belmonte et al., 2019; Vigouroux et al., 2021). Interestingly, ectopic expression of Zic2 in zebrafish RGCs leads to the appearance of an ectopic ipsilateral projection (Vigouroux et al., 2021), revealing that Zic2 is able to activate a transcriptional module that controls midline avoidance even in species that naturally lack an ipsilateral projection. Recent reports have shown that non-teleost bony fish also have an ipsilateral retinal projection (Vigouroux et al., 2021) but the function of this projection is still unknown and future experiments are needed to uncover this question and also to dilucidate the regulatory mechanisms that control this ancient ipsilateral projection.

Further functional experiments in chick and mice demonstrated that Zic2 does not only determines axon midline avoidance in the visual system but also in other types of ipsilateral neurons such as the thalamocortical projections and the late-born population of excitatory interneurons (dILB) located in the dorsal horns of the spinal cord. dILB neurons are born very close to the dorsal midline (Alaynick et al., 2011; Gross et al., 2002; Helms and Johnson, 2003; Lewis, 2006; Müller et al., 2002; Petkó and Antal, 2012). These cells but not their inhibitory counterpart dILA neurons that project locally and contralaterally (Escalante and Klein, 2020; Tulloch et al., 2019), express Zic2 which, in turn, is necessary and sufficient to define their ipsilateral trajectory (Escalante et al., 2013) (**Figure 2**). Chromatin immunoprecipitation experiments in a cell line and in spinal neurons, demonstrated that Zic2 is able to bind to the promoter of another Eph receptor, EphA4. Further functional experiments in chick and mice also confirmed that, instead of regulating EphB1 as in the visual system, in spinal neurons Zic2 controls the expression of EphA4 (Escalante et al., 2013; Luo et al., 2015; Morenilla-Palao et al., 2019). As EphB1, EphA4 binds to ephrinBs to mediate axon repulsion and it has been shown that ephrinB1, ephrinB2 and ephrinB3 are all expressed at the spinal cord midline (Kullander et al., 2001; Kullander et al., 2003; Escalante et al., 2013; Paixão et al., 2013; Klein and Kania, 2014; Haimson et al., 2021).

All together, these observations point to the existence of several gene programs that control axonal laterality in ipsilateral spinal neuron populations with dispar ontogeny. Early born dl1 neurons locate far away from the midline because the ventricle and the subventricular zone (SVZ), which is rich in progenitor cells, occupy the medial region of the dorsal tube. As progenitors exit the cell cycle, the SVZ shrinks and the somas of the late born dILB neurons locate close to the midline. In contrast to the dl1i population whose axons never approach the midline and their projection patterns rely on Lhx factors, dILB neurons are born in close contact with the midline and their axons need to be repelled as soon as they start growing in order to project ipsilaterally. Thus, it is not surprising that although both populations, dI1i and dILB neurons project ipsilaterally, they developed alternative strategies to control the

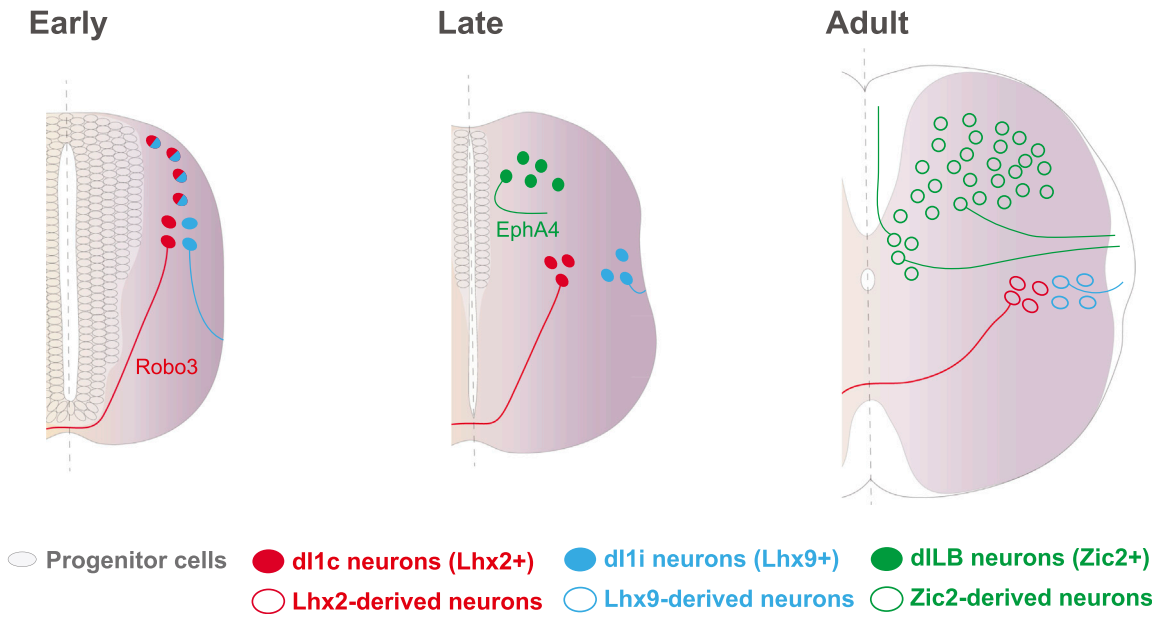

FIGURE 2 | Axon guidance strategies in different subtypes of spinal cord neurons. dI1 neurons are born early in neural tube development and are separated from the midline by the subventricular zone, populated by progenitor cells. Expression of Lhx2 in dI1 neurons activates a contralateral program, in part through the upregulation of Robo3. Ipsilateral dI1 neurons do never confront midline cues and project their axons into the ipsilateral lateral funiculus, likely through the expression of Robo2 and possibly mediated by Lhx9. Later, by the time that dILB neurons are born, progenitor neurons have already differentiated and postmitotic neurons distribute at both sides of the dorsal midline. In this scenario, EphA4 and likely other guidance molecules, are controlled by Zic2 to ensure midline repulsion and ipsilateral projection through the dorsal and lateral funiculi. These TFs are downregulated following development and are not expressed in adulthood.

guidance of their respective axons (Escalante et al., 2013) (**Figure 2**).

CONCLUSION

Despite the increasing number of rapidly emerging innovative techniques that largely facilitates research on the transcriptional mechanisms regulating gene expression, only a handful of TFs have been convincingly shown to control genetic programs involved in the regulation of axonal behaviors. In the last decade, the interest to understand how neural circuits function has exponentially increased and the development and application of genetically encoded, magnetic and thermal tools to manipulate neuronal circuits is helping us to disentangle brain connectivity and circuits function. However, it is surprising that in the era of next generation sequencing and single cell transcriptomic approaches (Escalante et al., 2020) there are still very few studies taking advantage of these technologies to elucidate the genetic programs that precisely control the definition of axonal trajectories. Incorrect circuit wiring during embryonic development may have a huge impact in the adult individual and we are still far from understanding how circuits are built in the first place. Future efforts devoted to understand the regulatory logic underlying neuronal trajectories will certainly contribute to prevent pathologies derived from neural circuits miswiring.

AUTHOR CONTRIBUTIONS

AE wrote the original draft. AE and EH revised subsequent versions of the manuscript.

FUNDING

This work was funded through the Junior Leader Programme of La Caixa Foundation (LCF/BQ/PI18/11630005) to AE. The laboratory of EH is supported by the following grants: PROMETEO/2020/007 from the Generalitat Valenciana, PID2019-110535GB-I00 from the National Grant Research Program, 20191956 from the Ramón Areces Foundation. The Institute of Neurosciences receives funding from the "Severo Ochoa" Program for Centers of Excellence in R&D (SEV-2017-0723).

ACKNOWLEDGMENTS

We thank members of the Herrera lab for thoughtful discussion and feedback, and Juan Antonio Sánchez Alcañiz and Carlos Sánchez Huertas for critical reading of the manuscript. We apologize to those researchers whose work could not be included in this manuscript due to space constraints.

REFERENCES

Alaynick, W. A., Jessell, T. M., and Pfaff, S. L. (2011). SnapShot: Spinal Cord Development. *Cell* 146, 178. doi:10.1016/j.cell.2011.06.038

Arlotta, P., Molyneaux, B. J., Chen, J., Inoue, J., Kominami, R., and Macklis, J. D. (2005). Neuronal Subtype-specific Genes that Control Corticospinal Motor Neuron Development *In Vivo*. *Neuron* 45, 207–221. doi:10.1016/j.neuron.2004.12.036

Avilés, E. C., and Stoeckli, E. T. (2016). Canonical Wnt Signaling Is Required for Commissural Axon Guidance. *Dev. Neurobiol.* 76, 190–208. doi:10.1002/dneu.22307

Avraham, O., Hadas, Y., Vald, L., Zisman, S., Schejter, A., Visel, A., et al. (2009). Transcriptional Control of Axonal Guidance and Sorting in Dorsal Interneurons by the Lim-HD Proteins Lhx9 and Lhx1. *Neural Dev.* 4, 21. doi:10.1186/1749-8104-4-21

Bermingham, N. A., Hassan, B. A., Wang, V. Y., Fernandez, M., Banfi, S., Bellen, H. J., et al. (2001). Proprioceptor Pathway Development Is Dependent on Math1. *Neuron* 30, 411–422. doi:10.1016/s0896-6273(01)00305-1

Bin Chen, B., Schaevitz, L. R., and McConnell, S. K. (2005). Fezl Regulates the Differentiation and Axon Targeting of Layer 5 Subcortical Projection Neurons in Cerebral Cortex. *Proc. Natl. Acad. Sci.* 102, 17184–17189. doi:10.1073/pnas.0508732102

Blockus, H., and Chédotal, A. (2015). "Disorders of Axon Guidance," in *The Genetics of Neurodevelopmental Disorders* (John Wiley & Sons), 155–194. doi:10.1002/9781118524947.ch8

Bravo-Ambrosio, A., Mastick, G., and Kaprielian, Z. (2012). Motor Axon Exit from the Mammalian Spinal Cord Is Controlled by the Homeodomain Protein Nkx2.9 via Robo-Slit Signaling. *Development* 139, 1435–1446. doi:10.1242/dev.072256

Broihier, H. T., Kuzin, A., Zhu, Y., Odenwald, W., and Skeath, J. B. (2004). Drosophilahomeodomain Protein Nkx6 Coordinates Motoneuron Subtype Identity and Axonogenesis. *Development* 131, 5233–5242. doi:10.1242/dev.01394

Butler, S. J., and Tear, G. (2007). Getting Axons onto the Right Path: the Role of Transcription Factors in Axon Guidance. *Development* 134, 439–448. doi:10.1242/dev.02762

Carreres, M. I., Escalante, A., Murillo, B., Chauvin, G., Gaspar, P., Vegar, C., et al. (2011). Transcription Factor Foxd1 Is Required for the Specification of the Temporal Retina in Mammals. *J. Neurosci.* 31, 5673–5681. doi:10.1523/jneurosci.0394-11.2011

Chédotal, A. (2014). Development and Plasticity of Commissural Circuits: from Locomotion to Brain Repair. *Trends Neurosciences* 37, 551–562. doi:10.1016/j.tins.2014.08.009

Chédotal, A. (2019). Roles of Axon Guidance Molecules in Neuronal Wiring in the Developing Spinal Cord. *Nat. Rev. Neurosci.* 20, 380–396. doi:10.1038/s41583-019-0168-7

Chen, A. I., de Nooij, J. C., and Jessell, T. M. (2006). Graded Activity of Transcription Factor Runx3 Specifies the Laminar Termination Pattern of Sensory Axons in the Developing Spinal Cord. *Neuron* 49, 395–408. doi:10.1016/j.neuron.2005.12.028

Colamarino, S. A., and Tessier-Lavigne, M. (1995). The Role of the Floor Plate in Axon Guidance. *Annu. Rev. Neurosci.* 18, 497–529. doi:10.1146/annurev.ne.18.030195.002433

Comer, J. D., Alvarez, S., Butler, S. J., and Kaltschmidt, J. A. (2019). Commissural Axon Guidance in the Developing Spinal Cord: from Cajal to the Present Day. *Neural Dev.* 14, 9. doi:10.1186/s13064-019-0133-1

Corradi, E., and Baudet, M.-L. (2020). In the Right Place at the Right Time: miRNAs as Key Regulators in Developing Axons. *Int. J. Mol. Sci.* 21, 8726. doi:10.3390/ijms21228726

Dasen, J. S., Liu, J.-P., and Jessell, T. M. (2003). Motor Neuron Columnar Fate Imposed by Sequential Phases of Hox-C Activity. *Nature* 425, 926–933. doi:10.1038/nature02051

Dasen, J. S., Tice, B. C., Brenner-Morton, S., and Jessell, T. M. (2005). A Hox Regulatory Network Establishes Motor Neuron Pool Identity and Target-Muscle Connectivity. *Cell* 123, 477–491. doi:10.1016/j.cell.2005.09.009

Dillon, A. K., Fujita, S. C., Matise, M. P., Jarjour, A. A., Kennedy, T. E., Kollmus, H., et al. (2005). Molecular Control of Spinal Accessory Motor Neuron/axon Development in the Mouse Spinal Cord. *J. Neurosci.* 25, 10119–10130. doi:10.1523/jneurosci.3455-05.2005

Ding, Q., Joshi, P. S., Xie, Z.-H., Xiang, M., and Gan, L. (2012). BARHL2 Transcription Factor Regulates the Ipsilateral/contralateral Subtype Divergence in Postmitotic dI1 Neurons of the Developing Spinal Cord. *Proc. Natl. Acad. Sci.* 109, 1566–1571. doi:10.1073/pnas.1112392109

Dominici, C., Moreno-Bravo, J. A., Puiggros, S. R., Rappeneau, Q., Rama, N., Vieugue, P., et al. (2017). Floor-plate-derived Netrin-1 Is Dispensable for Commissural Axon Guidance. *Nature* 545, 350–354. doi:10.1038/nature22331

Dorskind, J. M., and Kolodkin, A. L. (2021). Revisiting and Refining Roles of Neural Guidance Cues in Circuit Assembly. *Curr. Opin. Neurobiol.* 66, 10–21. doi:10.1016/j.conb.2020.07.005

Engle, E. C. (2010). Human Genetic Disorders of Axon Guidance. *Cold Spring Harbor Perspect. Biol.* 2, a001784. doi:10.1101/cshperspect.a001784

Erkman, L., Yates, P. A., McLaughlin, T., McEvilly, R. J., Whisenhunt, T., O'Connell, S. M., et al. (2000). A POU Domain Transcription Factor-dependent Program Regulates Axon Pathfinding in the Vertebrate Visual System. *Neuron* 28, 779–792. doi:10.1016/s0896-6273(00)00153-7

Escalante, A., and Klein, R. (2020). Spinal Inhibitory Ptf1a-Derived Neurons Prevent Self-Generated Itch. *Cell Rep* 33, 108422. doi:10.1016/j.celrep.2020.108422

Escalante, A., González-Martínez, R., and Herrera, E. (2020). New Techniques for Studying Neurodevelopment. *F1000prime Rep.* 9, 17. doi:10.12703/r/9-17

Escalante, A., Murillo, B., Morenilla-Palao, C., Klar, A., and Herrera, E. (2013). Zic2-Dependent Axon Midline Avoidance Controls the Formation of Major Ipsilateral Tracts in the CNS. *Neuron* 80, 1392–1406. doi:10.1016/j.neuron.2013.10.007

Fujioka, M., Lear, B. C., Landgraf, M., Yusibova, G. L., Zhou, J., Riley, K. M., et al. (2003). Even-skipped, Acting as a Repressor, Regulates Axonal Projections in Drosophila. *Development* 130, 5385–5400. doi:10.1242/dev.00770

Garces, A., and Thor, S. (2006). Specification ofDrosophilaaCC Motoneuron Identity by a Genetic cascade Involvingeven-Skipped, Grainandzfh1. *Development* 133, 1445–1455. doi:10.1242/dev.02321

García-Frigola, C., Carreres, M. I., Vegar, C., Mason, C., and Herrera, E. (2008). Zic2 Promotes Axonal Divergence at the Optic Chiasm Midline by EphB1-dependent and -independent Mechanisms. *Development* 135, 1833–1841. doi:10.1242/dev.020693

Gorla, M., Santiago, C., Chaudhari, K., Layman, A. A. K., Oliver, P. M., and Bashaw, G. J. (2019). Ndfip Proteins Target Robo Receptors for Degradation and Allow Commissural Axons to Cross the Midline in the Developing Spinal Cord. *Cel Rep.* 26, 3298–3312. e4. doi:10.1016/j.celrep.2019.02.080

Gowan, K., Helms, A. W., Hunsaker, T. L., Collisson, T., Ebert, P. J., Odom, R., et al. (2001). Crossinhibitory Activities of Ngn1 and Math1 Allow Specification of Distinct Dorsal Interneurons. *Neuron* 31, 219–232. doi:10.1016/s0896-6273(01)00367-1

Gross, M. K., Dottori, M., and Goulding, M. (2002). Lbx1 Specifies Somatosensory Association Interneurons in the Dorsal Spinal Cord. *Neuron* 34, 535–549. doi:10.1016/s0896-6273(02)00690-6

Guy, A. T., and Kamiguchi, H. (2021). Lipids as New Players in Axon Guidance and Circuit Development. *Curr. Opin. Neurobiol.* 66, 22–29. doi:10.1016/j.conb.2020.09.003

Haimson, B., Meir, O., Sudakevitz-Merzbach, R., Elberg, G., Friedrich, S., Lovell, P. V., et al. (2021). Natural Loss of Function of Ephrin-B3 Shapes Spinal Flight Circuitry in Birds. *Sci. Adv.* 7, eabg5968. doi:10.1126/sciadv.abg5968

Helms, A. W., Abney, A. L., Ben-Arie, N., Zoghbi, H. Y., and Johnson, J. E. (2000). Autoregulation and Multiple Enhancers Control Math1 Expression in the Developing Nervous System. *Development* 127, 1185–1196. doi:10.1242/dev.127.6.1185

Helms, A. W., and Johnson, J. E. (1998). Progenitors of Dorsal Commissural Interneurons Are Defined by MATH1 Expression. *Development* 125, 919–928. doi:10.1242/dev.125.5.919

Helms, A. W., and Johnson, J. E. (2003). Specification of Dorsal Spinal Cord Interneurons. *Curr. Opin. Neurobiol.* 13, 42–49. doi:10.1016/s0959-4388(03)00010-2

Herrera, E., Brown, L., Aruga, J., Rachel, R. A., Dolen, G., Mikoshiba, K., et al. (2003). Zic2 Patterns Binocular Vision by Specifying the Uncrossed Retinal Projection. *Cell* 114, 545–557. doi:10.1016/s0092-8674(03)00684-6

Herrera, E., Marcus, R., Li, S., Williams, S. E., Erskine, L., Lai, E., et al. (2004). Foxd1 Is Required for Proper Formation of the Optic Chiasm. *Development* 131, 5727–5739. doi:10.1242/dev.01431

Izzi, L., and Charron, F. (2011). Midline Axon Guidance and Human Genetic Disorders. *Clin. Genet.* 80, 226–234. doi:10.1111/j.1399-0004.2011.01735.x

Jie-Guang Chen, J.-G., Rasin, M.-R., Kwan, K. Y., and Sestan, N. (2005). Zfp312 Is Required for Subcortical Axonal Projections and Dendritic Morphology of Deep-Layer Pyramidal Neurons of the Cerebral Cortex. *Proc. Natl. Acad. Sci.* 102, 17792–17797. doi:10.1073/pnas.0509032102

Junge, H. J., Yung, A. R., Goodrich, L. V., and Chen, Z. (2016). Netrin1/DCC Signaling Promotes Neuronal Migration in the Dorsal Spinal Cord. *Neural Dev.* 11, 19. doi:10.1186/s13064-016-0074-x

Kaminker, J. S., Canon, J., Salecker, I., and Banerjee, U. (2002). Control of Photoreceptor Axon Target Choice by Transcriptional Repression of Runt. *Nat. Neurosci.* 5, 746–750. doi:10.1038/nn889

Kania, A., and Jessell, T. M. (2003). Topographic Motor Projections in the Limb Imposed by LIM Homeodomain Protein Regulation of Ephrin-A:EphA Interactions. *Neuron* 38, 581–596. doi:10.1016/s0896-6273(03)00292-7

Kania, A., Johnson, R. L., and Jessell, T. M. (2000). Coordinate Roles for LIM Homeobox Genes in Directing the Dorsoventral Trajectory of Motor Axons in the Vertebrate Limb. *Cell* 102, 161–173. doi:10.1016/s0092-8674(00)00022-2

Kawauchi, D., Muroyama, Y., Sato, T., and Saito, T. (2010). Expression of Major Guidance Receptors Is Differentially Regulated in Spinal Commissural Neurons Transfated by Mammalian Barh Genes. *Dev. Biol.* 344, 1026–1034. doi:10.1016/j.ydbio.2010.06.025

Keleman, K., and Dickson, B. J. (2001). Short- and Long-Range Repulsion by the Drosophila Unc5 Netrin Receptor. *Neuron* 32, 605–617. doi:10.1016/s0896-6273(01)00505-0

Klein, R., and Kania, A. (2014). Ephrin Signalling in the Developing Nervous System. *Curr. Opin. Neurobiol.* 27, 16–24. doi:10.1016/j.conb.2014.02.006

Komiyama, T., Johnson, W. A., Luo, L., and Jefferis, G. S. X. E. (2003). From Lineage to Wiring Specificity. *Cell* 112, 157–167. doi:10.1016/s0092-8674(03)00030-8

Kullander, K., Butt, S. J. B., Lebret, J. M., Lundfald, L., Restrepo, C. E., Rydström, A., et al. (2003). Role of EphA4 and EphrinB3 in Local Neuronal Circuits that Control Walking. *Science* 299, 1889–1892. doi:10.1126/science.1079641

Kullander, K., Mather, N. K., Diella, F., Dottori, M., Boyd, A. W., and Klein, R. (2001). Kinase-dependent and Kinase-independent Functions of EphA4 Receptors in Major Axon Tract Formation *In Vivo*. *Neuron* 29, 73–84. doi:10.1016/s0896-6273(01)00181-7

Kuwajima, T., Yoshida, Y., Takegahara, N., Petros, T. J., Kumanogoh, A., Jessell, T. M., et al. (2012). Optic Chiasm Presentation of Semaphorin6D in the Context of Plexin-A1 and Nr-CAM Promotes Retinal Axon Midline Crossing. *Neuron* 74, 676–690. doi:10.1016/j.neuron.2012.03.025

Kuwajima, T., Soares, C. A., Sitko, A. A., Lefebvre, V., and Mason, C. (2017). SoxC Transcription Factors Promote Contralateral Retinal Ganglion Cell Differentiation and Axon Guidance in the Mouse Visual System. *Neuron* 93, 1110–1125. e5. doi:10.1016/j.neuron.2017.01.029

Labrador, J. P., O'Keefe, D., Yoshikawa, S., McKinnon, R. D., Thomas, J. B., and Bashaw, G. J. (2005). The Homeobox Transcription Factor Even-Skipped Regulates Netrin-Receptor Expression to Control Dorsal Motor-Axon Projections in Drosophila. *Curr. Biol.* 15, 1413–1419. doi:10.1016/j.cub.2005.06.058

Lambot, M.-A., Depasse, F., Noel, J.-C., and Vanderhaeghen, P. (2005). Mapping Labels in the Human Developing Visual System and the Evolution of Binocular Vision. *J. Neurosci.* 25, 7232–7237. doi:10.1523/jneurosci.0802-05.2005

Landgraf, M., Roy, S., Prokop, A., VijayRaghavan, K., and Bate, M. (1999). Even-Skipped Determines the Dorsal Growth of Motor Axons in Drosophila. *Neuron* 22, 43–52. doi:10.1016/s0896-6273(00)80677-7

Layden, M. J., Odden, J. P., Schmid, A., Garces, A., Thor, S., and Doe, C. Q. (2006). Zfh1, a Somatic Motor Neuron Transcription Factor, Regulates Axon Exit from the CNS. *Dev. Biol.* 291, 253–263. doi:10.1016/j.ydbio.2005.12.009

Lee, K. J., Mendelsohn, M., and Jessell, T. M. (1998). Neuronal Patterning by BMPs: a Requirement for GDF7 in the Generation of a Discrete Class of Commissural Interneurons in the Mouse Spinal Cord. *Genes Dev.* 12, 3394–3407. doi:10.1101/gad.12.21.3394

Lewis, K. E. (2006). How Do Genes Regulate Simple Behaviours? Understanding How Different Neurons in the Vertebrate Spinal Cord Are Genetically Specified. *Phil. Trans. R. Soc. B* 361, 45–66. doi:10.1098/rstb.2005.1778

Lodato, S., Molyneaux, B. J., Zuccaro, E., Goff, L. A., Chen, H.-H., Yuan, W., et al. (2014). Gene Co-regulation by Fezf2 Selects Neurotransmitter Identity and Connectivity of Corticospinal Neurons. *Nat. Neurosci.* 17, 1046–1054. doi:10.1038/nn.3757

Luo, Z., Gao, X., Lin, C., Smith, E. R., Marshall, S. A., Swanson, S. K., et al. (2015). Zic2 Is an Enhancer-Binding Factor Required for Embryonic Stem Cell Specification. *Mol. Cel* 57, 685–694. doi:10.1016/j.molcel.2015.01.007

Marcos-Mondéjar, P., Peregrín, S., Li, J. Y., Carlsson, L., Tole, S., and López-Bendito, G. (2012). The Lhx2 Transcription Factor Controls Thalamocortical Axonal Guidance by Specific Regulation of Robo1 and Robo2 Receptors. *J. Neurosci.* 32, 4372–4385. The Official Journal of the Society for Neuroscience. doi:10.1523/JNEUROSCI.5851-11.2012

Marcucci, F., Murcia-Belmonte, V., Wang, Q., Coca, Y., Ferreiro-Galve, S., Kuwajima, T., et al. (2016). The Ciliary Margin Zone of the Mammalian Retina Generates Retinal Ganglion Cells. *Cel Rep.* 17, 3153–3164. doi:10.1016/j.celrep.2016.11.016

Molyneaux, B. J., Arlotta, P., Hirata, T., Hibi, M., and Macklis, J. D. (2005). Fezl Is Required for the Birth and Specification of Corticospinal Motor Neurons. *Neuron* 47, 817–831. doi:10.1016/j.neuron.2005.08.030

Morenilla-Palao, C., López-Cascales, M. T., López-Atalaya, J. P., Baeza, D., Calvo-Diaz, L., Gracia, A. G. D., et al. (2019). *Zic2 Abrogates an Alternative Wnt Signaling Pathway to Convert Axon Attraction into Repulsion*. Cold Spring Harbor: BioRxiv, 759407.

Morenilla-Palao, C., López-Cascales, M. T., López-Atalaya, J. P., Baeza, D., Calvo-Díaz, L., Barco, A., et al. (2020). A Zic2-Regulated Switch in a Noncanonical Wnt/βcatenin Pathway Is Essential for the Formation of Bilateral Circuits. *Sci. Adv.* 6, eaaz8797. doi:10.1126/sciadv.aaz8797

Moreno-Bravo, J. A., Puiggros, S. R., Blockus, H., Dominici, C., Zelina, P., Mehlen, P., et al. (2017). *Commissural Neurons Transgress the CNS/PNS Boundary in Absence of Ventricular Zone-Derived Netrin-1*. Cambridge: Development, 159400.

Müller, T., Brohmann, H., Pierani, A., Heppenstall, P. A., Lewin, G. R., Jessell, T. M., et al. (2002). The Homeodomain Factor Lbx1 Distinguishes Two Major Programs of Neuronal Differentiation in the Dorsal Spinal Cord. *Neuron* 34, 551–562. doi:10.1016/s0896-6273(02)00689-x

Murcia-Belmonte, V., Coca, Y., Vegar, C., Negueruela, S., de Juan Romero, C., Valiño, A. J., et al. (2019). A Retino-Retinal Projection Guided by Unc5c Emerged in Species with Retinal Waves. *Curr. Biol.* 29, 1149–1160. e4. doi:10.1016/j.cub.2019.02.052

Nakada, Y., Hunsaker, T. L., Henke, R. M., and Johnson, J. E. (2004). Distinct Domains within Mash1 and Math1 Are Required for Function in Neuronal Differentiation versus Neuronal Cell-type Specification. *Development* 131, 1319–1330. doi:10.1242/dev.01008

Nugent, A. A., Kolpak, A. L., and Engle, E. C. (2012). Human Disorders of Axon Guidance. *Curr. Opin. Neurobiol.* 22, 837–843. doi:10.1016/j.conb.2012.02.006

Paixão, S., Balijepalli, A., Serradj, N., Niu, J., Luo, W., Martin, J. H., et al. (2013). EphrinB3/EphA4-Mediated Guidance of Ascending and Descending Spinal Tracts. *Neuron* 80, 1407–1420. doi:10.1016/j.neuron.2013.10.006

Pak, W., Hindges, R., Lim, Y.-S., Pfaff, S. L., and O'Leary, D. D. M. (2004). Magnitude of Binocular Vision Controlled by Islet-2 Repression of a Genetic Program that Specifies Laterality of Retinal Axon Pathfinding. *Cell* 119, 567–578. doi:10.1016/j.cell.2004.10.026

Petkó, M., and Antal, M. (2012). Propriospinal Pathways in the Dorsal Horn (Laminae I–IV) of the Rat Lumbar Spinal Cord. *Brain Res. Bull.* 89, 41–49. doi:10.1016/j.brainresbull.2012.06.005

Quina, L. A., Pak, W., Lanier, J., Banwait, P., Gratwick, K., Liu, Y., et al. (2005). Brn3a-Expressing Retinal Ganglion Cells Project Specifically to Thalamocortical and Collicular Visual Pathways. *J. Neurosci.* 25, 11595–11604. doi:10.1523/jneurosci.2837-05.2005

Reig, G., Cabrejos, M. E., and Concha, M. L. (2007). Functions of BarH Transcription Factors during Embryonic Development. *Dev. Biol.* 302, 367–375. doi:10.1016/j.ydbio.2006.10.008

Roig-Puiggros, S., Vigouroux, R. J., Beckman, D., Bocai, N. I., Chiou, B., Davimes, J., et al. (2020). Construction and Reconstruction of Brain Circuits: normal and Pathological Axon Guidance. *J. Neurochem.* 153, 10–32. doi:10.1111/jnc.14900

Saba, R., Nakatsuji, N., and Saito, T. (2003). Mammalian BarH1Confers Commissural Neuron Identity on Dorsal Cells in the Spinal Cord. *J. Neurosci.* 23, 1987–1991. doi:10.1523/jneurosci.23-06-01987.2003

Saba, R., Johnson, J. E., and Saito, T. (2005). Commissural Neuron Identity Is Specified by a Homeodomain Protein, Mbh1,that Is Directly Downstream of Math1. *Development* 132, 2147–2155. doi:10.1242/dev.01781

Sabatier, C., Plump, A. S., Le Ma, L., Brose, K., Tamada, A., Murakami, F., et al. (2004). The Divergent Robo Family Protein rig-1/Robo3 Is a Negative Regulator of Slit Responsiveness Required for Midline Crossing by Commissural Axons. *Cell* 117, 157–169. doi:10.1016/s0092-8674(04)00303-4

Sharma, K., Sheng, H. Z., Lettieri, K., Li, H., Karavanov, A., Potter, S., et al. (1998). LIM Homeodomain Factors Lhx3 and Lhx4 Assign Subtype Identities for Motor Neurons. *Cell* 95, 817–828. doi:10.1016/s0092-8674(00)81704-3

Shirasaki, R., Lewcock, J. W., Lettieri, K., and Pfaff, S. L. (2006). FGF as a Target-Derived Chemoattractant for Developing Motor Axons Genetically Programmed by the LIM Code. *Neuron* 50, 841–853. doi:10.1016/j.neuron.2006.04.030

Srivatsa, S., Parthasarathy, S., Britanova, O., Bormuth, I., Donahoo, A. L., Ackerman, S. L., et al. (2014). Unc5C and DCC Act Downstream of Ctip2 and Satb2 and Contribute to Corpus Callosum Formation. *Nat. Commun.* 5, 3708. doi:10.1038/ncomms4708

Thor, S., Andersson, S. G. E., Tomlinson, A., and Thomas, J. B. (1999). A LIM-Homeodomain Combinatorial Code for Motor-Neuron Pathway Selection. *Nature* 397, 76–80. doi:10.1038/16275

Tsuchida, T., Ensini, M., Morton, S. B., Baldassare, M., Edlund, T., Jessell, T. M., et al. (1994). Topographic Organization of Embryonic Motor Neurons Defined by Expression of LIM Homeobox Genes. *Cell* 79, 957–970. doi:10.1016/0092-8674(94)90027-2

Tulloch, A. J., Teo, S., Carvajal, B. V., Tessier-Lavigne, M., and Jaworski, A. (2019). Diverse Spinal Commissural Neuron Populations Revealed by Fate Mapping and Molecular Profiling Using a Novel Robo3Cre Mouse. *J. Comp. Neurol.* 527, 2948–2972. doi:10.1002/cne.24720

Van Battum, E. Y., Brignani, S., and Pasterkamp, R. J. (2015). Axon Guidance Proteins in Neurological Disorders. *Lancet Neurol.* 14, 532–546. doi:10.1016/S1474-4422(14)70257-1

Varadarajan, S. G., Kong, J. H., Phan, K. D., Kao, T. J., Panaitof, S. C., Cardin, J., et al. (2017). Netrin1 Produced by Neural Progenitors, Not Floor Plate Cells, Is Required for Axon Guidance in the Spinal Cord. *Neuron* 94, 790. e3. doi:10.1016/j.neuron.2017.03.007

Vigouroux, R. J., Duroure, K., Vougny, J., Albadri, S., Kozulin, P., Herrera, E., et al. (2021). Bilateral Visual Projections Exist in Non-teleost Bony Fish and Predate the Emergence of Tetrapods. *Science* 372, 150–156. doi:10.1126/science.abe7790

Wang, S. W., Gan, L., Martin, S. E., and Klein, W. H. (2000). Abnormal Polarization and Axon Outgrowth in Retinal Ganglion Cells Lacking the POU-Domain Transcription Factor Brn-3b. *Mol. Cel Neurosci* 16, 141–156. doi:10.1006/mcne.2000.0860

Williams, S. E., Mann, F., Erskine, L., Sakurai, T., Wei, S., Rossi, D. J., et al. (2003). Ephrin-B2 and EphB1 Mediate Retinal Axon Divergence at the Optic Chiasm. *Neuron* 39, 919–935. doi:10.1016/j.neuron.2003.08.017

Wilson, S. I., Shafer, B., Lee, K. J., and Dodd, J. (2008). A Molecular Program for Contralateral Trajectory: Rig-1 Control by LIM Homeodomain Transcription Factors. *Neuron* 59, 413–424. doi:10.1016/j.neuron.2008.07.020

Wu, Z., Makihara, S., Yam, P. T., Teo, S., Renier, N., Balekoglu, N., et al. (2019). Long-Range Guidance of Spinal Commissural Axons by Netrin1 and Sonic Hedgehog from Midline Floor Plate Cells. *Neuron* 101, 635. e4. doi:10.1016/j.neuron.2018.12.025

Wurmser, M., Muppavarapu, M., Tait, C. M., Laumonnerie, C., González-Castrillón, L. M., and Wilson, S. I. (2021). Robo2 Receptor Gates the Anatomical Divergence of Neurons Derived from a Common Precursor Origin. *Front. Cel Dev. Biol.* 9, 1337. doi:10.3389/fcell.2021.668175

Yang, T., Huang, H., Shao, Q., Yee, S., Majumder, T., and Liu, G. (2018). miR-92 Suppresses Robo1 Translation to Modulate Slit Sensitivity in Commissural Axon Guidance. *Cel Rep* 24, 2694. e6. doi:10.1016/j.celrep.2018.08.021

Zelina, P., Blockus, H., Zagar, Y., Péres, A., Friocourt, F., Wu, Z., et al. (2014). Signaling Switch of the Axon Guidance Receptor Robo3 during Vertebrate Evolution. *Neuron* 84, 1258–1272. doi:10.1016/j.neuron.2014.11.004

Zhuang, M., Li, X., Zhu, J., Zhang, J., Niu, F., Liang, F., et al. (2019). The m6A Reader YTHDF1 Regulates Axon Guidance through Translational Control of Robo3.1 Expression. *Nucleic Acids Res.* 47, 4765–4777. doi:10.1093/nar/gkz157

Conflict of Interest: The authors declare that the research was conducted in the absence of any commercial or financial relationships that could be construed as a potential conflict of interest.

Publisher's Note: All claims expressed in this article are solely those of the authors and do not necessarily represent those of their affiliated organizations, or those of the publisher, the editors and the reviewers. Any product that may be evaluated in this article, or claim that may be made by its manufacturer, is not guaranteed or endorsed by the publisher.

frontiers in Cell and Developmental Biology

BRIEF RESEARCH REPORT
published: 22 February 2022
doi: 10.3389/fcell.2022.808045

FoxK1 is Required for Ectodermal Cell Differentiation During Planarian Regeneration

Pablo Coronel-Córdoba[1,2†], *M. Dolores Molina*[1,2†], *Gemma Cardona*[1,2†], *Susanna Fraguas*[1,2], *Eudald Pascual-Carreras*[1,2], *Emili Saló*[1,2], *Francesc Cebrià*[1,2*‡] *and Teresa Adell*[1,2*‡]

[1]*Department of Genetics, Microbiology and Statistics, Faculty of Biology, University of Barcelona, Barcelona, Spain,* [2]*Institute of Biomedicine of the University of Barcelona (IBUB), Barcelona, Spain*

OPEN ACCESS

Edited by:
Rosa Barrio,
CIC bioGUNE, Spain

Reviewed by:
Ricardo M. Zayas,
San Diego State University, United States
Jose Maria Martin-Duran,
Queen Mary University of London, United Kingdom

****Correspondence:***
Teresa Adell
tadellc@ub.edu
Francesc Cebrià
fcebria@ub.edu

‡*These authors share last authorship*

†*These authors have contributed equally to this work and share first authorship*

Specialty section:
This article was submitted to Morphogenesis and Patterning, a section of the journal Frontiers in Cell and Developmental Biology

Received: *02 November 2021*
Accepted: *25 January 2022*
Published: *22 February 2022*

Citation:
Coronel-Córdoba P, Molina MD, Cardona G, Fraguas S, Pascual-Carreras E, Saló E, Cebrià F and Adell T (2022) FoxK1 is Required for Ectodermal Cell Differentiation During Planarian Regeneration. Front. Cell Dev. Biol. 10:808045. doi: 10.3389/fcell.2022.808045

Forkhead box (Fox) genes belong to the "winged helix" transcription factor superfamily. The function of some Fox genes is well known, such as the role of *foxO* in controlling metabolism and longevity and *foxA* in controlling differentiation of endodermal tissues. However, the role of some Fox factors is not yet well characterized. Such is the case of FoxK genes, which are mainly studied in mammals and have been implicated in diverse processes including cell proliferation, tissue differentiation and carcinogenesis. Planarians are free-living flatworms, whose importance in biomedical research lies in their regeneration capacity. Planarians possess a wide population of pluripotent adult stem cells, called neoblasts, which allow them to regenerate any body part after injury. In a recent study, we identified three *foxK* paralogs in the genome of *Schmidtea mediterranea*. In this study, we demonstrate that *foxK1* inhibition prevents regeneration of the ectodermal tissues, including the nervous system and the epidermis. These results correlate with *foxK1* expression in neoblasts and in neural progenitors. Although the triggering of wound genes expression, polarity reestablishment and proliferation was not affected after *foxK1* silencing, the apoptotic response was decreased. Altogether, these results suggest that *foxK1* would be required for differentiation and maintenance of ectodermal tissues.

Keywords: FOXK, planarian, nervous system, regeneration, stem cell, differentiation

INTRODUCTION

Forkhead box (Fox) genes belong to the "winged helix" superfamily of transcription factors, showing a Forkhead DNA-binding domain. Over 2,000 Fox proteins, phylogenetically classified into 25 families (A to S), have been identified in a number of species of fungi and metazoans (Benayoun, Caburet, and Veitia 2011; Pascual-Carreras et al., 2021). Fox genes control essential processes such as cell death, cell cycle and cell differentiation during all stages of development and in adult tissues, although many members show a tissue/stage-specific expression and function (Benayoun, Caburet, and Veitia 2011). The function and the implication of some Fox genes in human diseases is well known, such as the role in the differentiation of endodermal tissues of FoxA factors, the control of the cell cycle by FoxM, the role of FoxO in regulating metabolism and longevity and the contribution to speech acquisition of FoxP (Golson and Kaestner 2016). Some Fox transcription factors, especially FoxA, FoxO and FoxI members, are shown to act as pioneer factors, which open compacted chromatin to facilitate the binding of other transcription factors at enhancer sites (Lalmansingh, 2012). However, the function of some Fox families has not been properly addressed. An example are the FoxK genes, which are characterized by containing a forkhead-associated domain (FHA) besides

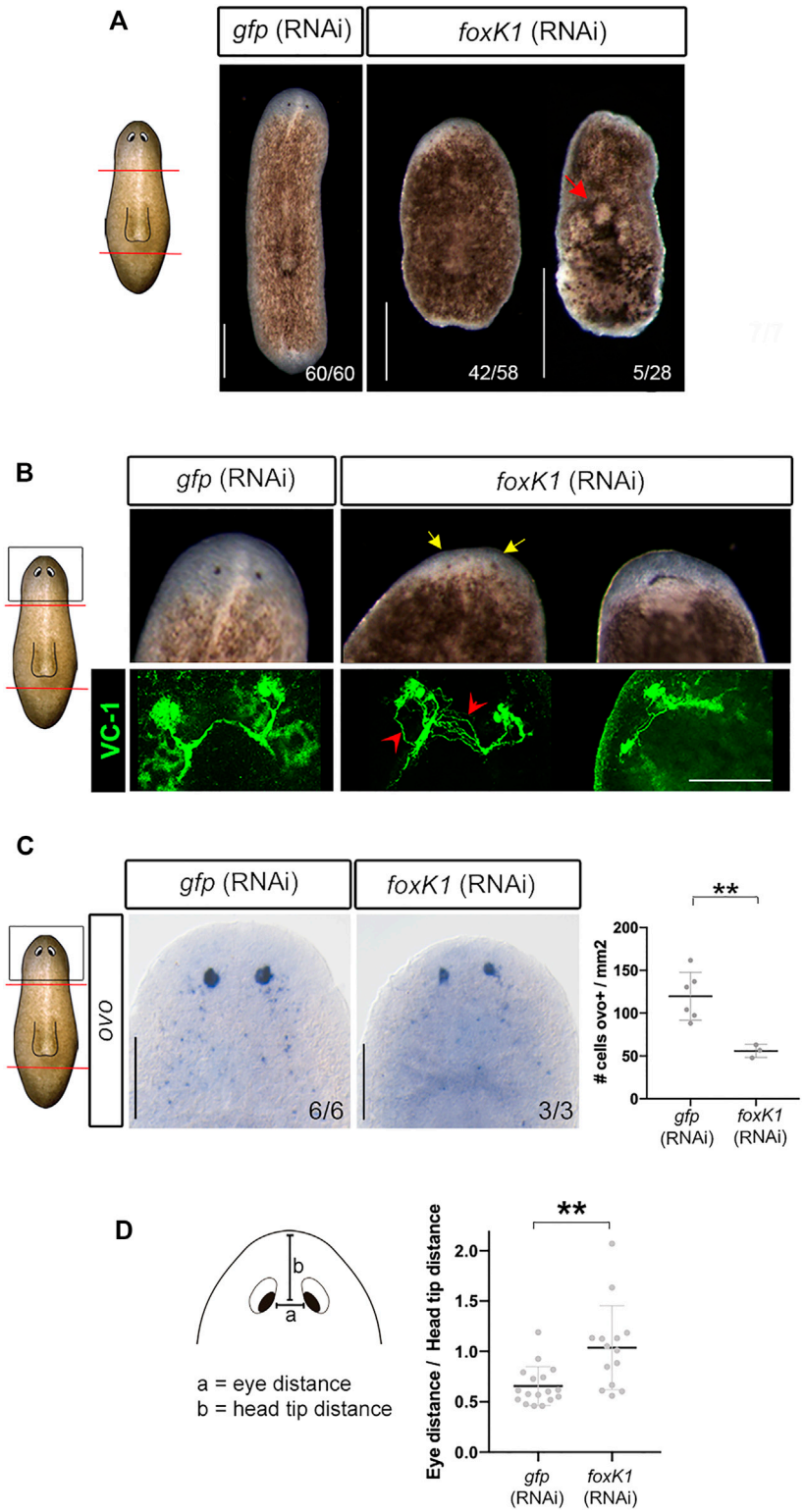

FIGURE 1 | *foxK1* silencing impairs planarian regeneration and eye differentiation. **(A)** *foxK1* RNAi animals present smaller anterior and posterior blastemas in comparison to controls. Red arrowhead points to the epidermal injuries observed in *foxK1* RNAi animals. Scale bar: 500 μm. **(B–D)** Aberrant eye regeneration after silencing *foxK1*. **(B)** *foxK1* RNAi animals present smaller eyes that differentiate closer to the pre-existing tissue in comparison to controls (yellow arrows). Visualization of the eyes with an anti-VC1 immunostaining reveals defects in eye regeneration and an incorrect guidance of visual axons (red arrows). Scale bar: 100 μm. **(C)** Whole-mount *in situ* hybridization analysis of the expression of *ovo* in *foxK1* RNAi animals. Scale bar: 200 μm. Quantification of *ovo* + cells/mm2 shows a significant decrease in

(*Continued*)

FIGURE 1 | the number of eye progenitor cells in *foxK1* RNAi animals ($n = 3$) compared to *gfp* RNAi animals ($n = 6$). Values represent the mean ± standard deviation [s.d]. $^{**}p$-value < 0.01. **(D)** Quantification of the eye distance/head tip distance ratio shows a significant increase in *foxK1* RNAi animals ($n = 14$) compared to control *gfp* (RNAi) animals ($n = 17$). $^{**}p$-value < 0.01. **(A–D)**: All animals shown and analyzed are at 7 days of regeneration after anterior-posterior amputation. In the schematic planarians, red lines indicate the amputation planes and black squares the region analysed.

the Forkhead DNA-binding domain, which mediates its interaction with multiple proteins (Ji et al., 2021). Few studies have been reported on the function of *foxK* genes, and they are mainly performed in mammals, which show two members (FoxK1 and FoxK2). From these studies, it is known that FoxK proteins are not tissue-specific but are ubiquitously expressed, and they regulate diverse biological processes, including cell proliferation, myogenic differentiation, cell cycle, autophagy, DNA damage and carcinogenesis (Liu et al., 2019).

Planarians are Lophotrochozoans well known for possessing pluripotent adult stem cells (called neoblasts) that confer them an extreme plasticity. They can regenerate any body part and change their size according to food availability (Wagner, Wang, and Reddien 2011; Baguñà 2012; Cebrià, Adell, and Saló 2018; Molina and Cebrià 2021). Previous studies of Fox genes function in planarians have demonstrated their evolutionary conserved role, and provided new data about their cellular function (Scimone, Lapan, and Reddien 2014; Vogg et al., 2014; He et al., 2017; Scimone et al., 2018). For instance, *foxA* was found to be essential for the maintenance of the pharynx and endodermal tissues (Koinuma et al., 2000; Adler et al., 2014) and *foxO* showed a conserved role in regulating metabolism during planarian regeneration and homeostasis (Pascual-Carreras et al., 2021). In a recent study, we identified 3 *foxK* paralogs in the genome of the planarian species *S. mediterranea* (*Smed foxK-1-2-3*). In this study, we aimed to analyze the function of *Smed-Fox* genes to provide new data about the role of this family in a model that, in contrast to mammals, displays stem cell-based tissue maintenance and regeneration.

We found that *foxK1*, expressed in neoblasts and their progenitors, is required for regeneration of neural and epidermal tissues. We hypothesize that *foxK1* may play a role in activating and maintaining lineage specific enhancers.

RESULTS

foxK1 RNAi Planarians Can Properly Regenerate Neither the Eyes nor the Nervous System

In a previous study, we identified 3 paralogs within the FoxK family in *S. mediterranea* (*foxK1-2-3*) (Pascual-Carreras et al., 2021). In this study, we have inhibited the three *foxK* genes by RNAi, showing that RNAi of *foxk1* generates the strongest phenotype (**Figure 1A**) (**Supplementary Figure S1A**). *foxk1* (RNAi) animals cannot regenerate proper anterior or posterior structures and 25% of them die after developing epidermal lesions after a single round of injection and amputation (**Figure 1A**). Prolonged silencing of *foxK1* eventually impaired the viability of all the treated animals.

FoxK1 RNAi planarians regenerated smaller blastemas and eyes (**Figure 1A**). In some animals, eyes were merged in the midline (**Figure 1B**). Immunostaining of photoreceptors demonstrated that visual axons were aberrant and not properly connected to form a correct optic chiasm (**Figure 1B**). The expression of *ovo*, a pan-eye marker (Lapan and Reddien 2011), corroborated the decrease in the number of both differentiated and progenitor eye cells (**Figure 1C**). It also showed that eyes were more separated and closer to the anterior tip in *foxK1*-silenced planarians (**Figure 1D**). A phototaxis assay showed that *foxK1* RNAi animals do not respond to the light stimulus, suggesting that although they could regenerate some photoreceptor cells (**Figure 1B**), these were not fully functional (**Supplementary Figure S1B**).

Analysis of the nervous system of *foxK1* RNAi animals through anti-synapsin and anti-α-tubulin immunostaining showed that cephalic ganglia did not regenerate, and only a few axons at the level of the neural nerve cords (VNCs) crossed the midline (**Figure 2A**). The analysis of the expression of markers of differentiated neural cells such as *gpas* (Cebrià, Nakazawa, and Mineta 2002; Iglesias et al., 2011), *pc2* (Collins et al., 2010) and *th* (Nishimura et al., 2007; Fraguas et al., 2011) corroborated that cephalic ganglia could not be formed (**Figure 2A**). The expression of *sim*, a marker of differentiated and progenitor neural cells (Cowles et al., 2013), was decreased in *foxK1* RNAi animals (**Supplementary Figure S2A**). Quantification of differentiated (*sim+*) and progenitor (*sim+*/PIWI1+) neural cells indicated that both populations were decreased in *foxK1* RNAi planarians (**Figure 2B**). The problem in regenerating the nervous system was not anterior specific, but it also affected the regeneration of proper posterior VNCs in the tail (**Figure 2C**).

According to the RNAi phenotype, *foxK1* was expressed in the nervous system of intact animals and during regeneration (**Supplementary Figure S1C**). Furthermore, the analysis of the expression pattern of *foxK1* in irradiated animals showed that it was expressed in differentiated cells and also in progenitors (**Supplementary Figure S1C**), which agrees with published single-cell RNAseq databases (Plass et al., 2018; Zeng et al., 2018) (**Supplementary Figures S1D–F**).

foxK1 RNAi Animals Cannot Regenerate a Proper Epidermis

foxK1 appears expressed in the neural and in the epidermal lineages according to the published single-cell RNAseq data (**Supplementary Figure S1C**). Furthermore, its inhibition produced epidermal lesions (**Figure 1A**). Thus, we analyzed deeper the integrity of the epidermal tissue in RNAi animals. Quantification of the nucleus demonstrated a decrease of cell density in the epidermis (**Figure 3A**). Interestingly, the nucleus

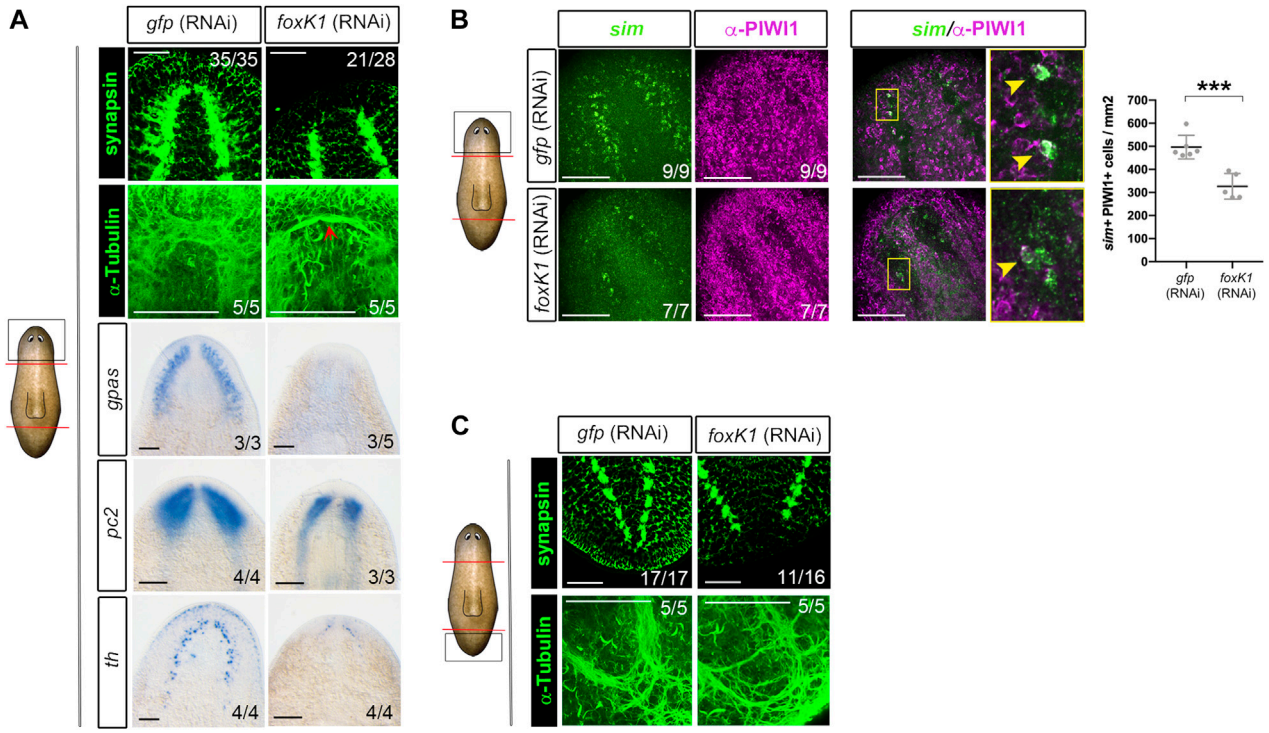

FIGURE 2 | *foxK1* silenced animals show a reduced number of neural progenitors and almost absent differentiated neural structures. **(A)** Whole-mount immunostaining and *in situ* hybridization analyses (WISH) of the anterior nervous system regeneration in *foxK1* RNAi animals 7 days post amputation. From top to bottom: immunostaining of the brain ganglia visualized with anti-synapsin which labels the brain synapsis; Immunostaining of the brain ganglia visualized with anti-α-tubulin which labels axons; WISH of *gpas, pc2 and th* which label differentiated neural cells. Scale bar: 100 μm. **(B)** Whole-mount fluorescence *in situ* hybridization analysis (WFISH) combined with immunostaining of the anterior blastemas in *foxK1* RNAi animals 7 days post amputation. From left to right: WFISH with *sim,* which labels both neural progenitors and differentiated neurons; immunostaining with anti-PIWI1 which labels stem cells; double *sim*+/PIWI1+ positive cells, which indicate neural progenitors; Scale bar: 100 μm. Quantification of *sim* + PIWI + cells/mm2 reveals a decreased number of neural progenitors in *foxK1* RNAi animals. Values represent the mean ± standard deviation [s.d] of a mean of 5 samples per condition. ***p-value < 0.001. **(C)** Whole-mount immunostaining analysis of the posterior nervous system regeneration in *foxK1* RNAi animals at 7 days post amputation. From top to bottom: anti-synapsin labelling the synapsis and anti-α-tubulin labeling the axons, showing defects in the posterior VNCs. Scale bar: 100 μm. In the schematic planarians, red lines indicate the amputation planes and black squares the region analysed.

appeared bigger in *foxK1* RNAi animals, as demonstrated by the quantification of their area (**Figure 3A**). Furthermore, the cilia of the epidermal cells in the dorsal midline were not properly regenerated (**Figure 3B**) and, in the ventral part, appeared disorganized (**Figure 3B**). Immunolabeling of adherens junctions with anti-β-catenin2 antibody indicated that these structures were not properly assembled in *foxK1* silenced animals, since the signal was dimmer and the pattern was irregular (**Figure 3B**).

On the other hand, other tissues such as the digestive or the excretory systems seemed not to be affected after *foxK1* inhibition (**Supplementary Figures S2B–D**).

Overall, these results suggest that *foxK1* is required for maintenance and regeneration of the epidermis in planarians.

Apoptotic Response is Affected in *foxK1* RNAi Animals

Regeneration of the missing tissues in planarians is preceded by the triggering of early signals that activate the expression of the early genes as well as the proliferative and apoptotic response (Saló and Baguñà 1984; Wenemoser and Reddien 2010; Wenemoser et al., 2012; Pirotte et al., 2015; Owlarn et al., 2017; Jaenen et al., 2021). Analysis of the expression of the early response gene *runt1*, as well as the polarity genes *notum* and *wnt1*, whose early expression is independent of polarity and occurs after any injury (Wenemoser et al., 2012; Sandmann et al., 2011; Petersen and Reddien 2009, 2011), indicated that the early gene response was not affected after *foxK1* inhibition (**Figure 4A**).

In addition, quantification of the proliferative response near the anterior and the posterior wounds showed that the dynamics of proliferation was not perturbed in *foxK1* RNAi animals, and the two mitotic peaks at 6 and 48 h described during planarian regeneration occurred normally (**Figure 4B**). It must be noted, however, that proliferation appeared to be increased in regenerating animals before amputation, but this did not interfere with a proper proliferative response after injury. On the other side, quantification of the apoptotic response showed a decrease in *foxK1* RNAi animals, both at early (4 h) and late phases of regeneration (7 days) (**Figure 4C**).

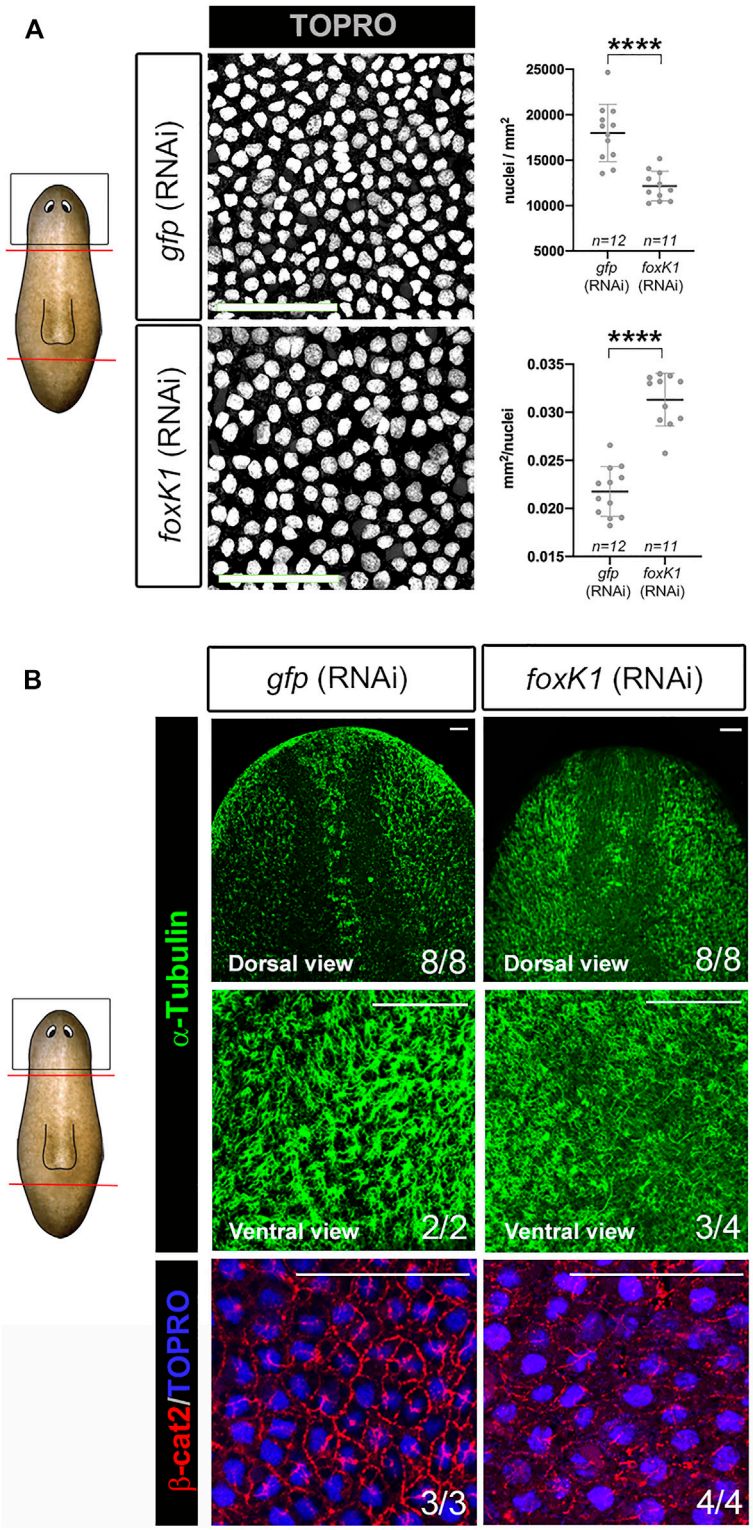

FIGURE 3 | *foxK1* silenced planarians show defects in the epidermis. **(A)** TO-PRO®-3 staining of the epidermis in anterior wounds and quantification showing that the epidermal nuclear density decreases (number of nuclei/mm2 of the area of the confocal section) while the size for each nucleus increases (average size in mm2 of each nucleus in the confocal section of every individual) after *foxK1* silencing. Animals at 7 days of regeneration are shown. All images are dorsal views. Values represent the mean ± standard deviation [s.d] of a mean of at least 11 planarians per condition. Scale bar: 50 μm ****p-value < 0.0001. **(B)** Immunostaining of the epidermis in anterior wounds. Anti-α-tubulin shows the aberrant regeneration of cilia along the dorsal midline and the ventral epidermis. Merge of the immunostaining of anti-β-catenin2 and TO-PRO®-3 in the dorsal region between the eyes showing a misorganization of the epithelial adherens junctions. Animals at 7 days of regeneration are shown. Scale bar: 50 μm. In the schematic planarians, red lines indicate the amputation planes and black squares the region analysed.

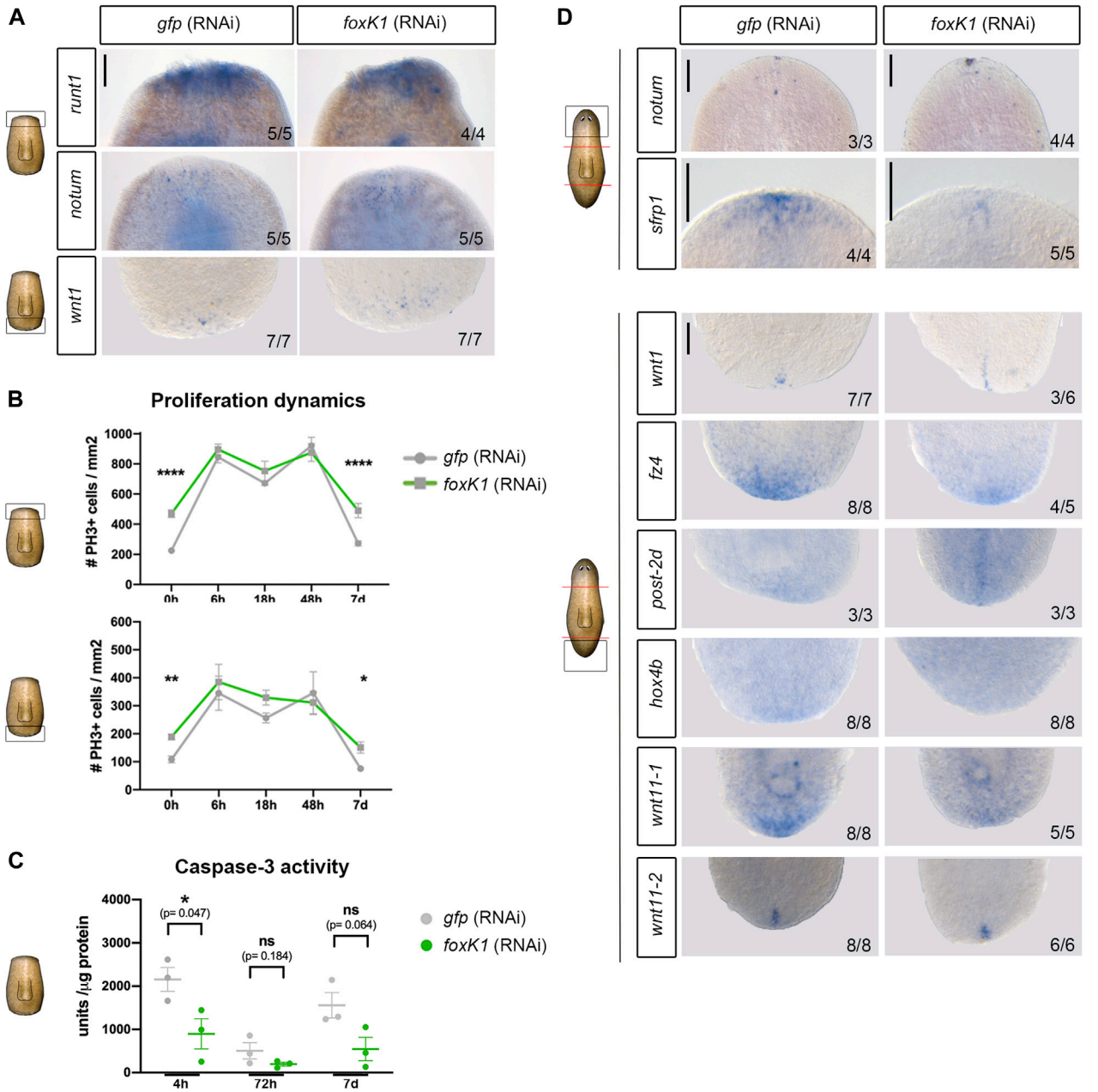

FIGURE 4 | Apoptotic response is affected in foxK1 RNAi animals, but the polarity establishment and proliferative response occurs normally. **(A)** Whole-mount *in situ* hybridization analysis of the expression of the early wound response genes in controls and *foxK1* RNAi animals 6 h post amputation (*runt1* and *notum*) and 12 h post amputation (*wnt1*). From top to bottom: *runt1* in anterior wounds, *notum* in anterior wounds and *wnt1* in posterior wounds. Scale bar: 100 µm. **(B)** Quantification of mitotic $PH3^+$ immunolabeled cells after silencing *foxK1* at several time points after anterior-posterior amputation. h, hours; d, days (**p*-value < 0.05; ** *p*-value < 0.01 *****p*-value < 0.0001. Student's *t*-test). Values represent the mean ± standard error of the mean [s.e.m] of a mean of at least 4 samples per time point and condition. **(C)** Quantification of caspase-3 activity after silencing *foxK1* at several time points after anterior-posterior amputation. h, hours; d, days (**p*-value < 0.05; Student's *t*-test). Values represent the mean ± standard error of the mean [s.e.m] of a mean of 3 biological samples per time point and condition. **(D)** Whole-mount *in situ* hybridization analysis of the expression of the genes responsible for establishing the anterior and posterior identity in controls and *foxK1* RNAi animals 3 days post amputation *(notum, wnt1, frz4, post2d* and *hox4b*), 6 days post amputation (*wnt11_1* and *wnt11_2*) and 7 days post amputation (*sfrp1*). Anterior polarity genes (from top to bottom): *notum* and *srfp1*. Posterior polarity genes (from top to bottom): *wnt1, frz4, post-2d, hox4b, wnt11-1 and wnt11-2*. Scale bar: 100 µm. In the schematic planarians, red lines indicate the amputation planes and black squares the region analysed.

These results indicate the only event found deregulated in *foxK1* RNAi animals during the early wound response is the activation of apoptosis.

foxK1 RNAi Animals Show a Correct Polarity Establishment

During planarian regeneration, the general early wound response is followed by a pole-specific response, which includes the expression of genes specific to anterior or posterior wounds that are required to specify the identity and to differentiate the proper missing tissue (Wurtzel et al., 2015; Cebrià, Adell, and Saló 2018). To clarify whether the problems of *foxK1* RNAi planarian regeneration could be associated with an incorrect pole-specific response, we analyzed several genes specific to anterior and posterior regeneration. The results showed that both anterior and posterior poles were properly formed in *foxK1* silenced planarians, since *notum* and *wnt1* were restricted to anterior and posterior wounds, respectively (**Figure 4D**) (Petersen and Reddien 2011; Adell et al., 2009). *post2-d* and *wnt11-2*, two positional control genes (PCG) (Witchley et al., 2013) that are specifically expressed in posterior facing wounds after *wnt1* (Adell et al., 2009; Currie et al., 2016; Tewari et al., 2019), also showed a proper expression in *foxK1* RNAi planarians (**Figure 4D**). However, the expression of some anterior and posterior PCG appeared decreased in *foxK1* RNAi animals, such as *sfrp1* in anterior; and *fz4*, *hox4b* and *wnt11-1* in posterior (Gurley, Rink, and Alvarado 2008; Petersen and Reddien 2008; Currie et al., 2016).

These results suggest that polarity was not affected in *foxK1* silenced planarians, even though the inability to regenerate a correct head and tail was associated with a decreased expression of some markers of anterior and posterior polarity.

DISCUSSION

In this study, we have found that inhibition of *foxK1* impedes correct regeneration of missing structures, while inhibition of *foxK2* or *foxK3* only produces mild defects. The strong phenotype observed after *foxK1*, but not *foxK2* or *foxK3* inhibition, could be due to the fact that the last two are mainly expressed in differentiated cells (Pascual-Carreras et al., 2021), while *foxK1* is also expressed in progenitors and in neoblasts. *foxk1* RNAi animals cannot properly regenerate the nervous system or the epidermis, which correlates with a decrease in the number of differentiated neural and epidermal cells. At least in the case of the nervous system, *foxK1* RNAi animals also show a decrease in the number of progenitors (*sim*+/PIWI1+) cells. However, the number of cycling cells is not decreased. This result could indicate that *foxK1* is required for maintenance and differentiation of the neural precursors and may be for specification of neoblasts towards the neural fate. This result agrees with a recent study in human ESCs, in which the FoxK2 transcription factor is found to be bound to thousands of regulatory regions and to act as a pioneer factor, playing a role in enhancer priming during differentiation (Ji et al., 2021). Thus, *foxK1* could also act as a pioneer factor during neural determination in planarians. This pioneer role has been already demonstrated for other Fox families, such as FoxA, FoxD or FoxH (Krishnakumar et al., 2016; Charney et al., 2017). In human ESCs, FoxK2 binding to enhancers is maintained as cells differentiate to neural precursor cell types (Ji et al., 2021). This could also be the case of *foxK1* in planarians. In contrast to other Fox factors, *foxK1* could be recruited not only in enhancer regions prior to their activation, but its binding could be retained as enhancers become activated during differentiation, since both progenitor and differentiated cells are decreased in RNAi animals.

Although the cephalic ganglia are more affected than VNCs in *foxK1* RNAi planarians, *foxK1* seems to be required for nervous system differentiation in general, since posterior fascicles of the VNCs appear thinner and the decrease in the expression of *sim* affects to all the body regions.

The defect in the eyes of *foxK1* RNAi animals is one of the first traits that can be observed, since they are the only structures clearly identified when planarians regenerate the head. With the analysis of specific markers, we demonstrate that eyes are not properly specified nor differentiated, since both eye precursor and eye differentiated cells are decreased. However, we cannot clarify whether this defect is due to an autonomous role of *foxK1* in the eye cells or it is linked to the inability of these animals to regenerate the cephalic ganglia, since the eyes connect to the brain while they both are regenerating. We have not observed the expression of *foxK1* in eye cells, but we cannot discard it.

FoxK1 RNAi animals die after developing epidermal lesions, thus it can be due to its role in the maintenance of the epidermal layer. We observed a decrease in epidermal cell density and an increase in the size of the nucleus, which agrees with the role of *foxK1* for correct terminal differentiation of epidermal cells. However, we cannot conclude whether *foxK1* is also required for maintenance and differentiation of epidermal progenitors, and whether it also acts as a pioneer factor in the epidermal lineage, since the number of epidermal precursors has not been analyzed. It is tempting to speculate that the increase in the size of the nucleus could be related with a decompaction of the chromatin, which would agree with the role of *foxK*1 as a pioneer factor, although it could also be due to other mechanisms.

FoxK1 expression is not neural or epidermal specific, thus it could be also required for specification or differentiation of other tissues. However, its RNAi inhibition apparently only affects the ectodermal lineages, as the digestive or the excretory system appear normal.

Despite in other models, as *Drosophila*, *foxK* has been involved in the control of proliferation of myogenic stem cells (Garry et al., 2000), our results indicate that in a stem cell-based model as planarians the FoxK family is not required for neoblast proliferation. *foxK2* and *foxK3* are not expressed in neoblasts, and *foxK1* is expressed in neoblasts but we have found that the bimodal proliferative response triggered by injury is correct in *foxK1* RNAi planarians, and in animals that have already regenerated there are more proliferative cells. This result agrees with the hypothesis that *foxK1* is activating neoblast and progenitor enhancers required for determination and differentiation, but it is not required for their proliferation. If

foxK1 is required to prime neoblasts, they would maintain their naive and cycling properties when *foxK1* is not functional, which would explain the increase in proliferation seen in regenerated animals that must maintain their tissues. However, the triggering of stem cell proliferation after injury is not dependent on *foxK1*.

foxK1 RNAi animals present a correct early mitotic response and early wound gene expression. However, we have found that inhibition of *foxK1* decreases the early apoptotic response at 4 h of regeneration, suggesting that this gene could have a key role in controlling apoptosis. In this study we have not been able to clarify the impact of the early apoptotic decrease in the phenotype observed. However, the fact that the apoptotic activity seems also reduced at later stages of regeneration in *foxK1* RNAi planarians suggests that the observed decrease in the number of neural progenitors and epidermal cells is not due to an increase in their cell death.

Polarity establishment is neither affected in *foxK1* RNAi planarians. Some PCGs are not correctly expressed, such as *sfrp1* in anterior and *fz4*, *hox4b* and *wnt11-1* in posterior. However, this could be associated with the inability to form a proper head or tail, but not to the incorrect pole formation, since *notum* and *wnt1* are correctly expressed at all regeneration stages. A possibility is that the expression of those PCGs genes could require the differentiation of a nervous system.

While several Fox proteins have been implicated in enhancer activation in a tissue-specific manner, the role of the FoxK has been associated to a range of biological processes apparently unconnected. This could be mainly due to its ubiquitous expression and to having an additional conserved domain, the FHA domain, which binds to multiple proteins. Analysing *foxK1* function in planarians we have been able to characterize a specific role of *foxK1* in the differentiation of the neural tissue, possibly by acting as a pioneer factor, as other members of the Fox family, which allows and maintains the activation of enhancers during differentiation of neural progenitors. Furthermore, the role of *foxK1* in controlling apoptosis deserves further attention, since a functional relationship between FoxK and apoptosis has only been suggested in cancer cells (Liu et al., 2019).

MATERIALS AND METHODS

Animal Maintenance

S. mediterranea from the asexual clonal line BCN-10 were used for all experiments. Animals were maintained at 20°C in 1X PAM water as previously described (Cebrià et al., 2007). Animals were fed twice per week with organic veal liver and were starved for at least 1 week before experiments. For irradiation experiments, planarians were exposed to 86 Gray (Gy) of γ-irradiation.

RNA Interference

Double-stranded RNA (dsRNA) for *Smed-foxK* genes were synthesised as previously described (Sánchez Alvarado and Newmark 1999). The region amplified by the *foxK1* specific forward primer 5′ AATCTCATTCTTTTATTCCT 3′ and reverse primers 5′ AGTATCGTTCATCAGTCCAT 3′ or 5′ TTGAGCGTATGAATATGGAGG 3’ was used to synthesize the dsRNA. The injection protocol consisted of 1 round of 4 consecutive days of injections or 2 rounds of 3 consecutive days of injections separated by a 4-days interval. A Nanoject II (Drummond Scientific, Broomall, PA, United States) was used to administer 3 injections of 32 nl of dsRNA (1 μg/μl) per day. Control animals were injected with *gfp* dsRNA. In each round, 1 day after the last injection, planarians were amputated to induce anterior and posterior regeneration.

Single-Cell Sequencing Data

FoxK1,2,3 genes expression profile (dd_Smed_v6_4500, dd_Smed_v6_5767 and dd_Smed_v6_7583, respectively) were obtained from the planaria single-cell database hosted by the Rajewsky lab at the Berlin Institute for Medical Systems Biology of the Max Delbrück Center, Berlin (Plass et al., 2018) and the planaria single-cell database hosted by the Sánchez Alvarado lab at Planosphere website (Zeng et al., 2018).

Whole-Mount *In Situ* Hybridisation and Whole-Mount Fluorescent *In Situ* Hybridisation

Whole-mount *in situ* hybridisation (WISH) (Currie et al., 2016) whole-mount fluorescent *in situ* hybridisation (WFISH) (King and Newmark 2013) were performed as previously described. Riboprobes for *in situ* hybridisation were synthesised using the DIG RNA labe ling kit (Sp6/T7, Roche) following the manufacturer’s instructions. Samples were mounted in 70% glycerol/PBS solution.

Immunohistochemistry

Whole-mount immunohistochemistry was performed as previously described (Ross et al., 2015). Treated animals were euthanised by immersion in cold 2% HCl in ultrapure H_2O for 5 min, washed with PBS-Tx (PBS +0.3% Triton X-100) at room temperature (RT), and placed in a fixative solution (4% formaldehyde in PBS-Tx) for 15 min at RT with agitation. Subsequently, samples were washed with PBS-Tx and bleached in 6% H_2O_2 (in PBS-Tx) at RT for 16 h under direct light. Bleached animals were then washed with PBS-Tx, incubated for 2 h in 1% blocking solution (1% BSA in PBS-Tx), and overnight at 4°C in the primary antibody (diluted in blocking solution). The following primary antibodies were used: anti-phospho-histone3 (PH3, Cell Signaling Technology) to detect mitotic cells, diluted 1:300; anti-SYNAPSIN, a pan-neural marker (anti-SYNORF1, Developmental Studies Hybridoma Bank), diluted 1:50; anti-VC-1, specific for planarian photosensitive cells (Sakai et al., 2000), diluted 1:15,000; anti-SMEDWI-1, specific for neoblasts, diluted 1:1,500 (Rouhana et al., 2010) (März, Seebeck, and Bartscherer 2013); polyclonal antibody against Smed-β-catenin-2 used to visualize adherens junctions (Chai et al., 2010), and used at a 1:2,000 dilution; the AA4.3 antibody (Developmental Studies Hybridoma Bank), specific for α-tubulin to visualize the epithelial cilia, diluted 1:20. The following secondary antibodies were used: Alexa-488-conjugated goat anti-mouse (Molecular Probes), diluted 1:400; and Alexa 568-conjugated goat anti-rabbit (Molecular Probes),

diluted 1:1,000. Samples were mounted in 70% glycerol/PBS solution. Nuclei were stained with DAPI (1:5000; Sigma-Aldrich) and TO-PRO®-3 (1:3,000, Thermo Fisher Scientific, Waltham, MA, United States).

Phototactic Assay

Phototactic assay was carried out using a modified version of the method described by (Inoue et al., 2004). Planarian behavior was recorded during 120 s using an overhead digital video camera (Canon EOS550D). The behavior analysis software SMART v.2.5.21 (Panlab, Spain) was used to quantify the time spent by the animals in each of the three virtual subdivisions of a transparent container of 60 × 30 × 10 mm, filled with planarian water. To obtain a light gradient, the container was protected by a black screen with a hole that allowed the entrance of 500 lux of white light from one side of the container.

Caspase-3 Activity Assay

The protein concentration of the cell lysates of three biological samples of 4–7 planarians each was measured using BioRad protein reagent. Fluorometric analysis of caspase-3 activity was performed as described previously (González-Estévez et al., 2007) using 16 μg of protein extract after incubation for 2 h at 37°C with the caspase-3 substrate Ac-DEVD-AMC. A Fluostar Optima microplate fluorescence reader (BMG Labtech) and a luminescence spectrophotometer (Perkin- Elmer LS- 50) were used to measure luminescence. The following settings were applied: excitation, 380 nm; emission, 440 nm. Three technical replicates were analysed per condition.

Microscopy, Image Acquisition, and Image Analysis

Live animals were photographed with an sCM EX-3 high end digital microscope camera (DC.3000s, Visual Inspection Technology). WISH, WFISH, and immunostained animals were observed with a Leica MZ16F stereomicroscope. Images were captured with the ProGres C3 camera (Jenoptik) and then processed in Photoshop CS6 for publication. Representative images of WFISH and immunostained animals were captured with confocal laser scanning microscopy (Leica TCS-SPE microscope) and processed in ImageJ2.3.0 and Photoshop CS6 for publication.

Statistical Analysis

All comparisons were performed using the unpaired Student's t-test, after first confirming data normality and homogeneity using the Shapiro-Wilk test.

DATA AVAILABILITY STATEMENT

The original contributions presented in the study are included in the article/**Supplementary Material**, further inquiries can be directed to the corresponding author.

AUTHOR CONTRIBUTIONS

PC-C, MDM, EP-C, FC, and TA contributed to the conception and design of the study. PC-C, MDM, GC, SF, and EP-C performed the experiments and statistical analysis. PC-C, MDM and TA wrote the first draft of the manuscript. ES, FC, and TA obtained funding. All authors contributed to manuscript revision, read, and approved the submitted version.

FUNDING

MDM has received funding from the postdoctoral fellowship programme Beatriu de Pinós, funded by the Secretary of Universities and Research (Government of Catalonia) and by the European Union Horizon 2020 research and innovation programme under Marie Sklodowska-Curie grant agreement No. 801370. EP-C was the recipient of an FPI (Formación del Profesorado Investigador) scholarship from the Spanish Ministerio de Educación y Ciencia (MEC). FC was supported by grants BFU 2015-65704-P and PGC 2018-100747-B-100 from the Ministerio de Ciencia, Innovación y Universidades, Spain. ES and TA received funding from the Ministerio de Educación y Ciencia (grant number BFU 2017-83755-P and PID2020-116372GB-I00). ES, FC and TA benefits from 2017SGR 1455 from AGAUR (Generalitat de Catalunya).

ACKNOWLEDGMENTS

We thank all members of the ESE, FC and TA laboratories for discussions. We thank H. Orii and Prof. K. Watanabe for providing anti-VC-1. We thank Dra. K. Bartscherer for providing anti-PWI1. Monoclonal anti-SYNORF1 and AA4.3 antibodies were obtained from the Developmental Studies Hybridoma Bank, developed under the auspices of the National Institute of Child Health and Human Development and maintained by the Department of Biological Sciences, University of Iowa, Iowa City, IA, United States.

SUPPLEMENTARY MATERIAL

The Supplementary Material for this article can be found online at: https://www.frontiersin.org/articles/10.3389/fcell.2022.808045/full#supplementary-material

Supplementary Figure S1 | RNAi silencing and expression pattern of the three *foxK S. mediterranea* paralogs. **(A)** *foxK2* or *foxK3* silenced planarians regenerate the missing head and tail. Scale bar: 500 μm. **(B)** Phototactic assay. Schematic representation of the position of treated planarians in each of the three subdivisions of 20 cm each after 120 s of light exposure. Red dots represent the position of *foxK1* silenced animals and blue dots the position of *gfp* RNAi control planarians. Graphical representation of the quantification of the velocity (meter/seconds) of *gfp* and *foxK1* silenced planarians showing the reduced mobility of *foxK1* silenced planarians. **(C)** Whole-mount in situ hybridization of *foxK1* in intact, γ-irradiated and planarians at 2 days of regeneration after anterior-posterior amputation. Scale bar: 200 μm. **(D)** Schematic representation of single-cell transcriptomic expression of *foxK* genes [according to (Plass et al., 2018)]. It must be noted that in a previous publication (Pascual-Carreras et al., 2021), these plots were not properly assigned, but this is

corrected in the present publication. **(E)** Schematic representation of single-cell transcriptomic expression of *foxK1* in all planarian neoblasts (Nb) subtypes [according to (Zeng et al., 2018)]. **(F)** Relative gene expression of *foxK1* and *piwi1* for the individual stages during differentiation of the epidermal and neuronal planarian cell lineages (in pseudotime) according to single cell analysis [https://shiny.mdc-berlin.de/psca/, (Plass et al., 2018)]. a.u, arbitrary units. In the schematic planarians, red lines indicate the amputation planes and black squares the region analysed.

Supplementary Figure S2 | Expression pattern of tissue-specific markers in *foxK1* RNAi planarians. **(A)** Whole-mount in situ hybridization of the neural marker *sim* (Cowles et al., 2013) reveals a decreased number of sim-expressing cells all along the planarian body of *foxK1* silenced planarians. Animals at 7 days of regeneration are shown. Scale bar: 100 μm. **(B)** Whole-mount in situ hybridization of *innexin10* (Nogi and Levin 2005) labeling the planarian excretory system reveals correct regeneration of excretory cells in *foxK1* silenced planarians. Animals at 7 days of regeneration are shown. Scale bar: 100 μm. **(C)** Whole-mount in situ hybridization of the gut marker *pk* (Fraguas et al., 2014) showing that treated planarians regenerate correctly the gut. Whole-mount immunostaining against α-tubulin showing a detail of the newly regenerated posterior gut branches. Animals at 7 days of regeneration are shown. Scale bars: 100 μm.

REFERENCES

Adell, T., Salò, E., Boutros, M., and Bartscherer, K. (2009). Smed-Evi/Wntless Is Required for β-catenin-dependent And-independent Processes during Planarian Regeneration. *Development* 136 (6), 905–910. doi:10.1242/dev.033761

Adler, C. E., Seidel, C. W., McKinney, S. A., and Sánchez Alvarado, A. (2014). Selective Amputation of the Pharynx Identifies a FoxA-dependent Regeneration Program in Planaria. *ELife* 3, 1–22. doi:10.7554/elife.02238

Baguñà, J. (2012). The Planarian Neoblast: the Rambling History of its Origin and Some Current Black Boxes. *Int. J. Dev. Biol.* 56, 19–37. doi:10.1387/ijdb.113463jb

Benayoun, B. A., Caburet, S., and Veitia, R. A. (2011). Forkhead Transcription Factors: Key Players in Health and Disease. *Trends Genet.* 27 (6), 224–232. doi:10.1016/j.tig.2011.03.003

Cebrià, F., Adell, T., and Saló, E. (2018). Rebuilding a Planarian: From Early Signaling to Final Shape. *Int. J. Dev. Biol.* 62 (6–8), 537–550. doi:10.1387/ijdb.180042es

Cebrià, F., Guo, T., Jopek, J., and Newmark, P. A. (2007). Regeneration and Maintenance of the Planarian Midline Is Regulated by a Slit Orthologue. *Develop. Biol.* 307 (2), 394–406. doi:10.1016/j.ydbio.2007.05.006

Cebrià, F., Nakazawa, M., Mineta, K., Ikeo, K., Gojobori, T., and Agata, K. (2002). Dissecting Planarian Central Nervous System Regeneration by the Expression of Neural-specific Genes. *Dev. Growth Differ.* 44 (2), 135–146. doi:10.1046/j.1440-169x.2002.00629.x

Chai, G., Ma, C., Bao, K., Zheng, L., Wang, X., Sun, Z., et al. (2010). Complete Functional Segregation of Planarian β-Catenin-1 and -2 in Mediating Wnt Signaling and Cell Adhesion. *J. Biol. Chem.* 285 (31), 24120–24130. doi:10.1074/jbc.M110.113662

Charney, R. M., Forouzmand, E., Cho, J. S., Cheung, J., Paraiso, K. D., Yasuoka, Y., et al. (2017). Foxh1 Occupies Cis -Regulatory Modules Prior to Dynamic Transcription Factor Interactions Controlling the Mesendoderm Gene Program. *Develop. Cel* 40 (6), 595–607. e4. doi:10.1016/j.devcel.2017.02.017

Collins, J. J., Hou, X., Romanova, E. V., Lambrus, B. G., Miller, C. M., Saberi, A., et al. (2010). Genome-Wide Analyses Reveal a Role for Peptide Hormones in Planarian Germline Development. *Plos Biol.* 8 (10), e1000509. doi:10.1371/journal.pbio.1000509

Cowles, M. W., Brown, D. D. R., Nisperos, S. V., Stanley, B. N., Pearson, B. J., and Zayas, R. M. (2013). Genome-Wide Analysis of the BHLH Gene Family in Planarians Identifies Factors Required for Adult Neurogenesis and Neuronal Regeneration. *Development (Cambridge)* 140 (23), 4691–4702. doi:10.1242/dev.098616

Currie, K. W., Brown, D. D. R., Zhu, S., Xu, C., Voisin, V., Bader, G. D., et al. (2016). HOX Gene Complement and Expression in the Planarian Schmidtea Mediterranea. *EvoDevo* 7, 7. doi:10.1186/s13227-016-0044-8

Fraguas, S., Barberán, S., and Cebrià, F. (2011). EGFR Signaling Regulates Cell Proliferation, Differentiation and Morphogenesis during Planarian Regeneration and Homeostasis. *Develop. Biol.* 354 (1), 87–101. doi:10.1016/j.ydbio.2011.03.023

Fraguas, S., Barberán, S., Iglesias, M., Rodríguez-Esteban, G., and Cebrià, F. (2014). egr-4, a Target of EGFR Signaling, Is Required for the Formation of the Brain Primordia and Head Regeneration in planarians. *Development (Cambridge, England)* 141 (9), 1835–1847. doi:10.1242/dev.101345

Garry, D. J., Meeson, A., Elterman, J., Zhao, Y., Yang, P., Bassel-Duby, R., et al. (2000). Myogenic Stem Cell Function Is Impaired in Mice Lacking the Forkhead/Winged Helix Protein MNF. *Proc. Natl. Acad. Sci.* 97 (10), 5416–5421. doi:10.1073/pnas.100501197

Golson, M. L., and Kaestner, K. H. (2016). Fox Transcription Factors: From Development to Disease. *Development* 143 (24), 4558–4570. doi:10.1242/dev.112672

González-Estévez, C., Felix, D. A., Aboobaker, A. A., and Saló, E. (2007). Gtdap-1 Promotes Autophagy and Is Required for Planarian Remodeling during Regeneration and Starvation. *Proc. Natl. Acad. Sci.* 104 (33), 13373–13378. doi:10.1073/pnas.0703588104

Gurley, K. A., Rink, J. C., and Alvarado, A. S. (2008). β-Catenin Defines Head versus Tail Identity during Planarian Regeneration and Homeostasis. *Science* 319 (5861), 323–327. doi:10.1126/science.1150029

He, X., Lindsay-Mosher, N., Li, Y., Molinaro, A. M., Pellettieri, J., and Pearson, B. J. (2017). FOX and ETS Family Transcription Factors Regulate the Pigment Cell Lineage in Planarians. *Development* 144 (24), 4540–4551. doi:10.1242/dev.156349

Iglesias, M., Almuedo-Castillo, M., Aboobaker, A. A., and Saló, E. (2011). Early Planarian Brain Regeneration Is Independent of Blastema Polarity Mediated by the Wnt/β-Catenin Pathway. *Develop. Biol.* 358 (1), 68–78. doi:10.1016/j.ydbio.2011.07.013

Inoue, T., Kumamoto, H., Okamoto, K., Umesono, Y., Sakai, M., Alvarado, A. S., et al. (2004). Morphological and Functional Recovery of the Planarian Photosensing System during Head Regeneration. *Zoolog. Sci.* 21 (3), 275–283. doi:10.2108/zsj.21.275

Jaenen, V., Fraguas, S., Bijnens, K., Heleven, M., Artois, T., Romero, R., et al. (2021). Reactive Oxygen Species rescue Regeneration after Silencing the MAPK-ERK Signaling Pathway in Schmidtea Mediterranea. *Sci. Rep.* 11 (1), 1–16. doi:10.1038/s41598-020-79588-1

Ji, Z., Li, Y., Liu, S. X., and Sharrocks, A. D. (2021). The Forkhead Transcription Factor FOXK2 Premarks Lineage-specific Genes in Human Embryonic Stem Cells for Activation during Differentiation. *Nucleic Acids Res.* 49 (3), 1345–1363. doi:10.1093/nar/gkaa1281

King, R. S., and Newmark, P. A. (2013). *In Situ* Hybridization Protocol for Enhanced Detection of Gene Expression in the Planarian Schmidtea Mediterranea. *BMC Develop. Biol.* 13 (March), 8. doi:10.1186/1471-213X-13-8

Koinuma, S., Umesono, Y., Watanabe, K., and Agata, K. (2000). Planaria FoxA (HNF3) Homologue Is Specifically Expressed in the Pharynx-Forming Cells. *Gene* 259 (1–2), 171–176. doi:10.1016/S0378-1119(00)00426-1

Krishnakumar, R., Chen, A. F., Pantovich, M. G., Danial, M., Parchem, R. J., Labosky, P. A., et al. (2016). FOXD3 Regulates Pluripotent Stem Cell Potential by Simultaneously Initiating and Repressing Enhancer Activity. *Cell Stem Cell* 18 (1), 104–117. doi:10.1016/j.stem.2015.10.003

Lalmansingh, A. S., Karmakar, S., Jin, Y., and Nagaich, A. K. (2012). Multiple Modes of Chromatin Remodeling by Forkhead Box Proteins. *Biochim. Biophys. Acta (Bba) - Gene Regul. Mech.* 1819 (7), 707–715. doi:10.1016/j.bbagrm.2012.02.018

Lapan, S. W., and Reddien, P. W. (2011). Dlx and Sp6-9 Control Optic Cup Regeneration in a Prototypic Eye. *Plos Genet.* 7 (8), e1002226. doi:10.1371/journal.pgen.1002226

Liu, Y., Ding, W., Ge, H., Ponnusamy, M., Wang, Q., Hao, X., et al. (2019). FOXK Transcription Factors: Regulation and Critical Role in Cancer. *Cancer Lett.* 458 (38), 1–12. doi:10.1016/j.canlet.2019.05.030

März, M., Seebeck, F., and Bartscherer, K. (2013). A Pitx Transcription Factor Controls the Establishment and Maintenance of the Serotonergic Lineage in Planarians. *Development (Cambridge, England)* 140 (22), 4499–4509. doi:10.1242/dev.100081

Molina, M. D., and Cebrià, F. (2021). Decoding Stem Cells: An Overview on Planarian Stem Cell Heterogeneity and Lineage Progression. *Biomolecules* 11 (10), 1532–1623. doi:10.3390/biom11101532

Nishimura, K., Kitamura, Y., Inoue, T., Umesono, Y., Sano, S., Yoshimoto, K., et al. (2007). Reconstruction of Dopaminergic Neural Network and Locomotion Function in Planarian Regenerates. *Devel Neurobio* 67 (8), 1059–1078. doi:10.1002/dneu.20377

Nogi, T., and Levin, M. (2005). Characterization of Innexin Gene Expression and Functional Roles of Gap-Junctional Communication in Planarian Regeneration. *Develop. Biol.* 287 (2), 314–335. doi:10.1016/j.ydbio.2005.09.002

Owlarn, S., Klenner, F., Schmidt, D., Rabert, F., Tomasso, A., Reuter, H., et al. (2017). Generic Wound Signals Initiate Regeneration in Missing-Tissue Contexts. *Nat. Commun.* 8 (1), 1–13. doi:10.1038/s41467-017-02338-x

Pascual-Carreras, E., Herrera-Úbeda, C., Rosselló, M., Coronel-Córdoba, P., Garcia-Fernàndez, J., Saló, E., et al. (2021). Analysis of Fox Genes in Schmidtea Mediterranea Reveals New Families and a Conserved Role of Smed-FoxO in Controlling Cell Death. *Sci. Rep.* 11 (1), 1–18. doi:10.1038/s41598-020-80627-0

Petersen, C. P., and Reddien, P. W. (2009). A Wound-Induced Wnt Expression Program Controls Planarian Regeneration Polarity. *Proc. Natl. Acad. Sci.* 106 (40), 17061–17066. doi:10.1073/pnas.0906823106

Petersen, C. P., and Reddien, P. W. (2011). Polarized Notum Activation at Wounds Inhibits Wnt Function to Promote Planarian Head Regeneration. *Science* 332 (6031), 852–855. doi:10.1126/science.1202143

Petersen, C. P., and Reddien, P. W. (2008). Smed- β Catenin-1 Is Required for Anteroposterior Blastema Polarity in Planarian Regeneration. *Science* 319 (5861), 327–330. doi:10.1126/science.1149943

Pirotte, N., Stevens, A.-S., Fraguas, S., Plusquin, M., Van Roten, A., Van Belleghem, F., et al. (2015). Reactive Oxygen Species in Planarian Regeneration: An Upstream Necessity for Correct Patterning and Brain Formation. *Oxidative Med. Cell Longevity* 2015, 1–19. doi:10.1155/2015/392476

Plass, M., Solana, J., Wolf, F. A., Ayoub, S., Misios, A., Glažar, P., et al. (2018). Cell Type Atlas and Lineage Tree of a Whole Complex Animal by Single-Cell Transcriptomics. *Science* 360 (6391). doi:10.1126/science.aaq1723

Ross, K. G., Omuro, K. C., Taylor, M. R., Munday, R. K., Hubert, A., King, R. S., et al. (2015). Novel Monoclonal Antibodies to Study Tissue Regeneration in Planarians. *BMC Dev. Biol.* 15 (1). doi:10.1186/s12861-014-0050-9

Rouhana, L., Shibata, N., Nishimura, O., and Agata, K. (2010). Different Requirements for Conserved Post-Transcriptional Regulators in Planarian Regeneration and Stem Cell Maintenance. *Develop. Biol.* 341 (2), 429–443. doi:10.1016/j.ydbio.2010.02.037

Sakai, F., Agata, K., Orii, H., and Watanabe, K. (2000). Organization and Regeneration Ability of Spontaneous Supernumerary Eyes in Planarians -Eye Regeneration Field and Pathway Selection by Optic Nerves-. *Zoolog. Sci.* 17 (3), 375–381. doi:10.2108/jsz.17.375

Saló, E., and Baguñà, J. (1984). Regeneration and Pattern Formation in Planarians. I. The Pattern of Mitosis in Anterior and Posterior Regeneration in Dugesia (G) Tigrina, and a New Proposal for Blastema Formation. *J. Embryol. Exp. Morphol.* 83 (October), 63–80. doi:10.1242/dev.83.1.63

Sánchez Alvarado, A., and Newmark, P. A. (1999). Double-Stranded RNA Specifically Disrupts Gene Expression during Planarian Regeneration. *Proc. Natl. Acad. Sci.* 96 (9), 5049–5054. doi:10.1073/pnas.96.9.5049

Sandmann, T., Vogg, M. C., Owlarn, S., Boutros, M., and Bartscherer, K. (2011). The Head-Regeneration Transcriptome of the Planarian Schmidtea Mediterranea. *Genome Biol.* 12 (8), R76. doi:10.1186/gb-2011-12-8-r76

Scimone, M. L., Lapan, S. W., and Reddien, P. W. (2014). A Forkhead Transcription Factor Is Wound-Induced at the Planarian Midline and Required for Anterior Pole Regeneration. *Plos Genet.* 10 (1), e1003999. doi:10.1371/journal.pgen.1003999

Scimone, M. L., Wurtzel, O., Malecek, K., Fincher, C. T., Oderberg, I. M., Kravarik, K. M., et al. (2018). FoxF-1 Controls Specification of Non-body Wall Muscle and Phagocytic Cells in Planarians. *Curr. Biol.* 28 (23), 3787–3801. e6. doi:10.1016/j.cub.2018.10.030

Tewari, A. G., Owen, J. H., Petersen, C. P., Wagner, D. E., and Reddien, P. W. (2019). A Small Set of Conserved Genes, Including Sp5 and Hox, Are Activated by Wnt Signaling in the Posterior of Planarians and Acoels. *Plos Genet.* 15, e1008401. doi:10.1371/journal.pgen.1008401

Vogg, M. C., Owlarn, S., Pérez Rico, Y. A., Xie, J., Suzuki, Y., Gentile, L., et al. (2014). Stem Cell-dependent Formation of a Functional Anterior Regeneration Pole in Planarians Requires Zic and Forkhead Transcription Factors. *Develop. Biol.* 390 (2), 136–148. doi:10.1016/j.ydbio.2014.03.016

Wagner, D. E., Wang, I. E., and Reddien, P. W. (2011). Clonogenic Neoblasts Are Pluripotent Adult Stem Cells that Underlie Planarian Regeneration. *Science* 332 (6031), 811–816. doi:10.1126/science.1203983

Wenemoser, D., Lapan, S. W., Wilkinson, A. W., Bell, G. W., and Reddien, P. W. (2012). A Molecular Wound Response Program Associated with Regeneration Initiation in Planarians. *Genes Dev.* 26 (9), 988–1002. doi:10.1101/gad.187377.112

Wenemoser, D., and Reddien, P. W. (2010). Planarian Regeneration Involves Distinct Stem Cell Responses to Wounds and Tissue Absence. *Develop. Biol.* 344 (2), 979–991. doi:10.1016/j.ydbio.2010.06.017

Witchley, J. N., Mayer, M., Wagner, D. E., Owen, J. H., and Reddien, P. W. (2013). Muscle Cells Provide Instructions for Planarian Regeneration. *Cel Rep.* 4 (4), 633–641. doi:10.1016/j.celrep.2013.07.022

Wurtzel, O., Cote, L. E., Poirier, A., Satija, R., Regev, A., and Reddien, P. W. (2015). A Generic and Cell-type-specific Wound Response Precedes Regeneration in Planarians. *Develop. Cel* 35 (5), 632–645. doi:10.1016/j.devcel.2015.11.004

Zeng, A., Li, H., Guo, L., Gao, X., McKinney, S., Wang, Y., et al. (2018). Prospectively Isolated Tetraspanin+ Neoblasts Are Adult Pluripotent Stem Cells Underlying Planaria Regeneration. *Cell* 173 (7), 1593–1608. e20. doi:10.1016/j.cell.2018.05.006

Conflict of Interest: The authors declare that the research was conducted in the absence of any commercial or financial relationships that could be construed as a potential conflict of interest.

Publisher's Note: All claims expressed in this article are solely those of the authors and do not necessarily represent those of their affiliated organizations, or those of the publisher, the editors and the reviewers. Any product that may be evaluated in this article, or claim that may be made by its manufacturer, is not guaranteed or endorsed by the publisher.

frontiers in Cell and Developmental Biology

BRIEF RESEARCH REPORT
published: 03 January 2022
doi: 10.3389/fcell.2021.749723

LanB1 Cooperates With Kon-Tiki During Embryonic Muscle Migration in *Drosophila*

Juan José Pérez-Moreno[1,2†], *Carmen Santa-Cruz Mateos*[1,3†], *María Dolores Martín-Bermudo*[1] and *Beatriz Estrada*[1,2*†]

[1]Centro Andaluz de Biología del Desarrollo, Universidad Pablo de Olavide/CSIC/JA, Seville, Spain, [2]Departamento de Biología Celular, Universidad de Sevilla and Instituto de Biomedicina de Sevilla (IBiS), Hospital Universitario Virgen del Rocío/CSIC/Universidad de Sevilla, Seville, Spain, [3]Department of Physiology, Development and Neuroscience, University of Cambridge, Cambridge, United Kingdom

OPEN ACCESS

Edited by:
Sofia J. Araújo,
University of Barcelona, Spain

Reviewed by:
Talila Volk,
Weizmann Institute of Science, Israel
Patricio Olguin,
University of Chile, Chile

***Correspondence:**
Beatriz Estrada
bestrada@us.es

†Present Address:
Juan José Pérez-Moreno; Beatriz Estrada, Departamento de Biología Celular, Universidad de Sevilla and Instituto de Biomedicina de Sevilla (IBiS), Hospital Universitario Virgen del Rocío/CSIC/Universidad de Sevilla, Seville, Spain; Carmen Santa-Cruz Mateos, Department of Physiology, Development and Neuroscience, University of Cambridge, Cambridge, United Kingdom

Specialty section:
This article was submitted to Cell Adhesion and Migration, a section of the journal Frontiers in Cell and Developmental Biology

Received: 29 July 2021
Accepted: 19 November 2021
Published: 03 January 2022

Citation:
Pérez-Moreno JJ, Santa-Cruz Mateos C, Martín-Bermudo MD and Estrada B (2022) LanB1 Cooperates With Kon-Tiki During Embryonic Muscle Migration in Drosophila. Front. Cell Dev. Biol. 9:749723. doi: 10.3389/fcell.2021.749723

Muscle development is a multistep process that involves cell specification, myoblast fusion, myotube migration, and attachment to the tendons. In spite of great efforts trying to understand the basis of these events, little is known about the molecular mechanisms underlying myotube migration. Knowledge of the few molecular cues that guide this migration comes mainly from studies in *Drosophila*. The migratory process of *Drosophila* embryonic muscles involves a first phase of migration, where muscle progenitors migrate relative to each other, and a second phase, where myotubes migrate searching for their future attachment sites. During this phase, myotubes form extensive filopodia at their ends oriented preferentially toward their attachment sites. This myotube migration and the subsequent muscle attachment establishment are regulated by cell adhesion receptors, such as the conserved proteoglycan Kon-tiki/Perdido. Laminins have been shown to regulate the migratory behavior of many cell populations, but their role in myotube migration remains largely unexplored. Here, we show that laminins, previously implicated in muscle attachment, are indeed required for muscle migration to tendon cells. Furthermore, we find that laminins genetically interact with *kon-tiki/perdido* to control both myotube migration and attachment. All together, our results uncover a new role for the interaction between laminins and Kon-tiki/Perdido during *Drosophila* myogenesis. The identification of new players and molecular interactions underlying myotube migration broadens our understanding of muscle development and disease.

Keywords: myogenesis, migration, adhesion, myotendinous junction (MTJ), drosophila, laminin, Kon-tiki, NG2

INTRODUCTION

Muscle development is a complex process where a series of cellular events need to be timely coordinated to render functional contracting muscles. First, myoblasts are specified, then they fuse with each other to form nascent myotubes, which migrate and attach to the tendons, then final differentiation takes place (Bate, 1990; Schulman et al., 2015). The formation of a stable myotendinous junction (MTJ) is key to withstand the strong forces generated by muscle contraction, and MTJ defects have been associated with myopathies in animal models and in human (Mayer et al., 1997; Bassett and Currie, 2003; Conti et al., 2008; Wang et al., 2008; Perkins et al., 2010).

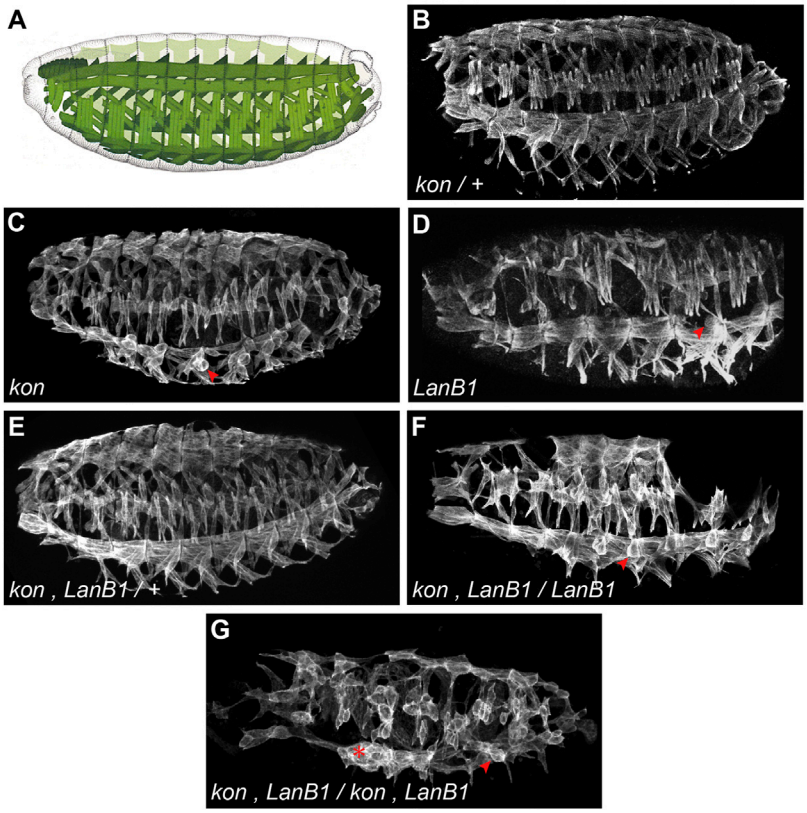

FIGURE 1 | Embryonic pattern of the body wall musculature. **(A)** Scheme of the *Drosophila* muscle pattern at the end of embryogenesis (adapted from Bate and Martinez Arias, 1993). **(B–G)** Representative examples of confocal projections of stage 16 embryos. In each case, a complete penetrance of the shown phenotypes was observed [$n = 12$**(B)**; $n = 9$**(C)**; $n = 4$**(D)**; $n = 5$**(E)**; $n = 5$**(F)**; $n = 24$**(G)**]. Muscles are labeled with anti-Tropomyosin; arrowheads indicate examples of myospheres; asterisk indicates accumulation of detached muscles.

Drosophila MTJ formation is a well-established model to study cell adhesion in organogenesis, where both the genes and cell behaviors are conserved. At late stages of muscle development, once muscle and tendons have physically contacted, final adhesion takes place by the assembly of a robust hemi-adherens junction between these cells (Schnorrer and Dickson, 2004; Schweitzer et al., 2010). This junction contains cell adhesion receptors and extracellular matrix (ECM) proteins (Valdivia et al., 2017), and the absence of these types of molecules leads to the formation of rounded muscles or myospheres. Myospheres can be observed in mutants of genes encoding cell adhesion receptors such as integrins (Martin-Bermudo et al., 1998) and Kon-tiki/Perdido (Kon) (Estrada et al., 2007; Schnorrer et al., 2007), as well as in genes encoding ECM components such as Tsp (Chanana et al., 2007; Subramanian et al., 2007), basement membrane proteins type IV collagen (Borchiellini et al., 1996) and laminins (Martin et al., 1999; Urbano et al., 2009; Wolfstetter and Holz, 2012). Although the formation of myospheres has been traditionally attributed to defects in the stabilization of the MTJ, defects in the earlier process of muscle migration towards tendon cells can also lead to the same phenotype (Kramer et al., 2001; Swan et al., 2004).

Myotube migration towards tendons depends on several factors, including the initial polarity of the muscle cell, local signals available during the migration, target recognition and terminating migration signals. It involves a cross-talk between muscles and tendons, where the latter not only serve as attachment sites but also provide guiding cues for the migrating myotube (Schweitzer et al., 2010). Then myotendinous contact and final adhesion takes place (Schnorrer and Dickson, 2004; Schweitzer et al., 2010). Although there have been shown a few genes involved in myotube migration and elongation (Maartens and Brown, 2015), very little is known about the underlying mechanisms regulating myotube migration. The conserved single-pass transmembrane proteoglycan Kon has been related not only with the assembly of the MTJ, but also with myotube migration. Muscles mutant in the gene *kon* fail to migrate in a directed manner being often lost or "perdidos" (in Spanish) and ending up as rounded unattached muscles (Estrada et al., 2007; Schnorrer et al., 2007; Pérez-Moreno et al., 2014). Kon interacts with PS2 integrin and the ECM protein Tsp in the formation of a stable muscle attachment (Pérez-Moreno et al., 2017) and it has been proposed to interact with αPS1 in the tendon (Estrada et al., 2007). Moreover, Kon contains a PDZ binding domain that forms

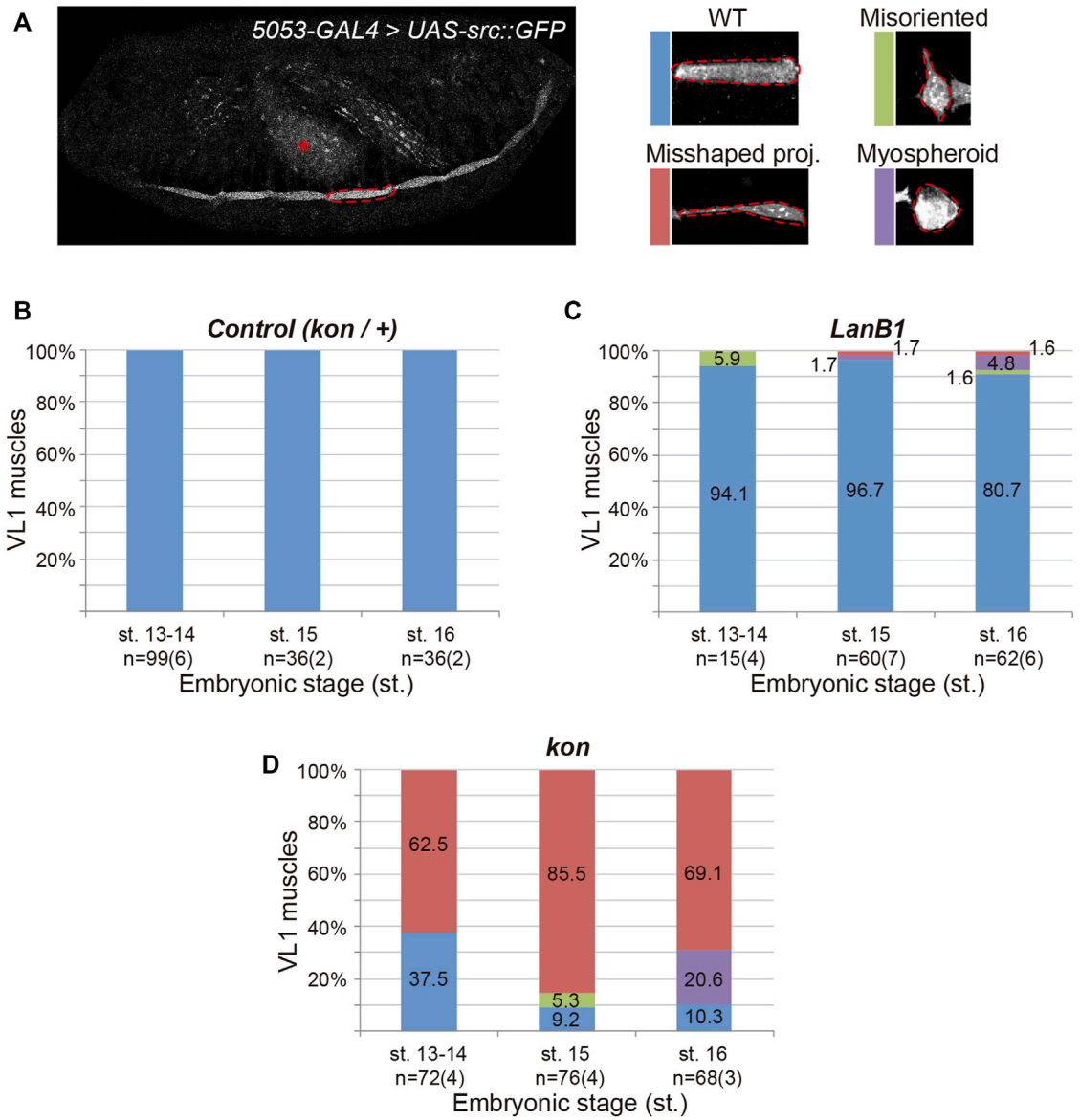

FIGURE 2 | Development of ventral-longitudinal muscle 1 (VL1). **(A)** Left panel shows a representative example of the confocal projection in a stage 16 embryo. *5053-GAL4* expresses the plasma membrane marker src:GFP in the VL1 muscle of each segment (dotted line indicates one example) and the gut (asterisk). Right panels show representative examples of the different morphological phenotypes observed in VL1 muscle for the genotypes indicated. **(B–D)** Quantification of the proportion of VL1 muscles according to their morphology at different embryonic stages for the indicated genotypes. Bar colors indicate VL1 muscle phenotypes: WT, blue; Misoriented, green; Misshaped projection, red; Myospheroid, purple. Sample size indicates the total number of muscles over the number of embryos indicated between parentheses.

a protein complex with the PDZ intracellular protein Grip, also involved in myotube guidance (Swan et al., 2004). However, it is still unclear which are Kon extracellular ligands during myotube migration. ECM molecules play important roles in embryonic cell migration (Walma and Yamada, 2020) but there are no ECM molecules yet identified to play a role in myotube migration.

Laminins are main basement membrane components, consisting of single α, *ß* and *γ* chains that coil to form a cross shape heterodimer, and are well-known integrin ligands (Hohenester, 2019). They are secreted and proposed to self-assemble into networks where they recruit other basement membrane components (Mouw et al., 2014). The *Drosophila* genome encodes only four laminin chains: two *α* chains (*α*1,2 and *α*3,5), one *ß* chain and one *γ* chain. These form two trimers, lamininA (*α*3,5; β1; *γ*1) and lamininW (α1,2; β1; *γ*1). Laminins are key regulators of embryonic morphogenesis, where they play different roles, such as migration processes. For instance, laminin *α*1,2-chain regulates embryonic tracheal migration and muscle-tendon adhesion (Martin et al., 1999), and LanA regulates axonal pathfinding (García-Alonso et al., 1996). Since laminins play a

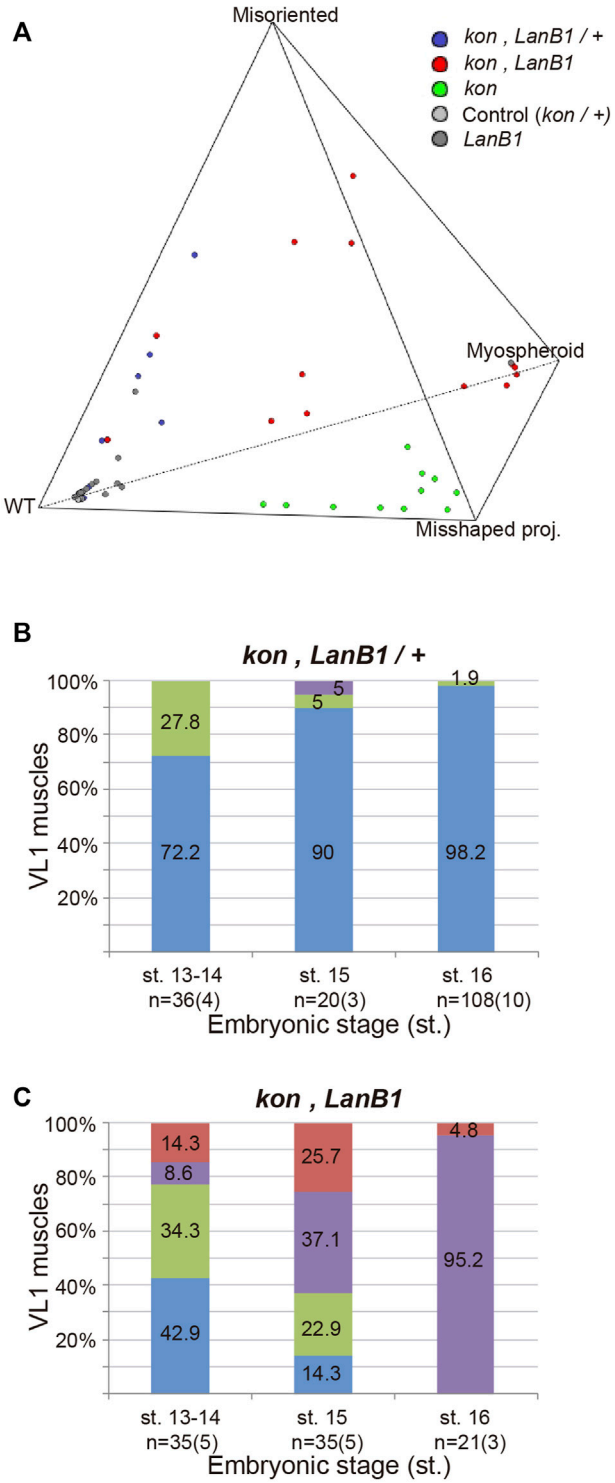

FIGURE 3 | *LanB1* and *kon* interaction during the development of the VL1 muscle. **(A)** Quaternary plot showing the embryo distribution among genotypes according to the morphology of their muscles. Multivariate analysis of variance (MANOVA) statistical test, $p < 0.00001$. **(B,C)** Quantification of the proportion of VL1 muscles according to their morphology at different embryonic stages for the indicated genotypes. Bar colors indicate VL1 muscle phenotypes: WT, blue; Misoriented, green; Misshaped projection, red; Myospheroid, purple. Representative examples of these phenotypes are shown in **Figure 2**. Sample size indicates the total number of muscles over the number of embryos indicated between parentheses. Binomial distribution test was performed for pairwise comparisons: misoriented muscles at st. 13, 14 between *LanB1* and *kon, LanB1/+*. $p = 0.046$; misoriented muscles at st. 13, 14 between *kon, LanB1* and *kon, LanB1/+*. $p = 0.55$; total abnormal muscles at st. 13, 14 between *kon, LanB1* and *kon*. $p = 0.60$; total abnormal muscles at st. 15 between *kon, LanB1* and *kon*. $p = 0.43$.

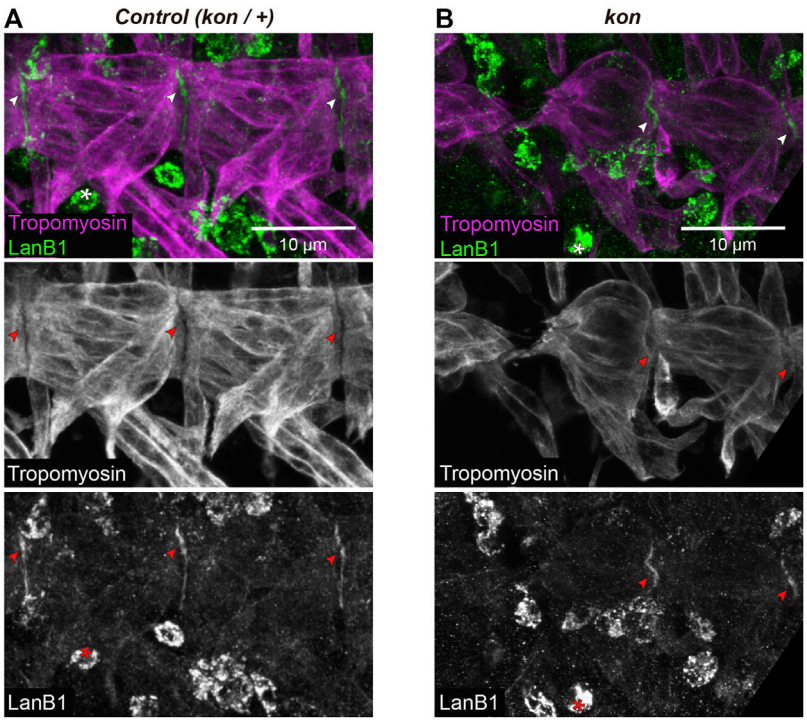

FIGURE 4 | LanB1 distribution at the MTJ. **(A,B)** Representative examples of confocal projections of st. 16 embryos, where the VL muscles of two hemisegments are shown. Muscles are labeled with anti-Tropomyosin; arrowheads indicate MTJ regions (intersegmental regions) showing LanB1 enrichment; asterisks indicate haemocytes. See **Supplementary Figure S2** for a detailed view of the corresponding confocal sections.

role in embryonic cell migration; are required for muscle-tendon attachment (Martin et al., 1999; Urbano et al., 2009); bind the tendon expressed αPS1βPS integrin (Gotwals et al., 1994), which might play a role in early events of the formation of the MTJ (Roote and Zusman, 1995; Estrada et al., 2007); and genetically interact with *Kon* (Wolfstetter and Holz, 2012), we aimed to study the potential role of laminins in myotube migration and its cooperation with Kon during this process. In particular, we analyze the role of *LanB1,* the only *Drosophila* gene encoding for the laminin *ß* subunit, present in both functional laminin *a-β-γ* heterotrimers. We show that *LanB1* plays specific roles in both muscle migration and attachment to tendon cells, as well as a strong genetic interaction between *LanB1* and *kon* during these processes. Our work suggests a key role for both muscle cell receptors and ECM components during different stages of MTJ morphogenesis.

MATERIAL AND METHODS

Drosophila Strains and Genetics

The following stocks were used: *kon* ($kon^{F1\text{-}3}$) (Estrada et al., 2007); $LanB1^{DEF}$ and $LanB1^{1P3}$ (Urbano et al., 2009); *5053-GAL4* (Bloomington *Drosophila* Stock Center: 2702) (Swan et al., 2004); *UAS-src:GFP* (Lesch et al., 2010). The *CyO, twist-GAL4, UAS-2EGFP* (Halfon et al., 2002), *CyO, ftz-LacZ* (Knoblich and Lehner, 1993), and *CyO, act:GFP* (Bloomington *Drosophila* Stock Center) balancer chromosomes, were used to identify homozygous mutants. In both **Figure 1** and **Figure 3**, we used the $kon^{F1\text{-}3}$, $LanB1^{DEF}$ (*Rec8*) recombinant chromosome to analyze double *kon* and *LanB1* mutation.

Embryo Immunohistochemistry and Microscopy

Embryo antibody stainings were carried out as described previously (Carmena et al., 1998). The following primary antibodies were used: 1:5,000 rabbit anti-*β*-galactosidase (Cappel, 55,976); 1:5,000 rabbit anti-GFP (Invitrogen, A-6455), 1:5,000 mouse anti-GFP (Invitrogen, A-11120), and 1:400 rat anti-Tropomyosin (Babraham Bioscience Technologies, MAC141). The following secondary antibodies were used: 1: 200 goat anti-rabbit-Cy2 (Jackson, 111-225-144), 1:200 goat anti-rat-Cy5 (Jackson, 112-175-143), 1:200 goat anti-mouse-488 (Life Technologies, A-1101), and 1:200 goat anti-rabbit-Cy5 (Jackson, 111-175-144). Confocal images were obtained using SP2 and Stellaris five confocal microscopes from Leica, and processed with Adobe Illustrator and ImageJ.

Data Analysis

The identification of specific embryonic stages was performed by following previous characterization (Campos-Ortega and Hartenstein, 1997). Stage 13–14 embryos showed head involution with retracting clypeolabrum, germ band retraction,

yolk sac protruding dorsally and dorsal closure of midgut and epidermis; Stage 15 embryos showed retracted clypeolabrum, completion of dorsal closure, and growth of the hindgut; Stage 16 embryos showed midgut constrictions and final pattern of somatic musculature was developed. In *LanB1* mutants there is a failure in midgut constriction so that staging of these embryos was based on the other morphologies. Quantification of phenotypes in VL1 muscle morphology was performed by counting the number of each type of phenotype per embryo. Image analysis was performed from both confocal z-stacks and maximal projections using ImageJ software.

Our VL1 muscles data consisted of relative proportions of *WT* and several types of muscle phenotypes across genotypes. Since the relative proportion of muscles in each category was not statistically independent from each other, we first conducted an overall compositional data analysis (Aitchison, 1982) using the package *CoDaPack* (Comas and Thió-Henestrosa, 2011). Visual inspection of the data distribution across the tetrahedron (**Figure 3A**) suggested that genotypes differed markedly in the proportion of abnormal muscles, which was confirmed statistically by a Multiple Analysis of Variance (MANOVA). Confirmed these overall differences across genotypes, we then tested for statistical differences between genotypes or within genotypes across stages in the proportion of specific muscle phenotypes. We tested such comparisons fitting Generalized Linear Models with a binomial error distribution and a logit link function, where the dependent variable was *number of muscles with a given phenotype vs total number of muscles* scored in a given embryo.

RESULTS

LanB1 and *Kon* Interact Genetically During the Development of the Myotendinous Junction in *Drosophila* Embryos

To study the role of laminins and their interaction with *kon*, during the development of the MTJ, we first studied the pattern of the body wall musculature at the end of embryogenesis, stage 16 (st. 16) (**Figure 1A**), in both control and mutant embryos. To study *kon* function, we analyzed embryos for the null mutant allele $kon^{F1\text{-}3}$ (hereafter referred as *kon*). In agreement with previous findings (Estrada et al., 2007; Schnorrer et al., 2007), we found that, while control embryos (*kon*/+) did not show any defect in the musculature (**Figure 1B**), some muscles from *kon* embryos, particularly the ventral-longitudinal ones (VL), formed myospheres, a term used to describe rounded shape muscles due to detachment from their tendon cells (Wright, 1960) (arrowhead in **Figure 1C**). To study laminin function, we analyzed embryos carrying a deficiency that eliminates the only *Drosophila* gene encoding the laminin *ß*-subunit, *LanB1*, hereafter referred as *LanB1* embryos (**Figure 1D**). Similar to *kon* embryos, *LanB1* mutant muscles also formed myospheres, particularly the VL ones (Urbano et al., 2009) (arrowhead in **Figure 1D**). Since loss of function of either *kon* and *LanB1* showed myospheres, we studied their cooperation during MTJ development by performing genetic interaction experiments. To do this, we generated flies with a recombinant chromosome for both mutations. Double *kon, LanB1* heterozygous mutants showed a wild-type muscle pattern (**Figure 1E**), suggesting that a single functional allele for each gene is enough to properly establish the muscle pattern. However, we found that the muscle detachment phenotype of *LanB1* embryos that were also *kon* heterozygotes, was dramatically enhanced compared with either *kon* or *LanB1* single mutants (**Figure 1F**). Moreover, complete loss of both *kon* and *LanB1* (hereafter referred as *kon, LanB1* embryos) led to a generalized presence of myospheres (**Figure 1G**) (quantification below). The high number of detached muscles in the mutant combination *kon, LanB1* (either partial or complete), resulted in the formation of gaps in the muscle pattern (**Figures 1F,G** and **Supplemetary Figure S1**). Since *LanB1* deficiency also removes the 5' UTR of the adjacent *CG72143* gene, we validated our results by recombining $kon^{F1\text{-}3}$ with a null allele for *LanB1*, $LanB1^{1P3}$ (Urbano et al., 2009). Consistently, these recombinant mutant embryos showed the same phenotype as the *kon, LanB1* embryos (**Supplemetary Figure S1**). Altogether, this data supports a cooperative role for *LanB1* and *kon* in the formation of the MTJ.

LanB1 is Required for Muscle Migration Towards Tendon Cells

The muscle detachment phenotype observed at the end of embryogenesis in *LanB1* embryos (**Figure 1D**) (Urbano et al., 2009) might be caused by defects in either muscle guidance and/or muscle attachment to tendon cells. To distinguish between these two possibilities, and to further characterize the role of *LanB1* in the formation of the MTJ, we characterized muscle migration and attachment in both control and *LanB1* embryos. Previous studies have shown that as muscles migrate towards their tendon cells they extend projections towards future attachment positions (Volk, 1999; Schnorrer and Dickson, 2004). The visualization of the complete body wall musculature (**Figure 1**) complicates the analysis of the morphology of individual muscles as they migrate, as well as their cellular protrusions. To solve this, we decided to label just one specific muscle, VL1, using *5053-GAL4* driver (Swan et al., 2004) to express a GFP-tagged plasma membrane marker, *src: GFP* (Lesch et al., 2010) (**Figure 2**). *wild type (wt)* muscles (**Figures 2A,B**) (Schnorrer et al., 2007) first project protrusions anteriorly towards their future attachment positions at the anterior segment border (st. 13–14). The posterior end does not migrate, as it is already placed near the posterior segment border, the other attachment point. Then muscles initiate (st. 15) and stabilize (st. 16) the attachment to tendon cells (**Figure 2A**). In *LanB1* embryos (**Figure 2C**), at early stages (13–14), 6% of the VL1 muscles showed misoriented projections, that is, muscles with projections oriented perpendicularly to the normal posterior to anterior direction of migration (**Figure 2A**). At st. 15, *LanB1* loss caused a few cases of myospheroid-shape muscles (rounded, and detached muscles) (2%) and of muscles with misshaped projections (2%), muscles whose projections were properly oriented but longer than normal, and presenting a small contact surface

with the attachment site (**Figure 2A**), which reflects a defect in the initial contact between muscle and tendon cells. Moreover, at st. 16, 5% of the muscles were myospheres, and some muscles showed misoriented or misshaped projections (2% each). Our data suggests that *LanB1* regulates muscle targeting to tendon cells at early stages and stabilization of muscle attachments later in embryogenesis. The fact that *LanB1* muscles send projections suggests that LanB1 is not required for the overall formation of filopodia during muscle migration, although we cannot distinguish if they are intact at this resolution.

As in *LanB1* embryos, we had observed that *kon* embryos also showed myospheres at the end of muscle development (**Figure 1**) (Estrada et al., 2007; Schnorrer et al., 2007). However, the specific analysis of VL1 muscle morphology at early and late stages revealed striking differences between both genotypes (**Figures 2C,D**) (Estrada et al., 2007; Schnorrer et al., 2007). At st. 13-14, *kon* mutants showed a remarkable proportion of muscles with misshaped projections (63%), already indicating an altered ability to initiate contacts with tendon cells. However, unlike *LanB1* mutants, loss of *kon* did not produce muscles with misoriented projections at these early stages (**Figure 2D**) (Estrada et al., 2007; Schnorrer et al., 2007). Later, at st. 15, *kon* embryos showed an increase in the number of misshaped projections (from 63 to 86%), supporting the known role of *kon* in mediating muscle-tendon attachment. Remarkably, *kon* mutants also showed some misoriented muscles at this stage (5%), likely consequence of failed attachment, as previously reported (Schnorrer et al., 2007). Finally, at st. 16, 69% of *kon* mutants showed misshaped projections and 21% myospheres, indicating respectively incomplete and failed muscle attachments. Together, this data supports that the myospheres observed in late *kon* embryos could be due to defects in muscle-tendon migration and/or attachment formation, while LanB1 additionally showed a specific role in projection orientation at the early stages of muscle migration.

Kon and *LanB1* Cooperate in Muscle Guidance and Attachment to Tendon Cells

To better understand the specific role of *LanB1* and *kon* and their interaction, we first analyzed, independently of the stage, VL1 muscle morphology in different dosages of mutant alleles for *LanB1* and *kon*. The spatial distribution of the observed muscles with different phenotypes within a polyhedron showed that there is a statistically significant difference in their distribution among genotypes. Specifically, loss of one or two copies of *LanB1* in a *kon* background caused the displacement of the *kon* phenotypes towards the misoriented muscle morphology, suggesting an interaction between *LanB1* and *kon* in muscle migration and attachment formation. This statistical analysis (**Figure 3A** and **Supplementary Movie**) (see Material and Methods for more details) allowed us to carry out the specific pairwise comparisons of the phenotypes among genotypes in different stages.

At st. 13-14, we observed that while embryos with only one functional copy of *kon* showed no alterations in muscle development (**Figure 2B**), the additional loss of one *LanB1* allele (double heterozygous) (**Figure 3B**) showed around one third (28%) of all muscles with misoriented projections. Interestingly, this was significantly higher than what we found in either *LanB1* (6%) or *kon* (0%) single mutant embryos (**Figures 2C,D**), supporting a cooperation between both *kon* and *LanB1* in muscle targeting. Moreover, *kon, LanB1* mutants (**Figure 3C**), presented a similar amount of misoriented projections than double heterozygote mutants (**Figure 3B**; 34 and 28% respectively), but the former additionally showed misshaped muscles and myospheres (likely unable to send projections). Together, this resulted in that more than the half (57%) of the muscles in *kon*, *LanB1* embryos presented some type of muscle phenotype at early stages. Therefore, our data supports a role for *LanB1* in muscle guidance and its cooperation with *kon* in this process.

At st. 15, comparing *kon*, *LanB1* (**Figure 3C**) with *kon* (**Figure 2D**) embryos, they both showed a similar proportion of total number of muscles with any of the described phenotypes (86 and 91% respectively), while this proportion was only 3% in *LanB1* mutants (**Figure 2C**). However, *kon*, *LanB1* mutants showed 37% myospheroids and 23% misoriented muscles, phenotypes which were respectively non-observed or milder (5%) in *kon* mutants. Therefore, the early formation of myospheres and the relatively high number of misoriented muscles in *kon*, *LanB1* embryos, suggest a cooperation between both genes to regulate the later stages of muscle migration and the attachment formation between muscle and tendon cells.

At st. 16, all the muscles were affected in *kon*, *LanB1* mutants (**Figure 3C**), where 95% were myospheres and 5% misshaped projections. The remarkable difference of the myospheres/misshaped projections ratio between *kon* (21/70) (**Figure 2D**) and *kon, LanB1* mutants (95/5) (**Figure 3C**), supports a strong cooperation between *kon* and *LanB1* in the stabilization of the myotendinous junction.

Kon is Not Essential for LanB1 Localization at the MTJ

The transmembrane proteoglycan Kon is a cell adhesion receptor that mediates the interaction between the muscle cell and the ECM (Estrada et al., 2007; Schnorrer et al., 2007; Pérez-Moreno et al., 2017). Therefore, the observed cooperation between *kon* and *LanB1* during the formation of the MTJ might suggests a potential role for Kon in localizing LanB1 at the MTJ. As previously reported in *wt* condition (Urbano et al., 2009; Wolfstetter and Holz, 2012), we observed that control embryos showed LanB1 enrichment at the MTJ (arrowheads in **Figure 4A** and **Supplementary Figure S2A**). In *kon* embryos, despite the decreased MTJ surface of attachment of VL muscles, we still detected accumulation of LanB1 where muscles were attached (arrowheads in **Figure 4B** and **Supplementary Figure S2B**). This result indicates that Kon is not essential to recruit LanB1 at the MTJ.

DISCUSSION

The development of the MTJ requires cell adhesion receptors and ECM components (Maartens and Brown, 2015; Valdivia et al.,

2017). This is supported by studies, mainly in *Drosophila*, showing that the loss of these types of molecules leads to MTJ disruption. The physical interaction between cell adhesion receptors, mostly integrins, and the ECM is well-known, as well as the requirement of this interaction in multiple cellular and developmental events (Walma and Yamada, 2020). However, the specific contribution of each of these components and interactions between them to the different cellular processes underlying MTJ development, such as migration, recognition and attachment, remains largely unknown. Here, we show that laminins, previously involved in muscle attachment, are also required for proper muscle migration to the tendon cells. Furthermore, our results support that *kon* interacts with laminins both during migration and attachment.

It has been reported that *kon* and *LanB2* interact genetically during the MTJ formation (Wolfstetter and Holz, 2012). We extended this analysis by exploring the interaction between *kon* and *LanB1*. Remarkably, we observed that double loss of *kon* and *LanB1* caused a more dramatic disruption of the body wall musculature than the previously reported in *kon, LanB2* mutants. The secretion of an individual laminin subunit has been only observed *in vitro* (Yurchenco et al., 1997), being widely studied that laminins are only secreted and functional as heterotrimers *in vivo* (Hohenester, 2019). Therefore, the different grade of disruption of the muscle pattern observed between *kon, LanB2* mutants (Wolfstetter and Holz, 2012) and *kon, LanB1* mutants (this work) might be due to differences in the genetic background of both studies. Here, we validated our data by analyzing the genetic interaction between *kon* and two different mutants for *LanB1* ($LanB1^{DEF}$ and $LanB1^{1P3}$).

Beyond its general role in MTJ formation, it was unknown whether laminin (and other ECM components) only accumulates at the MTJ to form and/or stabilize the junction, or whether it also participates during the earlier process of muscle guidance. To study this, here, we explored the effect of *LanB1* loss during MTJ development. First, we observed a requirement of LanB1 at the early stages of muscle development, supported by the presence of some misoriented muscles at stage 13–14 in *LanB1* mutants. The inability to polarize filopodia in the right direction could be due to a failure in sensing guidance cues, and it also suggests that LanB1 is not required for filopodia formation. Similarly, our previous studies have shown that while haemocytes from *LanB1* embryos can form protrusions they are not orientated in the direction of migration. Formation and stabilization of lamellipodia play a critical role in achieving directionally persistent migration in cell culture (Petrie et al., 2009). As we showed that haemocytes produced their own laminins, this led us to propose a role for laminins in reinforcing directional migration by stabilizing cellular protrusions locally. In the future, it will be interesting to analyse whether muscles can also produce their own laminins to enhance directional migration.

In contrast to the muscle guidance defects observed in *LanB1* mutants, early *kon* embryos (stage 13–14) only showed misshaped projections, what suggests that Kon plays a role in muscle-tendon recognition/attachment (Estrada et al., 2007; Schnorrer et al., 2007). Although *kon* embryos showed misoriented projections at stage 15, this might be a consequence of the failed muscle-tendon recognition/attachment observed at earlier stages. The genetic interaction observed between *kon* and *LanB1* further supports a role for both LanB1 and Kon in muscle guidance. It remains open, however, whether LanB1 only plays a role in muscle guidance or whether it has an additional role in the stabilization of the attachment. The observation of myospheres at late stages in *LanB1* embryos could be partially due to a LanB1 role during muscle guidance, but also to an additional role in muscle-tendon adhesion. However, the fact that practically all muscles form myospheres in late *kon*, *LanB1* embryos, cannot be only correlated with the proportion of misoriented muscles observed earlier in the same embryos. Since there are no muscle contractions at st. 15 and only isolated brief muscles twitches by the end of st.16 (Perenau et al., 2007; Crisp et al., 2008), the observed myospheres in our study are most likely due to failed formation of the MTJ and not to a contraction-derived detachment. Therefore, our data suggests that misoriented muscles, muscles with misshaped projections and also some muscles with no phenotype, detached from tendon cells in late *kon*, *LanB1* embryos, supporting a role for LanB1 in stabilizing the MTJ. This potential role is also supported by the progressive accumulation of LanB1 in the mature MTJ from st. 14 to 16 (Martin et al., 1999), and by the fact that LanA is required for the adhesion of the basement membrane to the muscle surface in the formation of a similar hemi-adherens junction, the one in the neuromuscular junction (Prokop et al., 1998; Tsai et al., 2012).

Despite the requirement of both LanB1 and Kon during muscle development, we propose they are likely acting in parallel. The strong genetic interaction observed suggests they are neither upstream/downstream of each other in the same pathway nor working together as ligand and receptor. In addition, we observed that LanB1 localization is not regulated by Kon. However, they still might be part of the same molecular complex, where loss of different components could affect its functionality. In fact, it has been shown that the Kon orthologue, NG2, can physically interact *in vitro* with laminin (Burg et al., 1996).

Cell receptors can influence the ECM which in turn feedback on cell adhesion through the receptors (Maartens and Brown, 2015). In fact, later in MTJ development, Kon localizes the ECM protein Tsp and enhances PS2 integrin adhesion (Pérez-Moreno et al., 2017). Both LanB1 and Kon have been shown to interact with integrins (Estrada et al., 2007; Maartens and Brown, 2015) but how these protein complexes are coordinated in regulating the intricate molecular mechanisms underlying muscle guidance and adhesion to the tendons needs to be further elucidated.

DATA AVAILABILITY STATEMENT

The original contributions presented in the study are included in the https://doi.org/10.17605/OSF.IO/JWHZU, further inquiries can be directed to the corresponding author.

AUTHOR CONTRIBUTIONS

Conceptualization: BE; Methodology: JP-M, CS-C, and BE; Formal analysis and investigation: JP-M and BE; Writing original draft preparation: JP-M and BE; Reviewing and editing: JP-M, BE, CS-C, and MM-B; Visualization: JP-M and BE; Project administration: MM-B and BE; Funding acquisition: MM-B and BE; Supervision: BE.

ACKNOWLEDGMENTS

This publication was funded by Grant IJC2019-038819-I, funded by MCIN/AEI /10.13039/501100011033. JP-M acknowledges the support from Grant IJC2019-038819-I; MCIN/AEI/10.13039/501100011033 and Proyecto de Excelencia of the Consejería de Economía, Innovación, Ciencia y Empleo, Junta de Andalucía (PO9-CVI-5058); CS-C acknowledges the support from CSIC (JAE intro 08-01103); MM-B acknowledges the support from Proyecto de Excelencia, Junta de Andalucía (PO9-CVI-5058) and Proyecto del Ministerio de Ciencia e Innovación (PID2019-109013GB-100); BE acknowledges the support from the Ramón y Cajal program, Proyecto del Ministerio de Economía y Competitividad (BFU2008-036550, BFU2011-26745), University of Pablo de Olavide and University of Seville; We thank the Bloomington Stock Center for fly stocks and Ivan Gomez-Mestre for help with the statistical analysis.

SUPPLEMENTARY MATERIAL

The Supplementary Material for this article can be found online at: https://www.frontiersin.org/articles/10.3389/fcell.2021.749723/full#supplementary-material

REFERENCES

Aitchison, J. (1982). The Statistical Analysis of Compositional Data. *J. R. Stat. Soc. Ser. B (Methodological)* 44, 139–160. Available at: http://www.ncbi.nlm.nih.gov/pubmed/12556452. doi:10.1111/j.2517-6161.1982.tb01195.x

Bassett, D. I., and Currie, P. D. (2003). The Zebrafish as a Model for Muscular Dystrophy and Congenital Myopathy. *Hum. Mol. Genet.* 12, R265–R270. doi:10.1093/hmg/ddg279

Bate, M., and Martinez Arias, A. (1993). *The Development of drosophila Melanogaster*. Plainview, N.Y., USA: Cold Spring Harbor Laboratory Press.

Bate, M. (1990). The Embryonic Development of Larval Muscles in Drosophila. *Development* 110, 791–804. Available at: papers3://publication/uuid/56CD762F-8D54-4E1A-A15E-9BA7EF9BA98F. doi:10.1242/dev.110.3.791

Borchiellini, C., Coulon, J., and Le Parco, Y. (1996). The Function of Type IV Collagen during Drosophila Muscle Development. *Mech. Develop.* 58, 179–191. doi:10.1016/S0925-4773(96)00574-6

Burg, M. A., Tillet, E., Timpl, R., and Stallcup, W. B. (1996). Binding of the NG2 Proteoglycan to Type VI Collagen and Other Extracellular Matrix Molecules. *J. Biol. Chem.* 271, 26110–26116. doi:10.1074/jbc.271.42.26110

Campos-Ortega, J. A., and Hartenstein, V. (1997). *The Embryonic Development of Drosophila Melanogaster*. Berlin, Germany: Springer.

Carmena, A., Murugasu-Oei, B., Menon, D., Jiménez, F., and Chia, W. (1998). Inscuteable and Numb Mediate Asymmetric Muscle Progenitor Cell Divisions during Drosophila Myogenesis. *Genes Dev.* 12, 304–315. doi:10.1101/gad.12.3.304

Chanana, B., Graf, R., Koledachkina, T., Pflanz, R., and Vorbrüggen, G. (2007). αPS2 Integrin-Mediated Muscle Attachment in Drosophila Requires the ECM Protein Thrombospondin. *Mech. Develop.* 124, 463–475. doi:10.1016/j.mod.2007.03.005

Comas, M., and Thió-Henestrosa, S. "CoDaPack 2.0: a Stand-Alone, Multi-Platform Compositional Software," in Proceedings of the 4th International Workshop on Compositional Data Analysis (2011), Girona, Spain, May 2011, 1–10.

Conti, F. J., Felder, A., Monkley, S., Schwander, M., Wood, M. R., Lieber, R., et al. (2008). Progressive Myopathy and Defects in the Maintenance of Myotendinous Junctions in Mice that Lack Talin 1 in Skeletal Muscle. *Development* 135, 2043–2053. doi:10.1242/dev.015818

Crisp, S., Evers, J. F., Fiala, A., and Bate, M. (2008). The Development of Motor Coordination in Drosophilaembryos. *Development* 135, 3707–3717. doi:10.1242/dev.026773

Estrada, B., Gisselbrecht, S. S., and Michelson, A. M. (2007). The Transmembrane Protein Perdido Interacts with Grip and Integrins to Mediate Myotube Projection and Attachment in the Drosophilaembryo. *Development* 134, 4469–4478. doi:10.1242/dev.014027

García-Alonso, L., Fetter, R. D., and Goodman, C. S. (1996). Genetic Analysis of Laminin A in Drosophila: Extracellular Matrix Containing Laminin A Is Required for Ocellar Axon Pathfinding. *Development* 122, 2611–2621. doi:10.1242/dev.122.9.2611

Gotwals, P. J., Fessler, L. I., Wehrli, M., and Hynes, R. O. (1994). Drosophila PS1 Integrin Is a Laminin Receptor and Differs in Ligand Specificity from PS2. *Proc. Natl. Acad. Sci.* 91, 11447–11451. doi:10.1073/pnas.91.24.11447

Halfon, M. S., Gisselbrecht, S., Lu, J., Estrada, B., Keshishian, H., and Michelson, A. M. (2002). New Fluorescent Protein Reporters for Use with Thedrosophila Gal4 Expression System and for Vital Detection of Balancer Chromosomes. *Genesis* 34, 135–138. doi:10.1002/gene.10136

Hohenester, E. (2019). Structural Biology of Laminins. *Essays Biochem.* 63, 285–295. doi:10.1042/EBC20180075

Knoblich, J. A., and Lehner, C. F. (1993). Synergistic Action of Drosophila Cyclins A and B during the G2-M Transition. *EMBO J.* 12, 65–74. doi:10.1002/j.1460-2075.1993.tb05632.x

Kramer, S. G., Kidd, T., Simpson, J. H., and Goodman, C. S. (2001). Switching Repulsion to Attraction: Changing Responses to Slit during Transition in Mesoderm Migration. *Science* 292, 737–740. doi:10.1126/science.1058766

Lesch, C., Jo, J., Wu, Y., Fish, G. S., and Galko, M. J. (2010). A Targeted UAS-RNAi Screen in Drosophila Larvae Identifies Wound Closure Genes Regulating Distinct Cellular Processes. *Genetics* 186, 943–957. doi:10.1534/genetics.110.121822

Maartens, A. P., and Brown, N. H. (2015). The many Faces of Cell Adhesion during Drosophila Muscle Development. *Develop. Biol.* 401, 62–74. doi:10.1016/j.ydbio.2014.12.038

Martin, D., Zusman, S., Li, X., Williams, E. L., Khare, N., DaRocha, S., et al. (1999). wing Blister, A New Drosophila Laminin α Chain Required for Cell Adhesion and Migration during Embryonic and Imaginal Development. *J. Cel Biol.* 145, 191–201. doi:10.1083/jcb.145.1.191

Martin-Bermudo, M. D., Dunin-Borkowski, O. M., and Brown, N. H. (1998). Modulation of Integrin Activity Is Vital for Morphogenesis. *J. Cel Biol.* 141, 1073–1081. doi:10.1083/jcb.141.4.1073

Mayer, U., Saher, G., Fässler, R., Bornemann, A., Echtermeyer, F., von der Mark, H., et al. (1997). Absence of Integrin Alpha 7 Causes a Novel Form of Muscular Dystrophy. *Nat. Genet.* 17, 318–323. Available at: http://www.nature.com/naturegenetics. doi:10.1038/ng1197-318

Mouw, J. K., Ou, G., and Weaver, V. M. (2014). Extracellular Matrix Assembly: A Multiscale Deconstruction. *Nat. Rev. Mol. Cel Biol.* 15, 771–785. doi:10.1038/nrm3902

Pereanu, W., Spindler, S., Im, E., Buu, N., and Hartenstein, V. (2007). The Emergence of Patterned Movement during Late Embryogenesis of Drosophila. *Dev. Neurobiol.* 67, 1669–1685. doi:10.1002/dneu10.1002/dneu.20538

Pérez-Moreno, J. J., Bischoff, M., Martín-Bermudo, M. D., and Estrada, B. (2014). The Conserved Transmembrane Proteoglycan Perdido/Kon-Tiki Is Essential for Myofibrillogenesis and Sarcomeric Structure in Drosophila. *J. Cel Sci.* 127, 3162–3173. doi:10.1242/jcs.150425

Pérez-Moreno, J. J., Espina-Zambrano, A. G., García-Calderón, C. B., and Estrada, B. (2017). Kon-tiki/Perdido Enhances PS2 Integrin Adhesion and Localizes its Ligand, Thrombospondin, in the Myotendinous junction. *J. Cel Sci.* 130, 950–962. doi:10.1242/jcs.197459

Perkins, A. D., Ellis, S. J., Asghari, P., Shamsian, A., Moore, E. D. W., and Tanentzapf, G. (2010). Integrin-mediated Adhesion Maintains Sarcomeric Integrity. *Develop. Biol.* 338, 15–27. doi:10.1016/j.ydbio.2009.10.034

Petrie, R. J., Doyle, A. D., and Yamada, K. M. (2009). Random versus Directionally Persistent Cell Migration. *Nat. Rev. Mol. Cel Biol.* 10, 538–549. doi:10.1038/nrm2729

Prokop, A., Martı´n-Bermudo, M. D., Bate, M., and Brown, N. H. (1998). Absence of PS Integrins or Laminin A Affects Extracellular Adhesion, but Not Intracellular Assembly, of Hemiadherens and Neuromuscular Junctions inDrosophilaEmbryos. *Develop. Biol.* 196, 58–76. doi:10.1006/dbio.1997.8830

Roote, C. E., and Zusman, S. (1995). Functions for PS Integrins in Tissue Adhesion, Migration, and Shape Changes during Early Embryonic Development in Drosophila. *Develop. Biol.* 169, 322–336. doi:10.1006/dbio.1995.1147

Schnorrer, F., and Dickson, B. J. (2004). Muscle Building. *Develop. Cel* 7, 9–20. doi:10.1016/j.devcel.2004.06.010

Schnorrer, F., Kalchhauser, I., and Dickson, B. J. (2007). The Transmembrane Protein Kon-Tiki Couples to Dgrip to Mediate Myotube Targeting in Drosophila. *Develop. Cel* 12, 751–766. doi:10.1016/j.devcel.2007.02.017

Schulman, V. K., Dobi, K. C., and Baylies, M. K. (2015). Morphogenesis of the Somatic Musculature inDrosophila Melanogaster. *Wires Dev. Biol.* 4, 313–334. doi:10.1002/wdev.180

Schweitzer, R., Zelzer, E., and Volk, T. (2010). Connecting Muscles to Tendons: Tendons and Musculoskeletal Development in Flies and Vertebrates. *Development* 137, 3347. doi:10.1242/dev.057885

Subramanian, A., Wayburn, B., Bunch, T., and Volk, T. (2007). Thrombospondin-mediated Adhesion Is Essential for the Formation of the Myotendinous junction in Drosophila. *Development* 134, 1269–1278. doi:10.1242/dev.000406

Swan, L. E., Wichmann, C., Prange, U., Schmid, A., Schmidt, M., Schwarz, T., et al. (2004). A Glutamate Receptor-Interacting Protein Homolog Organizes Muscle Guidance in Drosophila. *Genes Dev.* 18, 223–237. doi:10.1101/gad.287604

Tsai, P.-I., Wang, M., Kao, H.-H., Cheng, Y.-J., Lin, Y.-J., Chen, R.-H., et al. (2012). Activity-dependent Retrograde Laminin A Signaling Regulates Synapse Growth at Drosophila Neuromuscular Junctions. *Proc. Natl. Acad. Sci.* 109, 17699–17704. doi:10.1073/pnas.1206416109

Urbano, J. M., Torgler, C. N., Molnar, C., Tepass, U., López-Varea, A., Brown, N. H., et al. (2009). Drosophilalaminins Act as Key Regulators of Basement Membrane Assembly and Morphogenesis. *Development* 136, 4165–4176. doi:10.1242/dev.044263

Valdivia, M., Vega-Macaya, F., and Olguín, P. (2017). Mechanical Control of Myotendinous junction Formation and Tendon Differentiation during Development. *Front. Cel Dev. Biol.* 5, 1–8. doi:10.3389/fcell.2017.00026

Volk, T. (1999). Singling Out Drosophila Tendon Cells: A Dialogue between Two Distinct Cell Types. *Trends Genet.* 15, 448–453. doi:10.1016/S0168-9525(99)01862-4

Walma, D. A. C., and Yamada, K. M. (2020). The Extracellular Matrix in Development. *Development* 147. doi:10.1242/dev.175596

Wang, H.-V., Chang, L.-W., Brixius, K., Wickström, S. A., Montanez, E., Thievessen, I., et al. (2008). Integrin-linked Kinase Stabilizes Myotendinous Junctions and Protects Muscle from Stress-Induced Damage. *J. Cel Biol.* 180, 1037–1049. doi:10.1083/jcb.200707175

Wolfstetter, G., and Holz, A. (2012). The Role of LamininB2 (LanB2) during Mesoderm Differentiation in Drosophila. *Cell. Mol. Life Sci.* 69, 267–282. doi:10.1007/s00018-011-0652-3

Wright, T. R. F. (1960). The Phenogenetics of the Embryonic Mutant Lethal Myospheroid, in *Drosophila melanogaster*. *J. Exp. Zool.* 143, 77–99. doi:10.1002/jez.1401430107

Yurchenco, P. D., Quan, Y., Colognato, H., Mathus, T., Harrison, D., Yamada, Y., et al. (1997). The Chain of Laminin-1 Is Independently Secreted and Drives Secretion of its - and -chain Partners. *Proc. Natl. Acad. Sci.* 94, 10189–10194. doi:10.1073/pnas.94.19.10189

Conflict of Interest: The authors declare that the research was conducted in the absence of any commercial or financial relationships that could be construed as a potential conflict of interest.

Publisher's Note: All claims expressed in this article are solely those of the authors and do not necessarily represent those of their affiliated organizations, or those of the publisher, the editors and the reviewers. Any product that may be evaluated in this article, or claim that may be made by its manufacturer, is not guaranteed or endorsed by the publisher.

frontiers | Frontiers in Cell and Developmental Biology

CORRECTION
published: 13 April 2022
doi: 10.3389/fcell.2022.887432

Corrigendum: LanB1 Cooperates With Kon-Tiki During Embryonic Muscle Migration in *Drosophila*

Juan José Pérez-Moreno[1,2], *Carmen Santa-Cruz Mateos*[1,3], *María Dolores Martín-Bermudo*[1] *and Beatriz Estrada*[1,2]*

[1]Centro Andaluz de Biología del Desarrollo, Universidad Pablo de Olavide/CSIC/JA, Seville, Spain, [2]Departamento de Biología Celular, Universidad de Sevilla and Instituto de Biomedicina de Sevilla (IBiS), Hospital Universitario Virgen del Rocío/CSIC/Universidad de Sevilla, Seville, Spain, [3]Department of Physiology, Development and Neuroscience, University of Cambridge, Cambridge, United Kingdom

Keywords: myogenesis, migration, adhesion, myotendinous junction, drosophila, laminin, kon-tiki, NG2

A Corrigendum on

LanB1 Cooperates With Kon-Tiki During Embryonic Muscle Migration in *Drosophila*
by Pérez-Moreno, J. J., Santa-Cruz Mateos, C., Martín-Bermudo, M. D. and Estrada, B. (2022). Front. Cell Dev. Biol. 9:749723. doi: 10.3389/fcell.2021.749723

The original Funding and Acknowledgment sections were not formatted according to the institution's guidelines. This has now been rectified and the paragraph below replaces the previous version:

ACKNOWLEDGMENTS

This publication was funded by Grant IJC2019-038819-I, funded by MCIN/AEI /10.13039/501100011033. JP-M acknowledges the support from Grant IJC2019-038819-I; MCIN/AEI /10.13039/501100011033 and Proyecto de Excelencia of the Consejería de Economía, Innovación, Ciencia y Empleo, Junta de Andalucía (PO9-CVI-5058); CS-C acknowledges the support from CSIC (JAE intro 08-01103); MM-B acknowledges the support from Proyecto de Excelencia, Junta de Andalucía (PO9-CVI-5058) and Proyecto del Ministerio de Ciencia e Innovación (PID2019-109013GB-100); BE acknowledges the support from the Ramón y Cajal program, Proyecto del Ministerio de Economía y Competitividad (BFU2008-036550, BFU2011-26745), University of Pablo de Olavide and University of Seville; We thank the Bloomington Stock Center for fly stocks and Ivan Gomez-Mestre for help with the statistical analysis.

The authors apologize for this error and state that this does not change the scientific conclusions of the article in any way. The original article has been updated.

OPEN ACCESS

Approved by:
Frontiers Editorial Office, Frontiers Media SA, Switzerland

***Correspondence:**
Beatriz Estrada
bestrada@us.es

Specialty section:
This article was submitted to Cell Adhesion and Migration, a section of the journal Frontiers in Cell and Developmental Biology

Received: *01 March 2022*
Accepted: *02 March 2022*
Published: *13 April 2022*

Citation:
Pérez-Moreno JJ, Santa-Cruz Mateos C, Martín-Bermudo MD and Estrada B (2022) Corrigendum: LanB1 Cooperates With Kon-Tiki During Embryonic Muscle Migration in Drosophila. Front. Cell Dev. Biol. 10:887432. doi: 10.3389/fcell.2022.887432

Advantages of publishing in Frontiers

OPEN ACCESS
Articles are free to read for greatest visibility and readership

FAST PUBLICATION
Around 90 days from submission to decision

HIGH QUALITY PEER-REVIEW
Rigorous, collaborative, and constructive peer-review

TRANSPARENT PEER-REVIEW
Editors and reviewers acknowledged by name on published articles

Frontiers
Avenue du Tribunal-Fédéral 34
1005 Lausanne | Switzerland

Visit us: www.frontiersin.org
Contact us: frontiersin.org/about/contact

REPRODUCIBILITY OF RESEARCH
Support open data and methods to enhance research reproducibility

DIGITAL PUBLISHING
Articles designed for optimal readership across devices

FOLLOW US
@frontiersin

IMPACT METRICS
Advanced article metrics track visibility across digital media

EXTENSIVE PROMOTION
Marketing and promotion of impactful research

LOOP RESEARCH NETWORK
Our network increases your article's readership